TOPICAL SCIENTIFIC RESEARCHES INTO RESOURCE-SAVING TECHNOLOGIES OF MINERAL MINING AND PROCESSING

Multi-authored monograph

Publishing House “St.Ivan Rilski”, Sofia,
2020

UDC 622.002

Recommended for publication by the Academic Board of the National University of Water and Environmental Engineering, Ukraine. Minutes № 2, 28.02.2020

Reviewers: ***Dr. Mohamed Tafsir DIALLO***, Managing Director of Polytechnic Institute of Gamal Abdel Nasser University of Conakry, Republic of Guinea

Khavalbolot KELGENBAI, Professor, Head Department of Mineral processing and engineering Geology and Mining School Mongolian University of Science and Technology, Mongolia

Khalidilla YUSUPOV, Doctor of Science (Engineering), Professor**,** Professor of the Department of Mining, Satbayev University, Republic of Kazakhstan

Topical scientific researches into resource-saving technologies of mineral mining and processing. Multi-authored monograph. – Sofia: Publishing House "St.Ivan Rilski", 2020. - 446 p.

ISBN 978-954-353-408-1

The monograph considers potential technological development of ore mining and processing industries through updating mining machines and technologies
The book is intended for a broad mining audience of scholars, practitioners, postgraduates and students.

UDC 622.002

ISBN 978-954-353-408-1

Table of contents

PREFACE

We are glad to present the multi-authored monograph "Topical scientific researches into resource-saving technologies of mineral mining and processing".

The monograph deals with prospects of developing mineral raw material bases of different countries. There are analyzed specific features of technological advance in ore mining and processing industries as well as trends of their development in the world.

The necessity of modernizing operating mining enterprises and developing new deposits in regions with poor infrastructure is under consideration. There are determined stages of forming the basis for efficient mining of mineral deposits and parameters of operation of mining and processing enterprises through applying resource-saving technologies. Innovative effective technologies used in mineral mining and processing are under detailed analysis.

Chief editor,

Zinovii MALANCHUK - Doctor of Sciences (Engineering), Professor, Director Institute of Postgraduate Education, National University of Water and Environmental Engineering, Ukraine.

PHYSICAL-MECHANICAL AND TECHNOLOGICAL FEATURES OF AMBER EXTRACTION IN THE RIVNE-VOLYN REGION OF UKRAINE

Malanchuk Z.R.
National University of Water and Environmental Engineering (NUWEE), Professor, Doctor of Technical Sciences, Professor, Department of Development of Deposits and Mining, Ukraine

Soroka V.S.
National University of Water and Environmental Engineering (NUWEE), Associate Professor, Candidate of Agricultural Sciences, Associate Professor, Department of Transportation Technology and Technical Service, Ukraine

Lahodniuk O.A.
National University of Water and Environmental Engineering (NUWEE), Associate Professor, Candidate of Technical Sciences, Associate Professor, Department of Land, Cadastre, Land Monitoring and Geoinformatics, Ukraine

Marchuk M.M.
National University of Water and Environmental Engineering (NUWEE), Professor, Candidate of Technical Sciences, Professor, Department of Automobiles and Automobile Economy, Ukraine

Abstract

The main challenge facing the mining industry is to ensure the growth of minerals by enhancing mining in the most efficient open and underground way based on the widespread introduction of advanced technology and mining equipment.

In today's economic conditions, the efficiency of the mining equipment can be increased by substantiating the rational factors that affect the process of hydro mechanized production and improvement of existing technological equipment based on the application of the automatic control system of hydro-erosion. However, well-known mining technologies do not allow the full extraction of amber due to the imperfection and lack of effective technology for the complete extraction of amber from amber-containing deposits.

The complexity and the large number of possible production processes and the specifics of the operating conditions of the fields indicate that for the exploration and extraction of minerals there is a need for additional research of equipment complexes in the composition of hydro monitors. Increasing the efficiency of such

complexes by reducing energy costs while increasing the range and improving the quality of production requires scientific justification of the parameters of the components of the production complexes of a new technical level.

Physical-mechanical and technological peculiarities of amber extraction in Rivne-Volyn region of Ukraine are presented.

1.1. Physico-mechanical and chemical properties of Ukrainian amber

In the Rivne region, amber deposits are taken out by excavator at the Klesiv field. The extracted rock is delivered to the flushing unit located on the industrial site by road. Initially, the rock enters the loader, from which the conveyor is fed to the screen, equipped with a metal mesh with square cells with a diameter of 5 mm. Above the screen, at a height of 20 cm from the grid, there is a system of tubes into which water is pumped under pressure. It irrigates rocks, washes clay, sand, silicon, fragments of crystalline rocks and amber smaller than 5 mm, bringing them into a specially prepared quarry. Pieces of rock and gem of size 5 mm or more come to the conveyor for development. Here, the amber is separated manually from the breed containing it. Since 1980, more than 100 kg of mineral resources have been extracted from the field since 1980, 95% of the amber produced belongs to the category of jewelry [1-20].

The most energy-intensive and cost-effective process is the removal of cross-breed, which is of great value to the enterprise, but the cost of amber increases.

Amber is a high molecular weight organic acid compound containing an average of 79% carbon; 10.5% hydrogen; 10.5% oxygen (Fig. 1). It's formula $C_{10}H_{16}O$. In the amber, 24 chemical elements (Y, V, Mn, Cu, Ti, Zr, Al, Si, Mg, Ca, Fe, Nb, P, Pb, Zn, Cr, Ba, were detected in the amber (from traces up to 3%) , Co, Na, Sr, Sn, Mo, Yb). Of these, 17 were found in the lowland amber of the Klesiv deposit, 12 in the amber of the Beach section of the Primorsky deposit, 11 and 13, respectively, in the amber of the Curonian Spit and the Carpathian region. The least amount of chemical elements is contained in transparent amber. This mineral may be white, yellow, greenish, blue, red in color, but orange and golden yellow varieties are typical. The mineral is amorphous, soft (hardness of 2.2-2.5 points on the Moos scale), viscous, easily polished and polished. Its density is 1.05-1.096 g/cm^3. In terms of

classification, this mineral is representative of the group of combustible minerals - humus coal of the category "lipobiolites". Chemically, it is a high molecular weight compound of organic acids, usually with sulfur impurities. At a temperature of 150 °C amber softens, at more than 300 °C melts. It burns easily, giving off a resinous odor. The mineral has dielectric and heat-resistant properties, in nature occurs in the form of grains and pieces of size from 1 to 10-20 cm or more in diameter, but also find very large pieces - up to 10 kg in weight. The shape of the pieces can be any: drops, icicles, influxes of various irregular shapes, porous plates [13-15, 25].

Fig. 1. Polissya amber

The elemental composition of the amber of the Beach section of the Primorsky (South Baltic) and Klesiv(Ukraine) fields, the manifestations of the Carpathians is close. The average content of the main components (C and H) in them are respectively 80.78% and 10.12%; 78.05% and 9.55%; 79.68% and 10.07%; 78.26% and 9.99%. (Fig. 2).

The content of succinic acid in Baltic amber (succinate) ranges from 3 to 8%. Depending on the type of amber, it is distributed differently. In transparent amber, succinic acid contains from 3.2 to 4.5%, in Bastardo - from 4.0 to 6.2%, in bone amber - from 5.5 to 7.8%, in the oxidized crust - 8.2 %. Amber composition and structure continue to be studied. The volatile part (about 10% by weight) has been known for a long time. These are aromatic compounds - terpenes with 10 carbon atoms and sesquiterpenes with 15 carbon atoms in the molecule. According to mass spectrometric studies,

more than 40 compounds are included in amber. Many are not yet known. In amber form, abietic acid and its isomers are isolated from amber. They make up part (20-25%) of Baltic amber in organic solvents. Mineral inclusions in amber are represented by iron sulfide - pyrite and bituminous substance. Among the gas inclusions in the amber composition were found CO_2; O_2; H_2; Ar; Kr; Xe; No, nitrogen predominates. Amber residue, insoluble in any of the known solvents. IR- spectrometry data showed that "succinate" contains lactone (ester) groups, is an ester. In addition, the amber constantly contains succinic acid (about 4%) and impurities of salts (mainly succinic) potassium, calcium, sodium, iron (up to 1%). Thus, amber consists of three groups of compounds: volatile terpenes and sesquiterpenes; soluble organic acids; insoluble polyesters of these acids with alcohols formed from the same acids [12, 19-24].

Amber of Ukraine contains up to 3.19% of sulfur.

Rivne amber differs in its chemical composition. It is the most saturated with impurities and contains 18 chemical elements. In addition to silicon, magnesium, iron, calcium, which are present in almost all deposits, such as lead, zirconium and up to 3.19% sulfur are added. The ash content of Klesiv amber is 8.7%. This affects the quality and color of the cured resin. Amber is a mineral of the class of organic compounds, the coniferous tree resin in the main Paleogene period. Amber composition: volatile aromatic oil, two soluble resin fractions, succinic acid and 90% insoluble fractions. Its chemical formula is $C_{25}H_{40}O_4$. Amber is an amorphous polymer that has many colors, gives a specific IR spectrum (within 700-1900 cm^{-1}) that distinguishes amber from other similar resins. The melting point t=365-390 °C. Specific gravity - 1000-1100 kg/m^3 (in the Baltic states there are also 970 kg/m^3, and in the Carpathian region - 1220 kg/m^3). Well machined. It is insoluble in water (partially in alcohol - 20-25%, ether - 18-23%, chloroform - up to 20%), but it can swell and increase in volume up to 8% during long stay in it. Completely decomposes in hot concentrated nitric acid, can be softened at t=100 °C.

The cost of the amber depends on the uniqueness of the amber specimens and is determined by a peer review team.

To determine the cost, a technique has been developed that includes the classification of amber pieces by shape (shape A, B, C, D), size (1 to 5) and color (Color1, Color2, Color 3 and Color 4).

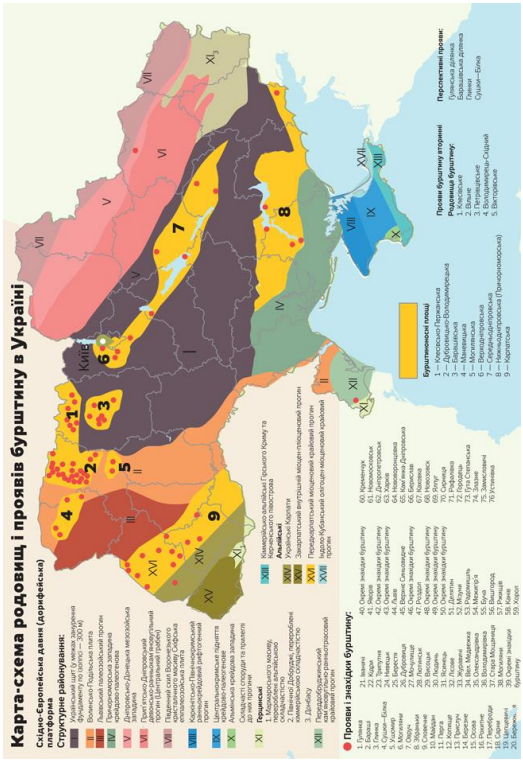

Fig. 2.. Map of amber manifestations in Ukraine

1.2. Geological features of the location of amber deposits

In nature, amber occurs in the form of amorphous bodies of various shapes and sizes. The weight of amber found in nature can range from grams to several kilograms. And the largest Burmese amber in the world can be seen in the Natural History Museum in London weighing 15 kg 250 grams.

Small deposits are located on the Gdansk Bay in Poland and on the North Sea coast in the Netherlands, Germany and Denmark. The content of the gem in the Stubbenfeld field on the island of Usedom is 0.357 kg/m^3. Depth of occurrence of blue earth 80-100 m from the surface.

The Paleogene layers of the Southern Baltic are only part of the vast amber horizon, which is exposed in Belarus (in the Minsk and

Grodno regions) and in Ukraine (the Klesiv deposit in the Rivne region). The presence of this horizon is confirmed by drilling operations carried out in Poland, in particular in the Eastern Seaside and in the vicinity of Braniewo, as well as in the Western Pomerania between Slupsk and Koszalin. The German researcher G. Conventz considers that amber breeds continue in the western direction to the coast of England [15-23].

Amber has been known in Ukraine for a long time. Its first developments are known near Kiev (Mizhgirya and Vyshgorod districts) and in Volyn (near modern Klesov). In 1870, 50 pieces of gem of different sizes weighing just over 800 grams were found in one layer near Kiev. Amber was washed by the Dnieper and other rivers with floods, carried away by melt and rain water from beams and ravines. In the distant times, its extraction not only satisfied local demand, but also made it possible to export it to ancient countries along the shores of the Mediterranean Sea and to the eastern states. However, the surface development of small Kiev deposits available for miners was gradually developed and forgotten [15-17].

Small manifestations of amber have long been known in the western regions of Ukraine on the territory of the present Lviv and Ivano-Frankivsk regions. In the tertiary deposits of Lviv and its environs, amber was found in the middle of the last century. Amber was not only mined in the Dnieper and its tributaries, in Volyn and Carpathian, but also cultivated in these places. Amber in composition and properties is not inferior to the Baltic. Therefore, it was sometimes called the Kiev succinates.

Amber is now found in Neogene deposits, which cover sulfur ores in the Yazivsky, Nemyrivsky, Rozdilsky and Podorozhny fields and in the Rechychansky sulfur manifestation. More than 2000 pieces of gem from millimeter to 25 cm have been accumulated in the quarry of the Yaziv deposit.

Amber is colorless, yellow-white, yellow, brown-yellow, light and yellow-brown, transparent, translucent and opaque. Changes in the degree of transparency of the stone by section were observed. Transparent amber is concentrated in its middle [15-19].

In geotectonic terms, the Klesiv Amber Zone is located at the junction of the northwestern slope of the Ukrainian Crystalline Massif, Volyn-Podilskyi Plate and the Pripyat Basin and has a two-

tier structure. The morphology of the present surface of the crystalline base is determined by its structural position on the northwest slope of the shield.

On the project area, the crystalline foundation is covered with Cenozoic and Quaternary sediments and has absolute marks of 130-170 m above sea level, gradually sinking in the northern and western directions with a slope of 10 m per 1 km. The general tendency to dive is complicated by some local elevations of the projections of the shield. The crystalline foundation is the ultra-metamorphic, metasomatic and intrusive formation of the lower and middle Proterozoic.

The outcrop nature of the relief of the foundation with the development of oval, isometric or irregular projections of Precambrian rocks with an area of 1 to 10 km, separated by relatively narrow (first hundreds of meters) and elongated (first kilometers) depressions, was established. In modern relief, they correspond to wetland valley sections, the relative excess of the projections of the basement over adjacent depressions averages 10-12 m. On the bark of weathering crystalline rocks lies a discontinuous layer of bluish-gray, sometimes greenish-gray, dense, viscous clay up to 2.5 m. The age of the clay is Lower Oligocene. Two layers of glauconite-quartz sands of oligocene age of different color shades, which are productive horizon, lie on the clays and in the places where they are absent, on the bark of weathering crystalline rocks. The lower layer of amber-bearing rocks is represented by fine-grained sands of dark gray, sometimes greenish in color and medium-grained sands of dark gray with a bluish-gray tint. The rocks are water-saturated, the thickness of the layer varies between 1.0-6.0 m. In the lower part of the section, thin (2-3 cm) layers of humus substance of black color are noted.

The upper amber-containing layer is represented by fine-medium-grained gray, light-gray sands, saturated with water, containing a considerable amount of humus substance, unevenly distributed throughout the formation. In the section there are small (1-3 cm) layers of lenticular clay layers, as well as plant residues and roots. The average layer thickness is 2.0 m. Oligocene sediments are covered by the Quaternary formations, which are represented by light yellowish-gray, gray, light gray fine-grained quartz sands of

fluvioglacial genesis. The thickness of the Quaternary sediment layer varies from 1 to 8 m.

The hydrogeological conditions of the Klesivskoye deposit are relatively simple, with the ubiquitous upper aquifer of groundwater, which is fed by atmospheric precipitation. Water-bearing rocks are represented by fine-grained sands of Quaternary and fine-grained sands of Oligocene age. The power of the horizon reaches 12 m. At the bottom it is a pressure swimmer. Most of the territory of the watershed is dark greenish gray clay of the Early Oligocene age or structured kaolinized crust of weathering crystalline rocks.

According to the Ukrainian geologist V.I. Panchenko [15-19] The Klesiv amber field is located in the framing zone of the Proterozoic crystalline rocks of the northwestern part of the Ukrainian Shield by sedimentary Paleogene formations. The placer consists of several sections, two of which are open pit. The productive horizon of the deposit consists of three sand layers composed of grained quartz sands, which are unequally enriched with clay, organic material and amber. The lower layer is sporadically enriched with glauconite, which gives the amber rock a blue tint. Amber pieces reach the size of 10 cm. According to V.I. Panchenko and O.S. Tkachuk, the content of amber in the field - from 15 to 310 g/m^3 and even 1000 g/m^3, the average - 50 g/m^3. The distribution of amber is uneven, the maximum concentration at the base is thicker. The annual extraction of amber at the Klesiv deposit does not exceed 140 kg. In a short time Klesovsky amber gained recognition in the domestic and foreign markets.

Unlike the Baltic amber, Klesiv is far from the sea. It can be predicted that at the Paleogene time near the village was the seashore. The position of the ancient coastal strip in Volyn is recorded by other amber finds in the area. It is known that vertical tectonic movements of the Earth's crust occurred at the boundary of the Eocene and Oligocene, which led to transgression (onset) and regression (indentation) of the sea. German researcher f. Kaunhoven found that in the tertiary period in the present Kaliningrad peninsula the interpenetration of sea and land changed 19 times.

In the post-Oligocene time, amber deposits were exposed to the effects of denudation factors; it was carried out by the waters to new deposits. In the glacial age in the south of the Baltic, part of the deposits was detached from the main deposit by a moving glacier.

Glacial waters and moraines spread pieces of amber rock across Europe. The yields of such rocks coincide with the boundary of glacial sediments, which lie on the boundary of tertiary and quaternary sediments. This process is associated with finding small amber deposits in Poland and Germany.

Amber-bearing rocks on the underwater slope of the Kaliningrad Peninsula are nowadays exposed to the active action of sea waves. A lot of amber is thrown on the beach on much of the southern Baltic coast. Researchers say that the fluvioglacial, marsh, and coastal sediments of Cenozoic age are associated with amber in Belarus. Two amber-bearing regions - Polissia and Mikashevichy-Zhytkovytska - have been identified in Belarus by the totality of paleotectonic, facial-paleogeographic data and the results of the experiment.

1.3. Technological features of amber extraction from amber-containing deposits in Ukraine

According to studies [15 - 23], three zones and four regions with industrial concentrations of amber have been identified in the Rivne region. All of them belong to the Pripyat Basin of sedimentation, which at the same time with the accumulation of marine sediments in the Oligocene epoch (about 35 million years ago) formed large-scale amber deposits. The total area of distribution of productive amber-containing horizons in the Rivne region is 3810 km^2, which is 18% of its territory.

Two fields of amber have been explored in the Rivne region: Klesiv in Sarnensky and Vilna in Dubrovytskyi districts, which are being developed today by the state enterprise “Amber of Ukraine” [15-19].

Further increase in amber reserves - raw is possible due to the completion of the stage of prospecting and prospecting and evaluation work on the sites "Fedorovska" and "reclamation" within the Klesiv field and sections of the Volodymyrets amber-containing zone, where the Rivne geologia field works.

The largest amber fields of "Klesiv", "Vilne", "Vladimir-Oriental" contain at least several hundred tons of amber raw materials, of which 128 tons of industrial reserves have been explored. Two of

them are operated: Of "Ukraine","Vladimir-East"- LLC" Center "Sunny Craft". Official amber production in 2015 was 4.5 tons.

In the Klesiv field, amber is extracted in open-pit mining (Fig. 3). Amber lies in sandy soil. Depth - up to 15m. A granite quarry with a large water supply is located near the deposit. The deposit is located close to roads and mains. During the six months of 2003, 230 kg of mineral was extracted from SE "Amber Mines". And for 2006, the extraction of amber is 3200 kg per year, achieved through the use of amber extraction of a new excavator ES-5/45 and stable funding from the state budget. In 2006, the volume of work in the quarry was: mines - 23.6t/m^3; rock mass - 17,466 t/m^3; reclamation per month - 0.5 ha. [45-53]

However, due to lack of financing, as of January 1, 2017, "Ukrburstin" is practically not functioning and is bankrupt.

Polissya amber differs in its chemical composition. It is the most saturated with impurities and contains 18 chemical elements. In addition to silicon, magnesium, iron, calcium, which are present in almost all deposits, such as lead, zirconium and up to 3.19% sulfur are added. The ash content of Klesiv amber is 8.7%. This affects the quality and color of the cured resin. The characteristic of amber is presented in item 1.2. [16-21].

Amber is used to make jewelry varnishes, paints, from amber to make medicines. In 1998, the first stage of the Rivne Jewelry Factory was put into operation, which, in addition to amber jewelry, produces succinic, glutaric acid and volatile aromatic oil, which is used in pharmacy.

Fig. 3. Preparation of the array for extraction of amber in the quarry by excavation

The potential amber reserves in the area are much larger. According to the results of the prospecting and evaluation work of the Rivne CCP of the SE “Ukrainian Geological Company”, the estimated resources of amber in the Dubrovytsf, Sarny and Volodymyrets districts are more than 1400 tons.

Number and total area of sites for which special permits for geological exploration were issued, including experimental and industrial development of subsoil for subsoil users as of the beginning of 2016: state - 3 and 46.5 km^2; private - 2 and 68.4 km^2, respectively. The total area of prospective sites for amber offered by "Ukrainian Geological Company" for geological study is about 800 km^2. Thus, 685 km^2 of amber sections of the region are not controlled and are the object of unauthorized development.

The total area of sites affected by unauthorized amber production as of 2010 was more than 500 ha. Now it is estimated to exceed more than 1000 hectares and growing, but their records and audits are not maintained.

1.4. Conditions for the formation of amber deposits in the Rivne-Volyn region of Ukraine

Amber accumulation conditions within the Oligocene sedimentation basin of the Rivne, Volyn, and Zhytomyr regions are determined by the peculiarities of the geological structure of the northwestern slope of the shield and the features of the structural and morphological structure of different parts of the Mezhigirsk Sea. The discovery of industrial amber deposits in Ukraine began with the discovery in 1980 of the Klesiv deposit, which is still active today. Further exploration and evaluation activities within the Klesiv amber-bearing area over the last 30 years have expanded information on its geological structure and conditions for the formation of primary amber deposits.

The Klesiv deposit in tectonic terms is located within the lowered part of the Osnitsky block - the Klesivsky ridge [15-19, 24]. The negative structure is small in size (according to geological survey work - 240 km^2), has a shape close to a regular quadrilateral and is bounded by faults. It is separated from the shield by Shakhinskaya [15], and in the west it is framed by Miliachka meridional local tectonic zones. Within this inherited decrease, mostly all (except for

the manifestation near Perebrody village in the north of the district and the Tomashgorod manifestation in the east) are located at the present time manifestations of amber within the Klesiv amber-bearing area.

The productive sediments of the Klesivskoye deposit cover a strip of width from 200 to 700 m, which can be traced from the southeast to the northwest between the outcrops to the domizhigir surface of small projections of the foundation. The length of the amber-enriched strip is more than 2 km. The outcrops of crystalline rocks among the inter-mountain deposits are insignificant in size and in the inter-mountain times represented numerous abrasion islands [15] with an area of about 50%.

Productive for industrial contents amber bearing thickness is the thickness of the sand of the early and middle Oligocene age [15-17]. The sediments are usually confined to paleosecretions between the crystalline projections of the basement and lie on low-thickness (up to 15 m) thick sediment deposits represented by glauconite-quartz sands and clays. The thickness of the sedimentary sediments decreases at paleo-elevations (see Fig. 4), where they are represented by clays or clays, which are underlain by sand with a small thickness. Amber sands are productive in amber, mainly fine-medium-grained, gray, dark gray, greenish-gray, sometimes containing up to 3-5% flint and fragments of crystalline rocks. Amber fragments of various shapes and sizes, with oxidation crust up to 1-2 mm. The sizes are preferably 1-2, rarely 5-10 cm. The capacities (according to the data of the Association "West Quartz Samotsvit") range from 1 to 420 g/m³.

Amber-containing deposits of this amber-bearing area contain a small (preferably 0.5-1%) amount of glauconite. According to the Institute of West Quartz Samotsvites [15-23], in the studies of the electromagnetic fraction of samples, the frequency of detection of glauconite is 69%, including 50% - in the light fraction. Glauconite of the light fraction is mostly rounded and rounded-angular, rarely - in the form of splices, which indicates the erosion and washing of bottom sediments formed in the conditions of the deeper deep shelf of the Obukh Sea.

According to the NGO "West Quartz Samotsvites" [15-19], the lower part of the horizon (700 m in length) of the Great Pugach of the Klesiv deposit is represented by sand of fine, medium-grained

mostly greenish-gray color, with a glauconite content of up to 5%. The power varies from 1-2 m to 5-6 m. Among the sand there are dark gray to black stripes (2-3 cm), enriched with scattered carbonaceous material and, preferably, with amber. Amber is mostly run-in. At the base of the horizon there are pebbles of foundation rocks and black flint (3-5%).

The upper part of the horizon is represented by sand of fine- to medium-grained gray, with light gray streaks; carbonaceous organic matter is scattered unevenly, clays of 1-2 cm thick are found and fragments of carbonaceous wood are chaotically arranged. Capacity from 0.5 to 1.6 m.

According to lithological and paleogeomorphological studies Maydanovich [15] clays mark the beginning of the transgression of the Berek Sea, and bluish-gray sands, which also revealed the broken fragments (1-5 cm) of flint and gray quartz, carbonaceous matter and amber, refer to its regressive stage.

However, during the last two decades, the materials of the search and evaluation works of the Rivne of the Ukrainian Geological Company on the manifestations of Oleksiyivka and Tomashgorod made it possible to investigate in more detail the structural and morphological conditions and the litho-facial conditions of the formation of amber in the northwest.

The lower part of the productive horizon is attributed to the terrigenous deposits of the shallow-coastal zone of the Kharkiv Sea, formed at the beginning of its regressive stage (inter-mountainous time). The upper part is thicker - to sediments formed in the open sea. The litho-facial section reflects the transition from sediments formed in the conditions of the channel of the sea to the sediments of the flooded coastal zone of the islands - mezhigirska thickness, represented by sand dark greenish-gray, fine-medium-grained (lower thickness), alternating with gray clay.), which is higher up the section and towards the Paleo Islands (w. 660) is replaced by sand bluish-gray, clayey. The sediments are represented by gray and bluish-gray sand formed simultaneously with the upper thickness within the blurred terrigenous zones of the Paleo Islands. Probably a bluish color of the sediment was acquired by erosion of the bark of weathering crystalline rocks.

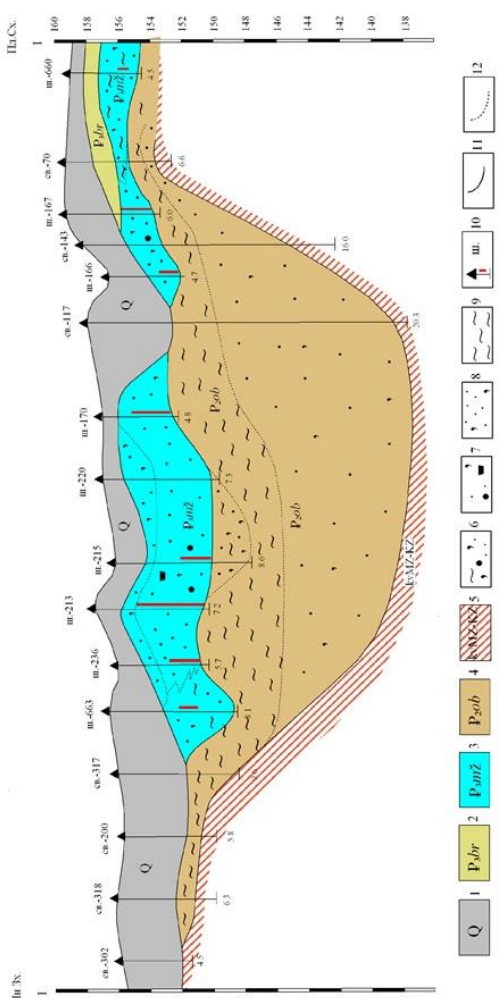

Fig. 4.. Lithologic-facial section of the Pugach section of the Klesiv deposit along line I-I: 1 - Quaternary deposits; 2 - sediments of the Upper Oligocene Berek world; 3 - facies of the terrigenous zones of the littoral of the open shallow shelf of the Mezhigirsk Sea; 4 - sediments of the Upper Eocene Obuchian world; 5 - bark of weathering of crystalline rocks; 6 - sand fine-grained, clay; 7 - sand: a) variegated; b) variegated with humus strips and fragments of wood; 8 - glauconite-quartz sand, fine-grained; 9 - clay; 10 - wells, their numbers and depths, amber detection intervals; 11-12 - borders: 11 - geological; 12 - lithological.

According to the Department of Fossil Flora of the Institute of Geological Sciences of the Academy of Sciences of Ukraine [45-49, 69], the age of the sands of the productive strata is lower-middle Oligocene.

To the northeast of the Pugach site, on the Dune site, the productive thickness forms a layer to local decreases in crystalline base. There is an increase in the power of the underlying clay and an increase in the capacity of the most productive thickness.

In terms of litho-facies, the Klesiv deposits are classified as terrigenous facies of the shallow-shelf coastal zone formed within the straits between islands and island beaches, as well as submerged terrigenous zones of islands.

At the Fedorovsky manifestation, located south of the Klesiv deposit, the productive sediments are represented by sands of fine-medium-grained mostly gray, dark gray color, with glauconite (up to 5%). There are also flint and fragments of crystalline rocks (3-5%) in the size of 0.4-1.5 cm, strips (1-15 cm) of black carbonaceous material with high amber content.

Within the manifestation there are pieces of amber (from 0.3 to 5 - 15 cm) and marked macrofossils - fossilized cones of Pinaceae. The thickness of the productive thickness varies from 0.5 to 11 m. Assuming productive deposits were formed during the flooding of the coastal parts by the sea and the massive removal of amber into the water area. South-east of this manifestation, a paleo-lowering is filled with inter-mountain deposits in the shield. According to Maidanovich I. [15] is the Fedoriv River Paleodolina, in which gray and dark gray inter-mountain deposits without amber are common. Sedations of the Fedorovsky manifestation are attributed [15] to shallow-sea lagoon-delta

Gypsometrically higher occurrence of amber deposits than within the Northern section, less power (Fig. 5) and variability of clayey sands in the southern part of the field with sands bluish-gray, dark-bluish-gray, greenish-gray, finely gray, fine the located fragments of amber indicate the formation of the latter at the base of the bar on the high seas.

Northeast of the Free deposit, with amber content from 0.60 to 242.7 g/m^3 (average 56.0 g/m^3), rubble amber was found on the Mochulishte manifestation (in 11 wells out of 22 passed, containing 1.0-36.5 g/m^3) and Khutirsky manifestation (in 17 holes of 99 traversed, containing 2.2-51.6 g/m^3) in dark gray sandy-clay sediments of the Lower Oligocene. Found amber usually flattened shape, mainly angular, slightly run-in and not run-in, with a peel of oxidation to 1mm. It is confined, in an overwhelming amount, to checks of clay and carbonaceous matter. These deposits are also

attributed to those formed during the accumulation of terrigenous material within the surface and underwater parts of the island bar, possibly extending from the field of Vilna in the northeast direction.

Fig. 5. Correlation scheme of inter-mountain deposits: *1* - Quaternary deposits; *2* - sediments of the Upper Oligocene Berek world; *3* - sediments of the inter-mountainous world of the Lower Oligocene; *4* - sediments of the Upper Eocene Obuchian world; *5* - bark of weathering of crystalline rocks of the foundation; *6* - medium-fine-grained sands: *a* - with glauconite; *b* - without glauconite; *7* - the sand is varied; *8* - sands of various types: with gravel, pebble, rubble, sulfide screeds, fragments of carbon or lignitized wood; *9* - sands: *a* - clay; *b* - with clay checks; *10* - clays: *a* - sandy; *b* - with sand checks; *11* - dense clays; *12* - workings (shur-shurf, st-well) and their numbers; *13* - findings of amber; *14* - borders of amber-bearing areas (*1* - Dubrovytsa; *2* - Volodymyrets; *3* - Klesiv); *15-16* - borders: *15* - different ages; *16* - age-old; *17* - break

References

1. **Bulat, A., Naduty, V., Korniyenko, V.** Substantiations of technological parameters of extraction of amber in Ukraine. *American Journal of Scientific and Educational Research*, **5(2)**, 591-597. (2014)

2. **Malanchuk, Y., Korniienko, V., Moshynskyi, V., Soroka, V., Khrystyuk, A., Malanchuk, Z.** Regularities of hydromechanical amber extraction from sandy deposits. Mining of Mineral Deposits, 13(1), 49-57, (2019). https://10.33271/mining13.01.049

3. **Korniyenko, V.Ya., Malanchuk, E.Z., Soroka, V.S., Khrystyuk, A.O..** Analysis of the existent technologies of amber mining. *Resources and resource-saving technologies in mineral mining and processing*, 209-232. (2018)

4. **Malanchuk Z., Korniienko V., Malanchuk Ye., Moshynskyi V.** Analyzing vibration effect on amber buoying up velocity. *E3S Web Conf. Volume* 123, (01018), Ukrainian School of Mining Engineering. (2019) https://doi.org/10.1051/e3sconf /201912301018

5. **Malanchuk Z. R. Moshynskyi V.S., Korniyenko V.Ya., Malanchuк E.Z., Lozynskyi V.H.** Substantiating parameters of zeolite-smectite puff-stone washout and migration within an extraction chamber. *Naukovyi Visnyk Natsionalnoho Hirnychoho Universytetu*. Preprint, (6), (2019)., 1-9

6. **Z. Malanchuk, V. Moshynskyi, Y. Malanchuk, V. Korniienko.** Physico-Mechanical and Chemical Characteristics of Amber. *Non-Traditional Technologies in the Mining Industry. Trans Tech Publications Inc. Solid State Phenomena*, **277** (2018). https://doi.org/10.4028/www.scientific.net/SSP.277

7. **Van der Werf, I.D., Fico, D., De Benedetto, G.E., Sabbatini, L.** The molecular composition of Sicilian amber. *Microchemical Journal*, **125**, 85-96.(2016) http://doi.org/10.1016/j.microc.2015.11.012

8. **Alekseev, V.I.** The beetles (Insecta: Coleoptera) of Baltic amber: the checklist of described species and preliminary analysis of biodiversity. *Zoology and Ecology*, **23(1)**, 5-12. (2013) https://doi.org/10.1080/21658005.2013.769717

9. **Antoljak, D., Kuhinek, D., Korman, T., Kujundzic, T.** Dependency of specific energy of rock cutting on specific drilling energy. *Rudarsko Geolosko Naftni Zbornik*, **33(3)**, 23-32. (2018) https://doi.org/10.17794/rgn.2018.3.3

10. **Belichenko, O., Ladzhun, J**. Complex gemological research of new types of treated amber. *Visnyk of Taras Shevchenko National University of Kyiv. Geology*, **4(75)**, 30-34. (2016) https://doi.org/10.17721/1728-2713.75.04

11. **Krek, A., Ulyanova, M., Koschavets, S..** Influence of land-based Kaliningrad (Primorsky) amber mining on coastal zone. *Marine Pollution Bulletin*, **(131)**, 1-9. (2018) https://doi.org/10.1016/j.marpolbul.2018.03.042

12. **Poulin, J., & Helwig, K.** The characterization of amber from deposit sites in western and northern Canada. *Journal of Archaeological Science: Reports*, **(7)**, 155-168. (2016) https://doi.org/10.1016/j.jasrep.2016.03.037

13. **Q. Y. Xing** et al. Study on the Gemological Characteristics of Amber from Myanmar and Chinese Fushun, *Key Engineering Materials*, **544** (2013). https://doi.org/10.4028/www.scientific.net/KEM.544.172

14. **Zakharenko, A. M., Golokhvast, K. S.** Using Confocal Laser Scanning Microscopy to Study Fossil Inclusion in Baltic Amber, a New Approach. *Key Engineering Materials*, **806** (2019). https://doi.org/10.4028/www.scientific.net/KEM.806.192

15. **Malanchuk Z., Korniienko V., Malanchuk E., Khrystiuk A.** Results of experimental studies of amber extraction by hydromechanical method in Ukraine. *Vostochno-Evropeyskiy zhurnal peredovykh tekhnologiy* [Eastern-European Journal of Enterprise Technologies], **3**, 10(81), 24-28, (2016). DOI: 10.15587/1729-4061.2016.72404

16. **Naduty V., Malanchuk Z., Malanchuk E., Korniyenko V.** Modeling of vibro screening at fine classification of metallic basalt. *Theoretical and Practical Solutions of Mineral Resources Mining*, 441–443, (2015). doi: 10.1201/b19901-77

17. **Malanchuk Y., Moshynskyi V., Korniienko V., Malanchuk Z.** Modeling the process of hydromechanical amber extraction. *E3S Web Conf. Ukrainian School of Mining Engineering*, **60**, (2018). https://doi.org/10.1051/e3sconf/20186000005.

18. **Malanchuk Z., Malanchuk Ye., Korniyenko V., Ignatyuk I**. Examining features of the process of heavy metals distribution in technogenic placers at hydraulic mining. *Vostochno-Evropeyskiy zhurnal peredovykh tekhnologiy* [Eastern-European Journal of Enterprise Technologies], 1(10), 45-51, (2017). http://nbuv.gov.ua/UJRN/Vejpte_2017_1(10)__7.

19. **Naduty V, Malanchuk Z., Malanchuk E., Korniienko V**. Research results proving the dependence of the copper concentrate amount recovered from basalt raw material on the electric separator field intensity. *Vostochno-Evropeyskiy zhurnal peredovykh tekhnologiy* [Eastern-European Journal of Enterprise Technologies], **5**, 5(83), 19-24, (2016). DOI: 10.15587/1729-4061.2016.79524

20. **Malanchuk Z., Korniienko V., Malanchuk Ye., Soroka V., Vasylchuk O.** Modeling the formation of high metal concentration zones in man-made deposits. *Mining of Mineral Deposits*, 12(2), 76-84, (2018). https://doi.org/10.15407/mining12.02.076

21. **Malanchuk Z., Korniienko V., Malanchuk Y**. Results of research into amber mining by hydromechanical method. *Mining Of Mineral Deposits*, 11 (1), 93-99, (2017). DOI: 10.15407/mining11.01.093

22. **Malanchuk Z., Malanchuk Y., Khrystiuk A.** Mathematical modeling of hydraulic mining from placer deposits of minerals. *Mining Of Mineral Deposits*, 10(2), 18-24, (2016). DOI: 10.15407/mining10.02.013

23. **Malanchuk Y., Malanchuk Z., Korniienko V., Gromachenko S.** The results of magnetic separation use in ore processing of metalliferous raw basalt of volyn region. *Mining Of Mineral Deposits*, 10(3), 77-83, (2016). DOI: 10.15407/mining10.03.077

24. **Nadutyi V., Korniyenko V., Malanchuk Z., Cholyshkina O.** Analytical presentation of the separation of dense suspension for the extraction of amber. *E3S Web of Conferences, International Conference Essays of Mining Science and Practice*, **109**, 00059, (2019). https://doi.org/10.1051/e3sconf/201910900059

RESEARCH OF ENERGY EFFECTIVE PARAMETERS OF THE PROCESS OF HYDRO MECHANICAL EXTRACTION OF AMBER FROM SANDY DEPOSITS

Moshynskyi, V.S.
National University of Water and Environmental Engineering (NUWEE), Professor, Doctor of Agricultural Sciences, Professor, Department Of Land, Cadastre, Land Monitoring and Geoinformatics, Ukraine

Korniyenko V.Ya.
National University of Water and Environmental Engineering (NUWEE), Professor, Doctor of Technical Sciences, Professor, Department of Development of Deposits and Mining, Ukraine

Khrystyuk A.O.
National University of Water and Environmental Engineering (NUWEE), Ph.D., Associate Professor, Department of Automation and Computer Integrated Systems, Ukraine

Solvar L.M.
Chervonograd State College of Mining Technology and Economics, Professor, Doctor of Pedagogical Sciences, Director, Ukraine

Abstract
The method of calculation of technological parameters of amber extraction from sand deposits by hydro mechanical method is presented. High energy efficiency of using hydro mechanical method of extraction of amber for sandy deposits has been confirmed. Methods for calculating the parameters of amber production have been analyzed. A calculation method of the amber production process that takes into account a significant number of parameters is proposed.

Introduction

The object of research is the process of the hydro mechanical method of amber extraction from sand deposits.

The existing technical means of implementing the process of hydro mechanical production of amber do not fully meet the requirements, namely, the developed technologies do not guarantee the completeness of extraction of the useful component from the host rocks and do not always use the working fluid efficiently. The efficiency of hydro mechanical mining plants, the amount of energy,

water, air consumption, as well as the number of useful component extracted, directly depend on the duration of hydro mechanical impact on the sandy mass, as on the speed at which particles of amber float to the bottom surface is proved.

Today, amber mining requires the latest technology and the improvement of technical and technological means to intensify the mining process, which achieves higher productivity and efficiency, as well as reducing the negative environmental impact. The most rational is the improving of a hydro mechanical method of amber extraction, which does not require expensive geological exploration and reclamation works, is characterized by minimal capital and operating costs, and has the potential to be improved by controlling the rate of emergence of the amber from sandy deposits by changing the flow rate and the oscillation frequency of the working body.

1. Experimental study

Experimental studies of amber-containing sands in laboratory conditions are performed to obtain the following indicators:

- type of soil;
- density of soil skeleton particles;
- natural soil moisture;
- coefficient of porosity in natural conditions;
- coefficient of porosity at hydro mechanical impact without supply of air;
- coefficient of porosity at hydro mechanical impact when supplying air at different flow rates;
- the resistance coefficient of sandy environment of a particle amber [1].

For laboratory experimental research use standard methods and tools required by regulatory documents, as well as developed by experts of the National University of Water and Environmental Engineering (NUWEE) pilot plant to simulate the process of transferring amber-containing sands to a fluid state by vibration and water and air supply (Fig.1).

The pilot plant consists of a glass box 1 (110 mm×110 mm in size and h=900 mm in height), which immerses two hollow cores 2 for water and air fixed on the plate 3, to which water and air lines are supplied from water meters. (“Rosa” SGR-1,5) 4 and air (G2,5) 7.In

each rod at an angle of 120° there are nozzles with a diameter of 1-1.5 mm. Water is supplied from the water supply network from 0 to 0.2 MPa The air with pressure of 0 to 0.2 MPa is supplied by the compressor. Valves 5 and 6 are installed to adjust the water and air pressure. Plate 3 is placed on suspensions 8. The glass box is placed on the frame 9. The oscillations of the rods are created by a shock mechanism with an eccentric 10, which is driven by an engine with a controlled speed.

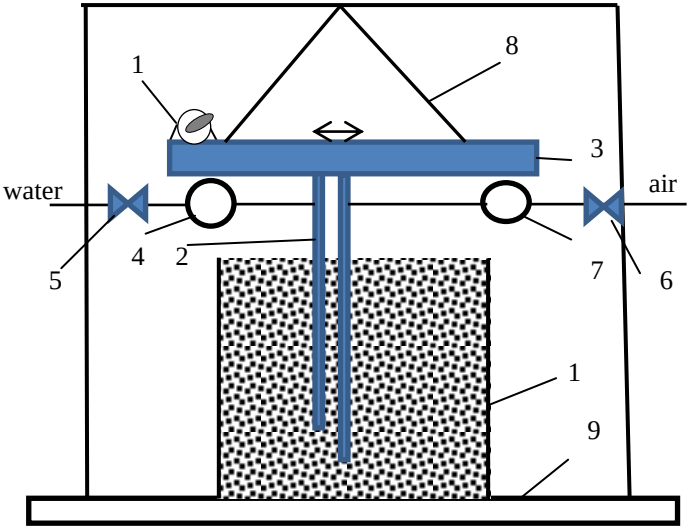

Fig 1. Pilot plant: *1* - glass box; *2* – rods with nozzles for water and air supply; *3* –плита; *4*, *7* - water meter "Rosa" SGR-1,5 andair meter G2,5; *5*, *6* - valves for regulation of water and air supply; *8* – flexible plate suspensions; *9* – fixed frame, *10* – shock mechanism with eccentric

Measurements of soil specific gravity in field and laboratory conditions to determine the density of sandy soil were carried out by volumetric method using electronic scales and a metal ruler. Amber lift time was measured with an electronic stopwatch. An air meter G2,5 was used to account for the passage of air into the sandy soil massif. Water meter "Rosa" SGR-1,5 used to determine the flow of water into the sand array. The pressure of water, air and hydraulic pressure supplied to the pump are determined by manometers: MP4-

U та OBMGnI-100. Roulette metal 5 m long and ruler metal 1 m long to determine the geometric parameters of the structure of the working body, working area, the depth of immersion of the amber in the sand array. Dynamic density gauge (impactor DorNDI) to determine soil strength. Other typical equipment and tools, installations and apparatus necessary to carry out and measure parameters during laboratory testing

In the course of experimental studies, the rods through which the air is blown through a nozzle of gas of varying intensity, in which a zone of boiling of the sandy mass with amber is formed, are immersed in a free-flowing sand medium with amber in a laboratory unit. The humidity of the sand varied due to the addition of water. The shape and size of the boiling zone and the motion of the amber in the array of amber-containing sand were studied.

During the study of the zone of boiling of the sandy mass at the laboratory installation when supplying water and air measurements of the porosity of the medium.

Studies at the laboratory facility were conducted using the following method:

- glass box with sandy medium was mounted on the frame, while measurements were made of the height of the sandy medium before and after the supply of water and air, the rate of emergence of amber;
- through the nozzles, sand, air were supplied through the nozzles, alternately and with changes in pressure and various costs, with the same measurements being made;
- studies have been carried out repeatedly.

The experimental data were processed using mathematical statistics methods [2-4].

When determining the dependence of porosity on the parameters of hydro mechanical impact, the purpose of processing the experimental data is to obtain a regression dependence of the following form

$$\varepsilon = \varepsilon_\omega \varepsilon_q , \quad (1)$$

$$\varepsilon_\omega = -\gamma' + \beta'\omega - \alpha'\omega^2 , \quad (2)$$

$$\varepsilon_q = \gamma + \beta q + \alpha q^2 , \quad (3)$$

where ε - the porosity of the array under vibration and air flow;

ε_ω - the porosity of the array under vibration without air supply;

ε_q - the coefficient of change of porosity during vibration due to the supply of air into the array.

When the values of the coefficient of resistance of the sandy medium of motion of the amber particles are determined, use the following formula

$$\varphi = \sqrt{1 + \frac{\alpha}{k_m \nu}} \left(1 - \frac{\rho_s}{\rho_c}\right), \tag{4}$$

$$\alpha = \begin{cases} Af, & A^2 f < kg \\ \dfrac{kg}{f}, & A^2 f > kg \end{cases}, \tag{5}$$

where ϕ - the drag coefficient of the sand medium of the amber particle motion [1];

ν - the rate of emergence of the amber particles;

g - the acceleration of gravity;

k_m - the coefficient of the coupled mass;

f - the frequency of oscillation of the working body;

ρ_s - the density of amber particles;

ρ_c - the density of water-sandy environment;

A - the oscillation amplitude of the working body;

k - the coefficient of friction.

Data obtained from laboratory experimental studies are used in the design and verification of the parameters of the process of hydro mechanical extraction of amber from sand deposits.

2. Methodology of calculating the parameters of the amber extraction process

The purpose of the design calculation of the parameters of the process of hydro mechanical extraction of amber from sand deposits is to determine the duration of the extraction process, the required flow of air and water, the diameter of the nozzle of the working body, indicators of the purpose of the pump for water supply.

The rate of emergence of the amber and the flow rate of air it provides are calculated, if known particle diameter, using the formu-

las

$$v = k_U d^2, \tag{6}$$

$$q = 0,0062 \frac{\Delta^{0,281}}{\sqrt{\varepsilon_\omega}}, \tag{7}$$

$$k_U = \frac{1-\phi}{3704K} \left(\frac{\rho_s}{\rho_g} \right)^{0,593} \frac{\gamma^m \nu_g^{0,47} \Delta^{1,86}}{\delta^{2,205} \varepsilon_\omega^{2,064}}. \tag{8}$$

$$\Delta = \frac{\rho_0}{\rho_s}, \tag{9}$$

$$K = \left(\frac{\sqrt[3]{g\nu_g} h_{dd}^2}{0,0003} \right)^{1,414}, \tag{10}$$

where δ - the particle diameter of the soil containing amber;

ρ_g - the air density;

ρ_0 - the density of water-saturated amber medium;

ν_g - the kinematic coefficient of air viscosity;

h_{dd} - the length of the conical part of the working body [5];

K - the dimensionless technological constant;

Δ - the ratio of the particle densities of the containing water-saturated soil and amber;

d - the diameter of the amber particles.

Calculate the time of emergence of amber from deposits

$$T_U = \frac{H}{k_U d^2}. \tag{11}$$

The losses for amber extraction from sand deposits are calculated, and the duration of field development is determined by the formulas

$$T = \left(2T_H + T_U\right)\eta\eta' + T_0\left(\eta - 1\right)\left(\eta' - 1\right), \tag{12}$$

$$T_H = \frac{H}{\upsilon}, \tag{13}$$

$$T_0 = \frac{A}{v_0}. \tag{14}$$

The fluid consumption required for the amber to emerge from the deposits is determined by the formula

$$Q_{рв} = \frac{ABv}{1+e}\left(\frac{\left(\rho_{ск}\left(1+W\right)-\rho_p\left(1+e\right)\right)}{\rho_p-\rho_в}\right), \quad (15)$$

and the diameter of the nozzle of the nozzle of the working body, which will allow to destroy deposits with such expense, is chosen according to the following conditions

$$D \le D_*, \quad (16)$$

$$D_* = \frac{6{,}347\sqrt{Q_{рв}}}{\sqrt[4]{c_0+\left(\sigma-p_m\right)tg\psi}}, \quad (17)$$

where D - the actual diameter of the nozzle of the working body;

D_* - the maximum possible diameter of the nozzle of the working body, which ensures the destruction of deposits;

c_0 - the specific adhesion of deposit particles;

$\mathrm{tg}\,\psi$ - the coefficient of internal friction of the deposit particles;

σ - the normal geostatic load on the deposit particles;

p_m – the pore pressure (pressure in free water contained in pores).

In order to supply the fluid flow required by the technology and calculated by the formula (15), the pump must create the following pressure difference

$$\Delta p = R_c Q_{рв}^{1{,}735} - g\rho_p H, \quad (18)$$

$$R_c = \frac{k\rho_p \nu_p^{0{,}265} L k_z}{2{,}74 D_L^{5{,}265}}, \quad (19)$$

where Δp – the difference in pressure of the liquid behind the pump at the outlet of the nozzle;

R_c - the coefficient of hydraulic resistance of the hose elements to which the fluid is supplied;

L - the length of hose;

D_L - the diameter of the hose;

k_z– the coefficient which taking into account local hydraulic supports [6];

k - the coefficient taking into account the change in length and diameter of the hose under the action of internal pressure (fig. 2) [6];

ν_p - the kinematic coefficient of water viscosity.

To determine the volume of processing of the soil massif, we take the performance of the vibrating hydraulic machine

$$П_{ex} = 3600 \cdot \frac{nW_e K_в K_{mov}}{t_p}, m^3 / period \quad (20)$$

$$t_p = T_U + 2T_H + T_0, \quad (21)$$

$$W_e = ABH, \quad (22)$$

where W_e - the amount of soil that is being processed by the mashine;

A, B - the width and length of oscillating soil massif;

H - the depth of fluidized bed of soil;

t_p - the time of device working;

n - the number of sinking and loss cycles from the soil massif;

$K_в$ - the coefficient that takes into account the use of working time;

K_{mov} - the coefficient that taking into account the time to reschedule the intensifier.

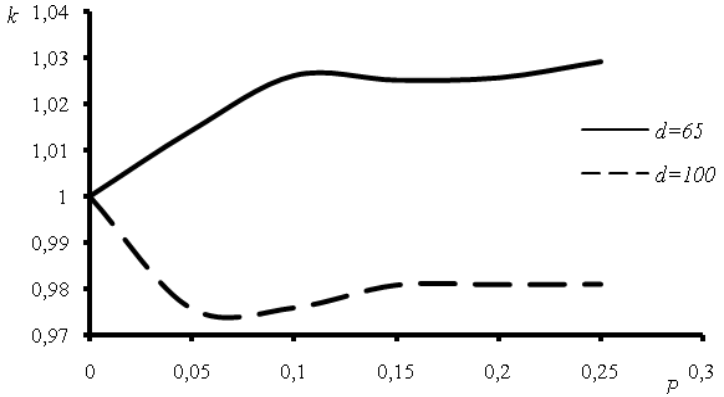

Fig. 2. Dependence of coefficient on internal pressure for hoses of different diameter [6]

Amber production is estimated by the formula

$$G = \varepsilon_H^d П_{ex}, \quad (23)$$

where G - amber production;

ε_H^d - the volume content of particles of amber with a diameter

less than d, which lie at a depth not exceeding H, kg/m^3.

The amount of fluid required to provide amber production with the duration of hydro mechanical exposure over time (11) is equal to

$$W_{рв} = \left(\frac{H}{k_U d^2} + 2T_H \right) Q_{рв}, \tag{24}$$

and specific water consumption, taking into account formula (20) - (24), is determined by the formula

$$w_{рв} = k_T k_\rho \left(\frac{\upsilon}{k_U d^2} + 2 + \frac{A\upsilon}{Hv_0} \right) \left(\frac{\upsilon}{k_U d^2} + 2 \right), \tag{25}$$

$$k_T = \frac{1}{3600 n K_в K_{пер}} \left(\frac{H}{\upsilon} \right)^3, \tag{26}$$

$$k_\rho = \frac{\rho_{ск} \frac{1+W}{1+e} - \rho_p}{\left(\rho_p - \rho_в \right) \varepsilon_H^d}, \tag{27}$$

$$e = \frac{V_n}{V_{ск}}; \tag{28}$$

$$W = \frac{V_{нв} \rho_в}{V_{ск} \rho_{ск}}; \tag{29}$$

where $W_{рв}$ - the amount of fluid needed to ensure amber production;
$w_{рв}$ - the specific water consumption;
V_n- thepore volume;
$V_{ск}$- the volume of soil skeleton;
$V_{нв}$-the volume of pore water;
$\rho_в$-the working fluid density;
$\rho_{ск}$- the density of soil skeleton.

3. Checking the calculation of the amber extraction process parameters

The purpose of verifying the parameters of the process of hydro mechanical extraction of amber from sand deposits is to determine the duration of the extraction process, the flow of air and water that will be in the existing pumping equipment.

The rate of emergence of the amber and the flow rate of air it provides are calculated, if known particle diameter, using the formulas

$$v = k_U d^2, \tag{30}$$

$$k_U = \frac{1-\phi}{3000K}\frac{\rho_s^{0,6}}{\delta^{2,2}}\frac{(\Delta-1)z^{1,3}}{\Delta^{0,407}\varepsilon_\omega^{1,414}}\left(1-\left[\gamma+\beta z+\alpha z^2\right]\varepsilon_\omega\right)^m, \tag{31}$$

Calculate the time of emergence of amber from deposits

$$T_U = \frac{H}{k_U d^2}. \tag{32}$$

The losses for amber extraction from sand deposits are calculated, and the duration of field development is determined by the formulas

$$T = (2T_H + T_U)\eta\eta' + T_0(\eta-1)(\eta'-1), \tag{33}$$

$$T_H = \frac{H}{\upsilon}, \tag{34}$$

$$T_0 = \frac{A}{v_0}. \tag{35}$$

The fluid consumption required for the amber to emerge from the deposits is determined by the formula

$$Q_{рв} = \left(\frac{\Delta p + g\rho_p H}{R_c}\right)^{0,576}, \tag{36}$$

$$R_c = \frac{k\rho_p v_p^{0,265} L k_z}{2,74 D_L^{5,265}}, \tag{37}$$

and the diameter of the nozzle of the nozzle of the working body, which will allow the destruction of deposits at such expense, must meet the following conditions

$$D \le D_*, \tag{38}$$

$$D_* = \frac{6,347\sqrt{Q_{рв}}}{\sqrt[4]{c_0 + (\sigma - p_m)tg\psi}}, \tag{39}$$

where D - the actual diameter of the nozzle of the working body;

D_* - the maximum possible diameter of the nozzle of the working body, which ensures the destruction of deposits;

c_0 - the specific adhesion of deposit particles;

$\mathrm{tg}\psi$ - the coefficient of internal friction of the deposit particles;

σ - the normal geostatic load on the deposit particles;

p_m - the pore pressure (pressure in free water contained in pores);

Δp - the difference in pressure of the liquid behind the pump at the outlet of the nozzle;

R_c - the coefficient of hydraulic resistance of the hose elements to which the fluid is supplied;

L - the length of hose;

D_L - the diameter of the hose;

k_z - the coefficient which taking into account local hydraulic supports;

k- the coefficient which taking into account the change in length and diameter of the hose under the action of internal pressure;

ν_p - the kinematic coefficient of water viscosity.

To determine the volume of processing of the soil massif, we take the performance of the vibrating hydraulic machine, m^3/cycle

$$П_{ext} = 3600 \cdot \frac{nW_e K_в K_{пер}}{t_ц}, \quad (40)$$

$$t_c = T_U + 2T_H + T_0, \quad (41)$$

$$W_e = ABH, \quad (42)$$

where W_e - the amount of soil that is being processed by the installation;

A, B - the width and length of oscillating soil massif;

H - the depth of fluidized bed of soil;

t_c- the time of device working;

n - the number of sinking and loss cycles from the soil massif;

$K_в$ - the coefficient that takes into account the use of working time;

$K_{пер}$ - the coefficient that taking into account the time to reschedule the intensifier.

Amber production is estimated by the formula

$$G = \varepsilon_H^d П_{ext}, \quad (43)$$

where G - amber production;

ε_H^d - the volume content of particles of amber with a diameter less than d, which lie at a depth not exceeding H, kg/m^3.

The amount of fluid required to ensure the production of amber, with the duration of hydro mechanical exposure over time (32) is equal to

$$W_{рв} = \left(\frac{H}{k_U d^2} + 2T_H \right) Q_{рв}, \tag{44}$$

and specific water consumption, taking into account formulas (43) and (44), is determined by the formula

$$w_{рв} = k_T k_\rho \left(\frac{\upsilon}{k_U d^2} + 2 + \frac{A\upsilon}{Hv_0} \right) \left(\frac{\upsilon}{k_U d^2} + 2 \right), \tag{45}$$

$$k_T = \frac{1}{3600 n K_в K_{пер}} \left(\frac{H}{\upsilon} \right)^2, \tag{46}$$

$$k_\rho = \frac{1}{\varepsilon_H^d} \left(\frac{\Delta p + g\rho_p H}{R_c} \right)^{0,576}. \tag{47}$$

The results obtained determine the energy-efficient parameters of the equipment for extracting amber from sand deposits.The presented method allows selection of equipment for amber extraction, which will provide high productivity of the process and will significantly reduce the costs of development of the field.

Conclusions

A method of calculating the technological parameters of amber extraction from sand deposits by a hydro mechanical method is proposed, which will allow to ensure a minimum duration of impact on the array and reduce energy consumption and water consumption of the extraction technology. The parameters of the hydro mechanical method of amber extraction have been verified.

When calculating the process parameters, the regularity between the particle velocity of the particle and the physical and geometric characteristics of the deposit, as well as the frequency of oscillation of the working body and the air flow are taken into account.

References

1. **Malanchuk Z., Malanchuk E., Khrystyuk A.** Mathematical modeling of hydraulic mining from placer deposits of minerals / Mining of Mineral Deposits. National mining university, 2016. № 10. pp. 18–24.

2. **Malanchuk Z., Malanchuk E., Khrystyuk A.** Results of experimental studies of amber extraction by hydro mechanical method in Ukraine / Eastern-European Journal of Enterprise Technologies, – 2016. Vol 3, №10(81). pp. 24–28. DOI: 10.15587/1729-4061.2016.72404

3. **Malanchuk Z.** Modeling the formation of high metal concentration zones in man-made deposits / **Malanchuk Z., Korniienko V., Malanchuk Ye., Soroka V., Vasylchuk O.** Mining of mineral deposits. ISSN 2415-3435, 2018, pp. 76-84 DOI: 10.15407/mining12.02.076.

4. **Malanchuk Z.** Results of experimental studies of amber extraction by hydro mechanical method in Ukraine / [**Z. Malanchuk, V Korniyenko, Y. Malanchuk and other.**]. // EasternEuropean Journal of Enterprise Technologies. – 2016. – pp. 24–28. DOI: https://doi.org/10.15587/1729-4061.2016.72404.

5. **Malanchuk Z.** Examining features of the process of heavy metals distribution in technogenic placers at hydraulic mining / **Malanchuk Z., Malanchuk Ye., Korniyenko V., Ignatyuk I.** Eastern-European Journal of Enterprise Technologies ISSN 1729-3774, 2017, pp. 45-51 DOI:10.15587/1729-4061.2017.92638.

6. **Arens, V.** (2001). Physical and chemical geotechnology: text-book (p. 656). Moscow: State. Mining University Press.

7. **Khrystyuk A. O.** Analiz isnuyuchykh sposobiv ta tekhnolohichnykh zasobiv hidromonitornoho rozmyvu / Visnyk Inzhenernoyi akademiyi nauk. Kyyiv, 2015. Vyp. № 1. C. 236–240.

8. **Malanchuk Z., Malanchuk E., Khrystyuk A**. Simulation of the comminution process to complex processing of metal-bearing basalt raw material / Cambridge Journal of Education and Science, 2015. No 2 (14), July-December. pp. 542–549.

9. **Malanchuk YE. Z., Khrystyuk A. O**. Matematychne modelyuvannya protsesiv sverdlovynnoho hidrovydobutku rozsypnykh korysnykh kopalyn / Visnyk Inzhenernoyi akademiyi nauk. Kyyiv, 2015. Vyp. № 4. C. 187–194.

10. **Khomenko O.Ye.** Principles of rock pressure energy usage during underground mining of deposits / **Khomenko, O.Ye., Sudakov, A.K., Malanchuk, Z.R., Malanchuk, Ye.Z.** / Naukovyi Visnyk Natsionalnoho Hirnychoho Universytetu, National Mining University of Ukraine, ISBN: 2071-2227, 2017, pp 34–43.

11. **Malanchuk Z. R., Malanchuk E. Z., Korniyenko V. Ya.** Modern geotechnical methods of management of the process of amber extraction / Multi-authored monograph:"Innovative development of resource-saving technologies of mining of minerals" Publishsng house «St. Ivan Rilsky» Mining and Mining University of Geology (Sofia, Bulgaria). – 2018. – P. 80–103.

12. **Malanchuk Z.** Physico-Mechanical and Chemical Characteristics of Amber / [**Z. Malanchuk, V Moshynskyi, Y. Malanchuk** and other.]. // Solid State Phenomena. – 2018. – pp. 80–89. DOI: https://doi.org/10.4028/www.scientific.net/SSP.277.80.

13. **Naduty V.** Research results proving the dependence of the copper concentrate amount recovered from basalt raw material on the electric separator field intensity / **Naduty, V., Malanchuk, Z., Malanchuk, Y., Korniyenko, V.** / Eastern-European Journal of Enterprise Technologies ISSN 1729-3774, 2016, pp. 19-24 DOI: 10.15587/1729-4061.2016.79524.

14. **Malanchuk Z. R.** Results of studies on amber extraction by hydro mechanical method / **Z. R. Malanchuk, V. Ya. Kornienko, E. Z. Malanchuk**. Mining of Mineral Deposits, 11(1), 2017, 93-99. DOI: http://doi.org/10.15407/mining11.01.093.

15. **Saik P.** Revisiting the underground gasification of coal reserves from contiguous seams / **P. B. Saik, R. O. Dychkovskyi, V. H. Lozynskyi, Z. R. Malanchuk, Ye. Z. Malanchuk.** Naukovyi Visnyk Natsionalnoho Hirnychoho Universytetu, №6, 2016, 60-66.

16. **Lozynskyi,V. G.** Experimental study of the influence of crossing the disjunctive geological fault on thermal regime of underground gasifier / **Lozynskyi,V. G., Dychkovskyi, R. O. , Falshtynskyi, V. S. , Saik, P. B., & Malanchuk, Ye. Z.,** Naukovyi Visnyk Natsionalnoho Hirnychoho Universytetu, 2016, № 5. - p. 21-29.

17. **Malanchuk, E., Malanchuk, Z., Korniienko, V., Gromachenko, S**. The results of magnetic separation use in ore processing of metalliferous raw basalt of Volyn region.*Mining of Mineral Deposits, 10*(3), 2016, 77-83.

28. **Malanchyk Z., Korniyenko V.** Modern condition and prospects of extraction of amber in Ukraine / Proceedings of the 1st International Academic Congress "Fundamental and Applied Studies in the Pacific and Atlantic Oceans Countries". (Japan, Tokyo, 25 October 2014). Volume II. "Tokyo University Press". – 2014. – P. 318–321.

19. **Bulat A., Naduty V., Korniyenko V.** Substantiations of technological parameters of extraction of amber in Ukraine / American Journal of Scientific and Educational Research. – No.2. (5) (July-December). Volume II. "Columbia Press". – New York. – 2014. – P. 591–597.

20. **Bulat A., Naduty V., Korniyenko V.** Features spread occurrence of amber deposits in the world / Oxford Review of Education and Science. – №1 (9), January-June 2015. – P. 60–65.

21. **Bulat A, Nadutyi V, Kornienko V.** Modern technologies of amber extraction from sand deposits/ Harvard Journal of Fundamental and Applied Studies, – No.1. (7) (January-June). Vol. VIII. "Harvard University Press".– 2015. – P. 514–519.

22. Promyslovi tekhnolohiyi vydobutku burshtynu. Monohrafiya / **Bulat A. F., Nadutyy V. P., Malanchuk YE. Z., Malanchuk Z. R., Korniyenko V. YA**. // – Dnipro–Rivne: IHTM–NUVHP. – 2017. – 237 c.

23. **Ye. Malanchuk, V. Korniienko, V. Moshynskyi, V. Soroka, A. Khrystyuk, Z. Malanchuk** Regularities of hydro mechanical amber extraction from sandy deposits MINING OF MINERAL DEPOSITS, – 2019. Volume: 13 Issue: 1 Pages: 49-57.

TIDAL PARK - MODELING AND CONTROL STRATEGY

Dr Mohamed Tafsir DIALLO

Institute Polytechnic-University Gamal Abdel Nasser of Conakry; M.Conférence- Managing Director,Guinea

Mamadou Oury Fatoumata DIALLO

Assistant -Institut Polytechnic-University Gamal Abdel Nasser of Conakry-Guinéa

Abstract

This article presents the modeling of a farm with 9 turbines. A synchronous permanent magnet machine (MSAP) with a nominal power of 2 MW is connected to a tidal turbine with a radius of 10 m for each of the turbines. The energy produced is injected into the 20 kV electrical network at a frequency of 50 Hz. The rectifiers of the various machines are interconnected on the DC bus before injecting power into the network, via an inverter. The proposed control strategies are implemented in Matlab/Simulink software for system simulation. The simulations are performed using the amplitude of the tidal current obtained from a hydrodynamic model, and the results obtained are presented and analyzed.

Key words - renewable energy; turbine; msap; farm; maximum power tracking (mppt); control strategy.

I. Introduction

Renewable energy

Faced with energy and environmental challenges, our society is turning more and more to renewable energy sources. European directives required producing 20% of these MRE, [1]. Estimates of tidal currents estimate the world energy potential at 450 TWh/year and a European potential evaluated between 15 and 35 TWh/year, [2]. Marine renewable energy (MRE) offer an opportunity to increase the energy mix. In terms of tidal current energy (energy captured by tidal turbine), France has the second potential for producing electrical energy from MRE behind the United Kingdom. According to EDF, in France the production potential is between 5 and 14 TWh/year. Or an installed power between 2.5 to 3.5 GW. It should be noted that the Raz Blanchard capitalizes around 50% of this national resource. Until now, the work carried out on tidal turbine has been based essentially on studies made on wind turbine; however they are different from the point of view of dimensions for the same power, [3,4,5].

Despite technical progress made in particular in the wind energy field, the installation of tidal turbines is still under study and important questions remain unanswered concerning interaction with the environment, placement of machines, and management of the energy produced over time. Technological barriers remain to be overcome so that this technology for producing electrical energy by tidal turbine is industrialized. Finally, it should be noted that there are many projects to set up tidal turbine west of the Cotentin and will have an industrial, social and economic impact on French territory.

The purpose of this article is to establish an equivalent electrical and/or mathematical model to describe the operation of a tidal turbine farm. This model must be adapted to the Raz Blanchard site and capable of fairly faithfully reproducing the production of electrical energy from tidal currents at this site. The characteristics of the Raz Blanchard site are indicated in [6].

Figures 1 and 2 show the profiles of the speed of the tides raised every quarter of an hour at the Raz Blanchard between January and June 2010, and in January 2010.

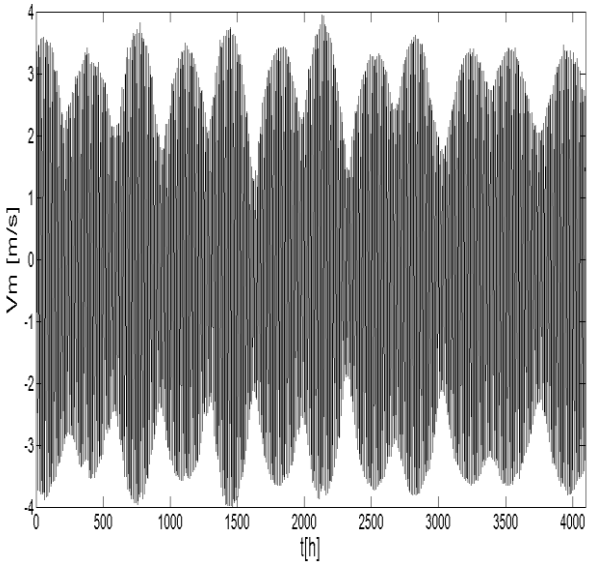

Fig.1. Diagram of the tidal speed profile from January to June 2010

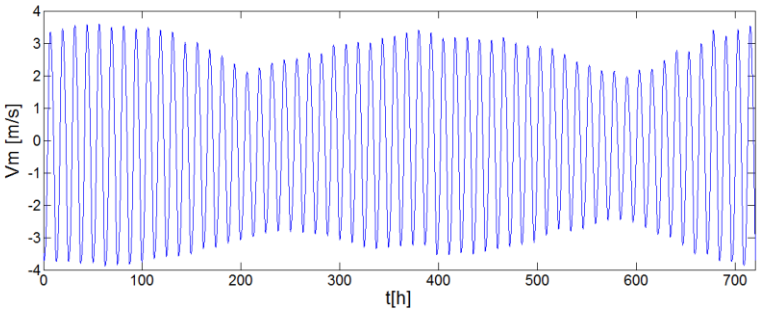

Fig.2. Diagram of the tidal speed profile in January 2010

The diagrams of the corresponding extracted powers are presented in Figures 3 and 4.

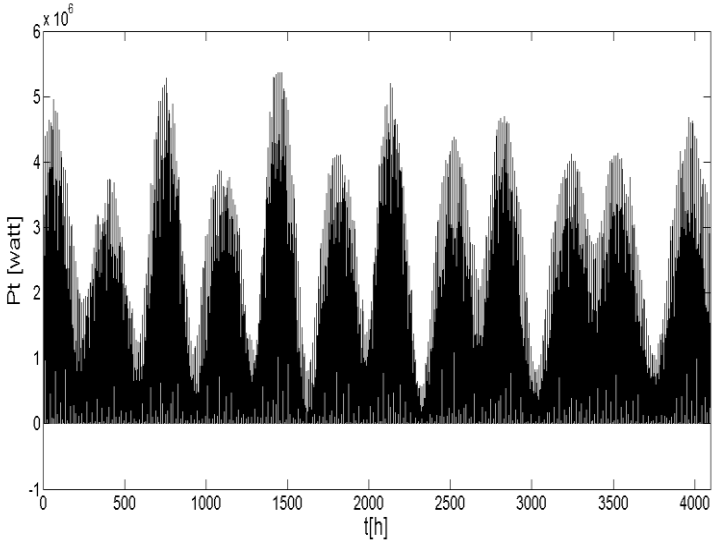

Fig.3. Power extracted from the tides from January to June 2010

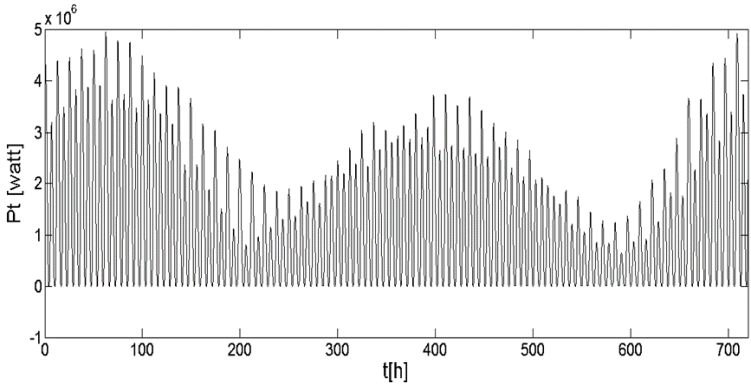

Fig4. Power extracted from the tides in January 2010

Fig:5 illustrated The tidal energy production system studied.

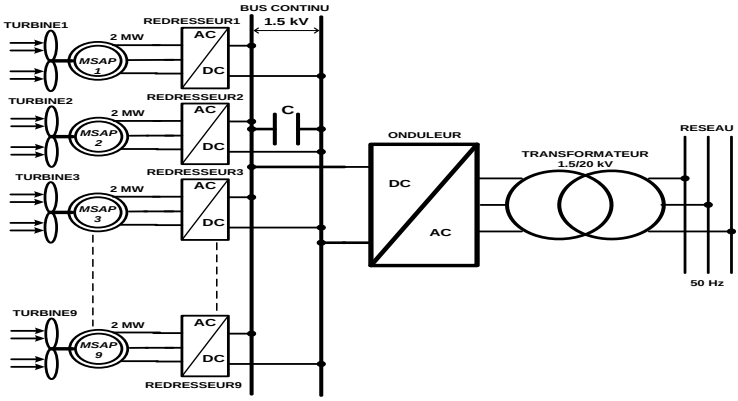

Fig.5. Diagram of the farm with 9 turbines

Modeling of the hydrolian energy production system PMSG

Modeling in the case of energy production by tidal turbines, the synchronous permanent magnet machine (m_{sap}) allows to optimize the power produced.in addition if for wind turbines, the mada is the most requested, for tidal turbines the msap is more interesting (absence of the multiplier, therefore less maintenance) [8] indeed, taking into account the behavior of the speed of the tidal currents, the pmsg makes it possible to compensate for these variations in acceptable proportions, while guaranteeing a good quality of the energy pro-

duced the dynamic model of the pmsg in the park coordinate system in (*d*, *q*) is expressed by equations (1) and (2), where r_s, l_d, l_q and Ψm represent the generator parameters.

Using (1) and (2), the dynamic model of the pmsg is represented by the differential equation (3), where *p* is the number of pole pairs, and ωm the speed of the machine.

$$\begin{cases} V_{sd} - R^s \times I_{sd} + \frac{d}{dt}(\psi_d) - p \times \Omega_m \times \psi_q \\ V_{sq} - R^s \times I_{sq} + \frac{d}{dt}(\psi q) - p \times \Omega_m \times \psi_d \end{cases} \quad (1)$$

$$\begin{cases} \psi_d = L_d \times I_{sd} + \psi_m \\ \psi_q = L_q \times I_{sq} \end{cases} \quad (2)$$

$$\frac{d}{dt}\begin{bmatrix} I_{sd} \\ I_{sq} \end{bmatrix} = \begin{bmatrix} -\frac{R_s}{L_d} & \frac{p \times \Omega_m \times L_q}{L_d} \\ -\frac{p \times \Omega_m \times L_q}{L_q} & -\frac{R_s}{L_q} \end{bmatrix} \cdot \begin{bmatrix} I_{sd} \\ I_{sq} \end{bmatrix} + \begin{bmatrix} \frac{V_{sd}}{L_d} \\ \frac{V_{sd} - p \times \Omega_m \times \psi_m}{L_q} \end{bmatrix} \quad (3)$$

In this model, the stator currents I_{sd} and I_{sq} are state variables, V_{sd} and V_{sq} the satatoric voltages in d_q.

The mechanical equation of a turbine is given in (4), where *f* is the coefficient of friction.

$$J \cdot \frac{d}{dt}(\Omega_m) = T_m - T_{em} - f \times \Omega_m \quad (4)$$

In this equation, Tm is the mechanical Torque and Tem, the electromagnetic Torque.

Model of a turbine

The mechanical power extracted by a hydro turbine is given in (5), where ρ is the density of the water (ρ=1024 kg/m^3); s is the area of the surface swept by the propellers of the machine; V_m is the speed of the tide [m / s], C_p (λ, β) is the power coefficient, which is the efficiency of the tidal stream.

$$P_{turb} = \tfrac{1}{2} \times C_p(\lambda, \beta) \times \rho \times s \times V_m^3 \quad (5)$$

The expression of C_p (λ, β), [9-10] is given in (6), where β is the pitch angle of the turbine blade

$$\begin{cases} Cp(\lambda,\beta) = (0{,}35 - 0{,}00167)\times(\beta-2)\times\sin\alpha \\ -0.00184\times(\lambda-3)-(\beta-2) \\ \alpha = \dfrac{\pi\times(\lambda+0{,}1)}{14{,}34-0{,}3\times(\beta-2)} \end{cases} \quad (6)$$

The expression of the specific speed which is the product of the speed-turbine radius and the speed of the tide is given in (7), where Rt is the radius of a blade.

$$\lambda = \left(\Omega_m \times R_t\right)/V_{tides}\ . \quad (7)$$

The mechanical torque of the turbine Tm obtained from the extracted power is illustrated in the expression.

$$T^m = P_{turb}/\Omega_m \quad (8)$$

C. Rectifier model

This section presents the analytical model of a rectifier. The rectified current of the 1st tidal turbine is illustrated in expression (9) .Considering figure 5, the currents measured in the DC bus make it possible to write equations (10) and (11), where S1, S2, S3 are rectifier control signals, C the capacitor of the DC bus capacitor; Iond is the inverter current, Ired the rectifier current, Icond, the current through the capacitor.

$$I_{red1} = (S_1 \cdot I_{s1} + S_2 \cdot I_{s2} + S_1 \cdot I_{s3}) \quad (9)$$

$$C \cdot \frac{dV_{dc}}{dt} = I_{red} - I_{ond} \quad (10)$$

$$I_{red} = I_{red1} + I_{red2} + I_{red3} + \Lambda + I_{red...} \quad (11)$$

A. Inverter model

The analytical expression of the inverter model is illustrated in (12), where Sa, Sb, Sc are the control signals of the inverter

$$\begin{cases} U_{Sa} = \dfrac{2 \cdot S_a - S_b - S_c}{3} \cdot V_{dc} \\ U_{Sb} = \dfrac{2 \cdot S_b - S_a - S_c}{3} \cdot V_{dc} \\ U_{Sc} = \dfrac{2 \cdot S_c - S_a - S_b}{3} \cdot V_{dc} \end{cases} \quad (12)$$

B. Network model

The analytical expression of the inverter model is illustrated in (13), where e_1, e_2, e_3 are the fem of the network.

$$\begin{cases} U_{sa} - e_1 = R_{res} \cdot I_{res1} + I_{res} + L_{res} \cdot \dfrac{dI_{res1}}{dt} \\ U_{sb} - e_2 = R_{res} \cdot I_{res2} + I_{res} + L_{res} \cdot \dfrac{dI_{res2}}{dt} \\ U_{sc} - e_3 = R_{res} \cdot I_{res3} + I_{res} + L_{res} \cdot \dfrac{dI_{res3}}{dt} \end{cases} \quad (13)$$

$$\Omega_{ref} = \frac{\lambda_{opt} \times V_{tides}}{R_i} \quad (14)$$

The control gains obtained from the PI regulators are presented in expression (15), where ω_{nd} and t_{sd} are the dynamics and the time constant of the system, respectively.

$$\begin{cases} K_p = \sqrt{2} \times \omega_{nd} \times J \\ Ki = \omega_{nd}^2 \times J \end{cases} \quad (15)$$
$$\omega_{nd} = 5{,}8 / t_{sd}$$

System control methods

The proposed control strategies include: - speed control of the 9 turbines using the MPPT technique; - Control of active and reactive powers using the inverter connected to the electricity grid; - Control of the DC bus voltage through the PMSG rectifier.

a. PMSG speed control with MPPT

The method used to control the speed of each turbine is based on the MPPT control strategy. The reference of the optimal speed is estimated in (14), where λopt is the specific speed of the turbine. It is obtained by the MPPT technique. The speed control strategy is illustrated in Fig. 6, where the electromagnetic torque Tem is estimated from the speed loop. The same method is described in [11-12].

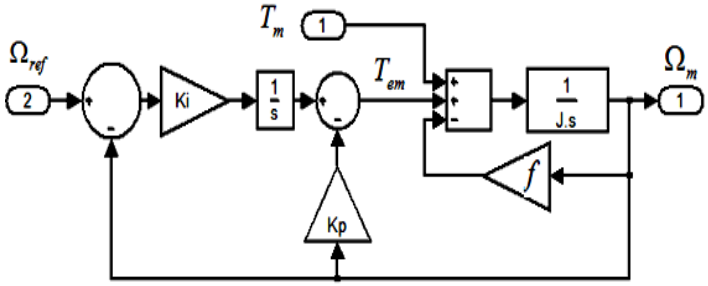

Fig.6. PMSG speed control loop

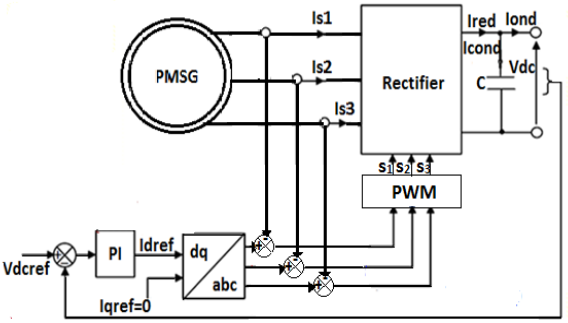

Fig.7. DC bus voltage control strategy

DC-bus Voltage Control Strategy

The strategy for controlling the DC bus voltage is illustrated in Fig.7, where the reference for the current Idref is obtained in the DC bus voltage control loop. Iqref is set to zero in order to obtain a power factor equal to 1. The expressions of the control gains are present-

ed in (16), where ω_{ndc} and t_{sdc} are respectively the dynamics and the time constant of the system.

$$\begin{cases} K_p = \sqrt{2} \times \omega_{ndc} \times C\omega_{ndc} = \dfrac{5{,}8}{t_{sdc}} \\ Ki = \omega_{nd}^2 \times C \end{cases} \tag{16}$$

b. **Active and reactive power control strategy**

The expression of the active and reactive powers exchanged with the network is presented in (17), where (V_{dg}, V_{qg}) and (I_{dg}, I_{qg}) are respectively the voltages and currents of the network in d_q.

$$\begin{cases} P_g = V_{dg} \times I_{dg} \times V_{qg} \times I_{qg} \\ Q_g = V_{qg} \times I_{qg} \times V_{dg} \times I_{qg} \end{cases}. \tag{17}$$

The strategy for controlling active and reactive power is presented in Fig. 8. The coefficients of the different regulators for the internal current loop and the power loop are illustrated in (18) and (19) respectively. In these equations t_{repir} and t_{repps} are the time constants for the internal and external loops, respectively; R_{res} and L_{res} are respectively the resistance and the inductance of the network.

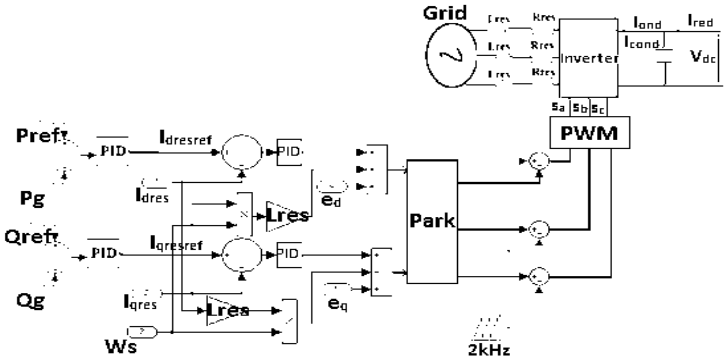

Fig.8. Active and reactive power control loops

$$\begin{cases} K_{pir} = (2{,}197 \times L_{res}) / t_{repir} \\ K_{iir} = (2{,}197 \times R_{res}) / t_{repir} \end{cases} \quad (18)$$

$$\begin{cases} K_{pps} = t_{repir} / t_{trepps} \\ K_{ipps} = 2{,}197 \times t_{trepps} \end{cases} \quad (19)$$

Simulation results

To evaluate the performance of the models, we present the simulation results based on the farm with 9 turbines composed of the same MSAP with a nominal power of 2 MW. Due to the limited performance of the computer used, the 24 hour tidal current speed profile (1st day of January) is used. Then the other profiles for the other 8 turbines are obtained by shifting the profile of the 1st turbine by 0.05 m/s successively. The DC bus voltage reference Vdcref is fixed at (2200 and 2000) respectively

The reference of the reactive power Qref is respectively fixed at (-400, 0 and 400) kVAr. The reference of the active power is fixed at 40% of the total power of the 9 turbines.

By convention, the sign of reactive power is assumed to be positive for the energy supplied, and negative for the energy consumed, [12]. The parameters used in the control loops are presented in the appendix.

The currents measured on the DC bus are shown in Fig. 11; or we find that the current of the inverter is equal to the sum of the rectified currents after the charging time of the capacitor. The results of control of the active and reactive powers are respectively presented in Fig.12 and Fig.13. These results allow us to conclude that the control strategy presented is adequate. It shows that variations in tidal speed are taken into account for the control of active power.

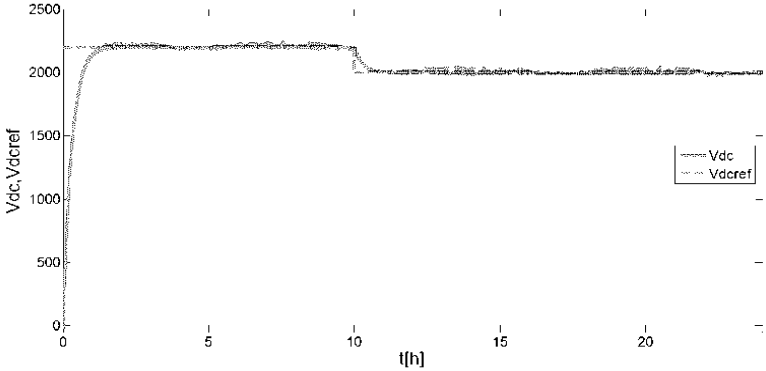

Fig.10. DC bus voltage control results

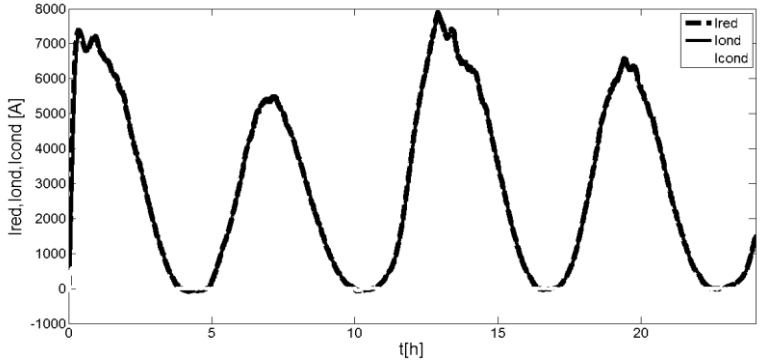

Fig.11. Current diagrams measured on the DC bus

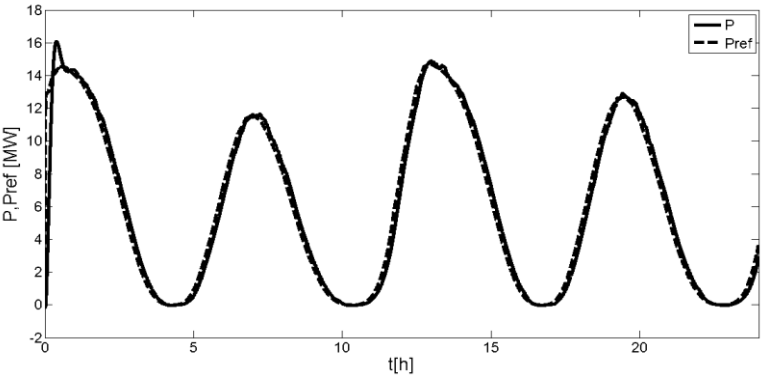

Fig.12. Active power control results

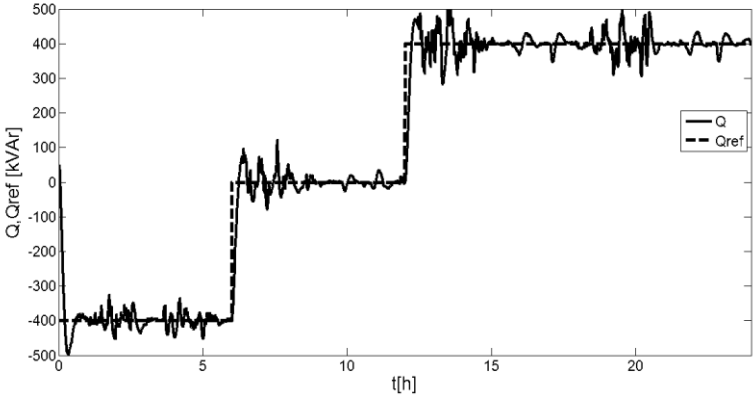

Fig.13. Reactive power control results

Conclusion

In this article we presented the architecture of the farm with 9 turbines and the results of simulation of the whole system.

A tidal energy production system based on the hydrodynamic characteristics was simulated using Matlab / Simulink. Each machine is driven by a turbine with a blade length of 10 m; and the different 24 hour tidal speed profiles are applied to them. Thus the DC bus voltage, the active and reactive powers have been controlled. The simulation results show that the proposed system is interesting for tidal turbine applications.

Appendix

Table 1

Simulation Parameters

Parametres	Valeurs
Radius of turbine, R_t	10 m
water density, ρ	1024 kg/m^3
Pitch angle, β	0°
Stator resistance, R_s	0.821 mΩ
Stator inductances in dq axis $L_{d,q}$	1.5731 mH
Rated rotor flux linkage, Ψ_m	4 W_b
DC-bus capacitor, C	50 m_F
Inductance of the grid, L_{res}	0.5 H
Resistance of the grid R_{res}	50 Ω
Total inertia moment J	1000 $kg.m^2$

Number of pole pairs P	52
Viscosity friction f	0.0022
PMSG speed control parameters	λ_{opt}=8; $C_p(\lambda_{opt,}0)$= 0.5120; t_{sd}= 0.05s; K_p=1.624·10^5; K_i=1.3456·10^7
DC - bus voltage control parameters	t_{sdc}= 0.02s ; K_{pdc}=20.3; K_{idc}=4205
$I_{d,q}$ currents control parameters	t_{repir}=0.011s;K_{pir} =99.8636; K_{iir} =9986.4
Active/reactive power control parameters	t_{repps} =0.13s; K_{pps} =0.0846; K_{ips}=0.2856

References

[1]. **Romain Luquet, David Bellevre, Didier Frechou** ‘’Developpement d’un concept novayeur d’hydrolienne’’, ATMA 2010

[2]. **Matthieu HAUCK**, Optimisation de l’architecture et de la commande de la chaîne électrique d’une hydrolienne fluviale : conception et réalisation’’, Décembre 2011.

[3]. **Seifeddine BENELGHALI** On multiphysics modeling and control of marine current turbine systems’’, décembre 2009.

[4]. **Michel Benoit, Jean-François Dhédin, Giovanni Mattarolo** ‘’Energies marines hydrolienne et houlomotrice.Exemples de projets et de travaux de R&D’’Conférence Institut Coriolis – 24 septembre 2010

[5]. **Ana Maria ANDREICA** Optimisation énergétique de chaînes de conversion hydroliennes modélisation, commandes et réalisations expérimentales’’16 juillet 2009

[6]. **M.O.F.Diallo, M.B.Camara, S.Youssef, J.Thiebot, H.Gualous, B.Dakyo**, “Energetic capability characterization for the tidal turbine farm implementation’’, IEEE-AFRICON 2013.

[7]. **M.O.F. Diallo, M.B. Camara, S. Youssef, H. Gualous, B. Dakyo** “Permanent Magnet Synchronous Generator for Tidal Turbine Application in Raz Blanchard - Modeling and Control Strategy’’, PEMC 2014.

[8]. **Benelghali, S. ; El Hachemi Benbouzid, M. ; Charpentier, J.F. ; Ahmed-Ali, T. ; Munteanu, I.** "Experimental Validation of a Marine Current Turbine Simulator: Application to a Permanent Magnet Synchronous Generator-Based System Second-Order Sliding Mode Control", IEEE Trans. on Industrial Electronics,Vol.38, Issue:1,pp:118- 126, 2011

[9]. **Tarak GHENNAM** ‘’Supervision d’une ferme éolienne pour son intégration dans la gestion d’un réseau électrique, Apports des convertisseurs multiniveaux au réglage des éoliennes à base de machine asynchrone à double alimentation’’, Septembre 2011

[10]. **Arnaud GAILLARD** Système éolien basé sur une MADA : contribution à l’étude de la qualité de l’énergie électrique et de la continuité de service’’, avril 2010.

[11]. **A.G. Sanchez, M.G. Molina, A.M. Rizzato Lede** "Dynamic Model of wind energy conversion system with PMSG-based variable-speed wind turbines for power system studies'', International Journal of Hydrogen Energy, vol.37, Issue 13, July 2012, pp: 10064–10069.

[12]. **Nantao Huang, Jiangbiao He, Nabeel A.O Demerdash** "Sliding Mode Observer Based Position self-sensing control of a Direct-Drive PMSG wind turbine system Fed by NPC Converters'', IEEE International on Electric Machines & Drives Conference (IEMDC) 2013

INSTITUTIONAL BASIS AND TRENDS OF MANAGEMENT OF THE USE OF THE SUBSOIL IN UKRAINE

Savina N.B.
National University of Water And Environmental Engineering (NUWEE), Doctor of Economics, Professor, Department of Labor Resources And Entrepreneurship, Ukraine

Malanchuk L.O.
National University of Water And Environmental Engineering (NUWEE), Candidate of Sciences (Economics), Assistant Professor Department of Public Administration, Documentation and Information, Ukraine

Ignatiuk I.Z.
National University of Water And Environmental Engineering (NUWEE), Candidate of Sciences (Economics), Assistant Professor, Institute of postgraduate education, Ukraine

Moshchych S.Z.
National University of Water and Environmental Engineering (NUWEE), Associate Professor, Candidate of Economic Sciences, Institute of Postgraduate Education, Ukraine

Abstract

In the conditions of overcoming the consequences of the economic crisis in Ukraine, effective subsoil use becomes of fundamental importance. Ukraine is one of the few countries in the world provided with its own natural resources, with the vast majority of required minerals. However, so far there is no reason to say exactly about all resources, perhaps not so much about already explored deposits, but about potential reserves. For example, it is the presence of native copper in the Rivne-Volyn region, which is reasonably predicted in the territory of Polissya. Activating

these resources by identifying specific fields and organizing their development is an urgent task today.

Scientists have determined the content of relations between state bodies that make and implement decisions and consumers of subsoil resources. The implementation of management decisions is carried out at the regional level, which necessitates the increase of responsibility and certain autonomy of territorial authorities. The regional level of utilization of MRs (mineral resources) is largely determined by the implementation of management functions to achieve strategic goals by performing operational tasks and types of work [2].

The main task of state regulation of subsoil use relations is to ensure the reproduction of the mineral base, its rational use and the protection of subsoil.

Introduction

Activity in the field of exploration, use and protection of mineral resources is an institutional activity based on the legislative and legal norms of activity of the relevant bodies of the Ukrainian state in the organization of the study of rational use of mineral resources to meet the needs of mineral resources and other needs of the economic complex, protection of the mineral resources in their close interaction and other natural objects and ensuring the safety of work when using the subsoil, as well as protecting the rights of businesses, organizations, institutions and citizens in this field.[3].

Relations arising from the study, use and protection of subsoil, and the use of waste from the mining complex and related processing industries (peat, sapropels and other specific mineral resources, including groundwater, salt lakes and seas), called mining relationships [2]. They are regulated by the Constitution of Ukraine, decrees of the President of Ukraine, as well as by resolutions of the Cabinet of Ministers of Ukraine on the study, use and protection of subsoil, the State Committee of Ukraine for Industrial Safety, Labor Protection and Mining Supervision, the Law on Environmental Protection, the Code of Ukraine on Subsoil , The Mining Law of Ukraine, the Laws of Ukraine “On the State Geological Service Ukraine”, “About concessions”, “About production sharing agreements”, “About oil and gas”, “About rent payments for oil, natural gas and gas condensate”, “About state regulation of production, production and use of precious metals and precious metals stones and control over operations with them”, “About the extraction and processing of uranium ores”, orders and other acts of the legislation of Ukraine [4-7].

The main task of institutional management of subsoil use relations is to ensure the reproduction of the mineral resource base, its rational use and the protection of subsoil.

The institutional system for the management of subsoil users is based on thorough scientific research conducted in different regions of Ukraine, which have their own specific features and peculiarities in these regions[8].

Overcoming the crisis in the Ukrainian economy on the basis of its structural restructuring is possible Overcoming the crisis in the economy of Ukraine on the basis of its structural restructuring can be done in a short time only based on the state resources: labor and natural, basic production funds, communications, etc. relying on state resources: labor and natural, fixed assets, communications, etc.

The mechanism of regulation in the field of subsoil use and environmental protection is a system of management measures, environmental legislation and economic incentives aimed at the rational use of nature.

The regulation of subsoil use is a real mechanism for incorporating environmental policy into the functioning of the economic system. There are several such regulators: regulatory and legal; organizational and managerial; economic (Fig.1.1).

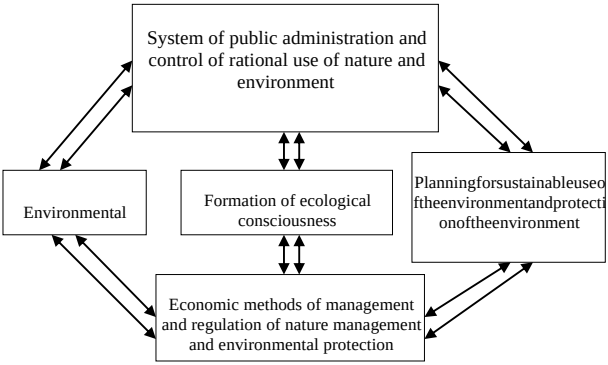

Fig. 1.1. The main levers of regulation of the process of rational use of nature and the protection of subsoil [1]

An important direction of increasing the efficiency of management activities in the field of environmental management and protection of the environment is the harmonization of economic and envi-

ronmental interests of enterprises, institutions, organizations, society as a whole and individuals. In order to ensure the economic and environmental interests of society, the state had to create the necessary and optimal conditions for combining economic development with rational use of nature and environmental protection, which is possible only through a combination of measures of administrative and legal influence on nature users and measures of economic regulation of nature use and environmental protection.

In order to methodologically correctly consider the issues of subsurface users' activities in the field of greening, it is necessary to define specific categories related to mining.

The public and community associations and organizations are also part of the institutional system for managing the greening of subsoil users. Citizens and their associations assist the Local Councils of People's Deputies and specially authorized bodies of the state executive in carrying out measures for the rational use and protection of subsoil. Enterprises, institutions, organizations, citizens of Ukraine, as well as foreign legal entities and citizens can be users of subsoil.

Actively cooperate with national subsoil users and international organizations, which are an integral part of institutional governance.

Exploring the institutional prerequisites for managing subsoil users, it is necessary to distinguish the levels of regulation of relations in this area. Depending on the object of regulation, mining can be divided into: mining for geological prospecting; mining on the use of subsoil; mining relations for the protection of subsoil.

The legislative segment of institutional support for subsoil users' activities is based on a number of legal acts and regulations. The Subsoil Code of Ukraine provides an approximate list of legal facts that give rise to mining relationships, that is, may be grounds for their occurrence, change and termination. In particular, in the course of implementation by the Councils of all levels, the Cabinet of Ministers, and other authorities in the field of geological exploration, use and protection of subsoil, which are envisaged by the Code on subsoil, they make decisions that are the basis for the emergence, change and termination of mining legal relations [5].

According to Article 4 of the Subsoil Code, subsoil is the exclusive property of the people of Ukraine and is provided only for use [3]. Agreements or actions that directly or covertly violate the own-

ership of the subsoil of the people of Ukraine are invalid. The people of Ukraine exercise their right to subsoil through the Verkhovna Rada of Ukraine and local councils of people's deputies. Separate powers regarding the disposal of subsoil by the legislation of Ukraine may be conferred on the relevant bodies of the state executive power (Fig. 1.2).

The main task of state regulation of subsoil use is to ensure the reproduction of the mineral base, its rational use and the protection of subsoil.

Subsoil use and protection control is one of the functions of the state environmental quality management, a system of measures aimed at organizing the monitoring of the geological environment, checking the compliance of individuals and legal entities with the requirements and rules for rational use of subsoil, protection of subsoil and environmental safety.

State regulation and control over the use and protection of subsoil within their competence in Ukraine is carried out by councils, state executive bodies on the ground, the Ministry of Nature of Ukraine, the Ministry of Emergencies and in matters of protection of the population against the consequences of the Chernobyl disaster and their bodies on the ground (Article 61 of the Code of Ukraine on bosom). State control over geological prospecting (state geological control) i carried out by the Ministry of Natural Resources of Ukraine and its bodies on the ground. State geological control bodies check the implementation of state programs of geological prospecting, the use of decisions on the methodological support of geological prospecting works, the validity of the use of methods and technologies, the quality, complexity, efficiency of work on the geological prospecting, the completeness of baseline data and the quality of reserves and jointly mineral resources.

Violation of subsoil legislation entails disciplinary, administrative, civil, criminal and criminal responsibility, and it is proposed to revitalize the activities of territorial executive bodies in planning the development of a regional mineral resource base.

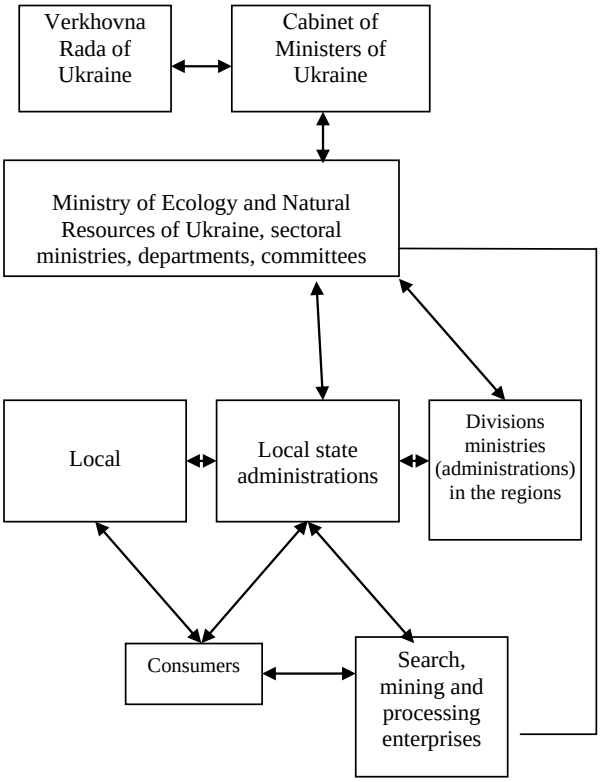

Fig. 1.2. Interaction of subsoil users with management bodies

The expediency of development of the strategy of subsoil utilization with the purpose of qualitative improvement and expansion of mineral resources base, reduction of raw material dependence of Ukraine, strengthening of ecological and energy security, determination of further ways of utilization of mineral resources of the country is proved.

The directions of its realization are as follows: determination of rational production volumes; creation of conditions for economically justified and technically possible increase of extraction of mineral resources; increasing the volume of investments in the mining sector; taking into account the tendency of changes in the internal and external markets of the MR, the environmental component of subsoil use;

diversification of energy supply sources of MR; transition to energy-saving technologies; creation of conditions for effective development and implementation of scientific and technical programs, introduction of high technology, including those that use man-made fields.

Public administration bodies in the field of use and protection of subsoil are divided into general and special government bodies.

Bodies of general government in the field of use and protection of subsoil are authorized bodies of the state executive power, which in addition to the general powers in the sphere of socio-economic development of the state also have functions to ensure the study, effective use and protection of subsoil. Such bodies, inparticular, are: President of Ukraine; National Security and Defense Council of Ukraine; Cabinet of Ministers of Ukraine; regional, district and city state administrations [6].

Bodies of special state management of relations of subsoil use - specially authorized bodies of the central executive power, carrying out the functions of management in the field of study, use and protection of subsoil, ensuring the safety of works in the use of subsoil, protection of rights of subsoil users, protection of the environment from pollution associated with subsoil use etc.

Bodies of special competence, which perform the functions of public administration in the field of study, use and protection of subsoil, by nature of their tasks and activities are divided into two main types: intersectional and sectorial (departmental).

Special bodies that regulate mining relations also include the State Service for Mining Supervision and Industrial Security of Ukraine, which is a specially authorized central body of executive power, which carries out state regulatory regulation of industrial safety issues in the territory of Ukraine, as well as special permits, supervision and control functions. The main task of this body is: organization and implementation in the territory of Ukraine of industrial safety and state supervision of all subsoil users and observance of requirements on safe conducting of works in industry; mining supervision; development and implementation of measures for the prevention of occupational injuries, etc.

In the regions of Ukraine, where prospecting and geological work is being done, territorial geological offices and trusts are created, boundaries of competence, which often do not coincide with the

boundaries of administrative regions and oblasts. The organization of prospecting and exploration operations is determined by the relevant instructions and regulations.

State control over the rational use and protection of subsoil is aimed at ensuring that all subsoil users comply with the established rules for the use of subsoil, legislation approved in accordance with the established standards, rules and regulations in the field of geological exploration, use and protection of subsoil, the rules of public accounting and reporting. It is carried out by bodies of state geological control in cooperation with bodies of state mining supervision, nature conservation and other control bodies [4,7].

State geological control bodies, within their competence, provide solutions to other geological prospecting issues and grant the right to; a significant reduction in the efficiency of work or lead to significant losses; to suspend the activities of enterprises and organizations engaged in geological exploration without the special permits (licenses) or in violation of the conditions stipulated by these permits; to give obligatory for execution of the instruction (prescriptions) on the elimination of defects and violations during the geological exploration of subsoil.

State geological control bodies in accordance with the legislation of Ukraine may be granted other rights to prevent and stop violations of rules and norms of geological prospecting. The task of state supervision of the safe conduct of work related to the use of subsoil is to ensure compliance with all subsoil users legislation approved in accordance with the established order standards, rules, rules for safe conduct of works, prevention and elimination of their harmful impact on the population, the environment and structures, as well as for the protection of subsoil [6].

State supervision of the safe conduct of work related to the use of subsoil is entrusted to the state mining supervisory authorities, which carry out their activities in cooperation with the state geological control bodies, nature protection and other control bodies, trade unions. In addition, industrial control over the use and protection of subsoil is carried out by enterprises, institutions and organizations (subsoil users), which are under the control of the relevant bodies.

The correctness of the development of mineral deposits is controlled by surveying, geological and other services. But the most ex-

tensive and comprehensive supervision of the correctness of exploitation and protection of subsoil, which includes the supervision of all uses of subsoil, is state mining supervision.

Conclusions

Institutional policy of subsoil use in Ukraine should have a sound legal basis. Regulatory legislative documents and by-laws of Ukraine, as a sovereign and independent state, have significant under-development, which are long-term use and are not able to fully protect natural resources from the mining and geological intervention of neighboring states. Each region (region) of Ukraine should have a "Concept of integrated industrial development of natural resources assigned to a given region", since after the collapse of the USSR the legal regime of nature management was violated, which caused considerable damage to the economy of the state and mineral dependence of Ukraine [7, 8].

References

1. **Savina N.B.** Investment support for the development of economic systems. Economics: realities of time. 2, 101-110.(2014)

2. **Antonov A.V., Savina N.B.** Mechanism of state management in the system of conservation of natural capital. Bulletin of the National University of Water Management and Environmental. Economics. 1, 255-264.(2018)

3. **Malanchuk L.O. Mexanisms of state regulation of subsoil use companies – subsoil users.** News of Science and Education. Economics. England: Sheffield Science and education ltd,. **16(16)**, 68 - 76.(2014)

4. **Malanchuk L.O.** Mechanisms of state regulation of subsoil use by subsoil users. Оралдын Ғылымжаршысы: scientific - theoretical and practical journal. Series "Economic Sciences. Public Administration. Kazakhstan, **37 (116)**, 35-45.(2014)

5. **Savina N.B. Serebryanaya V.** Energy policy-the essence and regularity of formation in Ukraine. Bulletin of the National University of Water Management and Environmental. Economics. 2, 181-190.(2018)

6. **Malanchuk L.O., Malanchuk Z.R, Malanchuk E.Z, Ignatyuk I.Z.** Strategic framework for the development of rational subsoil use in Ukraine. Australian and New Zealand Journal of Fundamental and Applied Studies, **1(15)**, 126-132 (2015)

7. **Malanchuk L.O., Malanchuk E.Z.** Current state of implementation of rational subsoil use in Ukraine. The 5th International Academic Congress «Science, Education and Culture in Eurasia and Africa». France, Paris, 23-25 March 2015. Vol. IV. «Paris University Press», 328-331. (2015)

8. **Malanchuk L.O.** Priority directions of development of mineral resources of Western Polesie. Internation journal of new economics and social sciences. Swinoujscie, **4(4).**(2016)

COLUMN FLOTATION MACHINE – INNOVATIVE AERATION, VIBRATORY – ACOUSTIC AND TECHNOLOGICAL RESEARCHES

Dedelyanova Kr. Y.
Dr. Eng., President, Scientific and Technical Union
of Mining, Geology and Metallurgy, Bulgaria

1. Introduction

During the past years a great efforts has been paid for improvement of the flotation process both mechanical equipment and the chemical interactions reagent – mineral. An important direction in this area is column flotation. The industrial experience shows that implementation of column flotation leads to decrease of the number of cleaning operations due to the improved selectivity.

G.M. Callow patented the first pneumatic flotation cell, which used air sparging through a porous bottom and horizontal slurry flow, in 1914. The first countercurrent column flotation device was designed and tested by Town and Flynn in 1919. Cross-current pneumatic flotation machines were widely used in industry in 1920's and 1930's, but were later replaced by the impeller-type flotation devices in mineral processing plants. Dissolved-air flotation became the main type of flotation for water treatment applications. These substitutions were the result of the absence of effective and reliable air spargers for fine bubble generation and by the lack of automatic control systems on the early columns. During this period, both the poor flotation selectivity and entrainment of slimes characteristic of impeller-type cells was offset by the use of complex flowsheets using large numbers of cleaner stages and recycle lines. Column flotation devices were re-introduced for mineral processing in the late-1960's in Canada by Boutin and Wheeler (1967) at which time wash water addition to the froth was used to eliminate entrainment of hydrophilic materials to the float product. By the late-1980's column flotation had became a proven industrial technology in the mineral industry. These separators are routinely used on their own or in conjunction with other types of devices within separation circuits

The flotation technique and technology developments are closely connected with the improvement of the flotation machines design.

The main road solving the task for flotation process intensification is the creation of high – productive flotation machines.

The contemporary requirements in the field of pulp aeration and bubble mineralization theories impose the design of pneumatic flotation machines of column type that find application at the flotation of ores of non-ferous, noble, rare and ferrous metals, coal and other mineral resources as well as wide use at purification of waste water from different productions. (Chernykh, 1996)

The column flotation machine wide practical introduction appears to be an important achievement during the last decade in the field of flotation concentration. The advantages of the column flotation machine in comparison with the mechanical and pneumomechanical are the following: increased productivity improved hydrodynamics, of concentrate with the required quality at minimal quantity purifying and control operations, production area decrease and economy of electric power.

The movement nature of the particle and the bubble is an important factor, which determines the probability of flotation complex formation, mineralization rate, flotation speed and the process power consumption. (Chernykh, 1996) The inertial forces which destroy the particle - bubbles complex in column are insignificant. This is connected with the absence of a stirring device and the pulp flow low turbulence.

The increase of the air bubbles flotation activity is connected with the increase of their conditioning time, i.e. the interval between the formation moment and the bubble mineralization. In consequence of the column considerable height the sojourn duration of the air bubbles in it is not longer than 20s, i.e. a mineralization process at optimal flotation activity of the bubbles is realized. The basic research field in column devices is the fine-grained pulp flotation. The absence of intensive pulp mixing, product purification zone, high position of the feeding level, and the thick froth layer contribute to the obtaining of concentrate of better quality in comparison with the impellers. (Rubbinshtain, 1989).

There is a bigger probability of capture and withstanding of the coarse particle to the bubble so in some cases the column flotation machine use could turn out to be expedient for coarse – grained material flotation, as well. (Foot, 1986)

The flotation machines work effectiveness depends on the conditions of the air dispersion. The aerators must provide a maximum gas content at an optimal average massiveness of the bubbles. The following claims are demanded to the aerators: providing for such a bubbles size that assures the flotation complex emerging, minimal pulp macrocirculation in the chamber, stable aeration characteristic.

The aerators designs developed in accordance with the requirements could be combined by the action principle as follows: pneumatic, hydraulic (swift - flowing) and pneumohydraulic.

The basic aerator type in the column flotation machine is the pipe device. An aerator representing a set of tightens in group hollow rings from porous (wool or porous polyethylene) or elastic (raw rubber) material is proposed for the aeration characteristics improvement. Changing the group tightening extent regulates the bubbles dispersive composition. The pulley aerator design is analogous. The ring pivot is vertically situated and the diameter increases from top to bottom. As a separate tendency the vibrating pneumatic flotation machines design should be mentioned. Their action principle is based on air dispersion by vibrations at its feeding to the aeration chamber. The pulp vibrating turbulent movement creation reinforces at the liquid flow through special lattices.

2. Experimental part

Dedelyanova and Metodiev (2002) presented a laboratory model of a vibratory column flotation machine constructed in the Laboratory of "Vibro-acoustic Intensification of the Technological Processes" at the Department of Mineral Technologies of the University of Mining and Geology "St. Ivan Rilski", Bulgaria.

It is realized on a modular principle, which provides a possibility for determination of the feeding device optimal height infinitely – variable regulation of the pulp level and precise determination of the necessary quantity of extra water for the froth layer irrigation. The vibratory column flotation machine basic elements are sensor (fig. 1-1), vibrator (fig. 1-2), air disperser (fig. 1-3), module for creation of single gas bubbles (fig. 1-4), feeding device (fig. 1-5), machine chamber (fig. 1-6).

The flotation batch tests were carried out in a laboratory vibratory column flotation unit – two meters high and 50 mm in diameter. It is

made of transparent plastic tube with internal volume 4.2 l. The sample for the tests is rougher copper concentrate. Due to the fact that the sample is already conditioned reagent collector is not used, only frothier – from15 to 25 drops in order to a high froth layer to be obtained.

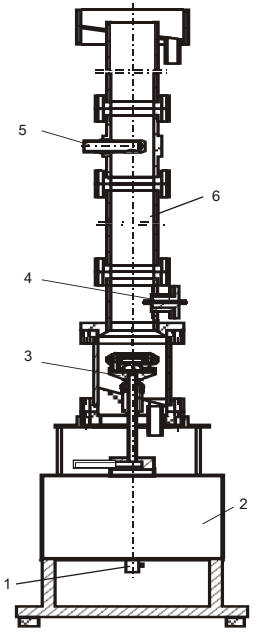

Fig. 1. Vibratory column flotation machine – scheme of principle

The vibratory disperser provides the opportunity of certain technological parameters research: gas bubble size change, change of the gas bubbles emerging speed and solid phase sedimentation speed, the influence on the opportunity of mineral particles attachment to the air bubbles, purifying of the froth layer from rock particles.

The vibrator is electrodynamic type, power 40 W and a possibility of a wide range frequency and amplitude change, overlapping the supposed range of vibratory parameters, required by the research.

Two modifications of the air- dispersing unit were constructed- for vertical and horizontal vibrations. The air-dispersing unit for vertical vibrations (fig.2-1-air) disperses air by its transition through an annular slot, which allows rate regulation within certain range and

production of gas bubbles of certain size by regulation of vibrations frequency and amplitude.

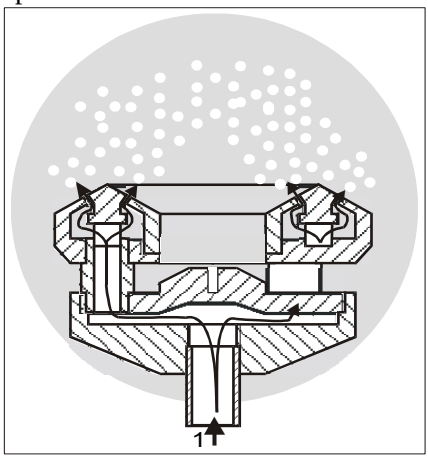

Fig.2. The air-dispersing unit for vertical vibrations

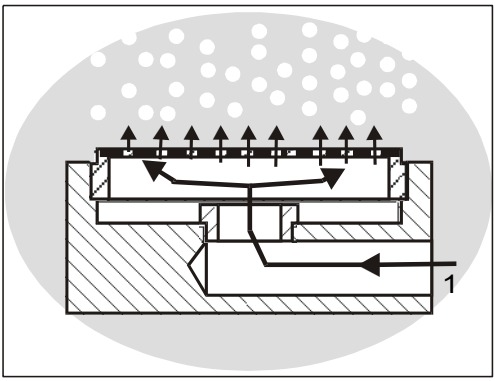

Fig.3. The air-dispersing unit for horizontal vibrations

Simultaneously, with the bubbles production, the vertical oscillations create a vibroacoustic field, which is distributed along the column height. The air-dispersing unit for horizontal vibrations (fig.3-1-air) produces gas bubbles through round holes, perpendicular to the direction of the vibratory field vector.

The feeding modulus allows pulp supply into the flotation machine and even distribution of pulp along the column section as well as filling with water for vibroacoustic measurements.

The commonly used quantity of air in the tests is 100 l/h.

The level of the pulp is adjusted based on the principle of connected vessels by vertical movement of overflowing ring. The tailings are discharged by plastic pipe and valve into a vessel.

The formed complexes particle-bubble are floating into the froth layer - about $30\text{-}40 \cdot 10^{-2}$ m high. The counter flow of fresh water is not necessary because the vibrating field cleans the complexes during their upward movement enough efficiently. The froth is collected also into a vessel for drying and assay. The time of flotation is 15 to 30 min. depending on the solids content. The tests are carried out at solids content of the slurry: 0,50, 0,51, 0,75, 1,10,1,50, 1,70, 2,10%, 2,50, 2,70, 2,90, 3,10, 3,80, 5,30, 5,90, 6,60, 10,30%.

The energy of vibrations could be characterized by the pointer – Af^2 and their influence upon flotation process is evaluated based on the difference in the grade and recovery of the valuable component into the concentrate compared to the zero test. The flotation tests were carried out at frequencies from 25 to 40 Hz, amplitudes 2.0, 2.5 and 3 mm and values of Af^2 respectively1500, 1800, 2250, 2450, 3200 and 3675.

3. Results and disscusion

The use of vibration impact on flotation process is based on the effects, caused by vibrations onto a heterogeneous media – effective decrease of viscosity of the liquid phase, vibrating of particles of the solid phase, periodic change in the shape of the gas bubbles. These effects displayed at the original design of column flotation machine having a big ratio between height and cross section diameter, should be determined at definite values of vibrations' frequency and amplitude so that the resonance phenomena to be displayed into the chamber. The batch tests carried out at this area should give the answer to the questions concerning the definite values of the effective interval of vibrations' frequency and amplitude for practical use in technological tests with definite products of the mineral processing industry.

During the tests are performed two types of tests: measurement of flotation speed of unique air bubble in calm and vibrating liquid me-

dia and calculation of the difference in their speed; measurement of the amplitude of vibrations along the column flotation machine as a function of the water height. These tests are carried out at different frequencies and amplitudes of vibrations of the vibratory-acoustic disperser.

3.1 Definition of the vibrations influence upon the speed of gas bubbles floating

The stream-lining character of the bubbles is substantially different to the stream-lining of the solid phase in the liquid. The smallest bubbles at Re < 1 keep their shape close to the spherical one because it is determined by the surface tension and the speed of flotation is defined by the Stock's low.

With increase of the bubbles diameter begins a process of deformation. This deformation violates the straightforward character of movement and changes its flotation speed.

The speed of flotation of the bubbles with deformed surface is bigger, which could be explained with the fact that thanks to the mobile border surface, the gradient of speeds in the liquid around the bubble are smaller than around the spherical one.

The decrease of speeds gradient leads to decrease in energy of dissipation in the liquid. The natural frequency of bubbles with diameter 1-4 mm is at the range of 200-500 Hz.

Therefore, the frequencies that have been researched at vibrating flotation are at the under-resonance range where stable amplitude of the bubbles vibration can be observed.

The general results of experimental determination of the flotation speed of gas bubble in vertical vibrating field are shown at the table 1.

The speed of flotation of gas bubble without vibrations is bigger than if they are applied. The decrease of speed depends on the amplitude of vibrations - with increase of amplitude the flotation speed decrease reaching to 13-14 % for bubble with diameter 4 mm. At the chart of these speeds at figs. 5 and 6 a sinusoidal dependence as a function of the frequency is definitely observed - the maximum is at 30 and 45 Hz and the minimum at 20 and 35 Hz.

Table 1

Velocity of bubble flotation without and with application of vibrations at water column 1.2 and 0.9 m and size – 4 mm

F, Hz	A, mm	V, m/s without vibrations	V, m/s with vibrations	Decrease in %	V, m/s without vibrations	V, m/s with vibrations	Decrease in %
20	0,5	26,43	25,21	3,7	26,55	25,86	2,6
	1,0	25,92	25,26	3,5	26,87	25,71	3,1
	1,5	26,43	25,26	3,5	26,47	25,28	4,7
	2,0	26,20	25,00	4,5	26,39	24,66	7,1
	2,5	26,30	24,84	5,1	26,39	25,00	5,8
25	0,5	26,14	25,42	2,9	26,47	25,42	4,2
	1,0	26,09	25,10	4,1	26,63	25,42	4,2
	1,5	26,32	25,00	4,5	26,55	24,66	7,1
	2,0	26,26	24,74	5,5	26,47	25,14	5,3
	2,5	26,03	25,10	4,1	26,32	25,21	5,0
30	0,5	26,49	25,59	2,2	26,55	24,66	7,1
	1,0	26,20	24,84	5,1	26,63	24,19	8,9
	1,5	26,20	24,44	6,6	26,55	23,94	9,8
	2,0	25,97	23,81	9,0	26,55	23,56	11,2
	2,5	26,09	23,12	11,7	26,39	23,32	12,1
35	0,5	26,61	25,81	1,4	26,87	26,16	1,4
	1,0	26,32	25,26	3,5	26,71	26,01	2,0
	1,5	25,97	24,39	6,8	26,55	25,35	4,5
	2,0	26,03	24,59	6,0	26,55	25,00	5,8
	2,5	26,03	24,69	5,7	26,47	25,07	5,5
40	0,5	26,32	25,37	3,1	26,71	25,77	2,9
	1,0	26,26	24,90	4,9	26,39	25,07	5,5
	1,5	26,14	24,05	8,1	26,63	24,73	6,1
	2,0	26,20	24,29	7,2	26,47	24,32	8,4
	2,5	25,97	24,29	7,2	26,47	23,75	10,5
45	0,5	26,55	25,53	2,4	26,87	25,94	2,3
	1,0	26,14	24,54	6,2	26,63	24,39	8,1
	1,5	26,09	23,81	9,0	26,63	24,00	9,6
	2,0	25,92	23,72	9,4	26,32	23,20	12,6
	2,5	26,03	23,76	9,2	26,32	22,84	13,9
50	0,5	26,67	25,92	1,0	26,63	25,28	4,7
	1,0	26,26	25,26	3,5	26,63	25,79	2,8
	1,5	25,97	24,29	7,2	26,55	25,00	5,8
	2,0	25,92	24,34	7,0	26,32	23,02	13,3
	2,5	25,92	24,44	6,6	26,32	22,78	14,2

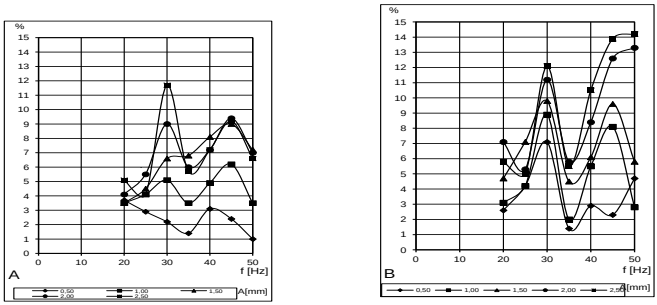

Fig. 4. Decrease of the speed of flotation of the bubbles in % as a subsequence of applied vibrating field: *A* - Height of the water column H=1.2 m and *B* - Respectively H=0.9 m

The decrease of flotation speed of the air bubbles in vibrating field is definitely connected with the amplitude of applied vibrations and is defined by the deformation of the bubble as a result of the processes of increase and decrease of pressure in the water column because of the pass of the wave processes. As a difference to the deformation of the bubbles during their free floating without vibrations, the deformation after application of vibrations is towards eliptical because of changeable pressure at the liquid. This pressure acts in vertical direction and diminishes the vertical size of the bubble enlarging the horizontal one, actually, the spherical bubble is changed into ellipsoid. The resistance to its floating is increased because of its increased horizontal diameter.

This behavior of the bubble ensures increase of the time for movement at the active zone of machine and increase the probability for contact with the particles of the solid phase. The contact bubble-particle is facilitated because of the difference in the vibration phases of the bubble and the solid particles and also makes easier the destruction of the hydrating layers which benefits the complex bubble-particle floating to the froth layer.

3.2 Hypothesis for the vibrations influence upon the speed of floating of gas bubble and elementary act of flotation

The smaller amplitude of vibrations at aeration of the water is explained by the loss of energy spent on change of the gas bubbles' shape. The changeable pressure caused by the front of the sound wave spreading along the height of column is the reason for resonance effects and on the other hand this pressure changes the shape of the bubbles from spherical to ellipsoidal with shorter vertical diameter and bigger horizontal one. This change in the shape explains the reason for the lower speed of flotation of the gas bubbles. The bigger diameter and the smaller height of the bubble lead to increase of resistance to the floating movement.

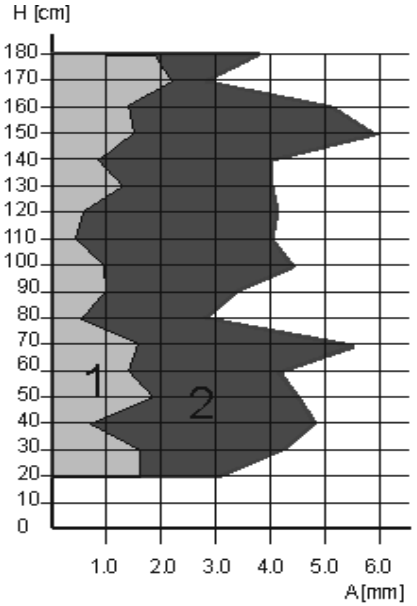

Fig. 5. Amplitude of vibrations along the height of column - *1* - with air bubbles; *2* - without them

The change in the shape of the bubbles is doing with the applied frequency - about 25-40 Hz. The decrease of the flotation speed practically increase the content of the gas phase and possibility for mineralization. The change of the diameter increases the possibility for contact with the sold phase during the process of mineralization – when the diameter increase the possibility for capturing of particles also increase. The vibration of the gas bubble determine the possibil-

ity for rejection of solid particles with hydrophilic surfaces. During the vibration of the bubble the perimeter of wetting is changing due to the changes of its diameter, leading to decrease of the capturing force and respectively the rejection of the hydrophilic particles.

The module for gas bubbles production provides the opportunity of air micrometric supply through changeable air nozzles of certain initial diameter. The pulp level is infinitely - variable regulated by the communicating vessels method.

4. The vibrations influence on the solid phase

Researches were carried out for the effect of frequency and amplitude of vibrations on speed of precipitation of mineral grains of different density. It was known that speed of precipitation decreases with the increase of intensity of oscillating, however the question of effect of diameter and relative weight of particles was still open. For that purpose a series of experiments were carried out with single mineral grains of a diameter from 0,09 to 0,155 and densities of different grains 2,65; 5,1 and 7,8 g/cm^3. Frequency of oscillation changes from 20 to 70 Hz, and amplitude - from 1,5 to 3,0 mm. Average results of experiments were presented in tables 2. Experimental researches involved the conclusion that vibrating media provided additional force of resistance, applied to the mineral particle, which provoked decrease of the speed of falling down. This force is a function not only of frequency of applied vibrations, where experimental values showed decrease of speed depending on density of particles. It was visually observed that when the particle did not reduce significantly its speed/for certain vibration parameters/, its amplitude of oscillation is approximately equal to the amplitude of oscillation of the liquid. When speed of a particle reduces significantly its amplitude increases visibly.

This dependency between speed of falling down of mineral grains into a liquid vibrating medium and parameters of vibrating field may be explained as an interaction between two oscillation motions - motion of mineral grains and motion of applied vibrations.

For lower frequencies of vibration reduction of speed is lower due to lower vibration speed. For particles of higher density reduction is higher due to higher speed, with which they meet the pulsing medium.

Table 2

Decrease of the speed of precipitation in dependence of density of particles

Frequency f [Hz]	Amplitude 2 mm, d=0.12 mm		
	Reduction of V [%] for density g/cm3		
	2,65	5,1	7,8
	%	%	%
20	1,54		
30	3,39	5,38	4,1
40	1,34	7,6	9,73
50	4,54	6,59	7,68
60	5,6	6	8,77
70	4,22	9,6	12,16

4.1. Experimental Research

Dedelyanova (2004) presented the results of research with vibratory column flotation machine with copper ore (cake taken from a control thickener).

The experiments have been carried out in a vibratory column flotation machine laboratory model with height 2000 mm and diameter 50 mm and effect of vibrations Af^2 1500, 1800, 2250, 2450, 3200, 3675, respectively, at a frequency of vibration from 25-40 *Hz* and an amplitude of 2.0, 2.5 and 3.0 mm.

Dispersion of air is through a vibration dispersant designed for vertical vibration. Along with the creation of bubbles, vertical oscillations create a vibro-acoustic field, which is distributed along the height of the flotation machine camera.

At values of vibration effect Af^2=3200 (f=40 *Hz*, A=2.0 mm) the copper content of the cake reaches 32.23% at a copper content in the sample output of 22.76%.

The content of copper in concentrate in the vibration increases 312%. The results are illustrated in Figure 6.

In summary, the effect of vibration Af^2=3675 (f=35 *Hz*, A=3.0 mm) and solids in the pulp 3.8%, that value is highest for this flotation experiments, extraction is highest at 90.68% and value of copper content in concentrate is also highest at 31.44%.

The copper content in concentrate increases 3-3.5%, and copper output from 23.31-27.89%.

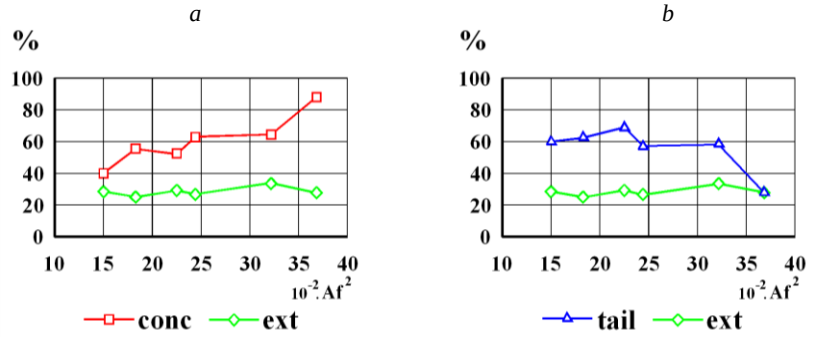

Fig. 6. *a* - dependence of copper content in concentrate and extraction from characteristic Af^2 - effect of vibrations; *b* - dependence of copper content in tail and extraction by characteristic Af^2

The vibratory effect on the gas bubble is applied after it detaches from the nozzle. The measurements results are presented in Figure 7. The gas bubble emerging velocity without vibrations is higher than that with vibrations. Vibrations contribute to the decrease in gas bubble emerging velocity and extend its stay in the column flotation machine.

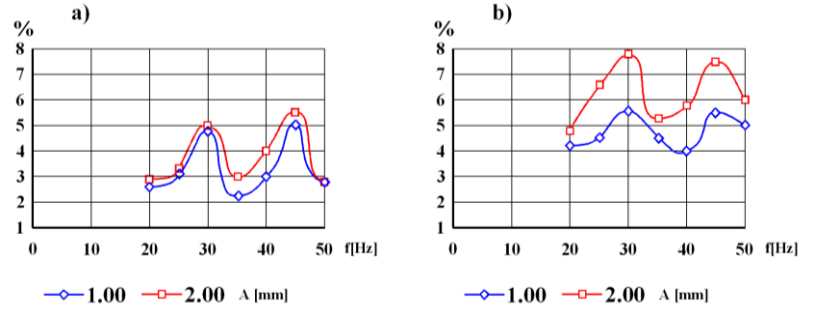

Fig. 7. Decreasing of emergence velocity of gas bubble in % from emergence velocity without vibrations: *a* - for the height of the water column *H*=120 cm and *d* = 3.5 mm; *b* - for *H*=90 cm and *d*=3.5 mm

According to Bogdanov (1990), forces acting on the bubble and the particles attached to it, accounted on the vertical axis are two types: forces acting on the particle and forces caused from the attachment of particle to the bubble. The first type of forces are gravity of particle and ejection Archimedean force, as follows: gravity

$P = -\pi d_p^{\,3} \rho_p g / 6$, where d_p is aligned particle diameter, ρ_p is the density of the particle and g is the gravity acceleration; ejection Archimedean force $F_A = \pi d_p^{\,3} \rho_l g / 6$, where p_i is the density of the fluid displaced by the particle. The second type of forces are the Laplace force F_L and capillary force F_k: Laplace pressure force that is acting on the upper wall of the particle is $F_L = -\pi d_p^{\,2} \Delta p / 4$ where $\Delta p = p_g - p_i$ is the Laplace pressure, p_g and p_i are respectively pressure in the gas and pressure in the liquid on the level of contact; capillary force $F_k = \pi d_p \sigma \sin\theta$, where σ is the surface tension recorded per unit length of contour of tangent wall of the particle and θ is the angle between the tangent wall of the particle and the surface of the bubble. The resulting equilibrium equation of bubble and attached particle is $P + F_A + F_L + F_K = \frac{\pi d_p^3 \rho_p a_l}{6}$, where $a_l = A\omega^2 \sin\omega t = 4\pi^2 A f^2 \sin\omega t$ is the acceleration of the liquid, due to the harmonious movement. To determine the angle θ the equilibrium equation is expressed in the form

$$\sin\theta = \frac{d_p^2 g\left(\rho_p - \rho_l\right)}{6\sigma} + \frac{d_p \Delta p}{4\sigma} + \frac{2\pi^2 d_p^2 \rho_p A f^2 \sin\omega t}{3\sigma}. \qquad (1)$$

The ratio of the hydrostatic pressure on the contact side of the particle to the Laplace pressure is defined as a form constant to the bubble near the particle.

$$\beta = \frac{\rho_l g d_b}{\Delta p} = \frac{\rho_l g d_b^2}{4\sigma} = \frac{\rho_l g d_0^2 \left(\frac{p_0}{p_0 + 4\pi^2 \rho h A f^2 \sin\omega t} \right)^{\frac{2}{3}}}{4\sigma}. \qquad (2)$$

From the equation (5) it follows that the size of the constant harmonic variation β is a function of effect of vibrations Af^2.

5. Collision efficiency in vibration

Productivity of flotation devices is determined by the flotation rate $(d\varepsilon/dt) = f'(t)$. For the case where the properties of the material in flotation conditions are constants (φ=const, N=const) then the equation assumes the shape $(d\varepsilon/dt) = k(1-\varepsilon)$. According to this equation, the flotation velocity is proportional to the mass of flota-

tion material 1-ε and is characterized by a probability *k* for flotation by one unit time. The solution of equation is $\varepsilon = 1 - e^{-kt}$, which determines the nature of the flotation process, reporting in time.

To obtain an integrated evaluation of the flotation machine efficiency, we must introduce the concepts of collision efficiency $E = (M_0 / M)$, where M_0 is the mass of particles that meet with bubbles and M is the mass of all particles that are located in the level of contact at a point in time *t*.

In (Ralston, 1999), the parameter k is called the flotation rate constant and is regarded as proportional to the defined collision efficiency E.

In Rubbinshtain, (1989) the parameter E is called the coefficient of grip. For two flotation processes labeled 1 and 2 for particles of different sizes and ceteris paribus, is presented the dependence:

$$\frac{\ln(1-\varepsilon_1)}{\ln(1-\varepsilon_2)} = \frac{E_1}{E_2}. \tag{3}$$

Rubinschayn (1989) presented multiple formulas determining the number of collisions N and collision efficiency E, divided in two groups:

1) a relatively small group - formulae derived by accepting the model of turbulent motion of bubbles and particles;

2) formulae derived by analyzing the deterministic description of the bubble and particle movement, processes of interaction and relevant forces governing these processes.

According to Derjaguin and Dukhin (1960), 3 zones can be defined around the bubble (Figure 8):

- Zone 1 – outermost part – of hydrostatic interaction;
- Zone 2 (of attachment) – area of effect of surfaces;
- Zone 3 - of stability efficiency of the bubble - particle aggregate

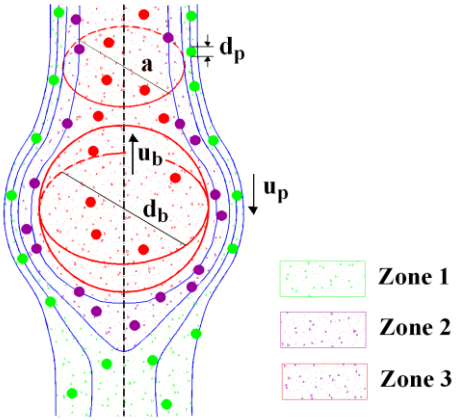

Fig. 8. Scheme of collision of the particles with the bubble

In accordance with the areas of interaction in the aggregate bubble - particle (zone 1 and zone 2) the effectiveness of a collision can be represented by $E = E_{il} + E_{vl}$, where E_{il} is efficiency of laminar (gravitation) flow (ideal liquid) and E_{vl} is efficiency of viscous flow (viscous liquid). Taking into account the formulas presented in (Bogdanov, 1990; Rubbinshtain, 1989) with some approximations, one can accept the formulae.

$$E_{il} = \frac{G}{1+G}\left(1+3\frac{d_p}{d_b}\right) \text{ and } E_{vl} = \frac{3}{2}\left(\frac{d_p}{d_b}\right)^2 f \text{, where } G = \frac{u_p}{u_b},\ f \in [0.1,1]. \quad (4)$$

From the ways of expressing the effectiveness of conflict, we can conclude that the vibrational motion of bubbles and particles is affected by the effectiveness of a collision. The impact is both through variable diameters of the bubbles and by the rate of ascent of the bubbles. Given that the collision efficiency is a dimensionless quotient of the ratio of the mass of the particle meeting the bubble and whole mass of flotation material, it is clear that we can not directly use formulae presented in the literature in the case of vibratory column flotation machine.

5.1. Determining the effectiveness of a collision at vibration impact

To determine the increasing of effectiveness of collision in the presence of vibration, we will use another approach. We will consider the model given by Bogdanov (1990) and supplement it with vibrational deformations of the bubble. We will also use results of experimental studies of Dedelyanova (2004).

For an analysis of the collision process, we accept a bubble as a sphere and and we consider a rotating body around a vertical axis, passing through the center of the sphere. We denote by d_b the aligned bubble diameter, d_p is the aligned particle diameter, and a is the diameter of the cylindrical areas include zones 1 and 2 before the level of collision.

The cross section of the cylindrical region in diameter a is $S_0 = \pi a^2/4$ and at the level of collision $S_b = \pi(d_b+d_p)^2/4$. Produced for the effectiveness of conflict $E = \frac{S_0}{S_b} = \left(\frac{a}{d_b + d_p}\right)^2$. The parameter E is a ratio from the section of the straight part of the area, including zones 1 and 2 to section at the center of the bubble. Because the bubble vibrates with sound frequency f, then the mean diameter d_b is the same as without vibration. Performing a harmonic cycle of bubble volume maintains the transition from sphere to rotating ellipsoid. When the bubble diameter is $d_b = 4\,mm$ and amplitude $A = 0.7\,mm$ extremes on the vertical axis of the ellipsoid are $z_{\min} = 3.3\,mm$, $z_{\max} = 4.7\,mm$ with horizontal axes, respectively $x_{\max} = y_{\max} = 2.48\,mm$ and $x_{\min} = y_{\min} = 1.72\,mm$. Due to the high velocity of the bubble oscillation at a given frequency f parameter a on Figure 8 reaches the diameter of the bubble d_b.

6. Conclusions

Although the basic concept of flotation column looks relatively simple, but the fundamental principles related to performance of flotation column are quite complex. The type of the relative motion of particles and bubbles is a major factor governing the probability of

bubble/particle attachment, bubble loading, flotation rate and power requirement of the processes.

Experimental research led to the conclusion that vibrating media provided an additional force of resistance applied to the mineral particle, which provoke a decrease of the speed of descent. This force is a function not only of the intensity of the vibrations of a complex variable vibration, but also of the frequency of vibration.

The use of vibrations enables the diameter of gas bubbles to be adjusted in dependence of the influence of vibrations parameters leading to a better dispersing of the gas phase at the column flotation machine. The decrease of floating speed of the gas bubbles ensures increase of the time for mineralization and also the probability for collision with the particles of the solid phase. The vibration of the gas phase also enables mechanically entrapped particles to be released.

As a logical consequence follows that at vertical vibrations the air disperser can disperse sufficient air quantity for the flotation process realization. The gas flow velocity decrease combines with the higher effective product content in the concentrate compared with that in the initial product that could be explained by the specific vibratory influence on the three-phase system.

From the analytical study of the collision efficiency are confirmed experimentally proven facts. It provides possibility to increase the residence time of the bubble in the zone of contact with the mineral particles. The vibrations of the hydrated layer allow for cost-effective implementation of the elementary act of flotation by providing larger relative velocities at the contact point between the bubble and the solid phase.

References

1. **Bogdanov, O.** (1990). Theory and technology of flotation. Moscow, Nedra.

2. **Chernykh, S.I.** (1996), Radical improvement of the designs of flotation machines based on the theory of pulp aeration and mineralization of air bubbles, Nonferrous metals, No. 4, 66-68

3. **Dedelyanova K., J. Dimitrov.** (2013). Investigation on the effectiveness of air bubbles collision in vibratory column flotation machine. XXIII World mining congress, 11-15 August 2013, Montreal, Canada

4. **Dedelyanova K., Metodiev M.** (2003). Determination of the influence of vibrations on velocity emerge of gas bubbles, Procedings of X Balkan Mineral Pro-

cessing Congress, Varna, Bulgaria, 15-20 June, 2003 Mineral Processing in the 21st century, pp. 117-120

5. **Dedelyanova, Kr.** (2004). Vibro-acoustic investigations in column flotation machine with vibratory air disperser (Doctoral dissertation), University of Mining and Geology, Sofia, Bulgaria.

6. **Derjaguin, B. V., & Dukhin, S. S**. (1960). Transactions of the Institute of Mining and Metallurgy, 70(1), 221.

7. **Finch, J.A., Dobby, G.S.** (1990), Column flotation, Pergamon press Canada Ltd., 29

8. **Foot, D.G., Mc. Kay, D.J., Hniatt, J.L.** (1986). Column flotation of chromite and fluorite ores., Canad. Metall Quart, V.25, N 1, 15-21

9. **Metodiev, M., & Dedelyanova, Kr.** (2003). Air bubbles creation and behavior in a vibratory acoustic field, Annual of UMG, Sofia

10. **Pisarev, A. V., & Ivanenko, A. Yu.** (2009). Mathematical model of particle – bubble flotation complex motion in vibration flotation, Theoretical Foundations of Chemical Engineering, 43(3), 337–340.

11. **Ralston, J.** (1999). Controlled flotation processes: Prediction and manipulation of bubble particle capture. The Journal of The South African Institute of Mining and Metallurgy (pp. 27–34). Retrieved from http://www.saimm.co.za/Journal/v099n01p027.pdf

12. **Rubbinshtain, U.B.**, (1989). Froth separation and column flotation, Moscow, Nedra

MAGNETIC FIELD ON ASPHALT, RESIN, PARAFFIN AND SALT DEPOSITS

Makarenko V.D.
National University "Yuri Kondratyuk Poltava Polytechnic"
DCs (Engineering), Professor, professor of the Department of Oil and Gas Engineering and Technology, Ukraine

Manhura A.M.
National University "Yuri Kondratyuk Poltava Polytechnic"
Senior Lecturer, Department of Oil and Gas Engineering and Technology, Ukraine

Lartseva I.I.
National University "Yuri Kondratyuk Poltava Polytechnic"
PhD in Technical Sciences, associated professor, associated professor of the Department of Oil and Gas Engineering and Technology, Ukraine

Manhura S.I.
National University "Yuri Kondratyuk Poltava Polytechnic"
Senior Lecturer, Department of Oil and Gas Engineering and Technology, Ukraine

Absract. The references of studies about the magnetic field effect on prevention of asphalt, resin, and paraffin and salt deposits formation in the oil are described in the article.

The effect of constant magnetic fields on the well production is currently one of the most interesting, leading to an increase in the overhaul period of the well. At the same time, this method is debatable, sometimes leading to ambiguous and contradictory results. In many cases, the nature of such effect is not properly studied. Often, according to some researchers, effect is discovered, whereas its intensity, on the basis of physical considerations, is clearly inadequate for the production of any useful effect. This refers to the type of magnetic effects, that is based on the principle of protection consisting in a sharp increase in 1000-100000 times the number of paraffins crystals nucleus by the action of static magnetic fields of topology and tension in the natural trace units - rod-shaped mineral oxides / hydroxides of iron are water, oil and gas production in the flow of production wells.

Key words: development of oil fields, asphalt, paraffins, resins, sediments, asphaltene deposits, salt deposits, the magnetic field, the magnetic anti-paraffin device.

Introduction.

Asphalt, resin, and paraffin deposits (ARPD) are one of the most serious complications in downhole oil production. They increase the filtration resistance of oil-bearing layers, clog the pores in the rock, and their deposits reduce the useful section of tubing and pipelines, while not taking countermeasures until their complete blockage. Asphalt, resin, and paraffins (ARP) decrease greatly overhaul period of the well (sometimes to 1-2 days), increase coasts and decrease the oil production [1].

The production of high-paraffin crude oil also creates significant environmental problems because of ARP are serious polluters of the environment. The deposits typically consist of the paraffins, resins and asphaltenes, wherein the total content of these components, the composition of each, and their ratio to various fields varies widely. Mainly, the composition consists of the paraffins (from 5 to 70 %); asphaltene and resin content may reach to 20%, moreover, in larger quantities of oil the latter are present in smaller amounts in comparison with resins [1].

Considerable problems in oil production can be created by the deposits of inorganic salts on the walls of tubing and equipment. Such deposits often form a very dense and mechanically strong layers, which not only reduce the cross-section of pipelines, but may even lead to jamming of moving parts (eg. submersible pumps), and its failure. To prevent, reducing the growth ARP and inorganic salts deposits and their removing, different mechanical, physical and chemical methods are used. Moreover, chemical methods became the most widespread. Thus, according to [1], a variety of chemical compounds are currently being processed about 10% of the wells complicated by ARP [1]. However, the use of chemical methods of protection against ARP deposits and organic salts, substantially increases the cost of oil, and often exacerbates environmental problems. However, the use of chemical methods of protection against deposits of paraffin and organic salts, substantially increases the cost of oil, and often exacerbates environmental problems.

Recent publications analysis. As experience of two decades shows, to improve the productivity and efficiency of high-paraffin crude oil, as well as to deal with the ARP deposits and inorganic salts are used magnetic devices are of high effectiveness.

In recent years there was published a large number of monographs, reports, articles in which lay emphasis primarily on the practical usefulness of magnetic treatment. There were held numerous conferences and meetings on the practical application of magnetic treatment in a wide range of industrial productions. Number of publications and patents on this subject is currently is calculated in the thousands, and even tens of thousands. An important role in maintaining interest in this direction was played by professor V.I. Klassen and academicians B.V. Deriahin and V.I .Lesin.

Emphasizing of recurring parts of the general problems. The simplicity of the procedure, consisting in the fact that the flow of the fluid flows through the gap between the poles of a magnet or the solenoid powered electric current, stimulated experimental work on a wide range of objects. Therefore, in the following years, magnetic treatment was applied not only for aqueous salt solutions but also for oil, motor fuels, solutions of polymers, drilling muds and cement, plant seeds, blood, etc. By using magnetic treatment the salinization was eliminated even when irrigation water with high salt content prevents the deposition of minerals and organic substances in the production and transportation of oil and water, achieved a significant reduction in viscosity slurries, etc. Widespread use of magnetic treatment was found in medicine to improve the condition of blood vessels, cleaning the blood from toxic substances, lowering a blood pressure [2].

However, in the early years, it was noted that the effects are not always repeated even for externally similar objects and processes. The effect of the magnetic field strength of several hundred oersteds on insensitive to such fields non-ferromagnetic materials - water, oil, blood, animal tissues and plants surprised greatly. All this has led to the fact that with respect to the magnetic effect two opposite opinions were formed: first - quackery and the result of "dirty" experiment, the second - at the heart of magnetic treatment are still unknown in the physics the fundamental properties of the matter. The scientific community is divided into the enthusiasts who continue to investigate the effects of magnetic treatment and the skeptics who did not take seriously the regular reports of the successful use of magnetic treatment [3].

Problem definition. In recent years, interest in the use of magnetic fields for the treatment of drilling fluid in order to prevent the ARPD has increased significantly, due to the appearance on the market of a wide range of high-energy magnets of rare-earth materials.

Basic material and the results. The most widely used were the devices found on the basis of permanent magnets. Structurally, they are comprised of one, two, three pairs of permanent magnets arranged in the case. The liquid flows through the gap between the two poles of the magnets.

However, in practice the application of magnets for specific oil fields, there are numerous cases where the magnetic treatment of oil does not give positive results. Available setbacks to some degree discredited the technology of magnetic treatment in the eyes of oil-industry workers. In fact, the problem complicating a widespread use of magnetic treatment is the absence of theory explaining the nature of the processes, particularly the physical and chemical mechanisms of a magnetic field effect on the flow of oil. Because of this, the conditions under which the magnetic field prevents the formation of solid ARPD, until recently, remained unclear. Considering the experience of these installations operation must meet the following requirements [4]:

- geometrically fit into the design of deep-pumping unit and does not to create a large hydraulic resistance;
- to ensure consistently the treatment of production fluid by a magnetic field with intensity of 20 - 40 kA / m, for at least 2-3 years;
- magnets should be secured and protected from aggressive action of products.

We proposed an original method for multi-reverse fields using a chain of permanent magnets. Using the device of this type, you can get multi-reversal (with a small number of reverse) magnetic field with predominantly perpendicular direction to the of fluid flow lines, with high intensity and gradient [5].

Devices of this kind are easily implemented with magnets installed into pipelines 2 (Fig. 1) and magnetized in a predetermined sequence, alternating directions of magnetization. Thus there is no difficulty in increasing number of reverses field. According to this principle a lot of magnetized devices were made. However, its use

creates difficulties in a regions greater length obtaining with high-gradient fields.

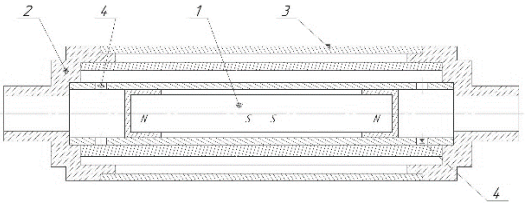

Fig. 1. MAPD construction:
1 – a chain of reverse unmagnetized permanent magnets;
2 – pipeline; *3* – outer casing; *4* – holes fluid input and output

Therefore, the regions of high-gradient fields usually constitute only a small part of the total channel length. Only in this small part of the length a fluids high magnetic treatment is carried out.

In this context, to improve the efficiency of magnetic devices and their mass and size characteristics, a special attention must be paid to the development of devices in which the areas of high-gradient magnetic field are placed inside of the unidirectional field.

Studies have shown that in passing water and in oil, even after their separation, always contain impurities of iron at a concentration of 10 to 500 g/t. These impurities are formed mainly with microcrystals of ferromagnetic oxides and hydroxides of iron in three crystalline forms, which are recorded in natural solutions of water and oil in the sediments. It was experimentally established the existence of ferromagnetic iron microcrystals formed by single microcrystals of a length 10-14 m.

It is experimentally established is the fact of aggregates disintegration of particles on individual particles under the influence of a magnetic field. These particles are additional centers of crystallization. In one tonne of oil total number of ferromagnetic microparticlesis in the range from 200 to 10 000 m^2, and the total surface area of one gram of particles is 20-40 m^2.

Microcrystalline ferromagnetic particles effect by electric charges, so that at their surfaces are adsorbed paraffins molecules, resins and asphaltenes which contained in the oil and which contain polar interclasts. In addition, due to the presence of water and heteroatomic impurities in the oil, water, gas mixtures such particles may exhibit

hydrophobic - hydrophilic properties, in conjunction with high surface curvature of such particles reduces the energy consumption for the formation of these bubbles of gas phase and thus contributes to the absorption as cores of micelles in paraffin molecules. The experience proved complete absence or minor effect by using distilled water, which also confirms the validity of the proposed mechanism of magnetic influence [1, 2].

In addition, there are also data on the efficiency of magnetic treatment of water and oil, which is extracted to improve and reduce ARPD. According to the research and industrial use, in most cases it was possible to completely prevent ARPD for the period of about one year, and in some cases it was possible to achieve prolongation of the well cleaning interval from 1-2 days to 10-20 months. Growth of the injection capacity of layers ranged from 30 to 100%.

There is a number of other useful effects (growth completeness oil displacement, increasing the waterless displacement, and etc.) that increase the productivity of oil. It can be assumed that the role of magnetic device for treatment of oil, water or oil system is to create more centers of crystallization. When oil refining by the magnetic field due to the formation of additional centers of crystallization, paraffin crystals do not grow on the walls of the equipment and the amount of oil that leads to the decrease of ARPD growth.

The magnetic anti-paraffin device has been developed (MAPD) with internal placement of magnets inside the pipe and with a consistently placed permanently magnetized magnets chain, alternating the directions of magnetization. In the proposed design, each of these magnets pairs placed around the axis of the pipe at 180° along the length of the channel's relatively to previous so that each side of the pipe polarity facing her pole magnets, taking turns produce a multireverse magnetic field with any necessary length of the interaction and any areas with a total length high-gradient field.

It is necessary to mention that, despite the high visibility and credibility of the proposed explanation of mechanism for preventing and reducing ARPD, and it is difficult to obtain the necessary practical conclusions on the magnetic parameters of corresponding magnetic devices [3-6].

It should be noted that the use of magnetic treatment of liquids in oil extraction, even in spite of the multiplicity of its objectives, and

achieved technical effects, does not use up the areas of its application.

MAD utilization increases between refining (overhaul) period of wells by direct magnetic field action. MAD mechanism is pointed at the subject of liquid viscosity change, that flows through the device (Fig. 2).

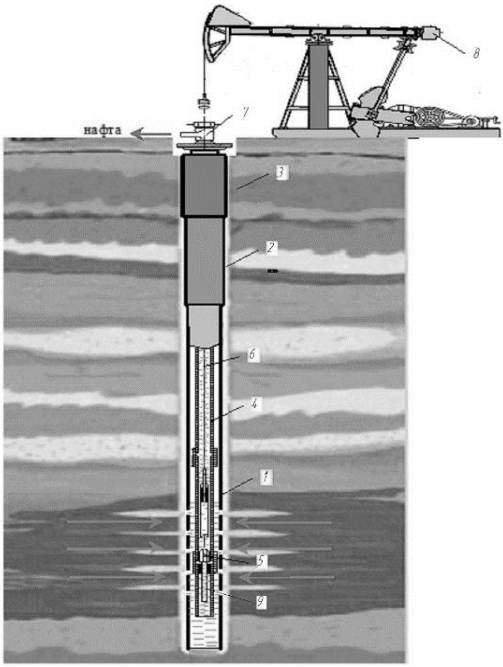

Fig. 2. MAD operational procedure in the well: *1* - capital string; *2* - intermediate string; *3* - surface casing; *4* - tubing; *5* - well pump; *6* - pump rod; *7* - tee; *8* - pumpjack; *9* - MAD

In MAD each of these pairs (blocks) magnets is rotated around the axis of the tube by 180° along of the channel's length in relation to previous so that each side of the pipe, polarity facing her pole magnets, alternating, create multi reverse magnetic field of any desired length of interaction region and with any total length of the sites with high gradient field.

The chain of cylindrical permanent magnets that is fixed in the conduit has reversible axial magnetization, created so that outer poles

have the same polarity and opposite polarity is formed in the middle of its length that makes it possible to receive multi reverse magnetic field mostly perpendicular to the direction of fluid flow lines with high intensity and gradient.

Results of MAD COMSOL Multiphysics software modeling

a - The distribution of the magnetic induction in the MAD:

Magnetic induction is a vector physical value, the main characteristics of the magnetic field strength and direction. Magnetic induction vector is usually denoted by Latin letter B. In the CGS system the magnetic induction field is measured in gauss (Gs) in the SI-system - in Tesla (T).

The distribution of magnetic induction can be observed in Fig. 3 and 4.

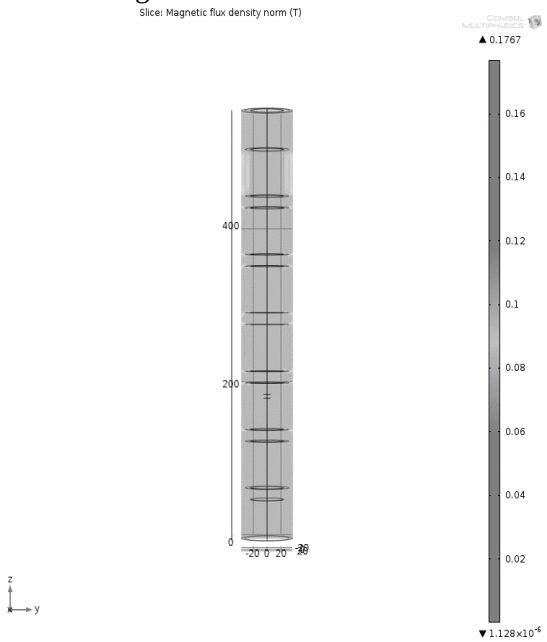

Fig. 3. The distribution of magnetic induction in the MAD

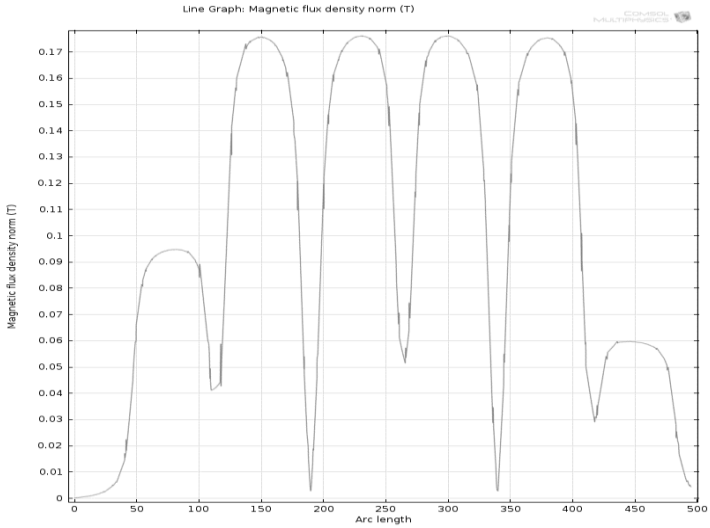

Fig. 4. The graph of magnetic induction distribution on the length of MAD

As a result of obtained values, we can see that while the maximum residual magnetic induction of 150 mT, which we pre-assigned in the initial terms in Figs 2 and 3, the maximum value after calculation is 187,5 mT. This change can be easily explained by the fact that the pipe is made of steel, which is ferromagnetic, i.e. the magnetic field strength increases, so we observe the pipe magnetization process.

When building a computer model of MAD, six blocks of axially magnetized permanent magnets were formed. The distance between them was 15 mm. The first pair of blocks has a magnetic induction of 50 mT and 150, respectively. The next pair was magnetized to the same values of 150 mT and was returned at 180° in relation to the previous block so that the second block of the first pair and the first block of the second pair were rotated to each pole of the same pole. The latter, the third pair of blocks was also returned at 180° relative to the previous and the first block of third couple had a magnetic induction of 150 mT, the second - 80 mT.

b - The distribution of the magnetic field in the MAD

The magnetic field strength is a vector characteristic that determines the magnitude and direction of the magnetic field at present point and present sample time.

It is usually denoted by Latin letter H, measured in Oersted in the CGS electromagnetic system and ampere-turns per meter ($A \cdot V/m$) in the SI system [7].

The distribution of the magnetic field depicted in Fig. 4 and 5.

After obtained results we can see that the concentration of magnetic field strength is observed at the end points of the magnets. On the graph is clearly observed a significant potential drop in the range of 190 and 340 mm due to the fact that the given points a pair of magnets rotated to each other with the same poles, i.e. there is some «compensation» of the magnetic field.

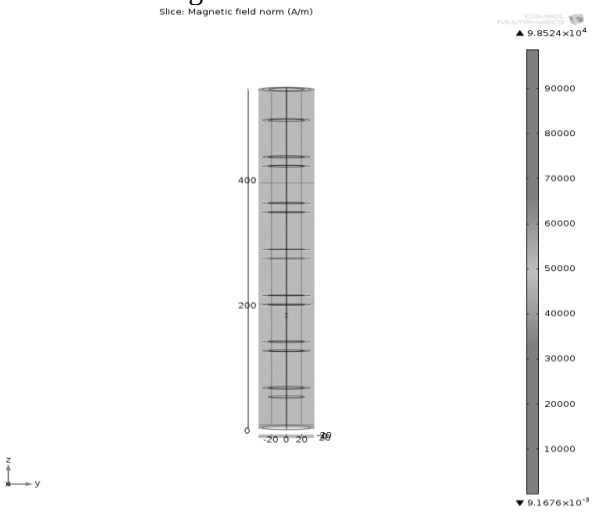

Fig. 5. The distribution of the magnetic field in the MAD

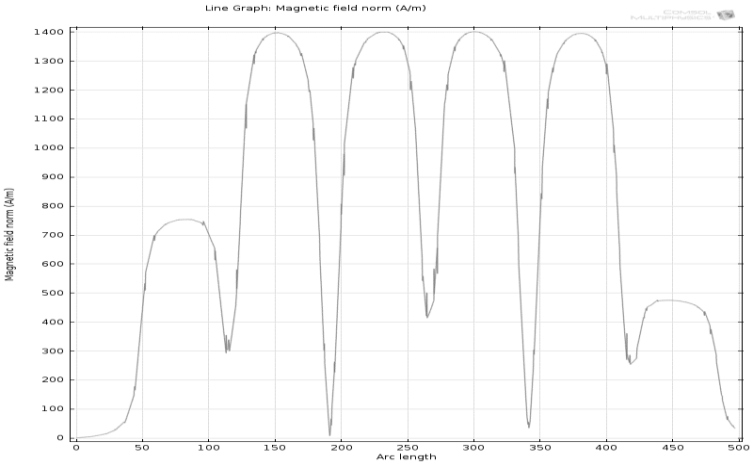

Fig. 6. Graph of the magnetic field distribution along the length of installation

c - Distribution of the scalar potential in the MAD

Vector field scalar potential A (often a potential vector field) - is a scalar function such that at all points of the domain of the field $A=\text{grad}\phi$ where $\text{grad}\phi$ denotes the gradient. In physics, potential is a magnitude, converse (force potential, power potential of the electric field).

Distribution of the scalar potential in the MAD is depicted in Fig. 7.

The maximum and minimum values of the scalar potential are observed in places where the magnetic blocks converge rotated to each other with the same poles [7].

d - Influence of MAD on mechanical impurities

Magnetic treatment of fluids long and widely used also to improve corrosion resistance of pipes and boiler equipment in water and heat to improve crop yield in agriculture irrigation systems for desalination of soil in irrigation systems to improve the effectiveness of drugs and medical procedures, and for many other purposes.

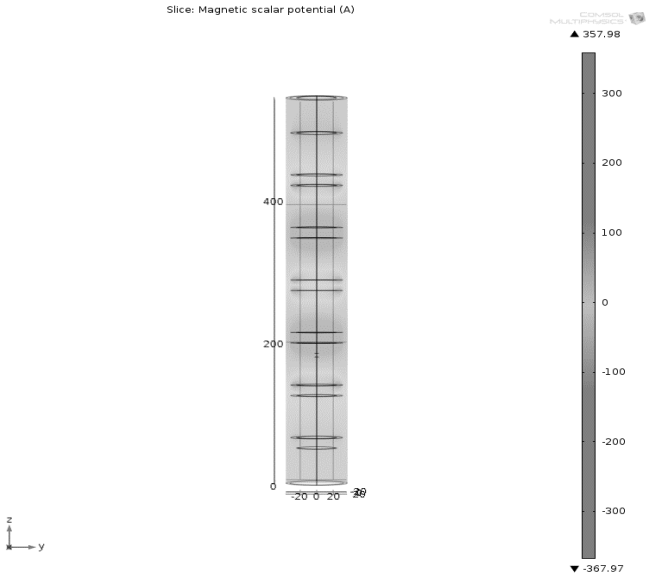

Fig. 7. Distribution of the scalar potential in the MAP

The presence of impurities in the flow of oil fosters formation of ARPD crystallization centers, so if you remove these elements from the stream, the rate of sediments formation will significantly reduce. In Figure 8 is depicted how the MAD effects on mechanical impurities. In the process of modeling into the liquid flow was put a piece of cylindrical metal in radius and height of 5 mm. Usually, these particle sizes in the oil are extremely rare, but for the visualization of magnetic field influence such simplification will to be appropriate.

As can be seen, the magnetic field affects the mechanical impurity that is evidenced by the line flow. Thus there is a definite change in the magnetic field around the metal impurities. This is the process of agglomeration and removal of fluid flow particles can serve to the formation of ARPD.

In Fig. 9, one can observe the patterns of magnetic field lines distribution. It should be noted that the magnetic field passes through the oil and has impact on the entire internal environment.

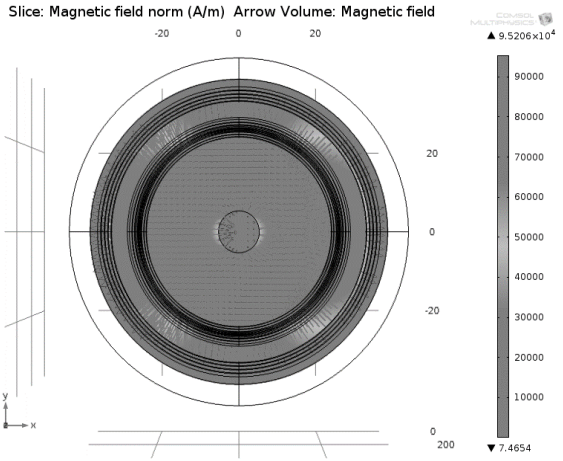

Fig. 8. Influence of magnetic field on mechanical impurities

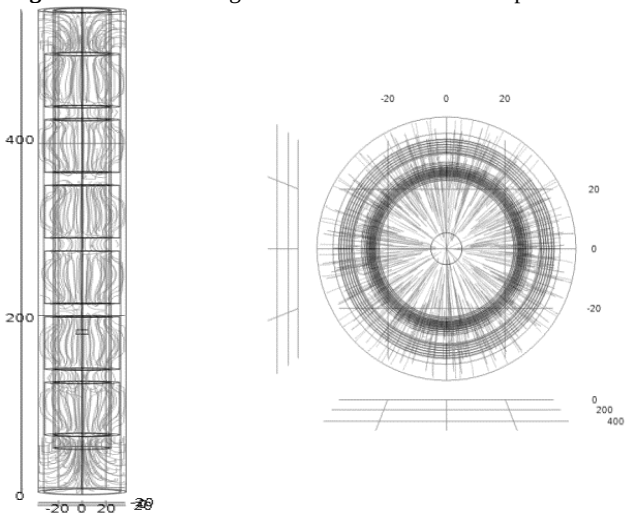

Fig. 9. Lines of the magnetic field

e - Graphs, showing the patterns of magnetic fields distribution

For better clarity, in Fig. 9 and 10 the magnetic field lines and the 3D model of the distribution of magnetic induction are exemplified.

Different color intensity of the first and sixth magnets caused by the fact that they have a magnetic induction of 50 mT and 80, respectively, and all the latest 150 mT. Also, on the border between 2-3 and 4-5 there is a significant drop in magnetic induction, due to the fact that these magnets are rotated to each other with the same poles.

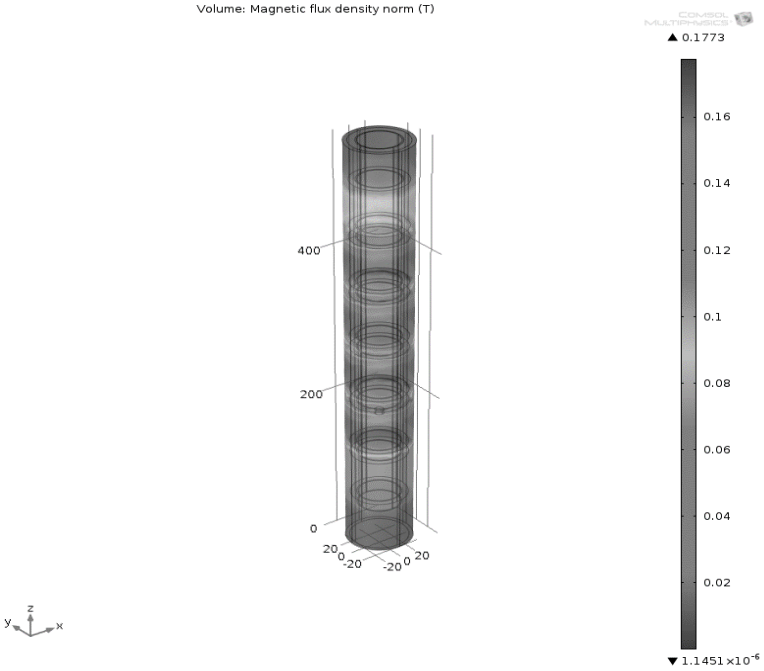

Fig. 10. 3D model of magnetic induction distribution

It is not clear, however, about the optimal parameters of the field that are needed to separate aggregates of microcrystals. It can be also assumed that at sufficiently high content of ferromagnetic microcrystal aggregates of iron in water oil system it may be quite sufficient the creation of necessary fields only in a limited part of the magnetic devices channel or magnetic treatment of oil. This helps to explain the practical effectiveness for devices with high performance magnetic fields only in small parts of the cross section of their working channel. Therefore, it should be emphasized that the presence of ferromagnetic particles is regarded as experimentally established fact.

This lists the application of magnetic treatment now can be considered as a well-established and traditional, with a wealth of accumulated experience in the development and operation of the relevant magnetic devices.

However, in recent years it began to appear a lot of new, innovative applications of magnetic treatment. These include, for example, increasingly spreading practice of using magnetic devices for natural gas and fuel for internal combustion engines. It is considered that the magnetic fuel treatment improves the completeness of its combustion, reduces costs, and simultaneously improves the sustainability of such engines. The new, innovative applications refer the usage of magnetic treatment for disinfection of water and other liquids, as well as for preserving food [7].

It is still difficult to apply some of the above hypotheses about the mechanisms of magnetic effect.

Conclusion. Thus, the application practicability and prospectivity of magnetic treatment is confirmed by the positive experience of its use and spreading in the various regions, not only in Ukraine but also abroad.

The description of magnetic devices modeling, ranging from theoretical concepts to the formulas used in the calculation, are exemplified in the work.

The theoretical and laboratory studies have allowed us to use the results of MAD on wells of highly paraffinic crude oil.

The modeling process of constant magnetic field on the fluid that moves through tubing, especially by the distribution of magnetic fields in the environment, has been held.

In the process of modeling various reservoir fluid properties have been used, as they affect the environment and the permeability and change the intensity distribution of the magnetic field characteristics in the flow of liquid.

The illustrative modeling results allow observing the work of the magnetic anti-paraffin waxes device.

References

1**. Chow, R., Sawatzky, R., Henry, D., Babchin, A., Wang, Y., Cherney, L., & Humphreys, R.** (2000). Precipitation of Wax From Crude Oil Under the Influence of a Magnetic Field. Journal of Canadian Petroleum Technology, 39(06).

2. **Gavriluk O.V., Glazkov O.V.** (2001) The application of magnetic liquide treatment in oil fields of West Siberia. IOR - 11th European Symposium on Improved Oil Recovery 19-25

3. **Ivakhnenko, O.P.,** (2006) Magnetic analysis of petroleum reservoir fluids, matrix mineral assemblages and fluid-rock interactions. Thesis, Institute of Petroleum Engineering, Edinburgh, UK, 210 pp.

4. **Klassen V.** (1982). Omagnichevanie vodnykh sistem. Khimiya, 1982.

5. **Kharchenko M., Manhura A., Manhura S., Lartseva I.** (2017) Analysis of magnetic treatment of production fluid with high content of asphalt-resin-paraffin deposits. Journal Mining of Mineral Deposits. Volume 11, Issue 2, pp. 28-33

6. **Suzuki, Hirofumi., Kodera, Sunao, Matsunaga, Hiroyuki, Kurobe, Toshiji** (1993) Study on magnetic field-assisted polishing (2nd Report) - effect of magnetic field distribution on removal distribution. Journal of the Japan Society for Precision Engineering. Nov; 59(11): 1833–1838

7. **Swapan Kumar** Das (2008) Electro Magnetic Heating in Viscous Oil Reservoir International Thermal Operations and Heavy Oil Symposium, 20-23 October, Calgary, Alberta, Canada

8. **Tung, N., Vuong, N., Bui Quang, K., Vinh, N., Hung, P., Hue, V., & Hoe, L.** (2001). Studying the Mechanism of Magnetic Field Influence on Wax Crude Oil Viscosity and Wax Deposition Reductions. Proceedings of SPE Asia Pacific Oil and Gas Conference and Exhibition.

9. **Wang L.J., Wang W., (**2014) Wax Depositing Mechanism and Prediction Methods of Wax Removal Cycle ", Applied Mechanics and Materials, Vols. 675-677, pp. 1512-1516

10. **Zhang, W.W., Wang, T.T., Li, X., & Zhang, S.C**. (2013). The Effect of Magnetic Field on the Deposition of Wax on the Oil Pipe. Advanced Materials Research, 788, 719-722.

11. **Zhang, W.W., Wang, D.D., Wang, T.T., & Zhang, S.C.** (2015). Study on the Mechanism of Magnetic Wax Control of Crude Oil Based on the Reorientation of Wax Crystals Induced by Magnetic Field. Applied Mechanics and Materials, 743, 137-141.

THE PROBLEM OF BEDS STABILITY IN THE CONDITIONS OF UNDERMINING HIGHER DEPOSITED BEDS IN THE CONTEXT OF SELECTED ANALYTICAL SOLUTIONS

Krzysztof TOMICZEK[1]

Ph.D. Eng. Krzysztof Tomiczek, Department of Geomechanics and Underground Building, Faculty of Mining, Safety Engineering and Industrial Automation, Silesian University of Technology, Gliwice, Poland

Summary. Underground mining of useful mineral deposits causes changes in the virgin rock mass stress state and may affects on rock masses and mining excavations damages. The result of exploitation may be tremors and rockbursts. Most often, in the case of deposits (of coal) exploitation, the higher lying beds are mined first. Sometimes, it is necessary to mining the lower lying bed first and undermining the upper bed. The clue is not to damage the undermined bed, and the damage raiser the distance between both beds is.

Keywords: rock mass stability, undermining, submining, rock damage, rock cracking, safety distance between mined beds

1. Introduction

Exploitation of on-bed deposits is associated with a number of problems related to technological and economic requirements as well as work safety in mines. One of the factors is the sequence of individual beds are mined.

The commonly used method of mining from shallow to deepest beds is profitable from the point of view of utilization the deposits. Under some conditions the sequence is not possible to use. In the event of a rockburst hazard, it is necessary to carry out rock burst prevention, which most often requires conducting stress relief exploitation of rockburst beds.

Under market economy conditions, economic criteria drive mines to select the deposits to be mined. The produced coal must correspond to specific, usually high quality requirements while maintaining the cheapest possible mining costs. That is why information

[1]Krzysztof.Tomiczek@polsl.pl , k.tomiczek@yahoo.co.uk
https://orcid.org/0000-0001-9227-310X Researchgate profile: Krzysztof_Tomiczek

about the impact of an already operated bed on the higher lying beds has fundamental importance. Information allows selection and sequence of mining bed.

Of the many cases of undermining coal beds, they are most often associated with ongoing anti-rockburst prevention.

Analytical methods for determining influence of undermining based on the past experience and theoretical solutions.

Extensive research material related to the problem of undermining coal beds was collected by Staroń (1975, 1979).

For the purposes of the analysis, Staroń distinguished three groups of mining impact of the mining lower bed lying on the upper bed.

Staroń qualified to the *first group* of cases for which no clear effects of undermining were found in the uplying bed during its exploitation, and assumed that the uplying bed did not have any influence from earlier exploitation.

The *second group* included the cases in which there were clear influences in the form of folding the bed floor and its cracking, but these changes did not cause significant difficulties in the mining of the bed earlier subjected to exploitation. The intensity of impact in the undermined beds included in this group were defined as the average influence.

The *third group* included those cases in which there were significant influences in the form of folding the bed floor and/or its cracking, which caused great difficulties in the mining of the undermined bed. The intensity of impact of the undermined beds in this group was defined as strong influence.

Data from the observations analysed by Staroń included over 60 cases of undermining of beds that were upper in deposits under the roof caving operation, distinguishing the scale of the observed characteristic undermining effects.

The discussed data cited by Staroń showed that when the distance between the mined and undermined beds was less than five times the thickness of the mined bed, strong influences were observed in the undermined bed.

In the case where the distance between the mined and undermined beds was between five and seven times the thickness of the mined beds, medium or no negative influences were observed in the under-

mined beds. If the distance between the mined and undermined beds was greater than seven times the thickness of the mined bed, no negative influences were observed in the undermined beds.

The research material discussed above indicates that the intensity of influence in the undermined bed is significantly influenced by the type and properties of rocks lying between the mined and undermined beds, the depth deposition of the bed and the distance between the beds.

The problem of determining the range and size of influence zone when undermining coal bed has been the subject of interest for researchers and engineers for many years. Due to the complexity of nature of the rock mass deformation process in the immediate vicinity of the mining exploitation, the hypotheses were based mainly on observations carried out in hard coal mines and were related to geometric quantities, such as thickness of the mined bed and distance between the mined and undermined bed. Attempts were also made to connect them with the strength properties of rocks lying between the beds and the depth deposition of the beds. The most important formulas for determining size and range of damage influences of undermining can be divided into the following groups:

- *group* I. - containing formulas for the required distance between mined and undermined beds as a function of the thickness of the mined bed,
- *group* II. - containing formulas for the required distance between mined and undermined beds as a function of mined bed thickness and rock loosening coefficient,
- *group* III. - containing formulas for height of the zone of the damage effects of exploitation of the undermined bed as a function of thickness of the mined bed, depth deposition of the beds and rock strength,
- *group* IV - containing formulas for determining the occurrence probability for damage effects of bed undermined bed.

Group I. including formulas for the required distance between mined and undermined beds M as a function of mined bed thickness g, includes solutions of:

- Czechowicz - the required safety distance between mined and undermined bed is:

$$M = 12g$$

where

g - thickness of the mined bed.

- Davidianz - the required safety distance between mined and undermined beds is:

$$M = 20g$$

- Dziunikowski, Rzempiel et al. - the required distance between mined and undermined beds is

$M = 8g$ for a regression factor of 0.144

$M = 12g$ for a regression factor of 0.229

- Kiliashkov – the required distance between mined and undermined beds

$$M = 12g + 3{,}5g^2$$

- Krupiński, Czechowicz et al. - the required distance between mined and undermined beds

$M = 12g$ for $g \leq 1.5$m

$M = 8g$ for $g > 1.5$m

The II. group including the formulas for the required distance between the mined and undermined beds M as a function of undermined bed thickness g and loosening coefficient k_r, includes, among others, work of:

- Chudek and Olaszowski - the required distance M between mined and undermined beds

$$M = \frac{g}{k_r - 1} \cdot \frac{1}{1 - \eta_1}$$

where

$$\eta_1 = \frac{k_r - k_r'}{k_r - 1}$$

k_r - rock loosening coefficient,

k'_r - loosening coefficient of the rocks after pressing the rocks in the caving zone,

g - mined bed thickness.

- Makeyev Research Institute - the required distance between mined and undermined beds

$$M = \frac{3g^2}{k_r - 1}$$

- Kuznetsov - the required distance between mined and undermined beds

$$M = \frac{(3+1{,}5g)g}{k_r - 1}$$

- Staroń - the required distance between mined and undermined beds

$$M = g\left[\eta_1 + \frac{4}{\pi(k_r - 1)}\right]$$

The III. group including the formulas for the required distance *M* between the mined and undermined beds as a function of thickness of the mined bed *g*, the deposition depth *H* and the tensile strength of rocks R_{rs} can include, among others Chudek's formula. Intensity of harmful effects of undermining is calculated from the formula:

$$M = 3{,}5g\sqrt{\frac{p_z}{R_{rs}}}$$

where

g - mined bed thickness,

p_z - vertical primeval stress,

R_{rs} - average tensile strength of rock (layers) lying between mined and undermined beds.

The IV. group including the formulas for determining the occurrence probability of undermining influences may include, among others, formulas of:

- Budryk and Bes - the probability of strong influence *p* is calculated as

$$p = 100\exp(-0{,}092\frac{M_H}{g})$$

and the probability of medium and strong influence *p*

$$p = 100\exp(-0{,}046\frac{M_H}{g})$$

where

M_H - distance between mined and undermined beds,

g - mined bed thickness;

- Staroń - the probability of loosening, the undermined bed (strong and medium influence *p*)

$$p = 100 \exp(-0{,}065 \frac{M_H}{g})$$

A large number of analytical solutions raises doubts, when choosing one of them to be used in a particular case. Before choosing a solution, it is important to know how they are related to observation in practice.

Comparison of cited analytical solutions with observations in mines can be made for individual groups. Comparing the results of calculations obtained on the basis of the formulas of group I, it can be stated that the largest required distances between the mined and undermined beds are obtained from the Davidianz's and Kiliashkov's formulas. These formulas show that the required distance between the mined and undermined bed is about 20 times the thickness of the mined bed; the smallest distances - Dziunikowski and Krupiński - 8 times the thickness of the mined bed.

Based on the observations in the coal mines, it can be stated that the calculations based on the formulas of the discussed first group give in an overwhelming majority of cases the results outnumbered. Studies show that if the distance between the mined and undermined beds is greater than seven times the mined bed thickness, no significant damage effects were found in the undermined beds (see Staroń, 1975).

Such a relatively small accuracy of matching the results of calculations carried out using the formulas for mine observations results, due to, among others, limiting only to geometrical factors (e.g. distance between beds, mined bed thickness) and omitting the geological structure of the rock mass, strength and deformation of rock properties.

Formulas of the second group have been expanded and in addition to only geometric factors, e.g. distance between the beds, mined bed thickness, they take into account the properties of rocks surrounding the beds by introducing so-called rock loosening coefficient.

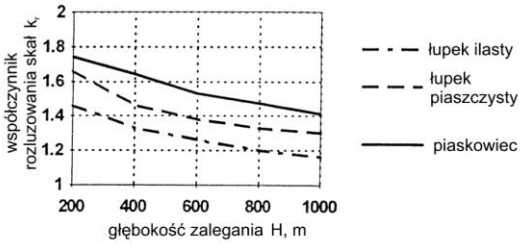

Fig. 2.1. Relationship between the rock loosening coefficient k_r (vertical axis) and the depth deposition H (horizontal axis) for different types of rocks; – · – · - shale, – – – - sand shale, —— - sandstone

Using the rock loosening coefficient, both the deposition depth of the beds and the type of rock surrounding the analysed beds, can be taken into account in a simplified way. On the basis of laboratory tests, the values of rock loosening coefficient has been determined for individual rock types for specific depths.

Figure 2.1 presents the variability of the rock loosening coefficient k_r depending on the depth of bed depth deposition H for three types of rocks: shale, arenaceous shale and sandstone.

The figure 2.1. indicates the highest value of the rock loosening coefficient k_r was obtained for shale, and the lowest - for sandstone. It means that if the roof layers are more difficult to cave in, then the rock volume increases strongly, and effect visibly increasing their loosening coefficient.

The second characteristic feature is the downward trend of the rock loosening coefficient k_r as the depth H increases. For depth H from 200 m to 1000 m, the rock loosening coefficient k_r takes values as follows:

- for shale 1.17-1.45,
- for arenaceous shale 1.30-1.65,
- for sandstones 1.40-1.75.

The loosening coefficient k_r of rocks significantly influences on the amount of required distance between the mined and undermined beds at which the undermined bed will not be damaged.

Figure 2.2 shows influence of the rock loosening coefficient k_r on the required distance between the mined and undermined beds.

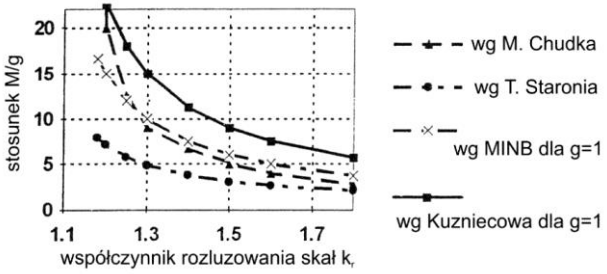

Fig. 2.2. The relationship between the rock loosening coefficient k_r (horizontal axis) and the ratio of the safe distance M between the beds and the thickness of the mined bed g (vertical axis); ▲- after Chudek, ● - after Staroń, x - after Makeyev Institute of Science and Research, ■ - after Kuznetsov

The characteristics presented in the figure, drawn on the basis of calculations carried out according to the formulas of Chudek, Staroń, Makeyev Institute of Science and Research and Kuznetsov, are of similar shape, however, the values of the required distance between the mined and undermined beds M are different, expressed as times the thickness of the mined beds M/g.

The graph shows that the smallest required distances M between the mined and undermined beds result from the formula given by Staroń, and the largest - from the Kuznetsov's formula. The results of calculations carried out according to the formulas of Chudek and Makeyev Institute of Science and Research are similar.

In order to compare the results of calculations carried out according to the formulas of the second group, Chudek's and Staroń's formulas were chosen.

Figure 2.3 shows the relationship between the thickness of the undermined bed m and the ratio of the safe distance M between the beds and the thickness of the mined bed g for different values of rock loosening coefficient k_r.

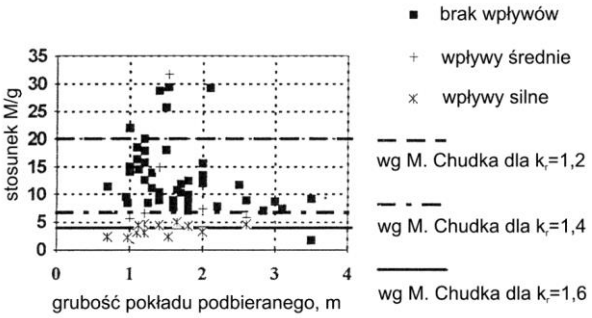

Fig. 2.3. The relationship between the thickness of the undermined bed *m* and the ratio of the safe distance between the beds *M* and the thickness of the mined bed *g* (vertical axis) for different values of rock loosening coefficient k_r (horizontal axis) according to Chudek; k_r=1.2, 1.4 and 1.6, ■ - no influence, + - medium influence, * - strong influence

It turns out that for the value of rock loosening coefficient k_r from 1.2 to 1.6 there is a large increase in the required distance between the mined and undermined bed *M*, e.g. for the loosening coefficient k_r equal 1.2, the required distance between the mined and undermined bed *M* is equal to 20 times the thickness of the mined bed, while for a coefficient k_r=1.6 the required distance is about four and a half times the thickness of the mined bed.

These results differ from those obtained on the basis of the formula given by Staroń (Fig. 2.4).

According to Staroń, for the rock loosening coefficient k_r=1.2, the required distance between the mined and undermined beds is equal to about seven times the thickness of the mined decks. For the rock loosening coefficient k_r=1.6, the required distance between the mined and undermined beds is approximately 3 times the mined bed thickness.

The presented analysis of formulas included in the second group shows that the required distance *M* between the mined and undermined beds determined on the basis of the Staroń's formula is definitely smaller than the calculated *M* values with all other formulas.

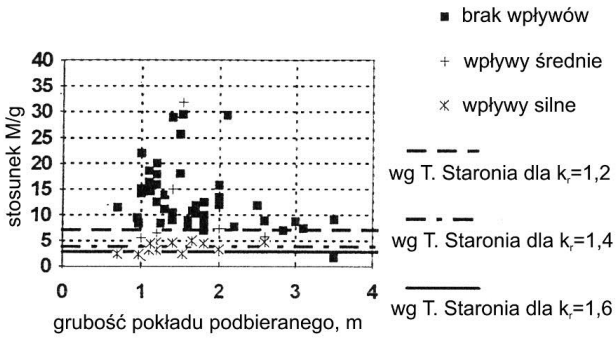

Fig. 2.4. The relationship between the thickness of the undermined bed *m* and the ratio of the safe distance *M* between the beds and the thickness of the mined bed *g* for different values of rock loosening coefficient k_r according to Staroń (k_r=1.2, 1.4 and 1.6); ■ - no influence, + - medium influence, * - strong influence

It should be assumed that for conditions of the Carboniferous rock mass with properties such as in the Upper Silesian Coal Basin, it will be most advantageous to determine the required distance *M* between the mined and undermined beds based on the formula developed by Chudek and Olaszowski.

Group III. includes the formula given by Chudek for determining the amount of damage impacts from mining during undermining.

The formula, the range of damage effects of mining on undermining depends on the thickness of the exploited bed, the depth of deposition expressed in the form of the primeval vertical stress in the virgin rock mass and on the average tensile strength of the rocks lying between the mined and undermined beds.

Figure 2.5 shows the relationship between the range of damage mining impacts *M*/*g* on undermining to the ratio of vertical primary stress in the virgin rock mass to the average tensile strength of the rocks lying between the mined and undermined beds p_z/R_{rs}.

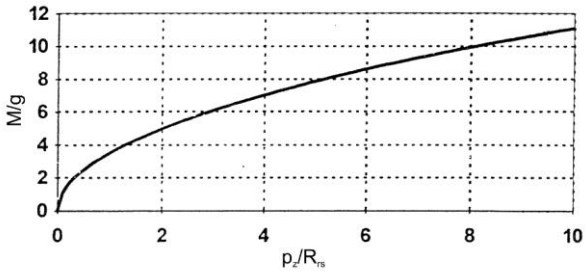

Fig. 2.5. The relationship between the ratio of the vertical component of the primary stress p_z and the tensile strength R_{rs} and the ratio of the safe distance M between the beds and the thickness of the undermined bed g

With the increase of the ratio of primeval stress p_z to the average tensile strength R_{rs}, the range of harmful effects of operation during picking up increases. It should be assumed that as the depth H increases, it is expected that the range of damage effects of undermining exploitation increases.

The IV. group includes formulas for determining the occurrences probability of undermining influences. Medium and strong influences were distinguished in the group. However, the criteria for qualifying specific consequences of undermining for strong or medium influences were not clearly defined.

Figure 2.6 compares the occurrence probability of undermining damage effects determined according to the formulas of Budryk and Staroń. The probability of strong damage influences as well as medium and strong influences is determined on the basis of Budryk and Bes's formulas. The probability of strong and medium influences is determined on the basis of Staroń's formula.

Comparing relevant characteristics, it can be stated that the probability values determined on the basis of the Budryk and Bes formula are higher than the probability values obtained on the basis of the Staroń's formula.

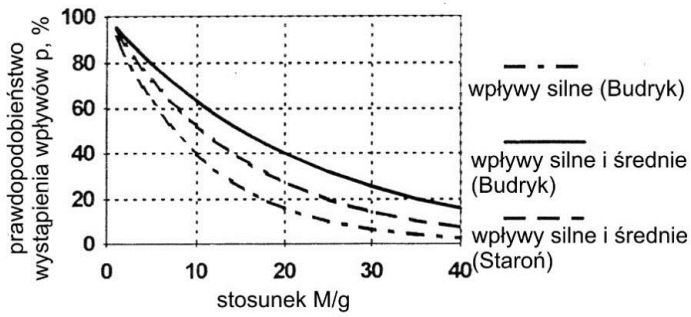

Fig. 2.6. The relationship between the ratio of the safe distance *M* between the beds and the thickness of the pick-up deck *g* and the probability of influences *p* according to Budryk and Staroń; -·-·-– strong influence (Budryk), —— - medium and strength influence, ---- medium and strength influence

3. Examples of calculations

3.1. Influence of undermining a 40I/D bed by mining the 41J bed

For the calculation of the influence of undermining the 41J bed by longwall 7-2 on the 40I/D bed, the following constant values were determined:

- bed 41I longwall 7-2,
- mining depth H=815÷850 m,
- bed thickness g_w=1.5÷2.2 m,
- height of the mining face g=2.2m,
- rock loosening coefficient k_r=1.23 (for clay and sandy shales after Fig. 2.2),
- the smallest assumed distance between the mined and undermined bed M_H=20 m.

Received results:

- required distance between mined and undermined beds:
  according to Chudek - Olaszowski (Fig. 2.1) M=15 m,
  according to Staroń (Fig. 2.2) M=13m,
  according to Staroń (Fig. 2.1) for k_r=1.23, ratio M/g=6.45, and M=14.2 m;
- probability of loosening the undermined bed:
  according to Budryk and Bes (strong influences) p=43%,

according to Budryk and Bes (medium and strong influences) p=66%,

according to Staroń (medium and strong influences) p=55%.

Analysis of results

I. The calculated values of the required minimum distance between 41J and 40I/D beds are smaller than the actual distance between both beds.

II. Comparing the obtained values with the data from observations carried out in Polish coal mines, it turns out that strong influences occurred when:

- the distance between the mined and undermined beds was less than five times the thickness of the mined bed,
- the probability of strong influences using the Budryk method was 65% higher,
- the probability of occurrence of strong and medium influences according to Budryk is equal to- or greater than 80%,
- probability of strong and medium influences according to Staroń is greater than 70%.

The distance between mined and undermined beds is much greater than 5 times the thickness of the mined bed (5g=11 m (12.5 m)), e.g. for B15E/1983, the distance between the 40I/D and 40I/C beds is about 36.4 m), and the obtained probability of influences p values are less than *borderline*. Therefore, strong influences should not be expected.

Average influences observed in coal mines appeared if the distance between the mined and undermined beds was in the range of 5÷7 times the thickness of the undermined bed, when:

- the probability of strong influences according to Budryk is equal to 50% to 65%,
- probability of occurrence of medium and strong influences according to Budryk from 70% to 80%,
- probability of medium and strong influences according to Staroń from 60% to 70% (Fig. 3.1).

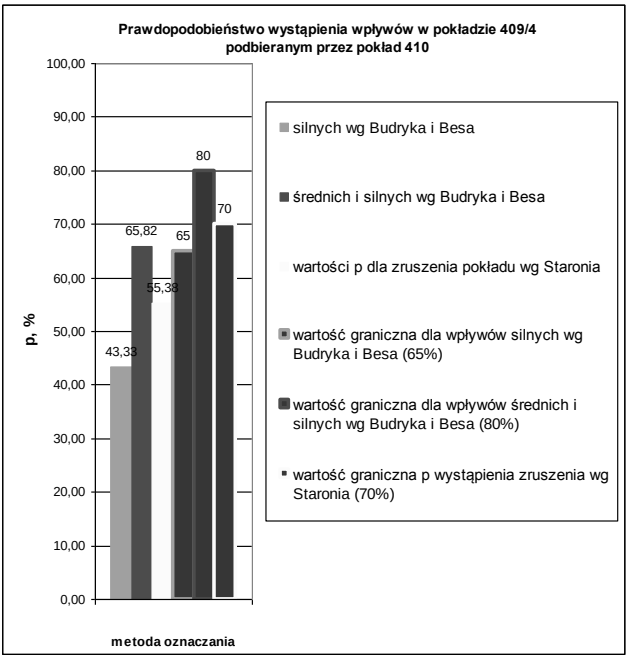

Fig. 3.1. The probability of influence *p* in the 40I/D bed undermined by 41J bed calculated by methods proposed by various authors (Budryk, Bes and Staroń); red (3 right bars) indicates the maximum "safe" p-values for the conditions in Polish coal mines and for the distance between the mined and undermined bed M_{minp} 5÷7

The obtained probability values of influences *p* are smaller than the *allowable* ones. Therefore, small, only locally medium influences are to be expected, which may cause slight folding of the bed floor and its cracking; these changes should not cause difficulties in the mining of the 40I/D bed.

3.2. Influence of undermining a 40I/C by mining the 2nd layer of 40I/D bed

For the calculation of the influence of the mining of the 41J bed with the G-B longwall on the 40I/D bed, the following fixed values were adopted:

- bed 40I/D lonwalls G-B, G-D, G-F, G-Fa,
- mining depth *H* (see Table 3.1),

- thickness of strata g_w,
- height of the longwall face g=3.0 m,
- loosening coefficient k_r=1.23 (for clay and sandy shales according to Fig. 2.2),
- smallest assumed distance between the mined and unmined beds M_H=18 m.

Tab. 3.1

Basic data on the mining of the 40I/D bed.

Bed	Longwall	Mining depth H, m		Longwall face height g, m		
		min	max	min	max	2nd layer (underfloor)
40I/D	G-B	775	835	3.80	5.00	3.00
	G-D	800	875	4.00	5.20	
	G-F	830	890	4.70	5.20	
	G-Fa	860	940	4.20	4.60	

Received results:

- required distance between mined 40I/D and undermined 40I/C beds:
- according to Chudek - Olaszowski (Fig. 2.1) M=20m,
- according to Staroń (Fig. 2.2) M=17.7m,
- according to Staroń (Fig. 2.1) for k_r=1.23, the ratio M/g=6.45, and M=19.35m;
- probability of loosening the undermined bed (Fig. 3.2):
- according to Budryk and Bes (strong influences) p=57.6%,
- according to Budryk and Bes (medium and strong influences) for the longwall probability p=75.9%,
- according to Staroń (medium and strong influences) p=67.7%.

Analysis of results

I. Based on exploratory borehole (e.g. B15E/1983), it was found that the distance between 40I/C and 41J/D beds ranges from about 18.0m to about 21.8m. Calculated values of the required minimum distance between 41J and 40I/D beds M is in the lower and middle parts of this range.

II. Comparing the obtained values with the data from observations carried out in Polish coal mines, it turns out that strong influences occurred when:

- the distance between the mined and undermined beds was less than five times the thickness of the mined bed,
- the probability of strong influences *p* using the Budryk method was 65% higher,
- the probability of occurrence of strong and medium influences *p* according to Budryk is equal to or greater than 80%,
- probability of strong and medium influences *p* according to Staroń is greater than 70%.

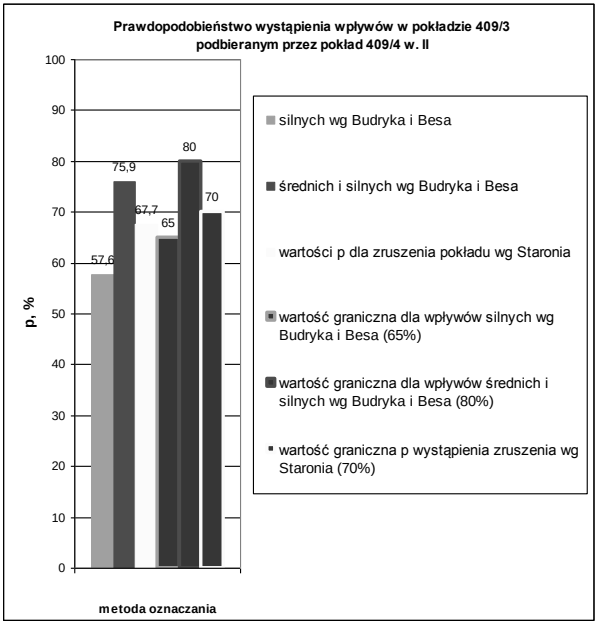

Fig. 3.2. Probability of occurrence of influences *p* in the 40I/C undermined bed by the 2nd layer of 40I/D bed calculated by methods proposed by various authors (Budryk, Bes and Staroń); red (3 bars on the right) indicates the maximum *safe p*-values for conditions in Polish mines and for the distance between the mined and undermined bed M_{minp} 5÷7

The distance between the mined and undermined beds is greater than 5 times the thickness of the mined bed (5*g*=15m), and the obtained probability *p* values are smaller than the *limit* values. Therefore, strong influences should not be expected.

Average influences observed in coal mines appeared if the distance between the mined and undermined beds was within the range of 5 to 7 times the thickness of the mined bed, when:

- the probability *p* of strong influences according to Budryk is equal to 50% to 65%,
- probability *p* of occurrence of medium and strong influences according to Budryk is 70% to 80%,
- probability *p* of medium and strong influences according to Staroń is from 60% to 70%.

The obtained probability values p belong to the central part of the *border* intervals. Therefore, at most average influences should be expected. They may cause folding of the 40I/C bed floor and its cracking, however, these changes should not cause significant difficulties in the mining the 40I/C bed.

3.3. A short numerical simulation of the influence of undermining a higher lying bed

In order to assess phenomenon of influence of undermining the bed uplying the bed below it, a simplified numerical rock mass model 1500m (W) × 300m (H_m) was built. A program FLAC v.5.0 based on the finite difference method (Itasca Consulting Groups, US) was used. The program has already been described many times. The part of rock mass was loaded by applying a vertical stress component σ_z equal to 11.0MPa to the upper edge, simulating the rock layers lying above. Two coal beds lay at a depth of -660.0m and -687.5m (floor). The thickness of both beds was 2.5m. The distance between two beds M_v was 25.0m, i.e. 10g. The rock mass was described by Coulomb-Mohr criterion. Rocks were assigned material properties characteristic of the Carboniferous sedimentary rocks of the Upper Silesian Coal Basin.

Mining with roof layers caving was simulated for mining face progress up to 600m. Figures 3.3-3.6 show selected maps of the maximum principal stresses σ_1 (which can be related to vertical stresses σ_z, Figures 3.3*a* and 3.6*a*) and damage zones in the rock mass (Figures 3.3*b*, 3.4, 3.5, 3.6*b* and *c*).

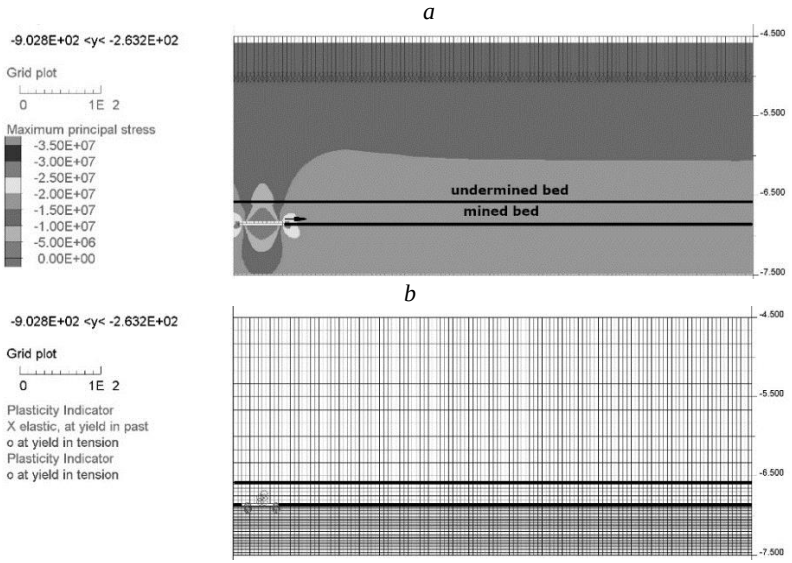

Fig. 3.3. Distribution of principal stress σ_1 (*a*) and damage zones (*b*) after face progress of the bed over a length of 50m; zones of plasticity and exceeding the tensile strength in Figure b have been marked with the signs ○ and ×

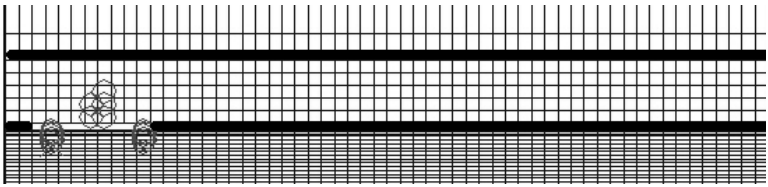

Fig. 3.4. Local view after face progress of the mined bed a length of 50m; zones of plasticity and exceeding of the tensile strength were marked with the signs ○ and ×

Limiting the comment to the range of rock mass damage zones above the mined bed, it should be stated that after exceeding the face progress length of 300 m, the damage zones covered the undermined bed. After the *finishing* of the 600 m mining, the damage zones reached 100 m above the mined bed and covered the entire undermined bed.

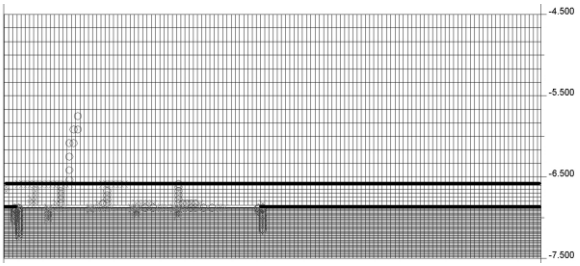

Fig. 3.5. Global view after face progress the mined bed over a length of 300m; places of plasticity and exceeding of the tensile strength were marked with the signs ○ and ×

a

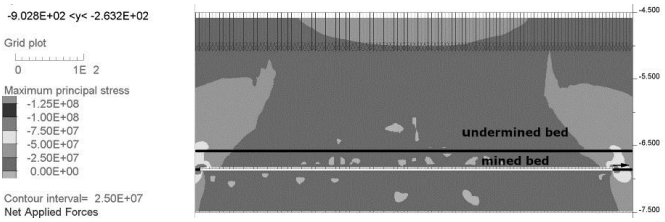

b

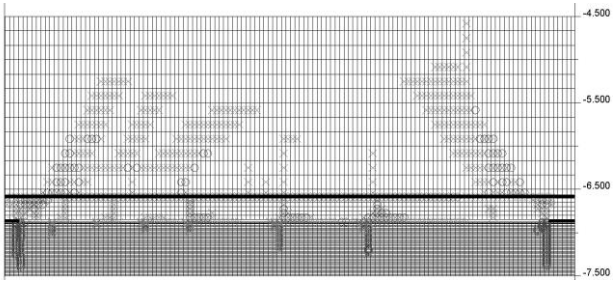

c

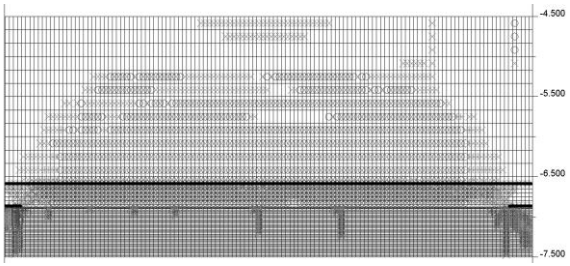

Fig. 3.6. Distribution of principal stresses σ_1 (*a*) and damage zones immediately after face progress of the mined bed over a length of 600 m (*b*) and the rock mass in equilibrium state (*c*); places of plasticity and exceeding the tensile strength in Figures *b* and c have been marked with the signs ○ and ×

The numerical model does not take into account the *support* of the filled post-mining void in caving zone- it was not *artificially* filled by adding blocks.

The obtained simulation results indicate that the extent of the damage zone above the mined bed is less directly affected by the strength and deformation properties of the rocks, and the process of filling the post-mining cavity void influenced critically.

4. Summary and final remarks

Undermining the 40I/D bed by mined the 41J bed should not result in significant influence on the 40I/D bed. The calculated values of the required minimum distance *M* between the beds (41J and 40I/D) is smaller than the actual distance between the two beds. Only small and locally medium influences may occur which may cause slight folding of the bed floor and its cracking; these changes should not cause difficulties in the mining the 40I/D bed.

Undermining the 40I/C bed by a longwall by mining the 2nd layer 40D/D bed will have some effect on the 40I/C bed. The calculated values of the required minimum distance *M* between the 40I/D and 40I/C beds is in the range of the actual distance between the two beds. The calculated values of the probability p of loosening the undermined bed indicate that there will probably be average influences. They may cause folding of the 40I/C bed floor and its cracking, however, these changes should not cause significant difficulties in the possible mining the 40I/C bed.

Due to the complexity of the problem of determining influences by the mined bed on the undermined bed, it is advisable to more completely determine the strength properties, including uniaxial tensile strength R_r and deformation properties, including Young's modulus E and Poisson's ratio □ for rocks lying between both beds and making mining computer simulation of both beds.

In turn, the numerical simulation results indicate that the extent of the damage zone above the mined bed is less directly affected by the strength and deformation properties of the rocks, and the process of filling the post-mining cavity void influenced critically.

Sources (selected)

1. **Borecki M. i Kwaśniewski M.:** Metody analityczne obliczania ciśnienia deformacyjnego oraz przemieszczeń lepkosprężystego górotworu izotropowego w sąsiedztwie wyrobisk korytarzowych na dużych głębokościach. Analytical methods for determining deformation stress and viscoelastic-isotropic rock mass displacement in the vicinity of headings at height depths. W: Metody i środki eksploatacji na dużych głębokościach. Wybrane zagadnienia. Wyd. Pol. Śl., str. 195-221, Gliwice 1982

2. **Budryk W. i Bes W.:** Prawdopodobieństwo uszkodzenia podebranego pokładu węgla. Probability of damaging the undermined coal bed. Archiwum Górnictwa, t. 1, z. I, Kraków 1956

3. **Chudek M.:** Zachowanie się skał stropowych nad wyrobiskiem ścianowym w świetle badań modelowych. Behaviour of floor rocks over the longwall excavation face in the context of model research. Zeszyty Naukowe Politechniki Śląskiej, Seria: Górnictwo, Zeszyt nr 30, Gliwice 1968

4. **Chudek M. i Staroń T.:** Współczynnik rozluzowania skał towarzyszących pokładom węgla w świetle badań laboratoryjnych. The loosening coefficient of rocks near the coal beds in the context of laboratory tests. Zeszyty Naukowe Politechniki Śląskiej, Seria: Górnictwo, Zeszyt nr 35, Gliwice 1969

5. **Chudek M., Pach A. i Olaszowski W.:** Wpływ ściśliwości zawału na warunki eksploatacji w pokładach podebranych. Influence of caving compressibility on exploitation conditions in undermined beds. Przegląd Górniczy nr 12/1969, Katowice 1969

6. **Drzewiecki J. i Piernikarczyk A.:** Dekoncentracja obszarów eksploatacji dla zminimalizowania liczby i energii wysokoenergetycznych zjawisk sejsmicznych. Deconcentrating of mining areas for reduction of the magnitude and Energy of high-power seismic phenomena. Przegląd górniczy Nr 5/2015, str. 3-9, Katowice 2015

7. Główny Instytut Górnictwa: Systemy eksploatacji węgla kamiennego. Hard Coal Mining Systems. Monografia polskiego górnictwa węglowego. Wydawnictwo „Śląsk", Katowice 1968

8. **Hoek E. and Brown E.T.:** Underground Excavations in Rock. Institution of Mining and Metallurgy, London 1980

9. **Jeremic M.L.:** Strata Mechanics in Coal Mining. Balkema, Rotterdam-Boston 1985

10. **Knothe S.:** Prognozowanie wpływów eksploatacji górniczej. Predicting the Influence of Underground Mining. Wydawnictwo „Śląsk", Katowice 1984

11. **Kołodziejczyk P., Musioł S. i Wesołowski M**.: Określenie zasięgu zniszczeń górotworu w otoczeniu wyrobiska ścianowego z wykorzystaniem modelowania numerycznego. Determination of range of rock mass damage in longwall surroundings using numerical modelling method Materiały konferencyjne, Warsztaty 2009: "Zagrożenia Naturalne w Górnictwie", str. 77-87, 2009

12. **Konopko W.:** Destrukcja górotworu w otoczeniu eksploatacji ścianowej. Rock mass destruction in the surroundings of longwall mining. Przegląd Górniczy, nr 2/2014, str. 1-11, Katowice 2014

13. **Kwaśniewski M.:** Badania nad mechanicznymi własnościami skał karbońskich dla potrzeb projektowania wyrobisk górniczych oraz prognozowania deformacyjnych i dynamicznych przejawów ciśnienia górotworu. Research on the mechanical properties of Carboniferous rocks for the design of mining excavations and predicting the deformational and dynamic manifestations of rock mass behaviour. W: "Metody i środki eksploatacji na dużych głębokościach. Wybrane zagadnienia." Proj. Resort. Min. Górn. i Energ. Nr 119 (1981-1985), Politechnika Śląska, Wydział Górniczy, Instytut Projektowania, Budowy Kopalń i Ochrony Powierzchni, str. 63-72, Gliwice 1987

14. **Kwaśniewski M.:** Numerical modeling of discontinuous rock masses and computer study of caving processes associated with longwall mining. Modelowanie numeryczne nieciągłych masywów skalnych i komputerowa analiza zjawiska zawału skał stropowych związanego z eksploatacją pokładów systemem ścianowym. Lecture at the Chinese University of Mining and Technology in Beijing, People's Republic of China, 2.03.1998.

15. **Kwaśniewski M.:** Numerical analysis of strata behaviour associated with longwall mining. Numeryczna analiza zachowania się górotworu poddanego wpływom eksploatacji podziemnej systemem ścianowym. Lecture at Instituto Técnico Superior in Lisbon, Portugal, 4.12.2002.

16. **Kwaśniewski M.:** Strength hypotheses and failure criteria for rocks. Hipotezy wytrzymałościowe i kryteria zniszczenia [warunki wytrzymałościowe] dla skał. Lecture at the Research Center for Large Depths at the National Institute of Advanced Industrial Sciences and Technology (AIST) in Tsukuba, Japan, 19.11.2004.

17. **Obert L. and Duvall W.I.:** Rock Mechanics and Design of Structure in Rock. Wiley, New York 1967

18. **Sałustowicz A.:** Mechanika górotworu. Rock Mass Mechanics. Wydawnictwo Górniczo-Hutnicze, Katowice 1955

19. Singh R.D.: Principles and practices of modern coal mining. New Age Int. (P) Ltd. Publ., Balkema, Netherlands 1985

20. **Staroń T**.: Studium nad zagadnieniem podbierania pokładów z zawałem stropu w świetle badań podziemnych i rozważań teoretycznych. A study on the problem of undermining beds with a roof caving in the context of underground research and theoretical considerations. Prace GIG, Komunikat nr 646. Katowice 1975

21. **Staroń T.**: Zasięg zruszania górotworu warunkujący podbieranie pokładów przy eksploatacji z zawałem stropu. The range of rock mass loosening determining the undermining of beds during mining with the roof caves. Prace GIG, Katowice 1979

22. **Tomiczek K.:** Krótka numeryczna analiza podbierania pokładu z zawałem stropu. Simple numerical analysis on the problem of undermining beds with caving. Zesz. Nauk. Pol. Śl., s. Górnictwo, z. 283, str. 301-312, Gliwice 2008

MANAGEMENT OF POLLUTION - PURIFICATION SYSTEM FOR MINING PLANTS

Safonyk A.P.
National University of Water and Environmental Engineering, Doctor of Technical Sciences, Professor, Department of Automation, Electrical and Computer-Integrated Technologies, Ukraine

Koziar M.M.
National University of Water and Environmental Engineering (NUWEE), Doctor of Pedagogical Sciences, Professor, Department of Theoretical Mechanics, Engineering Graphics and Mechanical Engineering, Ukraine

Martyniuk P.M.
National University of Water and Environmental Engineering (NUWEE), Doctor of Technical Sciences, Professor, Department of Computer Science and Applied Mathematics, Ukraine

Fylypchuk V.L.
National University of Water and Environmental Engineering (NUWEE), Doctor of Technical Sciences, Professor, Department of Occupational Health and Safety, Ukraine

Astract

A new mathematical model of the pollution-purification process in a river system has been developed to calculate changes in the range of quality values (concentration of pollution) of river water, including control of the pollution-purification process, with optimal profit for producers, taking into account fines for cleaning and maintenance permissible concentrations in the control areas.

Introduction

Water is one of the most valuable natural resources for human life. However, when the needs of mankind for mineral raw materials are met, its production leads to the pollution of a considerable amount of surface and groundwater. Yes, a significant amount of contaminated mine and quarry water is pumped daily during the development of ore deposits. At the same time, these waters are used to replenish reverse water supply systems of mining and processing plants, and their surplus is collected in ponds and storage facilities. Tailings come to process waters after the ore is enriched. At the final

stage of infiltration and displacement, they fall into groundwater and surface water, polluting them, making polluted water unsuitable for direct use in the economy. A significant amount of such water enters the riverbeds, causing pollution of the ecosystem, which is not always capable of self-healing or self-purification. Therefore, solving the problems of rational use of water resources in the extraction of minerals is an important and relevant scientifically practical task.

Many scientists have been involved in the processes of self-purification and dilution of sewage in rivers (in particular the dynamics of quality) over a long time [1-14]. Thus, [11] presents a mathematical model of the processes of self-purification and dilution of wastewater in a branched river system. Here, the object of simulation is the water quality indicator (*WQI*), for example, the concentration in the river of pollutants [1 - 12]. It is believed that a reduction in the value of WQI should be interpreted as an improvement in water quality or vice versa [3]. One of the most effective self-purifying processes for reducing WQI is dilution, which is to mix river water with polluted water. Usually, river water is much larger and is much cleaner than polluted water, which is why dilution makes the largest contribution to reducing the value of *WQI* for polluted waters. In order to emphasize the presence of other self-purifying processes, besides dilution, the term "self-purification and dilution" is often used [15-20].

In [18], general approaches to the management of ecological and economic systems are formulated. Hierarchical management techniques are proposed to enable the top-level entity to achieve the system's sustainability requirements. Examples of application of these methods in the annual water quality control system are given and their comparative analysis is given. But this model is homogeneous and a number of important process components remain unaccounted for (eg river shape).

The purpose of this work is to build a new model of the pollution-purification process in the river for management and decision-making, which is carried out under optimal profit of mining and processing enterprises (taking into account purification penalties) and ensuring permissible concentrations at the control sites.

General statement of the problem. Consider such a "traditional" formulation of a nonlinear singularly perturbed model problem of the pollution-purification process

$$\varepsilon\left(\frac{\partial}{\partial x}\left(\bar{D}(x,y,t,u)\frac{\partial u}{\partial x}\right)+\frac{\partial}{\partial y}\left(\bar{D}(x,y,t,u)\frac{\partial u}{\partial y}\right)\right)-v_x(x,y)\frac{\partial u}{\partial x}-$$
$$v_y(x,y)\frac{\partial u}{\partial y}+\bar{\Phi}(x,y,t)=\frac{\partial u}{\partial t},\ (x,y,t)\in G_z\times(-\infty,\infty); \quad (1)$$

$$u(M,t)\big|_{L_0}=0,\ \alpha_i(M,t)u+\beta_i(M,t)\frac{\partial u}{\partial n}\Big|_{L_i}=\gamma_i(M,t),$$
$$i=1,2,\ \frac{\partial u}{\partial n}\Big|_{CD}=0, \quad (2)$$

where G_z - curvilinear half-strip (river), bounded by the drainage interval $L_0=\{(x,y): x=-l_*, 0\le y\le l\}$ and "coastal" sections and *AB* and *CD* (see Fig. 1); $u=u(x,y,t)$ - concentration of pollution at a point (x,y) in time t, v_x, v_y - velocity vector components, $\vec{v}=k\cdot grad\varphi$, $div\vec{v}=0$, $k=(a+b\psi(Q-\psi))$, $\varepsilon\cdot\bar{D}$ - diffusion coefficient (ε– small parameter), $n=n(M)$ – normal, Q - full flow, M - running point of the corresponding curve, $\alpha_i, \beta_i, \gamma_i$ - continuous limited functions characterizing processes occurring in the coastal zone ($\alpha_i^2+\beta_i^2\neq 0$). Here $\bar{\Phi}(x,y,t)=\alpha_{jk}$, where $\alpha_{jk}=\alpha_{jk}^*$, if $(x,y)\in Z_j, t\in\left[t_k^*, t_{k+1}^*\right]$; $\alpha_{jk}=-\alpha_{jk}^0$, if $(x,y)\in O_j$, $t\in\left[t_k^0, t_{k+1}^0\right]$; $\alpha_{jk}=0$ - in other cases, α_{jk}^* - the intensities of industrial pollutants (Z_j - areas of their action, $j=\overline{1,N}$, N - the number of pollutants), α_{jk}^0 - the intensity of treatment plants (O_j - their areas of action), $\left[t_k^*, t_{k+1}^*\right]$, $\left[t_k^0, t_{k+1}^0\right]$- according to the time intervals of their action. We consider the current in the river to be near perfect. Through $\varphi=\varphi(x,y)$, $\psi=\psi(x,y)$, k We denote, respectively, by the quasi-potential, the flow function, and the dummy coefficient "(coefficients a, b characterize its dependence on coastal distances).

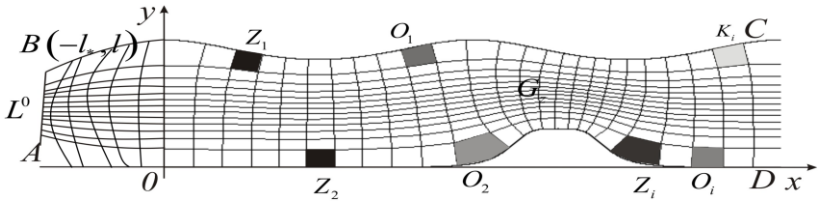

Fig. 1. The physical area of the river in question G_z

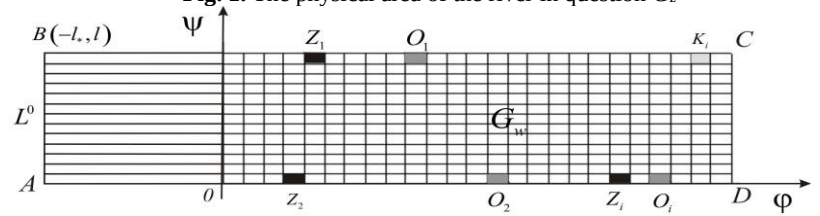

Fig. 2. Relevant G_z area of complex potential G_w

Since the rational use of natural resources, the introduction of new resource-saving technologies requires the transition to fundamentally new ecological and economic relations, which are based on the balance, proportionality of natural and industrial potentials, the environment should be in the system of socio-economic relations as one of its important elements. It is impossible to solve this problem without a comprehensive approach, which involves the creation of the concept of management of eco-economic systems, which should formulate the main tasks of management, the general structure of management systems and principles of their organization. Therefore, we complement the "traditionally" problem (1) - (2) by mathematically formalizing the control method based on the model of river water quality control.

We will assume that the activity of N pollutants located along the river is controlled by the State Environmental Security Authorities (SESA). The SESA regulates the quality of water in the river, eliminates pollution charges. The main goal of the SESA is to keep the river system stable. [12] There are several ways to achieve this. Therefore, in addition to the main goal, they are trying to maximize the proceeds from the enterprise.

In [12], the following options for specifying the objective function (obtaining the SESA funds) are considered

$$J_0 = \int_0^{\Delta} \left\{ -U_A\left(u\left(\bar{x},\bar{y},t\right)\right) + \sum_{i=1}^{N} \left[w_j\left(R_j\left(F_j\right) - VK_j\left(F_j\right) - H_j\left(F_j\right) - VS_j\left(\alpha_j^*, \alpha_j^0\right) - FN_j\right) + \right.$$
$$\left. + FN_j + FP_j + FS_j \right] \right\} dt \to \max\left\{KN_j, KS_j, q_j\right\}_{j=1}^{N}; \quad (3)$$

$$FP_j = \begin{cases} 0, if\ \left(1-\alpha_j^0(x,y,t)\right)\alpha_j^*(x,y,t) \le W1, \\ sKN_j\left(\left(1-\alpha_j^0(x,y,t)\right)\alpha_j^*(x,y,t) - W1\right), \\ if\ W1 < \left(1-\alpha_j^0(x,y,t)\right)\alpha_j^*(x,y,t) \le W2, \\ sKN_j\left(W2-W1\right), if\ W2 < \left(1-\alpha_j^0(x,y,t)\right)\alpha_j^*(x,y,t); \end{cases}$$

$$FS_j = \begin{cases} 0, if\ \left(1-\alpha_j^0(x,y,t)\right)\alpha_j^*(x,y,t) \le W2, \\ sKS_j\left(\left(1-\alpha_j^0(x,y,t)\right)\alpha_j^*(x,y,t) - W2\right), \\ if\ \left(1-\alpha_j^0(x,y,t)\right)\alpha_j^*(x,y,t) > W2, \end{cases}$$

where $\alpha_j^*(x,y,t)$ i $\left(1-\alpha_j^0(x,y,t)\right)\alpha_j^*(x,y,t)$ - the number of contaminants discharged into the river before and after the contamination of contaminated water at point (*x,y*) at time t; $\alpha_j^0(x,y,t)$ - part of the pollution that is extracted at the j enterprise in the process of purification of contaminated water (intensity of treatment facilities); FS_j, FN_j, FP_j - the functions of the pollutant payment for the discharge of pollutants within the limits set by the standard, as well as for the normative and extracurricular discharges respectively, these functions depend on the total amount of pollutants discharged into the river after the pollution of the polluted waters, incl. of magnitude $\left(1-\alpha_j^0(x,y,t)\right)\alpha_j^*(x,y,t)$; s, KN_j, KS_j - the amount of charge per unit of pollution that is dumped at the pollutant at point (*x,y*) at the time t of discharge within the prescribed limits, excess and extracurricular discharges, respectively; $W1, W2$ - norms of the legislation for discharge of pollution; $U_A\left(c(x,y,t)\right)$ - a function that reflects the material losses of society due to contaminated water (the cost of arranging new recreation facilities in other regions, the additional costs of river water treatment for consumer needs, etc.); $c(x,y,t)$ - total number of pollutants dumped

into the river; Δ - the time at which the review is under way; w_j - income tax rate at the mining and j processing plant; $R_j(F_j)$ - profit of the mining and j processing plant from the sale of products at the size of production funds F_j; $VK_j(F_j)$ - costs of basic production, which are included in the cost; $H_j(F_j)$ - total wages of basic and environmental industries; $VS_j\left(\alpha_j^*, \alpha_j^0\right)$ - environmental costs, which depend on the volume of pollutants dumped and the degree of contamination of the polluted waters; q_j - the minimum allowable degree of purification of contaminated water at the mining and j processing plant. Functions VK_j and H_j depend on the volume of production, that is, on the size of the production assets. Functions $VS_j\left(\alpha_j^*, \alpha_j^0\right)$ reflects the costs j of the enterprise to clean up contaminated water. In this paper it is assumed that the following relations are fulfilled

$$VK_j\left(F_j\right)+H\left(F_j\right)=\mu_j R_j\left(F_j\right);\mu=const;\ VS_j\left(\alpha_j^*,\alpha_j^0\right)=\alpha_j^* U_p\left(\alpha_j^0\right),$$

where $U_p\left(\alpha_j^0\right)$ - are the cost functions of the mining j and processing plant to clean up the unit of pollutants discharged into the stream. The purpose of the enterprise is to maximize the profit received during the production activity

$$J_j=\int_0^{\Delta}\left\{\left(1-w_j\right)\left(R_j\left(F_j\right)-VK_j\left(F_j\right)-VS_j\left(\alpha_j^*,\alpha_j^0\right)-FN_j\right)-FP_j-FS_j\right\}dt\to\max\left\{\alpha_j^0\right\} \quad (4)$$

The optimization problems in (3) and (4) in [12] are solved under the following constraints

$$q_j\le\alpha_j^0\left(x,y,t\right)\le 1-\mu, 0\le t\le\Delta, 0\le KN_j\le KN_{\max},\ 0\le t\le\Delta,\ 0\le KS_j\le KS_{\max},$$

where is the value of magnitude $KS_{\max}$ i $KN_{\max}$ given; $0<\mu<1$ - steel, which is determined by technological possibilities of water pollution at enterprises. The requirements of sustainable development of an ecological and economic system, which includes the flow, consists of the need to fulfill the following inequalities

$$0\le c\left(x,y,t\right)\le c_{\max},\ 0\le t\le\Delta,\ \frac{\alpha_j^*\left[1-\alpha_j^0\right]}{Q_j^0}\le Q_{\max}, 0\le t\le\Delta,$$

(j=1,2,...N, Q_i^0 - water consumption at j mining and processing plant; $c_{\max}$, $Q_{\max}$ - given), which are related to state standards for annual water quality and pollution.

One of the possible ways to set the objective function in the simplified form is as follows

$$\Psi = q\alpha^* - p\alpha^0 \to \max, \qquad (5)$$

where α^*,(α^0) - intensity of industrial pollutants (treatment plants), q,(p) - unit price of pollution (treatment). One of the "limiting" conditions when solving problem (1)-(5) is the following inequalities

$$\bar{c}\left(t,\alpha^*,\alpha^0\right) \le c_{kp},\ \bar{c}\left(t,\alpha^*,\alpha^0\right) = \frac{1}{S}\iint\limits_{(S)} c\left(\bar{x},\bar{y},t\right)d\bar{x}d\bar{y}; \qquad (6)$$

$$0 < \underline{\alpha} \le \alpha^* \le \bar{\alpha} < \infty,\ 0 < \underline{\underline{\alpha}} \le \alpha^0 \le \bar{\bar{\alpha}} < \infty, \qquad (7)$$

where (S) - the control area (territory), S - its area, c_{kp} - the set (critical) value of the concentration of pollution, $\underline{\alpha}, \bar{\alpha}, \underline{\underline{\alpha}}, \bar{\bar{\alpha}}$ – the positive real numbers are given.

The solution of problem (1)-(2) is found by introducing a quasi-harmonic function $\psi=\psi(x,y)$, complex conjugate to $\varphi=\varphi(x,y)$, and by replacing the last two boundary conditions (2) with the following conditions: $\psi\big|_{BC}=Q$, $\psi\big|_{AD}=0$, (Q - unknown parameter), replace this task with a more general conformal mapping task $w=w(z)=\varphi(x,y)+\mathrm{i}\,\psi(x,y)$ physical area G_z to the rectangle (area of complex potential) $G_w = \left\{w : \varphi_* < \varphi < \varphi^*, 0 < \psi < Q\right\}$ (see Fig. 2, we assume that the areas of contamination and cleanup of the area G_z are bounded equipotential lines of flow, hence their corresponding images in G_w are rectangles). Assuming that problem (1)-(2), by quasiconformal mapping G_z a G_w (or G_w a G_z) is decoupled, we replace the variables $x = x(\varphi,\psi)$, $y = y(\varphi,\psi)$ in equation (1) and conditions (2) and we arrive at the corresponding “diffusion problem” for the domain G_w

$$\varepsilon v^2\left(\left(\varphi,\psi\right)D\left(\varphi,\psi,t,c\right)\left[\frac{\partial^2 c}{\partial\varphi^2}+\frac{\partial^2 c}{\partial\psi^2}\right]+D_{\varphi}\left(\varphi,\psi,t,c\right)\frac{\partial c}{\partial\varphi}+\right.$$
$$\left.D_{\psi}\left(\varphi,\psi,t,c\right)\frac{\partial c}{\partial\psi}\right)-v^2\left(\varphi,\psi\right)\frac{\partial c}{\partial\varphi}-\Phi\left(\varphi,\psi,t\right)=\frac{\partial c}{\partial t}, \tag{8}$$

$$c\left(\varphi_*,\psi,t\right)\Big|_{L_0}=0,\ \left.\frac{\partial c}{\partial\psi}\right|_{\varphi=\varphi^*}=0,$$

$$\bar{\alpha}_1\left(\varphi,0,t\right)c\left(\varphi,0,t\right)+\bar{\beta}_1\left(\varphi,0,t\right)\left.\frac{\partial c\left(\varphi,0,t\right)}{\partial\psi}\right|_{L_i}=\bar{\gamma}_1\left(\varphi,0,t\right), \tag{9}$$

$$\bar{\alpha}_2\left(\varphi,Q,t\right)c\left(\varphi,Q,t\right)+\bar{\beta}_2\left(\varphi,Q,t\right)\left.\frac{\partial c\left(\varphi,Q,t\right)}{\partial\psi}\right|_{L_i}=\bar{\gamma}_2\left(\varphi,Q,t\right),$$

where $c\left(\varphi,\psi,t\right)=u\left(x\left(\varphi,\psi\right),y\left(\varphi,\psi\right),t\right)$,

$$\Phi\left(\varphi,\psi,t\right)=\bar{\Phi}\left(x\left(\varphi,\psi\right),y\left(\varphi,\psi\right),t\right),$$

$$D\left(\varphi,\psi,t,c\right)=\bar{D}\left(x\left(\varphi,\psi\right),y\left(\varphi,\psi\right),t,u\left(x\left(\varphi,\psi\right),y\left(\varphi,\psi\right),t\right)\right).$$

The exact solution to this problem $O(\varepsilon^{n+1})$ is sought in the following asymptotic series [17-19]

$$c\left(\varphi,\psi,t\right)=c_0\left(\varphi,\psi,t\right)+\sum_{i=1}^{n}\varepsilon^i c_i\left(\varphi,\psi,t\right)+\sum_{i=0}^{n+1}\varepsilon^i S_i\left(\xi,\psi,t\right)+\sum_{i=0}^{n+1}\varepsilon^{i/2}P_i\left(\varphi,\eta,t\right)+$$
$$+\sum_{i=0}^{n+1}\varepsilon^{i/2}\bar{P}_i\left(\varphi,\eta,t\right)+R\left(\varphi,\psi,t,\varepsilon\right), \tag{10}$$

where R - residual term, $c_i\left(\varphi,\psi,t\right)$ $(i=\overline{0,n})$ - members of the regular part of the asymptotics, $S_i\left(\xi,\psi,t\right)$ $(i=\overline{0,n})$ - are the boundary-type functions in the neighborhood $\varphi=\varphi^*$ (corrections at the outlet of the filtration flow from this layer G_z), $P_i(\varphi,\eta,t)$, $\bar{P}_i\left(\varphi,\mu,t\right)$ $(i=\overline{0,n})$ - boundary-type functions in the vicinity, respectively $\psi=0$, $\psi=Q$ (as amended on flow lines BC and AD), $\xi=(\varphi^*-\varphi)\cdot\varepsilon^{-1}$, $\eta=(Q-\psi)\varepsilon^{-1/2}$, $\mu=\psi\cdot\varepsilon^{-1/2}$ – relevant regulatory transformations (stretch variables), φ^*,φ_* - upstream (downstream) potentials, above sea level.

These functions are similar to [13-17] as a result of substitution (10) in (1)-(2), the application of the procedure of equalization of

coefficients at equal degrees ε, and the solution of the corresponding "split" problems. In particular

$$c_0(\varphi,\psi,t)=\begin{cases}\int_{\varphi_*}^{\varphi} v^{-2}(\phi,\psi)\Phi(\phi,\psi,\ f(\phi,\psi)+t-f(\varphi,\psi))d\phi, & t>f(\varphi,\psi),\\ \int_0^t \Phi(f^{-1}(f(\varphi,\psi)-t+\tau,\psi),\psi,\tau)d\tau, & t\le f(\varphi,\psi).\end{cases}$$

$$c_i(\varphi,\psi,t)=\begin{cases}\int_{\varphi_*}^{\varphi} v^{-2}(\phi,\psi)g(\phi,\psi,\ f(\phi,\psi)+t-f(\varphi,\psi))d\phi, & t>f(\varphi,\psi),\\ \int_0^t g(f^{-1}(f(\varphi,\psi)-t+\tau,\psi),\psi,\tau)d\tau, & t\le f(\varphi,\psi).\end{cases}$$

where $i=\overline{1,n}$, $f(\varphi,\psi)=\int_{\varphi_*}^{\varphi} v^{-2}(s,\psi)\,ds$ - is the time of passage of the selected particle along the flow line $\psi=\psi_0$ from the equipotential line $s=\varphi_*$ to the equipotential line $s=\varphi$, f^{-1}, - the function is inverted to the function f with respect to the variable φ.

Further, according to (6), we find $\bar{c}\left(t,\alpha^*,\alpha^0\right)$ and, for example, search the coefficients α^*,α^0 so that under conditions (6)-(7) the objective function J takes the maximum value.

Results of numerical calculations. Consider the case where the river is straight and neglect the diffusion and coastal components of the process, namely, we assume that $G_z=\{z:-1<y<0;\ 0<x<\infty\}$, $\varepsilon=0$, $\alpha_i=\beta_i=\gamma_i=0$, the process is stationary,

$$\bar{\Phi}(x,y,t)=g(x)=\begin{cases}\alpha, & x\in[\underline{a},\bar{a}],\\ -\beta, & x\in[\underline{b},\bar{b}],\\ 0, & x\notin\left([\underline{a},\bar{a}]\cup[\underline{b},\bar{b}]\right),\end{cases}$$

where respectively $[\underline{a},\bar{a}]$ - the source area of contamination, $[\underline{b},\bar{b}]$ - the treatment area, $[\underline{d},\bar{d}]$ - the control (operational) zone (see Fig. 3).

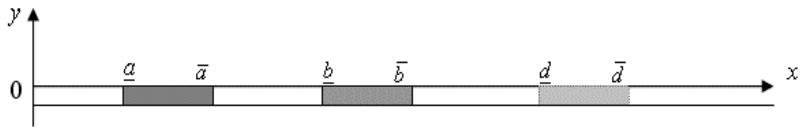

Fig. 3. River bed with appropriate areas of pollution, treatment and control

It's easy to see that

$$c(x,t)=c(x)=\begin{cases}0,\ x<\underline{a};\\ \alpha/v\cdot(x-\underline{a}),\ \underline{a}\le x\le\overline{a};\\ \alpha/v\cdot(\overline{a}-\underline{a}),\ \overline{a}<x<\underline{b};\\ \alpha/v\cdot\left(\alpha(\overline{a}-\underline{a})-\beta(x-\underline{b})\right),\ \underline{b}\le x\le\overline{b};\\ \alpha/v\cdot\left(\alpha(\overline{a}-\underline{a})-\beta(\overline{b}-\underline{b})\right),\ \overline{b}<x.\end{cases}$$

Figure 4 schematically depicts a corresponding graph of concentration distribution along the river.

By specifying a target function, for example, in the form $\Psi=q\alpha-p\beta \quad \left(\alpha\in[\underline{\alpha},\overline{\alpha}],\ \beta\in\left[\underline{\beta},\overline{\beta}\right]\right)$, and considering that $\frac{1}{v}\left(\alpha(\overline{a}-\underline{a})-\beta(\overline{b}-\underline{b})\right)\le c_{cr}$ (or $\alpha\le\frac{\overline{b}-\underline{b}}{\overline{a}-\underline{a}}\beta+\frac{vc_{cr}}{\overline{a}-\underline{a}}$), easily find the right optimal plan.

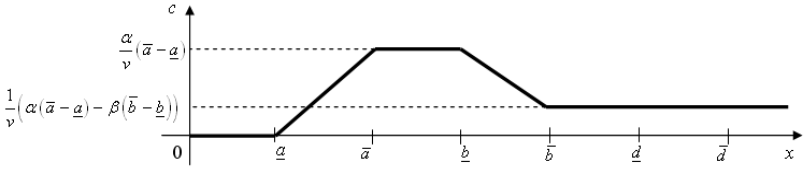

Fig. 4. Stationary concentration distribution in the pollutant-purifier-control system

Consider now a non-stationary process where the sources of contamination and purification (see previous example) only operate at intervals $\left[\underline{t}+n\underline{t},\overline{t}+n\underline{t}\right]$ and $\left[t_*+n\underline{t},t^*+n\underline{t}\right]$ respectively, where $n\in Z$, $\underline{t}$ - period. Here $g(x,t)=\alpha g_*(x,t)-\beta g^*(x,t)$, where

$$g_*(x,t)=\begin{cases}1,(x,t)\in\underline{D}=\left\{(x,t):x\in(\underline{a},\overline{a});\ t\in(\underline{t}+n\underline{t},\overline{t}+n\underline{t})\right\},\\ 0,(x,t)\notin\underline{D},\end{cases}$$

$$g^*(x,t)=\begin{cases}1,(x,t)\in\overline{D}=\left\{(x,t):x\in(\underline{b},\overline{b});\ t\in\left(t_*+n\underline{t},t^*+n\underline{t}\right)\right\},\\ 0,(x,t)\notin\overline{D}.\end{cases}$$

For convenience, we will consider a simpler case when *n*=0,

$$\frac{\underline{a}}{\underline{t}}=\frac{\overline{a}}{\overline{t}}=\frac{\overline{a}-\underline{a}}{\overline{t}-\underline{t}}=\frac{\underline{b}}{t_*}=\frac{\overline{b}}{t^*}=\frac{\overline{b}-\underline{b}}{t^*-t_*}=v,$$

$$\bar{a}-\underline{a}=\bar{b}-\underline{b}=\underline{b}-\bar{a}=\bar{d}-\underline{d}=2\left(\underline{d}-\bar{b}\right).$$

The solution of such a problem (as a characteristic of the interaction of sources of contamination and purification and the speed of convective transfer of particles) at certain points of time will be represented as follows: $c=(x,t)=0$ if $0<x<\underline{a}, -\infty<t<\infty$ and at $\underline{a}\le x\le\bar{a}$, $0<t<\underline{t}$; $c\left(x,\bar{t}\right)=\frac{\alpha}{v}\left(x-\underline{a}\right)$, if $\underline{a}\le x\le\bar{a}$, $c\left(x,\bar{t}\right)=\frac{\alpha}{v}\left(\bar{a}-\underline{a}\right)$, if $\bar{a}\le x\le\underline{b}$, $c\left(x,\bar{t}\right)=0$, if $x>\underline{b}$; $c\left(x,t_*\right)=\frac{\alpha}{v}\left(x-\bar{a}\right)$, if $\bar{a}\le x\le\underline{b}$, $c\left(x,t_*\right)=\frac{1}{v}\left(\alpha\left(\underline{b}-\bar{a}\right)-\beta\left(x-\underline{b}\right)\right)$, if $\underline{b}\le x\le\bar{b}$; $c\left(x,t^*\right)=\frac{\alpha-\beta}{v}\left(x-\underline{b}\right)$, if $\underline{b}\le x\le\bar{b}$, $c\left(x,t^*\right)=\frac{1}{v}\left(\left(\alpha-\beta\right)\left(\bar{b}-\underline{b}\right)-\beta\left(x-\bar{b}\right)\right)$, if $\bar{b}\le x\le\underline{d}$, $c\left(x,t^*\right)=0$, if $x\in\left(0,\bar{a}\right)\cup\left(\bar{b},\infty\right)$, $t^*=t_*+\left(\bar{t}-\underline{t}\right)=3\bar{t}-2\underline{t}$. Figure 5 shows the distribution of pollutants in the river at the time of the end of the purification process ($t=t^*$).

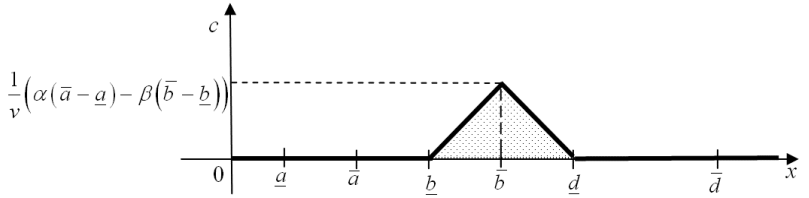

Fig. 5. Distribution of pollution concentration at time $t=t^*$

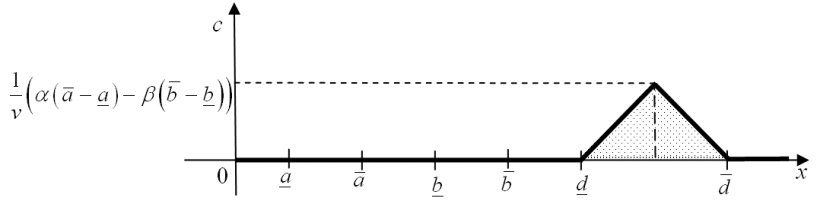

Fig. 6. Distribution of pollution concentration at time $t=t^*+2\left(\bar{t}-\underline{t}\right)$

Similar to the previous example, we find the optimal values a target function that allows you to control the process. Obviously, a "shaded" portion of contamination at time $t=t^*+2\left(\bar{t}-\underline{t}\right)$ "Stay" in

the control territory $\left[\underline{d},\bar{d}\right]$ (see Fig. 6). However, different limiting inequalities are possible: the maximum value of the concentration s should not exceed the specified critical value $c_{кр}^{(1)}$ $(\frac{1}{\nu}\left((\alpha-\beta)\left(\bar{b}-\underline{b}\right)-\beta\left(\underline{d}-\bar{b}\right)\right)\le c_{кр}^{(1)})$; average concentration in the control area at time $t=t^{*}+2\left(\bar{t}-\underline{t}\right)$ should not exceed its critical value, $c_{кр}^{(1)}$ ect.

Conclusions

Since conducting full-scale experimental studies is cumbersome and resource-intensive, mathematical modeling makes it possible to predict the impact of pollutants on the river system and to scientifically calculate and prevent pollution of rivers near settlements.

A new model of the pollution-treatment process in the river has been built to manage and make decisions based on optimal profit margins for producers (taking into account cleaning penalties), as well as ensuring acceptable concentrations of contamination at control sites; determine the time between the discharge of pollutants into the river and the beginning of the treatment process, the distance between contamination, treatment and control areas.

In the future, it is planned to apply this technique when solving the corresponding "diffusion perturbed" problems, as well as problems with specific boundary conditions.

References

1. **Nagara, G.** (2017). Perkembangan Sanksi Administratif Dalam Penguatan Perlindungan Lingkungan Terkait Eksploitasi Sumber Daya Alam (Studi Kasus: Sektor Perkebunan, Pertambangan, dan Kehutanan), Jurnal Hukum Lingkungan Indonesia, 3 (2), 19-47 pp.

2. **Grebin, V., Mokin, V., Kryzhanivskiy, Y., Afanasyev, S.** (2016). Optimization of hydrographic and water-management regionalization of Ukraine according to world approaches and principles of the eu water framework directive, Hydrobiological Journal, 52(5), 81-92 pp.

3. **Safonyk A., Martynov S., Kunytskyi S.** (2019). Modeling of the contact removal of iron from groundwater,International Journal of Applied Mathematics, vol. 32, no. 1, 71-82 pp.

4. **Safonyk A., Prysiazhniuk O, Prysiazhniuk I.** (2019). Modeling of the pro-

cesses of heat and mass transfer in the thin tube given the conditions of exchange with surrounding soil, Computer Science and Information Technologies: Proceedings of the XIV International Scientific and technical Conference CSIT 2019, vol. 1, 100-103 pp.

5. **Safonyk A., Prysiazhniuk O.** (2019). Modeling and simulation in engineering modeling of the electrocoagulation processes in nonisothermal conditions. Modelling and Simulation in Engineering, vol. 2019, Article ID 9629643, 6 p.

6. **James A.** (1978). Mathematical Models in Water Pollution Control, New York, Chichester, Brisbane, Toronto: John Wiley and Sons Ltd., 470 p.

7. **Biesen L., Cisneros Z., Chebreegziabeber T.** (2003). On the Application of the Power of GIS to Environmental Measurements for the Monitoring, Exploitation and Sustainable Environmental Management of Marine Ecosystems, XVII IMEKO World Congress — Metrology in the 3rd Millennium. Proceedings. — Dubrovnik, Croatia: HMD Croatian Metrology Society, TC19, 2110—2113pp.

8. **Lynott, J., Cullinane, R.** (2010). Administrative Sanctions, Irish Planning and Environmental Law Journal, 17 (1).

9. **Safonyk A., Targoniy I., Bomba A.** (2017). Development of an automated decision support system for the process of biological wastewater treatment, Computer Science and Information Technologies: Proceedings of the XII International Scientific and technical Conference CSIT 2017. Vol. 1., 71-75 pp.

10. **Bomba A., Safonik A.** Mathematical simulation of the process of aerobic treatment of wastewater under conditions of diffusion and mass transfer perturbations, Journal of Engineering Physics and Thermophysics, vol. 91, no. 2, 318-323 pp.

11. **Arya Utama, Nengah Suharta**. (2018). The Challenges of Water Pollution: Enforcement of Water Pollution Control. Faculty of Law, Udayana University, Indonesia, vol. 4 issue 1, 81-85 pp.

12. **Safonyk A, Targoniy I., Martyniuk Y., Bomba A.** (2018). Research and automation of the process of wastewater treatment electrocoagulation, Computer Science and Information Technologies: Proceedings of the XIII International Scientific and technical Conference CSIT 2018. vol. 1., 84-88 pp.

13. **Safonyk A., Martynov S., Kunytsky S., Pinchuk O.** (2018). Mathematical modelling of regeneration the filtering media bed of granular filters, Advances in Modelling and Analysis C, vol. 73, no. 2, 72-78 pp.

14. **Safonyk A., Bomba A., Tarhonii I.** (2019) Modeling and automation of the electrocoagulation process in water treatment, Advances in Intelligent Systems and Computing, vol 871, 451-463 pp.

15. **Safonyk A., Hrytsyna O., Voloshchuk V., Sereda V.** (2018) Mathematical modelling of heat and mass transfer processes in wastewater biological treatment systems, Bulgarian Chemical Communications, vol. 50, Special Issue K, 70–75 pp.

16. **Martynov S., Fylypchuk V., Zoshchuk V., Kunytskyi S., Safonyk A., Pinchuk O.** (2018). Technological model of water contact iron removal, Journal of Water and Land Development, no. 39, 93–99 pp.

17. **Bomba A., Safonyk A., Voloshchuk V.** (2018). Spatial modeling of multicomponent pollution removal for liquid treatment under identification of mass transfer coefficient, Mathematical Modeling and Computing, vol. 5, no. 2, 108-118 pp.

18. **Zhukovskyy V., Vlasyuk A., Zhukovska N., Safonyk A. (**2019) Method of Forensic Analysis for Carrier-lock Algorithm Compromising on 3G Modem Firmware, IEEE 2nd Ukraine Conference on Electrical and Computer Engineering, 1179-1183 pp.

19. **Burduk A., Grzybowska K., Safonyk A.,** (2019). The use of a hybrid model of the expert system for assessing the possibility of manufacturing the assumed quantity of wire harnesses, LogForum 15 (4), 459-473 pp.

20. **Safonyk A., Prysiazhniuk O., Prysiazhniuk I**. (2019) Modeling of the processes of heat and mass transfer in the thin tube given the conditions of exchange with surrounding soil, Computer Science and Information Technologies: Proceedings of the XIV International Scientific and technical Conference CSIT 2019. vol. 1, 100-103 pp.

RECENT DEVELOPMENTS IN THE FLOTATION OF SULFIDE ORES OF BASE METALS - BIOFLOTATION

Panayotova M. I.
University of Mining and Geology, Dept. of Chemistry,
PhD, Prof., Bulgaria

Panayotov V. T.
Bulgarian Academy of Sciences, Group on Technical Sciences,
D.Sci., Prof., Correspondent member, Bulgaria

Abstract

Bioflotation of sulfide minerals is being developed recently at laboratory scale. Different bacterial cells, cell parts and microbial metabolites have been successfully used as reagents (mainly biodepressants and biosurfactants) to separate by flotation pyrite, sphalerite, galena, chalcopyrite, arsenopyrite, molybdenite, pyrrhotite, etc. from mixtures of those minerals or from gangue minerals, such as quartz or calcite.

Influence of conditions for microorganisms' cultivation and of operating parameters (such as pulp density, pH and temperature, concentration of bioreagents and their nature, addition to the system of typical flotation reagents, such as xanthate or activators) has been widely studied. Changes in the system "mineral(s)/microorganism cells (cell parts or metabolites)" have been investigated by various methods, such as contact angle, electro-kinetic and zeta-potential measurements, Scanning Electron Microscopy/Energy Dispersive X-Ray Spectroscopy (SEM-EDS) and Fourier-transform infrared (FTIR) spectroscopy, sodium dodecyl sulfate - polyacrylamide gel electrophoresis (SDS-PAGE), etc. Different mechanisms of microbial action leading to minerals' surface biomodification have been raised, such as microbial cells attachment, occurrence of oxidation-reduction reactions on the interface

"mineral/microorganisms", adsorption and/or chemical reactions with microbial metabolite products. This paper briefly presents and discusses the above-mentioned issues.

Keywords: bioflotation, sulfide minerals, depression, activation

Introduction

Our society needs base metals for its sustainable development and this need will increase in the future. At the same time the rich ores deposits are practically depleted and the result is the need to process more and more low-grade ores. Economical extraction of valuable metals from such ores demands selective separation of minerals.

Flotation is widely applied for minerals separation. The process uses modifiers, collectors and depressants that modify the mineral surface properties, as well as frothers and dispersants to increase the flotation froth stability. Potassium and / or sodium cyanide is the most often used depressant for pyrite in complex sulfide mineral flotation systems. Cyanide is toxic and environmental regulations are stringent for final disposal of cyanide bearing effluents and waste. The other widely used depressant, namely sodium sulfide, also raises environmental concerns. Lime is typically used as a modifier to increase the pH to alkaline levels thus depressing pyrite.

Generally, the flotation selection of lower grade ores requires increased amount of reagents. This, besides related to the price of reagents and environment concerns, can lead to other negative economic results, such as depression of precious metals (gold, silver) that are lost with the gangue material. When lime is applied as pH modifier and the process is carried out with sea water, excess lime has to be used, due to the sea water buffering properties. In addition, the $Ca(OH)^+$ species that present at pH above 8, in combination with magnesium hydroxide species from sea water can readily adsorb onto the valuable mineral surface, such as molybdenite, considerably reducing its flotability [1].

The increased need of reagents, combined with the fact that some of them are not environmentally friendly and that a number of them lead to loss of valuable metals, means that the process is going to become increasingly unsustainable as ores become poorer. All mentioned facts lead to a necessity to develop alternative reagents.

Bioreagents possess the potential to mitigate the toxicity issues as they are generally easier to remediate, more biodegradable and as a

whole easier and at their mature technological development stage even cheaper to be produced than synthetic chemicals.

Bioflotation practically appeared in the eighties of the previous century as an answer of the above described problems. It is virtually very new branch, compared to over 150 years use of flotation. The bioflotation may be defined as process in which whole microorganisms or their parts or metabolites act as reagents (collectors, modifiers or surfactants) to facilitate the selective separation of minerals in an environmentally friendly manner [2-4].

Systematic studies on the bioflotation of sulfide ores practically began in the nineties of the previous century. Bacterial cells belonging to genera Acidithiobacillus, Leptospirillum, Bacillus, Mycobacterium, Staphylococcus, etc., and their metabolites such as extracellular polymeric substances (EPS), bio-surfactants, and nucleic acid have been used as reagents in the mineral flotation process [5].

The aim of this paper is to present the recent developments in the bioflotation of sulfide ores of base metals. Good examples of the use of whole cells or microbial metabolites are given. Mechanisms underpinning the good results of bioflotation are briefly discussed.

Use of whole cells as flotation reagents

Initial bioflotation investigations tested the bacterium *Thiobacillus ferrooxidans* (*T. ferrooxidans)* as a means for pyrite depression in the desulphurisation of coal [6].

Later it has been found that *T. ferrooxidans* sets off surface modification of sulfide minerals to enhance their hydrophilicity or hydrophobicity for the flotation of sphalerite and galena [7]. Higher bacterial growth was observed in the sphalerite suspension than in the galena suspension. It was found that the variables influencing the surface modification (and, thus, flotation response of the minerals) comprise the cell concentration used for bacterial conditioning, the period of biotreatment and the pulp density. Cell protein estimations suggested that more cells were attached on galena than on sphalerite. Flotation enhancement of galena obtained through sulfuric acid treatment was retarded by biotreatment at all cell concentrations. During the conditioning with sulfuric acid solution elemental sulfur is generated

$$ZnS \dashrightarrow Zn^{2+} + S + 2e^{-}$$

$$PbS \dashrightarrow Pb^{2+} + S + 2e.^{-}$$

It renders the mineral surfaces hydrphobic and hence increases their flotability. *T. ferrooxidans* is known to oxidize such elemental sulfur to form sulfate. At the pH of 2, the zinc sulfate formed on sphalerite surface is soluble, while lead sulfate formed on galena surface is insoluble. Availability of oxidized insoluble products on the surface of the sulfide mineral impedes the action of the collector leading to considerably decreased flotation recovery of galena observed after the biopretreatment. Such a decrease occurred for sphalerite only at cell concentrations enough high for bacterial attachment to the mineral surface, leading for a possibility for a differential flotation of sphalerite and galena [8].

Further, attempts were made to use *T. ferrooxidans* as pyrite depressant in sulfides ores flotation [9]. Bioconditioning of pyrite with *T. ferrooxidans* produced significant modification of the mineral surface. The flotability of pyrite was considerably reduced, depending on the bacterium concentration, conditioning pH, and the composition of the culture medium in which the bacterium was cultivated. Decrease in the pyrite floatability was attributed to the adhesion of *T. ferrooxidans* on its surface thus rendering the mineral hydrophilic and finally resulting in its depression, hydrophobic sulfur oxidation, and the formation of jarosite on the surface of pyrite.

Additional studies on mineral surfaces characterization using zeta-potential, contact angle, FTIR and FT-Raman spectrometry showed that a monolayer was formed on the pyrite and chalcopyrite surface in the presence of *T. ferrooxidans* [10]. The *T. ferrooxidans* adsorption began on pyrite at a much lower equilibrium cell population than on chalcopyrite. In the presence of *T. ferrooxidans* cells, the xanthate flotation of pyrite was completely depressed, whereas chalcopyrite flotation was unaffected, thus suggesting that chalcopyrite could be selectively floated from pyrite, at a neutral pH region, in the presence of *T. ferrooxidans* cells.

Nagaoka and co-authors studied the flotability of 5 sulfide minerals (pyrite, chalcocite, molybdenite, millerite and galena) upon addition of *T. ferrooxidans* [11]. They found that the flotability of pyrite was significantly depressed to less than 20%, while the addition of the bacterium had little or no effect on the flotabilities of the other minerals, even when they were present in relatively large

amounts. Their flotabilities remained in the range of 70 - 94%. Due to pyrite depression 84-95% of pyrite was removed from mineral mixtures, while 73-100% of non-pyrite sulfide minerals were recovered. The inhibition of pyrite flotability was assigned to bacterial attachment to its surface. The number of cells adhering to pyrite was significantly larger than the number adhering to other minerals.

The effect of *T. ferrooxidans* on the froth flotation of Iranian Sarcheshmeh copper ore was studied [12]. Pure strains of *T. ferrooxidans* were used to cause surface chemical changes in pyrite and chalcopyrite, and thus impact their flotation behavior. Pyrite was depressed in the presence of *T. ferrooxidans* - the recovery of was 50% lower than in the absence of any bacteria, and xanthate as collector. The flotability of chalcopyrite and other sulfide minerals were unaffected at natural pH.

The heterotrophic *Paenibacillus polymyxa (P. polymyxa*) bacteria was also studied in the sulfide minerals flotation [13]. A pure strain of *P. polymyxa* and mineral-adapted strains were used to cause surface chemical changes on pyrite and chalcopyrite. The adaptation was achieved by a repeated subculturing of *P. polymyxa*, carried out in the presence of pyrite and chalcopyrite until their growth characteristics became alike to the growth at the nonexistence of mineral. The results from Hallimond tube flotation with xanthate applied as collector reviled that pyrite was depressed when the tests were carried out after interaction with chalcopyrite-adapted *P. polymyxa*. Chalcopyrite was not depressed.

In further studies *P. polymyxa* was adapted also to galena and sphalerite. It was found that for the all mentioned minerals the mineral-adapted cells became more hydrophilic as compared to unadapted cells [14].

Santhiya and coauthors [15,16] studied the influence of cells of *Bacillus polymyxa* (*B. polymyxa*) on sphalerite and galena flotation. Flotation tests showed that galena was nearly entirely depressed after interaction with the cells both in the absence and in the presence of the collector. When collector and activator were added to sphalerite, which was initially interacted with the cells, its floatability was restored at and beyond pH 8.5. The selective flotation tests carried out with a synthetic mixture of galena and sphalerite confirmed that

sphalerite could be preferentially floated in presence of galena, the latter being depressed by the bacterial cells. Selective flocculation tests demonstrated that galena could be flocculated from sphalerite, which was dispersed in the presence of cells of *B. polymyxa* at pH 9–9.5. Adsorption experiments and FTIR spectroscopic data showed that a higher amount of the *B. polymyxa* cells was adsorbed onto galena compared to sphalerite. The adsorption density of the cells onto galena was practically independent of pH while that onto sphalerite was found to constantly decrease with increasing pH. Additionally, bio-dissolution studies carried out exposed the release of lead/zinc species from galena/sphalerite, correspondingly. The biosorption experiments proved interaction of cells of *B. polymyxa* with those metal ions. The highest amount of exopolysaccharides was found in the cells that had interacted with galena, while the cells that had interacted with sphalerite possessed the least. The cells interacted with sphalerite possessed the highest amount of protein while the cells interacted with galena possessed the lowest amount. The adsorption of xanthate onto galena was decreased in the presence of the cells whereas the xanthate adsorption on activated sphalerite was unchanged in the pH range 9-11. The cell surface hydrophobicity tests confirmed that the cells that interacted with sphalerite were more hydrophobic compared to the cells that interacted with galena. The elevated exopolysaccharides and lesser protein contents together with the hydrophilic nature of the cells interacted with galena were considered as the main factors causing the selective flocculation and depression of galena. The higher floatability and dispersion of sphalerite-interacted cells were assigned to the higher amount of protein and lower exopolysaccharides contents leading to bigger hydrophobicity.

Interaction with *B. polymyxa* was also successfully applied for selective separation of pyrite and galena from mixture of the two minerals [17].

Chemical changes on galena and sphalerite surfaces before and after interaction with *Thiobacillus thiooxidans* (*T. thiooxidans*) were studied [18]. The adsorption density of bacterial cells onto the two minerals was found to be independent of pH. FTIR studies showed that adsorption was due to hydrogen bonding between minerals and microbial cells. Higher number of cells was adsorbed onto galena

compared to sphalerite, causing galena depression. The sphalerite was made hydrophobic after interaction with the cells. Thus selective flotation and flocculation was realized leading to separation of galena from sphalerite after bacterial interaction.

Acidithiobacillus ferrooxidans (A. ferrooxidans) (formerly known as *T. thiooxidans*) was studied for its ability to ensure selective separation of pyrite from other associated ferrous sulfides [19]. It was found that due to the interaction with bacterial cells, pyrite was depressed even in the presence of collector (potassium isopropyl xanthate - PIPX) while chalcopyrite showed significant flotability. The separation achieved was significant both at acidic and alkaline pH. This selectivity was observed when the minerals were interacted with both bacterial cells and collector simultaneously. It was found that the initial interaction with collector followed by conditioning with cells improved the flotation of chalcopyrite [20]. Thus, with this sequence of interactions the pyrite recovery was considerably decreased while the recovery of chalcopyrite was above 80%. The bacterial cells were able to effectively depress collector interacted pyrite even when the minerals were conditioned together.

A. ferrooxidans was studied also for its ability to ensure effective separation of arsenopyrite from pyrite [21]. It was found that the adhesion of the bacterium to the surface of arsenopyrite was very slow compared to that to pyrite, causing a difference in surface modification of the minerals after their interaction with cells. *A. ferrooxidans* cells were able to efficiently depress pyrite flotation in presence of collectors, such as PIPX and potassium amyl xanthate. It was found that the flotability of arsenopyrite after conditioning with the cells was not significantly affected and the mineral rendered its good flotability in the presence of the same collectors. The activation of pyrite by copper sulfate was decreased when the minerals were conditioned together, while the copper activated arsenopyrite was able to retain its hydrophobicity in presence of cells due to poor attachment kinetics of cells to the mineral surface, thus resulting in better selectivity.

Further studies of the same authors included chalcopyrite [22]. It was found that the collector was able to render good flotability to chalcopyrite even after interaction with bacterial cells. Thus, by con-

ditioning with the cells and collector prior to flotation, it was possible to successfully depress pyrite from chalcopyrite and arsenopyrite.

Use of *A. ferrooxidans* instead of NaCN as depressant in the flotation of lean lead-zinc ore, bearing pyrite in high amounts, was studied [23]. *A. ferrooxidans* adapted to ore were used. The results showed that pyrite was significantly depressed in both galena and sphalerite concentrates, using *A. ferrooxidans* as depressant.

Completely new research shows that bacterium *A. ferrooxidans* can be used to depress pyrite in seawater flotation of copper sulfide at natural pH [24]. It has been found that biodepression of pyrite was improved by increasing the pH from 4 to 8, with a decrease in recovery from 92% to 36%. The improved depression is assigned to the increased density of bacteria attached on pyrite, from 2.58×10^8 bacteria/g to 1.99×10^9 bacteria/g at pH 4 and 8, respectively. It has been found that the collector produces a smaller increase in the hydrophobicity (contact angle) of pyrite when the mineral is preconditioned with *A. ferrooxidans* than when it is used alone in seawater. This implies that the bacteria prevent the action of the collector. The increased consumption of lime when seawater is used in flotation is avoided.

Leptospirillum ferrooxidans (L. ferrooxidans) is another studied microorganism [25]. The adhesion of *L. ferrooxidans* cells on pyrite and chalcopyrite minerals was studied by using adsorption, zeta-potential and diffuse reflectance FTIR measurements. The FTIR spectra of minerals treated with bacterial cells showed the presence of all the cell functional groups thus proving cells adsorption. The bacterial cells adsorption on chalcopyrite was higher compared with pyrite, which was in agreement with their greater depression effect on chalcopyrite flotation and pronounced flocculation behaviour in comparison with pyrite. The higher affinity of *L. ferrooxidans* to chalcopyrite was assigned to mineral's higher surface defects and consequently higher accessibility of iron available on mineral's surface as an energy source for the bacteria. Hallimond tube flotation tests, carried out under previously established optimum conditions showed that the flotation recoveries of both minerals were decreased in the presence of cells but the depression of chalcopyrite was much higher than that of pyrite. The depression of minerals was found to depend on cell concentration. At significantly higher *L. ferrooxidans*

concentration chalcopyrite showed floatability under the same conditions.

The behaviour of chalcopyrite and pyrrhotite in microflotation tests was studied using pure minerals and mixtures in the presence of *L. ferrooxidans* [26]. The results indicated that for chalcopyrite, the flotation rate significantly increased in the presence of bacteria in the first 10 min and use of thionocarbamate as collector.

B. subtilis was used for selective separation of galena and sphalerite [27]. The experiments showed that sphalerite can be preferentially (with a high selectivity index) floated from galena in the presence of the insoluble fraction of lysed *B. subtilis* cells initially adapted to sphalerite. Thermolysed sphalerite adapted cells showed enhanced selective recovery of sphalerite when compared to the intact sphalerite adapted cells.

Bacillus pumilus SKC-2 and *Alicyclobacillus ferrooxydans* SKC/SAA- 2, capable to produce biosurfactants and oxidize iron and sulfur, were studied with respect to their ability to act as bio-collector or depressant in sulfide bioflotation processes [3]. It was found that both bacteria strains were able to change the surface chemical properties of pyrite due to biosurfactant production and their adhesion on the pyrite surface. It was established that due to their capability of oxidizing iron and sulfur, the bacteria were also usable as depressants. SEM-EDS and FTIR data also proved the ability of the studied bacterial strains to change the pyrite surface properties to more hydrophilic or more hydrophobic in dependence of time of incubation.

Very recently halophilic bacteria have been studied as potential pyrite bio-depressants in Cu-Mo bioflotation [28]. Halophilic bacteria are a group of bacteria adapted to grow well at high salt concentrations (sea water), which are usually detrimental to the growth of bacteria. Halophilic bacteria are also known to produce EPS. Such bacteria are assumed to be beneficial if can be used in flotation processes in regions where sea water is applied in flotation. Microflotation experiments (using a Hallimond tube) have been carried out with pyrite and chalcopyrite with sodium isopropyl xanthate as collector and bacterial cells as depressant of pyrite as substitute for lime. Biodepression of pyrite is observed therefore at the natural pH of sea water (8.00-8.22) when *Halomonas boliviensis*,

Halobacillus sp. and *Halomonas sp*. were used (from around 68% to below 10% depending on the bacterium used.) It was supposed that the mechanism of adhesion to pyrite by halophilic bacteria was hydrophobic in nature (i.e. hydrophobic extracellular moieties interact with mineral's surface and depress it). Chalcopyrite flotation was unaffected under the same conditions as the pyrite flotation and in fact, it was enhanced by *Halobacillus sp*.

Use of microorganism metabolites as flotation reagents

The idea to use not only whole microbial cells in mineral separation but also to gain knowledge about the impact of specific bacterial metabolic products become essential in the beginning of our century. This was evoked by the need to understand the role of extra cellular polysaccharides and proteins in regulating microorganisms' attachment to minerals.

In one of the pioneering works the interaction of galena and sphalerite minerals with the metabolite obtained from *B. polymyxa* has been studied [29]. The carbohydrate component of the metabolite showed the highest adsorption on sphalerite at pH 6-7. For galena the adsorbed quantity increased with pH increase. The adsorbed amount of the bacterial protein on both minerals was reduced with pH increase. It was found that the adsorption affinity of carbohydrate and protein was higher for galena compared to sphalerite. Bioflotation tests exhibited selective depression of galena from its mixture with sphalerite. Entire depression of galena was observed in the pH range 3-11, in the absence or presence of PIPX, following conditioning for 15 min with *B. polymyxa* metabolite. Sphalerite was selectively floated at 3.3 (the natural pH of the metabolite) without application of any collector or activator. Sphalerite was floated in the pH range of 5-10.5 in the presence of $CuSO_4$, PIPX and metabolite. Bioflocculation studies showed that under appropriate conditions galena was selectively flocculated from sphalerite. Co-precipitation tests confirmed complexation of lead and zinc species with the metabolic products that present in the bulk solution.

B. polymyxa was also studied as a reagent in selective separation of pyrite from quartz and calcite via microbiologically induced flotation and flocculation [30]. It was shown that pyrite can be separated from quartz and calcite through either selective

flocculation or flotation after interaction with cells of *B. polymyxa* or bioproteins separated from the bacterial metabolite. This was due to the fact that cells of *B. polymyxa* exhibited higher affinity towards pyrite compared to quartz and calcite and the bacterial cell adsorption onto minerals followed the order pyrite>calcite>quartz. This phenomenon lead to the same order of the minerals' settling after the interaction with bacteria. Similar behavior was observed also with extracellular bacterial proteins. The study showed that through flotation pyrite could be efficiently separated from quartz after interaction with bacterial cells or extracellular bacterial protein. The efficiency of selective separation was increased by addition of small amount of amine collector to enhance the recovery of quartz.

The same authors used successfully cells and metabolic products of *B. polymyxa* in flocculation and flotation to remove chalcopyrite from quartz and calcite [31]. The adsorption studies showed that the cells of *B. polymyxa* exhibited higher affinity towards chalcopyrite and their adsorption density onto this mineral was the highest when compared to quartz and calcite. Extracellular bacterial protein and extracellular bacterial polysaccharides were isolated and their effects on minerals were studied through flocculation and flotation. Selective separation of chalcopyrite from quartz and calcite was realized through interaction with whole cells, as well as with extracellular protein. The protein flocculated chalcopyrite thus facilitating its settling and dispersed quartz thus decreasing its settling rate. It was found that chalcopyrite could be efficiently separated through flotation from quartz, after interaction with bacterial cells or extracellular bacterial protein. Further increase in the efficiency of selective separation was achieved by addition of small amount of amine collector to enhance the quartz recovery. The studies revealed that through microbially induced flocculation and flotation, both pyrite and chalcopyrite could be removed from oxide gangue minerals, like silicates and calcite, leading to their desulphurisation and consequently - environmental protection.

Cells of *P. polymyxa* and their metabolite products were also successfully utilized to separate selectively sphalerite from pyrite, through bio-flocculation and flotation [32]. It was suggested that the effective separation was due to significantly higher adsorption of cells of *P. polymyxa* onto pyrite compared to sphalerite - the phe-

nomenon observed beyond neutral pH range. Pyrite surface became more hydrophilic upon interaction with bacterial cells whereas sphalerite surfaces became hydrophobic at near neutral pH conditions. In addition, flocculation of pyrite and enhanced dispersion of sphalerite were observed in the pH range of 8–9 after interaction with either bacterial cells or extracellular bioproteins. All those phenomena facilitated the flotation selection with xanthate.

The same research group studied the affinity of different purified protein fractions of extracellular bacterial protein (EBP), isolated from *P. polymyxa*, to quartz, pyrite, chalcopyrite, sphalerite and galena [33]. EBP derived from *P. polymyxa* consisted of various kinds of amino acids (protein groups). Different protein fractions were separated from the EBP and characterized through controlled ammonium sulfate precipitation and SDS-PAGE. The obtained protein fractions exhibited varying adsorption capacity towards quartz, pyrite, chalcopyrite, galena and sphalerite. When bacterial cells were grown in the presence of the different minerals, mineral-specific proteins were squeezed. Protein fractions possessing significant affinity towards surfaces of different minerals were isolated and tested. Appropriate use of fractionated protein groups made pyrite and chalcopyrite hydrophilic while quartz, sphalerite and galena exhibited enhanced surface hydrophobicity after biotreatment. In a similar way protein preconditioning led to selective flocculation of pyrite and chalcopyrite, while galena, sphalerite and quartz were dispersed. Consequently, sphalerite, galena and quartz could be selectively separated from pyrite and chalcopyrite through prior interaction with bacterial proteins.

The above-described studies were limited mainly to use of pure cultures in microflotation tests. Govender and coauthors presented the first study demonstrating on a laboratory scale the potential use of free EPS, extracted from mixed bioleaching microbial consortia, as a viable flotation agent for bioflotation of sulphide minerals [34]. Analyses of the EPS extracted from different bioleach systems (operating at temperatures between 35 and 70 °C and using pyrite, sphalerite and chalcopyrite) showed that the EPS were composed mainly of carbohydrates, proteins and uronic acids. The EPS influence on the flotability of chalcopyrite was determined. The results from the micro-flotation tests indicated that free EPS were more

efficient as a flotation agent than the cells with bound EPS. Tests using free EPS achieved a chalcopyrite recovery of 77% when chalcopyrite was floated alone and 70% during the flotation of a mixture of pure chalcopyrite and pure pyrite, while the recovery was 32% when only sodium isobutyl xanthate was used. The results obtained suggested that free EPS, extracted from mixed bioleaching microbial consortia, can be used as flotation agent during bioflotation of sulphide minerals.

A selective flotation of sphalerite from a sphalerite-galena mineral mixture has been realized using the cellular components of *Bacillus circulans* [35]. Some bacterial species are able to secrete nucleic acids onto their cell surface. This double stranded DNA (dsDNA) has been designated as extracellular DNA to distinguish it from genomic DNA that is intracellular. Thermolysed genomic DNA is designated as single-stranded DNA (ssDNA). Experiments showed that flotation recovery of sphalerite over 80 % could be achieved by using ssDNA as a bio-collector in an anionic buffer. However, when pure ssDNA is used in the flotation of sphalerite from a sphalerite-galena mixture, the flotation recovery was reduced significantly compared to that of sphalerite alone. Even an addition of several fold excess of ssDNA did not enhance the flotation, possibly due to the preferential adsorption of ssDNA on galena than on sphalerite. However, it was found that in the presence of a large excess of other polyanionic species in the thermolysed cell-free supernatant (which consists of all the cellular non-DNA components), ssDNA was left free to bind with sphalerite and facilitate its flotation, while the non-DNA components (teichoic acids and polysaccharides) preferentially bound with galena. Polysaccharides have been found to possess a depressing action in the sulfide minerals flotation. The studies pointed out that the ratio of the bio-depressant and bio-collector likely regulated the flotation recoveries of sphalerite from the mixture of minerals.

A selective separation of sphalerite from a mixture sphalerite/ galena was realized by applying cells and extracellular secretions of *Bacillus megaterium* (*B. megaterium)* after the microorganism adaptation to these minerals [36]. The highest flotation recovery of sphalerite (with a selectivity index (SI) of 24.5) was achieved at using the extracellular secretions acquired after thermolysis of bacterial cells adapted to sphalerite. The amount of extracellular proteins secreted by sphalerite-adapted cells was bigger than that of galena-

adapted or unadapted cells. The hydrophobic proteins present in the soluble fraction of the thermolysed sphalerite-adapted cells facilitated the flotation selectivity of sphalerite. It was found that the protein profile for the unadapted and mineral-adapted cells differred distinctly leading to variation in the yield and nature of EPS. The changes induced in the bacterial cell wall components after adaptation to sphalerite or galena with respect to the contents of phosphate, uronic acid and acetylated sugars were quantified. The role of the dissolved metal ions from the minerals as well as that of the constituents of extracellular secretions (such as phosphate, e-DNA, and surface proteins) in modulating the surface charge of the bacterial cells and of the minerals under study was confirmed by applying different enzymatic analyses. It was discovered that zinc was mainly bioaccumulated, while lead was mainly biosorbed onto the bacterial cells. The sphalerite-adapted cells showed an increase in the phosphate content, while the glucosamine content was increased after adaptation to galena. The availability of additional molecular weight protein fractions as well as the higher amount of extracellular proteins and phosphate content, secreted after adaptation to sphalerite, compared to galena, facilitated the selective separation of sphalerite from galena.

The same authors studied also the role of extracellular constituents of *B. megaterium* as flotation biocollector in sulphide minerals separation [37]. Experiments on the flotation of the individual minerals showed that sphalerite was preferentially floated compared to galena. A SI of 11.7 was attained in the presence of the soluble fraction of the thermolysed cells. It was higher than that found with the intact cells (SI of 6.5) and the insoluble fraction of the thermolysed cells (SI of 9.6). The results of the enzymatic treatment tests revealed that extracellular DNA played a very important role in the selective flotation of sphalerite. It was found that the ssDNA had a higher biocollector capacity in comparison to the dsDNA, leading to higher flotation efficiency. About 95 % recovery of sphalerite could be achieved from the mineral mixture by the combined use of the ssDNA and the non-DNA components of the bacterial cells, resulting to SI of 19.1.

Cells and metabolic products of *Bacillus subtilis* (*B. subtilis*) were used in microbially-induced flocculation and flotation in an attempt

to separate pyrite from galena [38]. Bacterial cells showed an enhanced affinity towards pyrite compared to galena at neutral pH range. Extracellular (EP) and intracellular bacterial proteins were isolated from *B. subtilis* before and after interaction with the minerals and their profiles were established. It was found that the presence of galena during bacterial growth encouraged increased generation of EP that rendered hydrophobic the galena surfaces. The presence of pyrite resulted in enhanced production of exopolysaccharides that render pyrite more hydrophilic. Similar changes in galena and pyrite surfaces were observed also after interaction with cell free extract and EP. Such microbially-induced mineral surface chemical changes can be used to achieve a selective separation through selective flotation/flocculation of minerals without use of any conventional toxic collectors. The settling rate of pyrite was significantly increased after interaction with bacterial cells due to its nearly complete flocculation caused by the adsorption of exopolysaccharides. Settling rates for pyrite were found to be 85, 74 and 72% as a result of interaction with cells, cell free extract and EP respectively. Dispersion of galena was facilitated after interaction with cells, cell free extract and EP due to predominant adsorption of secreted hydrophobic proteins. Galena flotation yield was 92, 73 and 75% after conditioning with bacterial cells, cell free extract and EP respectively. Significant depression of pyrite was observed under similar conditions. Mineral-specific proteins (EP ones) were expressed when bacterial cells were grown in presence of galena. Generation and separation of such mineral-specific proteins points the way for development of suitable bioreagents for selective mineral separation.

Conclusions

Bioflotation of sulfide minerals has been developing during the recent 20-30 years as an answer of the scientific community to the need to extract metals in an environmentally friendly manner. Flotation separation of minerals like pyrite, sphalerite, galena, chalcopyrite, arsenopyrite, molybdenite, pyrrhotite, etc. has been studied. *A. ferrooxidans* (formerly known as *T. Ferrooxidans), T. thiooxidans, P. polymyxa, B. polymyxa, L. Ferrooxidans, B. Megaterium,* and *B. Subtilis* have been and are among the most used microorganisms in the sulfides ores beneficiation. Recently bacteria showing dual action

of biosurfactants and biodepressants, such as *Bacillus pumilus* SKC-2 and *Alicyclobacillus ferrooxydans* and halophilic bacteria (*Halomonas boliviensis*, *Halobacillus sp*. and *Halomonas sp.*) have also been investigated. Studies have included not only whole cells but also cells' parts and / or metabolites.

The interaction between microorganisms and minerals have been studied by means of different methods such as adsorption and flocculation, contact angle, electro-kinetic and zeta-potential measurements, SEM-EDS and FTIR spectroscopy, SDS-PAGE, etc.

Different mechanisms of microbial interaction with minerals' surface leading to essential changes in the surface characteristics of the minerals have been proposed but generally they may be classified as (*a*) microbial cells attachment to minerals surfaces, (*b*) proceeding of oxidation-reduction reactions on the interface mineral / microorganisms, (*c*) adsorption and/or chemical reactions with microbial metabolite products.

In order to go insight of the proposed mechanisms and to be able to direct them in a preferred course, systematic studies on both sides (biochemical and geochemical) of the mineral - bacteria interactions have to be carried out. Different scientific questions have to be answered, such as [39]: (a) Do and how bacteria exploit the energetic heterogeneities of the minerals surface to adhere and/or oxidize/reduce the mineral? (*b*) what is the influence of the mineral particle on the microbe adhesion and the rate of the biotically induced reactions with the participation of the mineral surface? (*c*) How the potential of the mineral (regulated either by pH or potentiostatically) influences the attachment of the whole bacteria cells or of the metabolites and the eventual heterogeneous charge transfer reaction? (*d*) How the presence of the bacteria and the potential of the mineral impact the collector adsorption, its forms and surface equilibria?

Influence of conditions for microorganisms' cultivation on their properties as bioreagents has been studied. It has been established that growth of bacterial cells in the presence of various minerals, i.e., bacteria preadaptation, may involve changes in cell morphology, qualitative and quantitative changes in the secretion of proteins and polysaccharides and surface changes in their levels. Such changes could be used to bring about increased selectivity and desired

mineral separation from multi-mineral mixtures. Currently these procedures are still expensive for an industrial application but represent an interesting perspective. This could pave the way for synthesis of specific environmentally friendly flotation reagents that can replace existing flotation agents.

Influence of operating parameters (such as pulp density, pH and temperature, concentration of bioreagents and their nature, addition to the system of typical flotation reagents, such as xanthate or activators) has been widely studied. However, to date, microbial flotation tests have been primarily carried out at laboratory scale by applying mainly modified Hallimond tube or Microflot tests. Experiments on larger scale are indispensably needed.

Nevertheless, there are more than enough evidences on the possibility to expand the eco-friendly bioflotation process in mineral processing industry.

References

1. **Castro S., Lopez-Valdivieso A., Laskowski J.** 2016, Review of the flotation of molybdenite. Part I: Surface properties and floatability, Int. J. Miner. Process., 148, 48-58.

2. **Rao K.H., Subramanian S.** 2007, Bioflotation and bioflocculation of relevance to minerals bioprocessing / **E. Donati**, **W. Sand** Microbial Processing of Metal sulfides - pp. 267-286. -Dordrecht: Springer.

3. **Sanwani E., Chaerun S.K., Mirahati R. Z., Wahyuningsih T.** 2016, Bioflotation: bacteria-mineral interaction for eco-friendly and sustainable mineral processing, Procedia Chemistry, 19, 666-672.

4. **Pollmann K., Kutschke S., Matys S., Raff J., Hlawacek G., Lederer F. L.** 2018, Bio-recycling of metals: Recycling of technical products using biological applications, Biotechnology Advances, 36, 1048-1062.

5. **Behera S.K., Bafubiandi A.F.M.** 2017, Microbes assisted mineral flotation a future prospective for mineral processing industries: A review, Mineral processing and extractive metallurgy review - An International Journal, 38 (2), 96-105.

6. **Townsley C.C., Atkins A.S., Davis A.J.** 1987, Suppression of pyritic sulphur during flotation tests using the bacterium *Thiobacillus ferrooxidans*, Biotechnol Bioeng., 30 (1), 1-8.

7. **Yelloji R.M.K., Natarajan K.A., Somasundaran P.** 1992, Effect of biotreatment with *Thiobacillus ferrooxidans* on the floatability of sphalerite and galena, Miner Metall Process, 9, 95-100.

8. **Yelloji R.M.K., Somasundaran P.** 1995, Biomodification of mineral surfaces and flotation. / **K.A. Matis** - Flotation science and engineering, Marcel Dekker Inc, New York, 455-472.

9. **Misra M., Bukka K., Chen S.** 1996, The effect of growth medium of *Thiobacillus ferrooxidans* on pyrite flotation, Minerals Engineering, 9 (2), 157-168.

10. **Sharma P.K., Das A., Hanumantha R.K., Forssberg K.S.E.** 1999, *Thiobacillus ferrooxidans* interaction with sulfide minerals and selective chalcopyrite flotation from pyrite. / **B.K. Parekh, J.D. Miller**, -Advances in Flotation Technology, SME/AIME, 147-165.

11. **Nagaoka T., Ohmura N., Saiki H.** 1999, A novel mineral processing by flotation using *Thiobacillus ferrooxidan*s, Process Metallurgy, 9, 335-342.

12. **Hosseini T.R., Kolahdoozan M., Tabatabaei Y.S.M., Oliazadeh M., Noaparast M., Eslami A., Manafi Z., Alfantaz A.** 2005, Bioflotation of Sarcheshmeh copper ore using *Thiobacillus Ferrooxidans* bacteria, Minerals Engineering, 18 (3) 371-374.

13. **Sharma P. ., Hanumantha R.K.** 1999, Role of a heterotrophic *Paenibacillus polymyxa* bacteria in the bioflotation of some sulfide minerals, Mining Metallurgy & Exploration, 16, 35-41.

14. **Sharma P.K., Rao K.H., Forssberg K.S.E., Natarajan K.A.** 2001, Surface chemical characterization of *Paenibacillus polymyxa* before and after adaptation to sulfide minerals, International Journal of Mineral Processing, 62 (1-4), 3-25.

15. **Santhiya D., Subramanian S., Natarajan K.A.** 2001, Surface chemical studies on sphalerite and galena using *Bacillus polymyxa*. Part I: Microbially induced mineral separation, J Colloid Interface Sci, 235, 289-97.

16. **Santhiya D., Subramanian S., Natarajan K.A.** 2001, Surface chemical studies on sphalerite and galena using *Bacillus polymyxa*. Part II: Mechanisms of microbe-mineral interaction, J Colloid Interface Sci, 235, 298-309.

17. **Patra P., Natarajan K.A.** 2006, Surface chemical studies on selective separation of pyrite and galena in the presence of bacterial cell and metabolic products of *Bacillus polymyxa*, J Colloid Interface Sci, 298, 720-729.

18. **Santhiya D., Subramanian S., Natarajan K.A.** 2000, Surface chemical studies on galena and sphalerite in the presence of *Thiobacillus thiooxidans* with reference to mineral beneficiation, Miner Eng 13 (7), 747-763.

19. **Chandraprabha M.N., Natarajan K.A.** 2004, Selective separation of pyrite and chalcopyrite by biomodulation, Colloids and Surfaces B, 37, 93-100.

20. **Chandraprabha M.N., Natarajan K.A.** 2006, Surface chemical and flotation behaviour of chalcopyrite and pyrite in the presence of *Acidithiobacillus thiooxidans*, Hydrometallurgy, 83, 146–152.

21. **Chandraprabha M.N., Natarajan K.A., Somasundaran P.** 2004, Selective separation of arsenopyrite from pyrite by biomodulation in the presence of *Acidithiobacillus ferrooxidans*, J Colloid Interface Sci, 276, 323-332.

22. **Chandraprabha M.N., Natarajan K.A., Somasundaran P.** 2005, Selective separation of pyrite from chalcopyrite and arsenopyrite by biomodulation using *Acidithiobacillus ferrooxidans*, Int J Miner Process, 75, 113-122.

23. **Mehrabani J.V., Noaparast M.** 2011, Evaluation of the replacement of NaCN with *Acidithiobacillus ferrooxidans* in the flotation of high-pyrite, low-grade lead–zinc ore, Separation and Purification Technology, 80 (2), 202-208.

24. **San Martín F., Kracht W., Vargas T., Rudolph M**. 2020, Mechanisms of pyrite biodepression with *Acidithiobacillus ferrooxidans* in seawater flotation, Minerals Engineering, 145, 106067.

25. **Vilinska A.K., Rao K.H**. 2008, *Leptosririllum ferrooxidans*-sulfide mineral interactions with reference to bioflotation nad bioflocculation, Trans. Nonderrous Met. Soc. China, 18, 1403-1409.

26. **Díaz-López C. V., Pecina-Treviño , Orrantia-Borunda E**. 2012, A study of bioflotation of chalcopyrite and pyrrhotite mixtures in presence of *L. ferrooxidans*, Canadian Metallurgical Quarterly, The Canadian Journal of Metallurgy and Materials Science, 51 (2), -, https://doi.org/10.1179/0008443312Z.00000000025

27. **Vasanthakumar B., Ravishankar H., Subramanian S.** 2017, Selective bio-flotation of sphalerite from galena using mineral - adapted strains of *Bacillus subtilis* Minerals Engineering, 110, 179–184.

28. **Consuegra G.L., Kutschke S., Rudolph M., Pollmann K.** 2020, Halophilic bacteria as potential pyrite bio-depressants in Cu-Mo bioflotation, Minerals Engineering, 145, 106062.

29. **Subramanian S., Santhiya D., Natarajan K.A.** 2003, Surface modification studies on sulphide minerals using bioreagents, Int. J. Miner. Process., 72, 175– 188.

30. **Patra P., Natarajan K.A.,** 2003, Microbially-induced flocculation and flotation for pyrite separation from oxide gangue minerals, Minerals Engineering, 16, 965–973.

31. **Partha P. Natarajan K.A.,** 2004, Microbially induced flocculation and flotation for separation of chalcopyrite from quartz and calcite, Int. J. Miner. Process., 74, 143– 155.

32. **Patra P., Natarajan K.A.** 2004, Microbially induced flotation and flocculation of pyrite and sphalerite, Colloids and surfaces. B, Biointerfaces, 36 (2), 91-99.

33. **Partha P., Natarajan K. A.** 2008, Role of mineral specific bacterial proteins in selective flocculation and flotation, Int. J. Miner. Process., 88, 53–58.

34. **Govender Y., Gericke M.** 2011, Extracellular polymeric substances (EPS) from bioleaching systems and its application in bioflotation, Minerals Engineering, 24, 1122–1127.

35. **Vasanthakumar B., Ravishankar H., Subramanian S.** 2012, A Novel Property of DNA – as a bioflotation reagent in mineral processing. PLoS ONE 7 (7), e39316. doi:10.1371/journal.pone.0039316

36. **Vasanthakumar B., Ravishankar H., Subramanian S.** 2013, Microbially induced selective flotation of sphalerite from galena using mineral-adapted strains of *Bacillus megaterium*, Colloids and Surfaces B: Biointerfaces, 112, 279-286.

37. **Vasanthakumar B., Ravishankar H., Subramanian S.** 2014, Basic studies on the role of components of *Bacillus megaterium* as flotation biocollectors in sulphide mineral separation, Applied Microbiology and Biotechnology, 98, 2719-2728.

38. **Sarvamangala H., Natarajan K.A., Girisha S.T**. 2013, Microbially-induced pyrite removal from galena using *Bacillus subtilis*, International Journal of Mineral Processing, 120, 15-21.

39. **Hanumantha R.K.**, **Vilinska A., Chernyshova I.V.** 2010, Minerals bioprocessing: R & D needs in mineral biobeneficiation, Hydrometallurgy, 104, 465-470.

SIMULATION OF SHOCK WAVES FROM EXPLOSION OF MIXTURE EXPLOSIVE CHARGES

N. Remez
National Technical University of Ukraine "Igor Sikorsky Kyiv Polytechnic Institute", Dr. Sc., Prof., Professor, Ukraine
A. Dychko
National Technical University of Ukraine "Igor Sikorsky Kyiv Polytechnic Institute", Dr. Sc., Prof., Professor, Ukraine
V. Bronytskyi
National Technical University of Ukraine "Igor Sikorsky Kyiv Polytechnic Institute", Ass., Ukraine
S. Kraychuk
Rivne State University of Humanities, Ph.D., Ass. Prof., Ukraine

The present paper provides the modelling of the explosion of the charges of the traditional (trotyl) and new blended explosive substances: polymix GR1/8 (74 %)+KRUK2 (26 %), compolite GS6, polymix GR4-T10. As a result of the research, it has been established that when using TNT a specific impulse is formed, which is by 40 % more than an explosion of new mixed explosives, and the safe distance from the source of the explosion of such explosives is increased by 25-50 %. On the basis of the established dependences of excess pressure, the specific impulse on the type and mass of charge, as well as the distance from the epicentre of the explosion, an engineering method has been developed for calculating dangerous parameters of the explosion impact on the environment.

Introduction

Due to an increase in volumes of mining operations and coming of quarry fields to protected ecosystems, there is a question about their safety regarding intense dynamic loads during the explosion of explosives (EX). However, blasting operations are characterised by a small coefficient of explosive energy use, an increase in the requirements of technological and environmental safety, and the economic inactivity of the use of expensive industrial EX. Therefore, in recent years several tens of new non-TNT EX mixtures have been developed. At the same time, conclusions about their technological efficiency and environmental safety are based on visual observation of experimental and practical results of explosions.

Special attention should also be devoted to the territory where, in

addition to environmental problems inherent in production processes, there are other types of hazards, for example, related to the carrying out military operations (bombing, explosives of military stockpiles of ammunition, mines, the use of phosphate mines, the destruction of infrastructure of settlements, etc.). Therefore, scientists urgently raise the issue of the safety of natural-technogenic environment in the spread of airborne shock waves.

In this regard, the study of parameters of airborne shock waves (ASW) affecting the protected ecosystems in the explosions of new blended EX, and prediction of the degree of damage of technogenic systems and living organisms represent actual scientific and practical tasks.

Literature review and problem statement

As it is known, the main parameters of the airborne shock wave (ASW), which determine its destructive and damaging effect, are excess pressure ΔP, Pa; speed pressure ΔPs, Pa; specific pressure impulse I, Pa·s; time of shock wave action, τ_+, ms.

Excess pressure at the front of the shock wave is the main parameter that determines the destructive force of the shock wave. This is the difference between the maximum P and the atmospheric pressure P_0: $\Delta P=P-P_0$.

For the determination of excess pressure in engineering practice, various modifications of the empirical formula of M.A. Sadovsky [1], [2], used for charge of TNT, are widely implemented. For other explosives, the so-called energetic TNT-coefficient is used to determine the equivalence of the explosive. However, these formulas do not correspond to the theory of dimensions and similarity; therefore, their application can lead to unsatisfactory results.

The works of many scientists are devoted to the research into the definition and assessment of the impact of airborne shock waves. Most of the research focuses on the underground and terrestrial explosions and examines the damaging factors of a nuclear explosion. Methods for determining the individual parameters of the explosion and assessing their impressive impact on objects of the environment during the explosion are developed by Ya.M. Eisenberg, A.N. Birbaer, V.V. Boyko, O.O. Vovk, K.V.Yegupov, Yu.I. Kalyukh,

M.A. Klyachko, S.V. Polyakov, Yu.I. Nemchinov, O.A. Savinov, A.E. Sargsyan, P.Z. Lugovoi, V.G. Kravets, V.S. Kukunaev, N.S. Remez, L.R. Stavnetsar, A.G. Tyapin, V.G. Bezdenkov, A.M. Trofimchuk, A.M. Uzdin, S.G. Shulman, N. Newmark, E. Rosenblueit and others.

The research of these scientists established such damaging for environment factors as funnel on the surface of the ground, the impact of the explosive shock wave, the seismic effect of the explosion on objects, the impact of the gas-dust cloud raised in the air during the explosion, thermal radiation, and the damaging effect of fragments and debris on security objects.

The studies of many scientists are devoted to the investigation of explosion damaging factors. Thus, in the publication [3], the estimation of the ASW action in an emergency explosion in the stock of ammunition is described, the main physical processes are described with the action of the ASW on surrounding objects, the basic parameters of the ASW are defined: excess pressure at the front of the ASW, impulse of pressure at the compression phase, action of the ASW and a safe distance at shock wave action. Formulas and dependences obtained in the research can be adapted and used to study an explosion case, for example, a terrorist act.

In the work by Vadulina, Achyvakov and Sanimov [4], the main bases of human life insurance during the explosion of the pipeline are considered, the dependence of the conditional probability of human damage on the change in excess pressure of the shock wave of the explosion is studied.

In the works [5]-[8], the influence of explosive lesions on the human organism is examined during technogenic catastrophes and terrorist acts.

The research by Chernozubenko, Kuprinenk and Bisik [9] provides the analysis of the damage factors on the human body after the explosion for the possibility of providing a complex system of personal protection. The distribution of injuries of body parts of military personnel during an explosion have been graphically depicted. The damage factors of the blow-ups of the explosive device have been considered, such as primary (fragments of an explosive device and a shock wave) and secondary factors (personnel fall from equipment, damage by buildings and structures, stress and heart attacks).

Study [10] helped establish the mechanogenes is of the impact of the damage factors of explosive devices on the human body. The results of the analysis showed that the main types of damage were injuries of the lower extremities, internal organs, and head.

Kryuchkova, Arzhavkina and Zhekalov in their research [11] presented results of studying dynamics of physical work ability and behavioural reactions of white rats at different intervals of the first day after damage by air shock wave of light and medium severity.

In the works by Luchko, Remez, Vorobiov, new types of EX were described [12]-[15]. The authors also compared different variants of charging pores and argued about the perspective use of these EX. However, the issue of the impact of air shock waves of new blended EX remains open.

Numerical modelling

The goal of the research is the theoretical substantiation of the parameters of air shock waves during explosions of charges of traditional and new blended EX to predict their destructive effect on the environment.

To achieve the goal, the following objectives are set:

- to carry out mathematical modelling of the process of propagation of air shock waves during explosions and their interaction with natural-technogenic ecosystems;

- to establish the mathematical dependences of parameters of air shock waves on the type and mass of the explosive and the distance from the source in order to calculate their effect on living organisms.

An explosion of the spherical charge of EX in the air is considered. The motion of detonation products and air is described by a system of differential equations that determine the laws of conservation of the amount of motion, mass and impulse [2]

$$\frac{\partial u}{\partial t}+u\frac{\partial u}{\partial t}+\frac{1}{\rho}\frac{\partial p}{\partial r}=0, \quad (1)$$

$$\frac{\partial \ln \rho}{\partial t}+u\frac{\partial \ln \rho}{\partial r}+\frac{\partial u}{\partial r}\frac{Nu}{r}=0, \quad (2)$$

$$\frac{\partial\left(\frac{p}{\rho^{\gamma}}\right)}{\partial t}+u\frac{\partial\left(\frac{p}{\rho^{\gamma}}\right)}{\partial r}=0, \quad (3)$$

where r - coordinate, u - speed, p - pressure; t - moment of time; γ - entropy index; ρ - density.

Expansion of detonation products takes place according to binomial is entropy [2]

$$P = A\rho^N + B\rho^{\gamma+1} \quad (4)$$

Constants in equation (2) characterise this type of EX. The initial conditions of this task are

$$u=0,\ p=p_n,\ \rho=\rho_n \text{ at } 0 \le r < r_0, \quad (5)$$

$$u=0,\ p=0,\ \rho=\rho_0 \text{ at } r_0 \le r, \quad (6)$$

where r_0 - charge radius, p_n,ρ_n - pressure and density of detonation products in the explosion, ρ_0 - density of air.

The boundary conditions are as follows: *1* - the condition of continuity of speed u and pressure on the moving contact boundary "products of detonation - air"; *2* - the condition of "non-penetration"- the speed on the charge axis is zero. For the approximation of the system of differential equations (1)-(3) with the corresponding initial and boundary conditions, the method of finite differences was used based on the finite-difference scheme of the type "cross" [13, 16-19] of the second order of accuracy in spatial and temporal coordinates.

To calculate the effect of traditional and new blended explosives on the shock wave parameters, the following EX are studied [12-14]: trotyl, polymyx GR⅛ (74%)+KRUK2 (26%), compolite GS6, polymix GR4-T10 (Table 1).

Table 1

Parameters of Explosion of TNT and New Blended EX

EX	Parameters						
	p_n, GPa	Q, KJ/kg	γ	ρ_0, kg/m^3	A	$B\cdot10^{-5}$	N
Trotyl	9.8	4184	1.25	1600			3.12
Polymyx GR1/8	4.54	3355.7	1.242	1000	59.35	0.604	2.48
Compolite GS6	1.75	3919.7	1.235	852	7.671	1.638	2.24
Polymix GR4-T10	2.71	3864.4	1.245	872	5.67	1.279	2.73

As a result of the numerical solution to the problem, graphic functional dependences of the change of excess pressure on the distances of the spread path for different charge radii of different types of EX were obtained. For example, in Fig. 1 r_0=0.2 m.

As a result of calculations, it is clear that excess pressure of air shock wave formed at explosion of traditional explosive substance TNT is much larger than during explosion of new blended EX.

At a distance of the air-shock wave spreadin1 m in the explosion of charges with a radius of 0.1 m and 0.2 m, the excess pressure for TNT is by 2 times greater than for new blended EX. At a distance of 1.5 m and 2 m, the difference is reduced to 90 %–75 %. At a distance of 5 m from the epicentre of the explosion, the excess pressures are almost the same. This is due to the fact that in the near area of explosion, TNT has significantly larger parameters of the explosion (pressure, density, heat of radiation, etc.), but with an increase in the distance from the explosive cavity the waves formed by the explosion of TNT expire considerably more intensively than from blended EX because in the explosion of the charges of TNT the energy losses at the front of the shock wave are much higher.

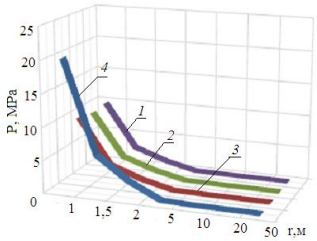

Fig. 1. Dependence of the change in excess pressure of the air shock wave on the explosion centre at r_0=0.2 m: 1 - polymix GR1/8; *2* - compolite; *3* - polymix GR4-T10; *4* - TNT

From this we can conclude that in the distant zone of the explosion, the parameters of air shock waves are weakly dependent on the type of EX, and are determined by the mass of charge.

Thus, it can be stated that a traditional explosive substance, such as TNT, forms a stronger excess pressure during the explosion, and therefore the force of destruction of surrounding objects is higher than in new blended explosives. The application of the polymix GR4-T10, the compolite GS6 and the polymix GR1/8 (74 %)+KRUK2 (26 %) during blasting works is safer in terms of excess pressure formation.

After comparing the explosion of charges of traditional and new blended EX charges with excess pressure at the shock wave front, an impulse for the same explosives was calculated. As an example, Fig.

2 shows the dependence of the impulse on excess pressure during the explosion of charges of polymix GR4-T10 with different radii.

As a result of calculations and graphic representation of the dependence of impulse on excess pressure, it is evident that with an increase in excess pressure the impulse of air shock wave increases.

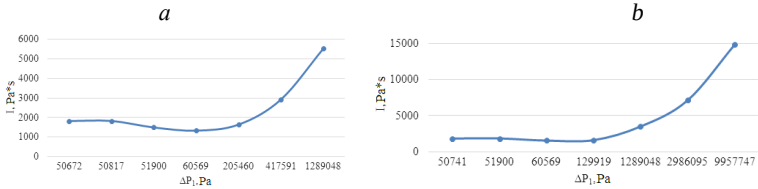

Fig. 2. Dependence of the impulse from the excess pressure in the explosion of charges of polymix GR4-T10 with different radii: *a* - at r_0=0.1 m; *b* - r_0=0,2 m

Impulse of the air shock wave formed during the explosion of a traditional explosive - TNT - is more by 40 % than during the explosion of new blended explosives for all investigated charge radii at a distance of 1 m from the epicentre of the explosion. At a distance of 1.5 m and 2 m, this difference is 30 % and 20 %, respectively. At a distance of 5 m, the value of the impulse is almost the same for charges with radii of 0.1 m and 0.2 m, but for a charge with a radius of 1 m - at a distance from the epicentre of the explosion from 1.5 m to 20 m, the difference is 40 %, and from 20 m - 20 %.

Consequently, a traditional explosive substance, such as TNT, forms a stronger impulse during the explosion, and therefore force of destruction of surrounding objects is higher than in new blended explosives. The application of the polymix GR4-T10, the compolite GS6 and the polymix GR1/8 (74 %)+KRUK2 (26 %) during blasting works is safer from the point of view of impulse formation.

The results of calculations of excess pressure were compared with the characteristics of the destruction of structures at the explosion of TNT and the new mixed explosives, depending on the distance of the propagation wave and the radius of charge (Tables 2, 3).

Table 2

Destruction (damage) of elements of constructures sensitive to maximum excess pressure at TNT explosion

Elements of constructures	Nature of destruction (damage)	ΔP_1, Pa	Explosive wave propagation distance, r_H, m		
			r_0=0, 1m	r_0=0,2 m	r_0=1m
1	2	3	4	5	6
Windows (large and small)	Glass beating; possible destruction of window frames	35000-70000	5 and more	10 and more	more 50
Lightweight wall filling with wavy asbestos panels.	Destruction	70000-140000	5	6,5-10	50
Wavy steel and aluminum panels	Disruption of connections with subsequent severe deformation	70000-140000	5	6,5-10	50
Brick walls of 20 - 30.5 cm thick (without reinforcement)	Destruction caused by shear deformation and displacement	490000-560000	1,5-2	3,5	17-18
Wall paneling made of wooden panels (standard design houses)	Disruption of connections and failure of wooden panels	70000-140000	5	6,5-10	50
Concrete or slag concrete walls of 20-30,5 cm thick (without reinforcement)	Destruction of the walls	140000-210000	2,5-3	5-6	25-31,5
Light ground vaulted structures made of corrugated steel panels of 6 - 7.5 m long, with thickness of soil shattering over 0.9 m above the vault	Complete destruction	2450000-2800000	1 and less	2	10,5-11
	Damage to the part of the vault from the side facing the explosion	2100000-2450000	less 1	2	11-11,5
	Deformation of end walls and arch; can damage the front door	1400000-1750000	1-1,5	2,5	25-27
	Damage to the ventilation system and the front door	70000-100000	5	6,5-8	50
Lightweight concrete ground or recessed shelter with soil crumbling at least 0.9 m thick (panels of 5-7.5 cm thick); beams are located at a distance of 1.2 m	Destruction of building	2100000-2450000	less 1	2	11-11,5
	Partly destruction of building	1750000-2100000	1-1,5	2-2,5	25-31,5
	Deformation of panels, formation of a large number	1000000-1750000	1-1,5	2,5	12-14

from each other	of cracks, depressions into separate panels				
	Formation of cracks, can cause damage to the front door	70000-100000	5	6,5-8	50
Planes on the ground	Complete destruction	420000	1,5-2	3-3,5	19-19,5
	Damage when restoration is not economic feasible	280000	2-2,5	4	22,5
	The plane needs major repairs to restore	210000	2,2-3	4,5	25-25,5
	No repair or minor one is required	70000	5	9,5-10	50

Table 3

Destruction (damage) of elements of constructures sensitive to maximum excess pressure at new EX explosion

Elements of constructures	Nature of destruction (damage)	ΔP_1, Pa	Explosive wave propagation distance, r_H, m		
			r_0= 0,1 m	r_0= 0,2 m	r_0= 1 m
1	2	3	4	5	6
Windows (large and small)	Glass beating; possible destruction of window frames	35000-70000	5-50	10-50	50 and more
Lightweight wall filling with wavy asbestos panels.	Destruction	70000-140000	2,5-4	5-8	24-40
Wavy steel and aluminum panels	Disruption of connections with subsequent severe deformation	70000-140000	2,5-4	5-8	24-40
Brick walls of 20 - 30.5 cm thick (without reinforcement)	Destruction caused by shear deformation and displacement	490000-560000	1,5	2,5-3	14-14,5
Wall paneling made of wooden panels (standard design houses)	Disruption of connections and failure of wooden panels	70000-140000	2,5-4	5-8	24-40
Concrete or slag concrete walls of 20-30,5 cm thick (without reinforcement)	Destruction of the walls	140000-210000	2	4-4,5	20

Light ground vaulted structures made of corrugated steel panels of 6 - 7.5 m long, with thickness of soil shattering over 0.9 m above the vault	Complete destruction	2450000-2800000	less 1	3,5	8,5-9
	Damage to the part of the vault from the side facing the explosion	2100000-2450000	less 1	4	9-9,5
	Deformation of end walls and arch; can damage the front door	1400000-1750000	less 1	4,5	10-10,5
	Damage to the ventilation system and the front door	70000-100000	2,5-3	6-8	29-40
Lightweight concrete ground or recessed shelter with soil crumbling at least 0.9 m thick; beams are located at a distance of 1.2 m from each other	Destruction of building	2100000-2450000	less 1	4	9-9,5
	Partly destruction of building	1750000-2100000	2	4-4,5	20
	Deformation of panels, formation of a large number of cracks, depressions into separate panels	1000000-1750000	1	5	10-11,5
	Formation of cracks, can cause damage to the front door	70000-100000	less 1	4,5-8	29-40
Planes on the ground	Complete destruction	420000	1,5	3	15,5
	Damage when restoration of plane is not economically feasible	280000	1,5-2	3,5	18
	The plane needs major repairs to restore	210000	2	4	20
	No repair or minor repair and replacement is required	70000	4	8	40

Comparison of the results of the calculations of the excess pressure formed during explosion of the TNT and the new mixed explosives indicates that, if the same pressure is generated with the same EX radius, the distance at which the structures are destroyed is more than for TNT. For example, when the walls are destroyed by the pressure of 140000-210000 Pa at r_0=0.1 m, the explosion of new EX occurs at a distance of 2 m, and during the explosion - at a distance of 2.5-3 m.

Thus, the use of explosives such as polymix GR4-T10, compolite GS6, and polymix GR⅛ (74%)+KRUK2 (26%) is safer to maintain the integrity of structures at greater distances.

Table 4 presents the results of calculations of the dependence of the degree of damage to people during the explosion of TNT and new blended EX on the distance of the spread of an explosive wave for different charge radii.

Table 4

The Degree of Damage to People in the Explosion of Different EX

Degree of damage	ΔP_1, Pa	Spread of an explosive wave, r_H, m (*)		
		r_0=0.1 m	r_0=0.2 m	r_0=1m
1	2	3	4	5
Death of people as a direct effect of ASW Death of people under the ruins of buildings Death of people as a result of smite from solid objects	190000	2.5-3 3-3.5	5-6 5,5-6,8	25-31,5 47-48
Serious damage as a result of ASW action Serious damage when the building collapses or the body moves by an explosive wave	69000-76000	4.5-6 4.7-7.8	9.5-10.5 7.3-8.5	49.5-50.5 more than 50
Serious damage as a result of eardrums and lungs under action of an explosive wave Defeat by fragments and ruins of the building	55000	8-9 10-11	16-16.5 more than 50	more than 50
Defeat by fragments and ruins of the building. Probability of rupture of drum chambers 10 %	24000	more than 50	more than 50	more than 50
Temporary loss of hearing or injuries as a result of secondary effects of an explosive wave (collapse of the building and body transference) Fatal or serious damage from direct exposure of an explosive wave is unlikely	16000	more than 50	more than 50	more than 50
Injuries associated with the destruction of glass and damage to the walls of the building	5900–8300	more than 50	more than 50	more than 50

* The numerator contains data for the TNT, in the denominator – for new compound substances.

From Table 4, it can be concluded that the use of such a traditional explosive like TNT is more dangerous to human health than the use of new blended explosives, as, for example, the death of people

as a result of direct exposure to ASW from the time of the explosion of EX with r_0=0.1 m at an excess pressure of 190 KPa for TNT will take place at a distance of 2.5-3 m, and during the explosion of new blended EX - at a distance of 3-3.5 m.

In work [20] with the experimental data, the degree of contusions (DC) in dogs caused by the action of air shock waves was analyzed, which came with the following values of maximum and average pressure. At the same time, the authors proposed the use of parameter $P_{ср}=I_{уд}/t$, equal to the ratio of the specific impulse to the time of action of the ASW because the spread of experimental data is much smaller than for P_{max}. In order to assess the damage of people in the explosion of EX, in emergencies or terrorist acts, it is important to assess the likelihood of getting a damage from the ASW and the degree of contusion, and the most acceptable is the class of parametric laws of damage (PLD) using the Weibull-Gnedenko distribution. To solve this problem, the recalculation of the degree of concussion at certain parameters of air shock waves was performed in the research.

For practical application of theoretical results of the spread of ASW and their effects on environment, the method of calculating the safe parameters of the explosion was developed.

To construct dependence of $P_{ср}$ from relative distance calculations were carried out, for example, for TNT they are given in Table 5.

Table 5

Dependence of the pressure on the relative distance for TNT

r,м	$\sqrt[3]{m}/r$			$\Delta P_{ср}$, *Pa*		
	m=6,7kg	*m*=13,4kg	*m*=6702kg	*m*=6.7kg	*m*=13.4kg	*m*=6702kg
1	1.885	2.375	18.848	$2.6\cdot10^6$	$20.13\cdot10^6$	$2.5\cdot10^9$
1.5	1.26	1.58	10.57	$0.8\cdot10^6$	$6\cdot10^6$	$7.44\cdot10^8$
2	0.943	1.188	9.424	$0.36\cdot10^6$	$2.6\cdot10^6$	$3.14\cdot10^8$
5	0.38	0.48	3.77	$70.7\cdot10^3$	$211\cdot10^3$	$2\cdot10^7$
10	0.19	0.24	1.9	$53\cdot10^3$	$60.7\cdot10^3$	$2.56\cdot10^6$
20	0.095	0.12	0.95	$50.9\cdot10^3$	$53.2\cdot10^3$	$0.36\cdot10^6$

On the basis of the established dependences of excess pressure, specific impulse from type and mass of EX, as well as distance from the source of the explosion, nomogram to determine the distances or masses of EX, safe for living organisms was built (Fig.3): *1* - trotyl, 2 - polymix GR⅛ (74%)+KRUK2 (26%), *3* - compolite GS6, *4* - polymix GR4-T10. Following degrees of concussion are marked: 1 - light, *2* - medium, *3* - hard, *4* - difficult edge, *5* - death.

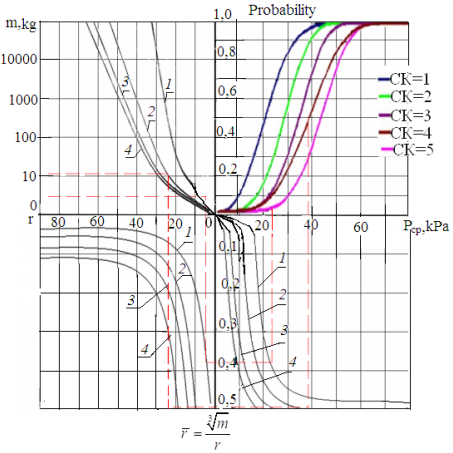

Fig. 3. Nomogram to determine the safe parameters of explosion of different EX for dogs, rabbits, pigs: *1* - trotyl; *2* - polymix GR⅛ (74 %)+KRUK2 (26 %); *3* - the compolite GS6; *4* - the polymix GR4-T10

Figure 4 presents nomograms for determining safe parameters of explosion for people in explosion of charges of different types of EX. Numbering of curves in Fig.4 corresponds to the numbering of Fig.3.

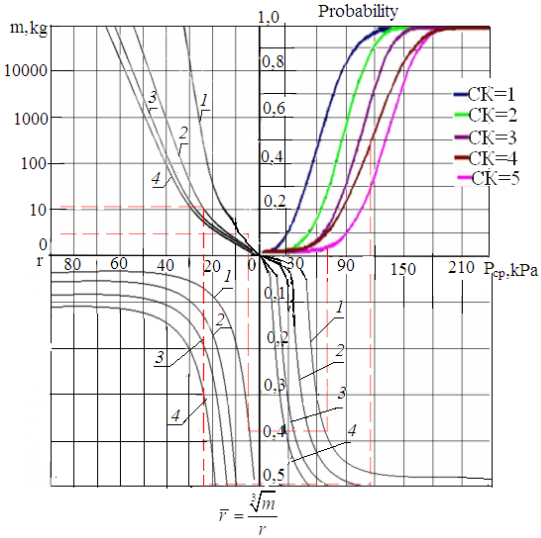

Fig. 4. Nomogram to determine the safe parameters of explosion of different EX for people: *1* – trotyl, *2* – polymix GR⅛ (74 %)+KRUK2 (26 %), *3* – the compolite GS6, *4* – the polymix GR4-T10

Results and discussion

As it is known, the main parameters of the air shock wave, which determine its destructive and striking effect, are excess pressure, speed pressure, specific impulse of pressure and action time of the positive phase of the shock wave.

Today, new non-TNT blended EX, the technical and economic efficiency of which is proven, become a widespread practice. However, there is no theoretical substantiation of the environmental safety of the use of these EX and the interaction of airborne explosive waves during explosive operations with elements of ecosystems.

On the basis of mathematical modelling, the research investigates the dependence of the change in parameters of air airborne explosive waves on the mass of charge of explosive at different distances from the epicentre of the explosion. For a charge weighting10 kg, the following dependences for the ASW parameters are established, i.e., for the TNT: excess pressure $y = 9901.3x^{0.7034}$, pressure of the speed throng $y=423.12x^{1.301}$, specific impulse $y=0.63x^{0.6667}$, action time of the positive phase of the wave $y=4.6171x^{0.1667}$; for the polymix GR4-T10: excess pressure $y=7932.4x^{0.647}$, pressure of the speed throng $y=250.87x^{1.2262}$; for the compolite GS6: excess pressure $y=7932.4x^{0.647}$, pressure of the speed throng $y=250.87x^{1.2262}$; for the polymix GR⅛ (74 %)+KRUK2 (26 %): excess pressure $y=7457.5x^{0.636}$, pressure of the speed throng $y=218.73x^{1.211}$.

For a charge weighting 50 kg, the following dependences for the ASW parameters are established, i.e., for the TNT: excess pressure $y=4\cdot10^{6}x^{-1,53s}$, pressure of the speed throng $y=5\cdot10^{7}x^{-2,00s}$, specific impulse $y=85,545x^{-1}$, action time of the positive phase of the wave $y=2,8025x^{-0,5}$; for the polymix GR4-T10: excess pressure $y=2\cdot10^{6}x^{-1,424}$, pressure of the speed throng $y=1\cdot10^{7}x^{-2.803}$; for the compolite GS6: excess pressure $y=2\cdot10^{6}x^{-1.426}$, pressure of the speed throng $y=1\cdot10^{7}x^{-2.806}$; for the polymix GR⅛8 (74 %)+KRUK2 (26 %): excess pressure $y=2\cdot10^{6}x^{-1.407}$, pressure of the speed throng $y=1\cdot10^{7}x^{-2.772}$.

Based on the comparison of the calculated results and the degree of damage we have, the use of an explosive such as TNT is more dangerous to human health than the use of new blended explosives because, for example, the death of people as a result of direct influence of ASW in explosion of EX with r_0=0.1 m at an excess pressure of 190 KPa for

TNT takes place at a distance of 2.5-3 m, while during the explosion of new blended EX -at a distance of 3-3.5 m.

Based on the established dependences of excess pressure, specific impulse from the type and mass of charge of EX, as well as the distance from the epicentre of the explosion, an engineering method was developed for calculating the dangerous parameters of the explosion on the environment.

Conclusions

1. The effective calculation method based on numerical simulation of the explosion of spherical charges of traditional and new explosives in the air has been developed, which allows obtaining the parameters of airborne shock waves, depending on time, distance, mass of charge and type of EX.

2. Based on the mathematical modelling of the spread of airborne shock waves and their interaction with natural-technogenic environment, the influence of traditional and new blended explosives on the parameters of ASW has been studied. As a result of numerical calculations, it has been established that during the explosion of charges of traditional EX (trotyl), a stronger excess pressure (by an average 85 %) than in the new blended EX is formed. Consequently, the use of the polymix GR4-T10, compolite GS6 and polymix GR⅛(74 %)+KRUK2 (26 %) during blasting works is safer in terms of excess pressure formation.

3. The functional (degree) dependences of excess pressure on the distance of the source of the explosion and the charge and impulse mass on the excess pressure and the charge radius for different types of EX have been determined.

4. It has been established that with an increase in excess pressure, the impulse of the airborne shock wave increases. When using TNT, a specific impulse is generated, which is much stronger (by 40 %) than that of blasting new blended explosives.

5. It has been established that the destructive and damaging effect of the explosion charge of TNT is much greater than of the new blended EX. The safe distance from the source of the explosion of such charges increases by25-50 %.

6. The engineering methodology has been developed for calculat-

ing the dangerous parameters of the explosion on the environment based on the established dependences of excess pressure, specific impulse on the type and mass of charge of EX, as well as the distance from the epicentre of the explosion.

References

1. **Sadovsky, M.A.** (1952). The Mechanical Action of Air Shock Waves of Explosion According to Experimental Studies: Physics of Explosion. Moscow: Publishing of Academy of Sciences of the USSR.

2. **Baum, F.A., Orlenko, L.P., Stanyukovich, K.P., Chelyshev, V.P., & Schechter, B.I.** (1975). Physics of the Explosion. Moscow: Science.

3. **Sidorenko, V.L., & Azarov, S.I.** (2008). Calculation of the effects of explosive shock waves on a person during an explosion in the stock of ammunition. Systems of Armament and Military Equipment, 1, 70-73.

4. **Vadulina, N.V., Achivakova, L.R., Salimov, A.O., Abdrakhmanova, K.N., & Abdullin R.S.** (2017). Insuring safety pneumatest of the pipeline. Oil and Gas Business, 4, 109–124. DOI: http://dx.doi.org/10.17122/ogbus-2017-4-109-124

5. **Minnullin, I.P., Fomin, N.F., & Nechaev, E.A.** (2010). Mine-explosive defeats – the global problem of humanity. Medicine of Catastrophes, 2, 34-36.

6. **Shapovalov, V.M., & Samokhvalov, I.M.** (2012). Explosive injuries due to man-made disasters and terrorist acts. War-Medical Journal, 1, 25-33.

7. **Kaptsov, V.A., Kulbacinskiy, V.V., Bazaz'yan, A.G., Romanov, V.V., & Semenchukov, A.V.** (2010). Probable injuries and specifics of preparedness planning for and management of acts of terrorism on railways. Medicine of Catastrophes, 1, 15-18.

8. **Shapovalov, V.M., Samokhvalov, I.M., & Lytaev, S.A.** (2012). Amazing factors, mechano-pathogenesis, clinical manifestations of explosive damage of peacetime. Quality Management in the Sphere of Health Care and Social Development,3, 46-51.

9. **Chernozubenko, A.V., Kuprinenko, A.N., & Bisyk, S.P.** (2014). Study of damaging factors sap mine explosive devices on the human body. Systems of Armament and Military Equipment, 2, 39-44.

10. **Ivanitski, A., & Petriko, H.** (2014). Assessment of consequences of impact of emergency explosion of fuel-air mixture on a person. Bulletin of the Command-Engineering Institute of the Ministry of Emergencies of the Republic of Belarus, 1 (19), 67-72.

11. **Kriuchkova, A.S., Arzhavkina, L.G., Zhekalov, A.N., Protasov, O.V., & Chernyavskiy, E.A.** (2015). Influence of blast wind injury of minor and medium severity on physical efficiency and behavioural reactions in animals. Herald of the Russian Military Medical Academy, 1 (49), 169-172.

12. **Luchko, I.A., Remez, N.S., & Luchko, A.I.** (2010). Wave processes in soil massifs during explosions of new blended explosives. Bulletin of NTUU "KPI". Series "Mining", 19, 24-25.

13. **Luchko, I.A., Remez, N.S., & Luchko, A**.I. (2011). Mathematical modeling

of the explosion in soils and rocks. Kyiv: NTUU “KPI”.

14. **Remez, N.S., Luchko, I.A., &Luchko, A.I**. (2006). Efficiency of application of new non-destructive explosives at consolidation of soil bases. SRI of Building Constructions, 64, 296-301.

15. **Vorobiov, V.D., &Tverda, O.Y.** (2012). Justification of the criterion for selecting a safe and effective type of explosives in mass explosions in quarries. Problems of Labor Protection in Ukraine, 22, 56–64.

16. Remez, N., Dychko, A., Kraychuk, S., Ostapchuk, N., & Yevtieieva, L. (2018). Simulation of seismic explosion waves with underground pipe interaction. Latvian Journal of Physics and Engineering, 3, 27–33. DOI: http://dx.doi.org/10.2478/lpts-2018-0011

17. **Remez, N., Dychko, A., & Yevtieieva, L.** (2018). Stress-deformed state of soil at the explosion of cylindrical charge of new industrial mixed explosives. In: Development of Scientific Foundations of Resource-Saving Technologies of Mineral Mining and Processing. Sofia: Publishing House St.Ivan Rilski.

18. **Remez, N., Dychko, A., Kraychuk, S., & Ostapchuk, N.** (2018). Interaction of seismic explosive waves with underground and surface structures. In: Resources and Resource-Saving Technologies in Mineral Mining and Processing (pp. 291–310). Petroєani, Romania: UNIVERSITAS Publishing.

19. **Isayenko, V.M., Vovk, O.O., Zaychenko, S.V., Remez N.S., & Vovk, O.O**. (2018). Methods of Forecasting and Monitoring of Technogenic Dynamic Processes in the Extraterritorial Territories. Kyiv: NAU.

20. **Guselskikov, Y.O., Vylokhin, S.A., & Ponikarov**, S.I. (2014). Study of effective parameters of an air shock wave. Bulletin of the Kazan Technological University, 9, 81-83.

ANALYSIS OF PRODUCTIVITY AND TECHNICAL EFFICIENCY IN GRANITE AGGREGATE PRODUCTION IN SELECTED QUARRIES IN SOUTH-WESTERN, NIGERIA

Melodi M. M.
PhD (Engineering), Associate Professor,
Department of Mining Engineering, The Federal University of Technology, Akure, Nigeria

Akande V. O.
Master's Student
Department of Mining Engineering, The Federal University of Technology, Akure, Nigeria

Abstract

This research analysed the productivity and technical efficiency in the granite aggregate production and also investigated the causes of inefficiencies in selected quarries across the south western region of Nigeria using stochastic frontier production function which incorporates a model of inefficiency effect. This was achieved through the collection of secondary data with a careful and thoughtful review of literature. The technical efficiency was estimated using Software for Statistics and Data Science (STATA). It was determined that the mean monthly granite production is 17,854.23 tonnes and about 86% of Mean production was influenced by the factors of production used in the study. The result also shows that 100% of the variation in quarries' output was due to inefficiencies on the part of the production processes rather than random variability. Variables such as total number of equipment, mean days of weekly use, number of skilled staff and quantity of fuel used per month, are factors which positively influence the output of the quarries, an investment on equipment would increase productivity and allows for continuity of operation against possible breakdown. The mean efficiency estimate of 68.4% is an indication that there is a chance to improve production. The implication of the study is that efficiency in granite aggregate production among the quarries could be increased by 31.6%. Factors such as age of equipment, availability of engineers for repair and number of working hours per day were found to be the sources of technical inefficiency. It is recommended that provision should be made by stakeholders investing in the quarries to provide access to affordable production inputs for an effective improvement in the level of efficiency among quarries.

Key Words: Technical Efficiency, Granite, Quarry, Productivity, stochastic frontier.

1. Introduction

Quarrying is the process of cutting or digging of stones, and related materials from an extraction site or pit. The different between mining and quarrying is that mining involves taking an economically

useful material from the ground while quarrying involves obtaining quarry resources usually rocks, found on or below the land surface (Banez *et al.*, 2010). However, quarry project is a capital intensive investment with many uncertainties (Opafunso and Ajaka, 2004) and the survival of a mine is determined by how efficient it is technically and in terms of cost.

The main concern of the extractive industry includes the productivity, effective use and maintenance of all types of machinery possessed by the company (Jaroslaw and Magdelena, 2018). Productivity is a basic and intuitive measure of performance (Machek and Hnilica, 2012).The effective utilization of mine machines is of utmost importance for the granite quarries as this is one of the major dictators of productivity despite the availability of all other input. This has motivated the managers of mining enterprises to take a series of measures, including activities aimed at enhancing effectiveness of the entire process of mining production. Consequently, this will result in the identification of areas which offer the possibility of increasing the effectiveness of the technical resources owned by mining enterprises. Conventional methods of granite quarrying are becoming increasingly expensive due to the sequence of diverse operations involved. Irrespective of the amount of granite aggregates produced, a quarry can operate technically efficiently only if the production is maximized with optimal use of input factors.

Technical efficiency measures the percentage of actual output relative to the potential output that is produced from the same set of inputs from a fully efficient firm (Aigner, 1968). This definition means that increase of technical efficiency can lead to profit maximization and improvement of the firm performance. Consequently, many granite aggregate quarries in Nigeria regards raising productivity as one of their main priorities because it is an important indicator to measure the developmental level of production systems. It reflects the utilization degree of various kinds of production factors such us resource, environment, capital, technology and energy sources (Liu *et al*., 2016). However, little has been done on how technically efficient is their operation. The above observations necessitated this research work in order to analyze the technical efficiency in the quarry operations in some selected quarries in Nigeria.

The quarry firm - level of efficiency of resource use has important implication on mining in Nigeria, since efficient quarry firms make better use of existing and available resources, producing maximum output at lowest possible cost (Melodi, 2019). However, the importance of analyzing the technical efficiency of an industry cannot be over emphasized because it plays a significant role in the economic growth of the firm. Thus, it is important to not only focus on how government must improve the business environment, studies have to be done to shed light on how to improve the efficiency of firms by analyzing their technical efficiency. The problem of measuring the technical efficiency of an industry is hence important to both the economic theorist and the policy maker and as a result of these factors, new technical and organizational solutions in mining have to be implemented.

2. Literature Review

Quarrying of granite consists of removing blocks or fragmented rock from an identified and unearthed geologic deposit. Differences in the particular quarrying technique used often stems from variations in the physical properties of the granite deposit such as density, fracturing/bedding planes, and depth, financial considerations, and the site owner's preference (Anaekwe, 2010). The operation process involves removal of overburden using heavy equipment (including transport to waste dump), drilling, cutting, splitting, and use of explosive charges, on-site transport of fragmented granite (run-off mine) using heavy equipment, crushing of run-off-mine to different aggregates sizes (Alaba and Agbalajobi 2017).

Productivity is a crucial factor in production performance of firms and nations, it is expressed as the ratio of output to inputs used in a production process, (Courbois and Temple, 1975). Efficiency is concerned with the relative performance of the processes used in transforming given inputs into outputs (Arene, 2008). Efficiency improvement is an important source of production growth in any economy. Productivity and efficiency studies have taken the attention of most mine economists and policy makers in recent years, since no meaningful economic development can take place in the absence of productivity growth (Sawaneh *et al.,* 2013).

Technical efficiency measures the ability of a firm to obtain the maximum output from given inputs. Technical efficiency is the suc-

cess with which an organization uses its resources to produce outputs, that is the ability to produce a given level of output with a minimum quantity of inputs under certain technology. Technical efficiency is a principal element in economic productivity and profitability

The concept of efficiency measurement begins with Farrell (1957) who define a simple measure of firm efficiency which could account for multiple inputs. The estimation of production frontier with the stochastic frontier approach is used in this study. This method appears to be superior because it incorporates the traditional random error of regression. In this case the random error, besides capturing the effect of unimportant left out variables and errors of measurement in the dependent variable, would also capture the effect of random breakdown on input supply channels not correlated with error of the regression. An appropriate formulation of stochastic frontier model (Battese, and Coelli, 1995) in terms of a general production function from t^{th} production unit is

$$(Y_i = f(X_{ij}\beta) + V_i - U_i), \quad (1)$$

where

Y_i = Output of ith quarry,

X_{ij}= the actual j^{th} input used by i^{th} quarry,

β= the regression coefficient to be estimated,

V_i= random variables outside the control of the quarry, and

U_i= error term under the control of the quarry.

3. Materials and Method

The study covered a total of twenty quarries from the four states (Ogun, Ondo, Oyo and Osun state).

Table 1

Quarry coordinates

S/N	Quarry Name	Coordinate
1	OGUN1	6º 45′ 31″ N, 3º 21′ 08″ E
2	OGUN2	6º 52′ 10″ N, 3º 16′ 23″ E
3	OGUN3	6º 38′ 21″ N, 3º 36′ 48″ E
4	OGUN4	6º 44′ 49″ N, 3º 47′ 06″ E
5	OGUN5	6º 54′ 53″ N, 3º 33′ 16″ E
6	ONDO1	7º 09′ 23″ N, 5º 42′ 06″ E

7	ONDO2	7º 01′ 08″ N, 5º 24 ′11″ E
8	ONDO3	7º 10′43″ N, 5º 12′ 43″ E
9	ONDO4	7º 06′ 03″ N, 5º 31′ 00″ E
10	ONDO5	7º 07′ 23″ N, 5º 19′ 14″ E
11	OYO1	8º 30′ 02″ N, 4º 35′ 26″ E
12	OYO2	8º 22′ 35″ N, 4º 28′ 45″ E
13	OYO3	8º 17′ 44″ N, 4º 24′ 39″ E
14	OYO4	8º 26′ 15″ N, 4º 33′ 20″ E
15	OYO5	8º 32′ 09″ N, 4º 20′ 00″ E
16	OSUN1	7º 51′ 46″ N, 4º 37′ 23″ E
17	OSUN2	7º 44′ 21″ N, 4º 55′ 00″ E
18	OSUN3	7º 32′ 48″ N, 4º 47′ 01″ E
19	OSUN4	7º 39′ 12″ N, 4º 30′ 43″ E
20	OSUN5	7º 41′ 01″ N, 4º 49′ 14″ E

Data Collection and Analysis

A well-structured questionnaire was used to collect the data of the quantity of granite aggregate produced per month and other production variables which includes; Number of equipment, Hours of daily use of equipment, Mean days of weekly use of equipment, Number of skilled staff, Number of unskilled staff, Quantity of fuel use per month, Age of quarry, age of the equipment, Availability of engineer for repairs, Total number of downtime, Number of working days per week, Number of working hours per day, Number of monitoring per month, Year of experience of quarry manager. Statistical Package for Social Sciences (SPSS) and Software for Statistics and Data Science (STATA) were used to analysis the data for the various objectives by using the appropriate models.

Productivity Estimation

In other to estimate the level of productivity of granite aggregates production in the study area, the productivity of each of the quarries was determined using the formula below;

$$\Pr oductiviti = Output(y)/Input(x) \quad (2)$$

The factors influencing the productivity of granite aggregates production in the selected quarries was also determined using multiple regression analysis. The principal components technique that was used maximized the sum of squared granite aggregates extracted.

Estimation of Production function:

A two stage stochastic frontier approach was used. In the first stage, stochastic production function and the technical efficiencies was estimated using the Maximum Likelihood Estimation technique. The stochastic frontier production function model is specified as

$$\text{Ln}Y_i=\ln\beta_0+\beta_1\ln X_1+\beta_2\ln X_2+\beta_3\ln X_3+\beta_4\ln X_4+\beta_5\ln X_5+\beta_6\ln X_6+V_i-U_i \quad (3)$$

Where Ln is Natural logarithm, Y_i is the Output of granite aggregates (tonnes), β_1, β_2, β_3, β_4, β_5, β_6 are unknown parameters to be estimated, $Z_1$is Total number of equipment, $Z_2$is Hours of daily use of equipment, $Z_3$is Mean days of weekly use of equipment, $Z_4$is Number of skilled staff, $Z_5$is Number of unskilled staff, $Z_6$is Quantity of fuel used per month, β_0 is a Constant term, V_i is random error component which is due to factors beyond the control of the quarry, U_i is the nonnegative technical inefficiency component of the error term.

According to Coeli *et al*. (2005), output oriented technical efficiency can be represented by

$$TE=\frac{Y_i}{Y_{\max}}=\frac{\exp\left(X_i\beta\right)v_i-u_i}{\exp\left(X_i\beta+v_i\right)}=\exp^{(-ui)} \quad (4)$$

TE = Technical Efficiency

In the second stage, the research used Censored Maximum Likelihood Estimation technique to investigate the causes of inefficiency. In this estimation technique the specific technical efficiency estimates were used as the dependent variable. The inefficiency of production U_i is modeled in terms of the factors that are assumed to affect the efficiency of the processor as follows

$$U_i=\delta_0+\sum_{n=1}^{8}\delta_n Z_n \quad (5)$$

$$U_i=\delta_0+\delta_1 Z_1+\delta_2 Z_2+\delta_3 Z_3+\delta_4 Z_4+\delta_5 Z_5+\delta_6 Z_6+\delta_7 Z_7+\delta_8 Z_8 \quad (6)$$

Where $U_i$is the nonnegative technical inefficiency component of the error term, δ_0 is constant term, $\delta_1,\delta_2,\delta_3,\delta_4,\delta_5,\delta_6,\delta_7,\delta_8$ are unknown parameters to be estimated, $Z_1$is Age of equipment, $Z_2$is Availability of engineers for repair, $Z_3$is Total number of down time, $Z_4$is Age of quarry, $Z_5$is Number of working days per week, $Z_6$is Number of working hours per day, $Z_7$is Number of monitoring visits per month, $Z_8$is Year of experience of quarry manager.

4. Result and Discussion Productivity Analysis

The productivity was estimated and the productivity statistics is shown in table 2, the major leading production variables are identified to be monthly granite production with a mean of 17,854.23 tonnes, monthly productivity per worker with a mean of 706.04 tonnes and monthly productivity per hour with a mean of 41.74 tonnes. From figure 1, the quarry with the highest productivity is identified to be OGUN1 (1,726.14) while the quarry with the lowest productivity is OGUN5 (256.83) indicting that among all the measured quarries, OGUN5 has the poorest combination of basic factors of production such as the ratio of the number of skilled staffs to that of unskilled staffs, number of workings days per week and the number of working hours pay day.

Table 2

Quarry production and Productivity statistics

Production variables	min.	max.	Mean	Std. Dev
Hours of daily equipment use	7.00	11.00	9.34	1.5312
Days of Weekly equipment use	5.00	7.00	5.82	0.9869
Skilled Staff (persons)	4.00	30.00	18.57	20.4936
Unskilled Staff (persons)	10.00	50.00	26.31	14.8210
Working Days per week	5.00	7.00	5.86	0.7422
Working Hours per Day	8.00	11.00	9.53	1.1034
Granite Production (tonnes/mth)	4,000	40,000	17,854.23	9534.6603
Productivity per worker (tonnes/pers/mth)	256.83	1,726.14	706.04	526.0782
Productivity per hour (tonnes/hr/mth)	485.17	3,636.40	41.74	729.5108

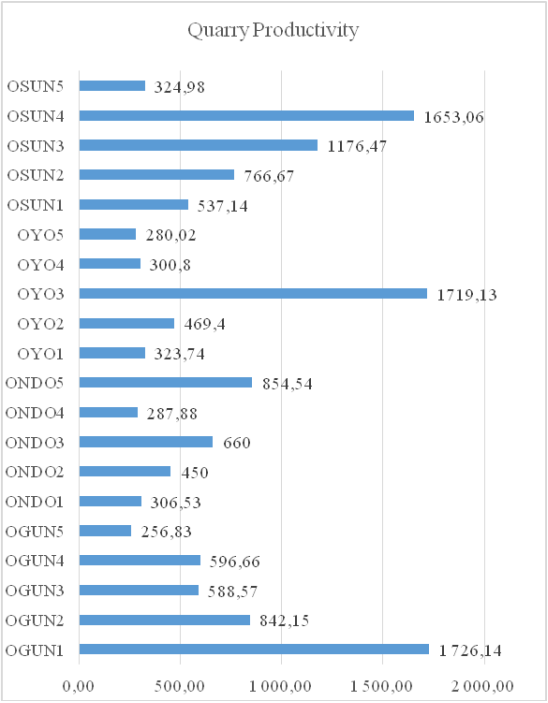

Fig. 1. Comparison of quarry productivity

Factors Affecting Productivity:

Multiple regression analysis was carried out to determine the factors influencing productivity in the selected quarries and the result is presented in Tables 3, 4 and 5.

The correlation coefficient (R) is calculated as 0.927, i.e. the correlation between the dependent (Mean Production of the quarries) and the independent variables (Mean age of equipment, Number of working days per week, Number of working hours per day, Age of the quarry, Number of skilled staff, Number of unskilled staff, Total repairs). The value of 0.927 implies a high and positive correlation between the dependent and the independent variables, the value also indicates a good level of prediction. The coefficient of determination (R-square) is estimated to be 0.859, which implies that about 86% of Mean production are accounted for by the included independent var-

iables. The remaining 14% is attributed to extraneous others factors that are not included in the model.

Table 3

Regression Model Summary

Model	R	R Square	Adjusted R Square	Std. Error of the Estimate
1	.927[a]	.859	.777	.51942

a. Predictors: (constant), Mean age of equipment, Number of working days per week, Number of working hours per day, Age of the quarry, Number of skilled staff, Number of unskilled staff, Total repairs he F-ratio in the ANOVA (Table 7) tests whether the overall regression model is a good fit for the data.

The table shows that the independent variables statistically significantly predict the dependent variable, F (7, 12)=10.438, p=0.000, significant at 5% level.

Table 4

Analysis of Variance Anova[a]

Model	Sum of Squares	df	Mean Square	F	Sig.
Regression	19.712	7	2.816.	10.4	000[b]
Residual	3.238	12	270	38	
Total	22.950	19			

a. Dependent Variable: Mean Production

b. Predictors: (Constant), Mean age of equipment, Number of working days per week, Number of working hours per day, Age of the quarry, Number of skilled staff, Number of unskilled staff, Total repairs.

The estimates of regression coefficients as presented in table 8, reveals that Number of working days per week, Number of working hours per day, Age of the quarry, Number of unskilled staff, Total repairs have direct relationship with the Mean production but only the estimated coefficients of Total repair is significant at 5% level i.e. Total repair $p(0.001)<0.05$. On the other hand, the estimated coefficient Mean age of equipment and Number of skilled staff have inverse relationship with the Mean production. Furthermore, the estimated coefficients reveals that a unit increase in number of working days per week results in 0.041 units increase in the mean production, also a unit increase in Number of working hours per day, Age of the quarry, Number of unskilled staff and Total repairs results in 0.241, 0.462, 0.408 and 0.768 units increase in the mean production respectively. However, a unit increase in the Mean age of equipment and

Number of skilled staff results in 0.154 and 0.160 units decrease in the mean production respectively.

Table 5

Regression Coefficients Coefficients[a]

Model	Unstandardized Coefficients		Standardized Coefficients	*t*	Sig.
	B	Std. Error			
(Constant)	-782	1.261.	-	-.620	.547
Mean age of equipment	-154	222	1.111	-.696	500
Number of working days per week	041	377	023	109	915
Number of working hours per day	241	410	097	587	568
Age of the quarry	462	218	410	2.121	055
Number of skilled staff	-160	133	-.214	-1.206	251
Number of unskilled staff	408	237	339	1.723	111
Total Repairs	768	179	702	4.301	001

Technical Efficiency Assessment

The statistics summary for the production variables used in the analysis are given in Table 2. The study shows that the mean granite stone production is 17,854.23 tonnes per month. The mean number of skilled and unskilled staff are 18.57 and 26.31 respectively which implies that there is dominant number of unskilled workers involved in granite production though the technical knowledge of the operation is required for efficient and effective production. Also the table reveals the mean hours of daily use and the mean days of weekly use of the equipment to be 9.34 hours and 5.78 hours. The mean age of equipment is 6.54 years, mean number of downtimes is 3.61 and mean availability of engineers for repair is 1.48.

Table 6

Statistics of the production variables used

Variables	min.	max.	Mean	Std. Dev.
Granite stone production (tonnes/mth)	4,000	40,000	17,854.23	9534.6603
Total number of equipment	5.00	15	7.15	3.9807
Hours of daily equipment use	7.00	11.00	9.34	1.5312
Number of skilled staff (persons)	4.00	30.00	18.57	20.4936
Number of unskilled staff (persons)	10.00	50.00	26.31	14.8210
Quantity of fuel used per month (litres)	3,500.00	101,760.00	39,374.63	38,944.16

Age of equipment (years)	2.00	12.00	6.54	1.0962
Mean days of weekly use of equipment	5.00	7.00	5.83	0.9869
Total number of downtime	1.00	8.00	3.61	1.6606
Availability of engineer for repairs	1.00	2.00	1.48	0.4743
Number of working days per week (days)	5.00	7.00	5.86	0.7442
Number of working hours per day (hours)	8.00	11.00	9.53	1.1034
Number of monitoring visit per month	1.00	4.00	2.66	2.7408
Year of experience of quarry manager	5.00	20.00	9.11	6.2795
Age of Quarry (years)	3.00	15.00	8.51	7.7872

From the stochastic frontier regression model that was carried out and presented in Table 10, the sigma-square σ^2 has an estimate of approximately 0.03 which attests to the good fit and correctness of the model. Also, the gamma γ estimate of approximately 1.00, this means that 100% of the variation in quarries' output was due to inefficiencies on the part of the production processes rather than random variability. The total number of equipment has a positive sign (0.0588), this indicates that a percentage increase in the total number of equipment available for use would result in 0.0588% increase in granite production. The estimated coefficient of mean days of weekly use of equipment is 5.4, which is significant at 1%, this means that an increase in days of weekly use equipment will equally lead to increase in the quantity of output of granite aggregates produced by the quarries. Number of skilled staff is positively correlated and insignificant with an estimate of 0.32 while quantity of fuel used per month (liters) also has positive estimated of 0.21 implying that increase in the use of these variables will also lead to increase in the output of the quarries if properly managed. The variable with negative coefficients such as hours of daily use of equipment which is significant at 5% and number of unskilled staff. This implies that as the hours of daily use of the equipment (-2.1) and the number of unskilled staff (-0.21) increases there is a negative effect on production efficiency.

Table 7

Maximum likelihood estimates of stochastic frontier for granite aggregate production

Variables	Parameters	Estimate	Std. error	t-value
Constant	β_0	6.2130	1.3754	5.9928
Total number of equipment	β_1	0.0588	1.2033	0.0521
Hours of daily use of equipment	β_2	-2.1572	1.1164	-1.9074
Mean days of weekly use of equipment	β_3	5.3921	0.9438	5.9882
Number of skilled staff (persons)	β_4	0.3160	0.2203	0.8469
Number of unskilled staff (persons)	β_5	-0.2075	0.4133	-0.4635
Quantity of fuel used per month (litres)	β_6	0.2109	0.2855	0.9257
Variance Parameters				
Sigma-squared	σ^2	0.0295	0.0324	0.8651
gamma	r	0.9863	0.0205	59.3
Log likelihood function		1.7812		
LR test of one-sided error		9.6035		

Technical Efficiency Estimates of the quarries

The estimated value of the technical efficiencies of each quarry is shown in Table 4, it can be deduced that the quarry with the highest technical efficiency is identified to be ONDO2 (0.9937) while the quarry with the least technical efficiency is OGUN5 (0.4352). This means that ONDO2 makes the highest output with its average given input while OGUN5 makes the lowest output with its average given input based on the variables considered. The mean technical efficiency is 0.6843.

Table 8

Technical Efficiency Estimates of the selected Quarries

Quarries	Efficiency Estimate
OGUN1	0.9554
OGUN2	0.8761
OGUN3	0.4728
OGUN4	0.9795
OGUN5	0.4352
ONDO1	0.6495

ONDO2	0.9937
ONDO3	0.8737
ONDO4	0.7840
ONDO5	0.8245
OYO1	0.5129
OYO2	0.4536
OYO3	0.5242
OYO4	0.6379
OYO5	0.4581
OSUN1	0.7735
OSUN2	0.4965
OSUN3	0.7329
OSUN4	0.6915
OSUN5	0.5607

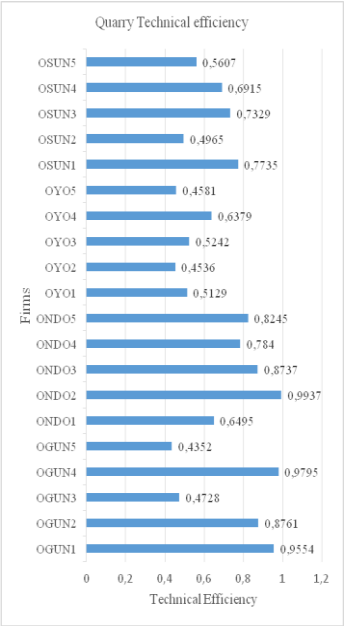

Fig. 2. Comparison of technical efficiencies

Technical Inefficiency

Table 5 describes the factors causing inefficiency in the study area. The coefficients for age of equipment (0.1653), availability of

engineers for repair (0.5935) and number of working hours per day (0.1847) was estimated to be positive which indicates an increase in technical inefficiency and consequent decrease in technical efficiency, i.e. as the age of equipment increases productivity efficiency of the quarries drops, the availability of workers to implement preventive and corrective maintenance on quarry equipment would positively affect technical efficiency and reliability on the equipment for production, thereby decreasing technical inefficiency. Consequently, an increase in working hours per day would improve productivity and technical inefficiency decreases. Factors such as total number of downtime (-0.906), age of quarries (-0.1847), number of working days per week (-0.2490), number of monitoring visit (-0.0315) and years of experience of quarry manager (-0.0448) were estimated to be negative implying that these variables led to decrease in technical inefficiency or increase in technical efficiency. Therefore from the result, the major factors contributing to technical inefficiency in the quarries are; age of equipment, availability of engineers for repair and number of working hours per day.

Table 9

Technical inefficiency factors

Variables	Parameters	Estimate	Std. error	*t*-value
Inefficiency effect model				
Constant	δ_0	0.1654	0.9971	0.1743
Age of equipment (years)	δ_1	0.1653	0.1764	0.9532
Availability of engineers for repairs	δ_2	0.5935	0.7824	0.9675
Total number of downtime	δ_3	-0.0906	0.1825	-0.6041
Age of quarry (years)	δ_3	-0.1847	0.1373	-1.6202
Number of working days per week (days)	δ_5	-0.2490	0.7450	-0.4680
Number of working hours per day (hours)	δ_6	0.1857	0.3918	0.7063
Number of monitoring visits per month	δ_7	-0.0315	0.1594	-0.0951
Year of experience of quarry manager	δ_8	-0.0448	0.0658	0.7414
Variance parameters				
Sigma-squared	σ^2	0.0295	0.0324	0.8651
gamma	γ	0.9863	0.0205	59.3
Log likelihood function		1.7812		
LR test of the one-sided error		9.6035		

Conclusion and Recommendation

Based on the findings, the mean monthly granite production is 17,854.23 tonnes, monthly productivity per worker is 706.04 tonnes and monthly productivity per hours is 41.74 tonnes/hr. However, these outputs can increase with the right combination of production variables.

The study further shows that about 86% of Mean production was influenced by the factors of production used. Consequently, the number of working days per week, Number of working hours per day, Age of the quarry, Number of unskilled staff and Total repairs all have positive influence on the production. However, factors such as Mean age of equipment and Number of skilled staff have negative influence on the production.

Out of all the quarries used for the study, ONDO2 has the highest technical efficiency while the quarry with the least technical efficiency is OGUN5 quarry. This means that ONDO2 makes the highest output with its average given input while OGUN5 makes the lowest output with its average given input based on the variables considered. The mean technical efficiency is 0.6843 which indicates that production can still be increased by 31.6% using available technology. This means that substantial opportunities should be explored to increase productivity and income of quarries through availability and efficient utilization of productive resources. Factors such as age of equipment, availability of engineers for repair and number of working hours per day were found to be the sources of technical inefficiency.

The following recommendations are made based on the findings and conclusion of this study;

1. For an effective improvement in the level of efficiency among quarries, provision should be made by stakeholders investing in the quarries to provide access to affordable production inputs such as latest equipment, standby engineer for repair, etc., and the practice of two shift in a day should be encourage.

2. More studies should be done on technical efficiency as very few published works has been carried out on technical efficiency in the mining industry considering the fact that it plays a significant role in the economic growth of the firm.

References

1. **Alaba, O., and Agbalajobi, S.** (2017). Profitability of Granite Quarry Operation in Akure South Local Government Area of Ondo State, Nigeria. *Daffodil International University Journal of Science and Technology*, *12*(1), *pp.96.*

2. **Aigner, D. J., and Chu, S. F.** (1968). On Estimating the Industry Production Function *American Economic Review, 58(4), pp.826*.

3. **Anaekwe, E. N.** (2010). How to Setup and Run a Granite Quarrying *Nigeria Business Forum, Switzerland*.

4. **Arene, C. J.** (2008). Determinants of profitability and willingness to pay for metropolitan Waste-use in urban agriculture of the federal capital territory Abuja, Nigeria. *Agro-Science, 7(1), pp.41*

5. **Banez, J. S., Mae, A., Bilolo, J. R., and Dailyn, J. M**. (2010). Assessment of the Environmental Effects of Quarrying in Ksofkin Kenya. *Environmental Monitoring Report and Assessment, pp. 38.*

6. **Battese, G. E., and Coelli, T. J.** (1995). A Model for Technical Inefficiency effects in a Stochastic Frontier Production Function for Panel Data. Empirical Economics, *20(1): pp.325*.

7. **Coelli, T. J., Prasada, D.S., Christopher J. O., and Battese, G.E.** (2005). An Introduction to efficiency and productivity Analysis. Springer, New York.

8. **Courbois, R., and Temple P.** (1975). The method of Surplus Accounts and its macroeconomics. 160 des Collect. INSEE, *Series C (35), pp.100*.

9. **Farrell, M. J.** (1975). The Measurement of Productivity Efficiency. *Journal of Royal Statistical Society A. 120(2), pp. 253-281*.

10. **Jarroslaw, B., and Magdalena, T.** (2018). Use of I.T Platform in Determination of Efficiency of Mining Machines. *XVIIth Conference of PhD Students and Young Scientist pp.7*.

11. **Liu, H., Yu, R., and Qin, X.** (2014). Productivity Analysis and Benchmark of X Mining Company by DEA. *Journal of Chemical and Pharmaceutical Research. 6(4), pp.162.*

12. **Machek, O. and Hnilica, J.** (2012). Total Factor Productivity Approach in Competitive and Regulate World, *International Conference on Asia Pacific Business Innovation and Technology Management, Social and Behavioral Sciences, 57(2), pp.230.*

13. **Melodi M. M.** (2019). Stochastic Estimation of Technical Efficiency and Productivity of Granite Stone Production in Edo State, Nigeria. *IOSR Journal of Research and Method in Education, 9(4), pp. 35.*

14. **Opafunso, Z., and Ajaka, E. (2004).** Application of geographic information system (GIS) to solid mineral resources information management. *Pakistan Journal of Science Industrial Research. 47(3), pp. 240.*

15. **Sawaneh, M., Latif, I. A., and Abdullah, A. M.** (2013). Total Factor Productivity of Rice Farming in Selected Southeast Asian Countries. *In Proceedings of the International Conference on Social Science Research.*

INVESTIGATION OF DISPERSED CONTAMINATES INFLUENCE ON THE HYDRAULIC ENERGY CONSUMPTION OF ELEMENTS OF GAS PIPELINE SYSTEMS WITH COMPLEX GEOMETRY

Doroshenko Ya.V.
Ivano-Frankivsk National Technical University of Oil and Gas, Candidate of Technical Sciences, Associate Professor, Associate Professor of the Department of Oil and Gas Pipelines and Storage Facilities, Ukraine

Karpash O.M.
Ivano-Frankivsk National Technical University of Oil and Gas, Doctor of Technical Sciences, Professor, Professor of the Department of Energy Management and Technical Diagnostics, Ukraine

Rybitskyi I.V.
Ivano-Frankivsk National Technical University of Oil and Gas, Candidate of Technical Sciences, Associate Professor, Associate Professor of the Department of Energy Management and Technical Diagnostics, Ukraine

Abstract. *The subject of the research* is the energy losses of gas pipeline systems of complex geometry (bends, tees) with consideration of different operational parameters (pressure, velocity of two-phase flow, volume fraction of the disperse phase).

Methodology. CFD (computational fluid dynamics) simulation was used to perform the research, which included a set of physical, mathematical and numerical methods designed to calculate the characteristics of gases and liquids. CFD modeling was performed in ANSYS Fluent R19.2 Academic software. The Eulerian approach and the Mixture model were used.

The purpose of the research is to determine the dependence of hydraulic energy losses of two-phase gas flow in elements of gas pipelines with complex geometry on the transmission mode of parameters, dispersed phase characteristics and the geometric parameters of the studied elements.

Research results. It is established that energy losses of gas pipeline systems elements with complex geometry are significantly influenced by the volume fraction of the dispersed phase. The most significant effect of such volume fraction was observed in bends with a large angle and a small bending radius. In particular, pressure drop values at the outlets increased at high multiphase flow velocities and

low pressures. Also, the energy losses of two-phase flow in small diameter bends are significantly increased.

With regard to tees, their hydraulic energy loss is affected by the volume fraction of the dispersed phase when the rounding radius of the connection between main line and the branch is the smallest or no rounding is present at all (welded branches). The increase in the volume fraction of the dispersed phase leads to a significant increase in pressure drop values in the tees, where the gas flow from the line transfers completely into the branch.

Introduction

Most of Ukrainian gas fields are in their final stages of development. At this stage, the extracted gas is characterized by a high content of formation water and carbohydrate condensate. Also, gas from wells removes rock particles, sand, sulphur and the like. These substances are transmitted to the separation plants by the gas-flow through the field gas pipelines. A large amount of harmful impurities is carried out through the separation installations due to the bumpers worn-out and many other reasons, into gathering pipelines and further to the main gas pipelines. Installation of new separation installations or their reconstruction considering the gas production reduction in Ukraine is inefficient.

Also, in the inner cavity of most gas pipelines, there is a scale that is detached from the pipes as well as products of intrinsic corrosion. When the dew point of the transferred gas is reached, the condensate occurs within the hydrocarbons.

If the velocity of the gas stream is a sufficiently high liquid drops and solid particles are trapped so that two- or multiphase flows occur. Compared to single-phase two- and multiphase flows are much more complex because they can have different structures (stratified, dispersed, etc.) and are described by different models.

Many researches were aimed to the study of multiphase flows in rectilinear sections of pipelines [1-4]. Researchers have found that dispersed harmful impurities in pipeline flows lead to an increase in hydraulic energy losses.

The problem of predicting energy losses of two-phase flows in elements of gas pipelines with complex geometry is much more complicated than in straight sections of pipelines, since the physical picture of the flow in such elements is extremely complex and clearly uncertain. This is especially true of bends and tees, which are the

most common elements of gas pipeline systems. In such elements, the direction of the two-phase flow changes, resulting in a centrifugal force, which leads to an uneven phase re-distribution and friction between the phases (the phase of higher density undergoes greater action by the centrifugal force), the momentum is lost, and secondary flows of force occur depending on the geometry curvature. All this causes a complex redistribution of speed and flow pressure, resulting in significant losses of hydraulic energy.

As the concentration of the dispersed phase increases, its influence on the movement of the transported medium and energy loss increases. In this case, the gas phase has a significant impact on the dispersal distribution processes. Therefore, when investigating the flow of pipelines, the mutual effect of the phases on one another must be taken into account.

Multiphase gas-dynamic processes and the amount of hydraulic energy losses depend significantly on the elements geometry of gas pipeline systems. There are many complex pipeline systems with a large number of complex geometry elements – bends, tees, fittings, etc. Hydraulic energy losses in such elements are quite significant. Given the large scale of the gas transmission system, even a slight reduction in energy losses in its individual elements can significantly reduce overall energy costs for transmission.

Today's energy efficiency requirements call attention to many aspects and issues related to the design, operation and reconstruction of gas pipeline systems. Therefore, the study of the dependence of the energy loss of two-phase gas flows in elements of gas pipelines with complex geometry on the modes of operation, improving the design of these elements to reduce hydraulic resistance is an urgent task.

As of today, there are few publications on the results of pressure drop studies, dynamics of two-phase flow concerning pipelines with complex geometry. Researchers have found that if the flow is two-phased, then the pressure drop values in such elements are greater than if the flow is single-phased. Moreover, the value of the pressure drop is largely influenced by the concentration of the dispersed particles. The value of the energy losses of a two-phase gas stream is not yet well understood, as it depends on many factors.

Most studies of two-phase flows have been performed experimentally in laboratory conditions [5-7], since such flows are three-dimensional and not available for any simplified theoretical analysis. There are the following disadvantages of the experimental approach:

– limited parameters of multiphase flows and geometric parameters of pipeline elements;

– small operating pressures and diameters of the studied pipeline systems elements;

– the obtained correlation dependencies do not cover all modes of transmission, geometric parameters;

– it is extremely difficult, and in many aspects it is impossible to study the physical picture of the multiphase flows transmission along the elements with complex geometry.

In recent years, computer modeling of pipeline flows, specifically CFD modeling [8-10], has become popular. CFD modeling is a powerful tool that allows to study the dynamics of single, multiphase flow, change all output parameters in a wide range, quickly obtain high-quality results, visualize the simulation results, which gives an understanding of the physical picture of multiphase flow inside pipelines elements. It can be effectively used to investigate the influence of mode and geometric parameters on gas-dynamic processes, design of minimally energy-consuming pipeline systems.

In order to determine the pressure drop in the elements of gas pipelines with complex geometry by CFD modelling, Eulerian approach was chosen in this work, which considers the dispersed phase as a continuum. Variable parameters of the experiment were the volume fraction of the dispersed phase, gas flow velocity, pressure, geometric parameters.

The results of CFD modelling were visualized by the creation of pressure fields in longitudinal cross-sections of simulated elements of gas pipeline systems with complex geometry. The pressure drop in the simulated elements and their dependence on the studied parameters of two-phase flows, geometrical parameters of the elements were determined.

1. Analysis of gas pipeline flows composition

Condensate, water, products of in-pipe corrosion, lubricant, scale, which were peeled off from pipes, particles of rocks, sand, are accu-

mulated in the internal cavity of gas pipelines, which have been operated for many years. Condensate and water are removed from the wells and occur when the dew point of the gas over water and hydrocarbons is reached. In gas pipelines, this occurs at a distance of more than 25 km from the compressor stations at the places where the pipeline route is lowered to the surface. The acidic environment created by the liquid accumulations in the internal cavity of the gas pipelines leads to an increase in the rate of in-line pipeline corrosion and, as a result, an increase in the content of metals and corrosion products in the internal cavity of the gas pipelines, which are solid harmful impurities. For example, the inspection results of an industrial pipeline with a diameter of 920 mm with a length of 45 km on the outskirts of Doha (Q_{atar}) revealed 7 tonnes of in-line corrosion products. [11]

Field and gathering gas pipelines contain much more impurities than main lines. The major contamination substances of such pipelines are formation water and hydrocarbon condensate. The type and qualitative composition of harmful impurities for each of the fields is specific and inherent only for the studied gas-bearing area:

- for Lviv region there is a presence of formation and condensation water with a considerable content of fine mechanical impurities as a corrosion by-product;
- for Poltava deposits - localization of condensate with different density;
- for the group of wells of Shebelinsky GCF in the area of CGPI-19 - clay-liquid suspension. [12]

The harmful impurities in the cavity of gas pipelines are one of the biggest problems of gas transmission organizations. They can accumulate at lowered sections, drop off at pipeline walls, or move in a stream. The accumulated and delayed harmful impurities exert additional hydraulic resistance, which leads to an increase in energy costs for gas transportation (compression at compressor stations) and a reduction in the extraction of hydrocarbons from the reservoirs.

The appropriate gas flow velocity is required in order the harmful impurities extracted from the well and accumulated in the internal cavity of field, gathering and main gas pipelines continue to move in the flow. According to J. Smart [13], the minimum velocity of flow when solid particles move through a pipeline depends on the proper-

ties of the substance of the stream, the diameter of the pipeline, pressure, density and particle size. For example, at a pressure of 7 MPa, the minimum flow velocity for moving solids is about 3 m/s for pipelines with a diameter of 200 mm, 4 m/s for pipelines with a diameter of 600 mm, and 4.2 m/s for pipelines with a diameter of 1200 mm. As soon as the solid particles start to move, the movement will continue until the flow rate decreases or the pressure is to be increased.

Transfer of droplets of liquid or solid particles in the gas flow, removal of liquid accumulations from lowered sections of the route leads to the occurrence of multiphase flows. Multiphase are called flows, which consist of a continuous phase (gas or liquid) and the dispersed phase (liquid and solids) mixed in it. The simplest case of multiphase flow is a two-phase one. The two-phase medium consists of a continuous phase and a dispersed phase, for example: gas - liquid droplets; gas - solid particles; fluid - solid parts; liquid - bubbles of steam.

The concentration of harmful impurities in gas pipelines in real time can be measured by an optical method. The optical device emits optical waves of different lengths within the infrared range into the gas stream. [14]

Two-phase flow leads to an increase in the loss of hydrodynamic flow energy in pipeline systems. These losses increase significantly in the elements of gas pipelines with complex geometry.

2 Elements of gas pipeline systems with complex geometry

Modern gas pipeline systems contain a large number of various elements with complex geometry. The most common of these are bends, tees, couplings. They are also called moulds or fittings. These shaped elements are produced by various manufacturers and have different geometry.

Specifically, many bends and tees are as a part of piping of various technological objects – compressor stations, gas refineries, underground gas storages, gas distribution stations, etc. The bends also contain compensators for above-surface pipe crossings, they are also located in places of sharp terrain breaks, pipeline route turns.

The bends are curves with an angle of 30, 45, 60 and 90° and small radius (Fig. 1*a*).

In welded tees, the connection of the main line (base line) and the

bend (side elbows) is made at right angles (Fig. 1*b*). In hot stamping tees, stamped tees, the branch connects with the main line by means of rounding (Fig. 1*c*). According to the requirements of SNiP 2.05.06 [15], the radius of curvature R must be not less than 0.1 $D_{o.b.}$, where $D_{o.b.}$ is the outer diameter of the branch.

Fig. 1. Elements of gas pipeline systems with complex geometry: *a* – bends; *b* – welded tee; *в* – stamped tee

The flow (separation) of the main pipe in tees is basically divided and the flows out of two pipes merged into one pipe.

In practice, there are a lot of tees, in which the flow moves in main line from which it flows completely into the branch. Such tees are a part of piping at the compressor stations of the main gas pipelines, underground gas storage, gas distribution stations and the like. In addition, in the place of technological crossings between gas pipelines, where all the flow from one line flows to another, as well as in case of multi-line offshore pipelines, where all the flow is transmissed by backup lines, etc.

3. Selection of research method

Multiphase gas flow in bends and tees is much more complicated

than single-phase. These elements of the gas pipeline systems change the direction of gas flow, resulting in an unequal redistribution of phases (the phase of greater density undergoes more centrifugal force), flow velocity and pressure, which cause hydraulic energy losses. The value of hydraulic energy losses depends on the mode and geometric parameters, the dispersed phase concentration. Quantitative determination of hydraulic energy losses of two-phase flows in bends and tees is a big problem during the design and hydraulic analysis of gas pipeline systems. There is very little experimental data in the literature. The reason for this is the large number and range of variable parameters of multiphase flows and geometric parameters of pipeline fitting elements. In addition, considering gas pipelines, especially main lines, it is extremely difficult to study experimentally multiphase flows, and in many aspects it is impossible. The reasons for this are the following:

- it is impossible to determine the exact value of velocity, pressure at any point in a complex 3D stream;
- it is impossible to visualize the flow of gas in the steel fitting element;
– gas pipelines are under high pressure and are explosive.

CFD modeling is an effective tool for quantifying the effect of multiphase flow parameters and geometric parameters of gas pipeline system elements on hydraulic energy loss. This method has become especially popular in the study of complex multiphase flows in recent years, when the computers' capabilities increased many times and the calculation time has decreased significantly. CFD modeling is mainly used for two purposes:

- research purposes - to gain an understanding of the various basic processes;
- designing purposes. The designer can predict what will happen in the design. Thus, it is possible to optimize the design, to create a new one without experimental research, which saves considerably time and costs.

CFD modeling gives an understanding of the complex dynamics of multiphase gas flows motion along the elements of gas pipeline systems, it visualize in detail the three-dimensional multiphase flow and study the pressure drop, phase distribution (volumetric particles), flow velocity, turbulence, kinetic energy and more. It is also possible

to change the initial mode parameters, element geometry under study and investigate their influence on the physical picture of multiphase flows movement, hydraulic energy losses. At any point in the 3D stream, the value of any parameter can be easily determined. Many of the above-mentioned aspects cannot be determined experimentally.

For the proper modeling of pipeline flows, CFD incorporates various complex multiphase models that have proven themselves to be more accurate than other models, especially when complex flow geometry is important. [16, 17]

It is best to use the Eulerian approach to study hydraulic energy losses in pipeline system elements. For multiphase flows, the concept of volume fraction, another additional flow parameter, is introduced. The Eulerian approach is applied when the volume fraction of the dispersed phase is significant. The Eulerian approach contains several models.

VOF model - surface tracking. This model is designed to model two or more streams of immiscible substances (stratified flows) with a clear extended (i.e., comparable in size to the size of the calculated geometry) interface (separation limit). The form of this interface is the only result of the simulation. The VOF model contains a set of momentum conservation equations and the tracking of the volume fraction of each of the fluids at each computational point of the entire 3D flow geometry. In this model, there is no sliding between the phases, and it is not possible to capture the flow dynamics for large slip coefficients. The simulation results are in good agreement with the experimental data up to the slip factor 20.

Mixture model is a multiphase model. The Mixture model is designed for two or more phases (liquid or solid). The phases are interpenetrating continua.

The Mixture model differs from the VOF model in two respects:

- the Mixture model allows the phases to penetrate each other. The volume fractions of the continuous phase q and the dispersed phase p can have any value from 0 to 1, depending on how much space they take;

- the Mixture model allows the phases to move at different speeds. The concept of slip speed is introduced for this purpose. It performs well at high slip ratios of over 262. Also, the phases can

move at the same speed and the Mixture model is then reduced to a homogeneous multiphase model.

Only one of the phases can be docked in the Mixture model.

The Eulerian model is a model of interpenetrating environments. The Eulerian model contains a set of n momentum and continuity equations for each phase. The equations are closed by coefficients of pressure and inter-phase exchange. Phases are interpenetrating continua. [18]

In this study the Mixture model will be used because it is designed to model dispersed multiphase flows where phases can move at different speeds, capable of simulating any number of phases (liquid or solids) and is relatively easier to be understood than the Eulerian model and is accurate enough.

CFD modeling will be performed by ANSYS Fluent R19.2 Academic software.

4. Mathematical model

The Mixture model contains continuity equations for mixture, momentum conservation and mixture energy, volume equation for dispersed phases, and algebraic expressions of relative velocities (if the phases move with different velocities).

Continuity equation for mixture:

$$\frac{\partial}{\partial t}(\rho_m) + \nabla \cdot (\rho_m \bar{v}_m) = 0, \quad (1)$$

where ρ_m – mixture density;

$\bar{v}_m$ – mixture average velocity.

Mixture density:

$$\rho_m = \sum_{k=1}^{n} \alpha_k \rho_k, \quad (2)$$

where α_k – phase k volume fraction;

ρ_k – phase k density;

n – phase number.

Mixture average velocity

$$\bar{v}_m = \frac{\sum_{k=1}^{n} \alpha_k \rho_k \varpi_k}{\rho_m}, \quad (4)$$

where $\bar{v}_k$ –average mass velocity of the phase k .

By adding individual momentum equations of each phase, the momentum equation of the mixture can be obtained

$$\frac{\partial}{\partial t}(\rho_m \bar{v}_m) + \nabla \cdot (\rho_m \bar{v}_m \bar{v}_m) = -\nabla p + \nabla \cdot \left(\mu_m \left(\nabla \bar{v}_m + \nabla \bar{v}_m^T \right) \right) + \\ + \rho_m \bar{g} + \bar{F} + \nabla \cdot \left(\sum_{k=1}^{n} \alpha_k \rho_k \bar{v}_{dr,k} \bar{v}_{dr,k} \right), \quad (5)$$

where $\bar{F}$ - bode force;

μ_m - mixture viscosity;

$\bar{g}$ - gravity acceleration;

$\bar{v}_{dr,k}$ - drift velocity of the dispersed phase k ;

Mixture viscosity

$$\mu_m = \sum_{k=1}^{n} \alpha_k \mu_k , \quad (6)$$

where μ_k – phase k viscosity.

Drift velocity of the dispersed phase

$$\bar{v}_{dr,k} = \bar{v}_k - \bar{v}_m . \quad (7)$$

The relative velocity (also called slip velocity) is the difference between the velocity of the dispersed phase *p* and the velocity of the continuous phase *q*

$$\bar{v}_{pq} = \bar{v}_p - \bar{v}_q , \quad (8)$$

where $\bar{v}_p$ – dispersed phase velocity;

$\bar{v}_q$ – continuous phase velocity.

The mass fraction of the dispersed phase *k*

$$c_k = \frac{\alpha_k \rho_k}{\rho_m} , \quad (9)$$

Disperse phase drift velocity is the difference between the slip velocity and the algebraic sum of the product of mass particles on the velocity of the dispersed phase

$$\bar{v}_{dr,p} = \bar{v}_{pq} - \sum_{k=1}^{n} c_k \bar{v}_{pk} . \quad (10)$$

The algebraic slip formula is used in the Mixture model. The basic assumption of the algebraic slip model of the mixture is that the

local equilibrium between the phases must be reached at a short spatial length. Then the relative velocity is equal

$$\bar{v}_{pq} = \frac{\tau_p}{f_{drag}} \frac{(\rho_p - \rho_m)}{\rho_p} \bar{a}\,, \tag{11}$$

where τ_p – relaxation time of the dispersed phase particles;

f_{drag} – function switch;

ρ_p – density of the dispersed phase;

$\bar{a}$ – acceleration of dispersed particles.

The relaxation time of the dispersed phase particles

$$\tau_p = \frac{\rho_p d_p^2}{18\mu_q}, \tag{12}$$

where d_p – diameter of dispersed particles;

μ_q – continuous phase viscosity.

Function switch

$$f_{drag} = \begin{cases} 1+0{,}15\,Re^{0{,}687} & Re \le 1000 \\ 0{,}0183\,Re & Re > 1000 \end{cases}, \tag{13}$$

Acceleration of dispersed particles

$$\bar{a} = \bar{g} - (\bar{v}_m \cdot \nabla)\bar{v}_m - \frac{\partial \bar{v}_m}{\partial t} a\,. \tag{14}$$

The particle acceleration is given by gravity and/or centrifugal force in the dispersive flow model. To account the presence of other particles, the particle relaxation time changes. In turbulent flows, the relative velocity must contain the diffusion component caused by the dispersion, which should be in the momentum equation for the dispersed phase. In the Mixture model, this variance is added to the relative speed

$$\bar{v}_{pq} = \frac{(\rho_p - \rho_m) d_p^2}{18\mu_q f_{drag}} \bar{a} - \frac{\nu_m}{\alpha_p \sigma_D} \nabla \alpha_q, \tag{15}$$

where α_p – volume fraction of the dispersed phase;

α_q – volume fraction of continuous phase;

ν_m – turbulent viscosity of the mixture;

σ_D – the Prandtl number.

The energy equation of the mixture

$$\frac{\partial}{\partial t} \sum_{k=1}^{n} (\alpha_k \rho_k h_k) + \nabla \cdot \sum_{k=1}^{n} (\alpha_k \bar{v}_k (\rho_k h_k + p)) = \nabla \cdot \left(k_{eff} \nabla T\right) + S_E\,, \tag{16}$$

where k_{eff} - effective conductivity;

h_k - enthalpy of phase k ;

S_E - energy transfer due to conductivity. S_E includes any other volumetric heat source;

From the continuity equation of the dispersed phase *p*, the volume fraction equation for the dispersed phase *p* can be obtained

$$\frac{\partial}{\partial t}\left(\alpha_p \rho_p\right) + \nabla \cdot \left(\alpha_p \rho_p \bar{v}_m\right) = -\nabla \cdot \left(\alpha_p \rho_p \bar{v}_{dr,p}\right). \text{[18]} \quad (17)$$

5. Geometric modeling

Both the multiphase gas-dynamic processes occurring in these elements and their hydraulic energy losses, depend significantly on the geometric shape and geometric parameters of the gas pipeline systems elements. Since multi-phase flows in elements of gas pipelines with complex geometry are extremely complex, and their physical transmission pattern is three-dimensional, the study should be performed using 3D geometric modeling.

3D geometric models of the internal cavity of gas pipeline system elements were designed in the academic version of the AutoCAD software. The shape and geometric dimensions of the elements are identical to the industrial designs and correspond to TU 27.2-05747991-001 [19] and OST 102-61 [20].

Modern pipeline systems contain a large number of various elements of gas pipeline systems of complex geometry such as tees, bends, fittings and the like. These elements are produced by various manufacturers and have different geometry.

The geometric parameters of the pipeline bends, on which the hydraulic energy losses of the multiphase flow depend, are the internal diameter of the bend D_{in}, the bending angle φ, and the bending radius of the bend R_B (Fig. 2*a*). The influence of these parameters on the hydraulic energy loss in gas pipeline branches has not been sufficiently investigated. Five different outside diameters were selected to perform such studies - 89 mm, 219 mm, 530 mm, 1020 mm and 1420 mm. For a diameter of 530 mm, bends were drawn with a bend radius equal to DN (DN - conditional bend diameter) and bending angles of 30°, 45°, 60° and 90°, as well as with an elbow angle of 90° and bending radii of DN, 1.5 DN, 2 DN, 2.5 DN and 3.5 DN. Bends were drawn with adjacent pipe sections.

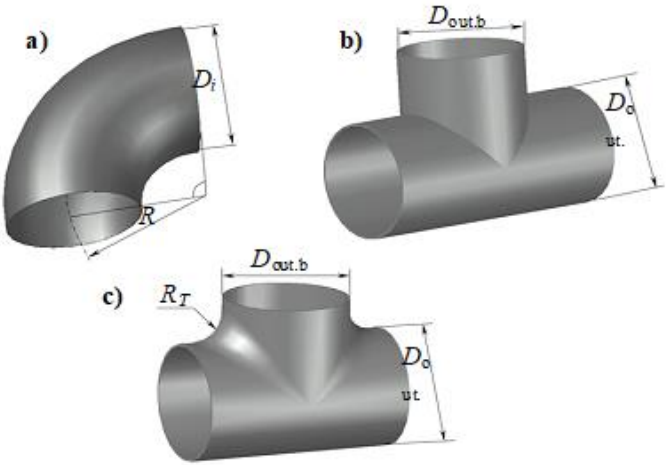

Fig. 2. Geometric models: *a* – bend; *b* – welded tee; *c* – stamped tee

The geometric parameter of the pipeline tees, on which the hydraulic energy loss of the multiphase flow largely depends, is the rounding radius of the connection between the main line and the branch. The effect of this parameter on hydraulic energy losses in pipeline tees has not been sufficiently investigated. To perform such studies, an internal cavity of the welded tee with an outside diameter of 530 mm was drawn, in which the connection of the main line and the bend is made at elbow angles (Fig. 2*b*). Also, an internal cavity of the stamped tees with an outside diameter of 530 mm was drawn, in which the transition from the bend to the line is made by rounding (Fig. 2, c). Since the rounding radius of the stamped tee R_T must be not less than 0.1 $D_{out.b}$, five models of the inner cavity were drawn, with a rounding radius varying from 0.1 $D_{out.b}$ to the maximum possible (53 mm, 95 mm, 136 mm and 178 mm).

The wall thicknesses of each bend, tee, and adjacent pipe sections were calculated for the appropriate pressure. According to the value of the nominal wall thickness of the taps and pipes, their internal diameter was determined.

Geometric models of bends and tees were imported from AutoCAD to Ansys Fluent.

6. Boundary conditions

In addition to the geometric shape and geometric parameters, the hydraulic energy losses in the elements of the gas pipeline systems are significantly influenced by the mode parameters of multiphase flow transmission and the characteristics of the dispersed phases, which were set in the ANSYS Fluent pre-processor. The continuous phase was selected as natural gas, which was accepted as a compressible medium. Steel was used as the material of the tee wall. The coefficient of equivalent roughness of tees and adjacent sections of pipes was set equal to 0.03 mm.

Experience of gas pipelines operation shows that the main cause of gas pipelines hydraulic resistance increase is liquid harmful impurities. Liquid contaminants may be condensate or water, which in large volumes are drawn from wells, fall out of gas when the dew point of the pumped gas is reached. The presence of condensate in the gas pipeline leads to the transmission of the two-phase mixture, which causes an increase in hydraulic energy losses. Therefore, the condensate density of 960 kg/m^3 was set as the dispersed phase. This value is close to the density of water.

The main transmission mode parameters, which have the greatest influence on energy losses, and the effect of which was studied are the velocity of multiphase flow and pressure. The velocity of the continuous and dispersed phase, which was assumed to be equal to each other, was set at the inlet of each bend, and the pressure was set at the outlet of the bend. The inlet velocity varied from 7 m/s to 19 m/s in 3 m/s increments and pressures was ranging from 3 MPa to 7 MPa in 1 MPa increments. A separate simulation was performed for each velocity and pressure values.

The temperature of the continuous and dispersed phases corresponds to the conditions of the gas pipelines operation and was set at 273 K. Also at the inlet and the outlet of the bend a turbulence intensity of 5% (for this value the flow is considered to be completely turbulent) and the hydraulic diameter were set. The hydraulic diameter was assumed to be equal to the inside diameter of the pipeline. The main characteristics of the dispersed phase, which have the greatest effect on energy loss, and the effects of which were studied are particles concentration and size.

The maximum diameter of the dispersed liquid phase droplets according to [21, (14.13)] is equal to

$$d_{liq}^{max} = 2D_{in}k_f^{-\frac{3}{5}}We^{-\frac{3}{5}}\left(\frac{\rho_{gas}}{\rho_{liq}}\right)^{\frac{2}{5}}, \quad (18)$$

where D_{in} - pipeline internal diameter;

k_f - coefficient of aerodynamic drag resistance, k_f =0,4;

ρ_{gas} - gas density;

ρ_{liq} - liquid phase density;

We – dimensionless parameter – Weber number

$$We = \frac{\rho_{gas}u^2 D_{in}}{\sum}, \quad (19)$$

where Σ - the surface tension of the liquid phase at the gas boundary.

The surface tension of the liquid phase at the gas boundary depends on the pressure and temperature of the gas and was determined according to [22, Tab. VI.2].

The maximum calculated (18) diameter of liquid phase droplets was about 100 μm. Therefore, the droplet diameters were assumed to be 100 μm, 50 μm, 10 μm, 5 μm, and 1 μm. The particle concentration in Ansys Fluent is given as the volume fraction of the dispersed phase, which varied from 0.1 to 0.3 in 0.05 increment. The volume fraction is determined by the amount of dispersed phase in the continuous. The volume fraction is taken to be a dimensionless value, which is the ratio of the volume of the dispersed phase to the total volume of the multiphase system.

In tees, the loss of hydraulic energy, in addition to the geometric shape and geometric parameters, is strongly influenced by the flow direction and the ratio of costs in the branch and main line. However, almost all theoretical and experimental studies in the laboratory are mainly concerned with the separation and merging of flows in tees. These results are incomplete because they do not cover all possible combinations of flow directions in tees found in various gas pipeline systems. The influence of tee geometry on hydraulic energy losses has not been established for the combinations of flow directions not covered.

In practice, there are a lot of tees in which a stream moves in a main line from which it flows completely into a branch. Such tees are a part of piping of the main gas pipelines compressor stations, underground gas storages, gas processing plants, gas distribution stations and the like. In addition, they are in place of technological overriders between gas pipelines, where all the flow from one line flows to another, in places of multiline underwater pipelines, where all the flow is transmissed by backup lines and the like. For such a scheme of flow movement in the tees, there is little information about the loss of energy in them today, not only considering multiphase flows, but also single-phase ones. In addition, as a result of the complete flow of gas from the main line to the branch, the gas flow from the wall at the beginning of the branch is detached, resulting in a significant vorticity, recirculation of the flow, and therefore the energy losses for this direction of flow of the tee will be maximum.

As tees were studied in which the gas flow from the main line completely flows into the bend, then the velocity of each phase was set at the branch inlet, and the pressure was set at the branch outlet. The velocity was set at 13 m/s and the pressure value was 5 MPa. The dispersed phase was given at spherical form with a diameter of 50 μm. The volume fraction of the dispersed phase was set to 0.2.

7. Research of hydraulic energy losses

Pressure losses of multiphase flow in gas pipelines elements with complex geometry are the main indicators by which their hydraulic energy losses can be estimated. Therefore, in the postprocessor of the ANSYS Fluent software, the results of each simulation were visualized by constructing a pressure field in the longitudinal cross sections of each bend and tee. For example, the outlet with an external diameter of 530 mm is considered. The continuous and dispersed phase velocity at the inlet is 13 m s, the outlet pressure is 5 MPa, the droplet diameter of the dispersed liquid phase is 50 μm, the volume fraction of the dispersed phase is 0.1 and 0.3. The pressure fields in the longitudinal cross sections of the bends are shown in Fig. 3.

Changing the direction of the multiphase gas flow in the bend leads to a complex pressure redistribution (Fig. 3). In the bend there is a radial pressure gradient, which is caused by the centrifugal force

acting on the multiphase flow. In addition to the radial pressure gradient, pressure losses in the bend are caused by turbulent vortices on the internal side of the bend after the bending place. By increasing of the volume fraction of the dispersed phase increases, the pressure drop in this place falls down (Fig. 3), which has a significant effect on the total pressure drop in the bend.

The pressure drop in the bend ΔP was determined by subtracting the inlet pressure and the outlet pressure at the bend. The greatest pressure drop occurs when the volume fraction α of the dispersed phase is 0.3 and these value equals to 17504 Pa. When the volume fraction of the dispersed phase α is 0.1, the pressure loss in the bend is 9864 Pa. As a result of volume fraction of the dispersed phase is increasing from 0.1 to 0.3, the pressure drop values in the outlet increase almost twice.

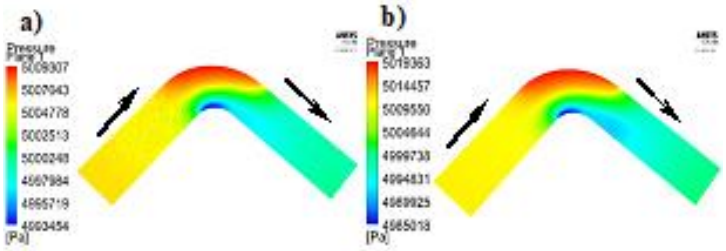

Fig. 3. Pressure field in the longitudinal cross sections of bends: *a* - volume fraction of the dispersed phase 0,1; *b*- volume fraction of the dispersed phase 0,3

The dependence of the pressure drop in the bends on their geometrical parameters (bend external diameter, radius and bending angle) was investigated at continuous two-phase flow mode parameters and unchanged dispersed phase characteristics. The speed of the continuous and dispersed phase at the inlet was set equal to 13 m/s, the bend outlet pressure was 5 MPa, the droplet diameter of the dispersed liquid phase was 80 μm. Only the volume fraction of the dispersed phase changed.

Pressure drop in bends of different diameters was determined for bends with an elbow angle of 90° and a bending radius equal to the nominal diameter of the bend DN. Fig. 3 shows the graphical dependence of the pressure drop in the bend ΔP on the bend outside

diameter $D_{out.b}$ for different volumetric fractions of the dispersed phase, namely 0.1, 0.2 and 0.3.

The results obtained show that with all other parameters being equal, the pressure drop in the bend increases with decreasing diameter for all volume fractions of the dispersed phase (Fig. 4). Moreover, the larger the volume fraction of the dispersed phase, the greater the pressure drop in the bend of the same diameter. It can also be observed that the increase in pressure drop in small diameters (less than 500 mm) is much more intense than in large diameters. Therefore, the influence of the bend diameter on the energy loss must be taken into account, especially with regard to the bend diameters less than 500 mm.

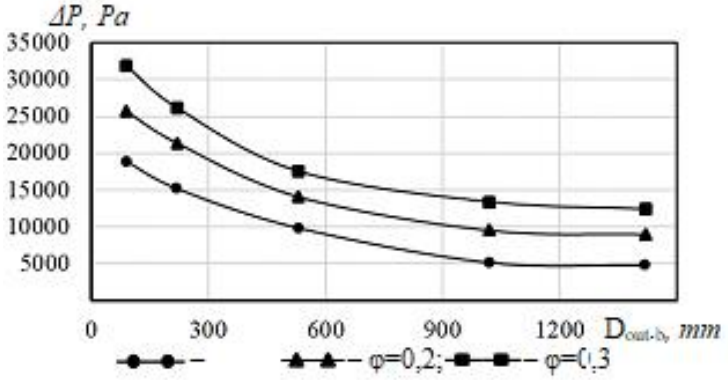

Fig. 4. Dependence of the pressure drop in the bend on the bend outside diameter for different volumetric fractions of the dispersed phase

Pressure drops in bends with different bending angles were determined for bends with an outside diameter of 530 mm with a bending radius equal to the nominal diameter of the DN bends. Fig. 5 shows a graphical dependence of the pressure drop in the bend ΔP on the its bending angle φ for different volume fractions of the dispersed phase, namely 0.1, 0.2 and 0.3. As we can see, as the bending angle increases, the pressure drop falls down with in a linear dependence for all volume fractions of the dispersed phase. Moreover, the larger the volume fraction of the dispersed phase, the greater the inclination of the straight line to the abscissa and the more intense the pressure drop in the bend.

Pressure drop in bends with different ratio of bending radius to nominal bending diameter was determined for bends with an outside diameter of 530 mm with an elbow angle of 90°. Fig. 6 shows a graphical dependence of the pressure drop in the bend ΔP on the ratio of the bending radius to the nominal diameter of the bend R_B/DN for different volume fractions of the dispersed phase, namely 0.1, 0.2 and 0.3. The bending radius of the bend has a significant effect on the pressure drop in it when it is less than 2.5 *DN*. There is a sharp increase in pressure drop in the bend while reducing the outside radius. Moreover, the larger the volume fraction of the dispersed phase, the more intense the pressure drop with decreasing the bend radius. At large radii of bend when it is more than 2.5 *DN* the pressure drop is minimal and practically does not change.

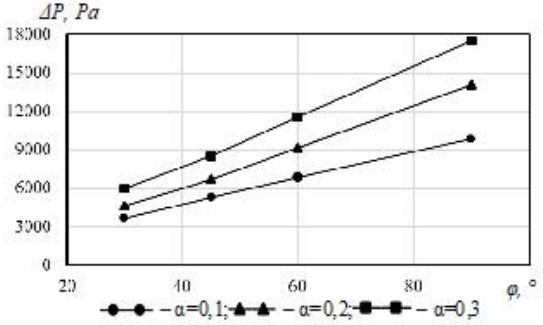

Fig. 5. Dependence of the pressure drop in the bend on the bending angle for different volume fractions of the dispersed phase

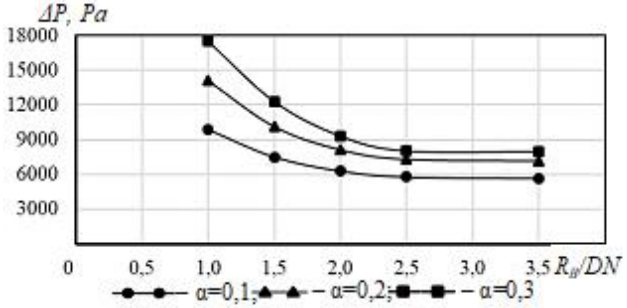

Fig. 6. Dependence of the pressure drop in the bend on the ratio of its bending radius to its nominal diameter for different volume fractions of the dispersed phase

The dependence of the pressure drop in the bend on the mode parameters of the two-phase flow, the characteristics of the dispersed phases were investigated at constant bend geometric parameters. The bend diameter was 530 mm, the bend elbow angle - 90°, the bending radius of bend was equal to the nominal diameter of the bend. The greatest pressure drop occurs in the bends with an elbow angle of 90° and a bending radius equal to the nominal diameter of the bend (Fig. 5, 6).

The dependence of the pressure drop in the bend ΔP on the velocity of the two-phase flow at the bend inlet *V* (Fig. 7) and the volume fraction of the dispersed phase α (Fig. 8) was investigated at a pressure at the bend outlet equal to 5 MPa and the diameter of the droplets of liquid dispersion phase equal to 80 μm.

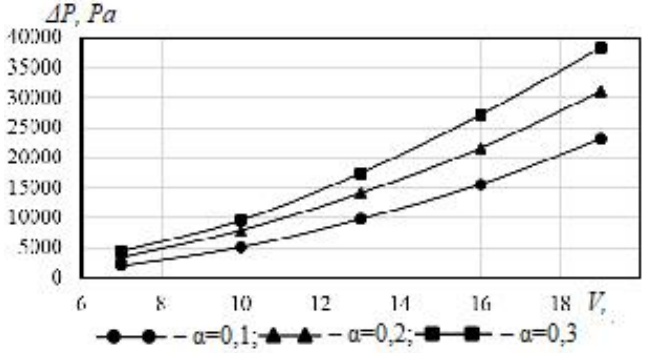

Fig. 7. Dependence of the pressure drop in the bend on the velocity of the two-phase flow at the bend inlet for different volume fractions of the dispersed phase

With the increase in the velocity of the two-phase flow there is a significant increase in the pressure in it (Fig. 7). Trends remain unchanged for all volume fractions of the dispersed phase. In the low velocity zone, the volume fraction of the dispersed phase has less influence than in the high velocity zone. Such a pattern can be better seen in Fig. 8. At low velocities of two-phase flow at the bend inlet (about 7 m/s), with the increase of the volume fraction of the dispersed phase, the pressure drop values do not increase significantly. Instead, at high velocities (about 19 m/s), there is a sharp increase of pressure drop values in the bend with an increase in the volume values of the volume fraction.

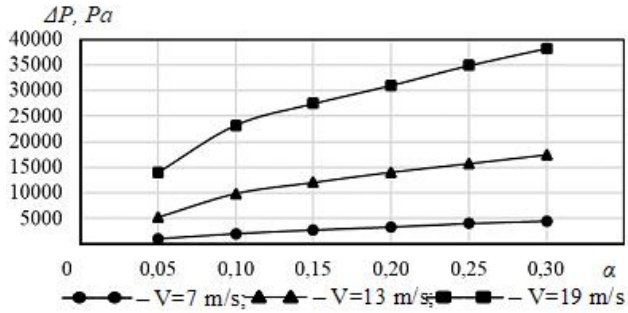

Fig. 8. Dependence of the pressure drop in the bend from the volume fraction of the dispersed phase for different velocities of two-phase flow at the inlet

The dependence of the pressure drop in the bend ΔP on the diameter of the dispersed particles d_p was investigated at the inlet for the two-phase flow velocity equals to 13 m/s and the pressure at the bend outlet equals to 5 MPa. As the diameter of the dispersed particles increases, their effect on the pressure drop in the bend increases with a linear dependence (Fig. 9). This trend is typical for all volume fractions of the dispersed phase. Only in the area of dispersed particles of small diameters with a volume fraction of the dispersed phase equal to 0.3 a sharp increase in pressure drop values was observed.

The dependence of the pressure drop in the outlet ΔP on the pressure at the bend outlet P was investigated with a velocity of two-phase flow at the inlet that was 13 m/s and the droplet diameter of dispersed liquid phase was 80 μm. As the pressure in the pipeline decreases, there is an increase in the pressure drop values in the bend for all volume fractions of the dispersed phase. (Fig. 10) Moreover, in the area of small pressures with decreasing pressure at the bend outlet, the pressure drop values in the bend are increasing more intensely.

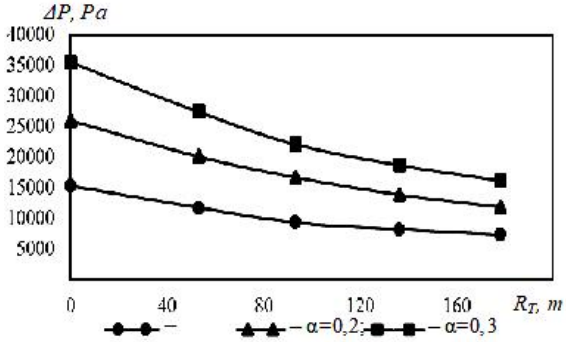

Fig 9. Dependence of the pressure drop in the bend on the diameter of the dispersed particles for different volume fractions of the dispersed phase

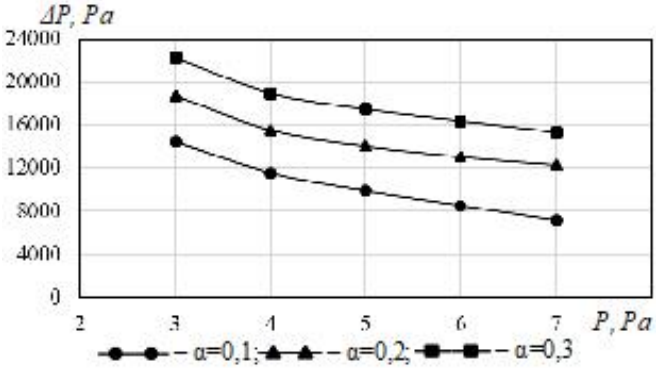

Fig. 10. Dependence of the bend pressure drop on the outlet pressure for different volume fractions of the dispersed phase

For tees, the effect of the rounding radius at the connection of the line and the branch R_T on the tee pressure drop for different volume fractions of the dispersed phase was investigated, namely 0.1, 0.2 and 0.3. The tee is equilateral with a diameter of 530 mm. The gas flow moves the tee main line from which flows completely into the branch. The speed of the continuous and dispersed phase at the inlet of the tee main line was set equal to 13 m/s, the pressure at the outlet of the tee outlet was 5 MPa, the droplet diameter of the dispersed liquid phase was 80 μm.

If the rounding radius connection between the main line and the branch is reduced, there is a significant increase in the tee pressure

drop values (Fig. 11). It has been found that the larger the volume fraction of the dispersed phase, the more intense the pressure drop will be in case of the rounding radius the connection between the main line and the branch being decreased.

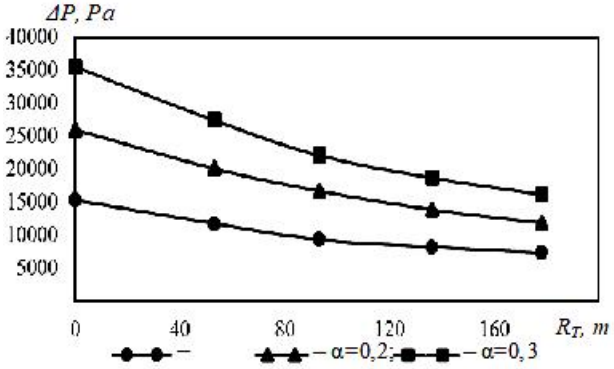

Fig. 11. Dependence of the pressure drop in the tee on the rounding radius of the connection between the main line and the branch for different volume fractions of the dispersed phase

Conclusions.

1. The performed researches give understanding of regularities of liquid dispersed harmful impurity influence in gas pipelines on hydraulic energy losses of gas pipeline systems' elements with complex geometry. The increase of the volume fraction of the dispersed phase leads to an increase in pressure drop values in the bends and tees. The most significant such effect of the volume fraction was observed in bends with a large angle and a small bending radius. In particular, pressure drops in bends increase at high multiphase flow velocities and low pressures. Also, the energy losses of two-phase flow in small diameter bends are significantly increased. In the case of tees, the most significant effect on the hydraulic energy loss is caused by the volumetric fraction of the dispersed phase when the rounding radius of the connection between the main line and the branch is the smaller or rounding is absent at all (welded tees). The increase in the volume fraction of the dispersed phase leads to a significant increase in pressure drop values in the tees, in which the gas flow from the main line transfers completely into the branch.

2. In order to minimize the energy losses of multiphase gas flow in gas pipeline elements, it is recommended, when designing new and refurbishing old gas pipeline systems, to give priority to bends with the largest possible bending radius and stamped tees with the largest rounding radius of the connection of the main line and the branch.

3. The obtained knowledge is useful for operators of gas pipeline systems that can optimize the operating parameters of two-phase gas flow transportation and can reduce the energy losses of pipelines, and engineers who can optimize the geometric parameters of bends and tees to minimize these hydraulic energy losses.

References

1. **Kumar, M., & Kaushal, D.** (2016). Modeling of sand-water slurry flow through horizontal pipe using CFD. *J. Hydrol. Hydromech*, Vol. 64, 3, 261-272. doi: 10.1515/johh-2016-0027

2. **Rizaldy, R., & Zarrouk, S.** (2016). Pressure drop in large diameter geothermal two-phase pipelines. *Proceedings 38th New Zealand Geothermal Workshop* (23-25 November 2016), Auckland, New Zealand.

3. **Hernández, F., Blanco, A., & Rojas-Solórzano, L.** (2008). CFD modeling of slurry flows in horizontal pipes. *8th Symposium on Applications in Computational Fluid Dynamics* (17-20 *August 2008*), Jacksonville, Florida.

4. **Uddin, S., Mohanty S., & Chandra G.** (2018). Numerical analysis of sand-water slurry flow through horizontal pipeline for various particle size at high velocity. *International Journal for Research in Applied Science & Engineering Technology*, Vol. 6, 5, 1577-1582.

5. **Auteea, A., & Girib, S.** (2016). Experimental study on two-phase flowpressure drop in small diameter bends. *Perspectives in Science*, 8, 621-625.

6. **Silva, S., Resendiz, L., Mariscal, C., & Eslava, T.** (2010). Pressure drop models evaluation for two-phase flow in 90 degree horizontal elbows. *Ingeniería Mecánica Tecnología y Desarrollo*, Vol. 3, 4, 115-122.

7. **Kumar, U.** (2015). Effect of added fines on relative pressure drop for narrow-sized silica sand slurry flow. *International Journal for Scientific Research & Development*, Vol. 3, 9, 591-595.

8. **Mazumder, Q.** (2012). CFD Analysis of the effect of elbow radius on pressure drop in multiphase flow. *Modelling and Simulation in Engineering*, Vol. 2012. doi.org/10.1155/2012/125405

9. **Mazumder, Q**. (2012). CFD Analysis of Single and Multiphase Flow Characteristics in Elbow. *Engineering*, Vol. 4, 210-214. doi.org/10.4236/eng.2012.44028

10. **Messa, G., & Malavasi, S. (**2014) Numerical prediction of particle distribution of solid-liquid slurries in straight pipes and bends. *Engineering Applications of Computational Fluid Mechanics*, Vol. 8, 3, 356-372.

11. Raghavan, V. (2017). Failure of 38" Dry gas injection pipeline Black Powder corrosion mechanism, November. Retrieved from https://www.researchgate.net/publication/321288112.

12. **Bratakh, M. I., Dobrunov, D. Ye., & Shkeir, A. (**2017). Vplyv hidravlichnoho stanu systemy promyslovykh hazoprovodiv na rezhymy roboty obiektiv hazovydobuvnoho kompleksu. Rozvidka ta rozrobka naftovykh i hazovykh rodovyshch, 65, 4, 59-64. [in Ukrainian]

13. **Smart, J.** (2007). Movement of Black powder in gas pipeline. *Pipeline and Gas Journal*, October, 82-85.

14. **Hosani, E., Meribout, M., Al-Durra, A., Al-Wahedi, K., & Teniou, S.** (2014). A new optical-based device for online black powder detection in gas pipelines. *IEEE transactions on instrumentation and measurement*, Vol. 63, 9, 2038-2252.

15. SNiP 2.05.06-85*. (2005). Mahystralnye truboprovody. Moscow: FGUP CzPP, 60. [in Russian]

16. **Zabaras, G., Menon, R., Schoppa, W., & Wicks III, M**. (2013). Large diameter riser laboratory gas-lift tests. *Offshore Technology Conference* (6-9 May 2013), Houston, Texas.

17. **Parsi, M., Vieira, R., Torres, C., Kesana, N., McLaury, B., Shirazi, S., Schleicher, E., & Hampel, U.** (2015). Experimental investigation of interfacial structures within churn flow using a dual wire-mesh sensor. *Int. J. Multiphase Flow*, Vol. 73, 155-170.

18. *The FLUENT User's Guide, Fluent Inc*. (2001). Vol. 2, Chapter 9, November.

19. TU U 27.2-05747991-001-2004. (2004). Detali ziednuvalni i zbirni odynytsi mahistralnykh i promyslovykh truboprovodiv na Pp do 10 MPa (100 khs/sm^2). Sumy : VAT "SMNO im. Frunze", 98. [in Ukrainian]

20. OCT 102-61-81. (1981). Detaly mahystralnykh truboprovodov stalnye pryvarnye na Ru do 10,0 MPa (100 khs/sm^2). Troinyky svarnye s usylyvaiushchymy nakladkamy. Razmery. Mosk-va: Mynysterstvo stroytelstva predpryiatyi neftianoi y hazovoi promyshlennosty, 32 [in Russian]

21. **Sinajskij, E.G.** (2002). Separatsyia mnohofaznykh mnohokomponentnykh system. Moskva: OOO Nedra-Byznestsentr. [in Russian] Separatsiya mnogofaznyih mnogokomponentnyih sistem. Moskva: OOO Nedra-Biznestsentr.

22. **Hymatudynov, Sh.K.** (1971). Fyzyka neftianoho y hazovoho plasta. Moskva: Nedra. [in Russian]

FEATURES OF METHANE EMISSION IN COAL MINES AT HIGH SPEED LONGWALL FACE ADVANCE

Skipochka S.I.
Institute of Geotechnical Mechanics named by N. Poljakov of National Academy of Sciences of Ukraine, Professor, Doctor of Technical Sciences, Head of Laboratory of Physics and Geomechanical Monitoring of Rock Massif, Ukraine

Krukovskyi O.P.
Institute of Geotechnical Mechanics named by N. Poljakov of National Academy of Sciences of Ukraine, Corresponding member of NAS of Ukraine, Doctor of Technical Sciences, Deputy Director of the Institute, Ukraine

Krukovska V.V.
Institute of Geotechnical Mechanics named by N. Poljakov of National Academy of Sciences of Ukraine, Senior Researcher, Doctor of Technical Sciences, Senior Researcher in Department of Dynamic Effects of Rock Pressure Control, Ukraine

Palamarchuk T.A.
Institute of Geotechnical Mechanics named by N. Poljakov of National Academy of Sciences of Ukraine, Doctor of Technical Sciences, Principal Researcher in Laboratory of Physics and Geomechanical Monitoring of Rock Massif, Ukraine

Abstract. The increase in coal mining is constrained by the gas factor. At high speed of wall advance, the current standards for the forecast of methane emission give significant errors. The goal of work is to study features of methane emission in coal mines at high speed longwall face advance.

The proposed method takes into account the geomechanics of the filtration region formation in the calculation of methane inflow. The method consists in sequential calculation of geomechanical parameters, rock permeability coefficients and methane filtration parameters. Established that the step of landing the main roof increases linearly with increasing speed of longwall advance. The blocks size increases and the fracturing rocks decreases. The size of the filtration area is reduced near the working stope. The front boundary of the filtration area moves closer to the longwall face.

Remote sources of gas emission go beyond the filtration area. The residual pressure of methane increases in undermined gas-bearing rocks and coal. The process of destruction and the emission of electrons decreases. This leads to a slowdown in methane desorption processes.

Thus, an increase in the speed of wall advance allows to reduce specific gas emission in the production sites. However, the requirements for the powered roof and drift supports are increasing due to the increase and redistribution of stresses in the rocks. This should be taken into account when choosing the optimal operating conditions for the mining section of a coal mine.

Key words: longwall, wall advance, geomechanical processes, gas dynamics, methane emission, desorption.

1 Introduction

During the design, the expected methane abundance of the mining sites is determined from the methane content of the coal seams and the host rocks. As a rule, their natural methane content for existing mines is determined by exploration data. Actual methane emissions are calculated by the mine ventilation service based on measurements of air flowrate and gas concentration.

Over the past 10-15 years, Ukrainian mines have switched to intensive coal mining technologies. Longwall average load was increased by 3-5 times. The requirements for monitoring the mine atmosphere were tightened. Analysis of the control results showed that with loads on the working face of more than 3 thousand tons/day, the forecast and control data differ significantly [1, 2]. Therefore, at the wall advance speed of more than 6 m/day, an uncertain situation occurs, which can lead to a decrease in mining safety. The reason for this phenomenon is rocks stress redistribution, rock deformation, and methane filtration. To date, research in this area has been episodic.

The goal of this work is to study features of methane emission in coal mines at high speed of the wall advance.

The objectives of the study included: determining the effect of the rate of mining on geomechanical processes in the rock massif; studying the mechanism of formation of the filtration area and determining the dependence of permeability on the rocks stress state; establishing the dependence of changes in the flowrate of methane into the lava at various speeds of its movement.

2 Methods

The problem was solved using analytical research methods based on continuum mechanics, elasticity theory, gas dynamics, and material resistance methods.

The methane filtration process in disturbed rocks in the zone of influence of the mine working was studied by the method of numerical three-dimensional modeling.

The methodology for studying the process of gas evolution from the host rocks into the mine workings included: calculation of geomechanical parameters; calculation of rock permeability coefficients depending on the components of the principal stress tensor; calculation of filtration parameters (methane pressure, filtration rate, methane flowrate).

The results were analyzed and summarized.

3 Results and discussion

3.1 The influence of the speed of longwall face advance on geomechanical processes in a rock massif

It is known that the dominant factor of geomechanical processes in the "longwall – rock massif" system is the formation of a rock console (plate) hanging over the waste [3]. Moreover, the increase in the speed of the movement of the coal face leads to an increase in the size of this console.

Let us evaluate the changes in the magnitude of the load on the clamping area of the rock-roof console. To simplify the calculations, we neglect the secondary features in the kinematics of the phenomenon under consideration. Since we are interested in the bending of the plate, we accept the hypothesis of direct normals. Therefore, when solving the problem, we use the following assumptions:

- until the plate is deformed, the set of points lying on a straight line normal to the elastic median plane remains on the straight line normal to the elastic deformation surface;

- the σ_{zz} component is small in comparison with other components of the stress tensor;

- when the plate is bent, the median plane is not deformed.

With these assumptions, we write the differential equation for the elastic surface of a curved plate in the form

$$\frac{Eh_p^{\,3}}{12(1-\nu^2)}\left(\frac{\partial^4 u}{\partial x^4}+2\frac{\partial^2 u}{\partial x^2}\frac{\partial^2 u}{\partial y^2}+\frac{\partial^4 u}{\partial y^4}\right)=q, \qquad (1)$$

where E is Young's modulus of elasticity, Pa; h_p is plate thickness, m; ν is plate Poisson's ratio; u is displacement, m; q is load intensity distributed evenly, N/m.

Let the plate be clamped by the load per unit length evenly distributed along the edges $y = 0$ (Fig. 1).

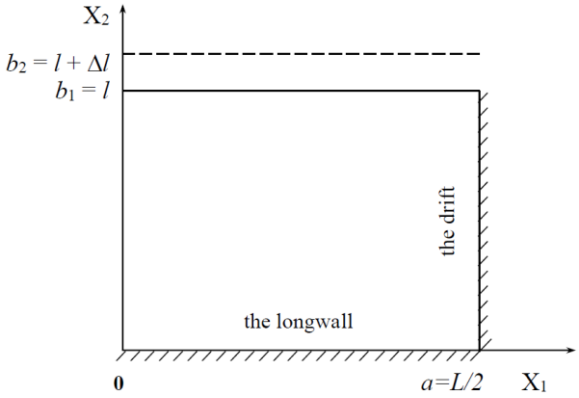

Fig. 1. The scheme for calculating the change in the magnitude of the load in the destruction zone of the face roof

We set the equation of the elastic surface in the form

$$u=\sum_{k=1}^{\infty}\sum_{n=1}^{\infty}A\sin\frac{k\pi x_1}{a}\sin\frac{n\pi x_2}{b}, \qquad (2)$$

where A is maximum displacement, m; a, b is plate length and width, m.

The displacement of the plate u and the speed of its displacement must satisfy the boundary conditions, which depend on the method of fixing the plate, and the initial conditions:

$$u=u_0(x_1,x_2); \quad \frac{\partial u}{\partial t}=v_0(x_1,x_2) \text{ for } t=0,$$

where u_0 is starting point (x_1, x_2) offset, m; v_0 is initial set speed at a point (x_1, x_2), m/day.

Let us consider the main roof with a thickness h_r in the form of a plate $h_r=h_p$, fixed on two adjacent sides a and b. The solution of equation (1) by the Runge-Kutta method in general is written as follows

$$\omega^2 = \frac{\pi^2 \delta}{a^2}\sqrt{\frac{D}{M^*}},$$

where $D = \frac{Eh_r^3}{12(1-\nu^2)}$ is plate bending stiffness, N/m; $M^* = \rho h_r$ is plate weight per unit area, kg/m^2; ρ is roof rock density, kg/m^3; δ is coefficient of the type of jamming of the roof contour.

For a plate with two adjacent rigidly fixed and two free sides, the circular frequency of its own oscillations is equal to:

$$\omega = 3{,}518\sqrt{\frac{1}{a^4} + (3{,}493 - 3{,}374\nu)\frac{1}{a^2 b^2} + \frac{1}{b^4}} \cdot \sqrt{\frac{D}{M^*}}. \qquad (3)$$

Given $\omega = 2\pi f$ and the velocity of the longitudinal acoustic wave in the plate is equal to

$$c_p = \sqrt{\frac{E}{\rho(1-\nu^2)}},$$

we rewrite formula (3) in the form

$$f = 0{,}145 h_p c_p \sqrt{\frac{1}{a^4} + (3{,}493 - 3{,}374\nu)\frac{1}{a^2 b^2} + \frac{1}{b^4}}.$$

The equations for determining bending moments are written as follows

$$M_{x_1} = -D\left(\frac{\partial^2 u}{\partial x_1^2} + \nu\frac{\partial^2 u}{\partial x_2^2}\right); \quad M_{x_2} = -D\left(\frac{\partial^2 u}{\partial x_2^2} + \nu\frac{\partial^2 u}{\partial x_1^2}\right);$$

$$M_{x_1 x_2} = -M_{x_2 x_1} = D(1-\nu)\frac{\partial^2 u}{\partial x_1 \partial x_2}.$$

Substituting solution (2) into these equations, we obtain for the values of the maximum bending moment

$$M_{x_1} = \frac{\zeta a^2 b^2 (a^2 + \nu b^2)\pi^2 \rho {h_p}^3}{b^4 + (3{,}493 - 3{,}374\nu)a^2 + a^4} \sin\frac{k\pi x_1}{a} \sin\frac{n\pi x_2}{b};$$

$$M_{x_2} = \frac{\zeta a^2 b^2 (b^2 + \nu a^2)\pi^2 \rho {h_p}^3}{b^4 + (3{,}493 - 3{,}374\nu)a^2 + a^4} \sin\frac{k\pi x_1}{a} \sin\frac{n\pi x_2}{b}. \quad (4)$$

For the case in question ζ = 0,245. Support reactions at the edges of the plates are equal to

$$R_{x_1} = \left(Q_{x_1} - \frac{\partial M_{x_1 x_2}}{\partial x_2} \right); \qquad R_{x_2} = \left(Q_{x_2} - \frac{\partial M_{x_1 x_2}}{\partial x_1} \right), \quad (5)$$

where Q_{x1} и Q_{x2} is values of cutting forces N equal to:

$$Q_{x_1} = \frac{\partial M_{x_2 x_1}}{\partial x_2} + \frac{\partial M_{x_1}}{\partial x_1} = -D \frac{\partial}{\partial x_1} \left(\frac{\partial^2 u}{\partial x_1^2} + \frac{\partial^2 u}{\partial x_2^2} \right);$$

$$Q_{x_2} = \frac{\partial M_{x_2}}{\partial x_2} - \frac{\partial M_{x_1 x_2}}{\partial x_1} = -D \frac{\partial}{\partial x_2} \left(\frac{\partial^2 u}{\partial x_1^2} + \frac{\partial^2 u}{\partial x_2^2} \right). \quad (6)$$

In view of equations (4)-(6), the support reactions fixed at the edges of the plate are equal to

$$R_{x_1} = \frac{\gamma h_p}{\pi a \left[\frac{1}{a^4} + (3{,}493 - 3{,}374\nu) \frac{1}{a^2 + b^2} + \frac{1}{b^4} \right]} \left(\frac{1}{a^2} + \frac{2 - \nu}{b^2} \right)^2 \sin\frac{\pi x_2}{b};$$

$$R_{x_2} = \frac{\gamma h_p}{\pi b \left[\frac{1}{a^4} + (3{,}493 - 3{,}374\nu) \frac{1}{a^2 + b^2} + \frac{1}{b^4} \right]} \left(\frac{1}{b^2} + \frac{2 - \nu}{a^2} \right)^2 \sin\frac{\pi x_1}{a}.$$

The resulting reaction will be expressed as

$$R = \frac{2\gamma h_p}{\pi \left[\frac{1}{a^4} + (3{,}493 - 3{,}374\nu) \frac{1}{a^2 + b^2} + \frac{1}{b^4} \right]} \left[\frac{1}{a} \left(\frac{1}{a^2} + \frac{2 - \nu}{b^2} \right) \right].$$

$$\cdot\int_0^b \sin\frac{\pi x_2}{b}dx_2 + \frac{1}{b}\left(\frac{1}{b^2}+\frac{2-\nu}{a^2}\right)\int_0^a \sin\frac{\pi x_1}{a}dx_1\Bigg] =$$

$$= \frac{4\gamma h_p}{\pi^2}\left\{ab + \frac{2(1-\nu)}{ab\left[\frac{1}{a^4}+(3{,}493-3{,}374\nu)\frac{1}{a^2+b^2}+\frac{1}{b^4}\right]}\right\}.$$

Let us evaluate how the load will change when the roof length is equal to half the length of the longwall face ($a=L/2$), and change b within $l \le b \le l+\Delta l$. Then, with $b=l$ and $h_p=h_r$

$$R^{\text{I}} = \frac{4\gamma h_r}{\pi^2}\left\{\frac{Ll}{2} + \frac{2(1-\nu)}{\frac{Ll}{2}\left[\frac{16}{L^4}+(3{,}493-3{,}374\nu)\frac{4}{L^2l^2}+\frac{1}{l^4}\right]}\right\}.$$

At $b = l + \Delta l$

$$R^{\text{II}} = \frac{4\gamma h_r}{\pi^2}\cdot\left\{\frac{L(l+\Delta l)}{2} + \frac{2(1-\nu)}{\frac{L(l+\Delta l)}{2}\left[\frac{16}{L^4}+(3{,}493-3{,}374\nu)\frac{4}{L^2(l+\Delta l)^2}+\frac{1}{(l+\Delta l)^4}\right]}\right\}.$$

Neglecting the terms of the second order of smallness, we obtain

$$\Delta R \approx \frac{4\gamma h_r \Delta l}{\pi^2}\left\{\frac{L}{2} + \frac{4(1-\nu)}{Ll(l+\Delta l)\left[\frac{16}{L^4}+(3{,}493-3{,}374\nu)\frac{4}{L^2l^2}+\frac{1}{l^4}\right]}\right\}.$$

From the expression it follows that the increment of the load at the point of clamping the face roof is directly proportional to the increment of its length, power, and also the speed of longwall movement (Fig. 2).

In addition, there are changes in the electrodynamics of the process. Electron emission decreases due to a decrease in the surface area of the resulting cracks [4, 5]. The energy of these electrons is sufficient to activate methane molecules bound by the Van der Waals forces. Consequently, the process of methane desorption with an in-

crease in the speed of movement of the longwall face also slows down.

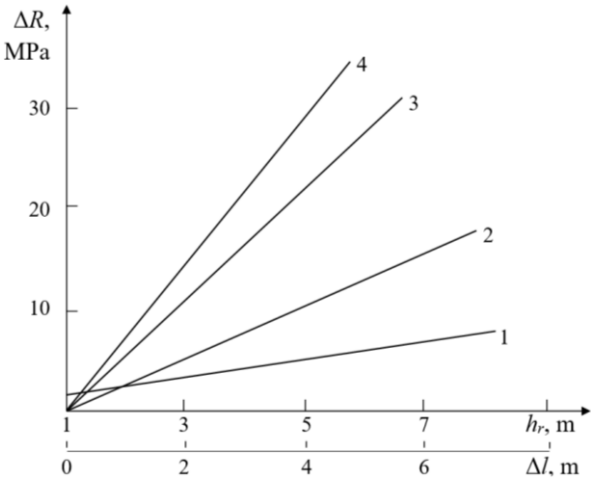

Fig. 2. The dependence of the increment of the load on the clamp of the roof on its thickness (*1*) and increase the length of the console when: *2* – h_r=2 m, *3* – h_r=4 m, *4* – h_r=6 m

Summarizing, we can draw the following conclusions.

1. In a transversely isotropic rock massif, the length of the longwall roof console is directly proportional to its thickness and elastic modulus of rocks, inversely proportional to the depth of mining and the degree of heterogeneity of the massif, it increases linearly with increasing speed of the face

2. In unstable and medium-stable rocks, with an increase in the speed of movement of the longwall from 0 to 12 m/day, the fall step of the main roof increases from 15-17 to 25-28 m.

3. With an increase in the speed of movement of longwall face due to a decrease in the intensity of formation of cracks, the methane desorption process slows down. This is due to a decrease in the activation of bound methane molecules by emitting electrons.

3.2 Simulation of methane filtration process

The most general model of a rocks is a fractured-porous, layered, and anisotropic medium within each layer. A gas flow consisting of

air, methane, and other gases we assume a continuous medium that fills the entire fractured-pore space of the massif.

Let's consider the conditions when the longwall moved away from the shaft furnace a sufficient distance and moves at a constant speed. The filtration area moves with the face at the same speed. In this case, the equations of deformation and filtration, boundary and initial conditions remain unchanged [6]. Therefore, we consider this processes as steady in a moving coordinate system associated with a moving longwall face.

Methane in sandstones and coal is in free and bound states [7, 8]. Thus, the methane desorption and its decay property in time have a significant effect on the filtration process. Methane desorption from disturbed coal seams and gas-bearing sandstones can be represented as the uniformly distributed methane sources $q(t)$. In the case of gas desorption from a coal seam, we assume that

$$q(t) = q_0 \cdot e^{-at},$$

where q_0 is initial gas emission, m^3/t; a is coefficient of accounting for properties of gas emission from a coal seam, 1/s; t is time from the start of gas emission, s.

Taking into account the speed of the wall advance V_{lw}, m/s, and the distance from the boundary of the filtration area z, m

$$q = q_0 \cdot e^{-a\frac{z}{V_{lw}}}.$$

The calculations take into account that exhaustion of emissions from gas-bearing sandstones occurs 4 times faster [9]. Coupled quasi-stationary three-dimensional processes of the rocks deformation and gas filtration in a disturbed area are described by a system of equations [10, 11]

$$\sigma_{ij,j} + X_i(t) = 0;$$
$$\frac{k}{2m\mu}\left(\frac{\partial^2 p^2}{\partial x^2} + \frac{\partial^2 p^2}{\partial y^2} + \frac{\partial^2 p^2}{\partial z^2}\right) + q(t) = 0;$$

where $\sigma_{ij,j}$ is the derivatives of the stress tensor components along x, y, Pa/m; $X_i(t)$ is the projections of the external forces acting on the

volume unit of a solid body, N/m^3; p is the gas pressure, Pa; k is the permeability coefficients, D; m is porosity; □ is gas viscosity, Pa·s; $q(t)$ is the gas release function.

The boundary conditions for the task set

$$u_x\big|_{\Omega_1} = 0; \quad u_z\big|_{\Omega_1} = 0; \quad u_y\big|_{\Omega_2} = 0;$$

$$p\big|_{\Omega_1} = p_0; \quad p\big|_{\Omega_2} = p_0; \quad p\big|_{\Omega_3} = p_0; \quad p\big|_{\Omega_4} = 0.1\ \text{MPa};$$

where □$_1$, □$_2$ is the vertical and the horizontal boundaries of the outer contours; p_0 is the methane pressure in the virgin rocks, MPa; □$_3$ is the boundary of the filtering area; □$_4$ is the internal contour (the mine working).

The problem is solved in an elastic-plastic formulation. For the mathematical description of the process of rocks changeover into a disturbed state, the Mohr-Coulomb failure theory is applied. To solve the problem, we used the finite element method.

Verification of the gas filtration model in the disturbed area was performed by comparing the calculated data on the gas release into the well with analytical solutions; comparison with experimental data on the distribution of gas pressure around the well and pressure changes in the dig up coal seam. The calculation error did not exceed 15 %.

Geomechanical parameters Q^* and P^* are used to analyze the stress state of rocks. Q^* - the parameter characterizing the diversity of the stress field components; P^* - the parameter characterizing the unloading of rocks from the rock pressure

$$Q^* = \frac{\sigma_1 - \sigma_3}{\gamma H}, \qquad P^* = \frac{\sigma_3}{\gamma H},$$

where σ_1, σ_3 is maximum and minimum components of the principal stress tensor, MPa; γ is the averaged weight of the overlying mine rocks, N/m^3; H is the mining depth, m.

3.3 Permeability of fractured rocks

The results of numerous experiments show that the permeability of the rock is a function of the acting stresses and has different meanings in different areas.

Permeability under elastic and uniform compression. Outside the zone of influence of mining, the rocks are in a state of compression with approximately equal components $\sigma_1 \approx \sigma_2 \approx \sigma_3$ ($Q^* < 0.6$). Compaction of rocks and overlapping of fissure-pore channels occur. The permeability filtration k is practically zero. The parameter P^* exceeds the threshold value $P^* = 0.1$, at which the deformation occurs in the regime of plastic or pseudoplastic flow [12]. With elastic deformation, the filtration properties of the medium do not significantly change [13]. We can assume that the zones of elasticity and uniform compression do not belong to the filtration area

$$k = 0 \text{ for } Q^* < 0.6;\ P^* > 0.25. \quad (8)$$

Permeability in the area of initial and intense cracking. For $\sigma_1 > \sigma_3$ ($0.6 < Q^* < 0.8$) microcracks begin to form. The increase in the permeability coefficient is insignificant, since this stage is characterized by the accumulation of single, non-interacting defects [12]. In this zone

$$k = k_{min} \text{ for } 0.6 < Q^* < 0.8. \quad (9)$$

Outside elasticity zone and when the ultimate strength is reached, which corresponds to the region of intense crack formation ($Q^* > 0.8$), uncontrolled crack growth occurs. At this stage, deformations rapidly increase due to the propagation of cracks and loosening of the rock [12]. With an increase in Q^*, the permeability coefficient increases by 2-3 orders of magnitude [14, 15]. A further increase in permeability beyond the ultimate strength occurs only due to the expansion of existing cracks. Using experimental data [16], the dependence of the permeability coefficient on Q^* was obtained

$$k = e^{0.26Q^* - 4.65} \text{ при } 0.8 < Q^* < 1.0. \quad (10)$$

Permeability in the rock destruction zone. When the rate of crack formation reaches a maximum, and the stresses of the ultimate strength of the rock, the process of macroscopic destruction begins. Destruction of geomaterials can be brittle, plastic or intermittent slip [12]. The permeability of the rock depends on this. The brittle fracture of the rock is characterized by an increase in deformations, loosening and, accordingly, the volume of the material. In the case of

plastic flow, material softening occurs without loosening it. Developing cracks are closed and their edges are tightly compressed. During compression deformation occurs with loosening for the condition $P^*<0.1$ [17]. In this case, the permeability coefficient takes the maximum values

$$k=k_{max} \text{ for } P^*<0.1;\ Q^*>1.0. \quad (11)$$

So the relationship between permeability coefficients in the disturbed rocks and geomechanical parameters is determined by relations (8)-(11).

3.4 An example of calculating methane filtration parameters for Pokrovskoye mine control conditions

Let us consider the rock area with 1st northern longwall (Fig. 3). The depth of mining is 570 m, the length of the longwall is 260 m. The thickness of the developed coal seam d_4 is 1.5 m. There are coal seam d_4^1 (0.15 m) 20 m above and coal seam d_4^2 (0.1 m) 38 m above.

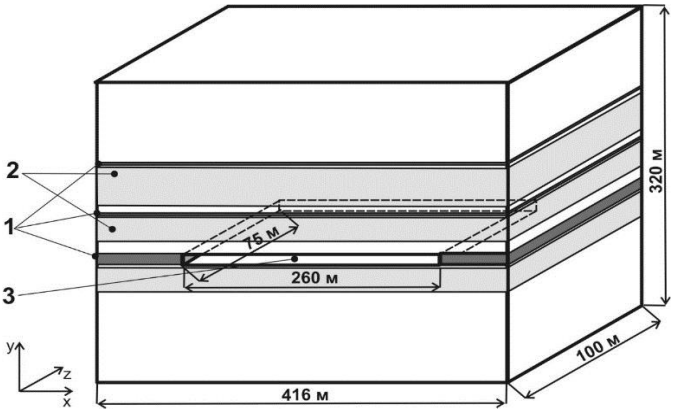

Fig. 3. Design model: *1* – the coal seams; *2* – the sandstones; *3* – the goaf

Potential sources of methane emissions are coal seams and sandstones. The natural gas content of coal is 20 m^3/ton, sandstones is 3.5 m^3/ton.

The fields of stress, permeability, distribution of methane pressure values and its filtration rates at each point of the studied area has been calculated. The calculations have been made for the wall advance speed V_{lw} 3, 6 and 9 m/day. The distribution of the relative

methane pressure p/p_0 in the central longitudinal section is shown in Fig. 4.

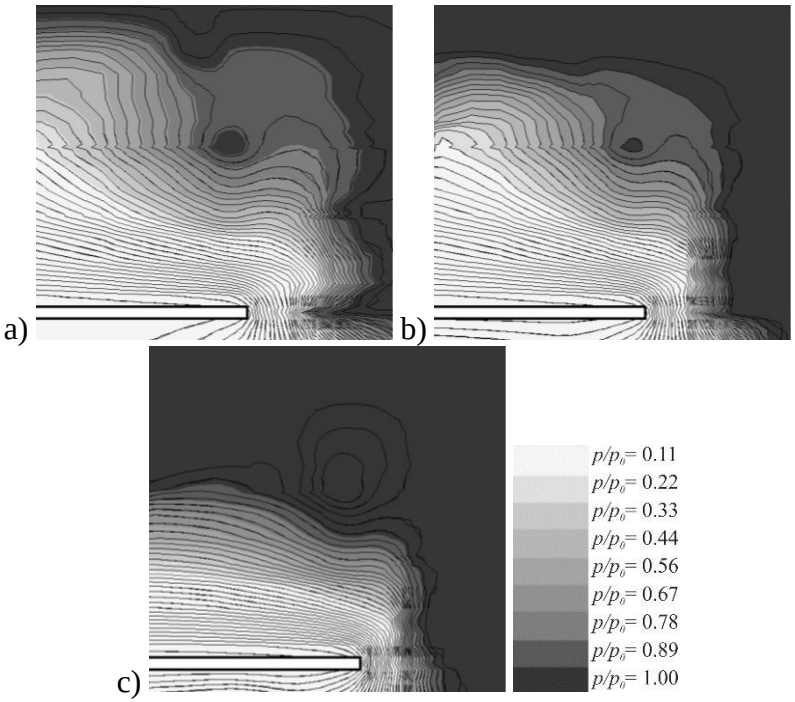

Fig. 4. Isobars of relative methane pressure in the central longitudinal section of the zone: *a* - V_{lw}=3 m/day; *b* - V_{lw}=6 m/day; *c*- V_{lw}=9 m/day

The p/p_0 distribution in the cross section z=50 m at a distance of 25 m behind the longwall face is shown in Fig. 5. It can be seen from the figures that in an untouched massif, the methane pressure remains equal to the pressure in the seam. Inside the filtration zone, the gas pressure is reduced. Methane partially moved to longwall atmosphere. With an increase in the speed of wall advance, the zone of reduced methane pressure decays, the rates of its desorption and filtration decrease as well. As a result, less methane is moved to the longwall.

a

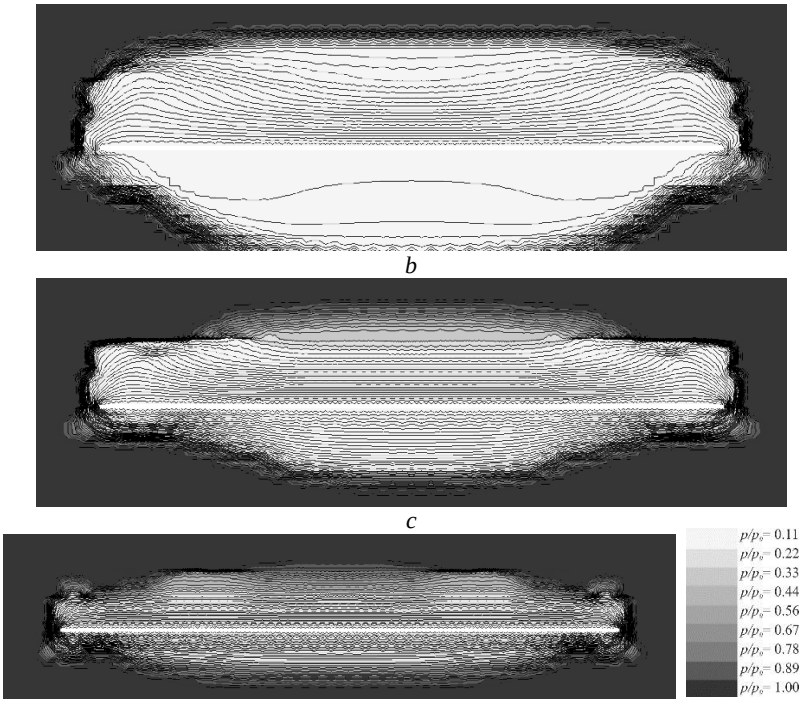

Fig. 5. Isobars of methane relative pressure in the cross section of the studied zone, *z*=50 m: *a* - V_{lw}=3 m/day; *b* - V_{lw}=6 m/day; c - V_{lw}=9 m/day

At V_{lw}=3 m/day in the roof of the longwall, two layers of gas-bearing sandstone and two coal seams will be inside of filtration area. The size of the sources of methane emission decreases with an increase in the speed of wall advance. At V_{lw}=12 m/day, the coal seam d_4^2 and the upper part of the gas-bearing sandstone are outside the filtration area. Its front border shifts closer to the longwall face. The volume of the filtration area at V_{lw} = 6 m/day decreases by 20 %, and at V_{lw}=9 m/day by 46 %.

The methane relative pressure (p/p_0) in the coal seams d_4^1 and d_4^2 at various speed of wall advance is shown on Fig. 6 и 7. Coordinate *z* of longwall face is 75 m.

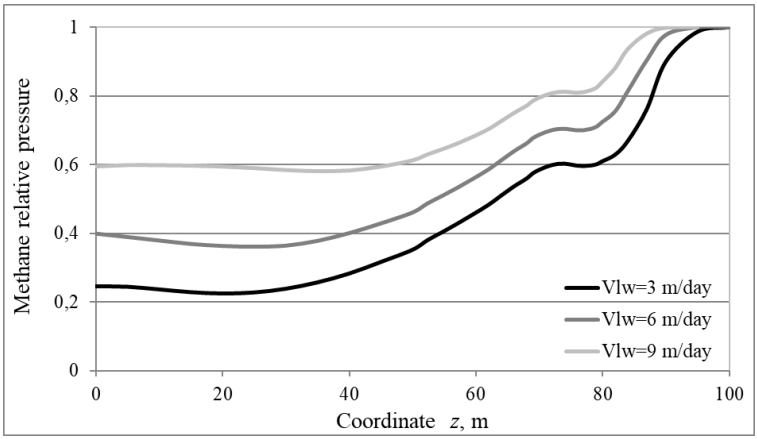

Fig. 6. Methane relative pressure in coal seam d_4^1 during its undermining

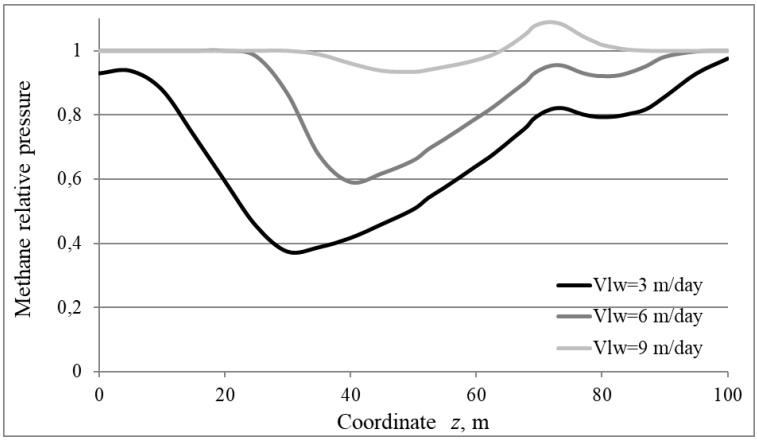

Fig. 7. Methane relative pressure in coal seam d_4^2 during its undermining

It can be seen from Figure 6, the methane pressure in seam d_4^1 is lower than in seam d_4^2. The coal seam d_4^1 is well degassed, unlike the one located above seam d_4^2. With an increase in the speed of wall advance, the relative residual pressure of methane increases from 0.25 to 0.6 (Fig. 6). The pressure in the upper coal seam at V_{lw}=9 m/day differs slightly from the pressure in the undisturbed seam (Fig. 7). Methane from it almost does not enter the longwall at such a speed of wall advance.

Increase in pressure with increase in the wall advance speed also slows down the process of desorption of methane from underworking coal seams.

Comparing the factual specific methane flowrates (Q/A, where Q – daily average methane inflow in longwall and adjoining mine workings, m^3; A – daily average coal production, t) in various mining sites with the calculated ones, we will see that specific methane flowrates decrease with increasing speed of wall advance in both cases (Fig. 8).

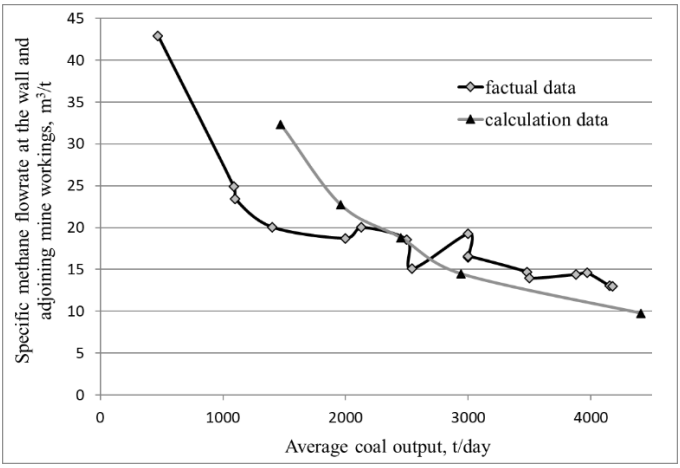

Fig. 8. Specific methane emission rate at the treatment area per ton of coal mined during coal production intensification

Thus, it was found that there is the reduction of methane specific emission at intensification of coal production from softly coal bed.

4 Conclusions

The length of the console hanging over the worked out longwall space is directly proportional to the thickness of the main roof and the modulus of elasticity of the rock, inversely proportional to the depth of mining and the degree of heterogeneity of the massif. With an increase in the speed of the wall advance, the length of this console increases linearly.

With an increase in the wall advance speed, the size of the blocks of destroyed sandstones increases, the process of formation of cracks in the roof rocks slows down. The size of the filtration area near the longwall is reduced. The front boundary of the filtration area shifts closer to the face. Remote sources of gas evolution completely or partially go beyond the filtration area. The residual pressure of methane in underworking gas-bearing rocks and coal seams increases. The cracking process slows down. For this reason, the emission of electrons from new cracks decreases, which activate methane molecules bound by the Van der Waals forces. This leads to a slowdown in methane desorption processes.

Thus, an increase in the speed of the wall advance can reduce the emission of methane in mine. However, due to the increase and redistribution of stresses in the array, the requirements for mechanized and drift supports increase. This should be taken into account when choosing the optimal operating conditions for the coal mine section.

Acknowledgements

The results are part of the program "Promoting the development of priority research areas" (KPKVK 6541230) of state funding for the National Academy of Sciences of Ukraine.

References

1. **Ilyashov, M.A., Agafonov, A.V., Kocherga, V.N., Bodnar, A.A., Skipochka, S.I., & Krukovskaya V.V.** (2009). The abundance of methane in mine workings during the intensive development of gently sloping coal seams. Geotechnical mechanics, 83, 14-25 [in Ukrainian].

2. **Bokiy, B.V., Kasimov, O.I., & Nazimko, I.V.** (2009). The effect of coal face movement speed on the stress-strain state and gas permeability of the massif. Coal of Ukraine, 11, 9-13 [in Ukrainian].

3. **Skipochka, S.I., Usachenko, B.M., & Kuklin, V.Yu.** (2006). Elements of geomechanics of coal and rock massif at high speeds of coal face movement. Dnepropetrovsk: Lira LTD [in Ukrainian].

4. **Skipochka, S.I., Usachenko, B.M., Ilyashov, M.A., Nazimko, V.V., & Mukhin, A.V.** (2004). The property of coal formation rocks in the process of their

destruction to exhibit additional desorption of bound methane molecules. Scientific discovery No. 275. Claimed on July 21, 2004; Priority 12/19/2002 [in Russian].

5. **Bulat, A.F., Skipochka, S.I., Palamarchuk, T.A., & Antsypherov, V.A.** (2010). Methanogeneration in coal seams. Dnepropetrovsk: Lira LTD [in Ukrainian].

6. **Barenblatt, G.I., Entov, V.M., & Ryzhyk V.M.** (1984). The movement of liquids and gases in natural seams. Moscow: Nedra [in Russian].

7. **Kush, O.A. & Kiriukov, V.V.** (2000). Perspectives for the development of gas-coal deposits in the Donbass. Geotechnical mechanics, 17, 23-29 [in Ukrainian].

8. **Shevelev, G.A.** (2000). Metano-intensity of sandstones containing coal seams. Geotechnical mechanics, 17, 204-207 [in Ukrainian].

9. **Malyshev, Yu.N., Trubetskoi, K.N., & Airuni, A.T**. (2000). Fundamental and applied methods for solving problems of coal seams methane. Moscow: Academy of Mining Sciences [in Russian].

10. **Basniev, K.S., Kochina, I.N., & Maksimov, V.M.** (1993). Underground hidromechanics. Moscow: Nedra [in Russian].

11. **Krukovska, V.V.** (2015). Simulation of coupled processes that occur in coal-rock massif during mining operations. Geotechnical Mechanics, 121, 48-99 [in Ukrainian].

12. **Vinogradov, V.V.** (1989). Geomechanics of massif condition control near mining. Kiev: Naukjva Dumka [in Ukrainian].

13. **Szlazak, J., & Szlazak, N.** (2004). Numerical determination of methane concentration in goaf space. Archives of mining sciences. Polish Academy of Sciences, Committee of Mining and Strata Mechanics Research Institute. Krakow, 49 (4), 587-599 [in Polish].

14. **Kulinich, V.S., & Kulinich, S.V.** (2000). The influence of the stress-strain state on the gas recovery of methane-bearing rocks. Geotechnical Mechanics, 17, 152-156 [in Ukrainian].

15. **Stavrogin, A.N., & Protosenia, A.G.** (1985). The strength of the rocks and of the workings stability at great depths. Moscow: Nedra [in Russian].

16. **Kulinich, V.S., Perepelitsa, V.G., Kurnosov, S.A., Ivanchishin, S.Ya., Shumeiko, A.M., & Kulinich, S.V**. (2003). The gas permeability of rocks in a multicomponent field of compressive stress. Geotechnical Mechanics, 42, 18-24 [in Ukrainian].

17. **Li S.P., & Wu D.X.** (1997). Effect of confining pressure, pore pressure and specimen dimension on permeability of Yinzhuang sandstone. Int. J. Rock Mech. Min. Sci., 34(3/4), 435-441.

STATISTICAL ANALYSIS OF EXPERIMENTAL DATA ON THE INDICES OF OPERATION OF THE LOADING UNITS OF THE BAUXITE COMPANY OF GUINEA (CBG)

Keita Daouda
Higher institute of mines and geology of Boké (ISMGB), PhD (Engineering), Senior Lecturer, Director General of the ISMGB in charge of education, Guinea

Pozdnyakov Valery
Gamal Abdel Nasser University of Conakry (UGANC), PhD (Engineering), Senior Lecturer, Senior Lecturer of the Department of Industrial Engineering and Maintenance of UGANC, Guinea

Bah Ibrahima
Gamal Abdel Nasser University of Conakry (UGANC), PhD (Engineering), Senior Lecturer, chief of the Department of Industrial Engineering and Maintenance of UGANC, Guinea

Abstrat

The natural resources, the technical level and the value of a nation's human resources largely determine its economic development.

The proper management of these resources requires reliable information on their nature, importance and conditions of existence in order to determine the most rational methods of exploitation.

In the specific case of the Republic of Guinea, bauxite is of prime importance because of its immense resources which can be exploited according to current technology. It is the country's largest mineral resource and the main source of foreign exchange.

Guinea is the world's second largest producer of bauxite after Australia, with an estimated bauxite potential of over 40 billion tons, which would ensure centuries of production at the current rate of exploitation. The bauxite deposits in the Republic of Guinea constitute a special geological phenomenon, which some have described as a "geological scandal".

The Bauxite Company of Guinea, which is the largest mining company, responsible for about 60% of the country's exports, exploits the exceptionally high-grade bauxite reserves of the Boke region. In recent years, the company's profit has decreased as a result of an increase in financial charges related to investments in the replacement and modernization of production machinery and equipment. Although the bauxite reserves of the region of Boke are no longer of the exceptional quality of the past, the quantity assessed on the site, still allows it to envisage a significant increase in production; however, each prospect of increase in production, necessarily entails a new investment.

This is a major handicap and raises questions: "How do we increase production with less expenditure?"

This is why, despite the large number of equipment and resources involved in mining, the CBG is still faced with problems of efficiency in order to increase its production in order to meet the demands of its customers.

In order to find a solution to this thorny problem, a systematic analysis of all the technical and natural factors affecting the efficiency of production equipment such as (availability factor, utilization factor defined and loading factor of the bucket of excavators having a direct influence on the cycle time;

Therefore, after evaluation of the current parameters of the operations by the statistical method to obtain their theoretical characteristics, these values are compared with their practical average or experimental values in order to estimate the efficiency of the operations.

As a result of this comparison, we found on average per day and per piece of equipment lost time deviations from the planned value. By relating these losses of time in the calculation of the technical production parameters, we have found a significant production margin; because when one proceeds to the reduction of the lost time of the cargo and transport units, one certainly ensures an improvement in the rate of use of the equipment. This ensures an average cycle of 28 minutes per race and per truck for 16 races per shift; an actual production margin of 30% of its planned value for the study period

Introduction

The harmonious development of science and technology would be impossible if man did not proceed to extract the useful minerals which today constitute the framework on which the technological progress of the world today is built.

Thus aluminum by its properties (non magnetic, ductile, light, decorative, good electrical and thermal conductor), by the diversity of its uses (thermite, Aeronautics, shipbuilding, civil construction...) to name only these is at present the most familiar of metals after Iron having a competitive price on the world market.

Demand for aluminum increased dramatically during and after the Second World War and remains strong for several decades of technological progress and economic growth in countries (from 1946 to the mid-1970 s).

Since the end of this period, demand has declined, as the market for aluminum products in the industrialized countries was approaching saturation point on the one hand and on the other hand due to the general economic recession in the world.

However, economic growth and the promising future of previous years led industrialists to build a large number of alumina and alumi-

num plants around the world. Since many of them were put into operation at the very moment when demand was falling, it was the imbalance between production capacity and demand that was the result.

Today the aluminum industry is increasingly cut with a large number of isolated alumina and electrolysis plants that sell their products on the open market.

These various opportunities have made the global aluminum industry intensely competitive. It is hoped that global demand for aluminum and therefore for alumina and bauxite will continue to grow. Each mining company today faces three major challenges.

In view of the increasing competition, a high-quality product must be supplied in sufficient quantity. ;

Economic issue: to maximize the gain, it is necessary to ensure the projected production at a competitive cost. ;

Technological challenge: in order to keep customers, it is necessary to reduce production time, by maintaining the efficiency of technological equipment and installations, correct planning and rigorous monitoring of production operations.

In addition to these main issues, there is also the issue of the environmental impact of mining, which ultimately determines the feasibility of all mining projects, regardless of their industrial value.

The Bauxite Company of Guinea, which is the largest mining company, responsible for about 60% of the country's exports, exploits the exceptionally high-grade bauxite reserves of the Boke region.

For years this company has contributed between $ 100 million and $ 200 million in revenue to the state budget, constituting a major part of the dividends that the government draws from its participation, despite all funding coming from outside.

As part of its commitment to provide quality and quantity bauxite that meets customer requirements and meets specification limits, any deviation from targets results in a loss of revenue that is detrimental to the company's profitability.

In recent years, the main objective of the Company des Bauxites de Guinee is to increase the value of its production each year by keeping the total cost of production constant.

It is in this perspective and in the perspective of making our modest contribution to the search for a solution to the problems related to

the management of the efficiency of the mining machines at the Company des Bauxites de Guinea (CBG) that we present this monograph, in which we have carried out a statistical analysis of the experimental data on all the technical indices of operation of the mining machines from:

Availability factor which characterizes the condition of the various types of equipment;

Utilization factor which characterizes the way in which the company's work is organized;

Load factor of the bucket of the loading units as well as the average number of buckets to load a bucket, having a direct influence on the duration of a run (production cycle).

Actual efficiency of loading units

Loading is a major technological operation affecting the technical and economic indices of exploitation. This is why, in order to ensure a better exploitation efficiency, it deserves special attention in the organization the management of the time of production.

At the Sangaredi mine (CBG), the loading of the damaged mass is carried out by two types of machines: hydraulic excavators (PC-1800 and PC-3000) and hydraulic loaders (Caterpillar 992-GK and Komat'su WA-900-3).

As an example we study the trend parameters of the statistical distribution of the real yields of the excavator PC-1800 in the month of April 2019 which are presented in Table №1.

Since this statistical series is linear, and contains several data, we proceed with the transformation of this linear series into a classified series.

For this, the number of classes is determined by the formula : $K=1+3.3 \log n$

where K - number of classes;

n - total number of employees in the series.

In our case $n=88$ then $K=1+3.3 \log 88 \approx 7$ so $K=7$

Let us calculate the class I interval by the following formula

$$I = \frac{Q_{max} - Q_{min}}{K},$$

where I-class interval;

- Maximum value of the yield (as of April 2019 equal to 2300t/poste) ;

- Minimum value of the yield (as of April 2019 equal to 200 t/poste). i=300

Following these results, we get the following table

Table 1

Absolute and relative frequency distribution
for the excavator PC-1800

Class no	Class	Center class	Effective	Relative frequency
1	200-500	350	8	0,09
2	500-800	650	20	0,23
3	800-1100	950	28	0,32
4	1100-1400	1250	22	0,25
5	1400-1700	1550	2	0,02
6	1700-2000	1850	7	0,08
7	2000-2300	2150	1	0,01
K=7			n=88	1

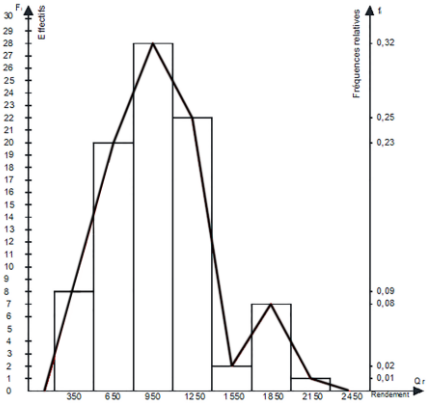

Fig. 1. Frequency range: excavator PC-1800

Determination of trend parameters of the series:

Arithmetic mean for the linear series it is calculated from the expression

$$\bar{X} = \bar{Q}_r = \frac{1}{n}\sum_{i=1}^{n} X_i$$

But for a classified series, it is accompanied by absolute frequencies such as

$$\bar{Q}_r = \frac{1}{n}\sum_{i=1}^{n} F_i Q_{ri} \quad (\text{for } n>30)$$

where n - sample size; F_i - effective or absolute frequency; X - Class center.

For our case we have

$$N>30\ \bar{Q}_r = \frac{1}{n}\sum_{i=1}^{n} F_i Q \text{ (t/p) or } \sum_{i=1}^{n} F_i Q = 88100$$

Table 2

Calculation of trend parameters of the series: Excavator PC-1800

Centre des classes	$\lvert Q_{ri} - \bar{Q}_r \rvert$	$\left(Q_{ri} - \bar{Q}_r\right)^2$	F_i	$F_i\left(Q_{ri} - \bar{Q}_r\right)^2$
350	651	423801	8	3390408
650	351	123201	20	2464020
950	51	2601	28	72828
1250	249	62001	22	1364022
1550	549	301401	2	602802
1850	849	720801	7	5045607
2150	1149	1320201	1	1320201
				12939680

Variance: calculated by the following formula

$$Q_r^2 = \frac{1}{n}\sum_{i=1}^{n} F_i\left(Q_{ri} - \bar{Q}_r\right)^2$$

Standard deviation: it represents the square root of the variance

$$\vartheta = Q_r \text{ thus } \sqrt{Q_r^2} = \sqrt{\frac{1}{n}\sum_{i=1}^{n} F_i\left(Q_{ri} - \bar{Q}_r\right)^2} \quad Q_r = 383{,}46 \text{ t/p}$$

The probability density function: the distribution is described by the probability density formula

$$\phi\left(Q_{ri}\right) = \frac{1}{Q_r^2\sqrt{2\pi}} e^{-\frac{\left(Q_{ri} - \bar{Q}_r\right)^2}{2\vartheta^2}}$$

According to the values of Q_{ri} we will have the values $\phi(Q_{ri})$ of in Table 3

Table 3

Summary of the values of the probability density function

Q_{ri} (t/p)	350	650	950	1250	1550	1850	2150
$\phi(Q_{ri})10^{-4}$	2,46	6,85	10,32	8,44	3,73	0,89	0,12

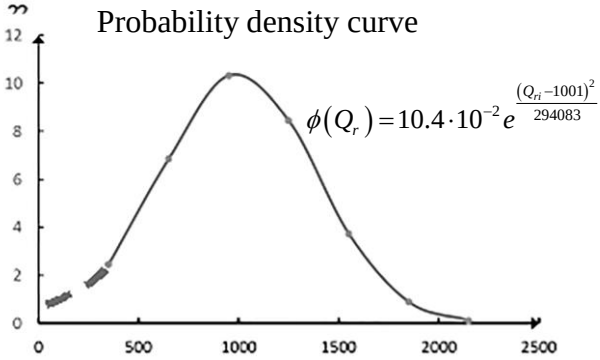

Fig. 2. Probability density curve for the excavator PC-180**0**

Theoretical data Distribution:

The theoretical distribution of data plays an important role in solving problems in many practical areas. Several laws of distribution are used for this purpose, such as : binomial law, poison law, uniform law, normal law among which the normal or Gaussian law is the most used because it can be exploited to solve a large number of problems of interpretation, namely the description of the distribution of experimental errors.

It can serve as a mathematical model for the representation of a large number of theoretical distributions.

This is why in our case if the actual Q_r performance meets the following conditions:

If Q_r is the result of several independent cases with additive effects and each of the cases has a negligible effect on the whole, then Q_r is distributed according to the normal law.

The probability density function in this case is as follows

$$Y = f\left(Q_r\right) = \frac{1}{Q_r\sqrt{2\pi}} e^{-\frac{\left(Q_{ri} - mQ_r\right)^2}{2Q_r^2}}$$

where mQ_r-mathematical expectation of the variable Q_r;

Q_r - standard Deviation of the variable

The curve Y is symmetrical with respect to the line perpendicular to the X-axis in $Q_r = mQ_r$;

On each side of the summit there are inflection points *A* and *B* from which the curve approaches the X-axis.

When Q_r tends to $\pm\infty$; *Y* tends to zero.

The probability density function at the center of symmetry of the curve is equal to

$$f\left(Q_r\right) = Y_{\max} = \frac{1}{Q_r\sqrt{2\pi}} e^{-\frac{\left(Q_r - mQ_r\right)^2}{2Q_r^2}}$$

when $Q_r = mQ_r$ we will have $e^{-\frac{\left(Q_r - mQ_r\right)^2}{2Q_r^2}} = e^0 = 1$

As well $f\left(Q_r\right) = Y_{\max} = \frac{1}{Q_r\sqrt{2\pi}}$

$$f\left(Q_r\right) = Y_{\max} = \frac{1}{383.46\sqrt{2 \cdot 3.14}}$$

$$Y_{\max} = 10.43 \cdot 10^{-4} \quad \text{t/p}$$

By integration, the cumulative normal function is equal to

$$F\left(Q_r\right) = \int_{-\infty}^{+\infty} f\left(Q_r\right) dQ_r = \frac{1}{Q_r\sqrt{2\pi}} \int_{-\infty}^{+\infty} e^{-\frac{\left(Q_r - \bar{Q}_r\right)^2}{2Q_r^2}} dQ_r = 1$$

If the change of origin and scale is done in the following way

$$t = \frac{Q_r - \bar{Q}_r}{Q_r}$$

We obtain the reduced normal centered variable defined on *R* by the probability density

$$Y = f\left(t\right) = \frac{1}{\sqrt{2\pi}} e^{-\frac{t^2}{2}}$$

Then the Laplace function defined by

$$Q(t) = \int_0^t Q(t)dt = \frac{1}{\sqrt{2\pi}} \int_0^t e^{-\frac{t^2}{2}} dt$$

$$Q(t) = \frac{1}{\sqrt{2\pi}} e^{-\frac{t^2}{2}} = 0.4e^{-\frac{t^2}{2}} \quad Q(t) = 0.4e^{-\frac{t^2}{2}}$$

According to the values of t in this function, the following table is obtained

Table 4

Summary of the values of the probability density function as a function of the reduced centered variable (t)

t	-3	-2	-1	0	1	2	3
f(*t*)	0,004	0,05	0,24	0,4	0,25	0,05	0,004

Kolmogorov-Smirnov hypothesis Test

In the statistical treatment of experimental data, it is usually assumed that the distribution of these data follows a certain theoretical law depending on the nature of the characters studied, which is a hypothesis.

Thus, the test of Kolmogorov Smirnov allows to answer the question: Can this hypothesis be applicable to these data or not or can one consider as true a sample drawn from a population of theoretical distributions of data?

Kolmogorov Smirnov's test is a means of comparing a theoretical and observed distribution.

According to the data in the table of values of the density function of the reduced centered variable (t) which is equal to

$$t = \frac{X_i - \bar{X}}{\vartheta}$$

where X_i - center classes; $\bar{X}$ - arithmetic average; ϑ - standard Deviation.

For the case of yields we will have

$$t = \frac{Q_{ri} - \bar{Q}_r}{\vartheta}$$

where Q_{ri} - class center; $\bar{Q}_r$ - arithmetic average; ϑ - standard deviation

For the theoretical and the observed frequency to have the same scale, the value of the function f(t) found in the table of values of the density function shall be corrected by the following scale coefficient:

$$K_{echelle} = \frac{n\omega}{\vartheta} = \frac{88 \cdot 250}{383.46} = 57.37$$

where n - total staff ; ω - class interval; ϑ - standard deviation

Table 5

Calculation of parameters to test the yield distribution. For the PC-1800 shovel

Q_{ri}	$\lvert Q_{ri} - \bar{Q}_r \rvert$	t	$f(t)$	Freq theoriq	Freq cum	Freq obse	Cumul	Ecart
350	651	1,70	0,3123	17,91	17,91	8	8	13,49
650	351	0,91	0,2637	15,12	33,03	20	28	1,85
950	51	0,13	0,3956	22,69	55,72	28	56	0,77
1250	249	0,65	0,3230	18,53	72,25	22	78	0,23
1550	549	1,43	0,1435	8,23	82,48	2	80	7,87
1850	849	2,21	0,0347	1,99	84,47	7	87	5,38
2150	1149	2,00	0,0044	0,25	84,72	1	88	0,70
$K_{\text{échelle}}$=57.37								

Of the maximum deviation found and the number of samples observed, the parameter λ_n is given by the following formula:

According to the table for the Kolmogorov-Smirnov test, we find the probability $P(\lambda_n)$. If $P(\lambda)$ is greater than 0.05 then we can say that the studied distribution follows the normal law. In our case the maximum deviation $Ecart_{\max}$=13.49; n=88

Then $\lambda_n = \frac{9.91}{\sqrt{88}} = 1.0564$ λ_n=1,06

Depending on the values of λ_n, the corresponding values of $P(\lambda_n)$ are chosen. So for λ_n=1,06 then $P(\lambda_n)$=0.2700

This value of $P(\lambda_n)$ is greater than its lower limit, so this distribution follows the normal law.

Confidence interval

The question can be answered as to the quality of the estimation of the mean m of the distribution by the mean of the sample.

If A and B are the random values, (a, b) is the confidence interval at the rate if the probability P. $P(a \le m \le b) \ge 1-\alpha$

Estimate the mean m at the rate of 95%, the confidence interval will be

$$\left(\bar{X}-1.96\frac{\vartheta}{\sqrt{n}};\bar{X}+1.96\frac{\vartheta}{\sqrt{n}}\right)$$

The precision is thus calculated by the formula

$$R=1{,}96\left(\vartheta/\sqrt{n}\right)$$

The above expressions are valid for sufficiently large samples (n>30).

Since in our case n is greater than 30 (n>30) we will have

$$\left(\bar{Q}_r-1.96\frac{\vartheta}{\sqrt{n}};\bar{Q}_r+1.96\frac{\vartheta}{\sqrt{n}}\right)$$

For an estimate of the average at the 95% rate, the precision is therefore

$$R=1.96\frac{383.46}{\sqrt{88}}=80.12\ \ R=80{,}12$$

So $\bar{Q}_r=1001\pm80.12$

In the same way, we have processed the experimental data on the actual performance of the three (3) other models of loading equipment, namely:

Excavator PC-3000; CAT – 992-GK Loader and Komat'su Wa – 900-3 Loader. The treatment results are shown in Tables 7, 8 and 9.

Table 7

Summary of the results of the calculation of the trend parameters of the distribution of the real yield of the three gears

Parameter / Gear	Average $\left(\bar{Q}_r\right)$ t/post	Variance (V) t/post	Standard deviation (Q_r) t/post
Excavator PC-3000	917	184019	429
Loader Caterpillar 992-GK	1036	185075	430
Loader Komat'su WA-900-3	1108	257460	507

Table 8

Summary table of the values of $P(\lambda_m)$ as a function of the values of λ_m

Parameter / Gear	$Ecart_{\max}$	$\Sigma F_i=n$	λ_n	$P(\lambda_n)$
excavator PC-3000	11,18	90	1,17	0,1122
Loader Caterpillar 992-GK	10,47	84	1,14	0,1777
Loader Komat'su WA-900-3	11,70	74	1,36	0,0681

In conclusion, all the values of the probabilities found $P(\lambda_n)$ are above the threshold of $P(\lambda_n)$=0,05; then we can affirm that the distributions of the real yield of the three (3) cargo gear according to the normal law.

Since the sample size is greater than 30 (N>30) for the three (3) loading units then we can estimate the average at the 95% rate with the following confidence interval

$$\left(\bar{X} - 1.96\frac{\vartheta}{\sqrt{n}}; \bar{X} + 1.96\frac{\vartheta}{\sqrt{n}} \right)$$

Table 9

Summary table of confidence intervals of the actual yield per shift of the three gears with 95% probability

Parameter / Gear	Arithmetic averages	Confidence intervals
Excavator PC-3000	917	917±89
Loader Caterpillar 992-GK	1036	1036±92
Loader Komat'su WA-900-3	1108	1108±109

Analysis of technical indices affecting the performance of loading units

The operating efficiency of loading units is calculated by the following formula

$$Q_{Ex} = \frac{3600 \cdot E \cdot T_p \cdot K_r \cdot K_u}{t_c \cdot K_f} \gamma \text{ t/p}$$

In the course of studies on the variation of the values of the actual efficiency of loading machines, we have found that there are three (3) main technical indices which directly affect the efficiency, depending on the condition of the slag mass (grain size, bulking, geometric dimensions, physical condition, etc.) and the way in which

- Utilization factor (K_u);
- Load factor (K_r);
- Duration of the working cycle (t_c);
- Coefficient of availability (K_d)

Utilization factor study (K_u)

The utilization factor represents the ratio between the time worked and the programmed time and is written as follows

$$K_u = \frac{T_{trav}}{T_{prog}} ; (\%)$$

où T_{trav} - time worked by post; T_{prog} - time programmed by post.

This formula is actually applied to find the utilization factor (K_u) at the first workstation. For the other two (2) items, the following expressions are used

$$K_{u_{II}} = \frac{Q_{II}}{Q_I} K_{uI} \text{ et } K_{u_{III}} = \frac{Q_{III}}{Q_I} K_{uI}$$

where K_{uI}, K_{uII} and K_{uIII} are the utilization factor for the 1st, 2nd and 3rd shift respectively.

Statistical processing of experimental data on coefficients of utilization of loading units

We treat the experimental data in the same way as the previous method applied to real yields. The results of the treatment are shown in Table 10.

Table 10

Summary of confidence intervals for shift utilization factors of loading units, with 95% probability

Parameter / Gear	Arithmetic average	Confidence interval
Excavator PC-3000	0,70	0.7±0.0294
Loader Caterpillar 992-GK	0,54	0.54±0.0337
Loader Komat'su WA-900-3	0,71	0.71±0.0305
	0,65	0.65±0.0373

These confidence intervals show that the value of each distribution is very close to the average of the utilization factors of each loading unit. This means that the organization of loading work at the Sangaredi mine affects the cycle time of the machines.

Study of the filling factor of the bucket

In practice, the extracted ore does not occupy exactly the geometric volume of the excavator bucket. Depending on The Shape of the load and the bulking of the rock, the actual capacity of the bucket may be lower or higher than its geometric volume. When the ore is well fractured during mining, the degree of bulking increases, which favors normal filling of the excavator bucket. But on the contrary,

when the cut Mass contains a high percentage of pieces of Rock whose dimensions are outside the gabarie, that is to say, exceeding the geometric dimensions of the bucket of the excavator, then the filling of the bucket of the excavator is called into question and the duration of the cycle of loading of the trucks will increase.

This is why, in calculating the efficiency of the machines, we have taken into account the degree of utilization of the capacity or the coefficient of filling of the excavator bucket expressed by the actual quantity of ore in the bucket compared to its geometric capacity

$$K_r = \frac{V_r}{E}$$

where K_r - filling factor of the bucket ;

V_r - actual volume of rock in excavator bucket;

E - capacity of the excavator bucket, given by the manufacturer.

To determine the values of this coefficient we used the results of the average tonnages loaded in the trucks during our research period (April 2019).

According to this method, the expression of the filling coefficient of the bucket becomes

$$K_r = \frac{Q_g}{Q_r}$$

where Q_g - actual quantity of ore in the bucket of the excavator; determined by the average tonnages put in the trucks, by the expression

$$Q_g = \frac{T_{moy}}{N_g},$$

where T_{moy} - average tonnage loaded in trucks during the month of April 2019; N_g - average number de godet pour charger un camion.

A cause de son impact sur le nombre de godet, la durée du cycle de chargement ainsi que le rendement d'exploitation des équipements, le coefficient de remplissage mérite une attention particulière

Analysis of the filling factor and the number of buckets in the loading units

This analysis is based on the study of the interdependence between the load factor and the average number of excavator buckets to fill the dump truck.

To determine the interdependence between these two parameters for each of the loading units, the actual values of these indices were used to determine their correlation using the correlation coefficients (table 11).

Table 11

Summary of the results of the calculation of the correlation coefficients

Loading units	Correlation Coefficients	Interpretation
Excavator PC-1800	- 0,82	Negative strong
Excavator PC-3000	- 0,90	Negative strong
Cat 992-GK loader	- 0,84	Negative strong
Komat'su WA-900-3 loader	- 0,91	Negative strong

On the basis of the results of the calculation of the correlation coefficient of these two technical indices, it can be confirmed that there is a strong but inverse correlation between the filling coefficient and the number of buckets.

Study of the availability factor of loading units

The availability coefficient is the ratio between the time available and the time programmed

$$K_d = \frac{T_d}{T_p},$$

where T_d - time available; T_p - time planned.

The treatment of the experimental data is carried out in the same way as the previous method applied to the utilization factor. The results of the treatment are shown in Table 12.

Table 12

Summary of the results of the calculation of the technical indices of loading units

Loading units	K_d real	K_d provide	K_u real	K_u provide
Excavator PC-1800	0,82	1	0,70	0,95
Excavator PC-3000	0,81	1	0,54	0,95
Cat 992 - GK loader	0,87	1	0,71	0,95
Komat'SU WA-900-3 loader	0,85	1	0,65	0,95

From this table it appears that the actual average values of the availability coefficient of the loading machines are below their forecast values of 18% which shows that, according to the data of our research period, the planned time management organization for the loading machines is not respected, because of the frequency of stoppages caused by unexpected breakdowns.

The utilization factors are lower than the planned values of 30%, which explains the decline in the production efficiency of loading units.

This phenomenon can be caused either by poor management of the available time, or by the poor physical quality of the ore or by the various conditions of use of the machines, such as: the state of the flat, the size of the slashed mass, the percentage of the big blocks, the incompetence of the operators.

Conclusion

Systematic study and analysis of production processes to improve the production of CBG is a very important and very complicated task from the point of view of the need to increase the efficiency of the machines without spending much. But the current practice of the CBG, other mining companies, and mining sector actors in this specific area of mining, shows us that almost 30% of equipment operating time is lost due to lack of rationality in time management and proper monitoring of production equipment.

The development of this work has enabled us to identify in general, the complexity of the organizational problems of the Bauxite Company of Guinea; but in particular the problems related to the management of the productivity of the machines as well as of the operating cycle at the Sangaredi mine.

Based on CBG's technical capabilities and production objectives under normal conditions, we have theoretically assessed all the parameters of the production sector in relation to planning, namely:

Yields, to estimate the productivity of production equipment;

Technical indices to measure their effects on gear performance.

Following this evaluation, we analyzed the values of these parameters under actual field conditions to determine the shortfall, comparing the results of the practical analysis with their theoretical values. This comparison enabled us to discover significant differ-

ences between these two values in terms of time, efficiency, production and the number of production equipment.

Thus, to reassure ourselves and confirm with certainty the existence of these important margins on all the parameters evaluated, we used an effective instrument for diagnosing technical procedures, called the statistical method.

This method enabled us, using the results of the statistical processing of the experimental data on yield and on all the technical indices having a direct or indirect influence on the yield of the loading units , to answer the question whether or not these loading units are capable of meeting the production objectives.

From these analyses it can be seen that the average values of the technical indices (coefficient of use, coefficient of availability ...) are well below their company's target average values, which gives the opportunity to increase production capacity with less expense.

It should also be noted that this study is characterized by a twofold interest:

Scientific: to provide useful information on the operating strategy and management of production equipment; possibility of using statistical methods to diagnose operating processes;

Economically: avoid spending unnecessarily on each production increase project by applying the principles of organization and management of the working time of each piece of equipment in order to improve their performance.

This would result in a production surplus of about 30% of the planned production at the Sangaredi mine.

Bibliography

1. **Bernard Barriau** : Métallurgie générale Paris, 1971
2. **Michel Kerfanto** : Technique statistique- Traitement des Solides ;1971
3. **Geliot** : Technologie d'appareil de l'industrie chimique. Paris 1976
4. **Pascal Montagneux** Manuel de boute feu Nitrobigford 2003
5. **Géologie Minière E**. Kazakov 1975
6. Echantillonnage et Préparation Christian 1999
7. Audit technique d'échantillonnage CBG/Sangaredi
8. Prospection Minière des gisements des minéraux utiles **Anatoly Bortinikov**
9. Procédé de contrôle qualité CBG 2003
10. Stratégie d'amélioration constante de la Qualité/ CB Juin 2001

11. Statistique Appliquée et outils d'amélioration de la qualité 2ème Edition 2001
12. Introduction aux méthodes statistique et contrôle qualité Edition SMGM.
13. Guide caterpillards « Matériel et méthodes, Edition 1990 »
14. Cours de contrôle statistique de procédé CSP enregistré au CDF de Kamsar 1993.
15. Traitement statistique des données expérimentales (Première partie) 2001
16. R**. Dorfman, P Samuelson et R Solow** : programmation linéaire et gestion économique.Dunod 1962 ;
17. **M Desplas** :Mathématique de la décision économique, complement et exercices Dunod 1967
18. **La prar Benayoun** : La pratique de l'optimisation dans l'entreprise PUF 1974
19. **R. Faure** : Guide de la recherche opérationnelle (tome 2) Masson 1990
20. **R faune**, Precis recherche opérationnel Dunod 1979
21. **B Guerrien et G Archinard** : Analyse mathématique pour l'économiste.
22. **AlBouy**. :La régularisation econopmique des entreprises Dunod 1982
23. François Monchy :Maintence : Méthode et organisation 2ème Edition Dunod 2007
24. **Cébo Maurice** GBILIMI : Cours de Statistique appliquée à la recherche et à l'exploitation minière 2003
25. **M. Kamien et N Schwartz** North Holland Méthodes et modele de la recherche opérationnelle 1981.
26. Rapport du plan minier :CBG 2015.
27. Gestion de la valeur dans le secteur minier : Wold Economic Forum 2013
28. **Hoover, H.C** 1909, Principles of Mining ; New York
29. **Vallée,M**. 1986 Mineral inventory ; from Resource reconnaissance and Evaluation
30. **Leigh, O.E** 1986 : Reportingon Reserves.
31. **Carlier A**. 1963 : Contribution aux méthodes d'estimation des gisements Paris France
32. Wold Class : 1989 : Editorial, The Northern Miner
33. **V.Giard** : Gestion de la production, économica. 1988
34. **D. Hague** : Economie du management. Dunod 1971
35. **I.Horowitz** : An introduction to quantitative busness analysis Mac. Graw Hill 1965
36**. L.Kantorovitch** : Calcul économique et utilisation optimale des ressources. Moscou 1960. Dunod 1963
37. **S.Sethi et G Thomson** : Optimal Control Theory. Application to management science : Martnus Nijh.

MODELING OF THE PROCESS OF MINING OF ZEOLITE-SMECTITE TUFFS BY HYDRO-WELL METHOD

Yevhenii Malanchuk
National University of Water and Environmental Engineering, Doctor of Technical Sciences, Professor of the Department of Automation, Electrical and Computer-Integrated Technologies, Ukraine

Sergiy Stets
National University of Water and Environmental Engineering, Candidate of Technical Sciences, Associate Professor, Associate Professor of the Department of Automation, Electrical and Computer-Integrated Technologies, Ukraine

Ruslan Zhomyruk
National University of Water and Environmental Engineering, Candidate of Technical Sciences, Associate Professor, Associate Professor of the Department of Automation, Electrical and Computer-Integrated Technologies, Ukraine

Andriy Stets
National University of Water and Environmental Engineering, Student, Ukraine

Abstract

The essence of the work is to study and model individual technological operations and determine the technological parameters of underground development of zeolite-smectite tuffs deposits by hydro-well method, taking into account the dominant factors of the process.

The work research the process of destruction of the massif under different conditions and methods of influence, identifies the main parameters that affect the process of hydrodynamic erosion of zeolite-smectite tuffs and established dependencies between the physical and technological indices of hydromonitor erosion of the massif rocks, determined the relationship between the indices of energy of erosion mineral consumption to optimize the extraction process.

The parameters of the technology of mining of the chambers of zeolite-smectite tuffs by hydro-well method deposits have been substantiated, the dependence of the flow transport ability on the flow rate of the hydromonitor under different conditions of movement of the destroyed tuff in the mining chamberhas been investigated and established. This will allow the effective extraction of zeolite-smectite tuffs for further use in various industries.

Introduction

Due to the widespread use of zeolite-smectite tuffs, the issue of using well hydrotechnology for their extraction is included in the state program of development of mineral resources of Rivne region [1-3].

To substantiate the parameters of well hydrotechnology for the production of zeolite-smectite tuffs in the work conducted research and proposed solutions that consist in establishing the laws of the process of erosion of rock, transportation in the flow of hydraulic mixture and the formation of mining chambers, which will be the basis of theoretical and technical solutions [4-7].

The novelty and the distinguishing features of the investigated and modeled methods of self-propelled hydraulic transport along the bottom of the extraction chambers is that the calculation is conducted with the condition of determining the qualitative and quantitative parameters of the erosion process: the amount of working agent required for erosion; the productivity of the erosion of the minerals, the coefficient of roughness of the bottom; radius and angle of the erosion sector.

Given that the creation of a common model of well hydrotechnology, mining is almost impossible due to methodological and technological difficulties, studies have been conducted for individual technological operations [8, 9].

Investigation of processes of erosion and fluidity of the hydraulic mixture

The movement of fluid in a jet is characterized by the movement of water particles in the absence of rigid boundaries of the channel. During the movement of a jet, when several liquids are mixed, different in density, as well as in multiphases, when the substance of the jet and the substance of the medium are in different physical states (in gaseous or dropping), and sometimes with the admixture of solids in the boundary layer of the jet, phenomena occur so complex that at the present stage there are no reliable methods for their analytical determination [10, 11].

The specificity of the formation of the jet in the well hydromonitor is such that as the flow of water to the nozzle, it meets on its way

various supports that contribute to the turbulence and cavitation of the flow, which impair the quality and parameters of the jet. The final formation of the jet occurs in the nozzle, the purpose of which is to convert the static pressure of water into the kinetic energy of the jet, and as the cross section of the nozzle at constant flow of water increases its speed. At the same time, the pressure loss in the nozzle, which is proportional to the square of the flow velocity, increases. In the final section of the nozzle, the static pressure takes into account the velocity head, taking into account the pressure loss [12].

The study of the distribution of the axial dynamic pressure of the jet along its axis with the central and lateral nozzles of the monitor head showed that the axial dynamic pressure of the jet from the lateral nozzle at a distance of 100-150 mm is 45-55% of this value for the central nozzle. This is due to the large losses of head when water enters the side nozzle, which significantly degrades the hydrodynamic characteristics of the jet.

The speed of rotation of the head of the monitor was determined on the stand (Fig. 1). Analyzing the research data, the dependence of the speed of rotation of the hydromonitor head on the pressure at different angles of rotation of the lateral nozzle is established, which is shown in Fig. 2.

The rotating motion of the head gives the centrifugal components of the reaction forces of the jet from the side nozzles. The speed of rotation of the head n was determined at different angles of rotation of the central jack nozzle relative to the axis of the head and at different values of the head of water H_0 at the inlet to the head. During the studies, the angle of rotation of the conveyor nozzle remained constant at α_2=15°.

Studies have also found that with increasing pressure from 0,4 to 1,1 MPa, the pressure loss on the sections of the telescopic shaft of the monitor is practically absent. The telescopic shaft also serves as a straight section that stabilizes the flow of water before the nozzle. Water costs for hydro screwdriver at the nodes of the telescopic shaft units were 15-18%.

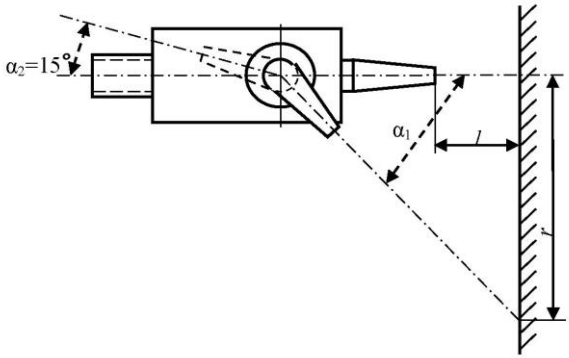

Fig. 1. Scheme of a stand for research of a hydromonitor head

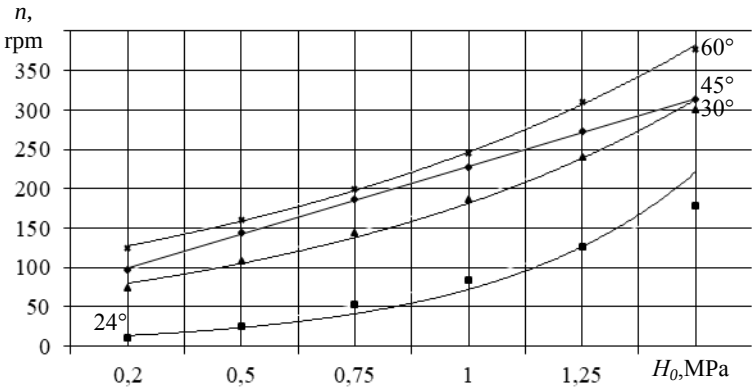

Fig. 2. Dependence of speed of rotation of the monitor head on the water head at different angles of rotation of the side nozzle $n=f(H_0)$

According to geological studies tuffs lie above the water saturation zone [1, 13]. In this regard, in our studies, we considered unfilled medium jet hydromonitor (1MPa - 4MPa) pressure.

When the action of the jet on a flat wall, located perpendicular to its axis, the impact force was calculated by the formula

$$P_0 = \rho_в \omega_0 V_0^2, \quad (1)$$

where $\rho_в$ - is the density of water, V_0– is the velocity of the jet at the outlet of the nozzle, and ω_0 - is the cross-sectional area of the jet.

In chambers, the erosion of the jet acts on a flat wall with a one-way outlet. The impact force of the jet in this case

$$P_0^I = P_0 K' , \quad (2)$$

where K'- is the coefficient taken within 1,3-1,4.

The specific pressure of the jet on the obstacle in all cases was determined by the formula

$$p_0^i = P_0^i / \omega_0 . \quad (3)$$

Pressure water jet has no solid particles, so as it moves away from the nozzle, it changes all its initial parameters – shape, diameter, speed, pressure. The reasons for this change are air resistance; aeration of the jet by air and its spraying, accompanied by an increase in diameter; the action of compressed air inside the jet; the presence of turbulent formations inside the jet; the effect of gravity.

The maximum pressure along the cross-section of the pressure water jet, ie axial dynamic pressure, as shown by studies, for all values, of the diameter of the nozzle and the pressure of water decreases with increasing distance from the nozzle and for low-pressure and medium-pressure water jets is determined by dependency

$$p_l^{oc} / p_0 = (l / l_n)^{-k'} , \quad (4)$$

where p_0 - is the jet pressure at the outlet of the nozzle, k' - is the coefficient characterizing the intensity of jet decay (for low-pressure water jets with a nozzle d_0=50-190 mm k'=0,5; for medium-pressure ones - k'=0,85).

As the distance from the nozzle pressure water jet due to the occurrence of transverse velocities and interaction with the air expands and its diameter increases. To calculate the diameter of the jet d_l at a distance l from the nozzle used the expression

$$d_l = d_0 \mu^{0,5} (l / d_0)^{0,115} (p_0 / p_l)^{0,25} , \quad (5)$$

where μ=0,93-0,96 - is the nozzle flow factor, p_l - is the average dynamic jet pressure at a distance l from the nozzle, calculated by the average pressure at the outlet of the nozzle

$$p_l = p_0 \cdot \varphi_l . \quad (6)$$

The following formula is used to calculate the parameters φ_l

$$\varphi_l = 320 / \left[(l / d_0)^{1,5} \sqrt[4]{H_0 + 320} \right]. \quad (7)$$

where H_0 - is the initial head.

The average velocity of the jet V_l at a distance l from the nozzle was calculated by the formula

$$V_l = 1{,}4 p_l^{0{,}5}. \quad (8)$$

Solving the flight range of a jet is of great practical importance, especially when determining the location of a hydromonitor with respect to a slope.

The theoretical jet flight range (excluding aeration and air resistance) was determined by the formula

$$L_{cmp}^{T} = (V_0^2 / g) sin 2\alpha_3, \quad (9)$$

where α_3 - is the angle of inclination of the jet to the horizon, deg.

From the conducted researches it follows that the maximum flight range of the jet will be at the angle of inclination of the jet monitor to the horizon α_3=30-45º.

To destroy rocks, the pressure of the jet on contact with the rock must be greater shear resistance.

For cemented tuffs and similar rocks the shear resistance is expressed by the Coulomb formula

$$\tau = c + (\sigma - p_{\Gamma}) \cdot tg\varphi_в, \quad (10)$$

where σ - is the total normal voltage; p_{Γ} - is a neutral voltage equal to the hydrostatic pressure of water in the pores; c - clutch coefficient (for loose tuffs it is possible to accept: c=0); $\varphi_в$ - is the angle of internal friction.

The decrease in shear resistance of zeolite-smectite tuff rocks during vibration is due to the change in stress state, as well as due to changes in the angle of internal friction or coefficient of friction. As a result, there is a violation of the structure of the rock due to the displacement of individual unstable particles. When the vibration is affected, there is a process of constant dilution: the first impulse changes the upper layer, which in turn causes the unloading of the lower layers and their transition to a rarefied state in subsequent vibrations [14, 15]. The dilution zone is constantly moving, extending into the depth of the layer.

Modeling of the process of pulp hydrotransport in the extraction chamber

The displacement of the hydromonitor tuff destroyed by the jet to the absorber of the dispenser occurs in the stream along the bottom of the chamber by self-propelled or pressure flow of water. In addition, self-propelled delivery can be effectively used on the surface, from minning wells to a map of the inwash or pumping dredge pump [16-19].

The erosion of the camera is carried out by sectors, which causes the presence of different specific costs of the working agent along the length of transportation and leads to variability of flow rates. Ultimately, the factor of variability of specific costs and velocities influences the transport capacity of the stream, which is minimal near the slope and increases in the direction of final production. On the other hand, the amount of minerals destroyed is maximum near the slope of the mining chamber and minimum near near of final production. Therefore, the loss of minerals near the slope is large enough, even at the first meters of the blasting radius of the extraction chamber, increasing (due to the imposition of previous floods) as the slope is advanced. Over time, this makes it impossible to transport the reflected mineral without repeated erosion the entire area of the sector. Increasing the transport capacity of the stream near the slope by increasing by increasing the work agent cost will not only lead to a significant cost overruns, but also to an increase in the productivity of hydroerosion. This creates the same problem - the inability to arrange at the periphery of the extraction chamber (near the slope) such flow rates that would allow the transport of all the amount of reflected minerals [20-22]. This significant difference is the basis of studies and calculations of hydraulic transport of mining in hydro-well.

The process of hydrotransporting the pulp to an automated well monitor or outlet is a separate element of the system, so the reliability of this link determines the efficiency of the entire technological complex. Knowledge of the nature and basic laws of this element will allow you to choose the optimal conditions of transportation of the hydraulic mix [23, 24].

It is worth noting another important fact: studies of hydrotransportation in related industries were carried out, as a rule, with the invariance of the flow of working fluid, whereas the hydrotransporta-

tion of the mixture under these conditions occurs at a variable flow of water. In addition, all known studies were carried out in the transportation of material that has no initial velocity (fixed on a trench or the bottom), which is significantly different from the conditions of erosion and hydraulic transport to the bottom of the chamber. Here, the eroded minerals have a considerable amount of kinetic energy when they fall to the bottom of the chamber. With a certain flow of working fluid and a sloping bottom, the initial speed of the hydraulic mix can have a predominant effect on the subsequent transportation at the bottom of the chamber.

It is characteristic that in the majority of studies the task of active interference in the process of formation and preservation of the dynamics and kinematics of the movement of the mixture was not put in order to obtain optimal conditions for self and forced hydraulic transport. The solution to the problems of hydrotransportation was basically to determine the transport capacity of the stream. This approach to the calculation of hydrotransportation under the conditions of well hydrotechnology is unacceptable, since the ability of hydrotransportation is based on the possibility of hydro fracture [25].

The absence of analogues and the need for efficient hydrotransportation require the identification and establishment of the following dependencies: the effect of water flow on the flow capacity of the stream; the influence of the slope of the bottom of the camera on the transport capacity of the stream; the effect of the roughness of the bottom of the camera on the transport performance; detecting the effect of the initial energy of the particles on the technological losses [26, 27].

The potential energy of the open flow of the pulp is spent on the interaction of: the working agent with the bottom and walls of the camera; fluid particles with each other (friction in a liquid); particles of moving rock with each other and overcoming local resistance. It is not possible to quantify energy consumption individually for each interaction, so the method of cumulative estimation of flow performance is adopted. The total work is expressed by the maximum transport capacity of the solid flow at a given inclination of the bottom of the chamber of extraction and consumption of the working agent [27].

It is extremely difficult to investigate the parameters of the technology of mining of minerals from the camera, so experiments were

carried out in a laboratory on a model stand (Fig. 3). It is practically impossible to perform absolutely appropriate modeling of well hydraulic production of tuffs, so the results of the studies are only quantitative.

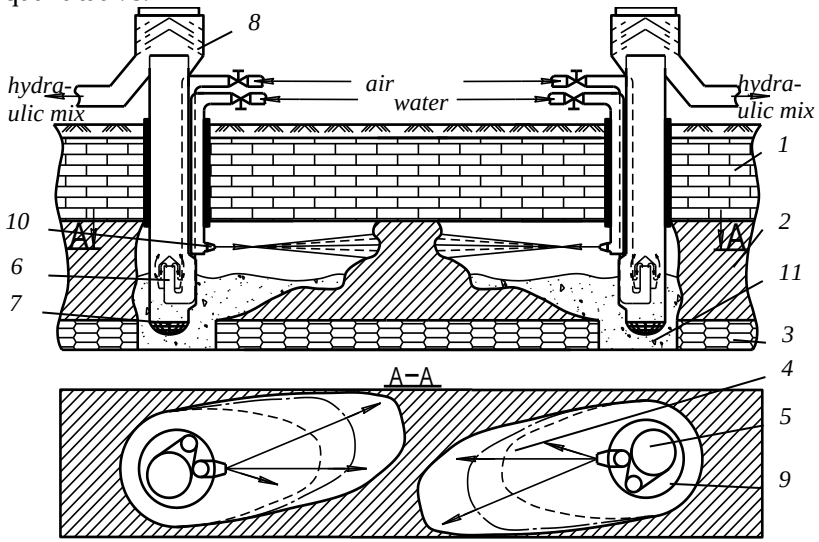

Fig. 3. Scheme of the stand for studying the technology of working out of the extraction chambers: *1* - rock of the roof; *2* - layer of zeolite-smectite tuff; *3* - the underlying rock; *4* - mining chamber; *5* - erlift; *6* - erlift nozzle; *7* - suction pipe; *8* - air separator plate type; *9* - casing string (well); *10* - a hydraulic monitor; *11* - hydraulic mi

The purpose of the research on the choice of the scheme of working out of the camera was to determine the most effective way of destruction and extraction of rock, the choice of the method of carrying out excavation works, as well as to determine the characteristics of the extraction equipment. Three schemes of working out of the chamber were studied: counter, back slope and circulating flow.

According to the first scheme, the extraction works were carried out by sectors around the production well.

In the second scheme, the drilling first occurred by beating the wells with a channel and then expanding it. In this case, the well hydromonitors work on each other, creating favorable conditions not only for the destruction, but also for the transportation of rock in the chamber,

as the jet energy is used most rationally in the coincidence of the movement of the hydraulic mixture and the promotion of the slope.

The third scheme is close to the first and provided for the formation of the primary chamber is not over the entire radius of effective action of the jet. The gradual and continuous rotation of the nozzle of the hydromonitor creates a circular circulation of the hydraulic mix in the bottom zone of the chamber. In this case, the jet energy is also used to transport the mixture to the dispenser.

The experiments were carried out at diameters of nozzles hydromonitor d_0 equal to 4,2 and 6,0 mm, changing the water pressure H_0 from 0,2 to 0,7 MPa and reservoir power 0,08-0,19 m. erlift performance 5 and density hydraulic mixtures 11 were measured by measuring capacities. Model layer 2 is represented by zeolite-smectite tuffs from the basalt quarry of the village of Ivanchi, selected from a depth of 15,2 m. Roof 1 and the bottom 3 of the reservoir were made in accordance with basalts and lavobreccia. The walls of the laboratory unit were made of transparent glass to accurately determine the shape and size of the chamber 4. The clamping lining created the ability to load the layer.

Averaged data of studies of tuffs by counter- slope are shown in Fig. 4.

Studies have shown that increasing the diameter of the nozzle and the water pressure increase the erosion rate and increase the efficiency of the extraction chamber (Fig. 4, Charts *1,2,3*), but the increase in efficiency is limited by the performance of the dispenser. Increasing the water pressure in the nozzle of the hydromonitor creates an increase in the density of the hydraulic mixture only up to a certain limit (ρ_h=1,3 g/cm^3).

Analysis of the results of the studies showed that of working out of layers from top to bottom in a single-well production scheme creates favorable conditions for the flow of hydraulic mixture to the dispensing device. The scheme of working out of the chambers by a back slope is promising only for the extraction of the rock in pillars. A limitation to its application is the small angle of deviation from the erosion axis.

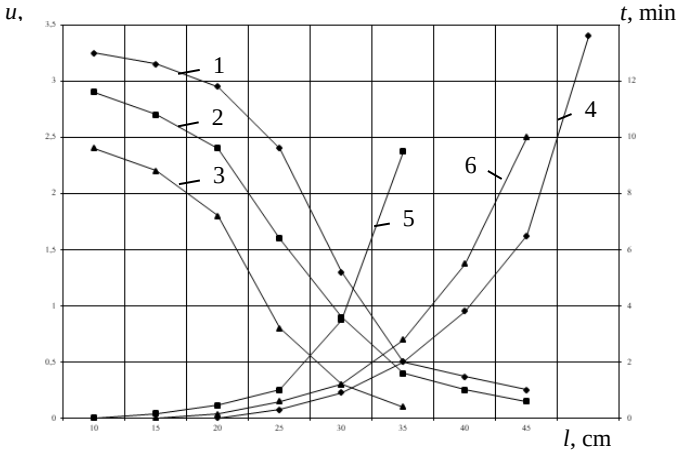

Fig. 4. Dependence of speed and time of erosion on the range of the slope: *1,2,3* - dependence of the speed of erosion u on the range of the slope*l*; *4,5,6* - dependence of the erosion time t on the range of the slope*l*; *1,4* - d_0=4,2 mm, H_0=0,7 MPa; *2,5* - d_0=6,0 mm, H_0=0,2 MPa; *3,6* - d_0=4,2 mm, H_0=0,2 MPa

The erosion of the reservoir and working out of the chambers by the circulation flow showed that, regardless of the power of the waste layer of rock, water pressure and diameter of the nozzle development stopped at a rotation of the nozzle 25° from the initial position.

The process of working out the chamber with undercutting the bottom was less effective due to the collapse of the ore and disturbance of the circulation flow. In the circulation scheme, it is preferable to increase the pressure on the nozzle to increase the working out. Flooding the camera dramatically reduces the efficiency of the discharge. Layered extraction by circulating flow under equal conditions reduces the working time of the camera of the same size by about 25%.

The circulation pattern is very sensitive to changing modes of operation of the hydromonitor and erlift and therefore it is advisable to apply it to the rock with a granulometric distribution. Due to the limitation of production sizes and low circulation stability in the bottom zone, the circulation scheme is less efficient compared to the previous two. Its effectiveness was noted only at the beginning of the formation of the extraction chamber.

Thus, as a result of the conducted research, it is established that the most effective and promising application of mining in hydro-well of zeolite-smectite tuffs is a single-well production scheme with a counter-slope in which the erosion occurs in sectors and round-shaped extraction chambers are formed. And considering that the roof of the zeolite-smectite tuffs are powerful layers of basalt, the most rational system of development is a chamber system with an open treatment space in which the extraction of tuffs will be carried out by layers. Layers should be designed with a slope sufficient for the self- propelled movement of the destroyed rock.

Studies have also found that for large particles (size 8-10 mm), the impact of flow growth occurs only until the liquid level increases to the height of the particle, that is, until it is fully immersed in the liquid. Further increase in flow creates a much smaller effect on the intensity of the action on the particle, since the surface of the liquid does not collide with the plane of the particle perpendicular to the velocity vector, and has an effect only on the flow plot. It can be assumed that with a further increase in the cost of transportation will increase, but the magnitude of the increase in cost will cause only a slight increase. This leads to the conclusion that there is a limit to the impact of increasing the cost of transporting particles of destroyed tuff.

The effect of falling pulp flow on the transport capacity of the stream was also investigated in the experiment. It is revealed that the initial energy of the falling pulp during the erosion intensifies the turbulence of the flow in the bottom space and thereby reduces the probability of sedimentation of the particles, creating an initial velocity of the incident particle. As a result of the blow, the particles of the reflected tuff rise, the pulp density increases and, as a consequence, the ejection force increases, which reduces the adhesion forces of the particle to the bottom.

When the level of the pulp in the bottom space of the chamber was high enough, the energy of falling particle with this layer was exhausted and the sedimented particles could not move. In other words, there must be turbulent motion at the periphery of the extraction chamber and the level of pulp optimal in terms of particle wear.

To create a level playing field transportation along the entire

length of the displacement of the reflected mineral in the extraction chamber, it is necessary to maintain a constant flow rate equal to the speed of reliable transportation. In this connection, it is necessary to create a rational, scientifically sound profile of the bottom of the extraction chamber, which must meet the following requirements:

- to create the optimum (effective in turbulence conditions) flow depth at the slope. If the depth of the pulp in the extraction chamber is large enough (as observed at small angles of inclination of the bottom), then the energy of the reflected particle of the rock will be exhausted upon fall and the deposited particles will not be able to be drawn into motion;
- to create the maximum force of rolling;
- have the optimum length of transportation of the reflected mineral.

Therefore, a rational profile should provide:

- constant flow velocity equal to the speed of reliable transportation;
- minimum losses of minerals during forming;
- the inability to settle the minerals at the bottom of the extraction chamber.

Analyzing the research data it is established that the flow transport properties are in most cases described by exponential dependencies or polynomials of the first order, ie linear functions, and the study of the transport capacity of the flow when changing the flow rate of the hydromonitor and the inclination of the bottom of the extraction chamber indicate that this process is approximated to an equation of this kind

$$Q_n(i, Q_{mp}) = 0{,}41 \cdot Q_{mp} \cdot i + 0{,}032 \cdot Q_{mp} + 15{,}7 \cdot i + 0{,}3. \qquad (11)$$

The maximum permissible relative error of approximation does not exceed 10%.

Conclusions

The process of hydraulic fracturing of the massif during the development of the zeolite-smectite tuffs deposit in the rivne-volyn region by the mining of zeolite-smectite tuffs by hydro-well method was investigated under various conditions and methods of influence and the dominant parameters affecting the hydrodynamic erosion technology were identified

In the erosion of the breed, the residence time in the rarefied state is determined by the thickness of the layer, its water permeability, the change in pores volume in the process of compaction, the placement of drainage and the duration of the dynamic load, destructive structure.

As a result of studies of the transportation process, it is established that the pulp falling to the bottom of the extraction chamber intensifies the turbulence of the flow in the bottom space by creating an initial speed of movement of the pulp to the suction nozzle of the dispenser, which reduces the subsidence of tuffs particles in the stream, the maximum height of which does not exceed two altitudes times the size of the largest fractions of the destroyed rock.

It is established that the dependence of the flow capacity on the flow rate of the hydromonitor and the slope of the bottom of the chamber for the destroyed zeolite-smectite tuff is linear in nature and directly proportional to the specified parameters.

References

1. **Malanchuk Z.R., Stets S.Ye., Malanchuk YE.Z., Zhomyruk R.V**., ta in. Tekhnolohiya i keruvannya hidrovydobutkom korysnykh kopalyn. Monohrafiya za zahalnoyu red. d.t.n., prof. Z.R. Malanchuka. Rivne: NUVHP, 2009. - 480 s.

2. **Malanchuk Ye.Z. Zhomyruk R.V. Stets S.Ye. Shvaher N.Yu. Kalynychenko V.A.** Rozrobka systemy avtomatychnoho upravlinnya sverdlovynnym hidrovydobutkom tufiv. Naukovo tekhnichnyy zbirnyk «Rozrobka rudnykh rodovyshch». – Kryvyy Rih: KTU.-2011 – Vyp. № 94.-S. 94-98.

3. Transportni systemy hirnychykh pidpryyemstv. **Z.R. Malanchuk V.Ya. Korniyenko V.S. Soroka, O.YU. Vasylchuk.** Navchalnyy posibnyk – Rivne: NUVHP, 2018, S. 190.

4. Spetsialni tekhnolohiyi vydobutku korysnykh kopalyn. **Malanchuk Z.R. Malanchuk Ye.Z. Korniyenko V.Ya.** Navchalnyy posibnyk – Rivne: NUVHP, 2017, S. 290.

5. **Malanchuk YE.Z. Zhomyruk R.V. Stets S.Ye.** Optymizatsiya parametriv avtomatyzovanoho kompleksu heotekhnolohichnoho doslidzhennya rodovyshcha. Zb. nauk. pr. „Heotekhnichna mekhanika". – Dnipropetrovsk: IHTM NANU. – 2011 – Vyp. № 92.-S.217 – 223.

6. **Malanchuk Ye.Z. Zhomyruk R.V. Stets S.Ye.** Vykorystannya metodu Fuzzy Logic dlya keruvannya protsesom sverdlovynnoho hidrovydobutku tufu. Tezy mizhnarodnoyi konferentsiyi "Éffektyvnost realyzatsyy nauchnoho, resursnoho y prom. potentsyala ", p. Slavske, Karpaty, 2011., S.165-167.

7. **Drevetsky V.V. Stets S.Ye.** Spetsialni vymiryuvannya i prylady. Navchalnyy posibnyk. – Rivne: NUVHP, 2012. - 288s.

8. **Stets S.YE. Hanzha O.O.** Modelyuvannya avtomatyzovanoho protsesu vydalennya vodnyu z produvnykh haziv syntezu amiaku. Teoretychnyy i naukovo-praktychnyy zhurnal inzhenernoyi akademiyi Ukrayiny. - Kyyiv. Visnyk IAU. – 2012 - Vypusk №1. – S. 265-270.

9. Physico-Mechanical and Chemical Characteristics of Amber / **Z. Malanchuk, V. Moshynskyi, Y. Malanchuk, V. Korniienko.** Non-Traditional Technologies in the Mining Industry. Trans Tech Publications Inc. Solid State Phenomena (Volume 277), 2018, pp. 80-89 doi: https://doi.org/10.4028/www.scientific.net/SSP.277.

10. **Stets S.Ye. Malanchuk Ye.Z. Prokopyuk O.M.** Matematychne modelyuvannya protsesu rozkladky midevmisnoyi hirskoyi porody. Visnyk NUVHP. Zb. nauk. pr. Vypusk 4 (48). Rivne.-2010.- S. 216 – 224.

11. Principles of rock pressure energy usage during underground mining of deposits. / **Khomenko O.Ye., Sudakov A.K., Malanchuk Z.R., Malanchuk Ye.Z.** Scientific Bulletin of National Mining University/ Scientific and technical journal. Dnipro. Ukraine, PP KF «Gerda». №2(158). 2017. – p. 34-43.ISSN 2071-2227 UDC 622.831.24.0010.

12. **Stets S.YE. Stadnyk V.S.** Systema avtomatyzovanoho keruvannya konusnoyi drobarky z konturom poshukovoho ekstremalnoho upravlinnya za tekhniko-ekonomichnym kryteriyem. Mizhnarodna naukovo-praktychna konferentsiya "Informatsiyno-obchyslyuvalni tekhnolohiyi, avtomatyka ta elektrotekhnika". Rivne. 2016. s. 249…251.

13. **Malanchuk Ye.Z. Stets S.Ye. Demyanchuk O.M.** Avtomatyzatsiya protsesu kondytsiyuvannya povitrya vyrobnychykh prymishchen. Visnyk Inzhenernoyi akademiyi nauk. Kyyiv 2014, Vyp.№1.-S.94-99.

14. Examining features of the process of heavy metals distribution in technogenic placers at hydraulic mining / Z**. Malanchuk, Ye. Malanchuk, V. Korniyenko, I. Ignatyuk** // Eastern – European Journal of Enterprise Technologies / PC «Technology Center», Kharkiv, Ukraine, - 2017. - № 1(10). - p. 45-51. Режим доступу: http://nbuv.gov.ua/UJRN/Vejpte2017 1(10) 7.

15. Modeling of vibro screening at fine classification of metallic basalt [Text] / **V. Naduty, Z. Malanchuk, E. Malanchuk, V. Y. Korniyenko** // Theoretical and Practical Solutions of Mineral Resources Mining, 2015. – P. 441–443. doi: 10.1201/b19901-77.

16. Stets S.YE. Malanchuk YE.Z. Trush M.P. Doslidzhennya avtomatyzovanoyi systemy teplovoho neruynivnoho kontrolyu obertovoyi pechi. Visnyk Inzhenernoyi akademiyi nauk. Kyyiv 2013, Vyp.№3-4.-S.121-126.

17. Revisiting the underground gasification of coal reserves from contiguous seams. / **Saik P.B., Dychkovskyi R.O., Lozynskyi V.H., Malanchuk Z.R., Malanchuk Ye.Z.** New Developments in Mining Engineering 2015: Theoretical and Practical Solutions of Mineral Resources Mining. №6. P. 60-66. ISSN 2071-2227.

18. Modeling the formation of high metal concentration zones in man-made deposits. / **Z. Malanchuk, V. Korniienko, Ye. Malanchuk, V. Soroka, O. Vasylchuk**. Mining of Mineral Deposits, 12(2), 2018, p. 76-84. https://doi.org/10.15407/mining12.02.076.

19. **Malanchuk Z., Korniienko V., Malanchuk Y.** Results of research into amber mining by hydromechanical method. Mining Of Mineral Deposits. V.: 11 (1) p. 93-99. DOI: 10.15407/mining11.01.093.

20. The results of magnetic separation use in ore processing of metalliferous raw basalt of volyn region. /**Malanchuk Y., Malanchuk Z., Korniienko V., Gromachenko S**. Mining Of Mineral Deposits. V. 10 (3) p. 77-83. DOI: 10.15407/mining10.03.077.

21. Regularities of hydromechanical amber extraction from sandy deposits. **Ye. Malanchuk, V. Korniienko, V. Moshynskyi, V. Soroka, A. Khrystyuk, Z. Malanchuk.** (2019). Mining of Mineral Deposits, 13(1), p. 49-57. http://mining.in.ua/2019vol13_1_6.html.

22. **Stets S.YE. Stadnyk V.S. Stets N.V.** Systema ekstremalnoho avtomatychnoho keruvannya protsesom droblennya rudy z vykorystannyam ekonomichnoho kryteriyu. Zb. nauk. pr. Visnyk NUVHP. - Rivne: NUVHP.-2016.-Vyp.№ 3 .(75).- S. 335-344.

23. Current status and problems of new technologies for coal mining in the western region Ukraine. / **Malanchuk Z., Zaiets V., Vasylchuk O.,Novak A.** Resources and resource-saving technologies in mineral mining and processing.Multi-authored monograph. – Petroșani, Romania: UNIVERSITAS Publishing, 2018. – P. 54-77.

24. Modern geotechnical methods of management of the process of amber extraction. **Malanchuk E.Z.Malanchuk Z.R.Korniyenko V.Ya.** Monograph: "Innovative development of resource-saving technologies of mining of minerals" "St. Ivan Rilsky»Mining and Mining University of Geology (Sofia, Bulgaria), 2018, - 439p., pp.80-103.

25. Efficiency of using magnetic separation for the processing of metal-containing basalt raw materials. Topical issues of resource-saving technologies in mineral mining and processing. **Malanchuk E.Z. Malanchuk Z.R. Korniyenko V.Ya.** Multi-authored monograph. – Petroșani, Romania: UNIVERSITAS Publishing, 2018. – 270 p., pp.65-89.

26. Analysis of the existent technologies of amber mining. **Korniyenko V.Ya., Malanchuk E.Z., Soroka V.S., Khrystyuk A.O.** Resources and resource-saving technologies in mineral mining and processing.Multi-authored monograph. – Petroșani, Romania: UNIVERSITAS Publishing, 2018. - 363 p., pp.209-232.

27. Mekhanika hirskykh porid. Laboratornyy praktykum. Navchalnyy posibnyk. **Z.R. Malanchuk, V.O. Kozyar, A.M.Polishchuk**. - Rivne: NUVHP, 2016. S.188.

DEVELOPMENT OF EXPERIMENTAL METHODS TO STUDY HETEROGENIC FLOWS IN THE CONTEXT OF HYDRAULIC HOISTING DESIGN

Samusia V. I.
Dnipro University of Technology, Dnipro, Dr. Sc. (Tech.), Professor, Head of Department of Mining Mechanics, Ukraine

Kyrychenko Y. O.
Dnipro University of Technology, Dnipro, Dr. Sc. (Tech.), Professor, Department of Mining Mechanics, Ukraine

Cheberiachko I. M.
Dnipro University of Technology, Dnipro, Cand. Sc. (Tech.), Associate Professor, Department of Mining Mechanics, Ukraine

Trofymova, O. P.
Dnipro University of Technology, Dnipro, Assistant Lecturer, Department of Mining Mechanics, Ukraine

Abstract

In view of rapid decrease of resources of raw-material base of continental formations, problems of ore field development in the World Ocean become absolutely essential. They are connected with the progress of topical research of resource-saving methods intended to extract solid minerals.

Construction of mining marine complexes on the basis of hydraulic systems for the extracted primary material hoisting is notable for high probability of their engineering implementation. Pump hydraulic hoisting and air-lift one are considered as the potentially productive alternatives to transport polymetallic concretions despite their high power intensity. The abovementioned sets the *relevant research and development problem* to improve accuracy of experimental methods.

Subjects of the study are vertical high-speed unidirectional annular flows and disperse flows within blading sections of deep-water hydraulic hoisting.

Objective of the research is to analyze the solid material transportability with the help of vertical three-phase flow in terms of annular and disperse flow structures as applied to hydraulic hoisting modeling. The objective is in the natural line with statement of the research and development problem.

The idea is to decrease power intensity of hydraulic hoisting and to improve its efficiency owing to selection of reasonable consumable parameters while advancing both experimental calculation techniques and theoretical ones as well as implementing innovative designs.

Originality is that for the first time the experimental methods have been developed to analyze three-phase flow with an active role of solid particles using the improved experimental and technical basis.

Innovative scientific finding is in the opening of previously unknown phenomenon titled conventionally «*change of a leader*» which is a definite stage in the development of dynamics of turbulent heterogeneous flows.

Introduction

Having analyzed and generalized their thirty-year experience in the design of deep-water pump and air-lift hydraulic hoisting, the authors believe that the available analytical methods are not efficient due to significant quantitative and qualitative differences in the end results of the modeling.

The efforts applied to improve theoretical models [4] in isolation from the currently unavailable experimental capability only result in unjustified losses of time and mental labour. As for the semiempirical models [10, 11], they are far from being reliable due to the use of closing empirical dependences generated exclusively with the help of short modeling facilities. The matter is that it is impossible to simulate the majority of determinant multiphase hydrodynamical processes, implemented in the deepwater hydraulic hoisting, using the short experimental devices since deepwater air-lift hoisting involves changes in structure of heterogeneous mixture flow, hundred-fold extension of a gaseous phase within a lift pipe, pressure nonlinearity, absorption and desorption processes under the conditions of high pressure gradients, multiscale turbulent fluctuations, specific features of a boundary layer as well as phase interaction etc.

Methodology to design deepwater hydraulic hoisting has been proposed. According to the methodology, at the current stage of marine facilities, the developers should focus on the upgrading of test benches and on the improving of experimental methods. Theoretical methods should be improved in parallel. The abovementioned is the research stage paradigm. One may say allegorically that theory has to step aside for systematic experiments.

Implementation of innovative techniques is the promising tendency to improve the efficiency of hydraulic hoisting [7, 9].

Since the experiments concerning three-phase flows are in the initial stage, it is possible to talk today only of the extension of area of

empiric analysis of sporadic results, and of verification of phenomenological hypotheses.

Experimental studies of annular and disperse structure

Experimental studies of vertical multiphase flow were carried out in the laboratory of hydraulics and hydraulic drive of the Rock Mechanic Department of the NTU "Dnipro Polytechnic" on the basis of the developed integrated experimental hydraulic bench (see Fig. 1). Experiments concerning projectile flow structure have been carried out earlier [1-3].

In view of the new object studies, certain units have been reconstructed and modernized which is described by certain specifications [8].

The bench design provides a possibility to simulate two- and three-phase flows, and to analyze trajectory parameters of sole solid particles as well as their groups within the blading sections of air-lift facilities. Moreover, the bench helps study the airlift behaviour when a value of relative geometric submersion of a mixer is 0.4-0.95 [5, 12]. In view of small dimensions, the experimental device can be only used to study morphology of certain structures of three-phase mixture flow within a vertical pipeline, transportation kinematics of solid particles in terms of different flow structures, and qualitative studies of metering characteristics of short airlifts.

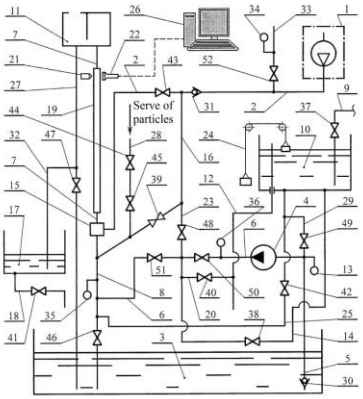

Fig. 1. Integrated experimental hydraulic bench

The authors do not set a goal to implement physical simulation of behaviour of powerful highly productive deepwater hoisting.

The research programme provided series of experiments for different groups of round particles of a monodisperse composition. Each particle group differed in diameters of the samples under study, and their densities. In this context, diameters of the particles being studied varied within the range of 0.002-0.014 mm and their densities varied within the range of 1100-1400 kg/m^3. In addition, groups of particles with similar diameters and varied densities were analyzed.

The complex experimental hydraulic bench consists of compressor unit *1* with pressure pipeline *2*; pool *3*; centrifugal pump *4* with intake pipeline *5*, and pressure pipeline *6*; lifting pipe *7* and feeding pipe *8* of airlift connected with pool *3*.

Pipeline *9* is connected with reservoir *10* through valve *37*. Air separator *11* is mounted on lifting pipe *7*. Pipeline *12* is connected with reservoir *10* and pool *3*. Intake pipeline *5* is equipped by one-way valve *30* and vacuum measuring transducer *13*. Compensatory pipeline *14* involves valve *38*; it is connected with pressure pipeline *6* and reservoir *10*. Mixer *15* is connected with pressure pipeline *2*, lifting pipe *7*, and feeding pipe *8*. Additional pipeline *16* involves valve 39; it is connected with pressure pipeline *2* and feeding pipe *8*. Metering reservoir *17* is connected with pool *3* through a casing neck *18*. Lifting pipe *7* includes an area made of transparent plastic (plastic pipe *19*). Connection pipe *20* is connected with compensatory pipeline *14* and pipeline *12*. Laser light source *21* and photoresistor *22* are fastened in the upper share on the diametrically opposed sides of pipe *19*. Connection pipe *20* includes valve *40*; casing neck *18* includes valve *41*. Bypass pipe *22* is connected with additional pipeline *16* and pressure pipeline *6*. Reservoir *10* is equipped with a float-type transducer to determine liquid level *24* connected with feeding pipe *8* through bypass pipeline *25*. Photoresistor *22* is installed in the frame, making safe from outer light; it is connected to computer system *26*. Outlet pipeline *27* is connected with air separator *11* and pool *3*. Bypass pipeline *25* includes valve *42*. Supplementary connecting pipe *28* is connected with additional pipeline *16* and atmosphere; additional connecting pipe *29* is connected with intake pipeline *5* and bypass pipeline *25*. One-way valve *31* and valve *43* are mounted within a pressure pipeline *2*; valves *44*, *45*, and *46* are mounted within supplementary connecting pipe *28* and feeding pipe *8* respectively. Outlet pipeline *27* includes valve *47*; it is connected

with metering reservoir *17* through separate pipeline *32*. Separate connecting pipe *33* is connected with atmosphere, gas meter *34*, and pressure pipeline *2*; feeding pipeline *8* is connecter with manometer *35*. Valves *48* and *49* are mounted within bypass connecting pipeline *23* and supplementary connecting pipeline *29* respectively. Pressure pipeline *6* is equipped with manometer *36* and valves *50* and *51*; separate connecting pipe *33* is equipped with valve *34*. The device provides the use of valves *37-40*, *42-47*, and *49-52* of ball type.

Basic regularities of the three-phase flow and its effects

Analysis of gas-liquid flows demonstrates definite achievements as for the two-phase flow theory development [6]. However, the data are hardly used for calculation of parameters for hydraulic hoisting of solid material since the processes are complex and poorly understood. The area cannot avoid extra deep analysis of the complicated physical phenomena as well as experimental results.

Vertical flow of a three-phase mixture (i.e. liquid, gas, and solid particles) arises within the marine air-lift. Availability of a solid phase varies significantly the structure of differential equations as well as ideology of the development of mathematical models and experimental methods.

It is possible to make a final conclusion concerning one or another method while comparing analytical results with the experimental data obtained using full-scale facilities. However, it is impossible to implement such efficient devices if a wide range of empirical problems were not solved at the stage of pre-design research.

Various structures of gas-liquid flow, differing in the interaction mechanisms of the flow phases, are of diverse potentials as for solid material transportation. In terms of a bubble flow structure, and a slug one, solid particles are transferred owing to high density of the mixture; in terms of annular structure and disperse one, stable hoisting of the particles is supported by high velocities of the flow.

The following can be considered as the basic difficulties while solving the problem [8]:

– the necessity to take into consideration relative phase velocity, depending upon the size of particles, their shape, surface roughness, concentration of the solid within sludge as well as effect of the pipeline walls, while determining density of the mixture, and its transportation velocity;

– since composition of the solid particles is not homogenous in terms of their sizes, availability of a boundary layer in the neighbourhood of the pipeline walls results in the origination of a radial force factoring into size separation of the particles;

– rotation of the particles and their mutual collision as well as collision with the pipeline walls initiate distortion in the liquid flow and in the increase of turbulent fluctuations.

Such a transition from one structure to another one takes place along with the increase in volumetric flow rate of a gas phase depending upon diameter of the pipeline and its length, physical properties of the liquid and its velocity as well as upon a number of other factors. The mechanism of structure transition may be interpreted as follows. When low-flow rate gas is supplied to a vertical liquid column, gas phase is distributed in the form of separate bubbles. If the bubbles are of rather small diameter, they move like solid spheres performing upward vertical motion. However, while achieving critical size (i.e. a value depending upon the mixture pressure) the bubbles start their deformation; their motion becomes zigzagged and randomized. Along with the increase in the bubble volume, their collision and slug formation take place. While achieving higher velocities, rod-like gas places within a central share of a pipeline pushing liquid away to a periphery. In this context, the liquid layer has undulating boundary line. Liquid waves fractionize and draw into the central gas column in the form of small components. Basically, the liquid moves up owing to resistance forces arising within a boundary line. In the process of further flow acceleration, the wall liquid layer drags into a gas core; a disperse structure of the mixture flow in the form of liquid drops is formed.

The data, represented fragmentally, involve the development of experimental methods as well as modernization of architecture of facilities in the context of the development of mining methods along with adequate equipment when sufficient experience of industrial hydraulic hoisting is accumulated.

The expanded conclusions

1. The current methods of deep-water hydraulic hoisting development should rely upon synthesis of classical scientific bases of liquid and gas mechanics with the latest advances in the empirical suspension theory, and engineering knowledge of the designers.

2. The experimental bench did not demonstrate ideal annular or disperse structures of the three-phase flow; their visualization is rather fuzzy and indistinct.

Maybe, the fact is explained by extra turbulization of the flow due to the availability of solid particles within the mixture being transported; specific features of boundary lines of the phases; and a nature of phase interaction. Thus, the unified disperse-annular model should be considered from the viewpoint of the applied calculation of deep-water hydraulic hoisting. In all cases, the flow under study involves numerous liquid drops compressing the gas core at the expense of mass exchanging processes.

3. Certain experiments demonstrated stable liquid plates and spacers shutting down gas core of the three-phase flow. In the context of Griffith's experiments, formation of such spacers is connected with a slug flow implementation [ ]. Disappearance of the plates coincides with a slug mode transition to an annular one. Probably, the experimental fact may be recommended a priori as a criterion of changes in flow structures in terms of three-phase flow as well. However, changes in the mode should involve greater value of actual gas content of the flow since certain share of the consumed energy is spent for the solid material transportation.

4. Visual studies of both annular and disperse modes have helped detect previously unknown phenomenon titled preliminary as a «*change of a leader»* being typical only for vertical unidirectional high-velocity three-phase flow. The phenomenon idea is as follows: if annular flow structure is applied then transportation of the majority of solid particles within high-velocity gas core leaves behind liquid located mainly at the pipeline periphery owing to the force interaction with walls. In the context of a disperse structure of the three-phase flow, liquid drops, which joined the total flow, leave behind solid particles owing to the difference of acting gravitational forces. The abovementioned results from the gas core destruction as well as from the intensive intermixing of upward phase trajectories. It goes without saying that the phenomenon needs more scrupulous and careful verification, and systematic performance of more delicate experiments.

Moreover, it is also possible to formulate additional useful effect according to which logic one may suppose conceptually that leveling

of profile of velocities of solid particles and liquid drops means indirectly changes in the flow structures.

Referens

1. **Kyrychenko, Y.O., Kyrychenko, V.E., & Evteev,V.V.(**2013). Teoriya i algoritmy rascheta snaryadnogo techeniya v erlifte. Dnepropetrovsk: Natsyonalnyi gornyi universitet [in Russian]

2**. Kyrychenko, Y.O., Goman, O.G., Kyrychenko V.Y., & Romanyukov, A.V.** (2012). Modelirovaniie dinamicheskikh protsessov v glubokovodnykh pnevmotransportnykh sistemakh. Dnepropetrovsk: Natsyonalnyi gornyi universitet [in Russian]

3. **Kyrychenko, Y.O.** (2009). Mekhanika glubokovodnykh gidrotransportnykh sistem v morskom gornom dele. Dnepropetrovsk: Natsyonalnyi gornyi universitet [in Russian]

4. **Kyrychenko, Y., Kyrychenko V., & Romanyukov, A.** (2011). *Research of dynamic processes in deep-water pumping hydrohoists lifting two-phase fluid*. Technical and Geoinformational Systems in Mining (pp. 115-124). London: CRC Press/Balkema, Taylor & Francis Group

5. **Kyrychenko, Y.O., Shvorak, V.G., Kyrychenko V.Y., & Yevteyev, V.V.** (2010). Dinamika glubokovodnykh gidropodyemov v morskom gornom dele. Dnepropetrovsk: Natsyonalnyi gornyi universitet [in Russian]

6. **Pivnyak, G.G., Kyrychenko Y.O. , Franchuk V.P**. (2008). *Problems of deep-water hydraulic lifting of solid mineral resources* . New technologies in mining 21st World mining congress (pp. 49-57). – Krakow

7. **Pivnyak, G.G., Kyrychenko, E.A. , Franchuk, V.P., Yevteyev, V.V., & Shvorak, V.G.** (2009). Sposib zapusku hlybokovodnoho erlifta (varianty) ta erliftna ustanovka dlia yikh realizatsii. UK. Patent № 91130 [in Ukrainian]

8. **Kyrychenko, Y.O., Goman, O.G., Kyrychenko V.Y., & Yevteyev, V.V.** (2014). Osnovy proiektirovaniia sistem gidrotransporta polimetallicheskikh rud Mirovogo okeana. Nikopol: FOP Feldman O.O. [in Russian]

9. **Pivnyak, G.G., Kyrychenko, E.A. , Franchuk, V.P., Yevteyev, V.V., & Shvorak, V.G.** (2009). Sposob zapuska i funktsionirovaniia morskogo erlifta i sistema dlia ego realizatsii. RF. Patent № 2346160 [in Russian]

10. **Kyrychenko, Y.O., Samusya V.I., & Kyrychenko V.E.** (2008). The technology of polymetallic concretions extraction and transporting. *Innovations in Non-Blasting Rock Destruction* (pp.169-178). − Freiberg

11. **Kyrychenko, Y., Kyrychenko V., & Taturevych A.** (2011). *Advanced method for calculation of deep-water airlifts and the special software development*. Technical and Geoinformational Systems in Mining (pp. 215-222). London: CRC Press/Balkema, Taylor & Francis Group

12. **Samusia, V.I., Yevteyev, V.V., & Kyrychenko, Y.O.** (2008). Eksperimentalnoie issledovaniie parametrov vertikalnogo dvukhkomponentnogo potoka primenitelno k erliftnomu techeniiu. *Naukovyi Visnyk Natsionalnoho Hirnychoho Universytetu* (12), 68-74 [in Russian]

MAGNETIC TREATMENT OF PRODUCTION FLUID WITH HIGH CONTENT OF ASPHALT-RESIN-PARAFFIN DEPOSITS

Makarenko V.D.
National University "Yuri Kondratyuk Poltava Polytechnic"
DCs (Engineering), Professor, professor of the Department of Oil and Gas Engineering and Technology, Ukraine

Kharchenko M.O.
National University "Yuri Kondratyuk Poltava Polytechnic"
PhD in Technical Sciences, associated professor, associated professor of the Department of Oil and Gas Engineering and Technology, Ukraine

Manhura A.M.
National University "Yuri Kondratyuk Poltava Polytechnic"
Senior Lecturer, Department of Oil and Gas Engineering and Technology, Ukraine

Petrash O.V.
National University "Yuri Kondratyuk Poltava Polytechnic"
PhD in Technical Sciences, associated professor, associated professor of the Department of Oil and Gas Engineering and Technology, Ukraine

Absract. Justification of magnetic fields treatment to prevent asphalt-resin-paraffin deposits (ARPD) on oil and gas equipment, and consider some current views on the state of ARPD problem on oilfield equipment and possible methods for its solution using magnetic treatment.

Analysis and generalization of magnetic treatment results of production fluid using COMSOL Multiphysics software.

The technology of magnetic fields effect to prevent asphalt-resin-paraffin deposits was introduced in the article. The results of production fluid magnetic treatment made it possible to use it in oil-wells equipped with oil-well pumping units and also at free flow production method or in wells operated by electric-centrifugal pump, as well as in oil pipelines.

The use of high energy magnets based on rare earth materials can reduce asphalt-resin-paraffin deposits in the oil equipment.

The proposed magnetic treatment creates opportunities for field exploitation at the later stages of development which are characterized by a high content of asphaltenes, resins and paraffins. Results of production fluid magnetic treatment have proved the efficiency of this treatment, which has doubled a turnaround time.

Keywords: development of oil fields, asphalt, paraffins, resins, sediments, asphaltene deposits, salt deposits, the magnetic field, the magnetic anti-paraffin device.

1. Introduction

Characteristic features of the current stage of oil industry development in Ukraine are the following: reduce of oil production volume, increase of inactive and low-debit wells, water cut production, scaling and solids, etc. Relevant industry task now is to reduce the number of inactive, not pumping and complicated wells.

It is known that the formation of asphalt-resin-paraffin deposits (ARPD) in producing wells is accompanied by accidents, mainly due to breakages of sucker rod and polished rod that repeatedly reduces their turnaround time (TT) and production volumes.

Different methods are used to control ARPD: the use of scrapers, well treatment by hot oil and water, flushing with distillate, organic solvents, aqueous solutions of surface-active agents (SAA), electric bottom-hole heating, magnetic treatment and inhibiting of borehole production, use of hydrocarbon oxidizing bacteria, etc. [1]

However, all the known methods of ARPD control are limited depending on conditions of specific fields. For example, biotechnological method is limited to high formation pressure and gas factors, a high content of hydrogen sulfide in the oil and temperatures above 40-50 °C and is recommended for wells operated by rod pumps.

Magnetic treatment has its own requirements to applicable environment, such as gas factor (20-300 m^3/m^3), the presence of ferromagnetic particles in well production, content of asphaltenes and resins no less than content of paraffin in oil and so on. Electrical methods have quite complex ground equipment for supplying electricity to underground heating equipment [1-3].

However, the problem of ARPD in the oil fields is actual and needs further improving methods for its solution. Research and experience have discovered the advantages and disadvantages of different ways of ARPD control in conditions of specific fields.

Many deposits of Ukraine are characterized by high temperature of oil saturation with paraffin that reaches 48-50 °C. In addition, a typical part of paraffin deposits is ceresine - crystalline high-paraffin, the number of carbon atoms in which reaches to 36-56 poorly soluble in oil, which melting point is 80-92 °C. The corresponding composition of paraffin is presented in Table 1.

Table 1

Homologous composition of paraffins

Components	Mass fraction of components in the wells of Boryslav OGCF, %			
Resins	2,33	1,55	3,53	2,47
Asphaltenes	2,19	3,96	5,49	2,30
Paraffins	23,82	26,54	56,29	30,57
Ceresin	5,00	11,00	34,00	25,00

Ceresin content in the composition of ARPD can be predominant. For example, according to the data in one of the production wells 70,5% of selected sediment was ceresin.

The industrial observations found that paraffin deposits in producing wells of Ukraine deposits decrease with increasing debits of wells and at insignificant water content in the oil.

There are two stages of ARPD formation and growth. The first stage is the crystal nucleation and growth of paraffin crystal directly in contact with the oil surface. The second stage – precipitating of larger crystals on the surface covered with paraffin.

The formation of ARPD is significantly affected by the following factors:

• reducing of pressure on the bottom hole and the related hydrodynamic equilibrium of gas-liquid mixture (GLM);
• intensive gassing;
• reducing the temperature in the reservoir and borehole;
• changing the speed of the GLM and its individual components;
• hydrocarbon composition in each phase of the mixture;
• ratio of phases;
• surface condition of the pipes.

The intensity of ARPD formation depends on the prevalence of one or more factors that may vary over time and depth, so the number and nature of the deposits are not permanent [4-8].

When bottomhole pressure is less than saturation pressure of oil aeration, the equilibrium system is disturbed, which increases the volume of the gas phase and liquid phase becomes unstable. This leads to the separation of paraffin not only in reservoir but also in a well, starting from the bottomhole.

When pumping an operating pressure at pump sunction may be less than the saturation pressure of oil aeration. This can lead to paraffin deposition in the receiving part of the pump and on the walls of the production string. In the tubing above the pump, there are two zones. The first zone - directly above the pump: the pressure increases dramatically and occurs more saturation pressure. The probability of deposition in the area is minimal.

Second - zone of pressure reduction to saturation pressure and below, where intensive paraffin precipitation starts.

In a flow wells while maintaining pressure in bottomhole, equal to saturation pressure, can be expected a paraffin precipitation in the tubing.

Practice shows that the main objects in which ARPD are formed are well pumps, tubing, flow line from the well, gathering stations [5].

The most intensive paraffin deposition is on the inner surface of the tubing. The thickness of sediments gradually increases from the starting point of their formation at a depth of 500-900 meters and reaches a maximum at a depth of 50-00 meters from the wellhead, and then reduced to the thickness of 1-2 mm in the wellhead (Fig.1).

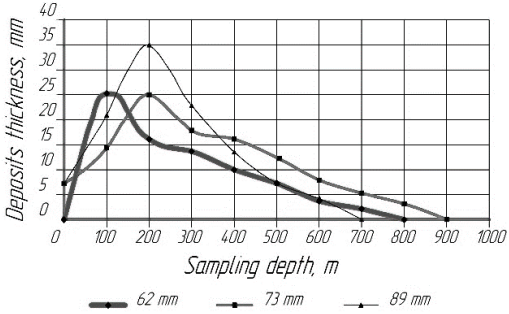

Fig.1. The deposition of ARPD on depth of well

With the decrease of depth is observed the reduction of asphalt-resins in ARPD and the increase of solids and solid paraffins (Fig. 2)

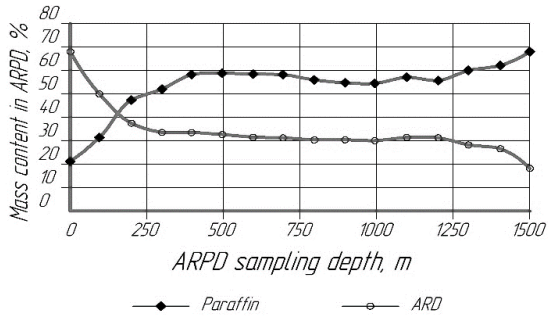

Fig.2. The deposition of ARD and paraffins on the depth of wells

The closer to the wellhead, the more ceresin in ARPD composition and, consequently, higher structural strength of deposits.

Oil is a complex mixture by chemical composition of components that, depending on the structure and the external environment may be in different states of aggregation. Temperature reduction causes a change in the physical state of the components, leading to the formation of paraffin crystallization centers and their growth.

Laboratory studies have shown that the rate of paraffins formation has an effect on allocation process and behavior of gas bubbles in the flow of mixture. It is known that gas bubbles have the ability to float suspended particles of paraffin. When bubbles contact with the pipes surface the paraffin particles come in contact with the wall and deposit on it.

In the following, the process of paraffin deposition increases because of its hydrophobicity. On the wall of the pipe is formed a layer of paraffin crystals and bubbles in the gas. The smaller gas-saturated layer, the greater density it has. Therefore, more dense sediments are formed at the bottom of the lifting pipes where gas bubbles are small and have greater strength adhesion to paraffin crystals and pipe walls.

The intensity of ARPD formation largely depends on the rate of fluid flow. At low flow rates, the formation of ARPD is quite slow. With speed increase (at transition to turbulent flow regime) deposits intensity initially increases. Further increase of liquid-gas mixture

speed (LGM) leads to decrease of ARPD intensity as the high rate of fluid flow allows paraffin to keep the crystals in suspension state and take them out of the well. Furthermore, the flow tears a part of deposits from the walls of the pipes, which explains the sharp decrease of deposits in the range of 0-50 m from the wellhead. At high speeds the flow of the mixture cools slower than at small. In turn at low speeds the formation ARPD slows [6].

On the formation of deposits also has an effect on the state of surface pipes. Microroughnesses are the sources of vortex formation, and speed retarders on the wall of the pipe. This is the reason for formation of crystallization centers, sticking of paraffin crystals to the surface of the pipe, blocking of their movement between the asperity and valleys of the surface.

The process of ARPD formation has an adsorption character. Adsorption processes are accompanied by the occurrence of double electric layer on the surface of paraffin contact with gas-oil flow.

When mechanical equilibrium violation of layer on the surface of the pipe or paraffin layer appear uncompensated charges of static electricity, in other words electrification takes place on the pipe surface and on the surface of paraffin crystals that intensifies the adhesion paraffin to metal.

It is assumed that magnetic fields effect is one of the most advanced physical methods. The use of magnetic devices to prevent ARPD began in the fifties of the last century, but because of low efficiency it did not become widespread. In particular, there were no magnets that could work long and steadily in well.

In a 1995-2015 the interest in the use of magnetic field effect on ARPD increased significantly, due to market appearance of a wide range of high-energy magnets from rare earth elements.

2. The main part

Recently, interest in the use of magnetic fields for treatment of production fluid to prevent ARPD increased significantly, due to the appearance at the market of a wide range of high-energy magnets from rare earth materials. It has been established that under the influence of a magnetic field in a moving fluid is the destruction of units consisting of submicron ferromagnetic microparticles of iron compounds, which are at a concentration of 10-100 g/t in the oil and associated water.

Each unit contains from several hundred to several thousands of microparticles, because the destruction of units causes a sharp (100-1000) increase in the concentration of paraffins crystallization and formation on the surface of ferromagnetic particles of micron size gas bubbles. As a result of units destruction paraffin crystals fall as finely dispersed, volume, stable suspension, and the growth of deposits rate is reduced proportionally to the reduce of average size of fallen paraffin crystals in the solid phase [7].

Formation of gas micro bubbles in the centers of crystallization after magnetic treatment provides, according to some researchers, the gas-lift effect, leading to the growth of wells production rate. Magnetic treatment of oil, including oil and gas mixtures produced in wells was intended to prevent (or significantly reduce) the formation ARPD and salts in the tubing and reduction of surface corrosion of pipelines [8].

One of the most important results of magnetic treatment is the occurrence of gas micro bubbles formed on the surface of the iron particles. Studies have shown that these micro bubbles have electric charge and high adsorption activity with respect to organic and mineral deposits.

After magnetic treatment such bubbles provide liquid detergent properties similar to those that occur when washing powder or soap are added to water. For effective magnetic treatment effect in a number of processes is necessary a combination of several factors. This explains the poor reproducibility typical for magnetic treatment [6-8].

However, the methods of analysis of the substance and hydrodynamic conditions of liquids flow make it possible to create or select technological processes in which consistently appear industrially important effects. It is possible to predict the expected effects in each case, and to prove from a physical point of view those already observed.

The effect of magnetic field on the formation of paraffin deposits in the lab helped to solve several problems in the selection of permanent magnets for this or that well in particular field.

Ferromagnetic particles test in borehole production - the first crystals seeds of ARPD by filtration of oils, can find out reasonability of magnetic field processing of the product. In the study of rheo-

logical behavior of oils after magnetic treatment was noted that magnetic field has an effect on their properties in different way (Table 2).

Table 2

Rheological parameters oil before and after magnetic treatment oil Boryslasv OGCF

Oil	η, мPa·s	τ_c,Pa	$E_{акт}$kJ/mole
Before magnetic treatment	778,1	303,2	12,84
After magnetic treatment	605,0	267,3	8,21

Decrease of rheological characteristics for oil are observed – dynamic viscosity by 28%, the yield stress at 13%, the activation energy of viscous flow by 56% [3].

In case of a sufficient content of asphalt-resinous substances and trace iron in the borehole fluid, the analysis of static magnetic field effect on it in the lab, makes it possible to determine the exact topology and the magnetic field and the desired temperature for effective operation of instrument that determines the previous installation depth of the magnetic device.

The magnetic device is convenient in operation because it does not require maintenance and supply of any kind of energy. The most effective is the use of magnetic devices immediately after wells cleaning from existing deposits [4].

Magnetic device for ARPD control is installed on the tubing string. Production fluid stream that passes through the activator comes under influence of strong magnetic fields of permanent magnets, which prevents the formation of deposits asphaltenes, resins, paraffins and salts on the inner surface of the tubing [1-5].

It is considered that the use of magnetic devices can increase the production of wells during overhaul period by 2-5 times, leading to considerable economy and can increase oil production.

The magnetic device is convenient in operation because it does not require maintenance and supply of any kind of energy. The most effective is the use of magnetic devices immediately after well cleanup from existing deposits.

Magnetic fluid magnetizing device consists of a body-pipeline with a soft magnetic material and fixed to the axis of the magnetic system, which is a consistent set of permanent magnets with sequential magnetization directions along a body-pipeline. These permanent

magnets have a circular shape and radial magnetization and placed on the magnetic circuit. On the outer surfaces of permanent magnets are fixed pole pieces, and magnets are placed between the pads of a nonmagnetic material [9].

The outer surface of the magnetic system with nonmagnetic spacers between the magnets and pole pieces placed on permanent magnets shaped like a cylinder and as a working channel for the treated liquid is the annular gap crossing between the magnet system and the body-pipeline. Figure 3 shows a diagram of the installation of a magnetic device in the well

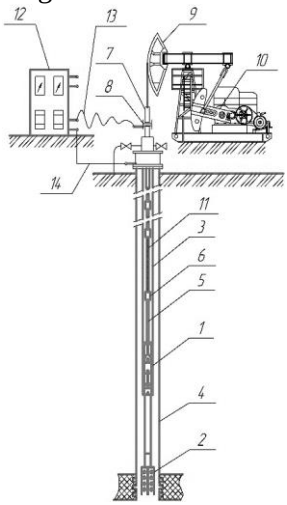

Fig. 3. ARPD control technology in the producing wells equipped with sucker-rod pumping unit: *1* - deep pump; *2* - magnetic device; *3* - tubing string; *4* - column casing; 5 - column rod (steel); *6* - centrators-protectors; *7* - polished rod; 8 - insulating insert; *9* - balance; *10* - drive unit; *11* - fiberglass rod; *12* - station of cathodic protection (power supply); *13* - cable (flexible); *14* - cable

Magnetic device is a body of ferromagnetic pipe. At one end of the pipe is fixed a sleeve joint for tubing. On the inner surface of the housing permanent magnets are fixed.

Device is installed in the tubing string under the bottom-hole pump or in the necessary part of the tubing string. With the passage of a mining fluid through the body it is treated by magnetic field.

Some characteristics of the magnetic device:

- the diameter of the device, mm - 73;
- working life, years, not less - 30;
- performance - explosion-protected;
- working pressure, MPa - up to 15;
- weight of magnetic device, kg – not more than 10;
- operating temperature range of production fluid – 10-120 °C;
- production fluid composition in which is guaranteed the efficiency of the magnetic device - watering at least 25%, mineralization of at least 150 g/kg [10].

The use of magnetic device increased the average turnaround time of wells complicated by the formation of emulsions and ARPD, on average twice. Chemical treatment of the wells was stopped.

At Boryslav OGCR the use of magnetic device made it possible to increase the turnaround period of wells in 2,2 times and to decrease the number of thermal and chemical treatments, respectively, in 2 and 5 times.

The use of magnetic device in wells complicated by ARPD allowed increasing their average turnaround time in 2 times at stopping chemical treatments of wells.

Magnetic treatment is aimed to increase turnaround period of wells by directional magnetic field effect [11].

The use of magnetic treatment can be effective, as in case of flowing, and the operation of the depth-rod, by centrifugal and diaphragm pumps and also on oil pipelines to increase their anti-corrosion resistance.

Payback of magnetic devices to prevent the ARPD formation depending on the turnaround period and geological characteristics of the particular wells ranges from one to three months.

3. Conclusions

In the article is proposed magnetic treatment of production fluid as a method of ARPD control. Magnetic device runs into the well and this ensures the effectiveness of magnetic treatment of the whole volume of liquid that passes through the device in the same conditions of high-gradient field with sufficient duration of treatment.

Magnetic treatment differs from other methods of treatment fluid so that work does not require any power supply to the unit, as it is based on permanent magnets.

Magnetic Anti-Paraffin Device can work in large diameter pipelines, thus providing the necessary magnetic field and magnetic induction. Therefore, in our opinion, it should be used in the wells with high content of ARPD deposits.

References

1. **Chow, R., Sawatzky, R., Henry, D., Babchin, A., Wang, Y., Cherney, L., & Humphreys, R.** (2000). Precipitation of Wax From Crude Oil Under the Influence of a Magnetic Field. Journal of Canadian Petroleum Technology, 39(06).

2. **Gavriluk O. V. , Glazkov O. V.** (2001) The application of magnetic liquide treatment in oil fields of West Siberia. IOR - 11th European Symposium on Improved Oil Recovery 19-25

3. **Ivakhnenko, O. P.,** (2006) Magnetic analysis of petroleum reservoir fluids, matrix mineral assemblages and fluid-rock interactions. Thesis, Institute of Petroleum Engineering, Edinburgh, UK, 210 pp.

4**. Klassen, V.** (1982). Omagnichevanie vodnykh sistem. *Khimiya*, 1982.

5. **Nalivaiko, O., Mangura, A., Mangura, S., Nalivaiko L.** (2015). Peculirities of magnetic anti-paraffin waxes device (MAD) modeling in Comsol multiphysics software. *Problems of Energy Saving and Nature Use*. 58-67.

6. **Pisareva, S.I., Kamenchuk, Y.A., Andreeva, L.N.** (2005) The Nature of Formation and Dissolution of Asphalt-Resin-Wax Deposits Chem Technol Fuels Oils 41: 480.

7. **Suzuki, Hirofumi., Kodera, Sunao; Matsunaga, Hiroyuki; Kurobe, Toshiji** (1993) Study on magnetic field-assisted polishing (2nd Report) - effect of magnetic field distribution on removal distribution. *Journal of the Japan Society for Precision Engineering*. Nov; 59(11): 1833–1838

8. **Swapan Kumar Das** (2008) Electro Magnetic Heating in Viscous Oil Reservoir International Thermal Operations and Heavy Oil Symposium, 20-23 October, Calgary, Alberta, Canada

9. **Tung, N., Vuong, N., Bui Quang, K., Vinh, N., Hung, P., Hue, V., & Hoe, L.** (2001). Studying the Mechanism of Magnetic Field Influence on Paraffin Crude Oil Viscosity and Wax Deposition Reductions. *Proceedings of SPE Asia Pacific Oil and Gas Conference and Exhibition*.

10. **Wang L. J., Wang W., (2014)** Paraffin Depositing Mechanism and Prediction Methods of Paraffin Removal Cycle ", Applied Mechanics and Materials, Vols. 675-677, pp. 1512-1516

11. **Zhang, W. W., Wang, T. T., Li, X., & Zhang, S. C**. (2013). The Effect of Magnetic Field on the Deposition of Paraffin Wax on the Oil Pipe. *Advanced Materials Research, 788*, 719-722.

12. **Zhang, W. W., Wang, D. D., Wang, T. T., & Zhang, S. C.** (2015). Study on the Mechanism of Magnetic Paraffin Con-trol of Crude Oil Based on the Reorientation of Paraffin Crystals Induced by Magnetic Field. *Applied Mechanics and Materials, 743*, 137-141.

INNOVATIVE MODEL OF DEVELOPMENT OF FUEL AND ENERGY COMPLEX OF UKRAINE

Kovshun N.E.
National University of Water and Environmental Engineering (NUWEE), Professor, Doctor of Economic Sciences, Professor, Department of Enterprise Economy, Ukraine

Ignatiuk I.Z.
National University of Water and Environmental Engineering (NUWEE), Associate Professor, Candidateof Economic Sciences, Associate Professor, Institute of Postgraduate Education, Ukraine

Moshchych S.Z.
National University of Water and Environmental Engineering (NUWEE), Associate Professor, Candidate of EconomicSciences, Institute of Postgraduate Education, Ukraine

Malanchuk L.O.
National University of Water And Environmental Engineering (NUWEE), Candidate of Sciences (Economics), Assistant Professor Department of Public Administration, Documentation and Information, Ukraine

Abstract

Prospects for the development of resource-saving technologies in mining are priorities, the state and further development of which depends on the existence of an independent Ukrainian state and the development of the energy sector of the economy. The essence of this process is that energy sector reforms should help integrate it into the EU energy space and at the same time create a positive foundation for reforming the entire economic complex of Ukraine, raising people's living standards to European standards. A special role in this is played by new technologies, the introduction of which is one of the main tasks of a steady progress in the strategy of development of the mining and processing industry. The solution to this complex problem is related to the introduction and increase of efficiency of resource-saving technologies of mining and processing of minerals.

The mining industry is currently in a difficult state, driven by both objective and subjective factors. Among the problems that need urgent solution is the reduction of the negative impact of the fuel and energy complex on the environment, which necessitates the improvement of the environmental management system with the use of new technologies.

Introduction

Ukraine as an independent state has not overlooked all the environmental problems that are characteristic of modern society. With a considerable list of works planned and completed during the years of independence, the state of the environment remains crisis with a tendency to deteriorate. For the sake of objectivity, it should be noted that Ukraine inherited from the Soviet Union an environmentally dangerous structure of the economic complex - dominated by metallurgical, mining, fuel and energy, chemical and petrochemical industries, extensively developed agriculture. The partial improvement of the environmental pollution and the reduction of harmful emissions observed since 2000 are not due to the systematic work of the authorities on environmental protection, but simply due to a significant drop in production in the basic industries. By and large, no progress has been made besides building a vertical of environmental watchdogs and establishing a specialized ministry in the executive branch. During the years of independence, Ukraine failed to address any of the environmental problems inherited from the Soviet regime.

The Ministry of Energy and Environmental Protection of Ukraine, which was established on December 9, 2010 through the reorganization of the Ministry of Environmental Protection of Ukraine, is functioning in Ukraine in 2019 and is joined by the Ministry of Energy and Coal Industry of Ukraine. The main purpose of such transformations is to ensure a comprehensive approach to public policy on the use of natural resources and energy, and to formulate a single policy to address the negative effects of global climate change. This approach is common in European and world practice, in particular in EU countries (France, Denmark, Greece, Portugaland Australia). In other words, the development of the country's energy supply and the preservation of the ecological balance are indispensable components of the sustainable development of society.

Mining is a major strategic prerequisite for the development of the economy, the basis for ensuring all types of social life

Therefore, defining and implementing the directions of its development are priority tasks in ensuring national security, political and energy independence, sustainable development.

Fuel and energy complex (FEC) of Ukraine covers the activities of exploration and production, processing and production, storage and transportation, transmission and distribution, trade and sale (sale) of energy products - fuel, electricity and heat. Formed in its time as an integral part of the fuel and energy complex of the USSR, it does not fully meet the conditions of energy functioning on the basis of sustainable development. Thus, the general structure of Ukraine's fuel and energy complex is shown in Fig. 1.

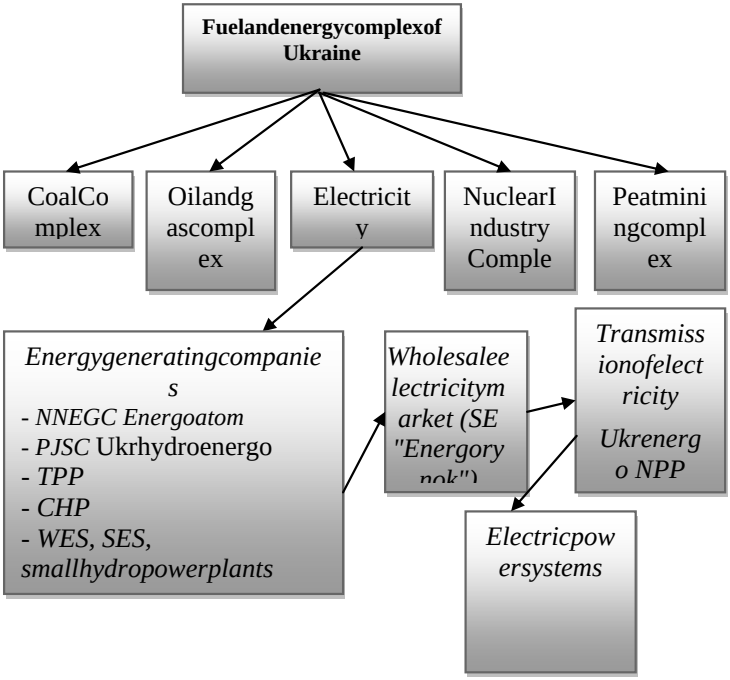

Fig. 1. FuelandenergycomplexofUkraine

Generally, the implementation of the state policy on the functioning of the fuel and energy complex occurs within the three spheres concerning fossil fuels; development of nuclear power; electricity complex. Ukraine's energy supply activities are carried out by the coal-industrial complex; electricity complex; nuclear-industrial complex; peat mining complex; oil and gas and oil refining complex.

The base for the fuel and energy complex of Ukraine is the coal industry. Analyzing the coal industry, it is worth noting that in terms of geological reserves of fossil coal, Ukraine ranks first in Europe and eighth in the world. Explored reserves amount to about 56 billion tons, forecast reserves - about 170 billion tons of coal of all brands - from brown to anthracite and coking [1].

Currently (excluding annexed territories) in Ukraine, coal reserves are operated by almost 50 mines. Some of them - 33 mines with a total production capacity of 11.7 million tons - belong to state-owned coal mines. The private sector is represented by 16 mines, the vast majority of which are in concession at DTEK LLC.

One of the main problems of the industry is the low technical development of production, the lack of widespread introduction of innovative technologies for field development. Currently, under the authority of the Ministry of Energy and Environmental Protection of Ukraine, only 1 mine (3%) has been operating for less than 30 years since the start of coal production. 6 mines (18.2%) have a lifetime of 30 to 50 years, 15 mines (45.5%) - 50-70 years, and 11 mines (33.4%) - more than 70 years. At the stage of liquidation are 13 unprofitable coal mines, 5 more mines are in the stage of preparation for liquidation. The two liquidated mines contain drainage complexes for the construction and reconstruction of which were foreseen by mine elimination projects[2].

The state scientific, technical and design potential of the industry consists of 8 institutes. The state of affairs in the field of coal-industrial complex is characterized by the following key indicators: volume of production at coal-mining enterprises, cost of 1 ton of finished commodity coal production (FCCP), number of employees at state-owned coal-mining enterprises, amount of budget support to cover losses and losses.

The trends of the mentioned indicators during 2016-2019 indicate an aggravation of the negative situations in the industry. For example, recent years are characterized by a general decline in production volumes, an increase in state support for coal mines to partially cover the costs of the cost of finished commodity coal products, import dependence, and a decrease in the number of employees of state coal mines.

In the current conditions, the problem of assessing the efficiency of functioning of state-owned enterprises in the coal industry complex is acute. During the period, the production of ordinary coal decreased by 9.7 million tons as a whole. at state-owned enterprises by almost 2 million tons. At the same time, the share of production by the private sector has increased, although the number of state-owned mines is almost double the number of private mines.

Thus, the share of coal production by state coal-mining enterprises in 2016-2018 is approximately 13% of the total production in Ukraine (Fig. 2). At state-owned coal-mining enterprises, the cost of 1 ton of GTVP for the 12 months of 2018 amounted to 3200 UAH, and for the first half of 2019 - 3860 UAH. However, in the cost structure, wages and salaries account for almost 50%. Costs of finished coal products for the first half of 2019 amounted to UAH 4,869.0 million and increased by UAH 345.5 million or 7.6% compared to the corresponding period of 2018. Budget support for state-owned coal mining companies in 2018 amounted to UAH 3 726 million, of which UAH 2,661 million to cover losses. In turn, only UAH 484 million was allocated for technical re-equipment and modernization.

The volume of finished commodity coal produced by state-owned enterprises for the first six months of 2019 amounted to 1 255.4 thousand tons, which is 85.3 thousand tons less than planned (-6.4% to the plan) and 89, 7 thousand tons to the corresponding period of 2018. The value of commodity coal products in the same period amounted to UAH 2 732.4 million, which is UAH 110.1 million, or 3.9% less than in the corresponding period of the previous year. Due to the increase in prices of coal products by an average of 3.0% compared to 2018, it allowed to receive UAH 292.4 million of additional income, but due to the loss of commodity output the positive result was reduced by UAH 402.5 million. Long-term deficit of own and budgetary funds for technical re-equipment of coal-mining enterprises registered and operating in the territory in which the state authorities fully exercise their powers (in 2013-2017, the financing of technical re-equipment from the state budget was not carried out at all) led to the fact that only 20 new treatment holes were commissioned in 2015 from the 32 lava coal mines; in 2016 - 15 new potholes; in 2017 - 25 lav; in 2018 - 16 lavas, compared to 73 introduced in 2013.

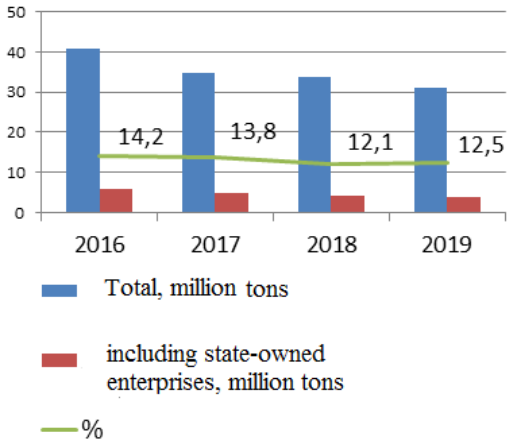

Fig.2. Dynamics of coal production in Ukraine

In 2019, the number of operating treatment holes is only 36 (with an operating line length of 5 896 m) against 48 holes (with a line of 7 814 m) in 2016. Due to the lack of mining equipment, coal is extracted from 11 treatment holes by jackhammers (SE "Mirnogogradvugillya", SE "Toretskugol", SE "Pervomaiskugol" and PJSC "Lisichanskugol"). There is no clearing front at the mines 1-3 Novogrodivsk, Privolnyansk and Novodruzhesk.

At the same time, it is burdened with a whole set of environmental problems. It has a complex man-made impact on the environment, namely changing natural hydrological regimes; remove large tracts of land for waste heaps and waste heaps from the standard environmental regime; stationary powerful sources of harmful emissions into the atmosphere and hydrosphere are created.

Peat-mining industry in Ukraine is represented by 9 peat-mining enterprises (in Volyn, Zhytomyr, Kyiv, Khmelnytsky, Rivne, Sumy and Chernihiv regions). They are united in the state concern Ukrtorf [3].

Ukraine is the southernmost European country in which peat resources are of industrial importance, making peat a real reserve for improving Ukraine's fuel and energy balance. The largest resources in peat are in the three regions of Polissja: Volyn, Rivne and Chernihiv. On their territory, 1051 fields were discovered and explored (36% of all country deposits), and the geological peat reserves amount to 1.09 billion tons (50% of Ukraine's reserves)[4].

The main negative trend during 2016-2019 is the gradual decline of the prepared for extraction of peat reserves due to the decrease of the areas set aside for the production activity of the land. The reason for this is the too complicated procedure of land allocation for the development of peat lands. Another factor that does not allow to increase peat production and production of peat briquettes is the moral and physical obsolescence of technological equipment at state peat mining enterprises. In order to stimulate the development of peat extraction and its processing, the following measures should be implemented:

• optimize the structure of the enterprises of the branch, liquidate the branches and subsidiaries, which have developed their own reserves or whose activities were unprofitable;

• concentrate equipment, machinery and mechanisms on prospective enterprises;

• involve representatives of the scientific community in the study and solution of the problems of the peat mining industry.

As for the development of the gas industry, it operates on a relatively small resource base - proven natural gas reserves in Ukraine amount to 1193 billion cubic meters, forecast resources - 3491 billion cubic meters. The largest stocks (43 percent of total forecast stocks) in Eastern Ukraine. The shelf of the Azov and Black Seas is also promising - up to 46% of forecast stocks. Potentially unconventional gas reserves are potentially promising:

- 1.2 trillion.shale gas cubic meters;
- 8.5 trillion.cubic meters of dense gas collectors;
- over 12 trillion. cubic meters of coal bed methane.

In the field of oil and gas condensate production there is a decrease in key indicators. Total oil and gas condensate production accounts for about 20% of Ukraine's total consumption of petroleum products. At the same time, there is a fall in production volumes by state-owned enterprises and an increase in production volumes by private enterprises. The problems of functioning of the gas industry are similar to the problems of oil production, but have specific features taking into account the transit capabilities of the gas transportation system of Ukraine.

Taking into account the current trends in the world, it should be noted that the use of renewable energy sources will save traditional

scarce energy resources and improve the ecology of production. However, the current lack of incentives by the state aimed at supporting the independent development of the peat mining industry does not allow it to ensure proper use of energy potential, which in turn puts obstacles in the way of reducing Ukraine's energy dependence on imported energy (natural gas, oil).FEC

There is no closed technological cycle of radioactive waste processing in the FEC of Ukraine. All operating nuclear power plants have their own temporary storage facilities for spent fuel and radioactive waste. Their filling is on average 60%. Liquid radioactive waste repositories are filled by 20-80%. These repositories are temporary and are not designed for long-term storage and increase of radioactive waste. For example, about 200 tons of irradiated and fresh nuclear fuel mixed with other components are concentrated at the Shelter facility of the decommissioned Chornobyl NPP.

The volume of radioactive waste in Ukraine is projected to increase due to:

- return of highly radioactive waste to Ukraine after the processing of spent nuclear fuel of Ukrainian NPPs in Russia;
- operation of operating NPPs as a result of their prolonged service life, introduction of new nuclear power units;
- accumulation of radioactive waste for temporary storage;
- the absence of a truly modern infrastructure for the treatment, storage and disposal of radioactive waste.

In general, in the years of Independence, with the tragic example of previously committed criminal negligence (Chornobyl NPP), all governments of Ukraine have postponed resolving the problems of radioactive waste management for an uncertain future. For a country with 15 nuclear reactors operating at 4 NPPs and technological dependence on the treatment of radioactive waste from Russia, the absence of an appropriate state program could lead to new catastrophic consequences in the near future.

So, as we can see, FEC of Ukraine does not meet the requirements for the energy complex of an independent state: two fundamental principles of energy, namely - reliable, sustainable energy supply and efficient use of energy resources, have been significantly violated. Due to inconsistent activities of the state authorities, not only the improvement and optimization of the fuel and energy com-

plex was not carried out, but also its technical condition, technological and raw material external dependence, as well as the increase of negative technogenic influence on the environment, despite the significant reduction of production volumes, production and production, resources in Ukraine.

Introducing the innovative model of development of the fuel and energy complex of Ukraine, foreign experience should be taken into account. Currently, about 18 countries on the European continent plan to completely stop coal production and combustion and thus reduce greenhouse gas emissions. Abandoning coal is an important step in the fight against global warming, because it is the dirtiest fuel.

For example, Germany is preparing to give up coal consumption by 2038; Great Britain by 2025, France by 2022; Greece - until 2028; Hungary until 2030. Japan, Portugal and the Netherlands also refused to develop the coal industry.

Analyzing the European experience, it can be noted that the abandonment of coal and the transition to renewable energy are a general trend towards a sustainable future and part of the climate change commitments made by the EU in the context of the ambitious European Green agreement "and the 2015 Paris Agreement.

The EU's transition to a climate-neutral economy is linked not only to the need to fulfill legal and political obligations, but also to a change in the mentality of Europeans and the massive climate strikes of young people. After all, the use of fossil fuels, in particular coal, is associated not only with the destructive effects on the atmosphere, land and water resources, flora and fauna, which is manifested in the collapse of the mountain range over treatment facilities, the drainage of aquifers, salinization and pollution of soil, soil and soil surface water, but also threatens the health of citizens.

Ukraine also has the Green Energy Transition Concept by 2050, which envisages the full replacement of coal generation and the transition of Ukraine's economy based on the use of fossil fuels - coal, oil, gas, to a climate-neutral economy in the long run. The main tasks of the Concept are:

- energy efficiency;
- reduction of the share of extractive industries in the economy and, accordingly, complete replacement of coal thermal power plants by 2050;

- integration of energy markets of Ukraine with the European ones.

Particular attention should be paid to minimizing the potential negative impact on the socio-economic and environmental situation in the coal mining regions. To this end, appropriate integrated programs aimed at social reconversion of regions should be developed and implemented; mitigating the social and environmental consequences of restructuring; development and implementation of employment measures and providing psychological support to former employees of coal mining enterprises; involvement of energy efficient developments and technologies in the process of restructuring of coal enterprises, taking into account the most successful experience of the EU Member States.

In view of the above, we believe that in order to achieve sustainable growth through the development of a more competitive low carbon economy, which requires efficient, rational use of resources, environmental regulation is a key element at this stage as a legal basis for the establishment and implementation of an environmentally friendly management process. , adoption and implementation of decisions enshrined in international, regional (European), national (state, corporate, international) sce, public) legislative and regulatory acts [5]. In Fig. 3 schematically shows an environmental management system that is guided by the principles, methods and tools of environmental regulation.

Analyzing the applied nature of the opportunities for energy of Ukraine, which will be opened by the implementation of the task of the NES for integration into the EU energy space, we mentioned above the planning of the strategic change of directions of electricity flows: from the existing scheme "Russia's Unified Energy System - Ukrainian Energy System" to the scheme "Ukrainian Energy System - EU Energy System" . Unfortunately, the political approach to this problem dominates the economic and (especially dangerous) over the technological. Abstracting from the analysis of possible economic losses, we will discuss in more detail the technological and organizational-legal problems of reorientation of electricity flows.

First, Ukraine's energy system is characterized by technological conservatism - that is, during the last two decades, there have been no significant changes in both the generation structure and the net-

work structure. Placement of generation capacity, base consumers, network capacity, structure of fuel resources have practically not changed. The unified power system of Ukraine operates in parallel with the energy associations of the Republic of Belarus, Moldova, the Russian Federation (OEC Center, UES of the South), except the so-called "Burshtynenergy" (Burshtyn TPP, Kaluskaya TPP and Tereble-Rickskaya Hydroelectric Power Plant), which is with the European grid.

Second, the fall in electricity consumption in Ukraine in the 1990s created an impression on government officials and experts about the artificial excess of generating capacity and slowed down the processes of modernization in electricity. In technological terms, Ukraine has fallen behind even its closest neighbors by decades. In accordance with the project, the scheme of capacity allocation of Zaporizhzhya NPP, Khmelnitsk NPP, Exactly NPP is not completed. The structure of the generating capacity is not optimized.

Third, state interference in power management is weakened, especially after two stages of so-called privatization of the industry have taken place, which has led to the domination of the interests of oligarchic groups over the interests of consumers. The Ministry of Energy and Coal did not become a source of energy policy in the country.

Fourth, the energy market management system, established over ten years ago, needs continuous improvement.

The analysis provided grounds for concluding generally about the positive trends in the relationship between energy development, overall economic growth and the reduction of the negative environmental impact of FEC.

However, their instability must be taken into account. And considering that the period from 2012 to the present is characterized by the deepening of the systemic crisis in the fuel and energy complex of Ukraine and its characteristic signs are the reduction of electricity production, reduction of oil and gas production, the curtailment of the work of coal-mining enterprises, we believe that in order to achieve the strategic priorities of national energy development, identified in the NES Ukraine project for the period up to 2035, some conceptual positions require correction and clarification.

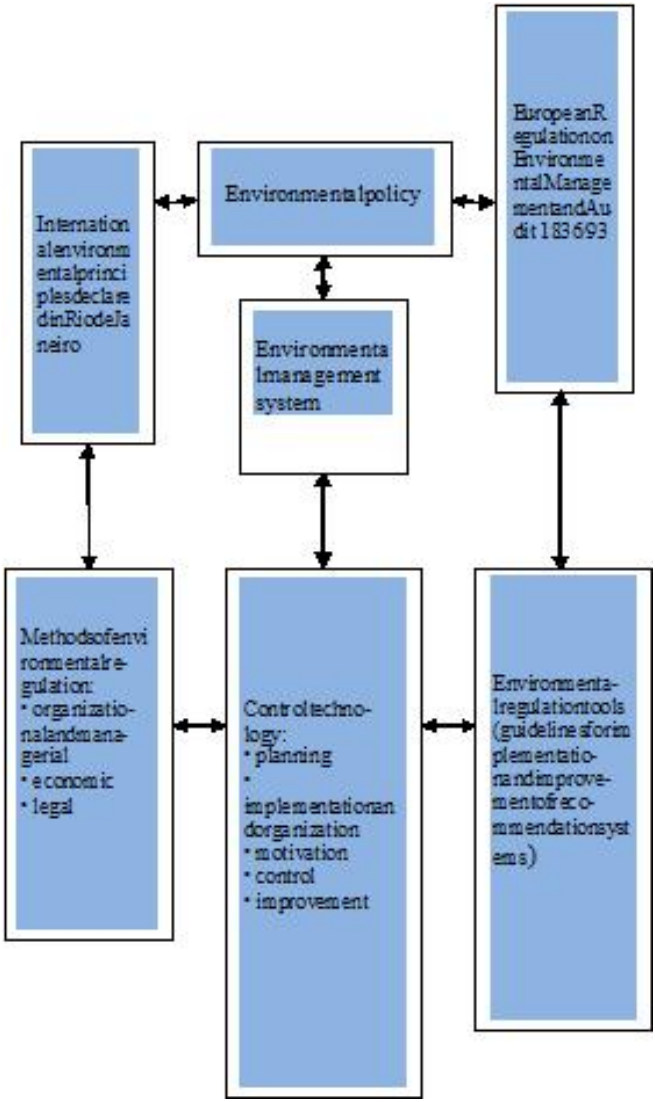

Fig. 3 - EnvironmentalManagementSystem

This, in particular, the accelerated achievement of energy independence, must be implemented taking into account the development of its own technological capabilities and environmental regulatory methods and mechanisms.

In independent Ukraine, a system of environmental regulation has been established, containing active legislative, administrative, economic measures and levers, which are used by public authorities of different levels to force pollutants to limit harmful substances, as well as to materially encourage conscientious environmental users.

To prevent the negative impact of anthropogenic activity on the environment and the rational use of natural resources in the system of organizational and management methods, special procedures were introduced at the state level: environmental expertise; environmental monitoring; standardization and standardization; target planning.

It is worth noting that integrated environmental programs are an effective way of solving nature conservation issues. They make it possible to provide the necessary concentration of economic, financial and production resources in priority areas of environmental policy. Forming government programs allows you to concentrate resources to solve a particular problem; unite the efforts of all stakeholders; set strategic goals and develop long-term strategies. However, in the context of inconsistent government policy, the results of the use of targeting methods do not meet the predicted possibilities.

In Ukraine, a system of state regulation of the state of the environment has been created, one of the key elements of which is the ecological regulation of the functioning and development of economic entities, including FEC (Fig. 4).

However, the implementation by the state authorities of the available capacity to regulate the state of the environment is insufficient.

It should be noted that today the innovative direction of development is the basic strategy for business, where knowledge together with social capital creates competitive advantages of individual countries and regions to a greater extent than their natural resources [6]. Innovation processes are becoming a major source of economic growth, especially in the context of the current paradigm of sustainable development and scarcity of natural resources, including energy [7]. Quality technological and organizational change is the basis of innovation.

Strategic directions of innovation activity are legislatively determined for the FEC of Ukraine modernization of power plants; new and renewable energy sources; the latest resource-saving technologies; protection and rehabilitation of the person and the environment.

Legally, the main task of the programs of innovation activity in the fuel and energy complex is to create the optimal fuel and energy balance of the state, taking into account energy security; diversification of sources of supply of energy raw materials and energy technologies; increase in the share of coal and electricity consumption by reducing the share of natural gas; development and implementation of the latest technologies of coal combustion and modernization of thermal power plants; creation of its own nuclear fuel cycle; development of the use of renewable energy sources.

Considering the technological level of the fuel and energy complex, the total need for innovative financing (according to experts) annually ranges from 8 to 12 billion UAH. Undertakings will not be able to obtain such financial resources without their own foreign investments.

Therefore, the problem of creating an attractive investment climate in FEC of Ukraine to activate innovation processes is of particular importance.

An objective indicator of the effectiveness of innovative activities in the fuel and energy industry, taking into account the requirements of environmental regulation, should be to achieve certain levels of baseline indicators that characterize the efficiency of the fuel and energy and its environmental impact.

As an option for possible evaluation, we propose a set of parameters, shown in table 1, formed using data from the National Institute for Strategic Studies [8-10].

Achieving these levels of benchmarks requires more than just boosting investment activity.

Ultimately, the environmental regulation of FEC (as well as other sectors of the economic complex) requires the construction of a new system of relationships in the chain: central government - regional government (local government) - the entity.

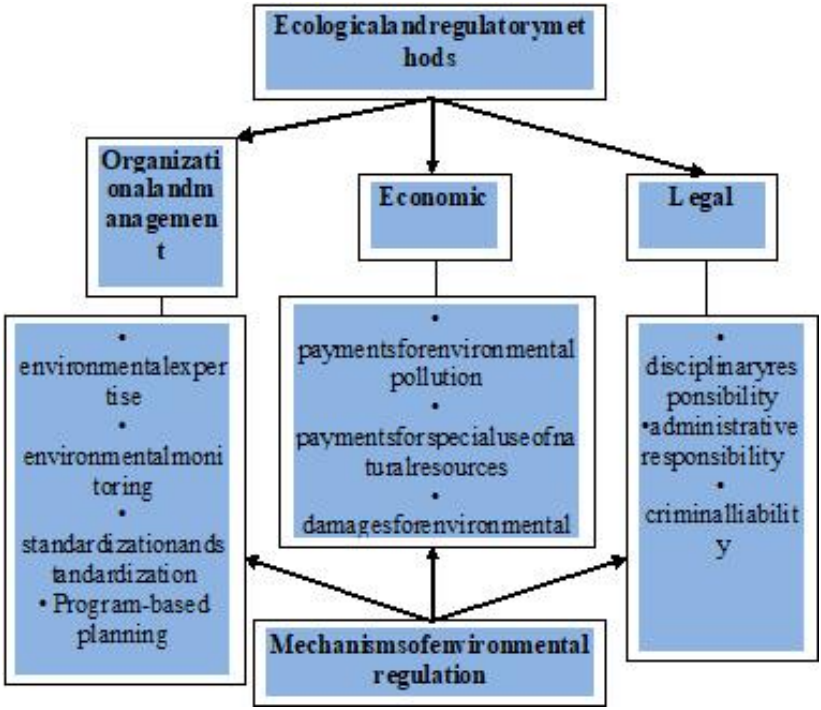

Fig. 4. Methods and mechanisms of environmental regulation

Table 2

Baseline performance indicatorsthe functioning of the FEC and its environmental impact

Indicators	2013 year	2020 year	2025 year	2030 year	2035 year
1. GDP energy intensity, kgc/$ 1 of GDP	0,33	0,27	0,23	0,20	0,17
2. Fuel consumption at TPP for electricity sold, gp/kWh.	396	384	367	353	334
3. The level of residual resource of FEC fixed assets,%.	20	30	50	60	80
4. The share of shunting power generating capacity of fuel and energy complex to the total installed capacity, %.	8,6	12	14	16	18
5. The share of losses in distribution grids,%.	12	11	10	9	8

6. The share of exchange trading in energy,% of domestic consumption, including electricity, coal, oil, gas and other fuels.	10	25	50	60	70
7. Share of renewable energy sources in gross final energy consumption,%.	4,5	11	15	18	20
8. The share of local alternative fuels in local fuel and energy balances,% to total consumption.		10	15	18	20
9. Reduction of CO_2 equivalent by end-use,% since 2010.		>5	>10	>15	>20
10. Reduction of CO_2 emissions in the production of 1 kWh,%, from 2010		>5	>10	>15	>20
11. Reduction of specific emissions in CO_2 equivalent in production 1 Gcal, %, from 2010.		>5	>10	>15	>20
12. The share of capacity in thermal generation that meets EU environmental requirements (SO_2, NOx, ash emissions), %.		20	40	80	100

However, the dominant role of central authorities in the implementation of the system of environmental regulation and control of this process has objectively encountered insurmountable difficulties in the current conditions, namely: lack of effective and objective environmental monitoring; poor control over the implementation of state environmental programs and a formal approach to monitoring the implementation of regional environmental programs.

At the same time, regional authorities and local self-government (unlike similar structures in EU Member States) do not consider the environmental issues of their territories as absolutely priority issues, focusing mainly on socio-economic issues, the state of housing and communal services, and employment.

Conclusions

The innovative model of the development of the FEC of Ukraine, taking into account the requirements of environmental regulation, requires a change in the system of relations between the authorities, strengthening the competence, activity and capacity of local authorities to solve environmental problems created by economic entities located in the territories of the respective communities, and euro adaptation and consistent investment from business entities, as well as EU budget support and financial assistance. Increased investment in environmental programs, effective control and monitoring, application of environmental management at the sectoral, regional levels and directly by economic entities will provide the process of reforming environmental regulatory tools for the Euro adaptation of national energy.

References

1. Formation and use of strategic reserves of fuel and energy resources in foreign countries. (2018). https://ua.energy/wp-content/uploads/2018/01/1.-Formuvannya-strategichnyh-zapasiv.pdf.

2. **Kulitsky S.** Coal industry of Ukraine: the state and problems of development in the context of national security. Ukraine: events, facts, comments. **21**. 62–74 (2019) http://nbuviap.gov.ua/images/ukraine/2019/ukr21.pdf.

3. **Kirichok OS, Shcherbak SD** Basic principles of public policy in the field of energy efficiency and renewable energy in Ukraine and in the world. The United Nations Industrial Development Agency (UNIDO) is supported by the Global Environment Facility (GEF). Kiev. P.49. (2015)

4. **Shershun M**. Ecological-economic problems of development of the peat industry in Ukraine / M. Shershun, I. Tymoshchuk, S. Moshchich // British journal of Science, Education and Culture. – London University Press,**1(7)**, Vol. 3. P. 240–247. (2015).

5. **Moshchych S.Z.** Organizational and managerial methods of ecological regulation and their application at international and national levels [Electronic resource] Global and national problems of economy: electronic science. kind. / The Nikolaev nat. them. V.O. Sukhomlinsky. - Nikolaev, (2016). **9**.553–558. http://global-national.in.ua/issue-9-2016

6. **Balatsky O. LukyanyinV., Lukyanykhina E.** Ecological management: problems and prospects of formation and development. Economy of Ukraine. **5**. 68-73.(2000)

7. **Christine Rosenberger**. Ukraine's Energy Policy [Electronic resource].Konrad Adenauer Stiftung. Access mode: http://www.kas.de/ukraine.

8. **MalanchukZ.., MalanchukE., IgnatyukI., MalanchukL., MoshchichS**. Strategic framework for the development of rational subsoil use in Ukraine. Australian and New Zeland Journal of Fundamental and Applied Studies. – Sydney University Press, **1 (15)**, V. 3. 126–132. (2015)

9. **Yakymchuk A.Y., Navrotskyi R.L., Kovshun N. E.** Natural resources potential as innovative and investment development prospect.Polesie Scientific Bulletin. **3 (11)**. V. 1. 179–186. (2017)

10. **Kovshun N.** Basis for the realization of sustainable development strategy in Ukraine. Economics of Sustainable Development: methodological approaches and practical solutions: collective monograph / by general edition of O. Kendikhov. – Kyiv : Center of educational literature,. 25–30.(2016)

DESIGN AND IMPLEMENTATION OF A JET PUMP DREDGE

Bondarenko A.O.
Doctor of Technical Sciences (D.Sc.), (Tech.), Professor of mining machines and engineering department, National TU Dnipro Polytechnic, Dnipro, Ukraine

Ostapchuk O.V.
Doctor of Technical Sciences (D.Sc.), (Tech.), Associate Professor at the Department of Renewable Energy National Technical University of Ukraine «Igor Sikorsky Kyiv Polytechnic Institute»

Purpose. Experimental confirmation of mathematical models obtained in previous studies, testing and industrial implementation of a jet pump dredger.

Methodology. Standard methods of experimentation with experimental and industrial mining of construction sand applied with different settings of the jet suction member.

Findings. The method for calculating the rational parameters of hydraulic ripper was introduced in the design of a jet suction member with a hydraulic ripper. The use of a jet working member as the main equipment of a jet pump dredger made it possible to efficiently mining a gravel bed during the development of the East-Bugsky-2 construction sand deposit. The industrial implementation of the jet pump installation using the example of an ejector dredger project showed the practical feasibility, technological and economic efficiency of the use of ejector dredgers in the mining of flooded and underwater sand and gravel deposits with a significant

content of coarse gravel. To confirm the reliability of the previously obtained analytical dependencies and determine the operational characteristics of the equipment, field experimental studies of the jet suction member were carried out.. An ejector dredger is used in the development of the East-Bugsky-2 sand deposit.

Conclusion. The use of a jet dredging member as the main equipment of a jet pump dredger made it possible to efficiently mining a gravel bed during the development of the East-Bugsky-2 field of construction sands.

Keywords: The jet pump dredger, jet suction member, hydraulic ripper, full-scale experiment.

Introduction

The existing variety of mining equipment for the mining of flooded and underwater sand and gravel deposits, domestic and imported, available on the market, allows you to choose equipment for the vast majority of options for the layout of mining complexes. At the same time, on the domestic market there are no offers of mining and transportation complexes applicable for the development of specific complex structural deposits, which include river, lake, flooded sand and gravel ore and non-ore deposits with a significant content of coarse gravel.

The development of such deposits, using traditional design suction dredges based on slurry pumps, due to their design features, is associated with a number of difficulties, which are mainly the impossibility of mining and hydrotransporting coarse gravel.

Objectives. The purpose of the work is **e**xperimental confirmation of mathematical models obtained in previous studies, testing and industrial implementation of a jet pump dredger.

Description of the research methodology. Is applied standard methods of experimentation with a full-scale and industrial mining of construction sand with different settings of the jet suction member.

Presentation of the main research. The solution to the problem of mining deposits with a significant content of coarse gravel can be accomplished by using pump dredgers with a jet system for forming a face, preparing pulp and hydrotransport (ejector dredger).

East-Bugsky-2 field of construction sands (Nikolaev region, Ukraine), is characterized by the presence of coarse gravel in minerals. For the mining of a gravel formation, during the detailed design, it is recommended to use an ejector dredger, which was designed by modernizing the melioration dredger MZ-8.

When modernizing the mining system of the MZ-8 dredger, the developed method for calculating the rational parameters of hydraulic disintegrants and the known methods for calculating jet pumps were applied [1, 2]. The project for the modernization of the MZ-8 dredger [3] provides for reconstruction and updating of: base vessel; engine room with the installation of a new pumping equipment, drive, stop valves, pipelines; cabs of the bagermaster with installation of start-up and control systems for the main electric drive, as well as equipment control systems for working movements of the working member. The work was carried out as part of the project №110025 «Justification of the rational parameters of the dredger MZ-8», 2009. After modernization, the dredger was named jet pump dredger. The work substantiates the parameters of the mining and hydrotransport systems, developed the design of the working member of the jet preparation system and hydrotransport of mined minerals. As a result of the rationale for rational parameters, the main elements of the water supply system of the jet suction member were chosen. The hydraulic system of the ejector dredger assumes the presence of a high-pressure water pump 1 with suction 2 and pressure 4 pipes (Fig. 1). To protect the suction pipe, a check valve 3 with a protective mesh is provided.

A valve 5 was used to start the pump and regulate the water supply. To control the pressure, pressure gauges are installed in the water supply system, directly behind the pump, and in the slurry pipeline. Pressure gauges are duplicated on the control panel in the cabin of the bagmeister. Working member with a jet pump and hydraulic ripper 7 is connected to the ship's water supply 4 and the slurry pipeline using flexible pipelines 6. The monitoring of the production process is carried out by means of a vacuum gauge, the sensor of which is installed on the suction pipe of the working member, and the device - on the control panel in the cabin of the bagmeister.

Fig. 1. The hydraulic system of the ejector dredger: *1* – water pump; *2* – suction pipe; *3* – check valve; *4* – pressure water supply system; *5* – valve; *6* – flexible pipeline; *7* – jet suction member; *8* – pressure slurry pipe

The hydraulic system of the ejector dredger works as follows: with a water pump 1 pressurized water is supplied by a water pipe 4 to a working member 7. The water pump is started after filling the system with water using the auxiliary pump with the valve closed 5. A protective mesh is provided to protect the system from large contaminants. Working member 7 implements the process of jet preparation of the minerals in the underwater bottom face and hydrotransport of the obtained slurry by the hydrotransport system 8 to the place of storage or processing. The recommended technology for the application of the developed working member, in which it is possible to achieve its maximum efficiency, has become pit mining technology.

The main element of the ejector dredger is a working member with a jet pump (Fig. 2). The design is developed using specialized computer programs (SolidWorks, MathCad).

In the summer of 2011, work on the manufacture, installation and completion of equipment was completed. Full-scale tests of the jet pump dredger took place in the conditions of the East-Bugsky-2 field of construction sands, which is located in the Voznesensk district of the Nikolaev region. Total area of the field – 32,25 hectare [4]. The territory of the quarry field is divided into four blocks. Approved mineral reserves amount to 3977 thousand m³. According to the peculiarities of the geological structure, the field belongs to the 1st group, such as reservoir, sustained in structure, capacity and quality

of the mineral. Within the limits of calculating reserves, the ineral is watered, the water level is at around 16,000 m. Mining and geological conditions of the field contribute to the development of open pit using floating dredgers. Overburden is represented by a soil-plant layer, loams, partially - by sandy loam. The average thickness of the soil-plant layer is 0,64 m, the loam layer is 1,26 m. Average minerals layer power in the overwater part is 8,13 m, and in the underwater part is 4,4 m.

During the tests, such mining and technical parameters were controlled:

H_B - pressure in a pressurized water pipeline, MPa;

H_B - vacuum in the suction pipe (the gauge is installed in the suction pipe of the working member), kPa;

$L_П$ - slurry pipeline length, m;

$h_П$ - geometric elevation of slurry above water level, m;

$h_З$ - geometric height of the slurry suction, m;

$d_Э$ – diameter of ejector nozzles, m;

$d_р$ – diameter of erosion nozzles, m;

$n_Э$ – number of ejector nozzles, pieces;

$n_р$ – number of erosion nozzles, pieces;

T – production equipment turning on time, min.

a

b

Fig. 2. Jet suction working member:a - general view; b - jet pump

To confirm the reliability of the developed analytical dependencies [1] and determine the operational characteristics of the equipment, full-scale field experimental studies were carried out. The full-scale experiment was carried out with a slurry pipe length $L_{П}$ of 80 m, mining depth $h_З$ of 2 m, geometric elevation of slurry above water level $h_{П}$ of 5 m. During the experiment, the volume concentration of the slurry was measured during discharge to the alluvium map. Productivity by slurry and minerals were determined by the volumetric method. The obtained experimental data of the full-scale experiment performed during pilot tests of the ejector dredger are shown in tables 1, 2 [5, 6].

The experiment was performed in two stages. The first envisaged the use of a simplified washout system for face jet preparation, while the cavity of the erosion nozzle had a direct connection with the pressure cavity of the working member, i.e., the pressure in the pressure cavity of the working member was 1,02-1,06 MPa (Table 1).

Table 1

The experimental data of a full-scale experiment. Pressure in the pressure cavity of the working member is – 1,02-1,06 MPa

Level in a measured capacity, mm		Slurry volume concentration, C_o	Pressure gauge, H_B, MPa	Vacuum Gauge H_B, kPa
slurry	sand			
1	2	3	4	5
The experimental data for: $d_Э$ – 19 mm, d_p – 7 mm, $n_Э$ – 8 pieces, n_p – 1 pieces.				
182	20	0,11	1,06	18-20
180	18	0,1	1,06	16-18
175	15	0,09	1,04	16-18
181	12	0,07	1,04	16-18
		C_o average – 0,09		
The experimental data for: $d_э$ - 19 mm, d_p - 7 mm, n - 8 pieces, n_p - 2 pieces.				
slurry	sand			
180	19	0,11	1,04	16-18
185	15	0,08	1,04	16-18
182	13	0,07	1,04	16-18
180	14	0,08	1,04	16-18
178	12	0,07	1,04	16-18
174	13	0,07	1,04	16-18
183	10	0,05	1,04	16-18
		C_o average – 0,08		

At the second stage, erosion of the soil in the face was performed by nozzles, in which, by throttling, the pressure in front of the nozzle was reduced to the calculated values, i.e., the pressure in the pressure cavity

of the working member was 0,5-0,6 MPa. The obtained experimental data are shown in table 2Table 2

The experimental data of a full-scale experiment. Pressure in the pressure cavity of the working member is 0,5-0,6 MPa

Level in a measured capacity, mm		Slurry volume concentration, C_o	Pressure gauge, H_B, MPa	Vacuum Gauge H_B, kPa
slurry	sand			
1	2	3	4	5
The experimental data for: $d_Э$ – 19 mm, d_p – 7 mm, $n_Э$ – 8 pieces, n_p – 1 pieces.				
180	3	0,02	1	22
180	7	0,04	1	20
180	15	0,08	1,06	18
180	17	0,09	1,06	18
180	13	0,07	1,06	18
185	5	0,03	1,06	18
		C_o average average – 0,06		
The experimental data for: $d_Э$ – 19 mm, d_p – 7 mm, $n_Э$ – 8 pieces, n_p – 1 pieces.				
185	25	0,14	1,06	16-20
185	20	0,11	1,04	16
170	15	0,09	1,04	18-20
170	17	0,10	1,04	18-20
170	26	0,15	1,04	15-18
180	30	0,17	1,04	14-16
185	27	0,15	1,04	14-16
185	25	0,14	1,04	14-16
180	25	0,14	1,04	14-16
170	12	0,07	1,04	14-16
		C_o average average – 0,12		
The experimental data for: $d_Э$ – 19 mm, d_p – 7 mm, $n_Э$ – 8 pieces, n_p – 2 piece				
180	33	0,18	1,02	10
180	31	0,17	1,02	12
185	29	0,16	1,02	12
175	26	0,15	1,02	10-12
170	28	0,16	1,02	10-12
180	29	0,16	1,02	11
180	29	0,16	1,02	11
180	27	0,15	1,02	11
		C_o average – 0,16		

Continuation of table 2

The experimental data for: $d_Э$ – 19 mm, d_p – 7 mm, $n_Э$ – 8 pieces, n_p – 3 pieces				
180	26	0,14	1,04	12

180	33	0,18	1,04	13
185	36	0,19	1,04	13
185	27	0,15	1,04	13
150	16	0,11	1,04	12
180	19	0,11	1,04	14
135	17	0,13	1,04	14
160	26	0,16	1,04	14
175	27	0,15	1,04	14
180	32	0,18	1,04	14
165	29	0,18	1,04	14
175	24	0,14	1,04	14
175	38	0,22	1,04	14
180	24	0,13	1,04	12
190	33	0,17	1,04	12
160	24	0,15	1,04	12
185	33	0,18	1,04	12
		C_o average – 0,16		

Comparison of experimental data indicates the effectiveness of the application of the developed calculation method for the design of jet systems for the minerals slurry preparation in the underwater bottom face of jet pump dredgers. The maximum average volumetric concentration of slurry for the first stage was C_o=0,09, for the second stage C_o=0,16. It is characteristic that the complete absence of the action of the erosion nozzles during the mineral slurry preparation for mining showed a minimum concentration of the slurry C_o=0,06 [7, 8].

Based on the results of full-scale tests of an ejector dredger, its operational characteristics were determined [9]:

- soil type - loose sand, gravel up to 120 mm;
- mining depth up to 6 m;
- horizontal transportation range - up to 250 m;
- pump drive - 160 kW;
- slurry productivity – 500 m^3/h.

The ejector dredger manufactured on the basis of the MZ-8 dredger, since 2011, has been used in the development of the East-Bugsky-2 sand deposit.

Conclusions. The developed method for calculating the rational parameters of hydraulic disintegrants was introduced in the design of the jet pump suction member with a hydraulic disintegrant. The use

of a jet dredging member as the main equipment of a jet pump dredger made it possible to efficiently mining a gravel bed during the development of the East-Bugsky-2 field of construction sands.

Referens

1. **Bondarenko, A. O.** (2012). Improving the erosion systems of pump dredgers: monograph. Dnipro. National Mining University, 105 p.

2. **Bondarenko, A. O.** (2012). Mining machines for underwater mining: textbook. Dnipro. National Mining University, 90 p.

3. **Bondarenko, A. O.** (2009). Justification of the rational parameters of the MZ-8 pump dredge: report on research. Dnipro. National Mining University.

4. **Bondarenko, A. O.** (2010). Quarry reconstruction for the development of East-Bugsky-2 sand deposit: working draft Dnipro. National Mining University.

5. **Bondarenko, A. O.** (2012). Mathematical modeling of soil dredger absorption processes in the underwater bottomhole. Metallurgical and Mining Industry, 3, pp. 79–81.

6. **Bondarenko, A. O.** (2012). Laws of determination of fine materials suction limits in submarine suction dredge face. *Naukovyi Visnyk Natsionalnoho Hirnychoho Universytetu*, 4, pp. 59–64.

7. **Bondarenko, A.O.** (2018). Theoretical bases of pulp suction process in the shallow dredge underwater face, Naukovyi Visnyk Natsionalnoho Hirnychoho Universytetu, 3, pp. 22–29. DOI: 10.29202/nvngu/2018-3/4.

8. **Bondarenko, A.O.** (2018). Modeling of interaction of inclined surfaces of a hydraulic classifier with a flow of solid particles, Naukovyi Visnyk Natsionalnoho Hirnychoho Universytetu, 4, pp. 13–20. DOI: 10.29202/nvngu/2018-4/5.

9. **Bondarenko, A.O., Naumenko, R.P.** (2019). Comprehensive solution of recycling waste from stone processing industry, Naukovyi Visnyk Natsionalnoho Hirnychoho Universytetu, 4, pp. 96–101. DOI: 10.29202/nvngu/2019-4/14.

RESEARCH OF DEPENDENCIES OF STOPE STRESS-STRAIN STATE CHANGE UNDER VARIOUS CONDITIONS OF PARTIAL STOWING OF DEVELOPED SPACE

Sotskov V.O.
Candidate of Technical Sciences, Associate Professor of the Mining Department, Dnipro University of Technology, Dnipro, Ukraine

Dereviahina N.I.
Associate Professor at Department of Hydrogeology and Engineering Geology, Dnipro University of Technology, Dnipro, Ukraine

Abstract. The main goal of the paper is to determine the optimal parameters of stope roof deformation depending on different mining and geological conditions for a selected technological scheme of stowing, as well as load distribution in structural elements of powered roof supports for selecting the optimal configuration of the stoperoof support unit. Modelling is performed for three variantsof stope stowing when the stope is developed through a thinly stratified rock massif under different mining and geological conditions in a three-dimensional representation with realization of conditions for mutual slipping of rock strata. It is determined that the designed unit of powered roof support allows overcoming structural features of a roof support used during partial stowing by increasing the safety margin of elements supporting the tail console. The safety margin increaseis achieved by introducing additional rigid structural elements what reduces the level of stress concentration in joints of a roof support structure.Using an integrated approach to determine the efficiency of selected roof supporting scheme allows estimating reliability of the selected modelling scheme when predicting changes in a state of a geomechanical system. This is a new method for evaluating the efficiency of various technological solutions. The results indicate that when using packs, a process of crack formation in an immediate roof of stopesis stopped by localizing areas and stress values that contribute to growth of main cracks.The optimal selection,from astandpointof dynamic stabilityof animmediate roof of stopes and packs, isselection of the minimum permissible height of extracted rocks while ensuring a statistical equilibrium of sides of packs.This allows determininga mechanism ofselection of stope movement velocity, a type and geometric parameters of erected packs.

Introduction

Mining and geological conditions of stope operation in Ukrainian mines needs solving complicated technological problems providing an opportunity of mineral mining [1-3]. Rock mass features, and mechanical characteristics of rocks, composing it, form the conditions

under which deformation of a mine working boundary may achieve up to 90% of its initial linear dimensions. Nature of such phenomena is as follows: even significant reinforcement of supports in mine workings cannot provide rock convergence decrease. Analysis of deformation features of geomechanical system of mine workings has revealed the two dominating alternatives of deformation development within the rock mass: deformations being oriented close to a vertical axis, and deformation, being oriented close to a horizontal one [1, 3]. It is obvious that nonhomogeneity of mechanical characteristics of rocks is the basic factor determining directions of the dominating deformations if only the mine workings were driven in the undisturbed rock mass. Mutual effect of the mine workings varies shaping conditions of a deformation field of the geomechanical system which results in the necessity of extra protective measures. In this context, the rocks, being cut in the process of selective coal mining and left within a production unit, may be used to erect protective structures providing satisfactory deformation mode of geomechanical system of a stope-mine working conjugation.

Efficiency of various structures of the powered support legs depends directly upon mining and geological conditions as well as upon technological conditions of a specific production unit. For instance, in terms of *Samarskaia* mine [1, 2] the powered support was reinforced with the help of pit props providing immediate roof holding within the operating area of a shearer. Hence, design characteristics of the powered support in the context of backfilling technique implementation have been determined for two alternatives – rigid alternative, and flexible one.

Statement of the problem. To carry out comparative analysis of the efficiency of different structural features of the powered support, a model of rock mass, corresponding to actual operation conditions, has been developed.

Longwall 4205 of C_4^2 seam is equipped with the powered complex КД-80, coal shearer КА-200, conveyor СП-251.14. The longwall length is 180 m. Ventilation scheme of the longwall is direct-flow 3-В-Н-г-пт. The first part of the simulation results is given in [3]. Modelling is performed for three variants of stope stowingwhen the stope is developed through a thinly stratified rock mas-

sif under different mining and geological conditions in a three-dimensional representation with realization of conditions for mutual slipping of rock strata. Deformational and mechanical characteristics of elements of the studied geomechanical massif are defined considering the results of laboratory studies and a natural experiment, which determine the behavior mechanism of a granular medium of stowing. The analysis of deformations of a geomechanical system allows determining the degree of influence of different variants of a technology of protecting a stope and deformational characteristics of a rock massif.

Analysis of a state of the disturbed rock mass

The identified discontinuities and areas of rock softening have been analyzed as for their interaction and integral effect on a stope support. As a consequence, 3-D model of the layered rock mass has been developed involving maximally each feature of strengthening characteristics and deformation characteristics of the rock and coal seam.

Stage one is the longitudinal stratification of a rock block, neighbouring the coal seam. The process takes place at the expense of the effect of a high-stress closed area occurring within the rock mass at the depth of 4-7 m down from the stope face. Stage two is the process when the forming blocks of layer one develops excessive pressure bearing on the lower plane of layer two from the top of the rock layer. Through a minor height of the layer, critical concentration of the deformation energy forms a plane of the block separation with 2.5-4.5 m intervals henceforth forming chain of plastic hinges providing smooth lowering of coal lumps. Stage three of rock block formation takes place owing to grouping of stress concentration areas being shaped within the upper boundary and lower boundary of a rock layer located as the third one from above the coal seam. Therefore, through different types of the geomechanical processes, formation of a block structure takes place within a stope roof. Parameters of the block structure are determined unmistakably in the process of the computational experiment which will provide in future adequate research as for the efficiency of the powered support sections with different designs [3].

Standard form of vertical stresses within the stratified rock mass accords well with general ideas concerning rock pressure formation

which can also be indirect confirmation of correctness of the parameters selected to describe geomechanical model for the computational experiment. The obtained curves of vertical stresses are separated into two areas of compressive stresses and tensile stresses by means of a parallel plane passing at the distance of 1.5 m from the stope face towards the mined-out area. Certain share of the analytical model, neighbouring the undisturbed rock mass, experiences compressive loads and the share, around the mined-out area experiences tensile loads. Ultimate compressive stresses are concentrated right behind the stope face.

Analysis of rock mass deformation development in terms of different backfilling methods.

Taking into consideration the computational experiment parameters, distribution of deformations within the rock mass is analyzed only from the viewpoint of qualitative evaluation if continuity of each component of the analytical model is preserved which excludes naturally origination of considerable rock mass deformations directed lengthwise stratification plane.

Figures 6 represent fragments of 3-D analytical model of geomechanical model of a stope-mine working conjugation in the process of use of packs and complete backfilling respectively.

Distribution of total deformation, if heights of the rocks being cut are 0.5 and 0.6 m, is similar which means lack of effect of backfilling alternatives on the processes of roof rock deformation under preliminiting conditions. Deformation nature of the undisturbed rock mass deformation coincides both qualitatively and quantitively. Hence, in the context of the computational experiment, the selected parameters of the powered support provide comparably effective resistance to the neighbouring rock mass deformation under various conditions of a stope backfilling.

Within the edges of parallelepipeds, distribution of deformations varies depending upon the selection of either packing or complete backfilling. In this context, the two specific areas of roof rock layers deformation can be singled out: upper rock layers of the model; and two rock layers neighbouring superiorly the coal layer. Behavior of the rock mass within the stope roof in the process of complete backfilling is of more complex structure in deformation area one, and in

deformation area two in the process of packing. Thus, determine two different approaches for the analysis of deformations within the areas – the generalized analysis in the selected vertical plane, and comparison of a certain rock layer along the stope.

Fig. 1. Total deformations of rock mass in front of the stope face in the process of complete backfilling if height of the rocks being cut is 0.7 m [3]

Fig. 1 represents distribution of deformations within a plane, selected in the process of stress pattern. The curves demonstrate that increase in height of the rocks being cut results in the decreased deformation value of roof rocks of a stope according to a law being close to linear one. Rock mass deformation in the neighbourhood of a mine working for the calculations, performed for partial backfilling, is of similar value and pattern. However, if calculations are made for 0.7 m height rocks, being cut, deformation value in the neighbourhood of a mine working decreases by 18%. The above is followed by the decreased deformations in the rock layer one of the immediate roof of the mine working.

Hence, due to the varied patterns of deformation distribution within the rock layers of a mine working roof, rock mass discontinuity along stratification plane is observed resulting in the formation of a local area with minor transverse strength inside o rock layers one and two. In this context, above rock layers form a block lowering uniformly into the mine working. In actual practice, partial failure of the immediate roof of a stope takes place with the transition to following state of stable equilibrium. The calculation results show: the greater the value of such a failure is, the less time it takes for stage two of the immediate roof failure in the process of packing.

It is typical for deformation curves to preserve quality of deformation distribution within a roof of a stope irrespective of the height of rocks being cut. However, 22% decrease in absolute deformation

values as for 0.5 m height of rocks being cut takes place to compare with calculations for 0.6 and 0.7 m heights. It means that in terms of complete backfilling, increase in the height of rocks being cut impacts bearing capacity of protective structures; as for the rocks, having low strength characteristics, selection of the parameter value is critical.

To compare with the calculation results concerning packing (see Fig. 2), in terms of complete backfilling, changes in height of rocks being cut factor into the increased deformations of rock mass in the neighbourhood of a mine working. If height of the rocks being cut is 0.5 m then roof rock deformations are comparable for packs and complete backfilling. If the heights are 0.6 and 0.7 m then the deformations experience 12-15% increase. Thus, mine working support takes up the increased wall pressure which worsens its operational characteristics [5, 6].

Effect of operational parameters of packs and complete backfilling

Deformation processes of a stope boundary takes place due to displacement of roof and floor of a mine working. That depends upon significant length of a stope together with minor height of the mine working. Roof fault and floor heaving follow the rule of plane-parallel displacements oriented perpendicularly to a gravity force axis [6, 9]. In such a case, vertical stresses become the dominating conditions providing equilibrium of geomechanical system of a mine working. The stresses also exert forming influence on other components of stress-strain state of the rock mass within areas neighbouring the stope and the mine workings.

Fig. 2. Vertical stresses in a cross section at 0.5 m distance from a mine working in the process of packing when height of rocks being cut is 0.5 m

Rapid growth of deformations, caused by vertical stresses within the mine working roof, results in the high-speed fissuring. Origination of the main cracks prevents from dissipation of the accumulated energy of rock deformation factoring into the uncontrolled breakdown of boundary rock layers. Stope advance gives rise to the increased rock pressure within the powered support area; loss of roof rock strength of the mine working takes place resulting in its performance degradation. Thus, to understand the processes involved in the deformation of boundary of the conjugated mine workings, it is required first to analyze the pattern of vertical stress distribution within the rock mass.

Start consideration of volumetric curves of vertical stresses from the degree of effect of operational parameters of packs within the mined-out area of a stope on SSS in a mine working wall. Fig. 3 explains stress pattern in a section, being cross relative to a stope face of rock mass located at 0.5 m distance from mine working-stope conjugation plane. A model of the powered support in the form of 1 m height and 5.5 m width parallelepiped in at the center. Undisturbed rock mass is to the left of the model; mine working with packs or complete backfilling is to the right. Such an arrangement is preserved for each further similar curve.

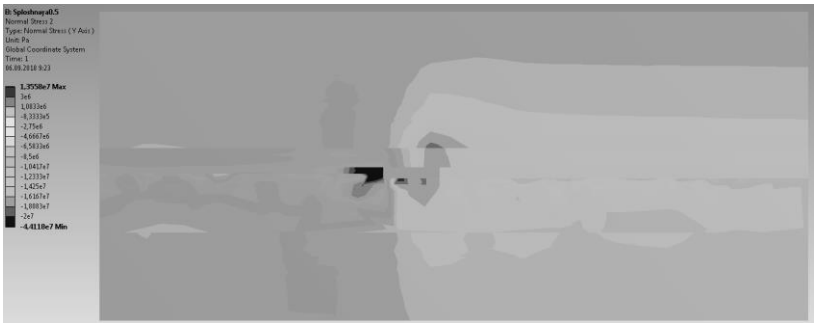

Fig. 3. Vertical stresses in a cross section at 0.5 m distance from a mine working in the process of complete backfilling when height of rocks being cut is 0.5 m

Total analysis of curves in Figures 2 and 3 has shown the following: more than 90 % of the analytical model experience compressive stresses to be correct for elastic problem statement while corresponding to conditions of vertical stress application to upper and lower edges of the model; maximum compressive stresses are in front of the stope face towards the undisturbed rock mass which corresponds to the practices of stress measurements under full-scale conditions; formation of tensile stress areas depends upon the effect of the powered support model on the neighbouring rock layers which is in the good agreement with its actual operational conditions [7]; and vertical stresses within the mine working roof exceed stresses in its floor and the fact is supported by operational practices of stopes in Western Donbas mines.

Range of maximum stresses for the three computational options coincides almost completely; less than 5% deviations are fall into the analytical error. Qualitative distribution of vertical stress is of the nature, being typical for all the calculations; however, both value and size of stress intensity gradient within a mine working roof increases from alternative 0.7 m height of the rocks being cut to 0.5 m height. In this context, stresses within the mine working floor decrease but the velocity drops twice.

Effect of the tensile stresses on the state of a mine working roof localizes within the area neighbouring the powered support. As a result, at 5 m distance from the powered support model, vertical horizontal directional stress gradient in the mine working roof is equal to zero.

Hence, use of packs to provide reasonable operational performance of a stope-mine working conjugation makes it possible to obtain uniform distribution of load on the support and on the protective structures of a mine working support in a vertical direction which should cut the likelihood of the main fissuring as well as dimensions of areas loss of strength within neighbouring rock mass. On the other hand, changes in height of the rocks being cut leaves invariant operation of the powered support and, having no influence on the stress distribution within the undisturbed rock mass behind the stope face.

Curves in Fig. 2 involve characteristic features, which are not typical for calculation options where packing is applied. Change in stress pattern within the stope roof in the area of rock mass neighbouring the powered support model is the principal distinction of the model.

First, the powered support effect on the stress distribution within the stope roof covers 10-15 m towards the mined-out area if increase in maximum stresses is 21-24% to compare with calculations concerning use of packing. It means that complete backfilling makes it possible to engage greater rock amount to a process of roof stabilization. However, the feature is neutralized completely by the increase in vertical stresses. Thus, accumulation of potential energy of roof deformation for the calculation options, demonstrated in Figures 2 and 3, is similar quantitively. At the expense of the varied value and geometry of vertical stress gradient, distance between the main fissures increases relative to packs if complete backfilling is applied which results in the formation of larger rock blocks [7].

Second, maximum compressive stresses are in front of a stope face within the undisturbed rock mass. Values of the stresses, obtained for packs, experience 20-50% exponential increase along with the increase of height of rocks being cut. In this context, a curve in Fig. 3 demonstrates abrupt jump of compressive stresses within the powered support model-stope roof contact zone. Such a feature is also typical for other curves represented in Fig. 3, which points to the varied nature of the powered support-rock mass interaction. Both front share of leg of the powered support and rare share are under the effect of alternate load, which increases the likelihood of “rigid” setting [8, 11]. Henceforward, the *alternate load* is understood as a state when a stress field, characterizing material compression and tension,

is formed simultaneously within the selected volume of analytical model.

The obtained results help conclude that the behaviour of boundary rock mass in the context of packing and complete backfilling is described with the help of linear regularities and exponential regularities stipulating difference increase in maximum vertical stresses depending upon the height of rocks being cut.

a

b

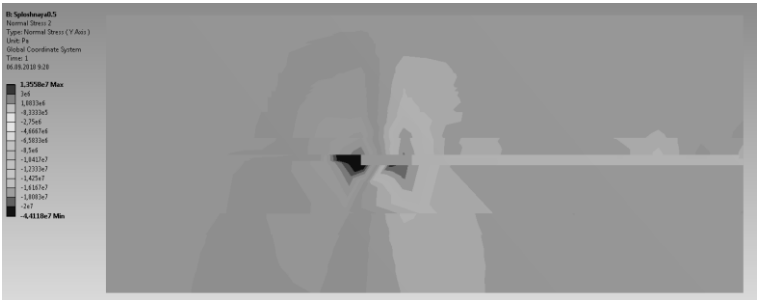

Fig. 4. Vertical stresses within the central cross section of a mine working at 0.5 m height of rocks being cut when: *a* - packing is applied; and *b* - complete backfilling is applied

If longwall length is 250 m, at 120 m distance from a stope-mine working conjugation, rock mass area is formed within which factors of technogenic impact on the rock mass stress-strain state are almost minimized. Hence, use the area to analyze stress distribution taking into consideration three typical longitudinal sections of packs: first – in close proximity to a pack within empty of a stope (see Fig. 4*a*); and second - along a side surface (see Fig. 4*b*).

Stress distribution within a roof in Fig. 10, a shows that it resists uniformly a displacement to the stope cavity lengthwise and the resistance is by 17% less to compare with floor resistance. Stress distribution within the stope floor is of regular nature with 9-12% stress value vibrations of maximum. Stresses, taken by the pack model, exceed greater vertical stresses than rocks neighbouring it; distribution of the stresses is of a regular nature as well.

Therefore, the pack operates like an equalizing damper in the process of effort transmitting from a roof to a floor. Minimum vertical stresses within the pack are located at the beginning at $L_н$=2.5 m distance from the edge of the powered support model. The $L_н$value is the determining parameter to select a velocity of a stope face displacement in the process of packing.

If the broken rock is laid down continuously along the stope in case of complete backfilling which results in natural compaction of the stowing, the formation of packs needs certain time interval, determined on the basis of mechanical disintegration conditions, during which the bulk rock will gain carrying characteristics. The characteristics can form naturally if only minimum external loads are available not initiating dynamic phenomena within the packs being formed. Hence,

$$v_{оп}=L_н \cdot t_{ст}, \quad (5)$$

where $v_{оп}$ s a stope advance; $L_н$ is a length of a pack area rejecting mine pressure; and $t_{ст}$ is stabilization period of the pack meter.

Stabilization period of a pack meter may be determined either experimentally or with the help of methods of extrapolation of findings obtained for different rocks and their failure conditions [10]. However, the parameter also depends upon the height of rocks being cut since it experiences effect by a value of total pack amount. Moreover, variation of the parameter, stipulated by the considered system state, is of nonlinear nature preventing from the use of mathematical scaling methods.

The calculations have shown that maximum $L_н$ value corresponds to 0.6 m height of rocks being cut reaching 3.4 m; if the height is 0.7 m then minimum value (i.e. 1.2 m) is obtained. Thus, the parameter has nonlinear characteristic too.

Ultimately, determination of a stope optimum advance in terms of a factor, providing carrying capacity of a pack, takes place according

to the results of full-scale experiments. The development of physical and mathematical model of the process needs further research which tendency and volume do not correspond to the area under consideration.

In Fig. 3, the coal seam and rock layers, neighbouring it, experienced high compressive stresses. At the mean, the stresses within the area are 4% higher than stress values in the undisturbed rock mass but the area extent is 18-22 m. Within the central cross-section plane (see Fig. 4*b*) such an area is not available and area of high vertical stresses formed vertically. Stress increase within the area is up to 12% of maximum theoretical values. Thus, in the context of complete backfilling, changes in vertical stresses along the stope are of qualitative and quantitative nature being expressed in the high stress area reorientation from horizontal to vertical as well as in 6-9% increase in the stress values.

Comparative analysis of the curves has explained that in the context of the two cases, geometry of the area of high compressive stresses is similar to a gradient value. Stresses, experienced by rocks of a stope (see Fig. 3), are 8% less to compare with those in Fig. 4*b*. In terms of complete backfilling alternative, no vertical floor stresses along the stope cross section are observed.

As a whole, when complete backfilling is used, rock mass loading is uniform; nevertheless, concentration of compressive stresses within the undisturbed rock mass is higher to compare with the use of packs. Thus, qualitative variations in stress distribution among curves, represented in Figure 4*a*, and Figure 4*b*, are as follows:

- in terms of computational alternative one, local stress concentration within the disturbed rock mass and within a stope floor is 22% less to compare with alternative two; and
- material at a wall surface of a pack takes stresses by 18% more to compare with complete backfilling.

The abovementioned points to the formation of conditions for dynamic phenomena origination in packs along the whole length of the mine workings. Loose rock thickening takes place under the effect of high rock pressure. Depending upon loading conditions, it may result in the geomechanical system stabilization or, instead, in the active development of the main fissures within immediate roof of the mine working. Determination of the geomechanical system stress-strain

state development under the conditions is a separate problem solved with the use of multiparameter system to analyze conditions of complicatedly structured enclosing rock mass [8-11].

In the context of complete backfilling, area of high compressive stresses to be calculated for 0.6 m and 0.7 m heights of rocks being cut is of a similar shape differing qualitatively from 0.5 m alternative. 1.5 times increase of compressive stresses in the stope immediate roof above the powered support is typical for such calculation options. Hence, increase in the amount of rocks being cut in the process of complete backfilling does not result in the change of stress-strain state of the rock mass. Nevertheless, pressure on the powered support also increases consistently for 0.5 m height of rocks being cut meaning incremental probability of a of "rigid" setting of the powered support legs.

Analysis of curves of vertical stresses has helped conclude the following: under the considered mining and geological conditions, operations of a mine working are provided better in the context of packing to compare with complete backfilling; if packing is used, changes in roof and floor of the stope follow a regular law along the stope advance axis and across it; height of rocks being cut effects the immediate roof state change during packing and complete backfilling but following different laws; and in the context of packing, vertical stress are distributed more uniformly along the stope face within the undisturbed rock mass to compare with complete backfilling being 12-16% less in terms of absolute values.

Analysis of stress distribution within stratification planes of rock mass along a stope advance

Under the conditions of high structuredness of rock mass, enclosing a mine working, horizontal stresses are among the basic factors determining parameters of the controlled roof rock caving during a stope advance. Changes in the stress values along the stope face as well as transversely to it identify both shape and time frame of the formation of a destructive breaking wave within the rock layers making a roof of the considered geomechanical system.

Following analysis is a comparison of horizontal stress characteristics in different sections of one and the same calculation. Determine backfilling effect on the state of the fine-grained rock mass

within a roof of geomechanical system of a stope and a mine working.

Availability of a vertical plane, oriented along the stope face and located above the powered support, is the common feature of the curves. Within the plane, analytical stress sign changes from compressive to tensile.

Parameters of the plane, its dimensions, and changes in its geometry (i.e. transformation into the curved surface) help determine dimensions of the rock mass being involved to a process of axial deformation of a stope roof.

Moreover, it is required to take into consideration variations of horizontal stresses in the depth of the undisturbed rock mass as well as from the worked-out area of the stope since it identify both degree and conditions of effect of maximum horizontal stresses on the backfilling method being applied in the specific case.

Hence, along with the stress analysis within the equilibrium plane, it becomes possible to determine the conditions of axial loading of a stope backfilling.

Comparison of Figure 5, a, and Figure 5, b helps understand that a height of alternate stresses increases by 27% from the mine working edge to a central share of the stope.

Local areas of high compressive and tensile stresses also increase towards the stope central share.

In terms of absolute values, the increase is 2 to 53% and change in dimensions of the areas achieves 145%.

However, the increase is observed only vertically.

Relying upon the results, it is possible to conclude that the increased height of the sign-variable plane results in the increase of horizontal stresses within the local area of a roof of the mine working neighbouring the powered support model pointing to the intensification of horizontal displacements depending upon distancing from the stope edge.

That factors into the formation of an ovoid-like front of the progress of the main fissures directed across the stope.

a

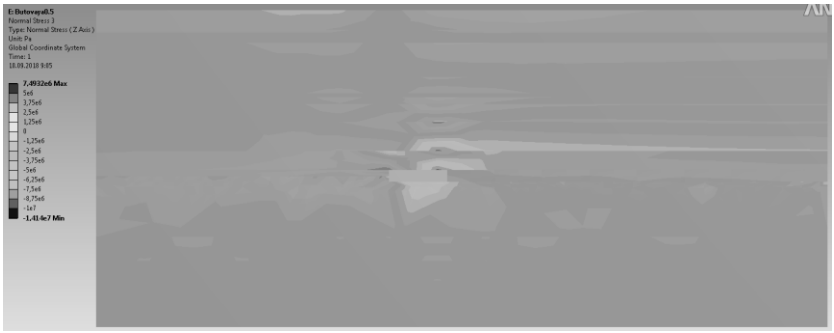

b

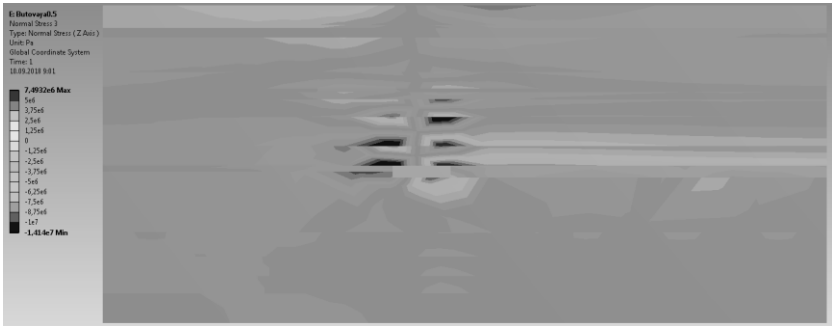

Fig. 5. Horizontal stresses in cross section in the process of packing when height of rocks being cut is 0.5 m: *a* - at 0.5 m distance from a mine working; and *b* - within a central transverse plane

To compare with curves in Fig. 5, Fig. 5*b* demonstrates increase in horizontal stresses within the undisturbed rock mass, and within the stope floor meaning the increased share deformations arising when rocks are converged to the stope cavity. If in the neighbourhood of the mine working effect of the undisturbed rock mass within walls of mine working helps decrease a level of horizontal stresses, significant distance neutralizes the effect. Thus, the less difference among stress distribution within sections in Figure 5*a*, and Figure 5*b* is, the more stable is the roof of the considered geomechanical system. Basing upon the statement, formulate rule one – optimum backfilling conditions are possible if only minimum deviations take place in the alternating-sign plane along the whole length of a stope.

Comparative analysis of curves in Fig. 6 has shown that 12% stress increase within the undisturbed rock mass in front of a stope results in 7% load increase on stowing within the mined-out area. Hence, for Ukrainian mines, the two factors are related and their connection helps evaluate strength degree of structural bearing capacity of protective measures as for the original rock mass. Thus, we obtain rule two – decrease in the difference of horizontal stress increment within the undisturbed rock mass in the context of packing or complete backfilling shows the increase in the bearing capacity of the protective structure to compare with other alternatives.

As for the calculation alternative, the intensity of changes in horizontal stresses along a stope is 1.3 times higher to compare with packing. Height of alternating-sign stress plane achieves upper boundaries of rock layers of the analytical model. Thus, mechanical state of rock layers within the considered geomechanical system deteriorates in the context of complete backfilling.

Stresses inside immediate roof of a stope within its central cross section (see Fig. 6) shape a pattern being close to a vertical section formation above the powered support legs. Within a central share of a stope, legs of the powered support resist to loads, increased by 40%, which are directed towards the mined-out area; i.e. despite complete backfilling, the mine working roof demonstrates intensification of deformation processes intended to separate certain share of the immediate roof along the stope face. It turns out that for complete backfilling conditions, stress-strain state of rock mass is less stable to compare with packing (see Fig. 5) but is still out of keeping the criteria of rock failure with the formation of the main fissures [13].

When complete backfilling takes place and height of rocks being cut is 0.6 m, sharp increase in the value of horizontal stresses is observed in the neighbourhood of a mine working as well as in the central share of a stope.

Shaping nature of the areas of high stresses remains invariable; nevertheless, their dimensions experience 17% increase. Therewith, in the neighbourhood of a mine working, average increase in tensile stresses is 14% and increase in compressive ones is 9 % which can be explained by sharp increment of load on the support and on protective structures of the mine working. The above mentioned may accelerate a process of rock heaving and arch lowering [9, 10].

a

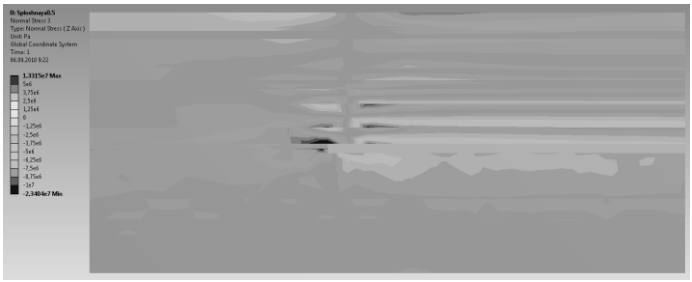

b

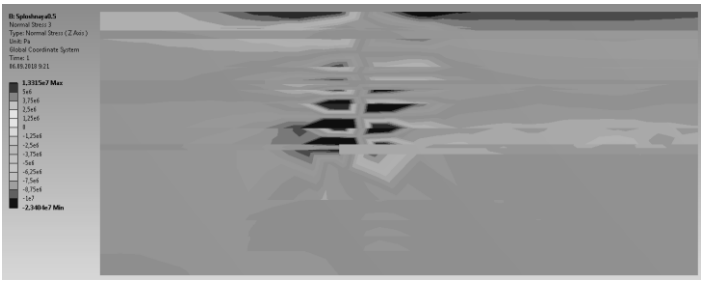

Fig. 6. Horizontal stresses in cross section in the process of complete backfilling when height of rocks being cut is 0.5 m: *a*- at 0.5 m distance from a mine working; and *b*- within the central transverse plane

In addition, a height of alternating-sign stress plane remains invariable for each computational alternative. That also means the lack of fundamental changes in the shaping of areas of ultimate rock state within the stope roof. Nevertheless, the constant increase in the absolute values of horizontal stresses shows that heightening of rocks being cut increases a risk of roof rock softening right above the powered support section. The dependence is nonlinear, and experiences its decrease in proportion to the heightening of rocks being cut.

In view of the fact that in the context of complete backfilling horizontal stresses within a roof of a stope are of maximum values, it is required to analyze specific features of their distribution in the immediate roof. In terms of the mining and geological conditions, immediate roof of the stope consists of three rock layers ordered in the analytical model from one to three starting from the coal seam being mined.

Findings

Assume a stope face-its central vertical section junction as the area to be analyzed. Levels one and three take up stresses with a wider scatter but degrees differ. Such a specific feature of the graphs denotes effect of rock deformation characteristics on the stress distribution within the rock mass substantiating indirectly the adequacy of the calculations.

However, there is a specific feature concerning horizontal stress distribution when heights of rocks being cut are 0.6 m, and 0.7 m. If in rock layer one, stress values increase gradually, in layers two and three, values of maximum stresses are less for 0.7 m height of rocks being cut to compare with 0.6 height meaning changes in the conditions of equilibrium state of the model of a stope roof. Such a change in maximum stress values is followed by partial transition of rock layers to the limit state resulting in the immediate roof softening under the effect of compressive horizontal stresses.

Analysis of graphs of tensile stresses (see Fig. 7) [3] demonstrates a pattern opposing the graphs of compressive stresses. If height is 0.5 m, then changes in maximum stresses in terms of rock layers of the immediate roof differ markedly from 0.6 and 0.7 m heights of rocks being cut; layer one is loaded greater and load, taken up by layer three, is quite lesser.

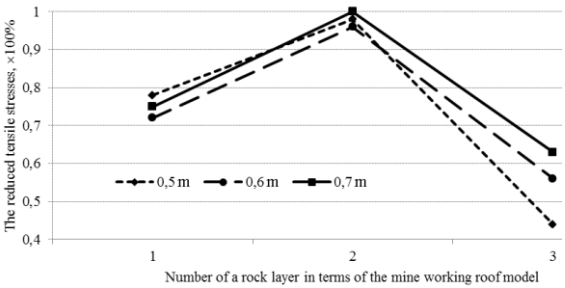

Fig. 7. Changes in the reduced maximum tensile horizontal vertical stresses on the stope face within the central share of the mine working in the process of complete backfilling in terms of different heights of rocks being cut [3]

On the whole, calculation alternative for 0.6 m height demonstrates indices of the limit efficiency state as for the provision of a stope immediate roof in the context of complete backfilling. Fur-

thermore, effect of compressive stresses on the stable state of a mine working immediate roof is greater to compare with the effect by tensile stresses.

Conclusions

1. Modelling is performed for three variants of stope stowing when the stope is developed through a thinly stratified rock massif under different mining and geological conditions in a three-dimensional representation with realization of conditions for mutual slipping of rock strata. Deformational and mechanical characteristics of elements of the studied geomechanical massif are defined considering the results of laboratory studies and a natural experiment, which determine the behavior mechanism of a granular medium of stowing. The analysis of deformations of a geomechanical system allows determining the degree of influence of different variants of a technology of protecting a stope and deformational characteristics of a rock massif.

2. It is established that a concentration of horizontal stresses directed along a stope face over a powered support in a roof of a mine working is the main factor affecting a mode of development of main cracks in a roof of a working during stowing. The interaction mechanism at junctions of a stope and another working is studied to determine a development mechanism of a stope roof collapse considering the influence of stowing parameters. Analysis of a stress-strain state of a stope roof by selected mining, geological, and technological parameters allows determining the conditions of rock strata interaction, the result of which is a roof collapse on packs.

3. It is determined that the designed unit of powered roof support allows overcoming structural features of a roof support used during partial stowing by increasing the safety margin of elements supporting the tail console. The safety margining crease is achieved by introducing additional rigid structural elements what reduces the level

of stress concentration in joints of a roof support structure.Using an integrated approach to determine the efficiency of selected roof supporting scheme allows estimating reliability of the selected modelling scheme when predicting changes in a state of a geomechanical system. This is a new method for evaluating the efficiency of various technological solutions.

4. The results indicate that when using packs, a process of crack formation in an immediate roof of stopes is stopped by localizing areas and stress values that contribute to growth of main cracks. The optimal selection, from a standpoint of dynamic stability of animmediate roof of stopes and packs, is selection of the minimum permissible height of extracted rocks while ensuring a statistical equilibrium of sides of packs. This allows determining a mechanism of selection of stope movement velocity, a type and geometric parameters of erected packs.

References

1. **Sotskov V.A., Malashkevich D.S. and Russkikh V.V.** (2016). Analysis of the influence of partial laying of the mined-out space on the VAT of a carbon-bearing massif during the selective mining of thin coal seams. Geotechnical mechanics, №129. 54–64.

2. **Fomychov, V.V.** (2012). Bases of calculation models plotting of bolt-frame support considering non-linear characteristics of physical environment behavior. Scientific herald of National Mining Ukraine, 4, 54-58.

3. **Fomichov V.V., Sotskov V.O., Dereviahina N.I. & Leonenko O.V.** (2019). Analysis of the results of a computational experiment to determine operational parameters for partial backfilling of the worked-out area. Modernization and engineering development of resource-saving technologies in mineral mining and processing. Multi-authotrf monograph. Romania: UNIVERSITAS Publishing. 410-430.

4. **Buzilo V.I., Sulaev V.I., Koshka A.G.** et al. (2013). The technology of mining thin layers with the laying of the developed space. Dnipropetrovsk.

5. **Ma, C., Yao, W., Yao, Y., Li, J.** (2018) Simulating Strength Parameters andSize Effect of Stochastic Jointed Rock Mass using DEM Method. KSCE Journal of Civil Engineering, 22 (12), 4872-4881.

6. **Fomychov, V., Sotskov, V.** (2018). Determination of parameters of non-uniform fractured rock massif in computing experiment. Journal of Geology, Geography and Geoecology, 26, 26-32.

7. **Fomichev, V.V., Sotskov, V.A., Malykhin, A.V.** (2014) Definition and analysis of changes in acceptable indicators of the stress-strain state of the elements of the frame-anchor lining of the dismantling drift when approaching the face. Naukoviy vísnik NGU, 1, 22 - 25.

8. **Bondarenko V.I., Russkih V.V. and Yarkovich A.I.** (2014). Materials On the issue of abandonment of rock in the worked out space of coal mines. Materials of the VIII international scientific-practical conference "School of underground mining", 19-24.

9. **Bondarenko V.I., Kovalevska I.A., Simanovich G.A., Koval O.I., Fomichov V.V.** (2012). Experimental studies of the stability of reusable excavation workings on the flat layers of the Donbass: Monograph. Dnepropetrovsk.

10. **Zakharov Yu.N., Kantovich L.I.** Interaction of mechanized roof supports with the roof during the development of the Starobinsky potassium salt deposit. Moscow.

11. **Li, J., Nie, Y.-F., Fu, K., Guo, J.-B., Xu, M.-X.** (2018) Experiment and analysis of the rock breaking characteristics of disc cutter ring with small edge angle in high abrasive grounds. Journal of the Brazilian Society of Mechanical Sciences and Engineering, 40(10), 505.

12**. Fomichev, V.V.** (2015). Scientific bases of control of geomechanical systems with the use of recursive methods in the underground development of deposits: Diss. … Doctor of Engineering. Sciences: 05.15.02. Dnepropetrovsk.

13. **Hu, F., Li, Z., Hu, R., Zhou, Y., Yue, R.** (2018) Research on the deformation characteristics of shear band of soil-rock mixture based on large scale direct shear test. Yanshilixue Yu Gongcheng Xuebao / Chinese Journal of Rock Mechanics and Engineering, 37(3), 766-778.

DETERMINATION OF BEARING CAPACITY AND CALCULATION OF THE GAIN OF THE DAMAGED SPAN OF A RAILWAY OVERPASS BY THE FINITE ELEMENT METHOD

Sakhno S.
Kryvyi Rih National University, Ph. D., Assoc. Prof., Ukraine

Liulchenko Y.
Kryvyi Rih National University, Ph. D., Assoc. Prof, Ukraine

Chyrva T.
Kyiv National University of Civil Engineering and Architecture, Ph. D., Assoc. Prof, Ukraine

Pischikova O.
Kryvyi Rih National University, Ph. D., Assoc. Prof, Ukraine

Abstract

The subject of the study the possibility of applying the finite element method to determine the bearing capacity of a damaged reinforced concrete structure and the subsequent selection of its reinforcement parameters with composite materials.

Research methodology – the studying of finite element models of the serviceable destroyed and restored structure and determination of design parameters of the structure before destruction, after the destruction, and after its strengthening.

The goal – identification of the possibility of further operation of the damaged structure using the finite element method, finding the most dangerous places in the construction, selection of parameters for its amplification.

Conclusion of the study. The proposed research method made it possible to more accurately and at a lower cost, identify the most dangerous areas in the damaged structure, and verify the effectiveness of the applied method of its restoration. The method showed high efficiency in assessing the bearing capacity of a structure with complex reinforcement in which part of the reinforcement is in a destroyed state.

1. Introduction

The need to restore the bearing capacity of reinforced concrete structures arises, usually in two cases. The first is due to the reconstruction of buildings and structures and the associated increase in the intensity of the operational load. The second case is due to the restoration of the bearing capacity lost during operation due to corrosion, mechanical damage, manufacturing, or installation defects.

One of the innovative ways to restore the load-bearing capacity of reinforced concrete structures is the method of constructing a reinforcing system made of composite materials [1-4]. This method successfully used throughout the world and is gaining great popularity in Ukraine.

Based on carbon fiber, composite materials usually used as an external reinforcement system in the construction industry for reinforcing the load-bearing construction structures of buildings and structures. The advantage of carbon composite materials is their manufacturability, low weight, relatively high strength, resistance to aggressive external factors, minimal material size, minimum requirements for installation work, high installation speed.

The main elements of the external reinforcement system of flexible reinforced concrete structures are fabrics and lamellas of various grades. They are gluing to the surface of building structures in a polymer matrix, which provides tight adhesion of the reinforcing filler to the reinforced structure. The most common reinforcement method is carbon lamellas. The article considers the calculation of the bearing capacity and reinforcement of a damaged reinforced concrete structure using the finite element method in the ANSYS software package.

2. Object of study

The strengthening calculation was made for the railway bridge overpass Zaporizhia Ferroalloy Plant. The three-span beam overpass has a longitudinal scheme -16.5 +13.5 +16.5 m. The angle of intersection of the overpass with the street - 39° (Fig. 1).

Fig. 1. General view of the overpass

Spans consist of two monolithic main reinforced concrete beams, which are connected by a slab and diaphragms. Longitudinal work-

ing reinforcement of class A-II ☛28 mm, located in 4 rows in height (9 rods in one row). Part of the rods does not reach the support and diverted into the compressed zone of concrete (Fig. 2).

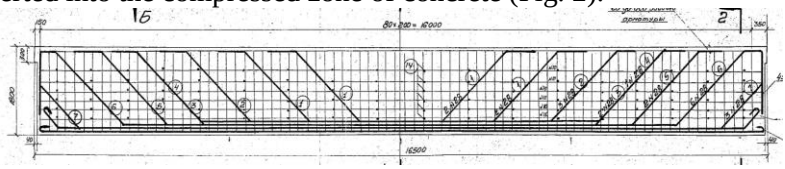

Fig. 2 Span beam reinforcement

Long consoles on which a railing installed arranged to create a ballast trough. The design load on the span construction — H 7.

The examination found that one of the spans, located on the side of the ferroalloy plant, has defects in the form of destruction of concrete in the stretched zone and destruction of part of the rods of the working reinforcement. In one rib, the torn two lower rows of reinforcement. The concrete strength of monolithic beams and diaphragms was determined using an ADA Schmidt Hammer 225 sclerometer and is in the range of 25.8-26.8 MPa, which is higher than the design grade of concrete - M250, except for damaged places where the average concrete strength was 18.8 MPa.

Damage (Fig. 3) occurred as a result of the transverse impacts of freight road transport on the lower edge of the beams due to a decrease in the size of the roadway. The reason for the decrease in size is an increase in the height of the carriageway during the repair of road works.

To checking the load-bearing capacity of the beam, 3D models were created in the ANSYS software package that takes into account the geometry of the structure before (Fig. 4) and after its damage (Fig. 5). The load C14 applied to the model following DBN B.1.2-15: 2009 [5] and DBN B.2.3-14: 2006 [6].

In the computational finite element model for numerical analysis, the symmetry of the computational domain taken into account. When creating the calculated finite element (FEM) model, the elements were used: for concrete (B35) - SOLID186, for reinforcement (A-300 steel) - REINF264. When generating a mesh of the reinforcement, the MESH200 element used.

Fig. 3. Damaged span beams

Solid186 - is a higher-order 3-D 20-node solid element that exhibits quadratic displacement behavior. The element defined by 20 nodes having three degrees of freedom per node: translations in the nodal *x*,*y*, and *z* directions. The element supports plasticity, hyperelasticity, creep, stress stiffening, large deflection, and large strain capabilities [7].

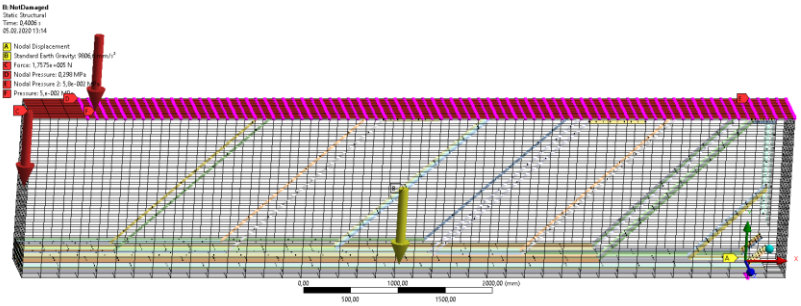

Fig. 4. FEM beam model before damage

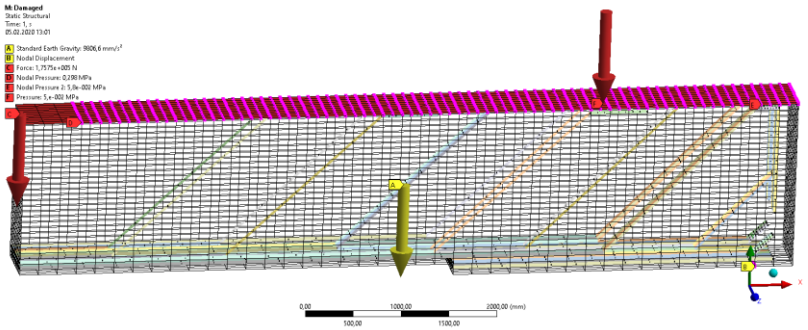

Fig. 5. FEM beam model after damage

Reinf264 used in the analysis of structural reinforcement of 3D beams, shells, and solid elements. The element is suitable for modeling reinforcing fibers with arbitrary orientation. Each fiber is modeled separately as an element that has only uniaxial rigidity. REINF264 has plasticity, stress stiffening, creep, large deflection, and large strain capabilities.

The characteristics of the materials used in the calculations shown in table 1.

Table 1

Structural characteristics of the materials used in the calculations

№	Parameter	Value
	Concrete	
1	Young's Modulus	22360 MPa
	Poisson's Ratio	0,18000
	Bulk Modulus	11646 MPa
	Shear Modulus	9474,6 MPa
	Compressive Ultimate Strength	41,000 MP
	Tensile Ultimate Strength	5,0000 MPa
	Structural Steel	
	Young's Modulus	2e+05 MPa
	Poisson's Ratio	0,30000
	Bulk Modulus	1,6667e+05 MPa
	Shear Modulus	76923 MPa
	Compressive Ultimate Strength	0 MPa
	Compressive Yield Strength	250,00 MPa
	Tensile Ultimate Strength	490,00 MPa
	Tensile Yield Strength	295,00 MPa
	Carbon fabric-tape-1000-12K-420.Ct-11083	
	Young's Modulus X direction	1,21E+05 MPa

	Young's Modulus Y direction	8600 MPa
	Young's Modulus Z direction	8600 MPa
	Poisson's Ratio XY	0,27
	Poisson's Ratio YZ	0,4
	Poisson's Ratio XZ	0,27
	Shear Modulus XY	4700 MPa
	Shear Modulus YZ	3100 MPa
	Shear Modulus XZ	4700 MPa
	Orthotropic Stress Limits	
	Tensile X direction	2231 MPa
	Tensile Y direction	29 MPa
	Tensile Z direction	29 MPa
	Compressive X direction	-1082 MPa
	Compressive Y direction	-100 MPa
	Compressive Z direction	-100 MPa
	Shear XY	60 MPa
	Shear YZ	32 MPa
	Shear XZ	60 MPa

3. Results of the research

As a result of the calculations, data obtained on the stress and strain states of concrete and beam reinforcement before and after damage (Fig 6 -15).

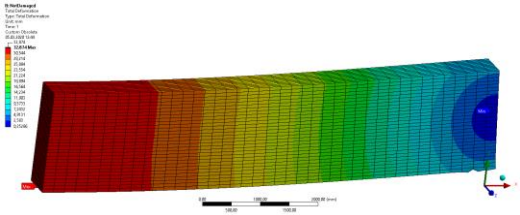

Fig. 6. Estimated beam deformation before damage

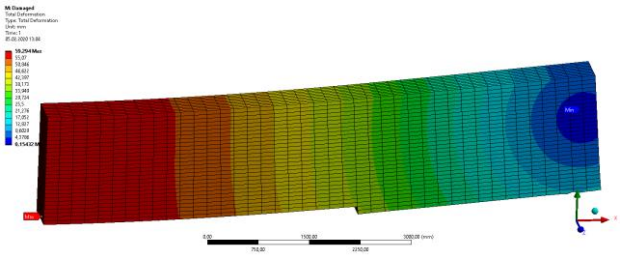

Fig. 7. Estimated deformation of a damaged beam

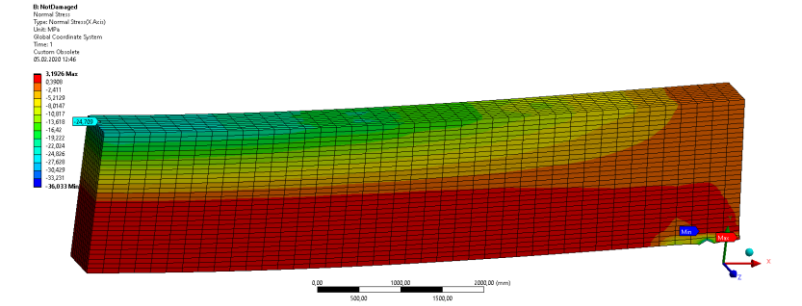

Fig. 8. Normal Stress distribution in the concrete of the beam before damage

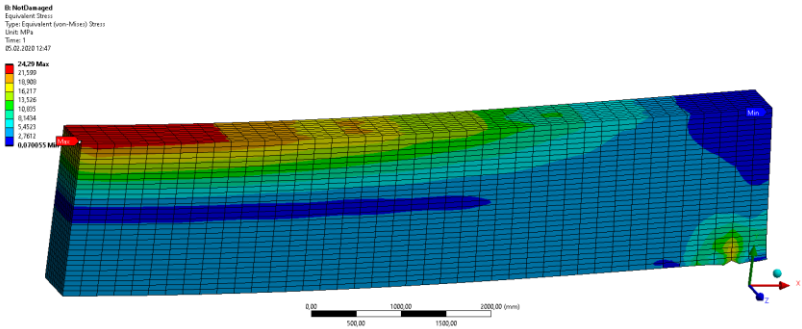

Fig. 9. Equivalent Stress distribution in the concrete of the beam before damage

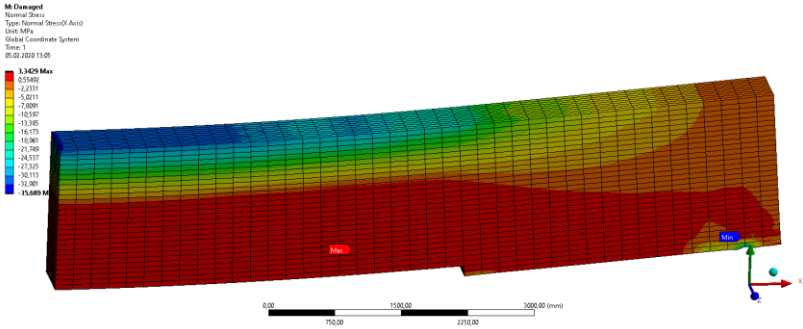

Fig. 10. Normal Stress distribution in the concrete of a beam after damage

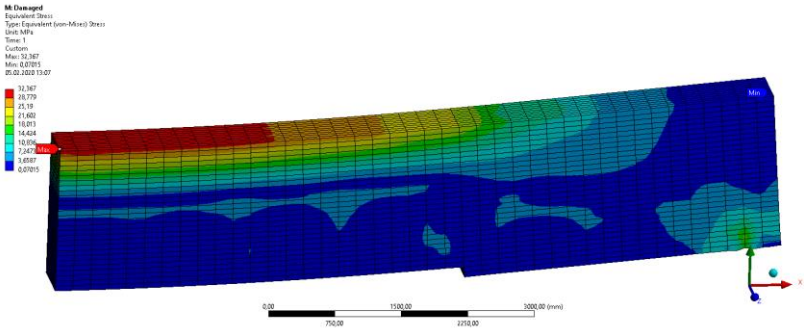

Fig. 11. Equivalent Stress distribution in the concrete of a beam after damage

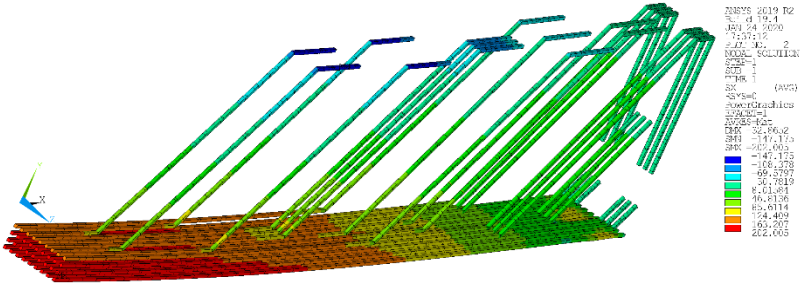

Fig. 12. Distribution of Normal Stresses in the beam reinforcement before damage

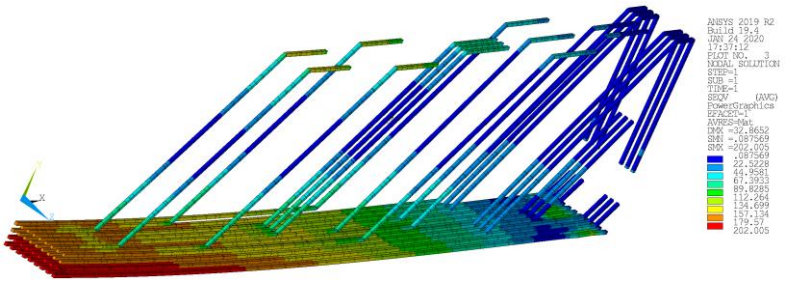

Fig. 13. Distribution of Equivalent Stresses in the beam reinforcement before damage

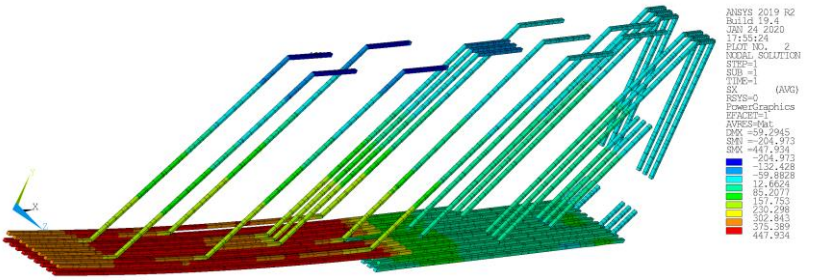

Fig. 14. Distribution of Normal Stresses in the beam reinforcement after damage

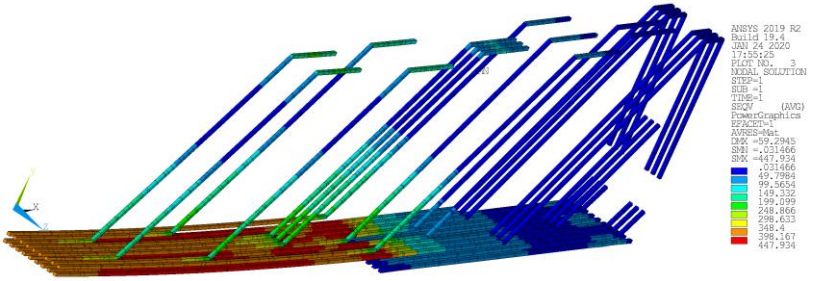

Fig. 15. Distribution of Equivalent Stresses in the beam reinforcement after damage

The maximum values of the data shown in table 2.

Table 2

Maximum deformations and stresses in the structure before and after damage

Maximum parameter value	Before damage	After damage	Δ, %
Beam deflection	32.87	59.29	59.1
Normal stress in concrete			
tension	3.2	3.3	0.3
compression	24.3	32.37	33.2
The normal stresses in the reinforcement	202.00	447.93	217.5

Although stresses in reinforcement after damage increased by almost two times, the static load-bearing capacity of the beam remains sufficient. However, the deflection of the damaged beam does exceed the permissible values.

To preventing further destruction of the beam to ensuring its bearing capacity and to preventing's corrosion of the reinforcement, additional reinforcement was developed by gluing a unidirectional carbon fiber Carbon fabric-tape-1000-12K-420.Ct-11083 onto the lower belt of the beam. The concrete coating restored in the zone of damage to the lower belt before gluing the CFRP. The structural characteristics of carbon fiber given in table 1 and figure 16.

The adhesive bonding of concrete and carbon fiber is modeled by Cohesive Zone Material (CZM) using Separation-Distance based Debonding. Contact algorithm: Penalty method. Contact detection at the Gauss integration point. The system generated elements SURF154 and SURF156 to implement the model.

The FEM model of the reinforced beam shown in Figure 17. The distribution of deformations and stresses in concrete and reinforcement shown in Figures 18-22.

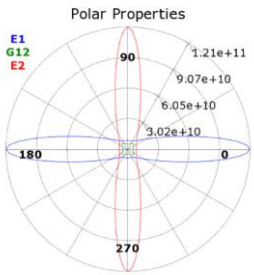

Fig. 16 . A properties of Carbon fabric-tape-1000-12K-420.Ct-11083:

E1 - Orthotropic Young's Modulus in-plane, in fiber direction;

E2 - Orthotropic Young's Modulus in-plane, orthogonal to fiber direction;

G12 - Orthotropic Shear Modulus in-plane, in fiber direction

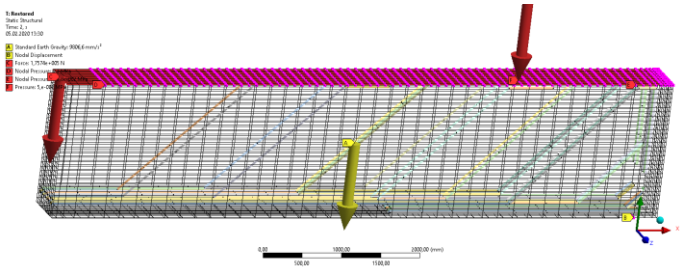

Fig. 17. Intensified beam design model

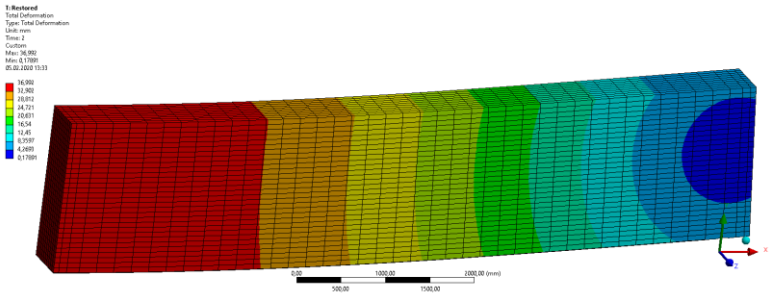

Fig. 18. Deflection of the intensified beam

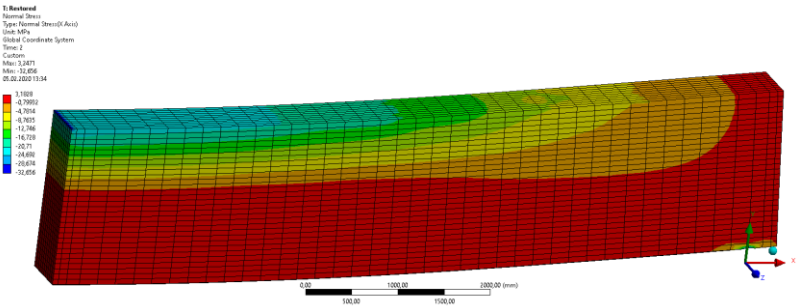

Fig. 19. Normal Stresses in the concrete of intensified beam

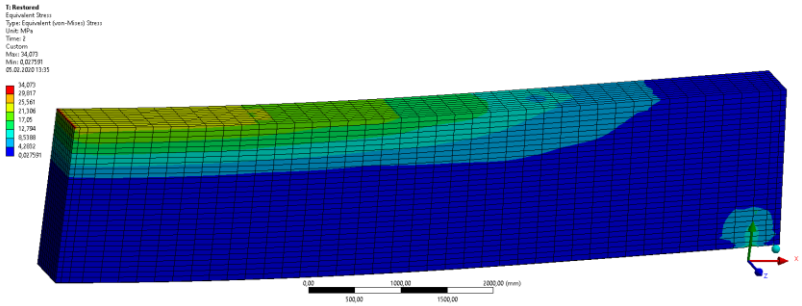

Fig. 20. Equivalent Stresses in the concrete of intensified beam

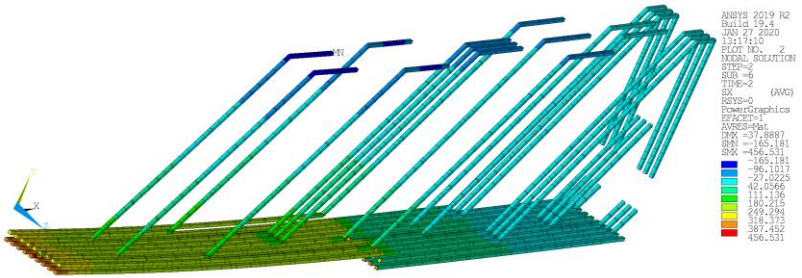

Fig. 21. Normal Stresses in the reinforcement of the intensified beam

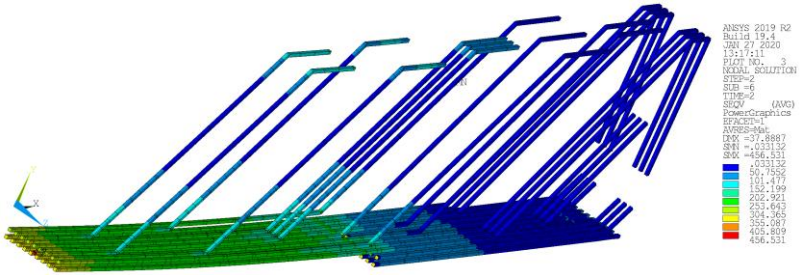

Fig. 22. Equivalent Stresses in the reinforcement of the intensified beam

The parameters of deformation and stresses in concrete and the reinforcement of intensified beams shown in table 3.

Table 3

Maximum deformation and stress in the structure before damage and after intensified

Maximum parameter value	Before damage	After intensified	Δ, %
beam deflection	32.87	38.5	17,1
normal stress in concrete			
tension	3.2	3.7	15.6
compression	24.3	26.3	8.2
the normal stresses in the reinforcement	202	345	70

An analysis of the results shows that reinforcing the structure with unidirectional carbon fiber with a thickness of 1 mm reduces the increase in deflection from 59 to 17 %, stresses in the stretched zone from 33 to 8 %, and in the reinforcement from 217 to 70 % compared with the unreinforced structure.

Analysis of the reinforced structure in the ANSYS software package revealed a picture of the normal stress distribution in the gain element, frictional stress between the gain element and the beam, and distribution of pressure in contact zone (Fig. 23-25).

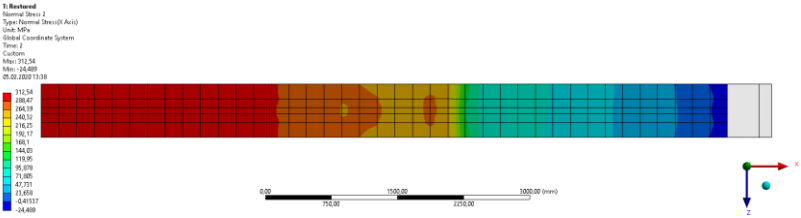

Fig. 23. Normal Stress in the carbon gain element

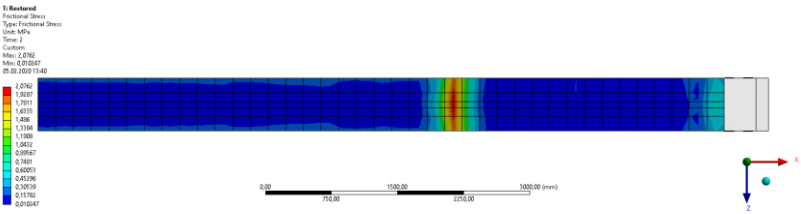

Fig. 24 .Frictional Stress in the carbon gain element

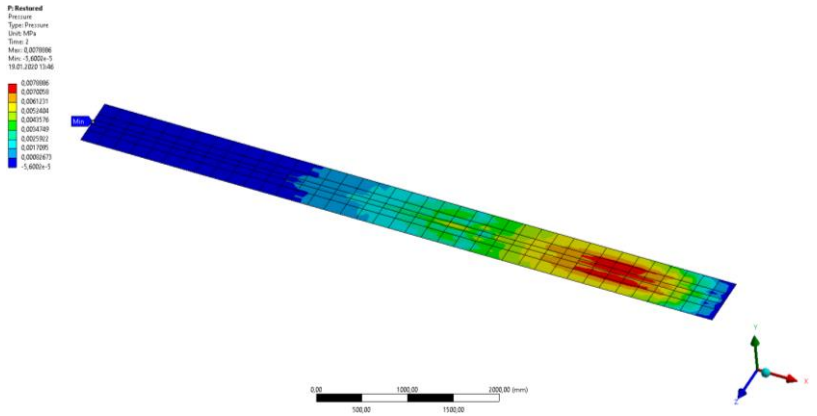

Fig. 25. Pressure in contact between concrete and carbon gain element

Analysis of the obtained data shows that the maximum stresses in carbon fiber do not exceed 20% of its bearing capacity. The maximum frictional stress between the beam and the carbon element is 3.25 MPa, and maximum pressure in glue is 0.008 MPa, which does not require bonding with high-quality epoxy adhesives.

Conclusions.

The use of the ANSYS software package in calculations of reinforcement of reinforced concrete structures allows a comprehensive analysis of the stress state of a damaged structure, to identify the most dangerous zones in the structure and to develop optimal schemes for its amplification.

Bibliography

1. **Onufriev N.M.** Usileniye gjelezobetonnyh construkciy promyshlennyh zdaniy i soorugjeniy. (Усиление железобетонных конструкций промышленных зданий и сооружений). M.: StroyIzdat, 1965. - 176 p.

2. **Shilin A.A., Pshenichny V.A., Kartuzov D.V.** Vneshneye armirovaniye gjelezobetonnih construkciy compozitnymi materialami (Внешнее армирование железобетонных конструкций композитными материалами). M.: OAO «Izdatelstvo «StroyIzdat», 2004. - 144 p.

3. **Malganov A.I., Plevkov V.S., Polishchuk A.I.** Vosstanovleniye i usileniye stroitelnyh construkciy avariynyh i reconstruiruemyh zdaniy. Atlas shem i chertegjey (Восстановление и усиление строительных конструкций аварийных и реконструируемых зданий. Атлас схем и чертежей). Tomsk : CNTI, 1990. 320 p.

4. Gunther Ruffert. Defecty betonnyh construkciy (Дефекты бетонных конструкций). M.: StroyIzdat, 1987. - 111 p.

ECONOMIC AND ENVIRONMENTAL IMPACTS OF ARTISANAL GOLD MINING ON NEAR-BY COMMUNITY OF SAUKA-KAHUTA, NIGERIA

Melodi M.M.
PhD (engineering), Associate Professor,
Mining Engineering Department,
The Federal University of Technology, Akure, Ondo State, Nigeria

Ojulari M.K.
HND, PGD (Mining Engineering),
Mining Engineering Department,
The Federal University of Technology, Akure, Ondo State, Nigeria

Oluwafemi V.I.
MSC Holder, Mining Engineering Department,
The Federal University of Technology, Akure, Ondo State, Nigeria

Abstract

Mining operations produce unequal socio-economic consequences and reward on its near-by communities. This study focused on economic and environmental impacts of artisanal gold mining on near-by community of Sauka-kahuta, Nigeria. Its objectives include examining the socio-demographic characteristics of artisanal gold miners; describing mining characteristics; and identifying the environmental and economic impacts of artisanal gold mining on nearby communities. Thirty one structured questionnaires were retrieved from forty questionnaires administered. The study revealed that a proportion of 71.0% of the artisanal respondents were between 21 to 40 years; male were 80.6%. Islam as religion (93.5%), primary education as highest education qualification (48.4%), Hausa by tribe (96.8%) and non-residence in nearby community (83.9%) were the dominant characteristics of artisanal miners in the study area. Increase in wealth status, creation of employment (100.0%) and improvement in household income (100.0%) were the confirmed socio-economic benefit of gold mining on the nearby community. Environmental effect of mining was observed to be substantially and severely negative; these include deforestation (67.7%), flooding (100.0%), poor assess road condition (71.0%), poor soil management practice (84.9%) and land degradation (100.0%). In conclusion, artisanal and small scale gold mining provide positive economic impacts through the provision of immediate means of livelihood for the residents of the community but the unskilled system adopted by the artisanal miners brought about environmental problems in the area studied. It is therefore recommended that community awareness and education be prioritized by governmental mining agencies and other relevant bodies to reduce exposure of residents to environmental dangers.

Key words: Artisans, gold, mining, community

1.0 Introduction

Gold mining is an age long economic activity in solid mineral exploration practices in Nigeria and around the world. Persistent hike in the price of gold caused by the increased competitiveness among its players and other gem stones were considered as the cause of the resurgence of this practice especially in the northern Nigeria. A number of negative environmental consequences and impact are associated with mineral exploration in Nigeria especially on the nearby communities of exploring sites. Literatures abound with reports of various devastating negative environmental impacts of gold mining in Nigeria; For example, devastating lead poisoning of children in Zamfara (Ajumobi *et al.* 2014; Haidara *et al.* 2017; Mejia 2015) and Niger States and environmental pollution due to significant emissions of mercury (used in processing) into the soil and air (Ajumobi *et al.* 2014).

Mining activities in Nigeria is characteristically artisanal and small scale accounting for well over 90% of mining activities most especially mineral types like gold, barite, lead, zinc etc. Their practices are always unguided and not regulated due to lack of proper policies in place to control their operations (Mallo, 2012). The uncontrolled actions of these informal miners have resulted in serious environmental degradations (Prasetyo et al, 2010; Girigisu *et al.* 2012), crude operational systems (Colins and Lawson, 2014, Hoadley and Limpitlaw, 2004) and loss of economy minerals (Mallo, 2012).

In regards to this, Ako *et al*, (2014) observed that most artisanal and small scale miners handling different mineral types, work in difficult and often hazardous conditions in the without the required safe mining regulations to safeguard their mining activities. Throughout history, it is believed that the exploration of heavy metals and other elements associating with the mining of gold expose the miners to toxicity present in these metals (Girigisu *et al*., 2012). Unlike some countries in West Africa, Nigeria does not have a well-developed, large scale mining companies with sustainable and structured operation policy, therefore the majority of gold mining in the country is carried out without due regulation by artisanal and small-scale miners.

Gold veins occurrence makes Minna and its environs in Niger State, Nigeria vulnerable to highly environmental hazards such as land degradation, de-vegetation, loss of aquatic plants and animals, water pollution and air pollution, resulting from the activities of artisanal and small-scale miners (Ako *et al*, 2014). Due to the migratory style of operations, the artisanal miners often leave the dug-out area not domesticated, and this pose various dimension of hazards to human beings and animals. Apart from safety and health impacts, mercury used in processing of mined gold-veins and lead associated with gold deposits impacts the environment detrimentally.

Up to 95% of mercury used is released into the environment (Environmental Law Institute, 2014). Unlike mercury, lead dusts does not travel very far, they settle out on the ground and can easily contaminate the soil. During periods of heavy rains, the lead dust can leach into groundwater systems and contaminate them. Most mine sites are located around farmlands where the harmful chemicals may contaminate the leaves and fruits of arable and cash crops through the soil resulting to severe heavy metal contamination of water sources and poisoning of humans and animals, if ingested (Eludoyin *et al*, 2017).

Economically, the activities in the mineral sector are not yielding the desired benefits because there are no records of payments of taxes and royalties to the government. Nigeria is losing lots of monetary value from the untapped mineral deposits and smuggling of the little that are mined out of the country. Many professionals such as geologists; mineral economists; mining engineers; etc. in the mineral industry in Nigeria believed that under the Nigerian soil are enormous wealth and riches of solid minerals but majorities of Nigerians are wallowing in abject poverty (Melodi, 2017).

The Nigerian Extractive Industries and Transparency Initiative [NEITI] (2012) stated that the Ministry of Mines and Steel Development (MMSD) has identified about 34 different kinds of solid minerals and precious metals buried in Nigerian soil waiting to be exploited that have potentials to contributing significantly to Nigeria's economic development. The commercial value of Nigeria's solid minerals has been estimated to be in hundreds of trillions of dollars, with at least 70 per cent of these buried in the bowels of Northern Nigeria (Eludoyin *et al*, 2017). The cost of health implications

outweighs benefits gained in mining operations especially when it comes to the issue of artisanal miners' activities (Melodi, 2017).

The Artisanal and Small-scale Mining (ASM) sector is growing rapidly around the Globe because the sector has potential to provide quick way to riches and means of ensuring daily sustenance (Hoadley and Limpitlaw, 2004). This sector also has a potential of creating profitable and productive employment, able to give economic sustenance to employees. In Nigeria, ASM is flourishing due to lack of rule of law and unscrupulous traders acquiring the minerals mined from artisanal miners cheaply and not ready to pay taxes or royalties due to government (Melodi, 2017).

Whether operating on a large or small scale, gold mining has potential of improving the standard of living of people in the community, which of course not without a price – series of health and environmental risks associated with their activities. The impact may even stretch several years beyond the life span of the mining operation. Gold mining operations has the potential to significantly improving the socio-economic living of the poor masses engaging directly or indirectly in artisanal mining in those communities by boosting their income level (Darma, 2016).

Hence, this study seeks to investigate the economic and environmental impact of artisanal gold mining on Near-by community in Nigeria. The specific objective of this study are to examine the socio-demographic characteristics of artisanal gold miners, mining characteristics, identify the environmental and economic impacts of artisanal gold mining on nearby communities.

2.0 Methodology

The study was carried out in Sauka-Kahuta residential layout, Niger State Nigeria. It lies within latitude $09^{0}35'22"$ North to $09^{0}30'36"$ North of the Equator and longitude $06^{0}28'11"$ East to $06^{0}32'13"$ East of the Greenwich Meridian (Amadi *et al*, 2015). The topography of the area is undulating drained by River Chanchaga and its tributaries. The gold mining pit is located on $09^{0}33'27.5"$ North and $06^{0}32'34.8"$ East and elevation of 228 meters. It covers about $6335.4m^2$ (1.5655 acres) in landmass having an orientation along north-south direction with a depth of about 8.4 meters.

Primary data used for this study were collected by simple random selection through the use of well-structured pre-tested questionnaires

and personal interviews, which addressed important data on artisanal miners' profiles, economic and environmental impacts (artisanal miners and residents' perspectives) of artisanal mining activities, perceived socio-economic impacts of artisanal gold mining in the study areas.

Five soil and nine water samples were taken at different locations around the mine site to adequately and effectively capture the impacts of the mining activities on both the domestic water available to the community and soil use for farmland around the mine area.

One sample was collected at upstream and used as "control" sample for the other four samples (one sample each on the overburden heaps on both sides of the pit and two samples at downstream with different distances from the waste dump).

Pitting sampling method were used to collect the soil samples. The mini-pit was dug to about 15cm to have access to fresh topsoil component before samples was collected. The collected samples was careful packed in polythene bags and labelled. The samples was sent to laboratory (National Geo-Science and Laboratory Research Center, Barnawa, Nigeria) for the testing of concentration of the selected six (6) heavy metals, namely: lead (Pb), cadmium (Cd), chromium (Cr), copper (Cu), zinc (Zn) and iron (Fe) with use of AAS (Atomic Absorption Spectrometry) machine. The AAS is an analytical technique that measures the concentrations of elements. Atomic absorption is so sensitive that can measure down to parts per billion of a gram ($\mu g\ dm^{-3}$) in a sample. The technique uses the wavelengths of light that is specifically absorbed by an element. It is particularly useful for measuring the presence and amounts of toxic metal cations in environmental samples, as well as interrogating the metal content of ores in the mining industry to evaluate the economical worth of pursuing their extraction.

Nine (9) water samples was collected for this study from three different water sources available within the study area; namely; well water, borehole water; and stream water. Three samples each from each water sources was collected using a 50cl plastic bottles and send to laboratory (Spectral Laboratory Services, Kaduna) for twelve (12) physico-chemical parameters analysis. The analysis of the water samples was also focus on the presence some of heavy metals present in the samples.

The well and borehole water samples was collected randomly from the residences, farms, and schools that are situated around the mine area. The stream water samples was collected from the only stream water available in the area. The first stream sample was collected at the upstream, second sample at some distance away from the first, and last sample at downstream.

Descriptive statistics was used to indicate artisanal miners' profiles, economic and environmental impacts of artisanal mining activities, perceived socio-economic impacts of artisanal mining of gold in the study areas. The analysis will involve the use of Analysis of Variance (ANOVA); mean, maximum, and minimum table; T-test; and frequency tables. Charts and flow diagrams was used to showing the different levels of heavy metals present in both the soil and water samples.

3.0 Results

3.1 Artisanal Miners' Profiles

Table 1

Socio-Economic Profile of Respondents (contd.)

	Mean	Minimum	Maximum
Residence (Years)	3.00	1	5
Experience (Years)	12.23	2	31
Family Size (Persons)	4.23	1	12

According to Table 1, resident respondents had a mean of 3 years of residence, working experience of 12.23 years keeping a family size of an average of 4.23 persons.

Most (71.0%) of the respondents interviewed for this study were between 21 and 40 years while very few (6.5%) were between 46 and 50 years. Male respondents (80.6%) were observed to be more than the female counterpart. This might be connected to the cultural believes and high energy demand involved in artisanal mining, making it not too fit for female participation.

The result further indicates that many of the miners are married (64.5%) while few (29.0%) of them are still single. A proportion of 58.0% of the artisanal miners respondents take the mining activities as full-time job, working as self-employed, while 25.8% are engaged in other non-mining economic activities which includes farming, cart-truck pushing, bike riding etc. Respondents, who were mainly

migrants (83.9%) attained primary school education as the highest level of education (48.0%) while 16.0% had secondary school education.

3.2 Economic Impacts of Artisanal Gold Mining Activities on Residents

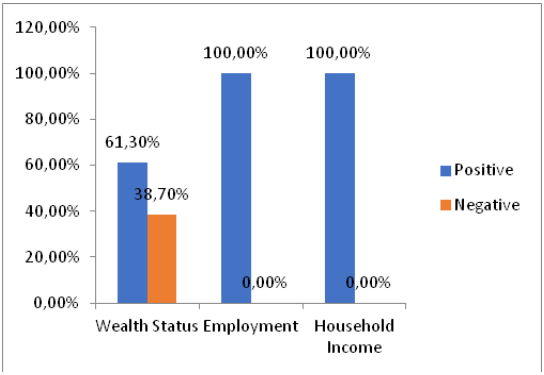

Fig.1. Nature of Economic Impact of Artisanal Gold Mining Activities

Figure 1 identified the general nature of economic impacts of artisanal gold mining activities at Sauka-Kahuta, Minna, Nigeria. Many (61.3%) of the respondents agreed to increase in their wealth status indicating a positive impact (above average). Most (100.0%) respondents agreed that the artisanal mining at the study area has help people of the community to be engaged in one job or another, which has equally improved the level (100.0%) of household income.

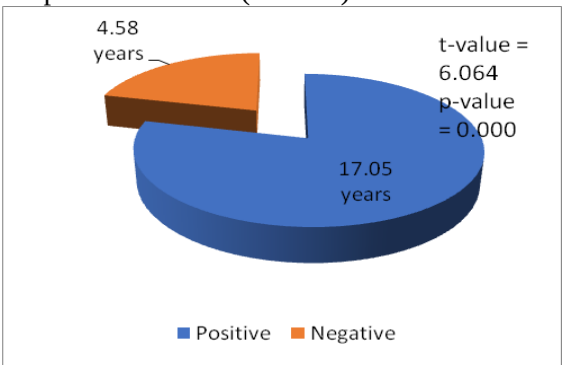

Fig. 2. Effect of Mining on Wealth Status across Means Years of Experience

This study identified that artisanal miners with much years (17.05) of experience agreed that they have had more cases of positive economic impacts of mining on their wealth status, while miners with fewer (4.58) years have a contrary experience. This variation is not farfetched from the fact that the respondents with many years of experience in artisanal mining have accomplished some prosperities in life that can be attributed to their engagement in this informal mining activities than those joining the trade newly. Therefore, it can be inferred that the activities of artisanal gold mining are perceived to be beneficial and positive by respondents having many (17.05years) years of experience. It was observed that the economic effect of artisanal gold mining in the study area was significant at 1% level. Individual artisanal miner with larger family size (5.26 persons) had positive impacts from the market formation created by the activities of the artisanal miners and have chances of raising a larger family than respondents with fewer (2.83) family size (Figure 2). This is because larger family size has high number of persons to participate in trading of essential commodities with artisanal miners and contribute more to the households' income than family with fewer persons. This difference is observed to be significant at 5% level.

3.3 Environmental Impacts of Artisanal Gold Mining Activities

3.3.1 Mining Methods and Characteristics

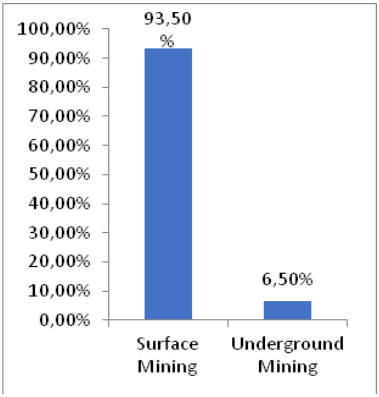

Fig. 3. Mining Methods Used

According to Figure 3, surface mining was the dominant mining method adopted by the artisanal miners in the study area. The number of pits dug to locate the veins was largely (89.7%) more than three. Most (67.7%) of the artisans do not care about the safely of dug out materials, although, some (10.3%) still believed the materials were not deposited safely.

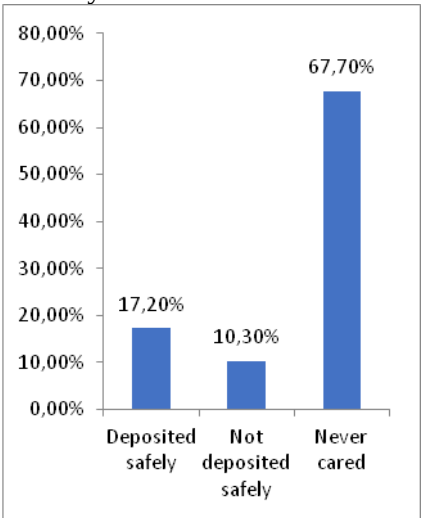

Fig. 4. Number of Pits Dug to get to Vein

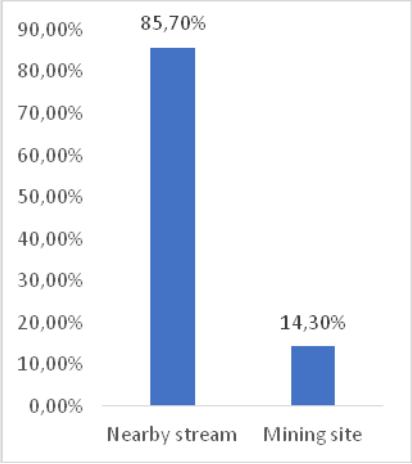

Fig. 5. Place of processing mined Gold

Processing of mined gold materials was carried out majorly (85.7%) at nearby stream (Figure 5); while few other miners have mined materials processed at mining site (14.3%). The type of processing method adopted by most (90.3%) of the miners was amalgamation method (Fig VIII) which involves dissolves of gold particles in mercury. The process includes the following: crushing and milling of gold-vein materials; sluicing and washing of sluice cloth; panning and adding of mercury; squeezing of amalgam; and burning of amalgam to remove the mercury from the bounded gold particles.

3.3.2 Perception of Residents

Table 2

Perception of Residents on Environmental Impact of Gold Mining

	Severity		
	Not Severe Freq. (%)	Severe Freq. (%)	Very Severe Freq. (%)
Water Pollution	**30 (96.8)**	1 (3.2)	0 (0.0)
Deforestation*	10 (32.3)	9 (29.0)	**12 (38.7)**
Flooding*	8 (25.8)	**23 (74.2)**	0 (0.0)
Poor Assess Road Condition*	9 (29.0)	**22 (71.0)**	0 (0.0)
Soil Management*	5 (16.1)	12 (38.7)	**14 (45.2)**
Noise	20 (64.5)	11 (35.5)	0 (0.0)
Air Pollution	18 (58.1)	13 (41.9)	0 (0.0)
Land Degradation*	0 (0.0)	0 (0.0)	**31 (100.0)**

* Environmental impact is severe

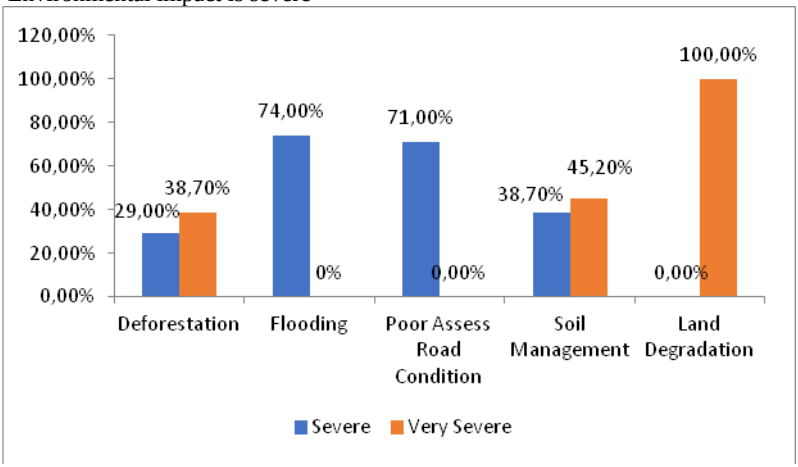

Fig. 6. Leading Perceived Environmental Impacts

Table 2 and Figure 6 revealed that there was severity (38.7%) of deforestation due to the activities of artisanal mining and building up of residential houses around the mining site. Some of these houses are already sited before the advent of artisanal mining activities in the study area. It was observed that the area was prone to flooding (74.2%), which has resulted in poor (71.0%) access road in the study area. The natural state of soil around the study area was observed to be affected (45.2%), which caused high (100.0%) land degradation.

The physico-chemical properties analysis of the water sources is depicted in Fig X to XXI. The results revealed that the mean concentrations of Cd, Mn, and Pb are higher compared to the World Health Organization's (WHO) standards (2017) for domestic water sources.

Ca, K, Mg, and Na values range from 0.01mg/l - 2.10mg/l, 2.10mg/l - 18.80mg/l, 5.0mg/l - 14.0mg/l and 123mg/l - 210mg/l with concentrations of 1.06mg/l, 7.63mg/l, 7.90mg/l, and 153.30mg/l respectively. The results also revealed that the mean values of Ca, K, Mg, and Na are lower compared the WHO's standards (2017) for domestic water sources. It revealed that both the borehole waters (BH) (2 PCU) and well waters (WW) (4.17 PCU) are lower compared to WHO's Standards (5 PCU), while the stream waters (SW) (6 PCU) is high.

The mean Total Dissolved Solids (TDS) values for all the water samples are lower compared to the requirements of the WHO (2017) for domestic waters. The average value for Turbidity of the water sources are higher compared to WHO's Standards (1.5 NTU), the WW (44.00 NTU); SW (17.67 NTU); and BH (2.77 NTU).

3.4 Socio-Economic Impacts

According to the perception of the residents of nearby community on the impact of artisanal gold mining in the area. Artisanal mining activities in the study area was noted to increase migration into the community (90.3%) for various reasons, which was observed to be a negative impact (90.3%). There was positive impact of market formation (83.9%) from sales of foods and other materials to the artisanal miners, which increased the households' income (100.0%). The study indicated that there were increased in the household wealth status and employment opportunities (100.0%), even though there was negative impact (100.0%) of social vices in the study area. The

cost of living was seen to be significantly high (87.1%) with positive impact in the standard of living (90.3%) of residents of nearby community. The cost of basic household's items is high (41.9%), which was observed to have negative impact (74.2%) on respondents. There was negative impact (74.2%) on water and land use from the activities of artisanal miners, which was observed to affect the environment negatively (71.2%)

4.0 Conclusion

It is no doubt that ASM provide positive economic impacts in the study area through the provision of immediate means of livelihood for the residents of the community but the unskilled system adopted by the artisanal miners has brought about environmental problems in the study area such as land deformation, destruction of farmlands, loss of soil enrichments, etc.

The chemical analysis of both the water sources and soil samples from Sauka Kahuta gold mining area showed that there is significant level of Cr, Cd, Pb, and Mn; and reasonable level of Zn, Cu, Ni, Ca, and Mg in the various water samples collected. These elements have contaminated the study area through the activities of the artisanal miners, if they are absorbed by the plants that are consumed by the residents and consumption of drinking water with these toxic materials there is possibility of health problems through the accumulation of these elements in the body tissues. This may result to kidney and liver damages and also carcinogenic diseases.

4.1 Recommendations

The environmental management regulations should be review to ensure that environmental problems caused by the activities of artisanal and small-scale miners are brought to barest minimum while putting into considerations the following recommendations:

1. Community awareness and education should be prioritized by governmental mining agencies to reduce exposure of residents to environmental dangers;
2. Training of artisanal miners by relevant agencies of government is important to adopt environmentally sustainable safer mining and trading practices;
3. Strengthening of "no child labour" campaign in the ASM sites;

4. Formalization of ASGM sector into a formidable economic entity is needed to adequately maximize the inherent economic benefit of gold mining.

References

1. **Ajumobi O.O., Ahmed T., Yango M., Aworh M.K., Anagbogu I.N., Mohammed A., Umar-Tsafe N., Mohammed S., Abdullahi M., Davis L., Idris S., Poggensee G., Nguku P., Gitta S., Nsubuga P.** (2014). High concentration of blood lead levels among young children in Bagega community, Zamfara- Nigeria and the potential risk factor. Pan African Medical Journal Vol. 18 (supp 1):14. pp. 1-4.

2. **Ako T.A, Onoduku U.S., Oke S.A., Adamu I.A., Ali S.E., Mamodu A., Ibrahim A.T.** (2014). Environmental Impact of Artisanal Gold Mining in Luku, Minna, Niger State, North Central Nigeria. Journal of Geosciences and Geomatics. Vol.2 (1) pp. 28-37.

3. **Amadi A. N., Akande W. G., Okunlola I. A., Jimoh M. O., Francis Deborah G.** (2015). Assessment of the Geotechnical Properties of Lateritic Soils in Minna, North Central Nigeria for Road Design and Construction. American Journal of Mining and Metallurgy Vol. 3(1), pp. 15-20

4. **Collins N. and L. Lawason.** (2014). Investigating approaches to Working with Artisanal and Small-scale Miners: A Compendium of Strategies and Reports from the Field. International Mining for Development Centre Action Research Report. Retrieved January 21, 2018, from www.im4dc.org pp. 7-8

5. **Darma M.R., Kankara I.A., Abdullahi S.** (2016). Effect of Artisanal Gold Mining at Maiwayo Environ Northern Nigeria: Implication for Environmental Risk. International Journal of Advance Studies in Ecology, Development and Sustainbility. Vol. 4(1), pp. 100-112.

6. **Eludoyin A.O., Ojo A.T., Ojo T.O., Awotoye O.O.** (2017). Effects of Artisanal Gold Mining Activities on Soil Properties in a Part of Southwestern Nigeria. Cogent Environmental Science. Vol. 3 (1305650). Pp. 1-11.

7. **Girigisu S., Ibeanu I.G.E., Adeyemo D.J., Okoh S.** (2012). Determination of Heavy Metals and Other Elements in Artisanal Gold Mining Soils. American Journal of Applied Sciences Vol.9 (7) pp. 1014-1019.

8. **Haidara A. M., Mudansiru A., Muhammad A.S., Yakubu M.S.** (2017). Lead Poisoning: An overview of Bagega Gold Mining Village in Zamfara State, Nigeria. MAYFEB Journal of Environmental Science Vol. 1, pp 11-17.

9. **Hoadley M., Limpitlaw D.** (2004). The Artisanal and Small Scale Mining Sector & Sustainable Livelihoods. A paper presented at the Mintek Small Scale Mining Conference September 9, 2004, NASREC, Johannesburg, Book of Proceedings pp. 1-9

10**. Mallo S.J.** (2012). Mitigating the Activities of Artisanal and Small Scale Miners in Africa: Challenges for Engineering and Technological Institutions. International Journal of Modern Engineering Research, Vol.2 (6), pp. 4714-4725.

11. **Melodi M.M.** (2017). Assessment of Environmental Impact of Quarry Operation in Ogun State, Nigeria. Journal of Engineering and Technology (FUOYEJET). Vol.2 (2), pp. 100-103.

12. **Praseyto B., Krisnayanti B.D., Utomo W.H., Anderson C.W.N.** (2010). Rehabilitation of Artisanal Mining Gold Land in West Lombok, Indonesia: 2. Arbuscular Mycorrhiza Status of Tailings and Surrounding Soils. Journal of Agricultural Science Vol.2 (2), pp. 202-203.

13. The Nigerian Extractive Industries and Transparency Initiative (2012). An Independent Report of Physical and Process Audit of Nigeria's Solid Minerals Industry 2007 – 2010 prepared by Haruna Yahaya & Co.

ENERGY SAVING MODES OF EXCAVATORS TYPE POWER SHOVEL

Kruchkov A.I.

National Technical University of Ukraine "Igor Sikorsky Kyiv Polytechnic Institute", Institute for Energy Saving and Energy, Department of geoengineering, Ph.D (Engineering) associate professor, associate professor, Ukraine

Besarabets Y.J.

National Technical University of Ukraine "Igor Sikorsky Kyiv Polytechnic Institute", Mechanical Engineering Institute, Department of Machine Design, Ph.D (Engineering) associate professor, associate professor, Ukraine

Yevtieieva L.I.

National Technical University of Ukraine "Igor Sikorsky Kyiv Polytechnic Institute", Institute for Energy Saving and Energy, Department of geoengineering, Ph.D (Engineering) senior teacher, Ukraine

Abstract

Taking into account the high actual energy intensity of excavation of the excavator type mechanical shovel, the idea of its reduction due to the information component is considered in the work - that is, optimization of the operating mode of the excavator according to the criterion of minimum energy intensity is used.

The purpose of the work is analytically and experimentally established dependence of the energy intensity of the excavation works on the performance of

the excavator, which is of extreme nature, which allows to establish its local optimal value, which corresponds to the minimum energy intensity of digging for different categories of rocks.

In system optimization, considering a quarry as a system of two or more working excavators, the mathematical model of their joint work is formulated as an Eulerian problem on conditional extremum, which includes a goal function and constraints using the method of indefinitely multiplying the solution Lagrange.

It has been found that the optimal local digging performance values for each excavation block do not coincide with the optimal values for system optimization for the career as a whole (the principle of emergence).

Thus, the system optimum mode of excavation allows to obtain the lowest energy intensity of the process of excavation in comparison with the local optimum mode, and even more so with the actual daily one.

Key words: Excavator, performance, power consumption, optimization, operating modes, local, system, minimum.

Introduction

For comparative evaluation of the performance of quarries for the extraction of building materials use the indicator of total cumulative cost, or other indicator, which includes the cash costs of production.

But the work of such enterprises over the last two decades has shown that in an unstable economy, the estimation of production efficiency by cost indicators leads to negative consequences. Under these conditions, a much better result is the use of natural indicators [1].

In this regard, the energy used in excavation works is used as an indicator of efficiency [1;2]. On the other hand, the introduction of such an indicator is due to the significant increase in the recent tariff for all types of energy, including electricity.

The most profound and systematic relationship of the energy intensity of the rock excavation process with the parameters of the excavation process was investigated by I.O. Tangayev [2]. The results of his research, carried out during the operation of the excavator on blocks with different mining and technological conditions, physical and technical properties of the rock mass and the parameters of the collapses, made it possible to recommend the energy scale of excavation of rocks for practical use.

Using the given classification of rocks by the energy intensity of the excavation, it is easy to set the table for each rock category as the

average performance of the excavator and the associated average energy of the excavation [2].

Comparing the energy intensity of the excavation process in domestic and foreign quarries is clearly not in our favor (2 to 2.5 times higher), which requires searching for operating modes that can reduce energy costs.

Thus, the purpose of the study is to determine the dependence of the energy intensity of excavation work on the performance of the excavator, which allows you to set its local value, which corresponds to the minimum energy intensity of digging for different categories of rocks.

To achieve this goal, the following scientific problems are formulated and solved:

Considering that the process of excavation is a random dynamic non-stationary dissipative process, for its mathematical modeling it is necessary to apply the principle of duality when moving mass in space [3], which allowed to consider the process of digging as a probable non-stationary motion of a body of variable mass in a solid medium in a solid medium from the mass and filling the volume of the bucket with the products of destruction, in the form of the Hamilton-Jacobi and Fokker-Planck-Kolmogorov (FPC) equations;

the analytical solution of these equations made it possible to determine the dependence of the exploitation energy of the excavation works on the productivity of the excavation, which is of extreme nature;

the study of the established dependence on the extremum has allowed to establish both the optimum values of the excavator productivity for the given conditions, and the minimum values of the energy of digging;

the developed approach allowed to consider the work of excavators of three main modes: actual average mode; local optimal mode; system optimal mode and perform a detailed analysis of these modes for different categories of rocks.

Excavator operating modes while optimizing the quarry process.

The scientifically grounded method of calculating the operational productivity of direct-excavator type excavators has made it possible to consider three basic modes of operation of the excavator:

- average actual mode of operation;
- local optimal;
- system optimal.

The theoretical calculations given in and experimental studies [2] have shown that energy costs for rock excavation are described by the Hamilton-Jacobi equation

$$\frac{\partial D(t)}{\partial t} - \frac{e_K K_B \Pi_K}{E_x} D(t) = 0 \qquad (1)$$

and FPK(Fokker-Planck-Kolmogorov) equation

$$\frac{\partial \omega(t)}{\partial t} = \frac{D}{2m} \nabla^2 \omega(t) + \frac{\nabla D}{m} \nabla \omega(t) + \frac{U}{D} \omega(t) \qquad (2)$$

where $D(t)$ is the mechanical action expended on the excavation of the specified number of meters of cubic mountain mass, $J \cdot s$; E_x is the energy of idle motion of the excavator, J.; e_K , - energy intensity of the digging process, J/m^3; K_B - the utilization coefficient of the excavator per shift; Π_K - excavation digging capacity, m/s; $\omega(t)$ is the non-stationary probability density of the bucket trajectory coordinates in the array; m is the mass of the ladle with the rock; U is the potential energy of the bucket with the breed, J.

The first-order solution of the initial equation can be written in the form

$$D(t) = E_x \cdot t_k \, exp\left[\int_0^{t_k} \frac{e_K K_B \Pi_K}{E_x} dt \right], J \cdot s. \qquad (3)$$

The power consumed by the drive to dig is described by the expression

$$N_E(t) = \frac{D(t)}{t_k^2} = N_x \, exp\left[\int_0^{t_k} \frac{e_K K_B \Pi_K}{N_x t_k} dt \right] = N_x \, exp\left[\frac{e_K K_B \Pi_K}{N_x} \right] (4)$$

By decomposing this expression into a power series and confining ourselves to a quadratic polynomial, we obtain

$$N_E = N_x + e_K K_B \Pi_K + \frac{e_K^2 K_B^2}{2N_x} \Pi_K^2 + \ldots$$

The solution of the FPK equation gives an analytical expression for the probability density $\omega(\Pi_K,t)$. Then the mathematical expectation for the power of digging is found by expression

$$\bar{N}_E = \int_0^{t_k} N_E \omega(\Pi_K,t)\, d\Pi_K = \int_0^{t_k} N_x \omega(\Pi_K,t) d\Pi_K +$$

$$+ \int_0^{t_k} e_K K_B \Pi_K \omega(\Pi_K,t)\, d\Pi_K + \int_0^{t_k} \frac{e_K^2 K_B^2}{2N_x} \Pi_K^2 \omega(\Pi_K,t)\, d\Pi_K .$$

Integrating this equation, we obtain

$$\bar{N}_E = \bar{N}_x + \bar{e}_K \bar{\Pi}_E + \frac{\bar{e}_K^2}{2N_x}\left[\left(1 - \frac{\Pi_0}{\bar{\Pi}_E}\right)^2 + \left(1 + \frac{\sigma_{\Pi E}^2}{\bar{\Pi}_E^2}\right)\right]\bar{\Pi}_E^2 \qquad (5)$$

where $\bar{N}_E$ - the average power of the excavator drives during operational productivity; $\bar{e}_K$ - average energy of the digging process; $\bar{\Pi}_E$ - mathematical expectation of the excavator's operational productivity; $\left(\bar{\Pi}_E = \bar{K}_B \cdot \bar{\Pi}_K\right)$; $\bar{N}_x$ - drive power at mode of idle moution; $\sigma_{\Pi E}^2$ - dispersion of excavator operating productivity; $\Pi_0 = \frac{\sqrt{2}N_x}{\bar{e}_K}$ - the optimum value of operational productivity.

The operational energy intensity of the excavation works is calculated by the expression

$$e_E = \frac{\bar{N}_E}{\bar{\Pi}_E} = \frac{A}{\bar{\Pi}_E} + B\bar{\Pi}_E + C \text{ , J/m}^3, \qquad (6)$$

where $A = N_x$; $B = \frac{e_K^2}{2N_x}\left[\left(1 - \frac{\Pi_K^0}{\bar{\Pi}_E}\right)^2 + \left(1 + \frac{\sigma_{\Pi E}^2}{\bar{\Pi}_E^2}\right)\right]$; $C = \bar{e}_K$.

Thus, depending (6), not only the deviation of the average productivity over cycles for change from the optimal value is taken

into account $(\Delta П_0)^2 = \bar{П}_E^2\left(\frac{\bar{П}_E - П_0}{\bar{П}_E}\right)^2$, but also the variance of productivity, both within the digging cycle and cycles per shift

$$(\Delta П_0)^2 = \bar{П}_E^2\left(\frac{\bar{П}_E^2 + \sigma_{ПЦ}^2 + \sigma_{\bar{П}}^2}{\bar{П}_E^2}\right) = \bar{П}_E^2\left(1 + R_{VЦ}^2 + R_{\bar{V}}^2\right)$$

Expression (6) has an extreme appearance, that is, the minimum value of the energy intensity corresponds to the optimal value of the excavator $P_E = P_0$ meets the minimum value of energy $e_{\min}$ (fig. 1).

The study of the dependence (6) on the extremum $\frac{\partial e_E}{\partial \bar{П}_E} = -\frac{A}{\bar{П}_E^2} + B = 0$ allows to determine the optimum value of the excavator's operational productivity, taking into account the random nature of oscillations of both the digging productivity on the cycle and the oscillations of the average digging productivity on the cycles per shift

$$П_0^{ф} = \sqrt{\frac{A}{B}} = \frac{N_x}{e_K} \cdot \frac{\sqrt{2}}{\sqrt{\left[\left(\frac{\bar{П}_E - П_0}{\bar{П}_E}\right)^2 + \left(1 + \frac{\sigma_{ПЕ}^2}{\bar{П}_E^2}\right)\right]}}, \qquad (7)$$

where $П_0 = N_x\sqrt{2}/\bar{e}_K -$ is the absolute optimum of productivity at $\sigma_{ПЕ} \to 0$, and $\bar{П}_E \to П_0$.

The minimum value of energy is the optimum value of the excavator's operating productivity

$$e_E^{min} = 2\sqrt{A \cdot B} + C = 2\sqrt{\frac{e_K^2 N_x}{N_x \cdot 2}\left[\left(\frac{\bar{П}_E - П_0}{\bar{П}_E}\right)^2 + \left(1 + \frac{\sigma_{ПЕ}^2}{\bar{П}_E^2}\right)\right]} + \bar{e}_K = \qquad (8)$$

$$= \bar{e}_K\left\{\sqrt{2\left[\left(\frac{\bar{П}_E - П_0}{\bar{П}_E}\right)^2 + \left(1 + \frac{\sigma_{ПЕ}^2}{\bar{П}_E^2}\right)\right]} + 1\right\}.$$

When digging automated process control possible mode in which $\bar{П}_E = П_0^{ф} \to П_0$, $\sigma_{ПЕ} \to 0$, $e_E^{min} \to e_0^{min}$ (fig. 1).

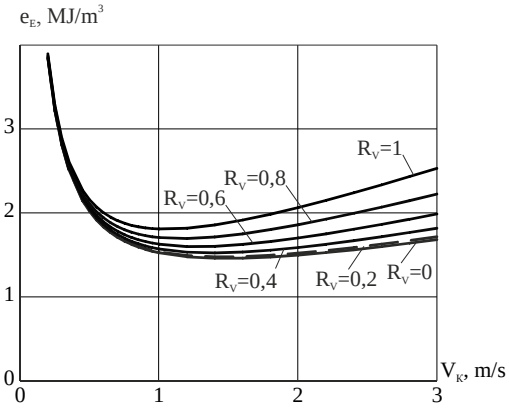

Fig. 1. Effect of random oscillations (R_V variations) of the digging velocity of the V_K of the excavator on the operational energy intensity of the e_E of the excavation process

When manually controlling the excavation process for optimum operation, the driver must: maintain at each cycle as close $\bar{V}_{KII}$ as possible to V_K^0; reduce digging fluctuations in each cycle to $\sigma_{IIE} \to \sigma_{IIE}^{min}$.

It follows from expressions (7) and (8) that both the optimum excavation $П_0^{ф}$, productivity and the minimum amount of operational energy e_E^{min} depend on the magnitude of the random fluctuations in the digging rate, which is estimated by the coefficient of variation R_V. The decrease in the coefficient of variation leads to a decrease in the energy intensity of the digging process and to an increase in the value of optimal productivity $П_0^{ф}$ (fig. 1).

Dependences of type (6) are calculated and constructed (fig. 2) for each rock category, taking into account the dynamic coefficient of digging resistance $K_F^{д}$.

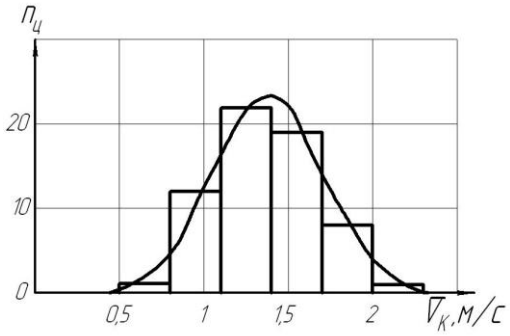

Fig. 2. Histogram of excavation speed distribution of excavator per cycle per shift ($n_ц$ = 60)

Considering these dependencies as an extreme task, the optimal productivity and corresponding minimum energy intensity e_E^{min} for each category (at $R_{VK} \rightarrow 0$) of the breeds are calculated.

Local optimal mode excavator

The analysis showed that to maintain the energy intensity of the excavation at a level close to the minimum for the rocks of the first and second categories, even a low qualification of the driver (fig. 1). The same can be said about working on rocks of the sixth category, when productivity close to optimal actually supports the drive itself.

A more difficult task arises when working on rocks (3 - 5) categories. Direct excavator type excavators are not equipped with a digging speed indicator, so only a highly skilled driver is able to maintain optimal digging. But in this mode he controls not the very speed of digging, which is close to the optimum V_0^{ϕ}, but the digging time t_0^{ϕ}, which corresponds to the optimal speed of digging, at approximately constant height of the ledge *H, s*

$$t_0^{\phi} = H_y / V_0^{\phi} \qquad (9)$$

Thus, a high-skill operator to operate the excavator in near-optimal mode must withstand as little as possible the deviation of the actual digging time from the optimum, s

$$\Delta t = \left(t_{\phi} - t_0^{\phi} \right) \to min \qquad (10)$$

which is equivalent to the condition $\Delta \Pi = \left(\bar{\Pi}_{\phi} - \bar{\Pi}_E^0 \right) \to min$.

The second condition is to reduce the variation of the digging speed to a minimum level, which depends on the dynamics of the excavator and the oscillation of the soil resistance to digging

$$\Delta \sigma_{VK} = \left(\sigma_{VK}^{\phi} - \sigma_{VK}^{min} \right) \to 0 . \qquad (11)$$

These two conditions are the prerequisites that ensure the digging mode is near the optimum. Unfortunately, the absolute optimum mode (at $\sigma_{VK} \to 0$) is almost impossible due to technical and geotechnological reasons.

To confirm these conditions, studies were conducted on the work of excavators with different qualifications (Table 1).

Table 1

Experimental data for the study of the parameters of the excavation cycle

№	Digging time t_K, s	Bucket turning time and unloading time $t_П$, s	The time of dipping the bucket into the slaughter t_0, s	Cycle duration,t_C, s	Cycle utilization rate of the excavator, $K_{ВЦ}$	Speed digging, V_K, m/s
1	7,0	6,5	4,5	28,0	0,25	1,42
2	7,0	10,0	12,0	29,0	0,24	1,42
3	8,6	9,0	13,0	30,5	0,28	1,16
4	9,0	9,0	14,0	32,0	0,28	1,11
5	6,5	7,5	10,5	24,5	0,26	1,66
…	…	…	…	…	…	…
53	6,0	10,0	13,0	29,0	0,20	1,66
54	7,0	8,0	12,0	27,0	0,25	1,42
55	6,0	9,0	14,0	29,0	0,20	1,66
56	5,0	10,0	14,0	29,0	0,17	2,00
57	5,0	9,0	14,0	28,0	0,17	2,00
58	6,0	13,0	12,0	29,0	0,20	1,66
59	5,0	12,0	12,0	29,0	0,17	2,00
60	7,0	9,0	12,0	27,0	0,25	1,42

The actual distribution of the digging velocity in the cycle $V_{КЦ}$ is analytically described by Gauss law. Then the distribution of the average speed of digging in cycles $\bar{V}_{КЦ}$ (fig. 2) with the mathematical expectation of the speed of digging per shift is $\bar{V}_{КЗ}$ calculated by the expression,m/s

$$\bar{V}_{K3} = \frac{1}{n}\sum_{1}^{n}\bar{V}_{KЦi} \qquad (12)$$

and variance

$$\sigma_{\bar{V}3} = \frac{1}{n-1}\sum_{1}^{n}\left(\bar{V}_{KЦi} - \bar{V}_{K3}\right)^2 . \qquad (13)$$

In our case, the values $\bar{V}_{KЦi}$ are given in table. 1 and in fig. 2 at n=60 cycles per shift. The value of $\bar{V}_{K3} = 1{,}40$ m/s, and the variance and the coefficient of variation $\sigma_{\bar{V}3} = 0{,}30$ m/s, $R_{\bar{V}3} = 0{,}21$ m/s, respectively. The optimal value for the rock of the third category $V_K^{\phi} = 1{,}45$ - m/s, ie the average speed of digging is close to the optimum. Fluctuations in digging speed both on cycle and on cycles per shift lead to an increase in energy intensity from 1.4 MJ/m^3 to 1.7 MJ/m^3. But this value is less than the operation of the excavator in the actual suboptimal mode e^{ϕ}=1.85 MJ/m^3 (according to Tangayev I.O).

Therefore, the operation of the excavator in the mode close to the optimum, is possible on rocks of all categories, if the driver of the excavator is sufficiently qualified.

The absolute optimum, that is $П_0^{\phi} \to П_0 = \frac{\sqrt{2}N_x}{\bar{e}_K}$ at $R_{ПЕ} \to 0$, can only be achieved with the use of automated digging mode control.

Comparison of the actual value of operational energy consumption (e_E^{ϕ}) with the minimum at local optimization (e_E^{min}) established: the energy intensity is affected not only by the average digging speed ($\bar{V}_K$), but also by its deviation from the optimal value (V_0^{ϕ}); the variation of the digging velocity (V_K) is influenced by both the change in the rock resistance of the digging cycle on the ledge height ($R_{VЦ}$) and the driver's qualification ($R_{\bar{V}}$).

The saving of electric energy in the process of digging due to the optimization of process parameters for six categories of rocks with the average qualification of the driver is shown in fig. 3 and fig. 4. Maximum savings on the fifth category. The smallest - on the rocks of the first category.

Reducing the magnitude of the digging velocities of the first and second types leads to a decrease in the energy intensity of the excavation process (fig. 1). On average, the energy intensity of the excavation process in the transition from the average actual excavation mode to the local optimum decreases from 10% to 25%.

Conducted experiments on the optimal control of the excavation process showed that in the mode closest to the optimum, a driver of even intermediate qualification on soils from the first to the sixth categories can work. The results of the experiment on soils of the third category for 60 cycles per change are shown in fig. 1 and in table. 2.

Table 2

The results of the experiment

category	K_F^{∂} MPa	$n_ц$	$\bar{\bar{V}}_K$ м/s	$\sigma_{\bar{V}}$ м/s	$R_{\bar{V}3}$	R_{VII}	V_0 м/s	e_K MJ/m^3	e_E^{ϕ} MJ/m^3	e_E^{min} MJ/m^3	Δe MJ/m^3
3	0,27	60	1,40	0,3	0,2	0,2	1,50	0,60	1,70	1,45	0,25

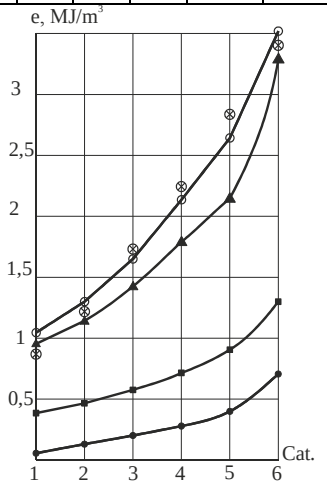

Fig. 3. Comparison of actual and calculated energy indices of the excavation process for different categories of rocks: ⊗ - actual operational energy of the excavation process (e_E^{ϕ}); ○ - estimated operational energy of the excavation; ▲ - energy consumption at optimum excavation mode; ■ - energy intensity of the digging process (e_K); • - coefficient of dynamic resistance of the breed of digging (K_F^{∂}).

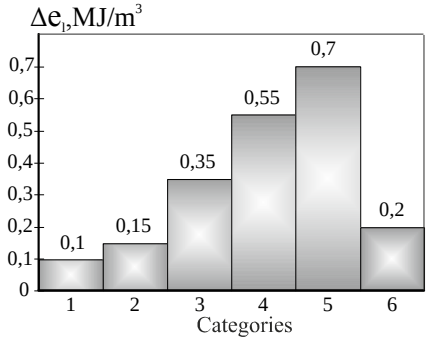

Fig. 4. Reduction of energy intensity of rock excavation at local optimization mode

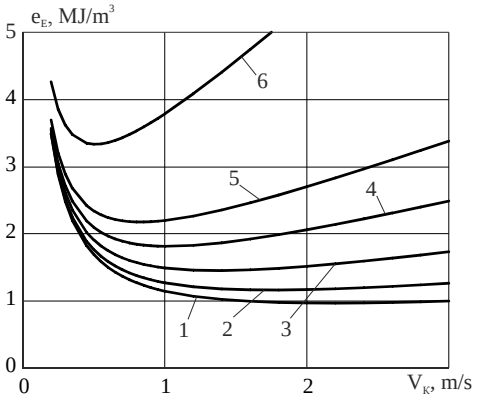

Fig. 5. Operational energy intensity (e_E) of the excavation process, depending on the speed of digging (V_K) for six categories of rocks: △ - actual mode; ○ - local optimal mode; □ - system optimal mode

System optimum operation of excavators

If two or more excavators work on the same quarry and are interconnected by a common transportation system, power supply system, common conditional costs and other connections, then the task is to establish the optimal productivity of each excavator, in which the total energy intensity of excavation works on the group of two excavators will be the smallest. In this case, the total career productivity should be equal to the sum of the two productivity of independently operated excavators [3].

In this approach, we obtain the classical Euler problem of conditional extremum. We find this solution by the method of undetermined Lagrange multipliers [3].

Mathematically, the model of this problem is written as

$$\bar{e} = \frac{e_{E1} \cdot \bar{\Pi}_{E1} + e_{E2} \bar{\Pi}_{E2}}{\bar{\Pi}_{E1} + \bar{\Pi}_{E2}} \to min, \text{ – target function;}$$

$$\bar{\Pi}_{E1} + \bar{\Pi}_{E2} = \sqrt{\frac{A_1}{B_1}} + \sqrt{\frac{A_2}{B_2}} \text{ – limitation.} \tag{14}$$

The energy intensity for each excavator is calculated by the expressions

$$e_{E1} = \frac{A_1}{\bar{\Pi}_{E1}} + B_1 \bar{\Pi}_{E1} + C_1, \text{ J/m}^3; \tag{15}$$

$$e_{E2} = \frac{A_2}{\bar{\Pi}_{E2}} + B_2 \bar{\Pi}_{E2} + C_2, \text{ J/m}^3. \tag{16}$$

Optimal productivity for each excavator when working independently (local optima)

$$\Pi_{E1}^0 = \sqrt{\frac{A_1}{B_1}}; \quad \Pi_{E2}^0 = \sqrt{\frac{A_2}{B_2}}, \text{ m}^3/\text{s}. \tag{17}$$

Minimum values of excavation energy consumption at local optima

$$e_{E1}^{min} = 2\sqrt{A_1 B_1} + C_1, \text{ J/m}^3. \tag{18}$$

$$e_{E2}^{min} = 2\sqrt{A_2 B_2} + C_2, \text{ J/m}^3. \tag{19}$$

To solve this problem, we construct a standard first-order Lagrangian function with the goal and constraint function

$$\bar{L}\left(\bar{\Pi}_{E1}, \bar{\Pi}_{E2}, \lambda\right) = \frac{\left(\frac{A_1}{\bar{\Pi}_{E1}} + B_1 \bar{\Pi}_{E1} + C_1\right)\bar{\Pi}_{E1} + \left(\frac{A_2}{\bar{\Pi}_{E2}} + B_2 \bar{\Pi}_{E2} + C_2\right)\bar{\Pi}_{E2}}{\sqrt{\frac{A_1}{B_1}} + \sqrt{\frac{A_2}{B_2}}} + \tag{20}$$

$$+ \lambda \left[\left(\bar{\Pi}_{E1} + \bar{\Pi}_{E2}\right) - \left(\sqrt{\frac{A_1}{B_1}} + \sqrt{\frac{A_2}{B_2}} \right) \right],$$

where λ is an indefinite Lagrange multiplier.

The study on the extremum of the function of three variables gives the following system of equations

$$\left.\begin{aligned}
&\frac{\partial L}{\partial \bar{П}_{E1}} = \frac{\left(2B_1\bar{П}_{E1} + C_1\right)}{\sqrt{\frac{A_1}{B_1}} + \sqrt{\frac{A_2}{B_2}}} + \lambda = 0;\\
&\frac{\partial L}{\partial \bar{П}_{E2}} = \frac{\left(2B_2\bar{П}_{E2} + C_2\right)}{\sqrt{\frac{A_1}{B_1}} + \sqrt{\frac{A_2}{B_2}}} + \lambda = 0;\\
&\frac{\partial L}{\partial \lambda} = \left(x_1 + x_2\right) - \left(\sqrt{\frac{A_1}{B_1}} + \sqrt{\frac{A_2}{B_2}}\right) = 0.
\end{aligned}\right\} \qquad (21)$$

The solution of these equations gives optimum productivity values for each excavator, but even with system optimization

$$\bar{П}_{E1}^{C} = \frac{2B_2\left(\sqrt{\frac{A_1}{B_1}} + \sqrt{\frac{A_2}{B_2}}\right) - C_1 + C_2}{2\left(B_1 + B_2\right)} \qquad (24)$$

$$\bar{П}_{E2}^{C} = \frac{2B_1\left(\sqrt{\frac{A_1}{B_1}} + \sqrt{\frac{A_2}{B_2}}\right) - C_1 + C_2}{2\left(B_1 + B_2\right)} \qquad (25)$$

From the last two expressions we can conclude that the optimum values of excavator productivity during system optimization do not coincide with the optimum values of local optima (the principle of emergence).

Local and system optimums will only coincide if two identical excavators will operate with drivers of approximately the same qualification under the same conditions, ie $A_1=A_2=A$, $B_1=B_2=B$, $C_1=C_2=C$.

Тоді $П_{01}^{ф} = П_{02}^{ф} = П_{0}^{ф} = \sqrt{\frac{A}{B}}$.

For Demidov quarry conditions, consider the operation of two EKG-5A excavators in the third category and the fifth category. Under these conditions, the average digging energy is $\bar{e}_{K1} = 0{,}60$ MJ/m^3, $\bar{e}_{K2} = 0{,}80$ MJ/m^3, and the actual average operating energy for two excavators is 2.23 MJ/m^3. The local optimum parameters for each of the excavators were calculated using expression (7) for opti-

mal productivity and expression (8) for minimum excavation energy consumption. The results of the calculation are given in table. 3 and fig. 5.

In system optimization, the optimum productivity for each excavator is calculated by expressions (24) and (25), and the substitution of these values into expressions (15) and (16) allows to obtain minimum values of energy capacities that do not really coincide with local optima (the principle of emergence). If, with local optimization, the weighted average energy consumption is 2.04 MJ/m^3, then in system optimization it will be lower by 0.34 MJ/m^3 and is 1.7 MJ/m^3, table. 3

Table 3

Excavator modes

Modes	Π_{E3} m^3/s	Π_{E5} m^3/s	e_{E3} MJ/m^3	e_{E5} MJ/m^3	$\overline{e}_E$ MJ/m^3	Δe_E MJ/m^3	ΔC UAH/m^3
Factual	0,11 (0,59)	0,09 (0,5)	1,72	2,85	2,23	–	–
local optimal	0,24 (1,5)	0,17 (0,92)	1,45	2,17	2,04	0,19	0,093
optimal system	0,27 (1,62)	0,14 (0,80)	1,46	2,2	1,70	0,53	0,300

Comparison of the parameters of the excavators in the three modes (fig. 5) shows the feasibility of reducing electricity costs by optimizing the parameters of the excavation process.

Thus, if you convert MJ to kW. hours, then when operating the excavator in the mode close to the optimum saving for the article "electricity" is from 0.10 to 0.30 UAH. / m3 on each cube of rock mass.

The implementation of the proposed optimal modes of operation of the excavator during the experiments on the Tovkachivsky quarry has resulted in savings of electricity costs in the amount of 70 thousand UAH. during the experiment. Expected savings are about 150 thousand UAH. / year for each excavator.

Conclusions

1. In work instead of cost criteria of production efficiency in the conditions of unstable economy the criterion of minimum energy intensity of excavation works was used.

2. The dependence of the energy intensity of the excavation works on the productivity of the excavator has an extreme nature, which allowed to establish the optimal productivity, which corresponds to the minimum energy intensity for all categories of rocks.

3. The work of the excavator is considered in three modes: actual average mode; local optimal mode; system optimal mode.

4. When operating the excavator in the local optimal mode, depending on the category of rocks, reducing the energy intensity of excavation compared with the average actual is from 0.15 to 0.40 MJ/m3, or from 8 to 20%.

5. Considering a quarry as a system of two or more excavation sites, it was found that the optimal productivity values of each site when working in the system did not coincide with the optimal value at local optimization, which allowed to reduce the average energy consumption by 20-40% compared to the average actual value, based on the fact that the total productivity does not change and ensure a minimum energy intensity of excavation work on the quarry.

6. Studies have shown that the driver of the secondary qualification excavator after proper training can work in a mode close to optimal not only on soils of the first and second categories, but also on soils from the third to sixth categories.

7. The energy saving during the operation of the excavator in the optimal mode is from 0.19 to 0.53 MJ/m^3, or from 0.10 to 0.30 UAH./m^3.

References

1. **Temchenko A.G.** Resource-saving technologies of mining production / A.G. Temchenko - Kryvyi Rih: Mineral, 2000. - 216 p.

2. **Tangayev I.A.** Energy intensity of mining and reprocessing of minerals / I.A. Tangayev - M .: Nedra, 1986. - 231 p.

3. **Kryuchkov A.I.** Optimizing the efficiency of excavators on the quarry by the energy intensity criterion / A.I. Kryuchkov, L.I. Evteyeva // Modern resource-saving technologies of mining. - 2014. - Vip. 1/2014 (13). - P. 97-103.

ENERGY SAVING THROUGH QUALITY OF TECHNICAL WATER: NEW TYPES OF MECHANICAL SCREEN FILTERS FOR VARIOUS LINKS OF WATER TREATMENT

Hryhorash M.V.
Director, Oceanmasenergo Ltd., Ukraine

Kuzminskyi V.P.
Ph.D. (Engineering) Deputy Director of R&D,
Oceanmasenergo Ltd., Ukraine

Ovchinnikova O.V.
Chief Designer, Oceanmasenergo Ltd., Ukraine

Kukhar V.Yu.
Ph.D. (Engineering)
Associate professor at the department of engineering and design in machinery industry of Dnipro University of Technology, Ukraine

Abstract

Energy saving in the industry is directly connected to the quality of water that is used in technical installations. One of the ways of technical water treatment of mechanical impurities is a screen filter. However, despite a diversity of existing automated filters, an analysis shows that not all links in a water treatment chain are equipped with automatic filters that meet corresponding requirements.

The object of research is constructive parameters of screen industrial mechanical filters, including special conditions of their operation.

The goal of the paper is to develop brand-new technical solutions on screen industrial mechanical filters, including special conditions of their operation.

Research methodology: detection of weak spots in characteristics of water treatment devices through an analysis of its separate links, development of main technical requirements to improvement or creation of new filters for these links, development of brand-new technical solutions that meet the developed requirements, development of methods of calculation of main elements of new filters.

Main paper conclusions: specific links of water treatment systems of industrial facilities are established, for which optimal technical solutions on screen filters are absent; technical solutions to new constructions of such filters are developed; theoretical justifications are performed and methods of calculation of constructive parameters of main elements of new filters are developed.

1. Introduction

Energy saving in the industry is directly connected to the quality of water that is used in technical installations. It is known from [1] that clogging of pipes and condenser plates leads to a reduction of coefficient of efficiency by 2-5% and more, which, in turn, leads to increased consumption of electric energy or to reduction of energy generation in power units.

One of the widely used modern ways of technical water treatment of mechanical impurities is automated filters.

Filtration is well-developed and is widely used in the industry as an element of technical water treatment. A multitude of automated filters is developed, which covers all ranges of flow rates, pressures, nominal filtration degrees, and conditions of filter usage.

However, an analysis of literary sources and real water treatment systems of Ukrainian and foreign manufacturers indicates that not all links of water treatment are equally equipped with automatic filters that meet the corresponding requirements.

Thus, creation of a new construction of industrial filters and a theoretical justification of their main constructive parameters is an actual scientific and technical problem.

The goal of the paper is a scientifically justified development of brand-new technical solutions on screen industrial mechanical filters, including their special operation conditions.

Solution methods of the formulated problem:

- detection of weak spots in characteristics of water treatment devices through analysis of their separate links;
- development of main technical requirements to improvement or creation of new filters for these links;
- development of brand-new technical solutions that meet the developed requirements;
- development of methods of calculation of elements of new filters.

2. Selection of filters, which require attention of specialists, analysis and development of technical requirements to filters

Consider some filters of the main links of water treatment, which require further improvement based on our analysis:

- water intake filters, through which the water is taken from reservoirs of different types;

- downstream pipeline filters, which are installed before the water consumers. These filters must provide coarse and fine filtration under given flow rates. They require large screen surface areas and large contaminant capacity, must be insensitive to large debris, so that there is no need for a cascade of filters in front of them;

- brush filters with a hydraulic drive based of filtrated water.

These filter types require further improvement based on our analysis.

2.1. Water intake filters. Water intake from rivers and reservoirs is the most crucial stage of water treatment for industrial installations. It should be noted, that water intake for the largest facilities is usually performed at a very high level of quality from a technical standpoint considering substantial financial investment. And it's hard to ignore the fact that large volumes of water from natural sources are consumed by smaller and medium facilities or separate pumping installations. Multiple water intake installations are put into operation in order to increase water intake for technical needs when the facility already runs.

Water intake automatic filters are the least developed and aren't generally shipped to facilities.

A screen stretched on a carcass and submerged in water is most often used as a water intake filter. Maintenance of such filters is complicated or almost non-existent.

Requirements to water intake filters:

- possibility to be installed directly into a reservoir and a discharge of filtering byproducts directly back to the reservoir;

- maintenance simplicity: filtering-purifying block must be in one piece and easily removable through an open top lid for maintenance at the surface;

- the drive must be a jet without a rotating shaft that reaches the surface and without electric power supply;

- one of the main requirements is that the filter must operate at low temperatures, at freezing reservoirs and have an easily removable filtering-purifying block.

New technical solutions on intake filters and a construction of a water intake filter are considered further (application number a 2020 01035 for an invention patent of Ukraine).

2.2. Multi-chamber automated filters with zig-zag-shaped screen.

A wide application of highly efficient, modern, and costly equipment in technological cycles requires ever-larger amounts of water finely treated of mechanical impurities.

Screen filters with a flat or cylindrical shape of the filtering element are simple and relatively inexpensive but in most cases cannot handle the increased requirements by the factor of contaminant capacity (amount of debris caught by the filtering element during the period between back-flushes).

It is well known that the smaller the nominal filtration degree, the larger the filtering element surface area must be in order to provide a required contaminant capacity and intervals of filter back-flushes [2].

The filtering block screen has a cylindrical shape in the known constructions of screen filters with a back-flush of the filtering element. The filter size increases proportionally to the size and surface area of the screen. However, the screen surface area, filter size, and its cost grow drastically when a fine filtration of large amounts of water is required. In order to provide the required flow rate, an array of filters is installed in one pipeline. Some manufacturers install a few filters in one filter body [3, 4].

The cost, general dimensions of such arrays of filtering installations, the cost of separate filtering installations and their maintenance are very high.

A trend to refusal of screen filter usage is outlined to solve the described problems with further transition to filters with a disc [5], a slotted spiral cone [6] and other filtering elements. Such filters are smaller, but require special complex technologies and equipment to produce these filtering elements. This conditions the high cost of technology development and the filters in general. In addition, the cost is much higher than the cost of screen filters, despite equal filtration quality.

The works on improvement of screen filters are systematic at Oceanmasenergo Ltd. (Dnipro, Ukraine) with participation of staff of the department of engineering and design in machinery industry of Dnipro University of Technology (Dnipro, Ukraine). The works indicate that the screen filters are still viable, and that the technical qualities of filters can be as high as of new filter types through de-

veloping new technical solutions while retaining relative simplicity and low cost, which are characteristic of screen filters.

Considering the indicated, it should be noted that the research of screen filters on substantial increase of screen surface area and contaminant capacity remains actual.

The authors together with other Oceanmasenergo Ltd. specialists have found new technical solutions on screen filters with a zig-zag-shaped screen, which allow significantly increasing screen surface area and contaminant capacity while the filter dimensions remain the same.

Technical requirements to new automated filters with a zig-zag-shaped screen and increased contaminant capacity can be formulated as follows:

- the filter must have a screen, a relatively simple construction and be easy to maintain;
- the screen surface area must be several times larger than the screen surface areas of similar filters with a cylindrical screen while the filter dimensions remain the same;
- the screen back-flush must be performed consecutively through different screen sections;
- large debris must be collected in special chambers and removed by a dirt collector, the filter must be insensitive to relatively large debris;
- filter body dimensions must be constant for filters of fine and coarse filtration of equal flow rate with a possibility of compact placement of screens of required surface areas.

New filters require new theoretical studies for their design, which are performed by authors and are presented further.

New automated filters with a zig-zag-shaped screen that correspond to all formulated requirements are developed by Oceanmasenergo Ltd. (FK filter series) and are shipped to industrial facilities (Patent of Ukraine number 109211 “Vitaliy Kuzminskiy Filter”).

It should be noted that filters with manual screen cleaning are used for cases of relatively clean water. The manual cleaning is performed through creating a reverse flow of water by switching the water flows manually.

Thus, the principle of zig-zag-shaped screen placement is also used during development of simple manual filters with a zig-zag-shaped screen (FZO filter series).

It is the most expedient to produce simple zig-zag-shaped filters with two chambers. The consecutive back-flush of each chamber with isolation of the currently back-flushed chamber from water intake makes screen cleaning exceptionally efficient compared to regular cleaning of the entire filter with a back-flush of water from filter inlet.

These filters can also be automated. To achieve this, the valves of filter must have drives and be controlled by a control box.

Two chamber filters with a zig-zag-shaped screen have substantial pros compared to other filters with a simple design. They provide large contaminant capacity and quality screen cleaning by consecutive cleaning of each chamber (application number a 2020 01034 for an invention patent of Ukraine).

2.3. New brush filters with hydraulic drive on filtered water. Brush filters are quite widely used just as filters with screen back-flush and filters with dirt collectors. Brush filter usage is conditioned by some specific features of solid debris in water, algae presence in water, water organics, and a relatively smaller price of these filters and other factors.

Brush filters are well-developed and showed good results in practice. Despite all this, there are things that require improvements. These are simplification of construction of the filtering block, change of arrangement of units in the filter aimed at simplification of its maintenance.

Despite this, it is expedient in many cases to have a brush filter with a hydraulic drive on water without electric power supply.

Thus, the main requirements to a brush filter are:

- the filtering block must be light, consisting of a screen stretched on a carcass of rings without transverse connections inside the screen so that they don’t interfere with brushes. This filtering block is easy to manufacture, maintain and repair;

- filtering and brush blocks must be united in a single filtration-cleaning block, which can be removed from the filter body for maintenance;

- the filter drive must exceed a force of total resistance of brushes moving along the screen, a resistance in rod guides of brushes considering water counter pressure, and a resistance that occur from the action of contaminants on the filtering element screen.

The first two requirements are realized and tested in real constructions of filter series FRU and in a representative of the second generation of brush filters – the filter of FB (Patent of Ukraine number 113232 Brush filter).

The brush is made in a shape of a disc; a hydraulic drive is installed inside the filter body in a form of a hydraulic cylinder, which operates on filtered water, in a new FBC series filter (application number a 2017 10068 for an invention patent of Ukraine). There are no issues with a required force value with this type of a hydraulic drive. A new method of filter calculation and hydraulic cylinder is developed. A series of hydraulic cylinders, which operate on water, is developed for brush filters.

3. New technical solutions on filters and new filter types

3.1. Water intake filters FZM

Water intake filters FZM of upstream pipelines are created considering all technical requirements to modern filters of pump upstream pipelines. FZM filters perform water intake from open reservoirs, including the ones that freeze in the cold season.

FZM filters (fig. 1) consist of a tubular body 1 with a watertight lid 2, an inlet nozzle 3, a removable filtering block 4, which is outside the body 1, and installed fixedly by the upper flange 5.

The upper flange 5 and the lower flange 7 are connected with each other through a cylindrical carcass 8. The screen 9 is stretched on the carcass 8; the ends of the screen are constricted by the metal plate 10 and screws.

The lower hub 11 with spokes is welded to the lower flange 7. The removable upper hub 12 with spokes is installed on the upper flange 5. Blind openings are made in the lower and upper hubs 11 and 12. The central pipe 13 of the jet dirt collector 14 with injectors 15 is put in the blind openings with a possibility of rotation. Injector axes are placed at a certain angle in order to be able to rotate the jet dirt collector by using the reactive force of water streams. Flushing water inflows through the opening 16.

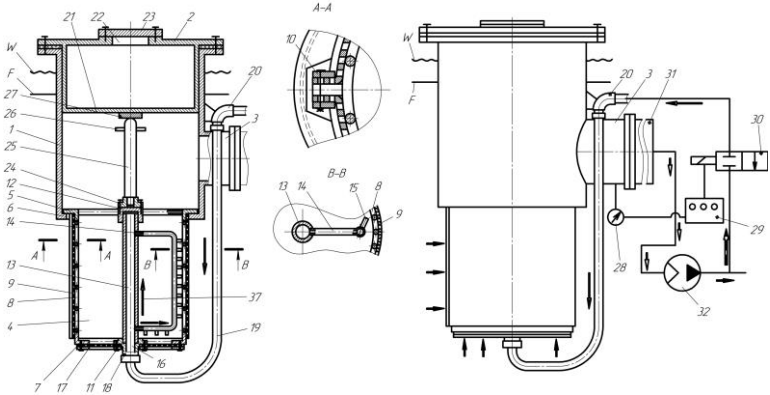

Fig. 1. Water intake filters FZM of upstream pipelines

The lower screen 17 and the fitting 18 are installed on the lower hub 11. The flexible flush pipe 19 is connected with the fitting 18 by one end and with the flush nozzle 20 by the other.

Water level W and the lower level of water freezing L in the reservoir in the filter installation zone are shown in fig. 1.

The cavity extruder 21 is at the bottom of the lid 2. The extruder enters the filter body 1 in such a way that when the lid is closed, the air and the water is pushed down from the filter cavity lower than the level of possible freezing F.

The opening 22 is made at the top of the lid 2 and is closed by the lid 23.

The shoe 24 is fixed on the upper hub 12. The shoe 24 has a threaded opening, in which the bar 25 is screwed, while resting on the buffer 27 with the upper end. The bar 25 pushes the filtering block 4 by the upper flange 5 to the inner flange 6 of the filter body when the lid 2 is shut.

The vacuum gauge 28 is installed on the inlet nozzle 3 of the filter. The gauge 28 sends the signal about the water vacuum value in the inlet nozzle 3 to the control box 29, which is electrically connected with a normally closed electromagnetic valve 30.

The filter is installed stationary at the reservoir, and the lid is located over the upper level of water surface W. Inlet nozzle 3 is located underwater, lower than the level of possible freezing F and is

connected with the inlet pipeline 31 of the pump 32, with which it is used. A pipeline is laid from the pump downstream pipeline through a normally closed electromagnetic valve 30 into the flush nozzle 20.

The cavity extruder 21 pushes the air and water from the filter cavity 1 down lower than the level of possible freezing F when the filter is installed and the lid 2 is closed. Because of this, there is no air in the filter body and the water doesn't freeze. The rotation of the jet dirt collector is performed by a reactive force of water streams of injectors 15.

The filter has two operating modes - **filtration mode** or **flushing mode**.

In the filtration mode the electromagnetic valve 30 is closed, pressurized water doesn't flow through injectors 15, the jet dirt collector 14 doesn't rotate. Vacuum is created in the filter body cavity 1 and in the filtering block cavity 4 from a suction pipe of the pump 32. Because of this, water from the reservoir is sucked through the screen 9 of the filtering block 4 and, already filtered, through the filter body cavity 1 and the inlet nozzle 3 enters the pump 32.

When operating in the filtration mode the screen 9 clogs, and because of this, the vacuum increases over time and the water pressure in the inlet nozzle 3 and in the inlet pipeline 31 decreases. Vacuum gauge 28 transmits a signal about pressure decrease to the control box 29, and when the vacuum reaches the pre-defined value, the control box switches the filter into the flushing mode. For this, the control box opens the normally closed electromagnetic valve 30.

In the flushing mode, pressurized water from the pressure pipeline of the pump 32 through the open electromagnetic valve 30, the flush nozzle 20, the flexible flush pipe 19, the opening 16 and the central pipe 13 enters the injectors 15 and flows out of them under pressure in a form of streams. At the same time, the jet dirt collector rotates under the action of reactive forces of jets. The streams from injectors 15 during the dirt collector rotation hit the screen 9 and the lower screen 17 with high velocity streams cleaning them. Due to the screen cleaning, the vacuum in the inlet nozzle is reduced, and when it reaches a pre-defined initial value, the control unit, having received a signal from the vacuum gauge 28, closes the electromagnetic valve 30. The filter switches back to the filtering mode. **The filtration does not stop during the flushing mode**.

Industrial implementation of FZM water intake filters of upstream pipelines. Sets of working design documentation for a series of FZM filters are developed (fig. 2). FZM filters cover flow rates through filters from 226 to 2700 m^3/hr and diameters of the inlet nozzles from 200 to 800 mm.

Thus, a scientific and technical problem of creation of a new construction of industrial **water intake filters of upstream pipelines** is solved. The main features of such filters are absence of a special electric drive for filtering element cleaning and a possibility of filter operation in open reservoirs, including the ones that freeze in the cold season.

3.2. Filters with zig-zag screen of filtering element.

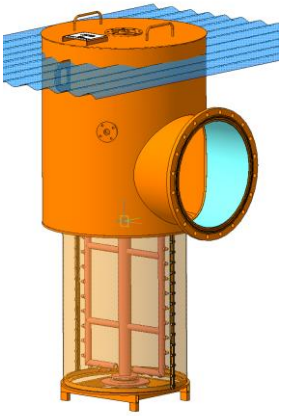

Fig. 2. 3D-model of water intake FZM filter of upstream pipelines

Filters with a zig-zag screen of a filtering element are created considering all technical requirements to modern filters for downstream pipelines (subsection 2.2)

Filters of FK series consist of a cylindrical body 1 (fig. 3), an inlet nozzle 2, an outlet nozzle 3, a flush nozzle 4, and also a filtering block 5, which is rigidly fixed on a central pipe 6. The central pipe is installed on a filter body pipe via bearings 7 and 8 with a possibility of mutual rotation with a filtering block.

An upper disc 9 and a lower disc 10 are parts of the filtering block 5, and are rigidly connected together via spacer rods. Band-shaped filtering screen 13 is stretched and wrapped around inner 11 and outer rods 12 in a zig-zag manner. The zig-zag filtering screen 13 is located between the upper disc 9 and the lower disc 10.

The filtering screen 13, stretched in this way, and the upper and lower discs form outer 14 and inner 15 chambers in the filtering block 5. Thus, the filtering block 5 is connected with the cavity 16 of the central pipe 6 via openings.

A static dirt collector 18 is fixed on the inner surface of the filter body 1. The dirt collector partially wraps the filtering block 5. The dirt collector is connected with the flush nozzle 4 via an opening 19. When the filtering block 5 rotates, its outer chambers consecutively connect with the flush nozzle 4.

The central pipe 6 is connected with an electric drive 20.

A flush valve 21 with an electric drive is installed on the flush nozzle 4. When opened, the flush valve connects the flush nozzle with the discharge.

The filter has two operating modes – filtration mode and flushing mode. When the flushing is active, the filtration does not stop.

Fig. 3 shows a water flow path in the filtration mode and a reverse water flow through the filtering element with arrows in a zone of the outer chamber 14, which is currently being flushed in the flushing mode.

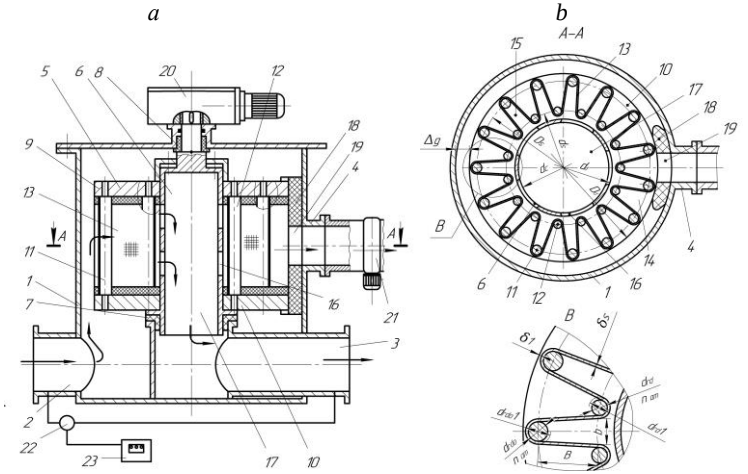

Fig. 3. FK series filter with zig-zag-shaped screen: a – vertical cross-section: b – lateral cross-section

In the filtration mode the flush valve 21 is shut and the electric drive 20 is switched off. The filter is installed in a downstream pipeline. Water with debris flows through the inlet nozzle 2 (fig. 3) into the cavity of the filter body 1. Then – through all outer chambers 14 of the filtering block and through the filtering screen 13 into the inner chambers 15 of the filtering block. It further flows, already purified, through openings 16, into a cavity 17 of the central pipe 6 and, lastly, into the outlet nozzle 3.

The filtering screen 13 gets clogged over time, which leads to an increase of the pressure drop between the inlet nozzle 2 and the outlet nozzle 3. A differential manometer 22 monitors this pressure drop and transmits an executive signal to the control box 23. When the pressure drop reaches a pre-determined value, which is a signal of

the filtering block 5 clogging, the control box switches the filter into the **flushing mode**.

In order to engage the flushing mode, the control box switches on the electric drive of the flush valve 21, which opens the valve, and switches on the electric drive 20, which starts rotating the central pipe 6 and the entire filtering block 5 together with it.

When the filtering block 5 rotates, every outer chamber 14 consecutively aligns with the opening 19 of the static dirt collector 18 and temporary connects with the flush pipe through an open flush valve 21. Water pressure inside the filter is higher than in the flush pipe, therefore a reverse flow (back-flush) of water occurs through the outer chamber 14, into the opening 19 and through the open flush valve 21 to the flush pipe. This reverse flow of water washes off and carries away the debris, which cakes up on sections of the filtering screen 13 in this outer chamber. Thus, when the filtering block 5 rotates, the entire screen and the outer chambers are flushed consecutively.

The debris is gradually washed off the filtering screen 13 as a result of the back-flush and the pressure drop between the inlet nozzle 2 and the outlet nozzle 3 reduces. When the pressure drop reaches the initial value, the control box shuts off the flush valve 21 upon the differential manometer signal. The filter is transferred to the filtration mode. And the cycle continues.

A method of calculation of FK filters is developed, which allows determining all geometrical and hydraulic design parameters of FK filter using initial data with empirical values.

The assumed filtration velocity V_f has a substantial role when designing a filter and is determined by the flow rate Q through the screen with a surface area S_s

$$V_f = Q / S_s \tag{1}$$

The correctly assumed filtration velocity provides a sufficient time interval between flushing cycles and an optimal value of a screen surface area S_s depending on the flow rate Q and the screen mesh size α.

Numerous research were previously conducted by Oceanmasenergo specialists on establishing filtration velocity. Filtration velocity that should be assumed when designing and selecting a

filter, linearly depends on the mesh size α for screen with a large mesh (a=0,5-5 mm and more), but for a screen with smaller mesh a=0,02-0,5 mm and in a range of real flow rates Q through the filter it has a more complex dependency, like

$$V_f = \int(a, Q) \tag{2}$$

An algorithm of selection of filter and its filtering screen surface area is shown in [2] for the basic assumed parameters – flow rate Q and a screen mesh size a.

The calculation order for each filter of the dimension type series is as follows:

- parameters, which are pre-obtained through project development and pre-calculations, are selected for each basic filter;
- all parameters of the filtering block of the basic filter are calculated (a=0,2 mm);
- particular parameters of screens of other filters of the dimension type series are specified (for the assumed a>0,2 mm);
- the rest of filter parameters are calculated.

After consideration of a series of geometric and hydraulic dependencies in order to determine five parameters, obtain the system of five equations (2), which connect these parameters. The parameters are: amount of rods n in the filtering element, inner diameter of the screen d_s, coefficient of screen width $k = B/H$, where B and H – height and width of the screen in one chamber respectively, b – maximum distance between the nearest screen sections (see fig. 3*b*), coefficient of flow rate for the flushing $\alpha = q/Q$, where q and Q – short-term flow rate for the screen surface flushing in one chamber and the entire screen respectively.

$$\begin{cases} \pi d_s - (b + d_{rd1})n \\ d_s = d_d + d_{rd1} + yb \\ 2\,jkH^2 V_f = Q \\ jbHV_b n = Q \\ \alpha = \frac{2\,jkH^2 V_f}{Q} \end{cases} \tag{3}$$

In this system of equations: d_{rd1} - diameter of the inner rod of the filtering block considering the thickness of the screen wrapped around it, d_d - the inner diameter of the disc of the filtering block, j - amount of filtering blocks, V_b - water flow velocity through a gap between the neighboring rods of the filtering block.

Obtain the main ratio for determining the amount of rods n in the filtering element through solving a system of equations with respect to unknowns

$$n = -\frac{p}{2} \pm \sqrt{\left(\frac{p}{2}\right)^2 - q_1} \tag{3}$$

where

$$p = \frac{A - \pi(d_d - d_{rd1})}{d_{rd1}} \tag{4}$$

$$q = -\frac{\pi A}{d_{rd1}} \tag{5}$$

And further, determine the other unknowns of the system of equations from the equation (3).

The parameters calculated in this way considering the assumed values during project development and pre-calculations allow determining other hydraulic and geometric filter parameters:

- outer D_s screen diameter $D_s = d_s + 2B$
- outer diameter of the filtering block disc $D_d = D_s + d_{rd1} + 2\delta_1$

gap between the filtering block disc and the filter body $\Delta_g \cong \frac{Q}{\pi D_d V_g}$ filter body diameter $D_b = D_d + 2(\Delta_g + \delta_b)$

Industrial implementation of filters with zig-zag screen of filtering element. Over 10 FK1.100, FK-1530 and FK-2700 filters have been produced and operated at PJSC "ArcelorMittal Kryvyi Rih" and PJSC CGOK (fig. 4) in 2014-2020 (numbers in filter type – nominal flow rate through the filter in m^3/hr). The filters have been operating for a long time, have fully confirmed their characteristics, and have been filtering water perfectly.

a *b*

Fig. 4. Automated self-cleaning filter FK: *a* –FK1.100; *b* – FK-1530

Thus, a scientific and technical problem of creating a new construction of a universal industrial filter with zig-zag shape of placement of a screen of filtering element. The main features of such filters are a zig-zag shape of screen placement, a formation of chambers for large debris with these 'zigs', and insensitivity to relatively large debris. These construction features provide high contaminant capacity of filtering elements while having relatively small filter body dimensions, longer intervals between back-flushes (compared to traditional flat or cylindrical filtering elements), and smaller water loss for filter back-flush.

3.3. Brush filters FBC with hydraulic drive on filtered water

Known brush filters are quite complex in regards to construction or they require special electric of pneumatic drives for brush dirt collector rotation. The problem of filter construction simplification can be solved by using a disc brush as a dirt collector. The disc brush is installed on a hydraulic cylinder rod with a possibility of cleaning the cylindrical filtering block during reciprocating motion of the dirt collector. The energy source for driving hydraulic cylinder operation is filtered water from a pipeline.

Brush filter consists of a filter body 1, an inlet nozzle 2, an outlet nozzle 3, a flush nozzle 4, and a lid 5. An inlet chamber 6 is under

the lid 5, and a debris bunker 7 is at the bottom of filter body 1. The inlet nozzle 2 enters the inlet chamber 6, and the flush nozzle 4 exits the debris bunker 7.

A screen with a cylindrical shape of the filtering element 8 is rigidly fixed in the filter body 1. A dirt collector 9 with a rod 10 is installed co-axially to the filtering element 8 with a possibility of reciprocating motion. The disc brush 11 is installed on the rod 10.

Hydraulic cylinder 12 is installed on a flange on the outer side of the filter body 1 bottom. Hydraulic cylinder 12 with a piston 13 and a bush neck 14 form rod cavity 15 and piston cavity 16. At the same time, the piston 13 is fixed on the rod 10, which is simultaneously a rod of the hydraulic cylinder 12. The bush neck 14 is a guide for the rod 10.

A normally closed flush electromagnetic valve 17 is installed on the flush nozzle 4. Valve 17 can connect the bunker 7 with the flush through the flush nozzle 4.

Normally closed electromagnetic valves 18 and 19 are provided for controling the hydraulic cylinder 12.

A differential manometer 20 is installed on the filter body.

All electromagnetic valves and the differential manometer 20 are electrically connected to a control box 21 via control cable lines 22, 23, 24, and 25.

The filter operates in one of two modes: long filtration mode or short flushing mode.

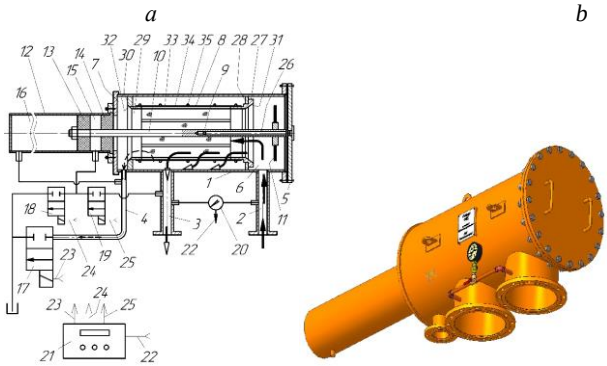

Fig. 5. Brush filter with hydraulic drive of disc dirt collector: *a* – filter cross-section with hydraulic scheme; b – filter 3D-model

In the **filtration mode** electromagnetic valves 17, 18, and 19 are closed, the dirt collector 9 and its disc brush are in the extreme right position.

Dirty water inflows through the inlet nozzle 2 into the inlet chamber 6 of the filter body 1, flows through the filtering element 8 from the inside and further, already purified, through the outlet nozzle 3. Debris is partially removed by water into the bunker 7, and partially sediments on the inner surface of the filtering element 8.

The filtering element 8 gets clogged over time, which leads to an increase of the pressure drop between the inlet nozzle 2 and the outlet nozzle 3. A differential manometer 20 monitors this pressure drop and transmits a signal to the control box 21. When the pressure drop reaches a value determined during filter installation, the control box 21 switches the filter into the **flushing mode.**

In order to engage the flushing mode, the control box opens the electromagnetic valve 17, which connects the bunker 7 for debris with the flush pipe through the flush nozzle 4, where the pressure in lower than in the filter.

A water flow already occurs from the filter inner cavity through the bunker 7, the flush nozzle 4, and through the flush pipe. This flow of water carries away the debris from the bunker 7 and the filter inner cavity to the flush pipe. A reverse flow of water occurs through the filtering element 8, which partially washes off the debris from the filtering element and carries it away to the bunker 7 and further to the flush pipe.

The debris that isn't washed off by the back-flush, stay on the inner surface of the filtering element 8. The disc brush 11 of the dirt collector 9 brushes off this debris from the filtering element 8 during its reciprocating motion along the filtering element 8 axis. In order to do this, the control box 21 opens the electromagnetic valve 19 already after the electromagnetic valve 17. The valve 19 connects the rod cavity 15 with the outlet nozzle 3, where high pressure is present, just as in the filter inner cavity. At the same time, low pressure like in the flush pipe is present in the piston cavity 16, which is constantly connected with the flush nozzle 4. This is because the flush electromagnetic valve 17 is open and the flush nozzle is connected with the flush pipe.

Pressurized water flows into the rod cavity 15 and moves the piston 13 right to left (fig. 5a). The dirt collector 9 and the disc brush 11 move together with the piston 13. At the same time, the disc brush 11 moves along the inner surface of the filtering element 8, while brushing the debris off the filtering element and exits to the bunker 7. The debris is carried out to the bunked by water and further to the flush pipe.

Control box 21 then closes electromagnetic valves 17 and 19 and opens the electromagnetic valve 18. The pressure in the rod cavity 15 gets as low as in the flush pipe. Pressure in the flush nozzle 4 after closing the electromagnetic valve 17 equalizes with pressure in the filter cavity, which is high. Water under high pressure flows into the piston cavity 16 from the flush nozzle 4, because it is constantly connected with the flush nozzle 4 via a pipeline. The piston 13 moves left to right because of the action of water under pressure, which flows into the piston cavity 16. The dirt collector 9 and the disc brush 11 move left to right together with the piston 13, while additionally cleaning the inner surface of the filtering element 8. The filtering element is clean, the differential manometer 20 sends the signal to the control box 21, and the control box closes all electromagnetic valves. The high pressure equal to the inner filter cavity pressure sets in the rod cavity 15 and the piston cavity 16 of the cylinder 12. Reciprocating motion of the dirt collector stops. The filter is transferred to the filtration mode.

A method of calculation of main elements of brush filters FBC is developed. When developing the method, theoretical achievements on designing the first generation of brush filters FRU are creatively used. This is why only main dependencies in regards to determining parameters of elements that are different from analogical elements of FRU filters are given. These elements are circular wire brush and water driving hydraulic cylinder.

A brush in the FBC filter loses contact with the screen at the end of each travel during the reciprocating rod motion along the longitudinal axis of the filtering element when screen cleaning is performed. Then, the brush contacts the screen again, but moves along the screen in the opposing direction. Each brush wire bends one way and then the other during motion along the screen.

The problem of calculating the brush is to select the brush parameters in such a way that the alternating bending stresses in wires are less than the yield strength of wire material. The calculated parameters are: brush wire material and permissible bending stress [σ], wire diameter *dw*, wire length *L*, wire protrusion length over the screen inner surface when not in contact with the screen (in brush extreme positions) *X*, wire deflection during movement along the screen *f*, an amount of wires in a bunch n_{bum}, a force, occurring in a bunch during movement along the screen P_{bum} (pre-defined).

Brush wire can be considered as a console beam of length *L* rigidly fixed at one end (fig. 6). The wire deflects by a value f when subjected to force *P*. At the same time, the free end of wire moves to the point *C* by the value *X*. The wires bend along a curve, which can be represented as an arc of a radius *R*. Considering a relatively small value of deflection *f*, this substitution doesn't introduce a substantial error to the solved problem.

Moment of resistance and deflection of a circular wire

$$J = \frac{\pi d_w^4}{64} \tag{6}$$

(7)

Assume the value *f* based on design considerations and prior developments.

Obtain the following from the triangles OAC and ADC by writing the expressions for determining the same line segment L_1 of the line AC and by excluding L_1

$$2R\sin\alpha = \sqrt{f^2 + (L - X)^2} \tag{8}$$

It can be seen in fig. 6, that

$$\alpha = arc\tan\frac{f}{L-X} \tag{9}$$

$$\alpha = \frac{360L}{4\pi R} = \frac{90L}{\pi R} \tag{10}$$

Equations (8), (9), (10) represent a system of equations with unknowns α,*R*,*X*.

Exclude *R* from the system. From (10)

$$R = \frac{90L}{\pi\alpha} \tag{11}$$

By transforming (8) and (11) denominate the following

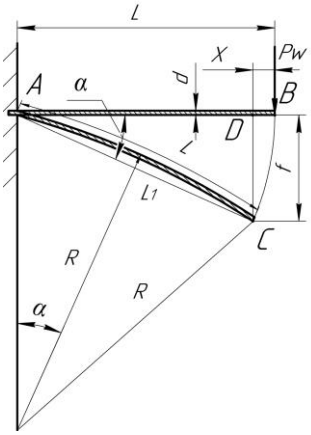

Fig. 6. Computational scheme of determining deflection of brush wire

$$A = \sqrt{f^2 + (L - X)^2}$$

$$B = \frac{180L\sin\alpha}{\pi\alpha}$$

By equating the two obtained equations and using the iterative method, determine the value of X (wire protrusion length over the screen inner surface when not in contact with the screen).

Obtain the following from the known dependencies of strength of materials and from fig. 6:

From the known dependences of the resistance of materials and from fig. 4 we get

- the moment bending a single wire $M_w = P_w L$;

- normal stresses that occur in a single wire under the bending moment action $\sigma = M_w / W$;

- moment of resistance of a wire cross-section: $W = 0{,}1 d_w^3$.

Determine a force that occurs at the end of a single wire during movement along the screen

$$P_w = \frac{\sigma W}{L} \tag{12}$$

Obtain the maximum force that occurs at the end of a single wire during movement along the screen from (12) and the condition of strength of material

$$P_{w.\max} = \frac{[\sigma]}{L} = \frac{0{,}1[\sigma] d_w^3}{L} \tag{13}$$

Obtain the expression for calculation of maximum permissible wire deflection by substituting the value of $P_{w.\max}$ from (13) to (7)

$$f_{\max} = P_w L^3 / 3Ej \tag{14}$$

The fulfillment of condition $f \leq f_{max}$ is checked by a value of f assumed earlier from design considerations.

The calculated value of the force occurring at the end of a single wire during movement along the screen

$$P_w = P_{w.\max} \frac{f}{f_{\max}} \quad (15)$$

The maximum calculated tractive force $P_{br.\max}$ for brush movement along the screen of the filtering element can be obtained in the first approximation by multiplying the value of P_w from (15) and the amount of wires in the disc brush.

The problem of calculation of the driving hydraulic cylinder, which operates on filtered but yet containing small debris particles water (fig. 7), is determination of operating diameters of the piston and the rod. The rod and piston diameters must be such that the tractive force output by the hydraulic cylinder is sufficient to provide traction to move the brush along the screen of the filtering element and to overcome friction forces in sealing systems of the hydraulic cylinder. When operating on dirty water, the dirt gets into the bush neck and piston and may jam the rod movement. Polyamide (PA) is selected as a material for the bush neck, the piston, and their seals in order to reduce wear. It is expedient to constructively combine the seals with the piston and the bush neck.

The piston must create a small gap in a place of interaction with the cylinder and the bush neck in a place of interaction with a rod to achieve the following goals:

- prevent jamming when the PA expands because of water;
- prevent jamming when small dirt particles get through the seals, especially when the seals are partially worn out, but yet water leakage through the seals remains permissible;
- allow a certain clearance in order to compensate the skewing during hydraulic cylinder installation on the filter body.

The axial forces output by the hydraulic cylinder when water under pressure p is pumped to the piston and rod cavities (fig. 7) must be determined considering friction forces in the sealing systems of the hydraulic cylinder.

Fig. 7. Schemes to calculation of water hydraulic cylinder:

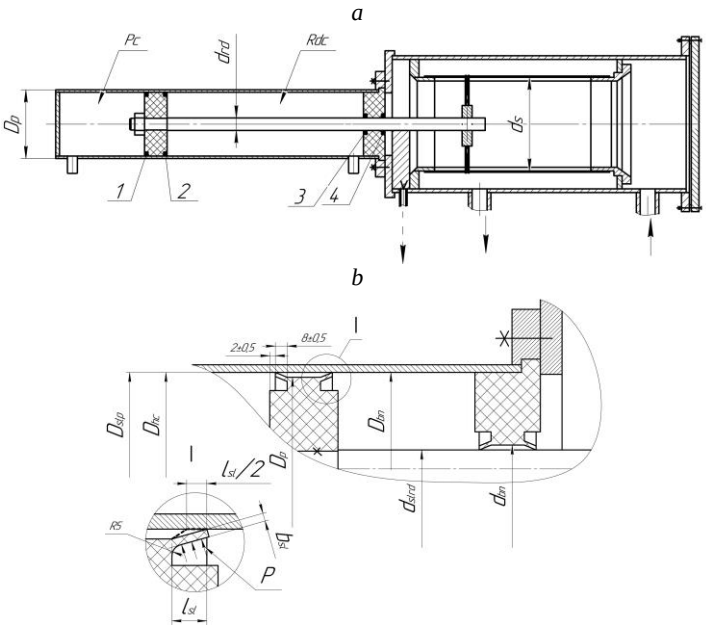

a – scheme to determining forces of rod movement; *b* – scheme to calculation of forces of friction in piston and bush neck

The seals are made of PA, are relatively rigid, have a thickness b_{s1}, and one of the seal sides is rigidly connected with the piston or the bush neck. Assume that under the pressure *p* just a half of the seal length $l_{s1}/2$ attaches to the support (hydraulic cylinder or rod) over the ring with surface area of $\frac{l_{s1}}{2}\pi D_p$ (for the piston) and $\frac{l_{s1}}{2}\pi D_{rd}$ (for the rod) and is pushed to them with a pressure *p*.

Then normal forces *N* at a pressure from the seals p, which create resistance to the cylinder movement due to friction, are determined from the expressions

$$N_1 = N_2 = \tfrac{1}{2}\pi D_p l_{s1} p \tag{16}$$

$$N_2 = N_4 = \tfrac{1}{2}\pi d_{rd} l_{s1} p \tag{17}$$

While under the pressure *p* in the piston cavity, the seals 1 and 4 create the resistance during the rod movement left to right (the brush returns to the

starting position, fig. 5*a*). While under the pressure p in the rod cavity, the seals 1 and 3 create the resistance during the rod movement right to left (the brush cleans the screen). The seal 4 is in the flush zone, since the flush valve is open.

Axial resistance to movement, created by the seals of the piston and the rod

$$F_{s1ap} = f(N_2 + N_3) \tag{18}$$

$$F_{s1ard} = f(N_1 + N_4) \tag{19}$$

or considering (16) and (17), the axial resistance from seals on the rod of the hydraulic cylinder during pressurized water inflow to the piston and the rod cavities respectively

$$F_{s1ap} = F_{s1ard} \cdot p - \tfrac{1}{2}\pi l_{s1}(D_p + d_{rd})p \tag{20}$$

The axial force, created at the rod of the hydraulic cylinder during pressurized water inflow to the piston cavity

$$F_{ap} = \frac{\pi D_p^2}{4} \cdot p - \frac{1}{2} \cdot \pi l_{s1} \cdot (D_p + d_{rd}) \cdot p \tag{21}$$

after transformations

$$F_{ap} = \frac{1}{4} \cdot \pi p \cdot [(D]_p^2 - \frac{1}{2} - 2l_{s1} \cdot (D_p + d_{rd})) \tag{22}$$

The axial force, created at the rod of the hydraulic cylinder during pressurized water inflow to the rod cavity

$$F_{ard} = \frac{\pi p \cdot [(D]_p^2 - d_{rd}^2)}{4} \cdot p - \frac{1}{2} \cdot \pi l_{s1} \cdot (D_p + d_{rd}) \cdot p \tag{23}$$

after transformations

$$F_{ard} = \frac{1}{4} \cdot \pi p[((D]_p^2 - d_{rd}^2) - 2l_{s1} \cdot (D_p + d_{rd})) \tag{24}$$

It is possible to calculate the unknown diameters of the rod d_{rd} and the piston D_p of the hydraulic cylinder from the conditions $P_{br.max} \leq F_{ard} \leq$ and $P_{br.max} \leq F_{ap}$ with known operational water pressure p in the pipeline.

Industrial implementation of brush filters with hydraulic drive on filtered water. Sets of working design documentation for a series of FBC filters (Fig. 8) and their driving hydraulic cylinders, which operate on filtered water, are developed. The series of filters

covers flow rates through filters from 170 to 2100 m^3/hr and diameters of the inlet nozzles from 200 to 700 mm.

Conclusions

1. The quality of technical water directly influences energy saving, specific links of water treatment systems are detected, which require improvement of filters for ensuring the required water treatment quality.

These are water intake filters, downstream pipeline filters of predominantly fine filtration at large flow rates, brush filters that are used predominantly in special conditions of water contamination (i.e. foliage, polyethylene film, etc.)

2. Through an analysis of literary sources and real water treatment systems of Ukrainian and foreign industrial facilities main requirements on development and improvement of constructions of the selected filters are detected and justified, main technical solutions on the constructions are suggested.

3. A construction of the new water intake filter with a jet drive and screen cleaning is developed, which does not have an electric drive (FZM type filter). The filter is installed in the open reservoir while providing simple maintenance by removing the filtering-purifying block through an open top lid.

The main feature of this filter is that it operates and is easily maintained even at frozen reservoirs.

4. The construction of a brand-new filter for downstream pipelines is developed. It has significantly larger screen surface area while the filter dimensions remain relatively small.

This is a filter with a zig-zag-shaped screen (FK type filter).

Theoretical justifications of calculation of such filters and their main geometrical and hydraulic parameters are developed.

The zig-zag-shaped screen allows creating chambers by its ‘zigs’, in which relatively large debris is collected before flushing. This allows using the filter without installing another one or a cascade of pre-treatment filters before it. The filter cleans itself automatically by a consecutive back-flush of chambers.

The filters are shipped to industrial facilities since 2014 and have operated very well (for example, during cooling of the blast furnace number 8 of PJSC “ArcelorMittal Kryvyi Rih”, Ukraine).

5. A new brush filter type is developed (FBC filter type). It has a hydraulic cylinder for a drive, which operates on filtered water, and a cylindrical brush operates together with a hydraulic cylinder.

A theory of calculation of FBC type filter is developed, which allows determining the necessary screen surface area, brush movement resistance considering the resistances from water and debris on the screen during cleaning.

A type range of hydraulic cylinders is developed, which can be used during filter designing.

FBC type filters don't have an electric drive, are suitable for fire systems, the filter data are requested by project organizations for usage in projects on fire systems.

6. Series of all types of filters (FZM, FK, FBC) are developed for the entire range of parameters required by industrial facilities.

The developer is ready for further shipping of any of the filters in the developed range.

References

1. New technologies of old thermal power station: boiler with circulating boiling bed, condenser ball cleaning system / Energosberezhenie №8. 2002, Editorial article, pp.6-9. [In Russian].

2. **Kukhar, V.J.** Broaden options industrial grid water filters / **V.J. Kukhar, V.P. Kuzminskyi, O.V.Ovchynnykova** // Underwater technologies. Industrial and civil engineering, №04. – Kyiv.: KNUBA, 2016. – Pp. 60 – 71.

3. Amiad Water System. Omega Series. Automatic self-cleaning filter with a multi-screen design.
http://amiad.com/downloads/brochures/Omega_Product_Page_En_04.2014.zip.

4. Hydac AutoFilt® RF3. Automatic Back-Flushing Filter for Process Technology
http://www.hydac.com/fileadmin/pdb/pdf/PRO0000000000000000000007709030011.pdf

5. Arkal. Disk filtration technology
http://amiad.com/ArkalCatalog/Industrial/Arkal_catalog.html

6. Filterelements of HYDAC http://www.hydac.com.ru/filterelements.html.

THE MODELING OF THE INTERACTION OF ROCK MASS AND COMPLIANT LINING WHILE IT IS EXPANDED

Didenko, M.
Candidate of Science,
associate professor of Mining sub faculty of Volodymyr Dahl East Ukrainian National University, Severodonetsk, Ukraine

Abstract

The bearing capacity of metal lining from a special interchangeable profile was studied under the conditions of its interaction with the rock mass both in expanding and in compliant modes. The purpose of research is the development of methods for managing the state of mine working by adapting its parameters to the rock pressure effects. The idea of the work is to numerically model the interaction of the rock mass and arched compliant lining during its expanding. In this case, the lining was imitated using a rod system of finite elements. As a result of the studies, the parameters of the lining are determined, which ensure the reliable functioning of the mine working throughout its entire service life. In order for the lining to work efficiently, the filling of voids beyond it is needed. In this case, however, the compliant elements must have the strength of resistance that higher than that of existing lining structures. The results of studies can be used in the construction of tunnel-like mine workings.

Introduction

Reducing the cost of coal is related to the problem of increasing the sustainability of mine workings, since the cost of their maintenance varies at different mines in the range of 25% to 45%. Basically, the Donbass mines use arch compliant lining. It is mounted with a large mounting gap, usually without filling the voids beyond the arch, so the lining does not come in contact with the rock outcrop for a long time and does not prevent the rock from exfoliation and loosening. From the point of view of resource conservation, the main bearing element in ensuring the sustainability of mine workings should not be lining, but its own bearing capacity of rocks. The lining of mine working should be used, first of all, as a means of controlling the deformation processes and increasing the strength of resistance to the destruction of rocks. The study of the possibility managing the condition of mine working by means of compliant lining that is able to expand is relevant, because it is of great scientific and practical importance.

Analysis of ways to manage the condition of mine working

Ways to manage the condition of tunnel-like mine working should provide [1]:

– continuous monitoring of the state of the rock mass throughout the life of mine working;

– rational management of the interaction of the lining and the rock mass in accordance with the form of loss of its firmness;

– workability, which is the ease of implementation;

– efficiency of impact on the rock mass;

– resource conservation, i.e. the economical use of materials.

Depending on the object of the control impact application, all methods for managing the state of the surrounding rock mass can be divided into four groups:

– methods of influencing upon the rock mass by the expanding of lining;

– methods of influencing upon the lining to regulate its parameters;

– methods of managing the contact conditions of interaction of rock mass and lining;

– complex methods of adaptive management of the mine working condition.

The principles stated earlier correspond to the method of forceful influence of a compliant lining upon the rock mass, which is carried out by the active expanding. The idea of this method was probably first expressed in DonNTU [2]. The idea was brought to the practical realization by prof. I.L. Chernyak [3], who checked it at a number of Donbass coal mines. With the help of mine experiments he proved the possibility of compaction of the destroyed rocks in the zone of inelastic deformation. However, while frame of lining is being expanded with hydraulic props it does not participate in the process of creating the packing force. Therefore, after the dismantling of the hydraulic props, the rocks will be exfoliated, i.e. the desired effect, which is only possible with the proper interaction of rock mass and lining, is not achieved. More effective are the methods of two-stage influence upon rock outcrop, proposed in DonSTU [4, 5, 6].

However, the problem of adequate calculation of the metal frame lining remains unresolved. Methods of calculation proposed in the

past based on the methods of construction mechanics and solid-state mechanics have not been widely used in practice. The main reason for this is that the complex and specific conditions of interaction the lining with the rock mass are still insufficiently studied, forcing the use of simplified hypotheses and numerous idealizations, which negate the practical value of such onerous calculation methods.

Known methods for determining the parameters of metal frame lining include, as a rule, three separate steps:

– determination of loads for lining and drawing up of the calculation scheme;

– calculation of internal forces and stresses, displacements and deformations in the structure of lining;

– design calculation of the lining, including the verification of its bearing capacity.

It should be noted that none of the known methods of calculating the lining does not allow for the active influence of arched lining upon the destroyed rocks in order to create the buffer zone of compacted rocks in the zone of inelastic deformation. Improvement of calculation methods should be aimed, first, at ensuring the mode of operation of the lining in its interaction with the rock mass; secondly, to take more fully into account the factors that determine the physical and mechanical properties of the rock mass, especially the formation of the zone of inelastic deformations; third, the widespread use of PCs, which allow the implementation of modern methods of computer simulation.

Beginning in the mid-1970s, the finite element method (FEM) has become the leading method of numerical solution of various geomechanical problems. Versatility and constancy of computational algorithms are the features inherent in the FEM that provided it a leading position in geomechanics. The approximation of the object being examined by a finite number of elements has a strongly marked physical nature, which increases the ease of perception of the calculation results. FEM allows modeling of plastic deformation and brittle fracture.

Setting of research objectives

The analysis showed that the problem of the mine workings is far from being finally resolved. Past studies on improving the stability of the mine workings have usually been limited to considering a sepa-

rate period of their existence and a particular method adapted to the particular form of the rock pressure effects. The overall purpose of this work is to develop a methodology for managing the condition of mine working and ensure their reliable functioning by adapting metal arch lining to the rock pressure effects. To achieve this goal, it is necessary to analyze the geomechanics of management of mine working condition by means of compliant lining that allow the expanding, than to perform theoretical studies on this basis to determine the patterns of joint deformation of rocks and compliant lining by FEM numerical modeling on the PC.

General methodological proposition of modeling

On the basis of testing different methods for calculating mounting as a core system for a given load, the licensed ЛИРА software was selected. The experience of its use in underground construction proved the prospect of its application [7, 8].

The basic design scheme is a two-hinged circular arch fixed with immobile hinges at the lower nodes (1 and 98). The width of the arch is 5154 mm and the height – 3477 mm, which corresponds to the typical cross-section of the tunnel-like mine working (Fig. 1). For modeling the frame of lining, a linear universal spatial-rod finite element КЭ-10 is used, the length of which is chosen to be about 10 cm. Thus, the frame of lining model consisted of 97 identical rod elements and 98 nodes. The parameters of the elements of the КЭ-10 are set corresponding to the parameters of the special interchangeable profile of the СВП-22 (F = 27,91 cm^2, I_y = 428,6 cm^4, I_z = 566,3 cm^4, I_k = 15,54 cm^4). Physically the rod elements is reproduced of ideally elastic material with Young's modulus $E = 2 \cdot 10^5$ MPa, which corresponds to the modulus of elasticity of structural steel.

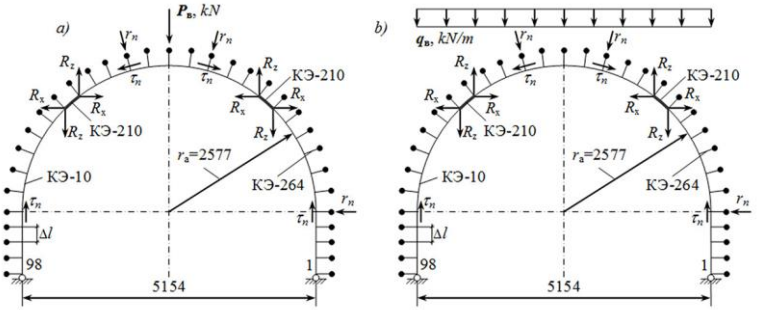

Fig. 1. Design scheme of arch lining loaded with concentrated force $P_в$ = 326 *kN* (*a*) and distributed force $q_в$ = 63,25 *kN/m* (*b*)

The presence of passive reaction of rock is the feature of the interaction of underground structures with rock mass that is surrounding their. For the simulation of rock reaction 98 physically bilinear two-node finite elements КЭ-264 are used. They have one-sided elastic bond of a given stiffness that is given taking into account the tangent displacements and friction. The resulting friction force is given as a parameter of the element КЭ-264, namely the coefficient of friction, which in the calculation is taken to be f = 0.3. The stiffness of the finite elements КЭ-264, mounted on the contour of the model of lining, is determined on the basis of the bedding value of the medium, which is equal to the ratio of pressure on its surface to displacement of the surface of the loaded area. In [9] it is stated that the bedding value depends on the displacement of the structure, and if displacements $U > 2$ cm then the bedding value is less than 20 MN/m^3. For loose filling, this factor can be up to 10 MN/m^3.

In the simulation, it was considered that the filling is present only in the sides of the mine working, and that filling is performed by the workers of the tunneling crew at human height (2 m). The mounting gap as a property of the element КЭ-264 is set equal to zero in the sides of the mine working, and equal to 50 mm in the roof.

The expanding of the lining is simulated with nonlinear rod finite elements КЭ-210 placed to the structure of lining frame (instead of elements КЭ-10) at the two areas that are correspond to the clamps of lining (four elements in each clamp, so the length of each clamp is 400 mm).

Nonlinearity was taken into account by setting the elements of the piecewise linear deformation law. The deformation diagram in the compression region was given by two segments: in the range $\varepsilon = 0\ldots0{,}0875 - \sigma = 0\ldots90$ MPa, which corresponds to the bearing capacity of the clamp 260 kN; in the range $\varepsilon = 0.0875\ldots\ 0.75 - \sigma = 90\ldots92$ MPa. In the stretching range, the deformation diagram was given by one segment in the range $\varepsilon = 0\ldots -0.75 - \sigma = 0\ldots -10$ MPa.

When calculating the mounting loads acting in the frame of the lining, which is mounted with the previous expanding, it was considered that due to the sliding of the frame by means of hydraulic jacks installed on the clamps of the lining, the top of arch interacts with the destroyed rocks of the roof, so the stiffness of the finite elements КЭ-264 of the working roof is taken to be equal to 2.5 MN/m, and the mounting gap is set at zero. The expanding force was assumed to be equal to 1000 kN and was modeled by the adding of concentrated forces to the nodes of the lining frame that correspond to the jacking points.

In the design schemas, the rock pressure iss set with different distribution laws (vertical concentrated force applied to the top of the arch, and vertically uniformly distributed load). The value of the load is set equal to $P_{в}$ =326 kN, which corresponds to the specific load $q_{в}$ = 63.25 kN/m.

Bearing capacity of the lining

The passive reaction of the rocks during the expanding of the lining is very unevenly distributed along the perimeter of the arch. Maximum normal $r_{п}$ and tangent force $\tau_{п}$ are observed directly at the point where the hydraulic jack is applied. With distance from the point of the application of the force, the tensile forces are reduced, reaching a minimum in the lower hinges and the top of arch. The higher the expanding force *R*, the greater the passive reaction of the rocks in the nodal elements, the value of which is proportional to the mounting load and is determined by the bedding value *c*. With the exception of local areas at load sites and end portions of lining legs, the expanding force is transmitted to the rocks relatively evenly and at the expanding force of 1000 *kN* the distributed normal load is approximately 300 *kN/m*.

Figures of internal forces in a compliant arch with a minimum reaction of the node of compliance (100 *kN*) under the action of con-

centrated force are shown in Fig. 2 ($P_в$=326 *kN*). The maximum positive bending moments are concentrated at the point of application of the vertical concentrated force and at the sites of action of the maximum load from the reaction of the rocks in the sides of the mine working. The longitudinal force is distributed almost evenly over the perimeter of the arch.

The internal forces in the arch of lining when the reaction of compliant nodes is 100 *kN* under the action of distributed load are presented in Fig. 3 ($q_в$ = 63.25 *kN/m*). The highest bending moment is observed in the roof of the mine working. The second unsafe area is located at the point where the peak of rock reaction is exposed, which is distributed unevenly at the contact area with the filling, especially under concentrated loading. The maximums of the lining reaction correspond to the points where filling ends.

The computational experiment showed that the load of arched lining with concentrated force without filling the voids outside the lining is the worst case of its work, but it is common in practice. The lining works as a rigid structure and collapses from bending moments at the top. In this case, the lining operation in the compliant mode is prevented by the negative moment at the location of the compliant node with the low value of the longitudinal forces, which remain much less than the bearing capacity. Therefore, in such conditions, the load of lining arches often does not work in the normal mode and fails before entering the compliant stage of work. In this case, the limit load at which the lining is destroyed is an order of much lower than the standard bearing capacity of the lining.

The filling of the voids outside the lining has significant influence on its work that as a result of the interaction rock mass and lining leads to the appearance of rocks reaction, which is very rarely taken into account in existing methods of designing lining. If the filling is carried out in part, only in the sides of the mine working, then at the end of its formation a second danger zone is formed as a result of the action of the peak reaction of the rocks, the value of which largely depends on the rigidity of the filling and the height of its area.

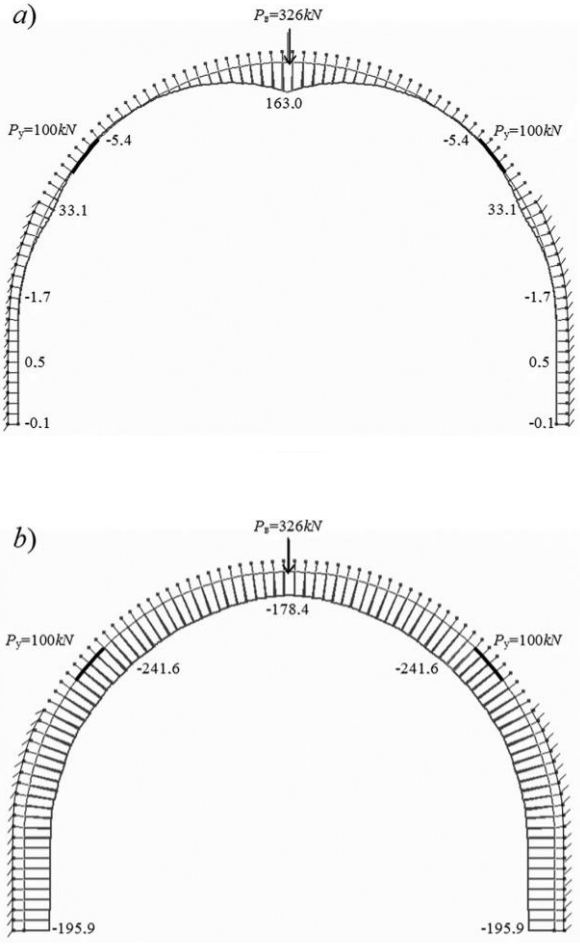

Fig. 2. Distribution of bending moments M, *kN/m* (*a*), longitudinal forces N, *kN* (*b*) in a compliant arch with a bearing capability of 100 *kN* under the influence of a concentrated force of 326 *kN*

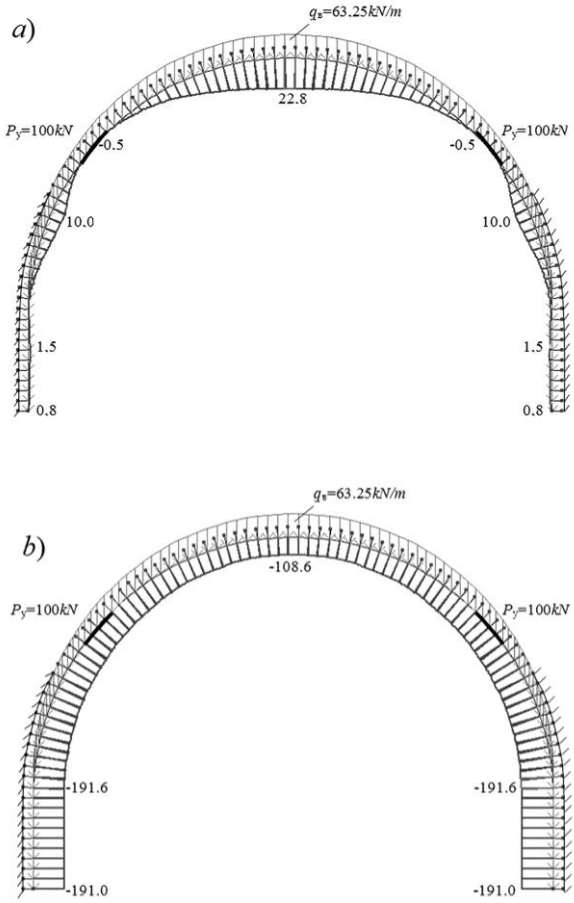

Fig. 3. Distribution of bending moments M, *kN/m* (*a*), longitudinal forces N, *kN* (*b*) in a compliant arch with a bearing capability of 100 *kN* under the influence of distributed load 63.25 *kN/m*

When the load is distributed, the bending moment in the clamps of lining decreases considerably, however, there is another dangerous cross section in the arch legs, where, in case of the absence of filling, the lining may be destroyed even before the implementation of the compliant operating mode. In order for the lining to work effectively, filling the voids beyond the lining is a prerequisite; however, the re-

sistance of the compliant nodes must be significantly higher than that of existing structures.

The calculation of the joint action of the load from the rock pressure and from the expanding (Fig. 4) is carried out only for the distributed vertical load $q_в = 63{,}25 kN/m$ when the expanding force is of 500 *kN*. Effect of concentrated force is not taken into account, since the purpose of expanding is, first and foremost, in the bringing of lining in contact with the rock mass overall the perimeter, and only then in the compaction of the destroyed rocks.

Under distributed load, the rocks are in contact with the lining over the entire length of the top, so when the arch is expanded by hydraulic jacks, the rock reaction will be more evenly distributed, and its value is determined by the amount of movement of the arch toward the rock mass and by the rigidity of the bonds, which for the destroyed rocks is 2.5 *MN/m*. An additional factor that causes the uneven distribution of the rocks reaction is the transition from the contact with the filling to the contact with destroyed rocks.

It should be noted that in the area of positive bending moments as a result of the lining deformation in the place of its contact with the rock will form a zone of exfoliation, i.e. special elements КЭ-264 should work only on shrinking. However, despite the declared properties of the one-sided operation of the finite element КЭ-264, the results of the test calculations did not confirm this possibility of ЛИРА software. Therefore, the action of the expanding force in the calculation was given in the form of reactive nodal loads of the rocks reaction r_n and τ_n that act simultaneously with the distributed load from the rock pressure and passive rock reaction formed at the location of the filling.

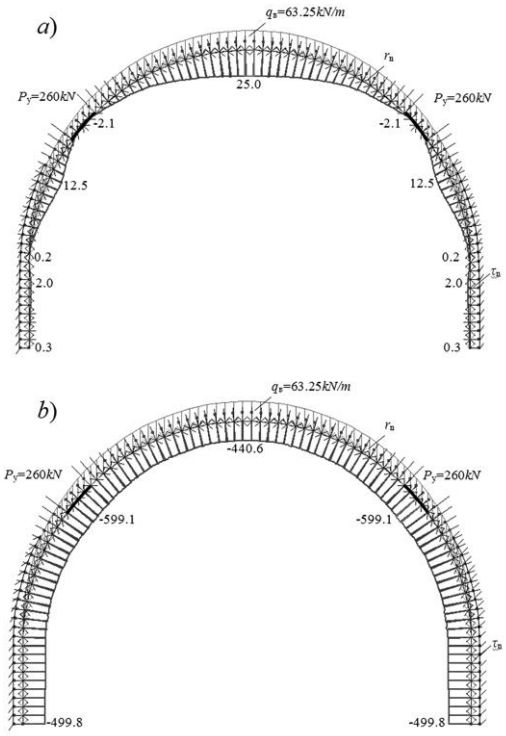

Fig. 4. Distribution of bending moments M, *kN/m* (*a*), longitudinal forces N, *kN* (*b*) in a compliant arch with a bearing capability 260 *kN* under the action of distributed force 63.25 *kN/m* and force of expanding of 500 *kN*

When the lining is expanded with the force of the 500 *kN*, the positive moments at the dangerous points (at the end of the filling) increase by a maximum of 10%, and the longitudinal force increases in the arch approximately 3 times. Therefore, the active expanding of the lining leads to an increase in bending moments and longitudinal forces in the arch, with the maximum load due to the joint action of the rock pressure and the expanding of lining is limited by the approach of the stage of steel yielding at the most dangerous point. However, the increase in internal forces in the lining during the arch expanding should be compensated by ensuring a more uniform application of the load from the rock pressure, as well as by the compacting of destroyed rocks in the zone of inelastic deformation. In

order to evaluate the observed effects, the calculation of the compliant lining must be performed taking into account the actual stress-strain state of the rock mass that interacts with the lining during its expanding.

The stress-strain state of the rock mass

The calculation of the stress distribution around the tunnel-like mine working with lining is performed using the ЛІРА software on an elastic spatial model consisting of 20120 finite elements and 11578 nodes. Due to the symmetry with respect to the vertical plane in which the line of mine working lies, the fragment of the rock mass is limited to half-space. The thickness of the model in the direction of mine working development is accepted equal to 4 m that allowed to place in the model 5 frames of lining with a step of 1 m. The dimensions of the model, 28.8 m wide and 57.6 m high, ensure that the initial conditions at the model boundary are met.

The rock mass was represented using prismatic finite elements of type КЭ-34 (spatial six-node finite element). In the simulation, six layers of rocks are simulated in accordance with their real occurrence. The Poisson coefficient for all rock layers except the sandstone underlying the mine working soil was taken to be 0.3. The properties of finite elements within the sandstone layer are set taking into account its deformation anisotropy; in the vertical direction, the Poisson coefficient is set equal to 0.3, and in the horizontal direction - 0.25. This achieves an additional concentration of stresses in this rock layer and its destruction, which is observed in natural conditions in the form of exfoliation and sudden lifting of the soil of the mine working. Young's modulus of longitudinal elasticity for the mudstone and siltstone are assumed E = 5000 MPa, for limestone E = 15000 MPa, for coal E = 1200 MPa. The zone of rock destruction is set artificially by reducing the Young's modulus for coal to 60 MPa and for sandstone to 200 MPa.

The hydrostatic load on the mine working is modeled outside the area where its face impacts. The value of the load is calculated based on the average depth of the mine working site (655 m) and the average value of the specific gravity of the rocks (2050 kgf/m^3), which is 13.16 MPa.

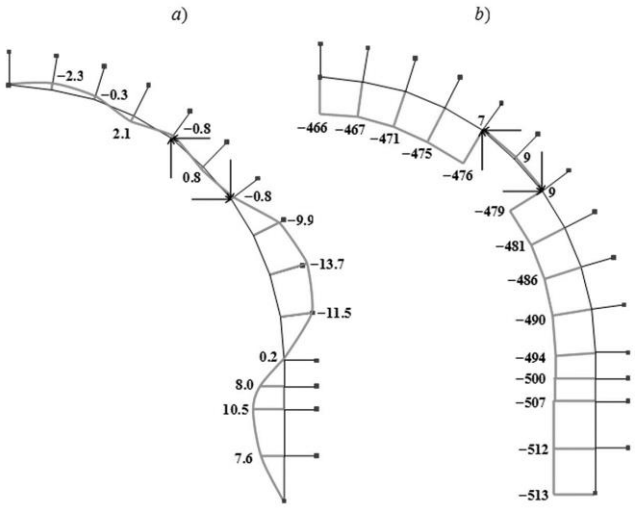

Fig. 5. Plots of distribution of bending moments (*a*), longitudinal forces (*b*) in the arched lining that interacts with rock mass during its expanding with force of 500 *kN*

The frame lining is modeled using the КЭ-10 universal space rod elements. The compliant of the lining frames is ensured by the putting into operation the physically nonlinear rod finite elements of the type КЭ-210, which simulates the clamps of lining. The load from the rock mass is transmitted to the lining frame by special finite element of the type КЭ-264 with single-sided elastic bond. The properties of the elements КЭ-10 and КЭ-264 are specified in the same way as in the previous calculations.

The expanding force from the hydraulic jacks is equal to 500 *kN*, is decomposed into vertical and horizontal components and applied in the form of concentrated forces to the extreme nodes of the lining clamps.

The analysis of the stress-strain state of the rock mass indicates that the stress distribution in the spatial problem is almost identical to the stress distribution in the flat model. As for the internal efforts, they do not correspond to those obtained in the previous calculations. This is due to the presence of a bond to the rock mass in the area of positive bending moments, which in reality is absent in the exfoliation zone.

Conclusions

As a result of the work the following results are obtained:

1) The FEM numerical modeling algorithms for the study of the stress-strain state of the rock mass around the tunnel-like mine working with the help of a flat model of the rock mass taking into account the extrinsic behavior of the rocks and their compaction during the expanding of the lining are substantiated.

2) By calculating the compliant lining allowed its expanding on the load from the rock pressure and the joint effect of the rock pressure and the expanding of the lining, the distribution of normal and tangential forces of rocks reaction along the perimeter of lining and the distribution of normal reactive resistance of the rocks in the sides of the mine working evoked by load from concentrated force and from uniformly distributed load depending on rigidity of filling, also the distribution of internal efforts, taking into account the load from expanding force and rock reaction in operating mode are investigated.

3) Based on the research it is found out that due to the distribution of vertical load of the lining, the bending moment in the lining clamps is reduced significantly, however, there is another dangerous section in the lining lags, where the destruction is possible in case of the absence of filling the voids outside lining.

4) In order for the lining to work effectively, filling the voids outside it is surely a prerequisite. Moreover, in this case, the resistance of the compliant nodes must be substantially higher than that of existing structures.

5) Based on the research, it is found out that the expanding force of 1000 kN corresponds to the maximum level of load on lining in order to not exceed the yield strength of the steels used for the production of special interchangeable profiles.

References

1. **Babiyuk, G.V.** (2012). Upravleniye nadezhnost'yu gornykh vyrabotok : monografiya. Donetsk, Ukraine : Svit knyhy.

2. **Zborshchik, M.P.**, **Morozov, A.F.** (1981). Certificate of authorship of USSR No. 887812. Retrieved from http://patents.su/3-887812-sposob-krepleniya-podgotovitelnojj-vyrabotki-podatlivojj-ramnojj-krepyu.html

3. **Kalimov, Yu.I.** (1981). Sovershenstvovaniye beztselikovoy vyyemki uglya. Ugol', 7, 20-24.

4. **Babiyuk, G.V.**, Litvinskiy, G.G., Stel'makh, V.I. (1996). Patent of Ukraine No. 10567 A. Retrieved from http://uapatents.com/2-10567-sposib-rozporu-ramnogo-piddatlivogo-kriplennya.html?do=download

5. **Babiyuk, G.V.**, Babiyuk, G.G., Toptun, N.I. (2001). Patent of Ukraine No. 35719 A. Retrieved from http://uapatents.com/7-35719-sposib-montazhu-ramnogo-piddatlivogo-kriplennya.html?do=download

6. **Babiyuk, G.V.** (2009). Patent of Ukraine No. 45127. Retrieved from http://uapatents.com/4-45127-adaptivne-ramne-kriplennya-girnichikh-virobok.html?do=download

7. **Litvinsky, G.G.**, Fesenko, E.V. (2012). Issledovaniye rabotosposobnosti shakhtnoy krepi s pozitsiy printsipov ravnoprochnosti. Forum hirnykiv-2012: Vol.2 (pp. 7-16). Natsional′nyy hirnychyy universytet.

8. **Litvinsky, G.G.**, Fesenko, E.V., Emetz, E.V. (2011). Raschet krepi gornykh vyrabotok na EVM : ucheb. posobiye. Alchevsk, Ukraine: DonDTU.

9. **Barchunova, T.N.** (2010). Koeffitsiyenty posteli, prinyatyye pri raschete gorizontal'no nagruzhennoy svai-kolonny s ushireniyem. Visnyk Odes′koyi derzhavnoyi akademiyi budivnytstva ta arkhitektury, 38, 35-41.

COMPLEX APPROACH TO RESEARCH AND SELECTION OF HYDROCARBON SOLVENTS FOR ASPHALTENE-RESIN-PARAFFIN-HYDRATE DEPOSITS CONTROL

Makarenko V.D.
National University «Poltava Yuri Kondratyuk Polytechnics»
DSc, Professor, professor of the Chair of Oil and Gas Engineering and Technology, Ukraine

Liashenko A.V.
National University «Poltava Yuri Kondratyuk Polytechnics»
Senior lecture of the Chair of Oil and Gas Engineering and Technology, Ukraine

Abstract

The article deals with the chemical methods of combating asphalt-resin-paraffin-hydrate deposits, in particular, the use of solvents. The influence of different chemicals on the dissolution of hydrates in the laboratory installation at different temperature-bar modes was carried out: the temperature varied discretely from -10 to + 40 ° C, the pressure from 0 to 10 MPa. To study the effect of hydrocarbon solvents on the process of removal of hydrate formations, we used the methods of regression analysis and mathematical planning of the experiment – simplex-lattice planning. The G-optimality criterion of the plan, including 22 experiments, was used. The measurement results are shown in the diagrams for each solvent separately. The

obtained data made it possible to substantiate a priori the choice of the optimal variant of the use of chemical reagents for complete dissolution and removal of hydrate formations from the surface of the downhole equipment. Analysis of the data shows that the highest solubility and efficiency for removal from the surface of the wellbore equipment of paraffin hydrate deposits are characterized by the solvents butyl cellosolve and ethylacetat, which are recommended for widespread use in the industries of Ukraine. An important fact is that the consumption of the proposed solvents for one well-operation is no more than 4 m^3, which is 2-3 times less than other domestic and foreign analogues. The use of new solvents also allows more than 2-3 times to increase the intercurrent well period, which reduces the cost of production.

Keywords: asphaltene-resin-paraffin-hydrate deposits, dissolvant, downhole equipment, chemical reagent, butyl cellosolve, ethylacetat.

Introduction. Since asphaltene-resin-paraffin and hydrates formations are deposited on the surface of the dowmhole equipment (casing and pumping tubes, pump housings, pump rods) it is necessary to use a universal reagent that would allow all types of such deposits to be dissolved and removed. In order to select such a chemical, we have conducted laboratory and industrial studies.

Formulation of the problem. The above data show that the most effective, economical and technologically simple to use are chemical methods, in particular, the use of solvents. It is known [1, 2, 6, 7] that the use of hydrocarbon solvents is one of the main methods of protecting wells and oilfield terrestrial communications from asphaltene-resin-paraffin deposits. The whole operational period of the wells, complicated by asphaltene-resin-paraffin-hydrate deposits, depending on the magnitude of the well cleaning interval without the use of chemical reagents can be divided into four groups [3-5]:

1 – well cleaning interval up to 10 days;

2 – well cleaning interval from 10 to 20 days;

3 – well cleaning interval from 20 to 30 days;

4 – well cleaning interval more than 30 days.

If in wells 1 and 2 groups the use of chemical reagents should be combined in a certain sequence when cleaning the underground equipment with reagents and dosage of inhibitors of paraffin deposits, then in the wells 3 and 4 groups is the most effective use of hydrocarbon solvents.

Presenting main material. First, on the laboratory installation, the schematic diagram of which is shown in fig. 1, studies of the ef-

fect of different types of chemicals on the dissolution of hydrates as the most soluble to remove. The experiments were carried out in the following temperature-bar modes: the temperature varied discretely from -10 to + 40 ° C, the pressure from 0 to 10 MPa, which most closely corresponds to the real regimes of the sheltered space of oil wells. In this case, the experiments were set up as follows: if the temperature was constant, for example, 0 ° C, the pressure discretely varied from 0 to 10 MPa and vice versa, at constant (fixed) pressure the temperature changed.

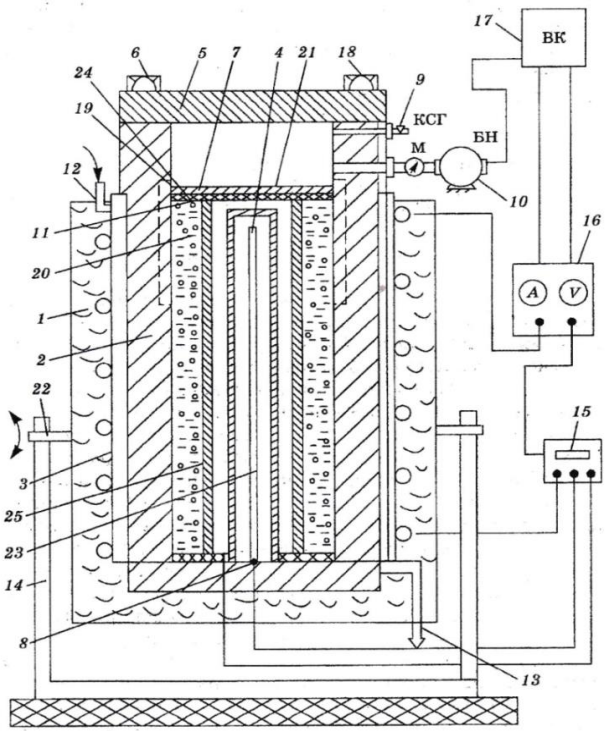

Fig. 1. Schematic diagram of the experimental installation:
1 – furnace; *2* - chamber of cylindrical shape; *3* – cooling jacket; *4* – tube; *5* – means of cover; *6* – squeeze bolts; *7* – insulation (textolite) gasket; *8*, *15* – electronic potentiometers; *9* – nipple; *10* – pump; *11* – grooves; *12* – special device; *13* – crane; *14* – frame; *16* – autotransformer with an ammeter and a voltmeter; *17* – computational complex; *18* – pulse tube; *19* – groove; *20* – reservoir water and gas fluid; *21, 25* – upper and lower walls; *22* – pins; *23* – electric heater; *24* – inner lid

Samples of tubing 1.4 m long, 72 mm in diameter, type of steel 36G2S and a reservoir-oil mixture were used as objects of study. As reagents used butyl cellosolve, ethylacetat, SNPH-7p and SNPH-7p-14, ethylbenzene and butylbenzene fractions. Chemical reagents were poured into the chamber in the amount of 1, 2, 3, 4 and 5 liters, based on the calculation of 10 - 50 liters per 1 m^3 of internal volume of the well. To study the effect of hydrocarbon solvents on the process of removal of hydrate formations from the wells, quantitative description of this effect and a significant reduction in the number of experiments, it is rational to use methods of regression analysis and mathematical planning of the experiment - simplex-lattice planning. Because specific hydrocarbon solvents cannot be implemented in the entire study area, they are subject to additional restrictions. As a result, the planning area becomes complex. In this area, it is advisable to use the G-optimality criterion of the plan [8], which includes 22 experiments and allows to minimize the maximum variance of the predicted values (fig. 2). The addition of a G-optimal plan ensures that there are no points in the planning area where the accuracy of the response surface estimation is not too low. The synthesis of the plan was implemented by numerous methods at the «Hewlett-Packard» computer.

According to the requirements of the plan, hydrocarbon solvents (22 brands of each system) were selected. The content of each solvent varied from 0 to 100%, while the total content of the three solvents remained unchanged and was 100%. As a result of the experiments, fifth order multiple regression equations (regression coefficients significant at the level) were constructed, which were used to construct the level lines on the triple diagrams. The adequacy of the obtained regression equations was tested using the Fisher F-test [9] at 5% significance level. The values of the correlation coefficients r=0.97-0.99, which indicates a good fit of the experimental data to the given regression equations and the possibility of using them as formal computational models.

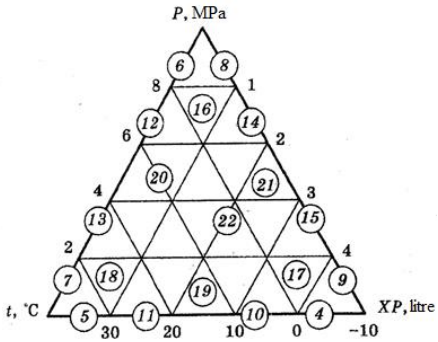

Fig. 2. Triple diagram experiment plan

The duration of the experiments was 12 hours. At the end of each experiment, the contents of the chamber were poured into the tank, and the sample tubing tubing and the inner surface of the chamber were carefully cleared of deposits, which were subsequently weighed on electronic scales to an accuracy of 0.001 g. The measurement results are shown in fig. 3-8.

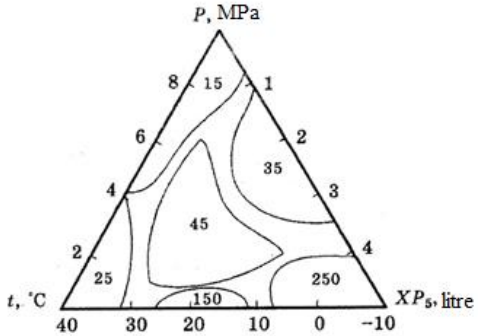

Fig. 3. The mutual influence of temperature, pressure and amount of chemical reagent ethylbenzene fraction on the value hydrate formation (g)

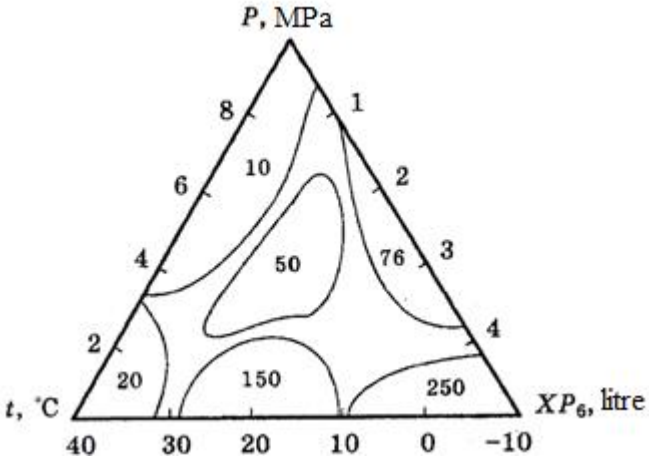

Fig. 4. The mutual influence of temperature, pressure and amount of chemical reagent of butylbenzene fraction on the value hydrate formation (g)

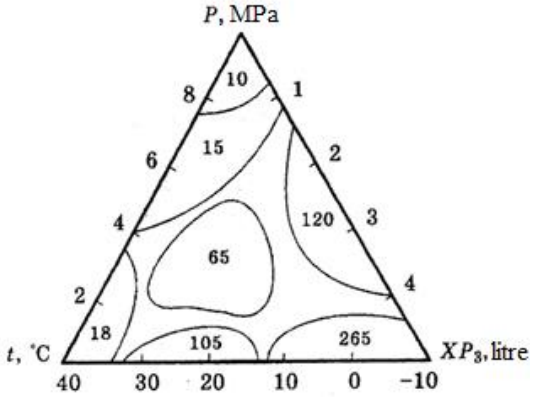

Fig. 5. The mutual influence of temperature, pressure and amount of chemical reagent SNPH-7p on the value hydrate formation (g)

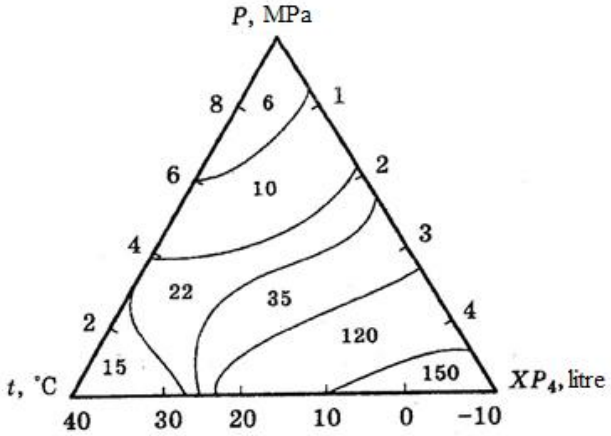

Fig. 6. The mutual influence of temperature, pressure and amount of the chemical reagent SNPH-7p-14 on the value hydrate formation (g)

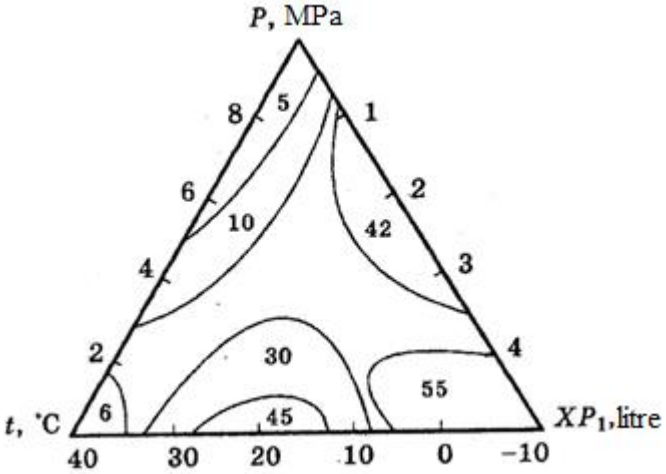

Fig. 7. The mutual influence of temperature, pressure and amount of the chemical reagent butyl cellosolve on the value hydrate formation (g)

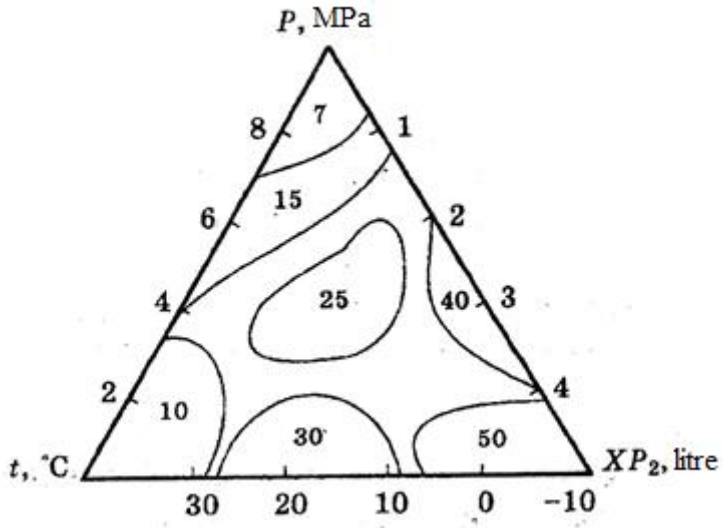

Fig. 8. The reciprocal effect of the temperature, pressure and amount of the ethylacetat chemical reagent on the value hydrate formation (g)

The analysis of the obtained data shows that the best dissolving properties have butyl cellosolve and ethylacetat in all investigated thermobaric modes. Their solubility reaches about 90-95 %. A fairly high solubility (40-60 %) showed composite hydrocarbon solvents SNPH-7p-14 and SNPH-7p.

Widely used in the artisanal chemicals – ethylbenzene and butylbenzene fractions – are characterized by very low solubility (an average of 15-20 %) hydration, although, as is known from practice, they dissolve asphaltene-resin-paraffin deposits quite well [10]. The obtained data made it possible to substantiate a priori the choice of the optimal variant of the use of chemical reagents for the complete dissolution and removal of hydrate formations from the surface of the downhole equipment, in particular, the injection into the well (inside the tubing and sheltered space) of solvents – butyl cellosolve and ethylacetat in the amount of 2-4 liters per 1 m^3 of well volume, ie an average of 2-4 m^3 per well depth of 1.5-2.5 km.

Conclusions.

1. Developed information-measuring system and equipment, which allow to fully approximate the conditions and modes of hydra-

tion formation to the real well processes and characteristics, which makes it possible to investigate hydration formation with a wide probability in a wide range of changes of temperature and pressure.

2. The statistical results of the experiments obtained with the help of the information-measuring system made it possible to determine the conditions required for hydration in the temperature range from -15 to +60 °C and pressures from 0 to 60 MPa, which are well confirmed by thermodynamic calculations of phase equilibria in the annulus of the well space known from the literature.

3. The influence of chemical reagents on the dissolution of paraffin hydrate deposits in a wide range of changes in temperatures and pressures was investigated using an information-measuring system using the method of mathematical planning of experiments. It is established that the most soluble and purifying ability is characterized by the chemical reagent butyl cellosolve and ethylacetat, which are recommended for widespread use in the industries of Ukraine.

The use of new solvents allows more than 2-3 times to increase the interworking period of the well, 5-10 times to increase the productivity of the well and up to 90 % to restore its initial properties.

References

[1]. **Troyanovskij Yu.V.** Osobennosti parafinizaczii promy`slovogo oborudovaniya i razrabotka mer po bor`be s otlozheniyami v usloviyakh mestorozhdenij Zapadnoj Sibiri: Avtoref. diss. kand. tekhn, nauk.- Tyumen`, 1971.

[2]. **Tronov V.P.** Mekhanizm obrazovaniya smoloparofinovy`kh otlozhenij i bor`ba s nimi.- M.: Nedra, 1970.-200 s.

[3]. Usloviya i zony` gidratoobrazovaniya v zatrubnom prostranstve neftyanoj skvazhiny`/ **M.G.Vyatchinin, N.K.Pravednikov, O.Yu.Batalin i dr**. // Neftyanoe khozyajstvo.- 1998.-t # 2.- S. 56-57.

[4]. Zakonomernosti gidratoobrazovaniya v zatrubnom prostranstve neftyanoj skvazhiny`/ **M.G.Vyatchinin, N.K.Pravednikov, O.Yu.Batalin i dr.** // Neftyanoe khozyajstvo.- 2001.- № 4.- S. 54-57.

[5]. **Vyatchinin M.G., Batalin O.Yu., Shhepkina N.E.** Opredelenie rezhimov i zon gidratoobrazovaniya v neftyany`kh skvazhinakh // Neftyanoe khozyajstvo.- 2000.- № 7.- S. 38-44.

[6]. **Khoroshilov V.A., Semin V.I.** Preduprezhdenie gidratoobrazovaniya pri doby`che nefti / Prirodny`e i tekhnogenny`e gazovy`e gidraty`.- M.: Nedra, 1990.- 220 s.

[7]. **Maganov R., Vakhitov G., Batalin O**. Optimal`naya tekhnologiya bor`by` s gidratoparafinovy`mi otlozheniyami // Neft` Rossii.- 2000.- # Z,- S. 96-99.

[8]. **Kasatkin O.G.** K voprosu postroeniya G-optimal`ny`kh planov na simplekse / Primenenie matematicheskikh metodov dlya issledovaniya mnogokomponentny`kh sistem.- M., 1974.- S. 64-69.

[9].https://www.itl.nist.gov/div898/handbook/eda/section3/eda359.htm

[10]. **Svetliczkij V.M., Demchenko P.N., Zariczkij B.V.**//Problemy` uvelicheniya proizvoditel`nosti skvazhin. - Kiev: Vid. Palivoda A.V., 2002. - 228s .

[11]. Code of Practice for Pipelines - Part 1 (2004) Steel Pipelines on Land, PD 41 8010, British Standards Institution, 44 p.

[12]. **Makarenko V.D., B.O. Korobko & Yu.L. Vynnykov** (2018) Innovatsiini materialy ta tekhnolohii v naftohazovii haluzi: monohrafiia . Nizhyn: NDU im. M. Hoholia. 233p.

INVESTIGATION OF THE OSCILLATIONS AMPLITUDES BASES AND FOUNDATIONS OF THE FORMING MACHINE

Mykhailovska O.V.
Ph.D., Senior Researcher, Associate Professor of the Department of Building Technology
National University «Yuri Kondratyuk Poltava Polytechnic»

Zotsenko M.L.
Doctor of Technical Sciences, Professor, Professor of the Department of Building Technology
Technology National University «Yuri Kondratyuk Poltava Polytechnic»

Abstract

Dynamic load equipment is a source of waves that propagate in the ground and affect nearby buildings and structures. Objects with equipment that are sensitive to vibration and operating personnel are not infrequently exposed to vibrations that do not rarely exceed the values set by regulatory documents. The foundations of molding machines from the influence of dynamic loads were studied experimentally, taking into account damage to the foundations. Also, the magnitude of the amplitude was influenced by the above mentioned soil properties, which arose during their operation, the physical and mechanical characteristics of the soil of the bearing layer, as well as the underlying layers.

To measure the amplitudes of oscillations and sediments of the foundations of the molding machines used modern measuring equipment It is determined that the amplitude of oscillation of the base under study when the machine is almost 2.3 times higher than acceptable. And at work of all machines at the same time the amplitude of oscillations of a certain foundation 13.7 times exceeds the allowable

one. The reason for the increased fluctuations of the foundations has been identified and substantiated. It was found that the foundations of the molding machines are made with deviation from the design decision (reduced size) and have damage during operation. Recommendations are given to remedy the identified shortcomings.

1. Introduction

It is almost impossible to prevent mechanical vibrations, which cause soil vibration in practice, because they are caused by production processes in enterprises, technology of construction work and other dynamic phenomena. Dynamic load equipment is a source of waves propagating in the ground and affecting nearby buildings and structures, vibration-sensitive facilities and equipment, maintenance personnel and not infrequently exceeding permissible values set by regulatory documents. Low-amplitude mechanical oscillations often cause the resonance of structural elements. Excessive vibrations of the foundations can cause premature actuation of machine parts, affect the growth of deformations and sedimentation of the foundations of machines, structures [1].

2. Basic investigation

2.1 Approaches to determining the characteristics of the foundation oscillations

Analytical methods of calculation are based on the use of some assumptions. There are two approaches to solving dynamic problems. Proponents of the first approach used the Lagrange dynamic method to explain the phenomenon [2]. The calculations were performed using the characteristics of vibrations, materials and soils. This method required preliminary determination of the mechanical energy of the system, which consisted of: kinetic energy of vertical, horizontal displacement and rotational motion, potential energy of deformation of the soil in the plane of the sole of the foundation. If the foundation was designed deep into the soil, then the potential energy of deformation of the lateral compression of the soil was determined, the reduction of potential energy due to the decrease in the center of gravity of the inertia. As a result of the calculations, differential equations of the forced plane harmonic oscillations of the foundation were obtained.

Other authors used the principle of J. d'Alembert [3], that is, in addition to the active forces added forces of inertia, and regarded the

system as being in equilibrium. This method is called the method of kinetostatics. This method is simpler, so it is most common. Calculating the foundation in this way, the following assumptions were applied: under dynamic loads, the substrate was assumed to be linearly deformed, perfectly elastic-viscous and devoid of mass (soil inertia not taken into account). The viscosity of the substrate is due to the properties of the damping soil. The foundation was regarded as absolutely solid.

Carrying out a number of transformations, the differential equations of the forced oscillations of the foundation-base system were obtained with one degree of freedom based on them. According to the approach to solving the differential equations of dynamics, the methods of calculating the amplitudes of oscillations of the bases and foundations of the machines are distinguished (Fig. 1). The deformation method was used to calculate the foundations for the machines. Turning to the basic system of the deformation method, I.V. Urban assumed anchoring structures at the center of gravity, and based on this he formulated unknown amplitude displacements that impeded vertical and horizontal displacements as well as rotation. The conditions of symmetry of the structure were taken into account in the calculation, but the deepening of the foundation was not taken into account.

In the works of VB. Shvets [5,6], the dependences for the calculation of the displacements of the foundation and the machine, the system "base - foundation - machine" are proposed, which is considered as two - mass, taking into account the inelastic resistances of the base and the over - base laying. However, dependencies are cumbersome for use in engineering calculations without the use of computers. VB The cobbler is recommended to calculate the foundations for the molding machines, to carry out the hammer taking into account the elastic pads under the shaking part of the machine, which significantly affects the amplitude of the oscillations of the foundation. Yu.O. Kirichek [1], E.O. Lando at Finite element method (FEM) performed the analysis of the interaction of combined solid-plate foundations with the base. Such modeling has advantages in terms of complexity and cost in comparison with full-scale and experimental studies on models. In addition, using this numerical

method, it is possible to simulate processes that cannot be experimentally investigated.

A.V. Grishin [7], S.M. Novak noted that this simple and versatile approach worked great. A.V. Grishin [7] investigated with the help of ITU a concrete slab lying on a deformed base under the action of impulse loading, taking into account elastic-plastic properties of concrete and soil base. For the base he used an elastic-plastic model under the condition of Mora - Coulomb. In the numerical solution of the nonlinear elastic-plastic dynamic problem, the sampling of the initial equations was carried out both in time and in the area occupied by the slab and the base.

Eight and five nodal infinite isoparametric elements were used to sample the initial equations. Infinite elements were used to sample the infinite boundaries of the substrate to avoid the reflection of waves. The following is an iterative process. The calculation scheme is shown in Fig. 1.

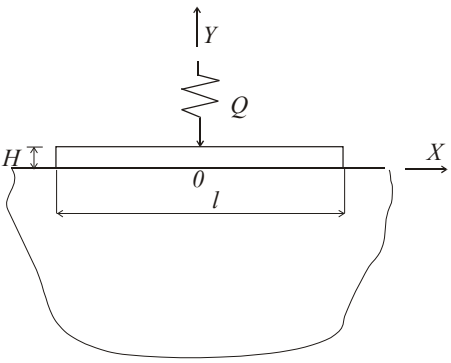

Fig. 1. Calculation scheme of the concrete slab, which is deformed on the basis of the impulse load

A.M. Uzdin [8] used infinite finite element modeling to use "infinite finite elements" (IFE). The base area is divided into two subdomains. The interior adjacent to the foundation of the structure is separated from the outer circle and divided into traditional finite elements. The outer area is divided into IFE limited by the circle and the radii of this circle. This technique can be recommended to calculate the foundations of deep-loading for the action of dynamic loads.

Recently, the market for software for engineering calculations offers a lot of both domestic and foreign developments based on FEM, which allow to carry out calculations of bearing structures fairly reliably. Unfortunately, the area of calculations related to geotechnical engineering which underlies the processes of interaction between foundations and soils is much less developed. Each program

has both advantages and disadvantages in terms of solving a specific problem. Multipurpose programs include the following: "Lyra", "MSC.Nastran", "APM Dynamics", "Dynamics - 3", "NONSAP", "Selena", "SCAD", "ABAQUS", "Zenith-95" " VESNA "and others. These software systems allow you to perform static, dynamic design calculations.

Programs suitable only for the dynamic calculation of any design are "ANSYS LS-DYNA", "LS-DYNA", "MSC / DYTRAN" "T-Flex / Dynamics". Narrow profile software complexes are intended for dynamic calculations of individual types of foundations and foundations. Such programs include "Dynardo". With the Dynardo program you can perform dynamic analysis of foundations (pile and slab) in conjunction with the ground for the effect of wind load. "Dynamics" is a software complex for the calculation of port hydraulic structures, machine foundations.

When calculating the FEM of dynamic problems on the basis of computers, the developers of software complexes are tasked with increasing the accuracy of the calculation of oscillation parameters. However, it is necessary to pay attention to the possibility of taking into account cracks and defects, changing the properties of the soil during operation during the calculation of the foundation. This area needs detailed study in the design and reconstruction of the foundations of machines [9].

Thus, the purpose of the study is to investigate the foundations and foundations of molding machines against the effects of dynamic loads, taking into account the damage to the foundations, the given properties of the soil that arose during their operation, the physical and mechanical characteristics of the soil of the bearing layer, as well as the underlying layers.

2.2. Experimental study of oscillation amplitudes of foundations of molding machines during reconstruction.

The molding and steelmaking workshop of the DniproVagonMash plant in Kamianske was investigated. The territory of the section of the steel-and-steel shop of the DniproVagonMash plant in Dneprodzerzhinsk is located about 200 m from the Dnipro River. Its relief is generally equal, substantially altered by human activity. Absolute Earth Marks: 62.00 - 63.50.

Adverse physical-geological processes and phenomena within the site include:

- thick (10 m or more) bulk soils (IGE - 1 and IGE - 2), which are very heterogeneous both in length and in depth of the massif. In terms of characteristics, such soils should be considered very compact. Very compact soils include litter soils (IGE - 3);

- dynamic impact on soils within individual sections of the site, in particular, the molding department.

The hydrogeological conditions of the territory are caused by the hydraulic connection of the groundwater with the water level in the Dnieper River.

The level of groundwater at the time of the survey (12.04.2005) was 8.60-8.80 m from the surface of the earth. Its fluctuations are fixed within 1.5 - 2 m.

Within the surveyed area the following engineering-geological elements (IGE) are highlighted:

IGE - 1 - bulk soils (industrial waste - slag, ash, ie products of complex thermal transformation of rocks and burning of solid fuel) are loose, from medium degree of water saturation to saturated with water, with sandy filler (sand of medium coarse, non-uniform) and uniform. ;

IGE - 2 - bulk soils (industrial waste - slag, ash and slag) loose, saturated with water, with sandy aggregate (sand dusty, inhomogeneous) and fragments of rocks;

IGE-3 - silt alluvial, greenish-blue-gray (saprolite - the final product of weathering of granites), with the inclusion of small fragments of crystalline rocks, from fluid-plastic to fluid;

IGE - 4 -granite is greenish-gray, medium-grained, slightly stained, non-softening in water, medium to durable.

Soil samples (IGE − 1a), which were passed directly next to and under the sole of the forming machine 3, were also selected.

IGE - 1*a* - bulk soils (industrial waste - slag, ash and slag) of small degree of water saturation, with sand filler (medium size sand, inhomogeneous) and rock fragments, subsidence. The filler content of sand up to 95%, dust content up to 5%. It should be noted that the IGE-1 under the sole of the foundation has been substantially altered by compaction during machine operation. This should have been manifested in significant deformations of the foundations in the past.

According to the values of its characteristics, such soils should be considered as very short [10-12].

To determine the amplitudes of oscillations and depositions of the foundations of the molding machines, measurements were made with the help of a measuring device - the vibrometer 107B (Fig. 2).

Fig. 2. Instrument for measuring oscillation parameters "Vibrometer 107B": *1* - accelerometer; *2* - probe; *3* - the vibrometer

Vibrometer 107V is a stand-alone microprocessor-based vibration measuring device designed to measure vibration parameters (vibration acceleration, vibration speed and vibration displacement).

At the same time, a spectral analysis of the vibration signal was performed. For digital signal processing (DSP), Fourier analysis is used - discrete Fourier transform (DFT), which operates a discrete time sampling of a periodic vibration signal. The exponential averaging was used in the calculation of the mean square value of the measured value. The Hanning weighting function was used to process the input signal. The main element of the device is a processor unit that provides control of measurement circuits, measuring signals, displaying information on the display. The device is operated using the keyboard. Dynamic vibration measurement ranges: 1-5000 microns. Sensitivity of the accelerometer: 0.1 to 500 pcl c^2/m.

The manufacturer of such molding machines is Kamyanske. The main parameters: dimensions in the plan 2730-3500 mm (Fig. 3), height - 2500 mm; weight - 4000 kg; vibrators - 2 pcs; shaking mechanism with an average number of blows: 200-250 beats/min; the course of the table when shaking: 30-60 mm.

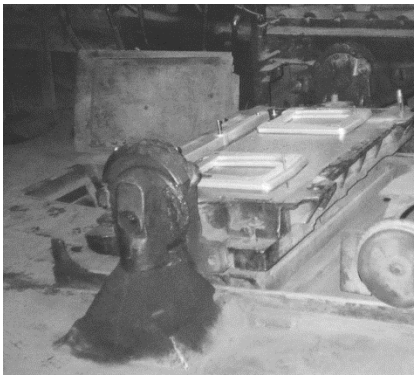

Fig. 3. Model 405 Forming Machine

The hollow folding was carried out by pneumatic hoist, with a load capacity of 1.5 t. from 3.25 to 3.75 m.

Reinforced concrete foundations for molding machines are made jointly with the floor. The condition of the foundation F-3 on the revealed defects indicates the impossibility of its safe operation, therefore, the study of the amplitude of the oscillations of the foundation, taking into account cracks and damage to the foundation during reconstruction. Structurally, the foundation is a massive base (bottom), on which the perimeter wall wall is installed along the perimeter and the base is connected in one. Cracks have been found in the area of connection of the foundation with the floor (Fig. 4).

Fig. 4. Horizontal reinforcement and corrosion of reinforcement in the wall of the base F-3

The lower massive part of the foundation had significant defects and damage during the 2005 survey, namely:

- through horizontal and vertical cracks on the front surface of the supporting part of the foundation;
- the presence of loose soil of the backfill of the foundation;
- destruction of the reinforced concrete base due to the impact of the equipment mounted on it;
- separation due to displacement of the central part of the foundation relative to its side walls.

Such damage is caused by the long operation of the foundations of the molding machines and does not allow full use of the foundation, so it must be reconstructed.

Table 1

Amplitude data of the vertical oscillations of the F-3 foundation for the molding machine of the molding shop

Data	Amplitude	
	mkm	mm
All disabled	17	0,017
Only the first machine is included	67,99	0,068
Only the second machine is included	248,1	0,248
Only the third machine is included	1153	1,153
Only the fourth car is included	136	0,136
The second and third machines are included	1852	1,852
The third and fourth machines are included	1657	1,657
Included are first, second, third, fourth machines	8878	8,878

To evaluate the impact of foundation fractures during operation, measurements of the dynamic characteristics of the foundations of the foundations of the forming machines were measured. The accelerometer sensor, when measuring the amplitude of the oscillations of the foundation, was mounted on the mortar and directly on the concrete surface.

The amplitude of oscillation of the base of the F-3 at the operation of the machine No. 3 was 1.15 mm - 0.5 mm - the value is almost 2.3 times higher than the permissible one [13,14]. And for all machines at the same time, the amplitude of the oscillations of the base F-3 - 8,878 mm - 0,65 mm is 13.7 times higher than acceptable. The foundations of the molding machines are made with deviation from the design decision (reduced sizes); between the foundation structure and the frame of the machine, the elastic gasket is missing or does not meet the requirements of regulatory documents; the wall around the perimeter of the foundation was combined with the floor design of the shop, which contradicts the requirements [13, paragraph 5.10.]. That is, these facts influenced the increase in the amplitude of the oscillations of the foundations, as evidenced by full-scale studies of the foundations.

3. Conclusions

1. The condition of the foundation F-3 on the detected defects indicates the impossibility of its safe operation, therefore, the study of the amplitude of the oscillations of the foundation, taking into account cracks and damage to the foundation during reconstruction.

2. To study the amplitudes of oscillations and sediments of the foundations of the molding machines, measurements were made with the help of a measuring instrument - the vibrometer 107B.

3. The oscillation amplitude of the F-3 foundation when operating the machine was almost 2.3 times higher than acceptable. And at work of all machines at the same time the amplitude of oscillations of the base F-3 13,7 times exceeds the allowable one. This is due to the fact that the foundations of the molding machines are made with deviation from the design decision (reduced size) and have damage during operation. Therefore, it is necessary to carry out the project of reconstruction of the foundation of the machine.

References

1. **Kirichek, Yu. A**. (2001) *Combined Massively Slab Foundations. Resource-saving methods of calculation and design*. PSASA, 2001. - 207 p.

2. **Pyatetsky, V.M.** (1988), Simplified formulas for the calculation of massive and walled foundations for machines with dynamic loads. Foundations, foundations and mechanics of soils. - 1988. - № 3. - P. 14- 6.

3. **Novak, S.M.** (1990) Vibration and noise protection in construction: K .: Builder, 1990. - 184 p.

4. **Zaporozhets, E.V.** (2005) *Calculation by the finite element method of flexible circular plates freely lying on an elastically low-viscosity base.* Prydnipr. state. Acad. building and arch. - 2005. - № 4. - P. 9-14.

5. **Shvets, V.B.** (2005) *Experience of the study of regional soil bases and deformations of the foundations of buildings and structures under static and dynamic impacts.* Prydnipr. state. Acad. building and arch. - 2005. - №7 - P. 113- 21.

6. Foundations of industrial, civil and transport structures on layered soil bases / [**Shvets V.B, Shapoval V.G, Petrenko V.D**, etc.]. Dnepropetrovsk: 2008. - 274 p.

7. **Grishin, A.V.** (2005) Nonlinear dynamics of port hydraulic structures: abstract. diss. for the sciences. Doctor of Engineering. Sciences: 05. 23.01. - Odessa, 2005.

8. **Nesterova, O.P, Uzdin, A.M, and Fedorova, M.Y** (2018) *A method for calculating highly damped systems with disproportionate damping* // Engineering and construction journal. 2018. No. 5 (81). Pp. 64–72. doi: 10.18720/MCE.81.7.

9. **Bandurina, O.V.** (2007) *Analysis of the dynamic state of the foundation of the molding machine* // Mechanics and physics of destruction of building materials and structures. - Lviv: Stonecutter, 2007. - Issue. 7. P. 388-395.

10. Engineering geology. Soil mechanics, foundations and foundations: Textbook / **M.L Zotsenko, V.I Kovalenko, A.V Yakovlev, O.O Petrakov, V.B Shvets, O.V Shkola, S.V Bida , Yu. L. Vinnikov**. - Poltava: PNTU, 2004. - 568 p.

11. **Kholmyansky, M.L** (2007) Calculation of displacements of the base at periodic load // *Foundations, foundations and mechanics of soils*. - 2007. - №5. - P. 2-6.

12. **Taranov, V.G.**(2005) *Some problems of the founding of the powerful turbo-generator sets* / V. G. Taranov, N. S. Shvetz, V. B. Shvetz // Pros. 16 ICSMGE.- 2005.- Osaka. - vol. 3. – P. 1567- 1570.

13. SNiP 2.02.05–87 Foundations of machines with dynamic loads:− Adopted:01/01/1985. - 32 c.

14. DSTU B B.2.1-17: 2009. Foundations and foundations of buildings and structures. Soils. Methods of laboratory determination of physical properties. Adopted: 02/08/2018 Date: 01/01/2019 - 36 p.

PHYSICAL-CHEMICAL AND TECHNOLOGICAL PARAMETERS OF IMPROVING PROFITABILITY OF UNDERGROUND COAL BURNING

Inkin O. V.
Doctor of Technical Sciences, Professor at Department of the Hydrogeology and Engineering Geology, Dnipro University of Technology, Dnipro, Ukraine

Puhach A. M.
Doctor of Public Administration, Dnipro State Agrarian and Economic University, Dnipro, Ukraine

Dereviahina N. I.
Candidate of Technical Sciences, Associate Professor at Department of Hydrogeology and Engineering Geology, Dnipro University of Technology, Dnipro, Ukraine

Abstract. Currently, coal is the main natural energy carrier in Ukraine due to its limited resources of oil and natural gas. A promising method for extracting coal is underground gasification using thermochemical and mass-exchange processes. Objective of the paper is to substantiate and implement the integrated approach aimed at the studies of filtration and mass-transfer processes within roof rocks of coal seams in the context of their underground gasification. Integrity of the studies is substantiated by the use of analytical calculations as well as physical and numerical modeling. Zones with different permeability have been determined and values of specific water inflow have been identified basing upon the performed numerical modeling and involving multicomponent transformations within roof formation.The research data actuality is in the studies of spatial and temporal dynamics of rock technogenic rock permeability above gasification channel depending upon their geological structure which will favour the substantiation of efficient engineering solutions to control a process of underground coal gasification under difficult hydrogeological conditions. It has been substantiated that almost all disturbing factors

have negative effect on gas calorifity whereas parameters of blast rate increase and static pressure growth in a gas generator have the most positive effect among the controlling factors. Aspects concerning the increase in loss of the produced gas that may reduce economic efficiency and environmental safety of underground coal gasification have been considered as well. Using the results, we improved the UCG technology by using the condensing products of gasification in the overburden.

Introduction. The necessity to make a technique of coal extraction, conversion, and use more ecologically feasible on the crucially new basis, while minimizing the environmental impact and reducing waste volume, is one of the topical problems to be solved by energy sector of Ukraine. Underground coal gasification (UCG) is the innovative solution to the problem. The process relies upon the transition of a mineral into a movable gas-condensate state within its occurrence by means of thermochemical and mass-exchange reactions. Gasification is followed by the loss of gas, being formed, into enclosing rocks which value is influenced by a number of factors. In this context, gas loss may achieve 30% affecting ecological compatibility and efficiency of UCG significantly. Thus, object of the paper is to study the parameters affecting the process of underground coal gasification as well as gas loss into roof rocks of underground gas generator.

Statement of basic material of the research. Relying upon domestic and the world practices, as well as scientific research [1-4], following basic factors, affecting the efficiency of underground coal gasification, can be singled out:

- mining and geological environment of the deposit occurrence;
- amount of water, involved into the gasification process;
- mineral composition of coal;
- characteristics of blast delivered to the gas generator; and
- arrangement of wells. The factors may be divided into controllable (those which can be varied during UCG process), i.e. blast characteristics, and arrangement of wells; and initial factors (which cannot be varied), i.e. mineral composition, and coal seam thickness.

Coal seam thickness, its depth as well as tectonic disturbance of enclosing rocks are among the mining and geological conditions affecting UCG process. Increased seam thickness results in the decreased heat loss in the environment, decreased specific water inflow, and ultimately, in the increased gas heat as well as gasification

process efficiency. However, specific gas output lowers due to the decreased seam mining as for its thickness. Thus, according to operation data of gas generators №№5, 5*a*,*b* and 6 of *Yuzhno-Abinskaia* station of *Podzemgaz* [5], gas heat output, obtained within *Vnutrenni IV* seam with 9 m thickness, is 1-1.5 MJ/m^3 higher to compare with *Vnutrenni VIII* seam with 2.2 m thickness. In this context, specific gas output is less by 1 m^3/kg and gasification efficiency of thicker seam is 10-15% higher.

Coal seam shallowness results in gas loss through overlying rocks; in turn, significant coal seam depth results in sharp efficiency decrease. Availability of faults, tectonic disturbances, and complicated seam hypsometry troubles the development of a reaction channel as well as control over a combustion source. Less than 100 m depth of a coal seam occurring within undisturbed rocks is optimum for its mining by means of UCG technique making gasification process more stable [2].

In the process of UCG, water balance is formed of natural coal humidity, inflows of water to a gas generator, water, containing in the blast, and water, being formed in the process of carbon, hydrogen, and methane combustion as well as CO conversion. Low water within the coal as well as nonavailability of water inflows may results in moisture lack which will decelerate gasification process; among other things that gives rise to the decreased CO formation during reduction reactions. Much water decelerates coal seam degassing, and reduces heat content of gas, being generated, due to its increased water ratio (Fig. 1).

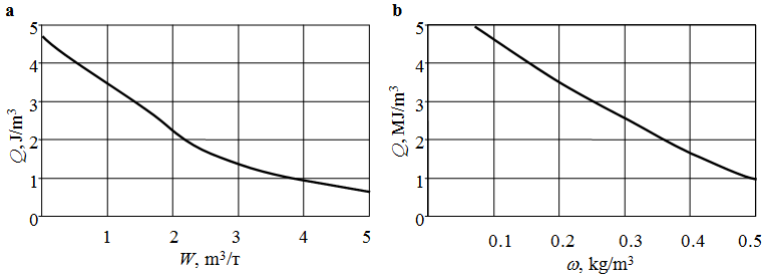

Fig. 1. Dependence of gas heat output (*Q*) upon: *a* - specific water inflow to the seam (*W*); and *b* - gas water content (ω)

Hence, the amount of water, involved in UCG process, should be controlled strictly depending upon specific conditions. The main procedures to control amount of water, participating in UCG process, are: preliminary dewatering of a deposit by means of drain wells; increased pressure of the blast to displace moisture from the gas generator; increased oxygen content within the blast; and increased air to be supplied.

Changes in characteristics of blast, delivered to the gas generator as well as chemical content of the blast, delivery rate, and delivery pressure are the important factors effecting gasification procedure [6-7]. Analysis of the results of coal seams gasification shows that blast oxygenation increases temperature within combustion area; delocalizes it; and intensifies heat output of the gas, being generated. If oxygen content of the blast to be delivered is two times higher than atmospheric one, then the content of CO and H_2 experiences 1.5 to 2 times increase. Water vapour with 0.15-0.2 kg/m^3 content added to air blast (within the drained deposits) intensifies reduction reactions increasing CO, H_2, and CH_4 output. Combined use of oxygen and water vapour (i.e. vapour-oxygen blast) is more efficient. A Table demonstrates the influence of blast content on the heat output of the generated gases in the context of different UCG stations.

Experiments, concerning the effect of blast intensity on the gasification process were carried out within gas generator #1 of *Yuzhno-Abinskaia* station of *Podzemgaz* during its different operation periods. To begin with, blast consumption was increased from 1000 to 6500 m^3 per hour; then, it was decreased gradually from 6500 down to 1000 m^3 per hour. Fig. 2 explains changes in the content and gas heat output in terms of various consumption of blast delivered for gasification.

The graph demonstrates that gas heat output increases depending upon the increase in the blast consumption. Moreover, the increase in heat value depends on carbon monoxide mainly. Carbon dioxide content within the gas reduces moderately while blast intensity increasing; at the same time, content of other components remains constant being more or less independent of the blast consumption.

Experiments have determined [8] that in addition to the blast intensity, interrupted blast to a reaction channel is one of the factors intensifying heating value of gas as well as the efficiency of UCG

station. Fig. 3 represents a graph of changes in gas composition in the context of Gorlovka *Podzemgaz* station.

Table 1

Influence of the blast chemical composition on the gas heat output

Blast type	Station	Gas heat output, MJ/m^3
Air blast	Lisichanskaia	3.1
	Podmoskovnaia	3.6
	Yuzhno-Abinskaia	4.6
Oxygen blast	Lisichanskaia	5.3
	Podmoskovnaia	7.3
Vapour-air blast	Yuzhno-Abinskaia	6.3
Vapour-oxygen blast	Podmoskovnaia	6.8

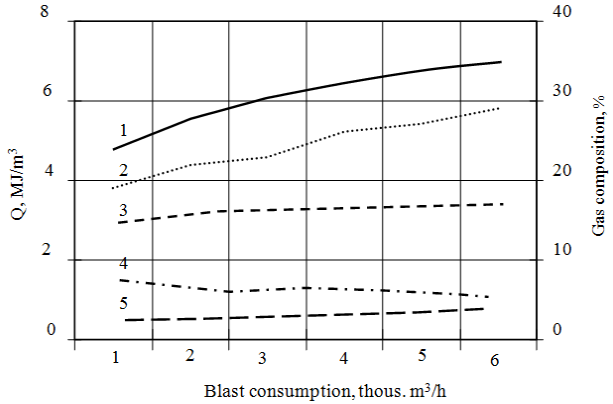

Fig. 2. Changes in gas heat output *Q* (1) and its composition CO (2), H_2 (3), CO_2 (4), CH_4 (5) in terms of various blast types

When gasification channel operated with the use of air blast (section *A*), H_2+CH_4 content within the gas was 15-18% in the context of 4.8 MJ/m^3 average heating value. After blast was interrupted to the gasification channel, intensive increase in H_2+CH_4 content started; the increase continued during the whole blastless period (section *B*). Then, when blast was restarted, composition of the gas, being generated, varied sharply. After 80 minutes it came up to the level when the channel operated with the use of air blast, i.e. H_2+CH_4≈15-18 % (section *C*). During blastless period, the peak H_2+CH_4 content was 58%, and heat output was up to 11 MJ/m^3.

Ash washing off coal surface, decreased aerodynamic drag factor, and increased coal loosening are the advantages of pulsating blast delivery. Use of the technique intensifies a process of gas release, and reduces the influence of negative factors arising with uniform blast.

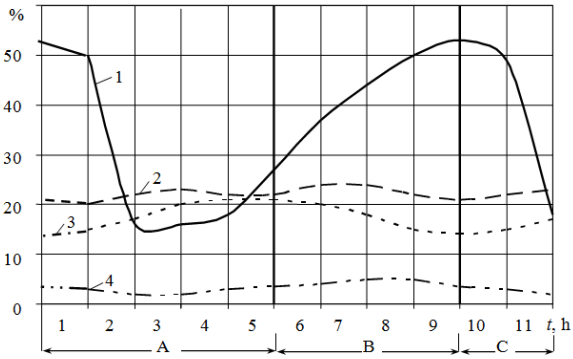

Fig. 3. Changes in the concentration of gas components (*1* - H_2; *2* - CO_2; *3* - CO; *4* - CH_4) during blast and blastless periods of underground gas generator operation

Effect of static pressure within gas generator on gas heat output and loss value was analyzed at *Podmoskovnaia* station of *Podzemgaz* during 1954-1956 [9]. During the period, static pressure varied significantly; averaged data can help estimate its change influence (Fig. 4). As it is seen in the graphs, increased pressure results in the increased heat output as well as in the increased gas loss. Average 10^4 Pa pressure increase results in 0.25 MJ/m^3 gas heat output increase and in 5% gas loss increase.

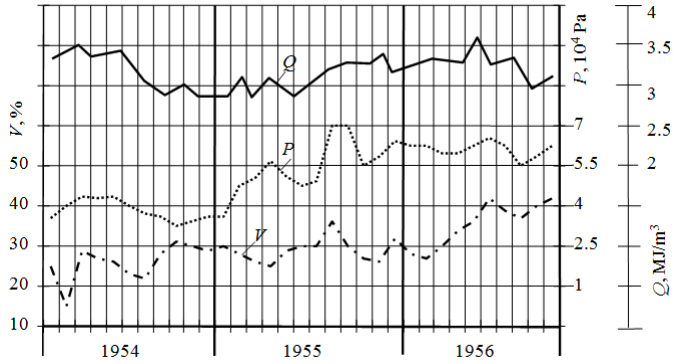

Fig. 4. Changes in static pressure (P), heat output (Q), and gas loss (V) in Podmoskovnaia station of Podzemgaz

Fig. 5 shows changes in gas humidity depending upon static pressure. Increase of static pressure results in certain forcing out of formation water owing to which moisture content of the gas reduces. The data confirm the dependence of the increased pressure upon the increased heat output. Moreover, high static pressure within gas generator prevents from rock roof caving and reaction channel filling up with molten rock.

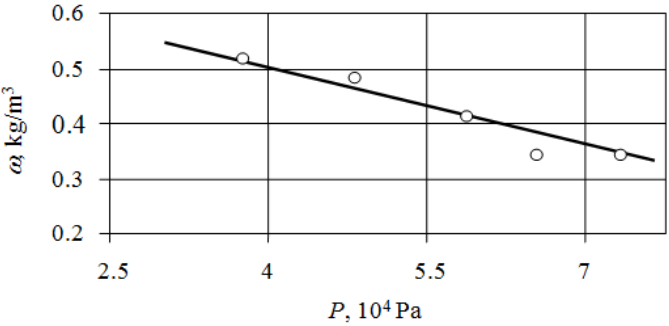

Fig. 5. Dependence of gas humidity (ω) upon static pressure (P)

Analytical approach to study temperature field distribution within rock mass during underground coal gasification (UCG). It is known that modes of conductive and convective rock mass heating may arise within underground gas generator in terms of different un-

derground water pressure-gas pressure ratios. Consider a situation when pressure within gas generator is less than water pressure; thus, gas effusion doesn't originate and heat transfer is of conductive nature, mass transfer with surrounding rock mass is minimal being carried out at the expense of diffusion.

In terms of static position of two rock mass phases (i.e. rock+water), thermal flow from gas generator may be reduced to axisymmetrical consideration of temperature field described by an equation of the type [11]

$$T(r,t)-T_0=\frac{q}{\lambda}R_2\left\{\frac{R_2^2}{R_2^2-R_1^2}\left[2\frac{at}{R_2^2}-\frac{1}{4}\left(1-2\frac{r^2}{R_2^2}\right)-\frac{R_1^2}{R_2^2}\left(\ln\frac{r}{R_1}+\frac{R_2^2}{R_2^2-R_1^2}\ln\frac{R_1}{R_2}+\frac{3}{4}\right)\right]+\right.$$

$$\left.+\sum_{n=1}^{\infty}\frac{\pi}{\mu_n}\frac{I_1\left(\mu_n\frac{R_1}{R_2}\right)I_1(\mu_n)}{I_1\left(\mu_n\frac{R_1}{R_2}\right)I_1(\mu_n)}\cdot\left[I_0\left(\mu_n\frac{r}{R_2}\right)Y_1\left(\mu_n\frac{R_1}{R_2}\right)-Y_0\left(\mu_n\frac{r}{R_2}\right)I_1\left(\mu_n\frac{R_1}{R_2}\right)\right]\cdot e^{-\mu_n^2\frac{at}{R_2^2}}\right\} \quad (1)$$

where q is specific heat flow capacity; R_1 and R_2 are radius of a gas generator radius and its depth relative to earth's surface respectively; r is distance from the gas generator axis to a reference point; t is time baseline period; T_0 is background rock mass temperature; μ_n are characteristic first-order numbers of Bessel function for boundary values R_1 and R_2; λ is heat conductivity factor of water-saturated rock mass.

Heat-transfer problem considering relative displacement of one of the rock mass phases in the context of analytical version is extremely difficult.

One-dimensional solution in terms of finite differences for static case and taking into consideration liquid phase transfer is represented by means of the equations

$$T_i^t=\frac{1}{2+\frac{\Delta x^2}{a\Delta t}}T_{i-1}^t+\frac{1}{2+\frac{\Delta x^2}{a\Delta t}}T_{i+1}^t+\frac{\Delta x^2}{2a\Delta t}T_i^{t-\partial t} \quad (2)$$

$$T_i^t=\frac{\frac{\lambda}{\Delta x^2}-\frac{C_wV_w}{\Delta x}}{\frac{C_r}{\Delta t}-\frac{C_wV_w}{\Delta x}+\frac{2\lambda}{\Delta x^2}}T_{i+1}^t+\frac{\frac{\lambda}{\Delta x^2}}{\frac{C_r}{\Delta t}-\frac{C_wV_w}{\Delta x}+\frac{2\lambda}{\Delta x^2}}T_{i-1}^t+\frac{\frac{C_r}{\Delta t}}{\frac{C_r}{\Delta t}-\frac{C_wV_w}{\Delta x}+\frac{2\lambda}{\Delta x^2}}T_i^{t-\Delta t} \quad (3)$$

where a is temperature conductivity coefficient; Cr, and Cw are heating capacities of rock and water respectively; and Vw is actual velocity of water flow; the mentioned specifications have already been involved.

To use the solutions correctly, certain features of the set problem should be mentioned.

Nonlinear temperature within axisymmetrical thermal flow is: temperature gradients decay at the distance of 3-4 radii of a thermal source reduced to a cylindrical form. In the context of the layer, practical evaluations can not involve difference between one-dimensional and axisymmetrical flows.

Formula (1) is true for boundary second-type conditions when a function of a heat flow is known. In terms of sensible temperature difference between thermal source (T_s) and absorptive medium (T_0), the function becomes constant

$$q = \sigma \cdot C(T_s - T_0), \tag{4}$$

where σ is Stefan-Boltzmann constant; and C is a coefficient depending upon capability of the medium to absorb thermal energy.

Underground gas generator emits thermal flow which temperature achieves 1000°C; as a rule, it means that condition (4) has been applied. It is obvious that within rock masses, being typical for coal deposits, a value of thermal flow according to condition (4) can be obtained from equation (1) on the experimental temperature measurements. To do that, use actual data from [12].

Results of variant calculations of dynamics of a temperature field in roof rocks of an underground gas-generator, confirmed by convergence with the actual data [12] create a possibility to evaluate the influence of hydrogeological conditions on it more differentially. The highest temperature distribution indexes in a five-meter contour are typical for a condition of rocks at natural humidity, i.e. when a massif is pre-drained. The smallest range of distribution of a temperature field is typical for conditions of water-saturated filtration flow at a filtration rate of 0.4 m/day, which is typical for location of sandstone rocks in a roof of a gas-generator. The study of distribution of a temperature field allows applying accurate corrections to change in

physical and mechanical properties of rocks when creating numerical mathematical models.

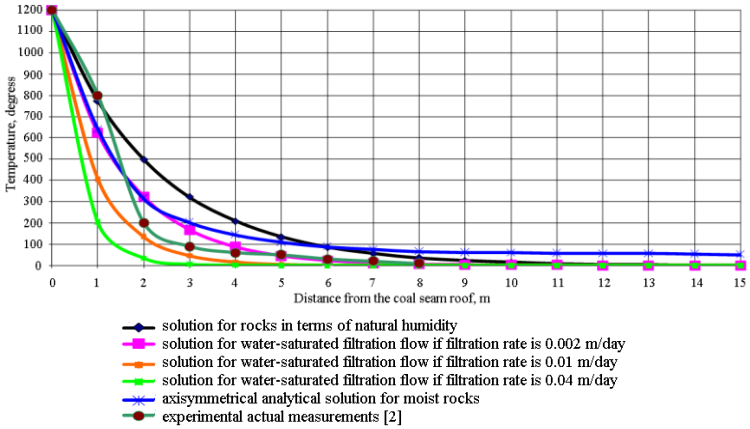

Fig. 6. Demonstrates results of variants calculations showing dynamics of temperature field within roof rocks of underground gas generator

Experimental procedure and results of the experiments in the context of physical modeling

Experimental module to study a process of distribution of temperature field of overburden rocks and their permeability (Fig. 7) was developed and manufactured taking into consideration the calculated similarity coefficients. Modeling of coal seam degassing process was performed within clear thermal-resistant tube with 1 m length and 0.04 m diameter. Compressor was used to supply air into combustion chamber. Air consumption was similar during the whole experiment. Pressure difference was recorded with the help of a manometer; temperature was recorded with the help of microthermocouple elements. Temperature within a medium being modeled (i.e. fine sand) was controlled from a combustion zone to combustion products extracted to atmosphere through a hydroseal. Gas consumption was recorded with the help of flow rate meter.

Source excess pressure providing air supply while igniting, was $1.013 \cdot 10^5$ Pa. The ignition was provided by means of thermal heat of coal. After the coal started firing, the ignition device removed and combustion rate was supported with the help of air supply. After filtration, the gas was extracted through a hydroseal to the atmosphere [6].

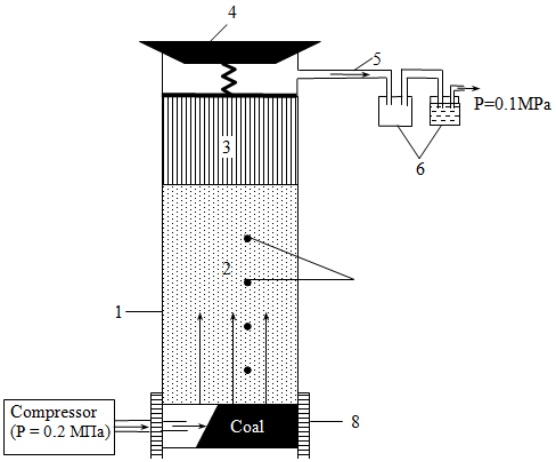

Fig. 7. Scheme of experimental facilities: *1* – clear thermal-resistant tube; *2* – roof rock of a coal seam (sand); *3* – laboratory cotton; *4* – a stopper; *5* – interconnector; *6* – moisture collector and hydroseal; *7* – thermocouple elements; and *8* – ignition device

The experiment involved visual observation of changes in the state of the coal seam and overburden rocks. Its period was limited by time of coal combustion (i.e. 45 minutes); then the medium, which has already been saturated by gasification products, is ejected from the thermal-resistant tube for the analysis of filtration properties.

To evaluate filtration parameters of the medium, its particle composition was studied with the help of grain-size analysis. Since effective diameter is 0.1 to 3 mm and heterogeneity coefficient is less than 5, nomogram of N.N. Bindeman has been applied to determine a filtration coefficient of the medium being modeled [13-14]. A value of the filtration coefficient was κ_f =3 m/day. Permeability coefficient k_p has been identified according to the dependence [15]

$$k_p = \frac{k_f \cdot \mu}{\rho \cdot g}, \tag{5}$$

where k_f is filtration coefficient; μ, and ρ are dynamic viscosity and water density. The calculated value of sand permeability within the experimental facilities was determined as $4.46 \cdot 10^{-11}$ m^2.

Permeability coefficient was also evaluated according to data obtained during the experiment relying upon formula (6) [16]

$$\kappa_p = \frac{2\mu P_{at} QL}{F\left(P_1^2 - P_2^2\right)}, \quad (6)$$

where P_{at} is atmospheric pressure ($1.013 \cdot 10^5$ Pa); Q is consumption of air being pumped to a combustion chamber ($4 \cdot 10^{-5}$ m^3/s; L, and F are a seam thickness and sectional area of overburden rocks (0.5 m and $1.25 \cdot 10^{-3}$ m^2); μ is average dynamic viscosity of filtering gas ($1.481 \cdot 10^{-5}$ Pa·s); and P_1, and P_2 are intake pressure and output pressure on the exit from a layer of gas-permeable rocks respectively ($2.026 \cdot 10^5$ Pa and $1.013 \cdot 10^5$ Pa).

The k_p value, determined on (6), was $3 \cdot 10^{-12}$ m^2. Difference between the obtained values of permeability coefficient is allowable taking into consideration empiric data of granular sand composition. The obtained experimental value should be used in the context of subsequent calculations.

In the course of the experiment, temperature was recorded in certain points of the model at the distances of 5, 10, 12, 15, and 20 cm from the combustion source. The temperature was recorded continuously with the help of identical thermal couples connected to multichannel recorder H-307. The thermal couples have been calibrated relative to hyperthermal temperature gauge ТУ-31А № 433 with ±2 °C error. Figures 8 and 9 demonstrate over-time temperature variations within the filtering medium.

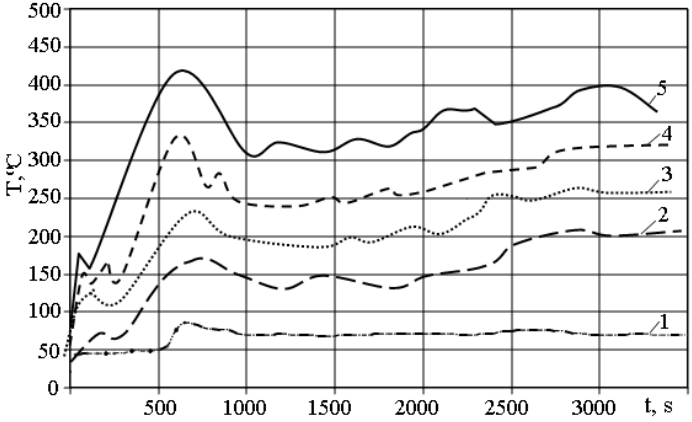

Fig. 8. Temperature variations within the filtering medium: 1,2,3,4 and 5 are temperature variations in a roof at the distance of 20, 15, 12, 10, and 5 cm from the top edge of the combustion zone respectively

The coal seam state as well as overburden rocks state was observed visually synchronous with temperature recordation; as a result, the following was determined:

- a zone of coal combustion is convex towards air motion; its geometry depends upon a supply rate;
- combustion zone-overburden rocks contact is unstable; overlying sand material penetrates into the combustion zone;
- in due course, the filtering medium (i.e. sand material) becomes grey with point distribution of black microinclusions;
- through the microscope, films of resinous substances, thickening within irregularities, are seen at the surface of the sand grains; and
- an arch is formed right above the zone of coal combustion; its stability depends upon the number of carboniferous inclusions and dimensions of the zone is determined with the help of the coal-combustion process duration.

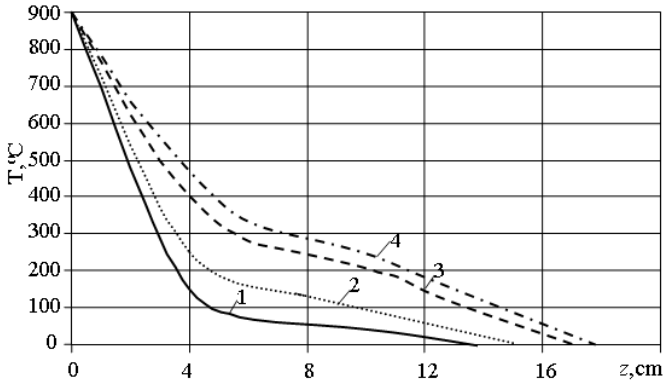

Fig. 9. Heating intensity of overburden rocks: *1*, *2*, *3*, and *4* are temperature distribution within a roof after 200, 400, 600, and 2500 s from the experiment beginning respectively

The data, obtained during the experiments, have helped conclude that rocks of immediate roof, occurring closer to the combustion zone, become of higher temperature and start varying first. Temperature increase within overburden rocks is followed by changes in their physical and mechanical characteristics. After rock heating, evaporation of natural and bound moisture starts. The evaporation originates

at the temperature of 100 °C; when the temperature achieves 200 ^{0}C and exceeds it, chemical moisture is liberated from roof rocks. Temperature increase up to 600 °C results in agglomeration and further decomposition of certain elements of overburden rocks (Fig. 10).

Fig. 10. Samples of sandy deposits and argillaceous deposits of Dnieperbas after 400 °C and 650 °C temperature field effect on rock mass

Analysis of curves (Fig. 7 and 8) means that roof rock heating process is intensive during the first 600 seconds from coal ignition within a combustion zone. Further heat transfer is a very slow process. The phenomenon can be explained by the fact of the decreased thermal conductivity of overburden rocks at the expense of changes taking place in their physical state (i.e. agglomeration, expansion, pore mudding) under the effect of high temperature and chemical effect of escaping gas. Insignificant temperature variations during the experiment can be explained by the unstable burning process and, consequently, temperature fluctuations within inlet boundary.

In the context of the medium, being modeled, vertical temperature distribution is nonlinear process. Distribution of temperature within certain areas (Fig. 8) corresponds to the processes of rock variations, condensation of filtering gas, and circulation of gas flows with constant temperature.

Both physical and filtration properties of the medium, saturated during the experiment, were calculated and determined from its different areas by means of a technique of cutting cylinders [10]; Table 2 contains the results.

The analysis shows that migration of gasification products (GP) within filtering medium results in nonuniform filling of pore space

with the formation of several zones. First of all, GP distribution depends upon temperature distribution. Poriness of overburden rocks and their permeability vary owing to mechanical blocking of pores by means of unburnt combustibles as well as physical and chemical *GP-rock* interaction. A zone of thermally altered rocks with solid carboniferous inclusions is the closest to the degassed area. In consideration of geometrical similarity coefficient (C_1=25), thickness of the zone will not be more than 0.5 m under full-scale conditions. Above the zone (at the distance of 0.5-2.5 m) a condensation zone is located which porous space is filled with resinous products. Within the overlying zone of undisturbed rocks, constant-temperature gas flows circulate.

The determined regularities coincide qualitatively with the data obtained at Shahtinsk station *Podzemgaz* [18, 19]. Thus, after gasification of a coal seam *Rozovy* with 0.4 m thickness, upper share of overburden rocks was melted layer containing unburnt combustibles with up to 20 cm thickness. Above the layer (at the distance of 0.2-1.5 m) rocks transferred gradually from melted (i.e. red colour) to undisturbed (deep blue ones).

Table 2

Structure and properties of overburden rocks saturated by gasification products (according to the data of physical modeling)

Zone	Distance from a coal seam roof, m	Prevailing processes	Permeability, m^2	Poriness, %	Density, kg/m^3
3	>2.5	Filtration gas flow (undisturbed rocks)	$3 \cdot 10^{-12}$	33	1510
2	0.5-2.5	Filtering gas condensation (pores are filled with liquid carbohydrates)	$1.6 \cdot 10^{-12}$	27	1630
1	<0.5	Rock melting (slagged and agglomerated rock with the inclusion of unburnt combustibles)	$9.2 \cdot 10^{-13}$	21	1740

Temperature above the layer being characterized was 700-800 °C; it dropped gradually down to 500 °C. Then, the temperature became

150-200 °C within a zone where the rocks transferred from heat-dried state to water-saturated one.

Zones of immediate roof annealing of *Rozovy* coal seam were located closer to a rock boundary of the underground gas generator to compare with the zones selected for the experiment. Their eliminating can be explained by slower decrease in the parameters of gas being filtered within the medium under modeling (sand material) and, consequently, by its greater permeability and heat transfer to compare with *Rozovy* seam roof (shale).

Numerical modeling of filtration parameters in the context of two-layer rock formation within a roof of a gas generator

If a coal seam roof contains water-proof argillaceous rocks (even with carbonaceous component) and up to 0.01 m/day values of filtration coefficient being typical for them (Fig. 11), the values of specific water inflow in the context of shear deformations of the rock formation [10,20] are within 0.11-0.23 m^2/day when gas generator operates.

The evaluation of changes in hydrodynamic mode of the complicated rock formation, containing gas generator, has shown that formation of filtration parameters depends directly on the changes in rock lithology under the effect of temperature field, geomechanical processes, and residual hydraulic pressure.

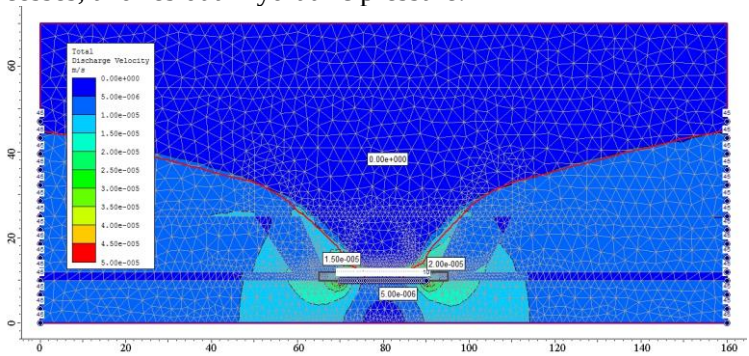

Fig. 11. Distribution of filtration rates within foliated rock mass disturbed by operation of the gas generator if waterproof layer is available within a roof of a coal seam, m/s

On the basis of numerical simulation, under conditions of a complex lithological structure of roof rocks [21], it is possible to deter-

mine the values of specific water inflows into the channel of a gas-generator at various stages of its formation with sufficient accuracy. The solution of this problem is possible only with a complex approach based on previously obtained data on the transformation of physical and mechanical properties of rocks under the influence of temperatures, and a change of geofiltration parameters in a geomechanically disturbed massif.

Conclusions

1. The studies concerning the factors, working upon the efficiency of underground coal gasification, have shown that perturbing factors are not equal to controlling ones in terms of their degree of influence. All the perturbing factors with the exception of a coal seam thickness have an adverse effect on gas heating power; in turn, blast characteristics are the most favourable ones among controlling factors. Hence, increased blast consumption and increased static pressure within a gas generator are the most active controllable factors working on the efficiency of UCG process. Conversely, that results in the increased gas loss which may decrease both profitability and environmental safety of UCG.

2. It is established that the zone of intensive thermal transformation of rocks reaches 2.5 m, which is confirmed by the results of physical simulation. The decrease of the temperature field to 100°C occurs in an interval from 1.5 to 4.5 m, and is non-linearly distributed vertically. These patterns coincide qualitatively with the data obtained at Shakhtynska station of "Podzemgaz".

3. The temperature increase in covering rocks is accompanied by a change in their physical and mechanical characteristics. Evaporation of natural and bound water begins after the warming of rocks. At a temperature above 200 °C, the release of chemical moisture from the roof rocks begins, and a temperature increase to 600 °C leads to sintering and further disintegration of individual components of covering rocks and a change in their permeability.

4. The physical modeling results have helped determine permeability coefficient for different roof zones above gasification channel. Difference between the obtained values of the permeability coefficient is allowable on the basis of granular sand composition.

5. Zones with different permeability have been determined and values of specific water inflow have been identified basing upon the performed numerical modeling and involving multicomponent transformations within roof formation.

References

1. **Korolev, I.V.** (1962). Dependence of the UCG process on geological and hydrogeological conditions at coal deposits. VNIIPodzemgaz, nauchnyye trudy. Podzemnaya gazifikatsiya ugley. № 8, 64 – 70.

2. **Yefremochkin, N.V**. (1960). Features of the groundwater regime in terms of coal gasification at the Shatskoye field. VNIIPodzemgaz, nauchnyye trudy. Podzemnaya gazifikatsiya ugley. № 3, 29 – 33.

3. **Yudin, I.D., Grigor'yev, V.V.** (1958). Underground gasification of coal in Kuzbass. Moskva. Ugletekhizdat, 28.

4. **Saik, P., Petlovanyi, M., Lozynskyi, V., Sai, K. and Merzlikin, A.** (2018). Innovative Approach to the Integrated Use of Energy Resources of Underground Coal Gasification. Solid State Phenomena, 277, 221-231.

5. **Nusinov, G.O., Brushteyn, N.Z., Kulakova, M.A., Dotsenko, P.N.** (1963). Underground gasification on the water-filled areas of a coal seam. VNIIPodzemgaz, nauchnyye trudy. Podzemnaya gazifikatsiya ugley. № 9, 85 – 88.

6. **Arinenkov, D.M., Markman, L.M.** (1960). Underground coal gasification. Donbass: Knizhnoye izdatel'stvo Stalino. 94.

7. **Inkin, O., Dereviahina, N**. (2018). Study of the migration processes in the roof of an underground gas-generator. Dniprop. Univer. bulletin, Geology, geography. 26 (1), 64-70.

8. **Kulish, Ye. D.**, 1958. Underground gasification of Moscow brown coal. Moskva. Ugletekhizdat. 36.

9. **Garkusha I. S**. 1964. Podzemnaya gazifikatsiya uglya [Underground coal gasification]. Trudy instituta i proizvodstvennyy opyt. Moskva. Nedra. №12, 36. (in Russian).

10. **Sotskov, V.O., Demchenko, Yu., Salli, S.V. & Dereviahina N.I.** (2017). Optimization of parameters of overworked mining gallery support while carrying out long-wall face workings. Naukovyi Visnyk Natsionalnoho Hirnychoho Universytetu. №6, 34-40.

11. **Russo, Yu.V.** (1957). Heat losses in the side rocks during the underground gasification of thin gentle and inclined coal seams. Podzemnaya gazifikatsiya ugley, (5).

12. **Kreynin, Ye.V.** (2004). Non-traditional thermal technologies for the extraction of hard-to-recover fuels: coal, hydrocarbons. Moskva: OOO "IRTS Gazprom".

13. **Tishkov, V.V.** (2014). Assessment of water inflow into the channel of an underground gas generator, when changing the permeability parameters of the massif, in the conditions of the Dnieper basin. Mining of Mineral Deposits. 8(4), 409-413. https://doi.org/10.15407/mining08.04.409

14. **Sadovenko, Í.O., Timoshchuk, V.Í., & Tíshkov, V.V.** (2010). Investigation of the influence of the stress-strain state of the host rocks on their filtration properties during underground gasification of coal seams. Naukovyi Visnyk Natsionalnoho Hirnychoho Universytetu, (3), 32-33.

15. **Sadovenko, I.A., Polyashov, A.S., & Inkin, A.V**. (2004). Experimental studies of the mechanism of filtration of gasification products. Gírnichodobuvna

promislovíst Ukraĭny í Polshchí: Aktualní problemy í perspektivy: Mater. Ukraĭnsko-Polskoho forumu hírnykív, 598-603.

16. **Mironenko, V.A.** (1983). Groundwater Dynamics. Moskva: Nedra.

17. **Semenenko, D.K., Russa, Yu.V., & Ovchinikov, V.M.** (1959). Gas permeability of a gas-filled space filled with slagged rocks. Podzemnaya gazifikatsiya ugley, (4), 19-21.

18. **Lomtadze, V.D.** (1952). Laboratory methods for the physicomechanical properties of sandy and clay soils. Moskva: Gosgeolizdat.

19. **Skafa, P.V.** (1960). Underground Coal Gasification. Moskva: Gosgeolizdat.

20. **Sotskov, V.O., Demchenko, Yu. I., Salli, S.V., & Dereviahina, N.I.** (2017). Optimization of parameters of overwoked mining gallery support while carrying out long-wall face workings. Naukovyi Visnyk Natsionalnoho Hirnychoho Universytetu, (6), 34-40.

21. **Fomichov, V., Sotskov, V., Pochepov, V., & Mamaikin, O.** (2018). Formation of a calculation model determining optimal rate of stoping face movement with a large deformation of a rock massif. ARPN Journal of Engineering and Applied Sciences, 13(7), 23 81-2389.

22. **Sotskov, V., & Saleev, I**. (2013). Investigation of the rock massif stress strain state in conditions of the drainage drift overworking. Annual Scientific-Technical Collection - Mining of Mineral Deposits, 197-202. https://doi.org/10.1201/b16354-36.

Scientific edition

TOPICAL SCIENTIFIC RESEARCHES INTO RESOURCE-SAVING TECHNOLOGIES OF MINERAL MINING AND PROCESSING

Multi-authored monograph

First publication

Chief editor **Zinovii MALANCHUK**,
Doctor of Sciences (Engineering), Professor, Director Institute of Postgraduate Education, National University of Water and Environmental Engineering, Ukraine.

Deputy chief editor **Serhii CHUKHAREV**,
PhD (Engineering), Associate Professor.

Technical editor **Elena SAMOILUK**

Signed to print 04.02.20. Format A5.
27 conventional printed sheets.
The printing run is 300 copies.

Publishing House "St.Ivan Rilski", Sofia, Bulgaria
University of Mining and Geology "St.Ivan Rilski" 1,
Prof. Boyan Kamenov Str